

Flame Retardant FRP Additives and Pyrolysis Modeling Software

A Major Qualifying Project Report

Submitted to the Faculty

of the

WORCESTER POLYTECHNIC INSTITUTE

In partial fulfillment of the requirements for the

Degree of Bachelor of Science

By:

Tanner Buxton

Elias Miner

Austin Payret

Jizhang Xu

April 2015

Project: NAD FN14

Professor Nicholas Dembsey, Advisor

Professor David DiBiasio, Co-Advisor

Abstract

Fiber Reinforced Polymers (FRPs) continue to grow in popularity as building materials, while manufacturers continue to develop additives, treatments, and manufacturing methods to improve their flame-resistant performance. Cone calorimeter tests, according to ASTM E1354, can be implemented to cost-effectively analyze these materials. These tests serve to compare the performance of flame resistant additives and treatments against currently marketed materials. Additionally computer models such as G-Pyro have been developed to simulate combustion reactions. This type of software offers the potential to simulate the effects of different additives or treatments on a given material at without costly lab tests. However, this software is new and relatively untested, and has not yet been implemented as a design tool. Through analysis of laboratory test results and computer generated test results, this project evaluated the effectiveness of new flame-retardant additives as well as the feasibility of implementing pyrolysis computer modeling in commercial research and development applications.

Acknowledgements

We would like to thank the following individuals and companies, without which we would not have been able to complete the project.

Professor Nicholas Dembsey – for providing the team with the necessary resources and advising the team on all challenges encountered throughout the project

Professor David DiBiasio – for supporting and co-advising the team throughout the research process

Randall Harris – for his help in the Fire Protection lab at WPI, and coordination of the team's lab time and equipment

Chris Lautenberger – for developing G-Pyro and providing supporting material, enabling our team to continue research and analysis of pyrolysis modeling software

Kreysler & Associates – for providing the real world inspiration for this project and furnishing the project team with all needed test samples

Authorship

Tanner Buxton	TB
Elias Miner	EM
Austin Payret	AP
Jizhang Xu	JX

Abstract	AP
Introduction	AP
Background	EM, AP
Cone Calorimeter Testing	EM, AP, JX
Lab Test Results	EM, JX
Standard Test Simulation	EM, JX
Computer Simulation	TB
Conclusion	TB, AP
Appendix A	EM
Appendix B	EM
Appendix C	TB, JX
Appendix D	TB, EM, JX
Appendix E	TB, AP, JX
Appendix F	TB, AP, JX
Appendix G	TB
Editing	TB, EM, AP

Table of Contents

Abstract	2
Acknowledgements	3
Authorship.....	4
List of Figures	7
List of Tables.....	8
1.0 Introduction.....	9
2.0 Background	9
2.1. Fiber Reinforced Polymers	9
2.2. Industry Standard Testing.....	10
3.0 Cone calorimeter Testing	10
3.1. Procedure.....	10
3.2. Samples Tested.....	11
4.0 Lab Test Results.....	11
4.1. Average Value	12
4.2. Comparison	12
4.3. Conclusion.....	14
5.0 Standard Test Simulation	15
5.1. International Building Code (IBC)	15
5.2. Flammability Parameter	15
5.3. ASTM E84 Screening Tool	16
5.4. Flame Spread Index (FSI).....	16
5.5. Smoke Developed Index (SDI).....	17
5.6. Results and Conclusion.....	18
6.0 Computer Simulation.....	18
6.1. G-Pyro	18
6.2. Governing Equations	19
6.3. Inputs.....	19
6.3.1. General Settings.....	19

6.3.2.	Properties.....	20
6.3.3.	Altering Microstructure	21
6.4.	Results.....	22
6.4.1.	Validity of G-Pyro.....	22
6.4.2.	Varying ATH.....	23
6.4.3.	Varying Coating Thickness	24
6.4.4.	Varying Layering Style.....	25
6.5.	Conclusions.....	26
7.0	Conclusions	27
8.0	Works Cited.....	28

List of Figures

Figure 1: Mass Loss Rate - 3A.....	12
Figure 2: Mass Loss Rate Comparison - Series 3.....	13
Figure 3: Mass Loss Rate Comparison - Neat.....	14
Figure 4: Comparison between a simulated test and a physical cone test.....	23
Figure 5: Comparison of G-Pyro results with varied levels of ATH.....	24
Figure 6: Comparison of G-Pyro results with varied coating thickness.....	25
Figure 7: Visualization of the effects of layering on G-Pyro results.....	26

List of Tables

Table 1: International Building Code Classes	15
Table 2: Summary of Average Flammability Parameter Values.....	16
Table 3: Summary of Prediction of Standard Tests	18
Table 4: Solid properties input for G-Pyro.....	20
Table 5: Kinetic properties input for G-Pyro	21

1.0 INTRODUCTION

This project looked at the affect that additives such as Alumina Trihydrate (ATH) and an exterior gelcoat had on the thermal and flame properties of fiber reinforced polymers (FRP). The samples provided by Kreysler and Associates were tested using a cone calorimeter. There was also a computer simulation element to the project. G-pyro is a pyrolysis simulator that was used to model the experiments that were completed throughout the course of the project. Overall these experiments and computer simulations were intended to evaluate the effectiveness of some of the innovations in flame retarding techniques and to further industry understanding of computer-based methods of material analysis.

2.0 BACKGROUND

To understand the relevance of fiber-reinforced polymers and the importance of their relative fire resistance, it is important to be familiar with the common applications of these materials as well as the codes and test standards that apply to them as used in building construction.

2.1. Fiber Reinforced Polymers

Fiber Reinforced Polymers, or FRPs are composite materials consisting of a polymer matrix reinforced with fibers. Usually, they consist of a fiber weave laminated with layers of resin or epoxy. Polyester resin is typical, although FRPs can also be made with epoxy, vinyl ester. The fiber weave is usually composed of glass fibers, though although fibers such as carbon fiber are also common (Crane 2013).

This family of materials offers numerous advantages. They are relatively lightweight, flexible, strong, durable structures that can easily be molded into a wide variety of shapes. They can be made to have a variety of visual appearances, from a glossy shine to a rough concrete-like finish, and can even be translucent. There are however, some disadvantages to FRPs in construction applications. The industry as a whole has less experience in working with them, they can be complex to design and manufacture, and they are combustible. Recent advances in the FRP technology have led to additives that allow

these materials to pass accepted industry standard tests such as ASTM E 84 and NFPA 285 (Kreysler, 2013). For more information about FRP technology and varieties, see Appendix B.

2.2. Industry Standard Testing

The International Building Code (IBC) is a technical manual for engineers, designers, and construction professionals worldwide that provide standards and best practices for the design and construction of many types of buildings. It focuses on public health, safety and welfare, including fire safety. In the chapter regarding interior finishes, the IBC establishes standards for fire-retardant performance for wall coverings. These standards address two primary factors: how quickly the flame actually spreads on a material, and the volume and thickness of the smoke produced. To test both of these factors, the IBC specifies the standard test ASTM E 84 (2012 International building code handbook).

The ASTM E 84 is a large-scale fire performance test designed to evaluate the suitability of materials to be used as interior finishes. In essence, this test exposes a large sample of material to an intense propane-gas fire and measures the smoke produced as well as how far the flame travels along the sample. From this test, materials are sorted into three classes based on fire performance – A, B, or C. A-class materials have the best flame-retardant performance, B is moderate, and C is relatively basic performance. Commonly the IBC specifies A-class material for primary means of egress such as fire escape stairwells, B for secondary corridors, and C for rooms and enclosed spaces (ASTM, 2015). For more information on the IBC, ASTM E 84, and other common industry standard fire-performance tests, refer to Appendix A.

3.0 CONE CALORIMETER TESTING

3.1. Procedure

The cone calorimeter is a piece of equipment that was used to test, as per ASTM E 1354, the thermal properties of the samples provided (ASTM, 2014). The cone consisted of an electric heater that, for the duration of all the experiment that were conducted, to an incident heat flux of 50 kW/m². This type of testing is highly beneficial to any company that cannot afford to run large scale ASTM E84 tests for all iterations of a development project.

The cone calorimeter can run a high volume of bench scale tests that are relatively inexpensive and still comparable to the large scale tests.

The apparatus exposes a four inch by four inch square of FRP or epoxy resin to the aforementioned heat flux in order to burn the sample. As the sample burns the cone calorimeter directly measures mass loss rate, smoke obscuration, and heat release rate. These results are presented in a spread sheet layout that can be used to see trends in the data via graphing. Resulting graphs can then be examined to compare one material to another to see larger, overarching patterns throughout all the samples.

3.2. Samples Tested

Kreysler and Associates provided sixteen varieties of material to test, with many samples of each variety. These samples were sorted by finish and Alumina Trihydrate (ATH) content. They were sorted into four Series 2, 3, 4, and 5. Series 2 is pure epoxy with no glass, series 3 is epoxy and glass, series four is epoxy and glass with gelcoat, and series five is epoxy and glass with gelcoat and a sand finish. For each finish type, Kreysler and Associates provided samples with 0%, 5%, 10%, and 20% ATH. Letters are used to designate ATH concentration with “a” referring to 0%, “b” referring to 5%, “c” referring to 10%, and “d” referring to 20%. So for example, 5b is a sample with a gelcoat and sand finish containing 5% ATH.

4.0 LAB TEST RESULTS

52 tests of 16 different samples were conducted on the cone calorimeter, including series 2,3, 4, and 5. All of the samples tested from series two during exhibited strongly intumescent behavior, each sample from this series expanded to roughly 45mm from around 7mm. Because the cone calorimeter depends on samples being roughly geometrically stable, series 2 did not yield valid data from cone calorimeter tests. Therefore, only the results of series 3, 4, and 5 will be reported in the paper.

For each specimen tested on the cone calorimeter, the team conducted three tests runs, to isolate human, systematic, and conditional errors. Our team summarized and analyzed five parameters. These parameters included mass loss rate, heat release rate, heat of combustion, extinction coefficient, and specific extinction area. Due to the concern of

space, only mass loss rate will be shown in this section. For a comprehensive summary of the data recorded, refer to appendix E.

4.1. Average Value

To analyze the performance of the various samples, all three test runs for each type of sample were averaged, and then these averaged results were compared to the averaged results for other types of samples. This allowed the team to accurately study the performance of the various samples relative to each other.

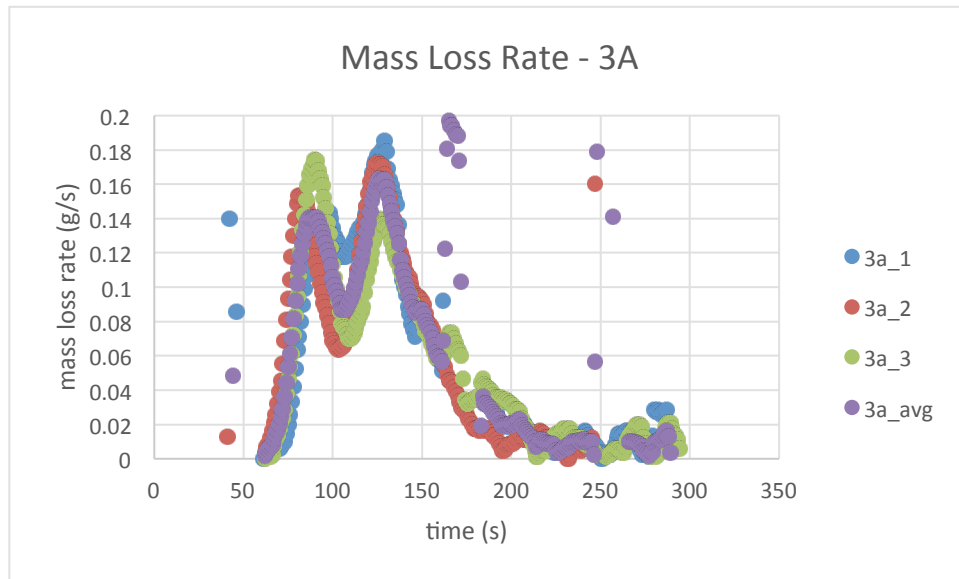


Figure 1: Mass Loss Rate - 3A

The figure above shows an example of data averaging, using our three test runs for sample 3A, glass and epoxy with no added ATH or gelcoat. As can be seen, the averaged curve (in purple) accurately reflects the data the team collected for the three test runs. For all tests, data was refined with the strategies: limiting the magnitudes into a reasonable range, using 9-point average method to smooth the curve, and selectively throwing out inconsistent test runs. Refer to Appendix D for a detailed explanation of our data handling strategy.

4.2. Comparison

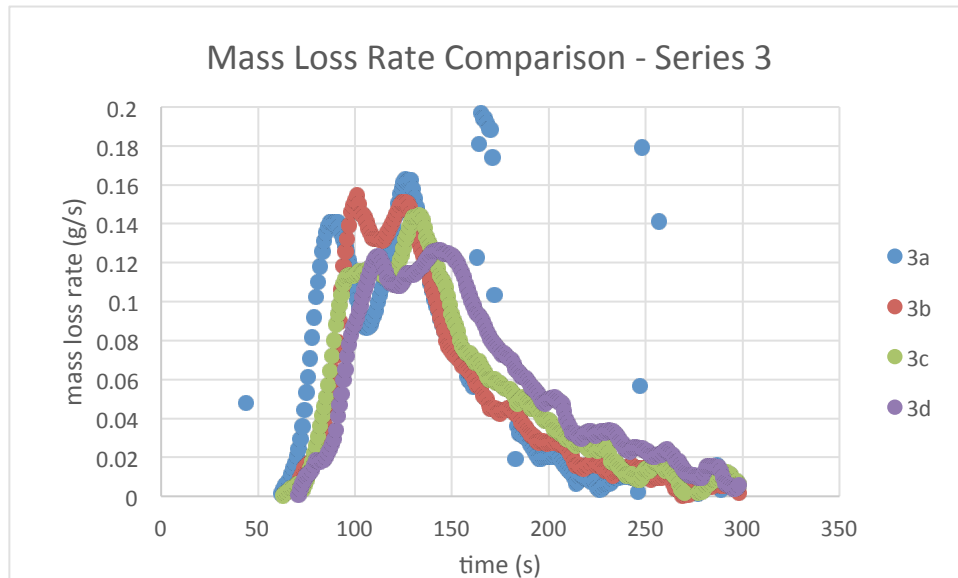


Figure 2: Mass Loss Rate Comparison - Series 3

The graph shown above is an example of an in-series comparison, which is a comparison between samples with the same type of fire block and varying ATH concentration. These comparisons were conducted for every sample series we tested to isolate the impact of ATH on flame-retardant performance. Note that each curve represented above is an average curve, found in the manner indicated above. Refer to Appendix E for in-series comparisons for the series tested.

The figure above also offers some insight into the performance of the specimens tested, particularly by comparing the peak and overall burn time of each sample. Increasing the concentration in the ATH sample lowered the peak of the curve, indicating a less energetic burn. Although it does indicate a less energetic burn, the difference is still relatively small indicating that ATH is not a significant factor. Burn time was largely unaffected. To conserve space, only series three (glass and epoxy) is shown here. Series four and five, both with varying types of gelcoat, exhibited similar results with respect to ATH concentration. For more data and more comparisons, refer to Appendix E.

Figure 3 below is an example of cross-series comparisons, which are comparisons between samples with the same ATH concentration and different types of fire block, showing the effect of the type of fire block. Below, 3a, 4a, and 5a are compared. See Appendix E for all the cross-series comparisons.

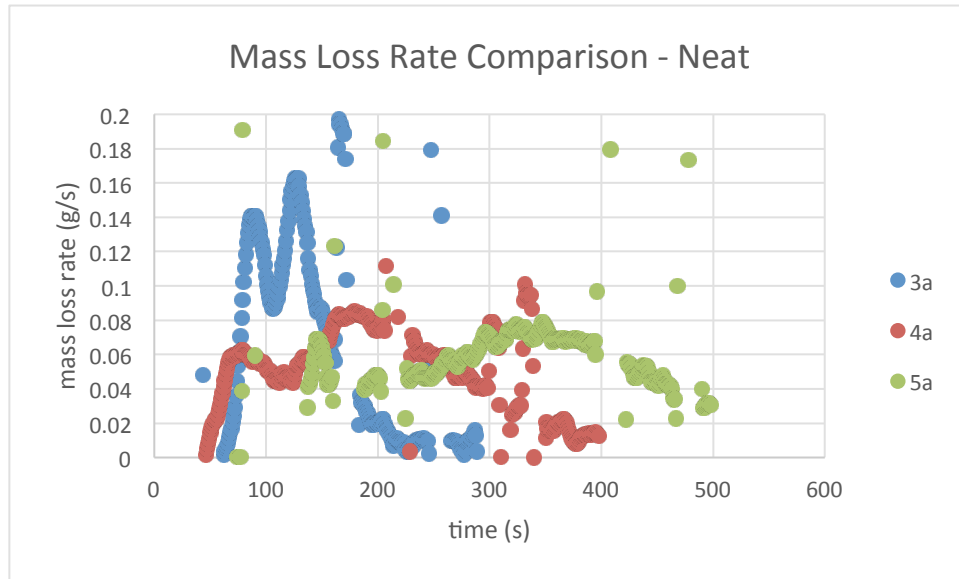


Figure 3: Mass Loss Rate Comparison - Neat

Figure 3 shows that the samples constructed with gelcoat perform significantly better than samples without. The gelcoat was shown to significantly slow the reaction, as can be seen by the lower peaks and longer overall curve. The gelcoat (4a) and sand-finish gelcoat (5a) had roughly similar peaks, although the sand-finish gelcoat did have a slightly longer overall burn. The samples with other concentrations of ATH exhibited similar behavior to the samples shown above. From these results, the team concluded that gelcoat significantly improved the fire-retardant performance of the materials tested. For more data and more cross-series comparisons, refer to Appendix E.

4.3. Conclusion

It was found that both gelcoat and ATH additives improved the flame-retardant performance of the materials tested. The gelcoat proved to be very effective, regardless of the presence or absence of the sand finish. The ATH concentrations we tested did improve the performance, but only minimally so.

5.0 STANDARD TEST SIMULATION

Any material used as an interior finish needs to meet IBC standards for safety. One of the primary applications of FRP materials is interior finish, so it was important to extrapolate the results of the team's lab tests to industry standard tests such as ASTM E 84.

5.1. International Building Code (IBC)

The Flame Spread Index (FSI) is a measure of material's propensity to burn rapidly and spread flame, and Smoke Developed Index (SDI) is a measure of the intensity of smoke a material emits as it burns. The IBC categorizes materials into three classes based on FSI and SDI.

Table 1: International Building Code Classes

	FSI	SDI
Class A	0-25	less than 450
Class B	26-75	less than 450
Class C	76-200	less than 450

5.2. Flammability Parameter

Flammability parameter, referred to by the Greek letter β (Beta), is a term used by the theoretical predictions of Mowrer and Williamson (1991). These predictions are based on the concurrent flow flame spread model developed by Cleary and Quintiere (1991). When the flammability parameter has a positive value, it represents flame spread acceleration, and a negative value represents a decelerating spread. The parameter can be calculated based on direct and indirect measurements of cone calorimeter:

$$\beta = k_f \dot{Q} - \frac{t_f}{t_{bo}} - 1 \quad (1)$$

In the Equation 1, t_f (seconds) is the time to ignition of the sample under the given Incident Heat Flux (IHF), t_{bo} (seconds) is the burn duration and \dot{Q} (kW/m²) is the Heat Release Rate Per Unit Area (HRRPUA). The parameter k_f is a constant related to the flame length or forward heating distance and is assumed to be 0.01 (m²/kW).

The 2014 cone calorimeter MQP group studied three different combinations of input needed for Equation 1: peak HRRPUA and visual burn duration, average HRRPUA and visual burn duration, and average HRRPUA and burn duration based on total energy released. Their results showed that the two combinations based on the average HRRPUA showed the most consistent outputs (Anaya, et al). Therefore, our team decided to use average HRRPUA and visual burn duration to calculate the flammability parameter.

Table 2: Summary of Average Flammability Parameter Values

ATH (%)	Series 3	Series 4	Series 5
0	0.10	-0.10	-0.06
5	0.14	-0.24	-0.09
10	0.04	-0.22	-0.08
20	0.02	-0.25	-0.21

As shown in Table 2, all samples without gelcoat (series 3) showed accelerating flame spread, and all the samples with gelcoat (series 4 & 5) showed decelerating flame spread. The results shown above additionally suggested that the relative concentration of ATH does have an effect, although it is relatively insignificant. The results also showed that the presence of a gelcoat significantly reduced the flammability parameter, with or without the sand finish (series 4 or 5, respectively).

5.3. ASTM E84 Screening Tool

Both FSI and SDI are typically measured using the ASTM E 84 tunnel test. For more information on the ASTM E 84 test, refer to Appendix A. Because of the extreme cost associated with this test, results from cone calorimeter tests were extrapolated mathematically to compare FSI and SDI. The method used is the one developed by 2013 MQP team (Acosta, et al).

5.4. Flame Spread Index (FSI)

In regular ASTM E 84 tests, the FSI is calculated from the time integral of the flame extension utilizing the following equations:

$$FSI = 0.515 \cdot A_T \quad A_T \leq 97.5 \quad (2)$$

$$FSI = \frac{4900}{195 - A_T} \quad A_T > 97.5 \quad (3)$$

In the Equations 2 and 3, the flame extension, A_T , has a unit of $ft \cdot min$

A screening tool has been developed to simulate flame extension in the tunnel test by the 2013 MQP Team (Acosta, et al). This tool works on the basic assumption that the fire during the ASTM E 84 test can be modeled as a basic 2-D fire with a point source. Though this tool provides useful data, it is limited because these calculations carry an uncertainty of 30%, due to the dramatic scaling that is necessary. The 2013 team developed two different versions of the tool, to be used with FRPs with or without additional coating.

$$L_{f-coated} = \left(0.2322 \cdot \left(\frac{0.6\dot{Q}+88}{0.43} \right)^{0.6496} \right) - 4.5 \quad (4)$$

$$L_{f-noncoated} = \left(0.1574 \cdot \left(\frac{0.6\dot{Q}+88}{0.43} \right)^{0.6496} \right) - 4.5 \quad (5)$$

Where L_f (ft) is the simulated flame extension, and \dot{Q} (kW/m²) is the HRRPUA from the cone calorimeter test results. For each test, L_f was calculated for each recorded time step based on HRRPUA. To find FSI, the team integrated L_f over the time of the test, and averaged the results of three test runs. Zero flame extension was assumed before the time to ignition. Refer to Appendix F for more details about this calculation.

5.5. Smoke Developed Index (SDI)

In the ASTM E 84 test, the SDI is calculated using the smoke thickness, measured by recording light obscuration through the smoke. This value is integrated over the time of the test and then is compared in a ratio to established standards to find the value for SDI. These calculations follow the Janssens model, and follow the equations shown below (2008).

$$SDI = \frac{(\int_0^{10 \text{ min}} (100 - T\%) dt)_{specimen}}{(\int_0^{10 \text{ min}} (100 - T\%) dt)_{red oak}} \times 100\% \quad (6)$$

$$T\% = \frac{100}{\exp\left(\frac{22.268 \cdot k}{0.645\dot{Q} + 125.6}\right)} \quad (7)$$

In the Equations 6 and 7, k (m⁻¹) is the extinction coefficient, \dot{Q} (kW/m²) is the HRRPUA, and $T\%$ is the light transmission. For each test, $T\%$ was calculated at each time step based on time-varying HRRPUA and extinction coefficient. SDI was calculated based off of these calculations repeated for each identical test run and then averaged. The

uncertainty of the calculation was about $\pm 20\%$. Refer to Appendix F for further details about this calculation.

5.6. Results and Conclusion

Table 3: Summary of Prediction of Standard Tests

ATH	Series 3			Series 4			Series 5		
%	FSI	SDI	Class	FSI	SDI	Class	FSI	SDI	Class
0	30	325	B	15	345	A	27	320	B
5	32	340	B	14	335	A	31	325	B
10	28	330	B	13	325	A	32	315	B
20	27	310	B	15	305	A	32	285	B

The table above shows the ASTM E 84 predictions for the samples this team evaluated. All of the samples tested have an SDI that places them in class A, and for FSI all samples are class A or on the low end of B class ratings. From the results, it was found that the relative concentration of ATH does improve the flame-retardant performance of the samples, although minimally. In contrast, the gelcoat significantly improves the performance. Interestingly, it was found that series 5 (gelcoat with sand) performed poorly when compared to series 4 (gelcoat no sand). This may be due to the slightly different calculation technique utilized, because the sand finish on series 5 means that we needed to follow the procedure for a coated FRP. With all of these calculations, it is important to remember that the FSI indices have an uncertainty of roughly 30%, and the SDI indices have an uncertainty of roughly 20%. Although many of the samples fell into the B class rating, with uncertainty they could fall into an A class rating. Therefore, all of the samples tested were either class A or marginally B class.

6.0 COMPUTER SIMULATION

6.1. G-Pyro

G-Pyro Version 0.700 is a young program that simulates thermo-chemical processes occurring in thermally stimulated solids. It models pyrolysis and acts as a property estimation program that can analyze properties based on Thermogravimetric Analysis and Differential

Scanning Calorimetry lab results. For the purpose of this project, G-Pyro was used for its pyrolysis modeling capability. Considering the previous work explained using the cone calorimeter, in order to achieve results equitable to the ASTM E 84 test, computer modeling would ideally be able to reduce further the necessity of spending larger amounts of money on testing. In order to be able to consider G-Pyro not only as a pyrolysis model or property estimation program, but also instead as a design tool, an understanding of G-Pyro had to be developed. After understanding the equations being used in G-Pyro, the next step was to learn how to use the software. With the ability to manipulate and understand the inputs and outputs, analysis on G-Pyro could begin. G-Pyro was critiqued on its ability to model fire similar to how the cone calorimeter does, how well it modeled compared to known results, and finally, whether it could actually be considered as a feasible design tool and what recommendations could be made. The sections below focus on the necessary steps in order to achieve the specified results, but for more information on the general aspects of G-Pyro as well as additional graphs for the results refer to Appendix: G-Pyro.

6.2. Governing Equations

At its heart, G-Pyro uses several governing equations to model fire behavior. Some equations used include several conservation equations for mass and energy, a gas phase momentum equation, reaction rate equations (Arrhenius), and equations of heat of reaction, absorption, and release. For a detailed description of the equations that G-Pyro operates please refer to the G-Pyro Technical Reference Guide (Lautenberger 2009).

6.3. Inputs

G-Pyro is highly dependent on user knowledge in order to be used effectively. The inputs themselves require an understanding of the material properties associated with each substance in the sample, the reaction properties, the physical makeup of the sample, the conditions of the simulation, and general settings for operating G-Pyro. The G-Pyro User's Guide (Lautenberger, 2009) can provide a more complete description of the required inputs and operation of G-Pyro.

6.3.1. General Settings

When utilizing G-Pyro the general default settings for the simulations were kept the same, but only a few important changes were made. Incident heat flux of every test was set to 50

kW/m^2 . The duration of the simulation was also changed for each test to ensure that the sample had burned out. BC_Patches was turned on and set so that the radiative cooling was turned on by setting reradiation to true. The outputs can also be changed in order to get profile and point data at any thickness and any time. Possible outputs include temperature, bulk density, porosity, composition, conversion, reaction rate and mass loss rate. The only output that is shown in this section is the mass loss rate, which can be used to best compare simulated results to cone results. Other outputs for each result can be found in Appendix: G-Pyro.

6.3.2. [Properties](#)

There are two major sets of properties that were required to create a sample in G-Pyro: solid properties and reaction properties. The solid properties refer to innate properties of the components that are used in the samples. One of the initial difficulties with acquiring the properties of the components that were to be simulated was that they could not be obtained easily or quickly. This required the use of an alternate that would model similarly hopefully, while also not compromising later analysis. With that in mind, a hybrid material was developed that combined properties of a modified acrylic and an unsaturated polyester FRP.

Component	Resin	Resin Residue	ATH	ATH Residue	Glass
Thermal Conductivity, k [W/m*K]	0.23	0.19	1.220	0.240	0.18
Density, ρ [kg/m ³]	1200	253	2300	1558	2600
Heat Capacity, c [J/kg*K]	1400	1900	1200	1200	400
Emissivity, ϵ	0.84	0.90	0.81	0.89	0.88
Radiation absorption, κ [m ⁻¹]	$1 \cdot 10^6$	$1 \cdot 10^6$	$1 \cdot 10^6$	$1 \cdot 10^6$	$1 \cdot 10^6$
Radiation across pores, γ [m]	0	0.00348	0	0.00475	0.00769

Table 4: Solid properties input for G-Pyro

Kinetic Properties of the new hybrid were based on the reactions of the unsaturated polyester from Esther Kim's 2014 paper, Parameter Estimation for Comprehensive Pyrolysis Modeling: Guidance and Critical Observations.

Reaction	Pre-Exponential Factor [s ⁻¹]	Activation Energy [kJ/mol]	Heat of Vaporization [J/kg]	Order of reaction
Resin -> Resin Residue	5.0 ¹³	195	172000	1.125
ATH -> ATH Residue	2.5 ¹¹	140.1	1000000	1.24

Table 5: Kinetic properties input for G-Pyro

The above properties are from the work of the 2014 MQP group (Gillespie, 2014).

6.3.3. [Altering Microstructure](#)

After the properties of the materials were outlined, the physical make up of the samples were then defined. The samples were capable of being varied in several manners. Each sample can be made up of several layers. For each layer, the thickness, composition, and back face contact resistance could be specified. Several different variations were considered when creating the electronic sample. The thickness of each sample was kept constant at 9 millimeters for all final tests, unless a coating was added which added to the overall thickness of the sample. The sample was considered to be well mixed, which eased some constraints with regards to consistency between samples. Not all the samples weighed the same due to the fact that volume was kept constant and the density of the samples changed.

The samples were created in order to compare to cone calorimeter results from previous MQPs, which would hopefully line up more closely with the hybrid properties, the results of the previously discussed cone calorimeter results, and possible changes that would highlight limitations of G-Pyro. The samples simulated include variations in ATH composition, coating thickness, glass composition, and glass layering. For variation in ATH, the sample was a single layer made up of 91 cells for a total thickness of 9mm. The composition was changed so that a simulation was run for compositions of 0, 5, 10, and 20 % ATH. The coating samples were

designed to have 91 cells plus an additional 1 cell for each 0.1 cm. The variation in layering consisted of 91 cells which was made up of a top and bottom layer of 0.395 mm, alternating glass layers of 0.5 mm and resin/ATH layers of 0.785 mm. Illustrations of the simulated materials can be found in Appendix: G-Pyro.

6.4. Results

In order to properly compare the simulation results to cone results, the samples were all compared with regards to their mass loss rate history. The ignition times were aligned in order to make the comparisons on an equal basis. All simulations were run at 50 kW/m^2 , which is equivalent to incident heat flux of all the cone tests. All tests when not specified otherwise used a composition of 50% glass, and 100:133 parts resin:ATH, at a thickness of 9mm.

6.4.1. Validity of G-Pyro

The first simulation that was compared was a straightforward evaluation of how well G-Pyro could model a sample burning based off previous work done with materials similar to the hybrid that was created. The results of the simulation versus the cone data from 2014 cone calorimeter MQP Team are shown below (Anaya, 2014).

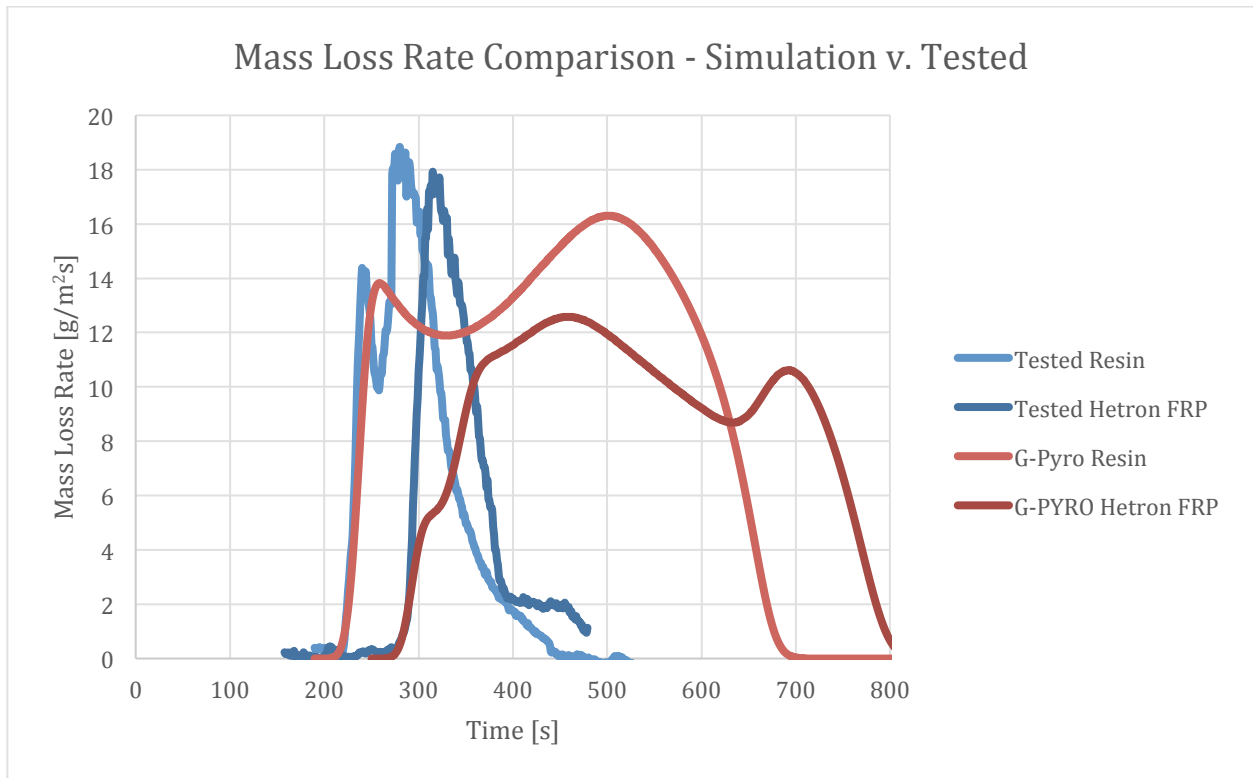


Figure 4: Comparison between a simulated test and a physical cone test

There are three primary discussion points that can be formulated based on the above graph. The first is the initial spike that occurs due to ignition and how well the simulation follows it. The initial spike and the general slope line up well. The peak of each simulated curve does not match the peak of the tested curve. The final point is the overall length of the burn, which is significantly longer for the simulated cases. A possibility for the difference may stem from the nature of a simulation and how it is idealized. The tested samples may have burnt out before all the resin had burned away as is the case in the simulated version. With these results, it is clear that G-Pyro is not quantitatively accurate enough to be valid for exact comparisons, which is reasonable due to the difficulty associated with pyrolysis modeling and the age of the program.

6.4.2. Varying ATH

With the knowledge that G-Pyro is not a quantitative tool, further study was done to determine its capability as a qualitative tool. Using some of the results of the cone tests earlier, a simulation was done to determine how well G-Pyro could record changes and also how close the changes were. The two main factors in the earlier tests were the variations of ATH and of

coatings. Below is a graph showing the results of the simulations where ATH was varied with the same respects as in the cone samples.

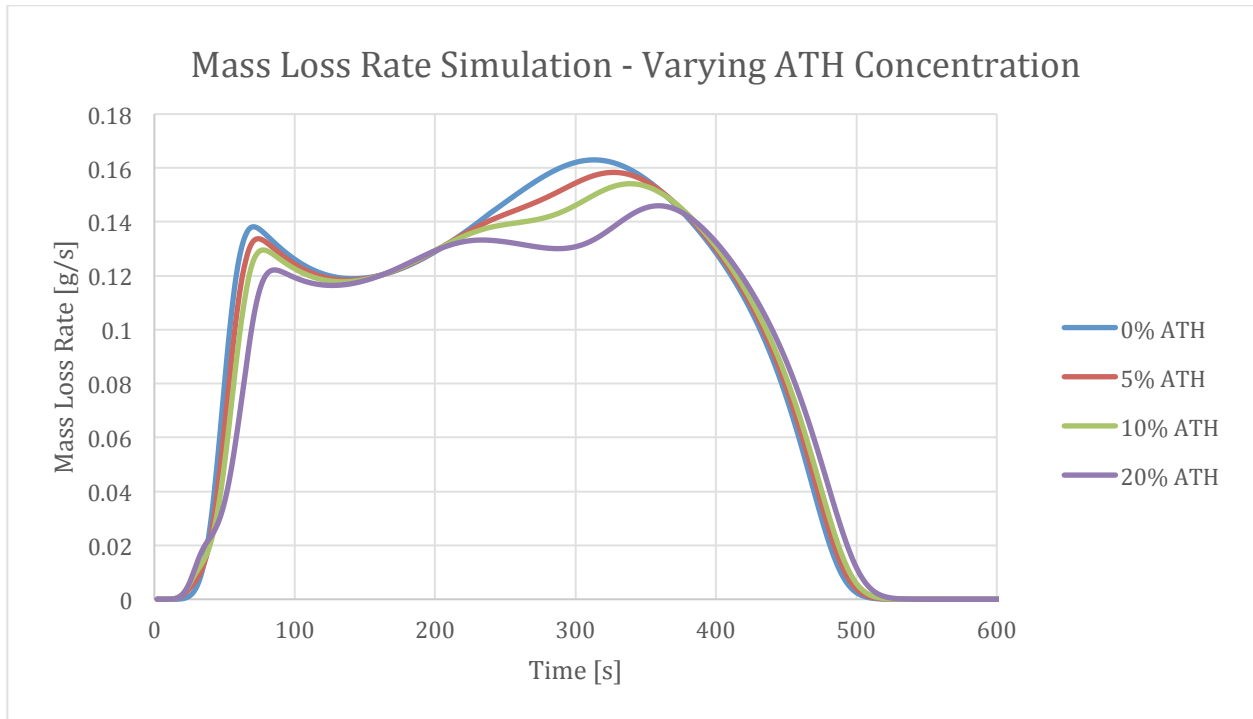


Figure 5: Comparison of G-Pyro results with varied levels of ATH

The results of this simulation show that G-Pyro was capable of picking up the slight differences, and like in physical tests, it can be seen that there is little effect in changing the level of additive at these magnitudes. Variation from the 0% ATH sample in the simulation was 11% (approximately 0.4 g/s), whereas in the cone test it was closer to 23%. This again reinforces the idea that G-Pyro cannot get quantitative results, which may be a result of different properties used in this comparison. It can however make reliable comparisons when a single parameter is being varied as seen in the results from varying ATH.

6.4.3. Varying Coating Thickness

After testing the variation in ATH, the next step was considering the effects that adding a coating may have, as was seen with the gelcoats in the cone samples. The immediate problem that arose was the lack of any gelcoat properties. In an attempt to still model the effects, glass was used as an inert coating to hopefully provide similar results to the gelcoat used earlier. The resulting mass loss rate profile is shown below.

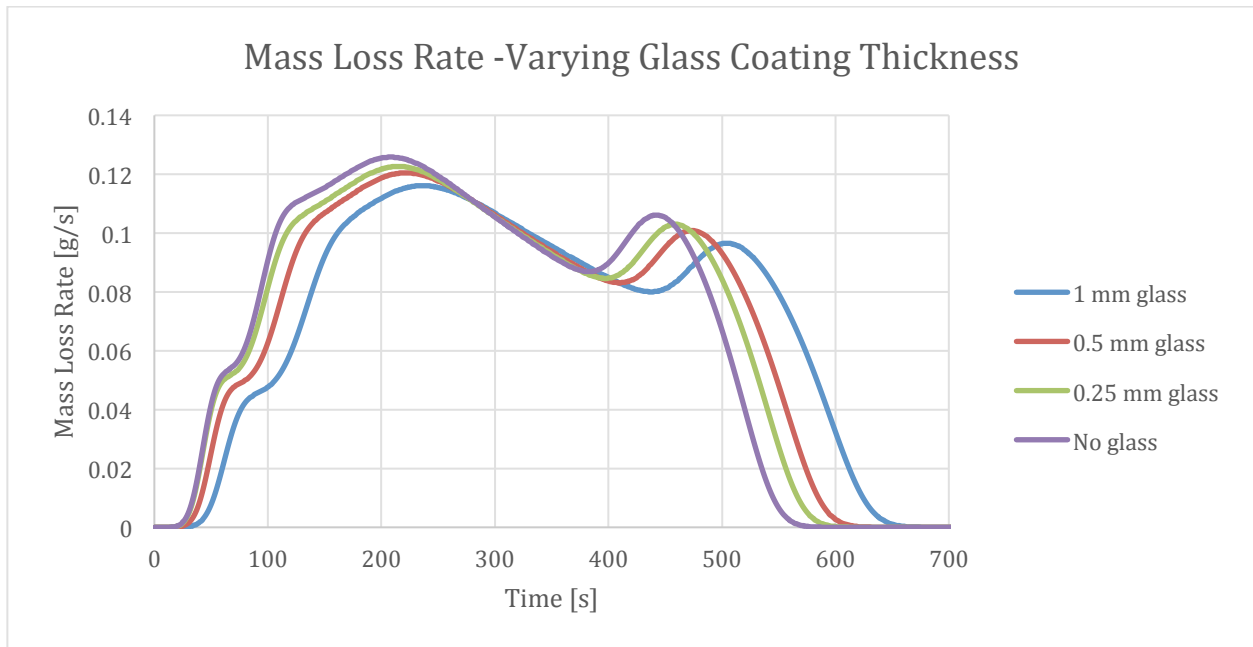


Figure 6: Comparison of G-Pyro results with varied coating thickness

The graph above shows that there is minimal effect when changing the thickness of a glass coating, when compared to no coating. The glass does lengthen the required time to burn the same amount of sample, but there is no dramatic drop in the mass loss rate curve as was seen with the gelcoat. This comparison is not as effective as previous tests, but it does demonstrate the need to have material properties when inputting into G-Pyro.

6.4.4. Varying Layering Style

One of the final variations that were considered was the imperfection of cone samples compared to the perfectly mixed samples that were created in G-Pyro. In order to determine the effects of layering and whether there was reason to consider all tests illegitimate based on this, a layered sample was created consisting of 15 alternating layers of glass and non-glass within the same 9mm sample that has been used. The sample was designed to represent a more realistic FRP, while also being easy to generate in the program. The results of the layered sample were compared to a perfectly mixed sample shown below.

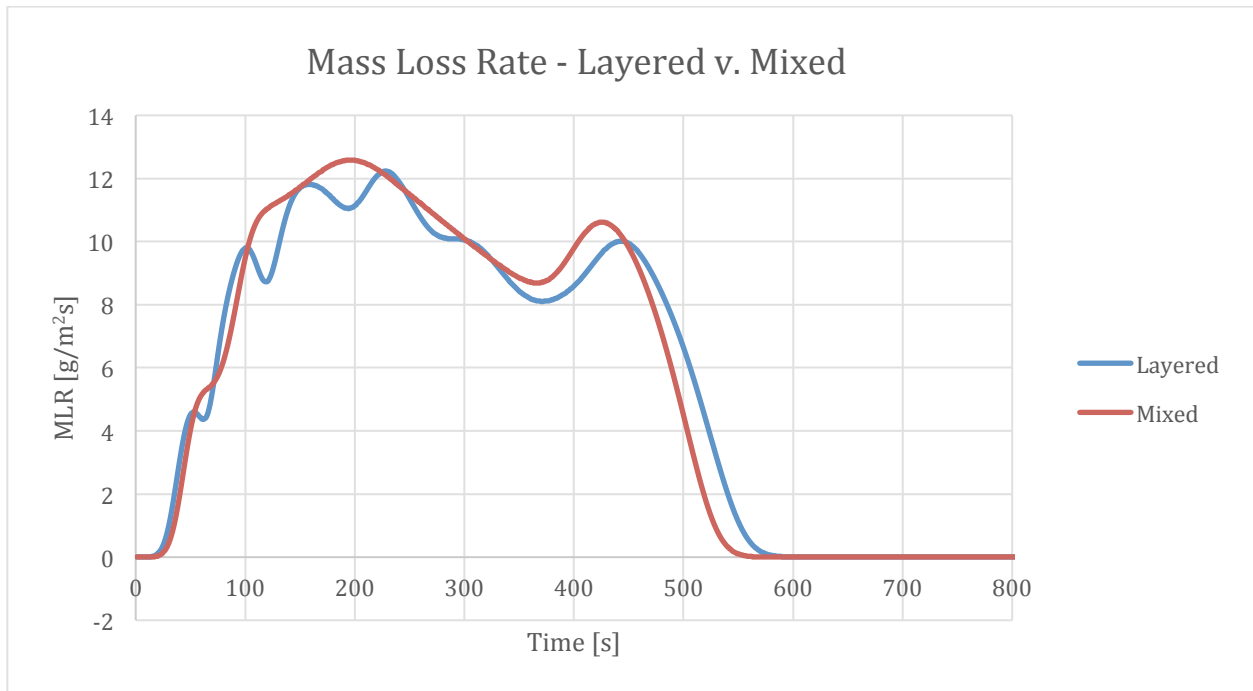


Figure 7: Visualization of the effects of layering on G-Pyro results

The curve of the layered simulation closely followed the mixed simulation curve, except for the jumps, which are indicative of the glass layers. Based on the similarity of these results, it proved that doing a perfectly mixed system did not greatly affect the analysis that was performed.

6.5. Conclusions

G-Pyro's ability to model fire properly was effective in some respects, but ineffective in others. The program itself was capable of modeling the general trends from changing certain parameters, but there is not a quantitative reliance associated with G-Pyro yet. A major benefit was the ability to reliably model the effects of varying certain characteristics on a qualitative level. With these two considerations in mind, G-Pyro, in its current state, is not yet ready to be used specifically for design. Some limitations with regards to G-Pyro are the necessary properties that are required in order to properly simulate anything. The properties required are not easy to obtain, especially when using complex materials that have many different components. The next limitation faced with G-Pyro is the learning curve associated with it. It is not a simple program to use even with the technical reference and users' guide that accompany it. A simplified user interface and a simpler terminology

may assist a new user in being able to use G-Pyro more effectively. Despite these limitations on the operations of G-Pyro, it can still be developed further and may some day be more useful as a quantitative design tool.

7.0 CONCLUSIONS

Over the course of this project it has been determined that the ATH and gelcoat are effective means to improve the fire performance of FRP's. The gelcoat and the sand finish applied performed particularly well. They reduced the mass loss rate very effectively, especially the gelcoat which halved the rate and almost doubled the burn time. This is directly responsible for increasing the performance of the sample in a fully-fledged ASTM E84 test. It is important to remember that the equations used to scale up the cone calorimeter tests

The computer simulations ran also showed strong correlation to the lab data - showing that the technology does have potential and could be developed further into a useful design tool. That being said, G-Pyro is still very early in its developmental stages and over the next five or ten years there is a very real possibility that it can be used to design materials and model their burns. At the moment though, it is only good at qualitatively examining the samples as opposed to quantitatively generating useable results. From a research and development perspective there is potential for this to become a great design tool.

8.0 WORKS CITED

- Acosta, Mahoney, Nava, Wright, and Dembsey, N.. "Evaluation of Fiber Reinforced Polymer Bench Scale Specimen Sizes and Prediction of Full Scale Flame Spread Testing for Building Applications," WPI. Worcester, MA (2013). Undergraduate Major Qualifying Project.
- Anaya, Herrera, Morgan, and Dembsey, N. "FRP Resin and Additive Effects on Fire Performance for Quality Control Planning", WPI, Worcester, MA 01609 USA, Kreysler & Associates, American Canyon, CA 94503 USA (2014). Undergraduate Major Qualifying Project.
- ASTM E 1354. (2014, October 1). Standard Test Method for Heat and Visible Smoke Release Rates for Materials and Products Using an Oxygen Consumption Calorimeter. Retrieved April 30, 2015, from http://compass.astm.org/EDIT/html_annot.cgi?E1354 14e1
- ASTM E 84. (2015, January 1). Standard Test Method for Surface Burning Characteristics of Building Materials, Designation: ASTM E 84-15. Retrieved April 27, 2015, from http://compass.astm.org/EDIT/html_annot.cgi?E84 15#s00083
- Cleary, T., and Quintiere, J.G. "A Framework For Utilizing Fire Property Tests," Fire Safety Science - Proceedings of the Third International Symposium, Elsevier Applied Science, London, UK (1991), 647-656.
- Crane. (2013, January 13). FRP Encyclopedia. Retrieved April 27, 2015, from <http://www.cranecomposites.com/pdf/7606.pdf>
- Gillespie, B., Long, M., McMillan, N., Walde, C., & Dembsey, N. (2014). *Determining Limitations of Kinetic Models for Pyrolysis Simulation of Fiber Reinforced Polymer Composites*. Worcester, Massachusetts: Worcester Polytechnic Institute.
- Janssens, M., Huczek, J. and Saucedo, A. "Development of a Model of the ASTM E 84 Steiner Tunnel Test," Fire Safety Science - Proceedings of the Ninth International Symposium, International Association for Fire Safety Science, London, UK (2008) 279-289.

- Kim, E., Dembsey, N., & Shivkumar, S. (2014). Evaluating effects of applying different kinetic models to pyrolysis modeling of fiberglass-reinforced polymer composites. Worcester, Massachusetts: Worcester Polytechnic Institute.
- Kim, E., & Dembsey, N. (2014). Parameter Estimation for Comprehensive Pyrolysis Modeling: Guidance and Critical Observations. Worcester, Massachusetts: Worcester Polytechnic Institute.
- Kreysler. (2013, August 13). Architectural Composites. Retrieved April 27, 2015, from <http://www.kreysler.com/wp-content/uploads/2013/08/FRP-General-Info-2013-07-311.pdf>
- Lautenberger, C. (2009). *Gpyro – A Generalized Pyrolysis Model for Combustible Solids Technical Reference* (Vol. .700). Berkeley, California: University of California Berkeley.
- Lautenberger, C. (2009). *Gpyro – A Generalized Pyrolysis Model for Combustible Solids User's Guide* (Vol. .700). Berkeley, California: University of California Berkeley.
- Mowrer, F., and Williamson, R.B. "Flame Spread Evaluation for Thin Interior Finish Materials," Fire Safety Science - Proceedings of the Third International Symposium, Elsevier Applied Science, London, UK (1991), 689-698.
- NFPA. (2012). NFPA 285: Standard Fire Test Method for Evaluation of Fire Propagation Characteristics of Exterior Non-Load-Bearing Wall Assemblies Containing Combustible Components (2012 ed.). National Fire Protection Association.
- Thornburg, D., & Henry, J. (2013). 8. Interior Finishes. In *2012 International building code handbook*. McGraw-Hill Professional.

Appendix A: International Building Code and Test Standards

International Building Code

The international building code (IBC) is a document produced by the International Code Council (ICC) that establishes standards for the construction of buildings regarding design, materials, and installation. The objective of the IBC is to provide for public health, safety, and welfare while facilitating innovation. It references and specifies standards for different aspects of building construct, requiring buildings to meet any number of given standards. The American Society for Testing and Materials (ASTM) controls many of the standards referenced by the IBC.

Chapter 8 of the IBC addresses interior finishes, focusing on fire safety. This chapter of the IBC evolved out of necessity, specifically referencing events such as the 1942 Coconut Grove nightclub fire in Boston, a disaster that took 500 lives. The chapter cites two primary concerns: excessive flame spread that may physically obstruct exits and trap building occupants, and excessive thick smoke that would obscure exits and exit signs. To test and approve interior finishes, the IBC specifies the ASTM E 84 test standard.

Corresponding to ASTM E 84, the IBC specifies particular performance requirements for different areas within a building. These performance ratings fall into three classes – A, B, and C, with A class having superior fire resistance, B intermediate, and C minimal. These class ratings are directly related to results of the ASTM E 84 test. The below diagram shows an example of what these ratings would be for a non-sprinkler equipped office building. Typically, A class finishes/materials are specified for primary means of egress, such as exit stairways, exit passages, and exit ramps. Class B is often specified for other corridors, and non-primary egress stairways. Class C is typically specified for other rooms and enclosed areas.

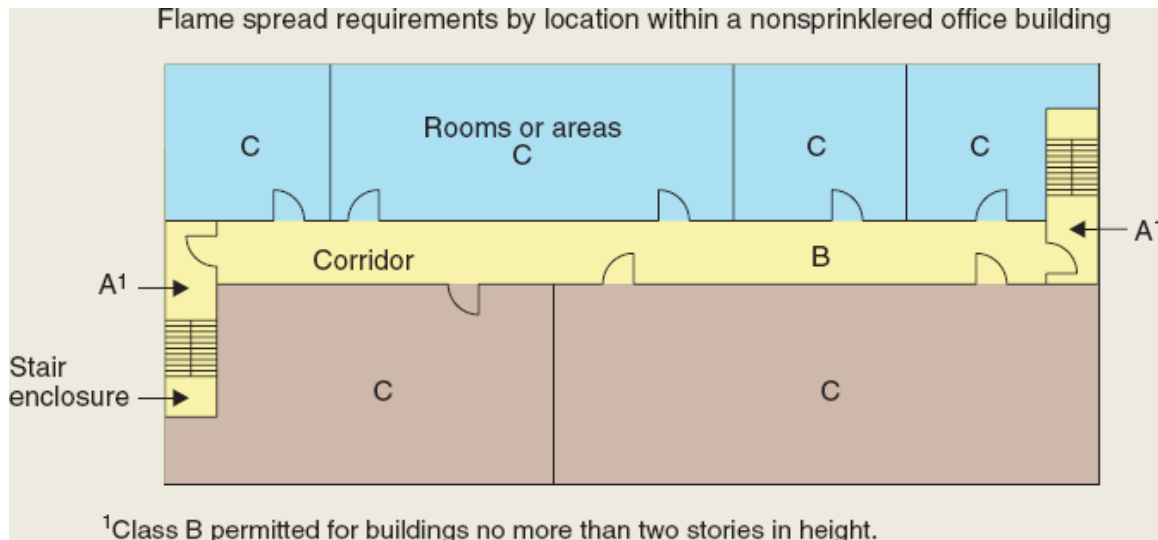


Figure 8-Example of International Building Code Requirement

ASTM E84

Surface Test Method for Surface Burning Characteristics of Building Materials

This document establishes testing procedures for fire testing samples of various building materials, such as those used for interior walls and ceilings. It outlines the application, properties, procedures, and analysis of the method and mechanism used to test these materials (ASTM, 2015).

Use

“The purpose of this test method is to determine the relative burning behavior of the material by observing the flame spread along the specimen” (p. 1). It is meant to be a simple gauge of how materials respond when exposed to fire. It is dependent on two primary metrics: flame spread and smoke density. Though these variables are related, they are not necessarily interdependent (ASTM, 2015).

Apparatus

The apparatus defined in this documentation utilizes a fire test chamber resembling a long duct, approximately 17 inches wide and 12 inches deep. A long plank of test material is laid into the machine, with one side of it exposed to burn. The overall length of the test chamber is 25 feet. Along the length of the test chamber, insulating brick line the walls and several double pane glass windows allow the operator to view the specimen. The support surface for the specimen is made up of ledges capable of withstanding the heat of the furnace. At one end of the furnace, two gas burners are positioned to direct flame against the surface of the test sample. An air intake shutter located approximately 54 inches away from the burners controls the air flow into the test chamber. This shutter is also designed to provide air turbulence as air enters the system. On the other end of the test chamber, and is fitted with a rectangular to round to transition piece routed to ducting pipe. A photometric system (lamp and sensor), mounted approximately 36 inches apart in the exhaust pipe, monitor the physical qualities of the exhaust gas, such as concentration of smoke and particulate. Additionally, other systems are used to monitor and control the test chamber,

such as thermocouples to monitor temperature and a draft regulating valve to control exhaust flow. A water column manometer is used to monitor pressure in the exhaust line (ASTM, 2015).

Specimens

Samples for this system should be relatively large, approximately 20 inches wide and 24 feet long. It is intended to test materials as they would be installed in the wall or ceiling. It is designed for testing a variety of samples, such as wood planks, fiberboards, or sheetrock type materials (ASTM, 2015).

Calibration

Conduct calibration by initially placing a ¼" piece of fiberboard in the device, adjusting the draft readings to a predetermined settings and ensuring a proper seal in the chamber. Monitor and record air velocity through a series of 3 tests, with varying internal air vane configurations, while the predetermined draft setting is maintained. Next, the gas is connected and set so as to provide 5000 Btu. The gas pressure, pressure differential across the orifice plate, and the volume used is recorded. Under these circumstances, the flame should extend 4 ½ feet down the face of the test specimen. The test chamber is preheated, with the fiberboard in place. Continue preheating until the floor thermocouple at the far end of the test chamber reached approximately 150 degrees Fahrenheit. During preheating, record the temperature at the vent end thermocouple every 15 seconds. Compare these values to the time-temperature curve for preheating given in the ASTM E84 manual. If there is significant variance, adjustments based on red oak calibration tests can be made to correct it (ASTM, 2015).

After each test allow the furnace to cool to about 105 degrees (at the floor thermocouple). After the furnace is cool, conduct a series of tests using 23/32" red oak flooring samples and ¼" fiber-cement board. During the oak board tests, record observations at intervals of 2 feet or less, and at time intervals of no more of 30 seconds. Record the time when the flame reaches the end of the test specimen. Additionally, record the photoelectric cell output at intervals of 15 seconds or less. Conduct similar tests with ¼" fiber-cement board. Plot all these variables against time and compare them to the correspond charts given in the ASTM E84 manual. If there is significant variance, or the burn time for the flame to reach the end of the sample is outside of the specified window, readjust the settings and repeat until the results are accurate. Maintain a record and running average of the last five calibrations (or max number available) using red oak boards to provide calibration data or future tests (ASTM, 2015).

Procedure

With the furnace draft operating, place the test specimen in place and close the top of the machine. After 120 seconds with the furnace draft operating, ignite the burner flame. Record the distance and time of maximum flame travel, continuing the test for ten minutes. The test can be ended before ten minutes if the test area is completely consumed in fire. Record the photoelectric cell output before and throughout the test. Also record the gas pressure, gas pressure differential across the orifice plate, and the volume of gas used. After the test is finished, shut off the gas supply, and record the smoldering and other conditions on the specimen. Plot the flame spread distance, temperature, and change in photoelectric

cell output for the length of the test as a function of time. These will be used to determine the flame-spread and smoke-developed indexes (ASTM, 2015).

Interpretation.

The flame spread index (FSI) is determined by first approximating a curve on the plot of the flame distance vs time chart. Flame recession is ignored for this calculation, a straight line with zero slope is continued from the highest point of flame progression and is continued either until the end of the test or until the flame passes that point. Find the total area under that curve. If that area is equal to or less than 97.5 feet*min, the FSI is .515 times the total area. If the area is greater than 97.5 feet*min, then the FSI is 4900, divided by 195 minus the total area ($FSI = 4900/(195-A)$). The final number is rounded to the nearest multiple of five to get the FSI. Cement board has an FSI of 0, while red oak has an FSI of 100.

The smoke index is calculated in a similar manner, first find the total area under the curve. Divide that area by the same area for the red oak board tests (from calibration runs), then multiply it by 100. This number is then rounded to the nearest multiple of five. If this number is over 200, round to the nearest multiple of 50. Compare to the values of cement-fiber board and red oak, which are established at 0 and 100 arbitrarily (ASTM, 2015).

NFPA 285

NFPA® 285 Standard Fire Test Method for Evaluation of Fire Propagation Characteristics of Exterior Non-Load-Bearing Wall Assemblies Containing Combustible Components 2012 Edition

Overview

This document outlines a different flammability testing method, specifically for exterior (non-load-bearing) wall assemblies. This is a large scale test intended to test how flame will propagate through a structure, including both lateral and vertical flame progression. This would help determine how a structure would resist flame spreading from one story of a building to the next through the exterior walls (NFPA, 2012).

Apparatus and Facility

Unlike the test mentioned in the ASTM standard above, this test requires a large facility designed for large scale combustion tests. The test facility required must have at least 30 feet x 30 feet x 23 feet high. To conduct the test, the structure to be evaluated is actually to be constructed and placed in the test facility. The test structure/specimen is mounted directly to the front of the test apparatus, and is to be at least 17.5 high by 13.5 feet wide. The test apparatus is steel and cement story structure, with the stories separated by a permanent cement floor, so as to limit the test to the wall material. Each room (upper and lower) is built with three heavy walls, and a 10 by 10 foot floor space. On the first story, a window opening is built into the test specimen. The window opening is 78 inches wide and 30 inches tall. The system uses two burners, with one placed inside the lower room, and the other near the top of the first story window opening. The one inside the room is four feet away from the wall and about 2.5 feet above the ground. The window burner is placed within ½” of the wall above the window (NFPA, 2012).

Thermocouples are strategically placed through the test apparatus and specimen to track the progression of the fire. On the wall itself, thermocouples are placed in line down the front of the wall, with varying positions. Some are placed both one inch away from the exterior surface, others are placed inside the wall cavity or insulation. Thermocouples are also placed along the interior of the test specimen and below the first floor ceiling. Additionally, gas flow meters are attached to each burner to measure flow rate and overall gas use (NFPA, 2012).

Calibration

A calibration test is performed by burning a simple wall of two layers of gypsum wallboard set on steel studs. The joints of the specimen should be sealed (with tape or caulk), and the wall should be at least 18 feet high and 11 feet wide. When the wall is built and in place, the paper of the gypsum wallboard is burned away by turning up the burners for approximately five minutes, before the start of the calibration test. During the actual calibration test, the burners are ignited and thermo couplers are used to monitor the temperature of the sample throughout. The thermo coupler values are recorded and are compared to given values for the test that are found in the test manual. After the test is completed, the window burner is moved away from the test sample and tested for flame height independently. This calibration procedure is performed when major maintenance is performed to the system, there are any changes in the setup, or on a yearly basis (NFPA, 2012).

Test Procedure and Performance

The test procedure is comparable to the calibration procedure. The fire is started with the interior burner, and after about 5 minutes a second burner is turned on near the window. After 30 minutes or less, both burners are shut off via the gas supply. Data is collected through video recording, visual observations, and measurements from thermocouples and other devices installed in the test facility.

Throughout the test, thermocouple data is recorded, photos and videos are taken periodically. After the test is complete, the specimen is allowed to smolder for at least ten minutes. Within the test document, various maximum allowances are prescribed for the test outputs to determine the relative performance of the specimen. For different applications, different criteria are listed in detail.

This test standard is referenced in international building code, section 1403.6, vertical and lateral flame propagation. Certain varieties of walls that are 40 feet or higher must meet the standards prescribed in this test procedure (NFPA, 2012).

Heat Transfer

From the NFPA Manual:

| Table 4.4.13 Calibration Gas Flow Rates (Based on Natural Gas)

Time Interval	Room Burner				Window Burner			
	SCFM	m ³ /min	kW	Btu/min	SCFM	m ³ /min	kW	Btu/min
0:00–5:00	38.0	1.08	687	39,064	0.0	0.00	0	0
5:00–10:00	38.0	1.08	687	39,064	9.0	0.25	163	9,252
10:00–15:00	43.0	1.22	777	44,204	12.0	0.34	217	12,336
15:00–20:00	46.0	1.30	831	47,288	16.0	0.45	289	16,448
20:00–25:00	46.0	1.30	831	47,288	19.0	0.54	343	19,532
25:00–30:00	50.0	1.42	904	51,400	22.0	0.62	398	22,616

Figure 9-Calibration Gas Flow Rate (Based on Natural Gas)

Appendix B: Overview of FRPs (Fiber Reinforced Polymers)

Definition and Construction

Generally, the term FRP refers to a composite made up of a polymer matrix **material** reinforced with fibers. The polymer provides the base for the material, and the fibers provide much of the strength and structure. Typically during manufacturing, the fiber weave is laminated with sheets of polymer. Typically the polymer is made up of polyester resin, though epoxy, vinyl ester, or other types of resins can be used. Glass fibers are typically used, though other fibers (such as carbon) can be used for specific applications and requirements. This type of material allows for lightweight, flexible, strong structures that are relatively easy to manufacture. They can be made to have nearly any type of finish, from glossy to rough and cement-like, and can be any color (including translucent) depending on composition and molding method. FRPs have significant advantages for construction, including their lightweight, flexibility, customizability, and durability. However, there are certain disadvantages associated with FRPs, including potential issues with market acceptance/lack of knowledge in the industry, potential combustibility, and complexity (Kreysler & Associates, 2013).

Materials

There are two basic types of polymers (plastics) used today, thermoplastics and thermosets. FRP composites usually utilize a thermoset. In thermoplastics, the individual molecules are not cross-linked from one to another. This makes the plastic more flexible when heated, and allows the material to deform, melt, and flow when heated. In thermosets however, the molecules are cross-linked during manufacturing. Though this can make manufacturing more difficult, it makes the material resistant to deforming when heated (Crane, 2013).

Many FRP materials use fiberglass to bolster the mechanical properties of the material. Fiberglass is made by extruding molten glass into thin fibers, these fibers are then bundled together and wound into what is essentially a rope – called a roving. This roving is then used to create the FRP – either by being woven into a sheet, or used throughout the material in long or short sections.

Gelcoats are a thin layer of plastic resin applied to the surface of FRPs (or other materials). This layer is not reinforced with fiber, and can be colored or translucent. They can be used to create a desired finish, or can be used to augment the durability and of the material (Crane, 2013).

Fire Resistance

Though polymers are not naturally as resistant to flame as some conventional building materials, such as steel or concrete, they can be made to meet standards with proper additives. Several different additives can be used to improve fire resistance. A higher concentration of glass, ranging from 30% to **70%** can be used to improve flame resistance. Additionally, incorporating resins or additives including compounds that contain halogens (such as bromine or chloride) or phosphorous also contribute to fire resistance. Modern

FRP's are capable of achieving **Class A** ratings in smoke development and flame spread in the ASTM E-84 Surface Burning Characteristics test. They are also capable, when assembled into an appropriate structure, of passing the NFPA 285 test, which is meant to evaluate the fire resistance of external wall structures (Kreysler, 2013).

Appendix C: Operating Cone Calorimeter

This section will introduce the procedure used in order to operate the cone calorimeter located in WPI's Fire Protection Engineering Laboratory in Gateway Park. Several experiments were performed before beginning testing of the specimens provided by Kreysler, to confirm the accuracy and reliability of cone calorimeter tests. The materials that have been tested include: poly methyl methacrylate (PMMA), red oak, white pine, architectural composite, bathroom tile-like FRP, and 2c fiber reinforced polymer (2c FRP).

Firstly, an understanding of what the cone calorimeter and the cooperating software VI were doing was important. Both direct and indirect measurements were reproduced, which also showed up on the summary reported by the VI based on the raw data collected by the cone calorimeter. By doing the reproduction and comparing it with the VI's results, a comprehension of the procedure and ability to recreate the results of the experiment were demonstrated.

Secondly, the reliability of the tests needed to be critiqued. Limited specimens from the sponsor, as well as the need to provide concrete results demanded effective and careful testing. To achieve this, several materials were tested multiple times to determine if the results were reproducible or not. If similar results were achieved through repetition, then a conclusion could be made justifying that the procedure was effective and the data was reliable

Cone Calorimeter Samples

Images from Cone Tests

Not Photographed: 2B, 2C, 2D, 2E



Figure 10-Pre and post burn comparison of sample 2A

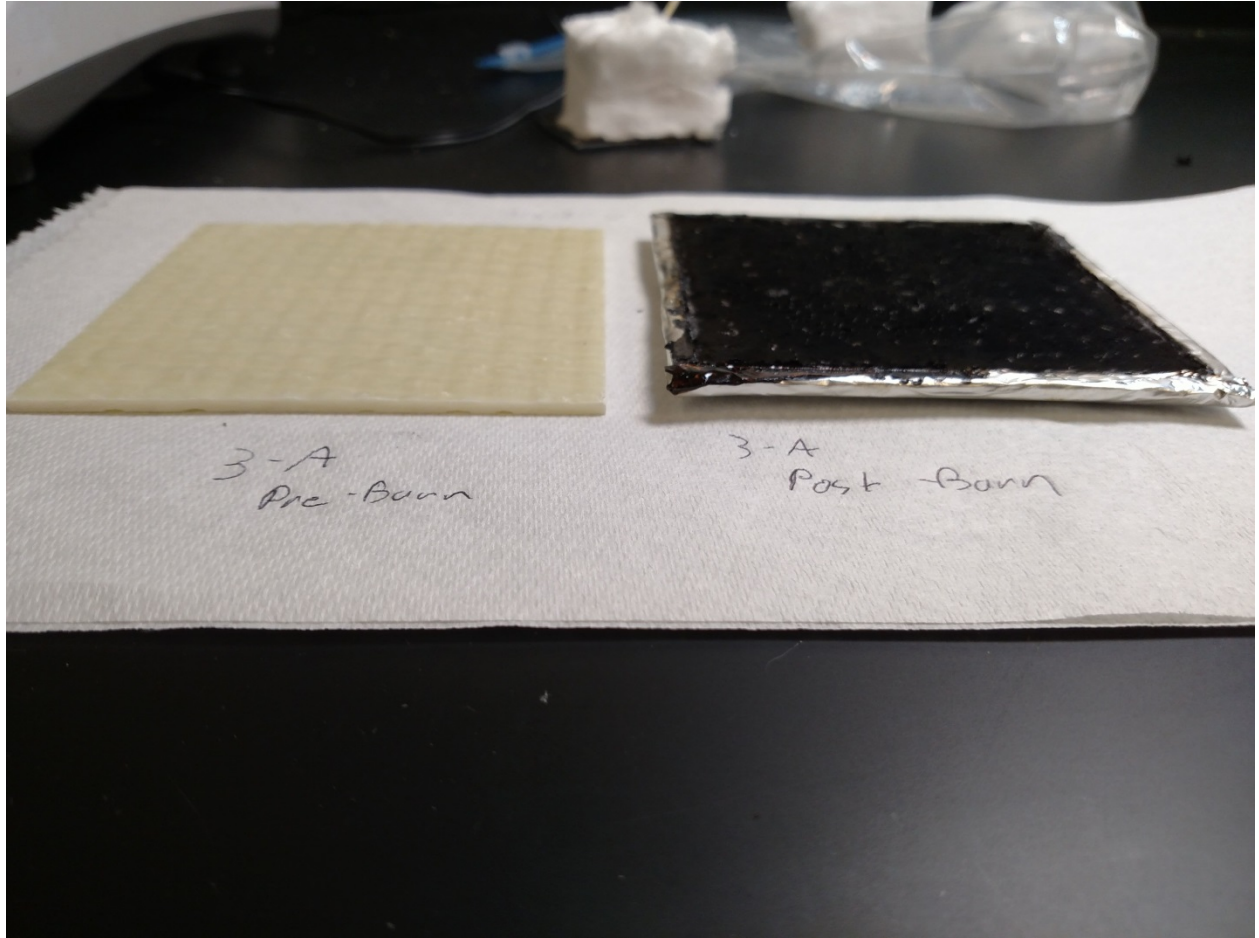


Figure 11-Pre and post burn comparison of sample 3A

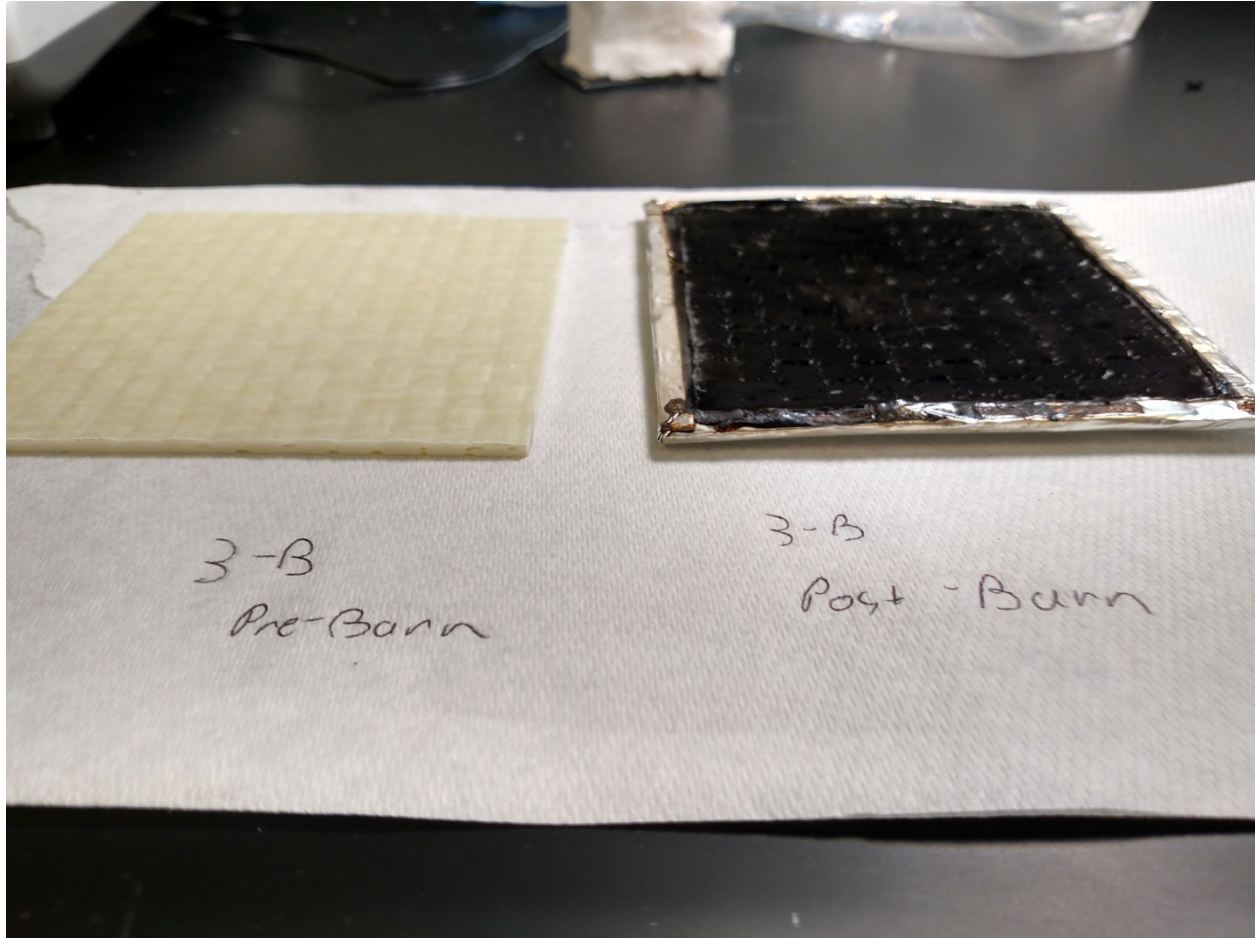


Figure 12-Pre and post burn comparison of sample 3B

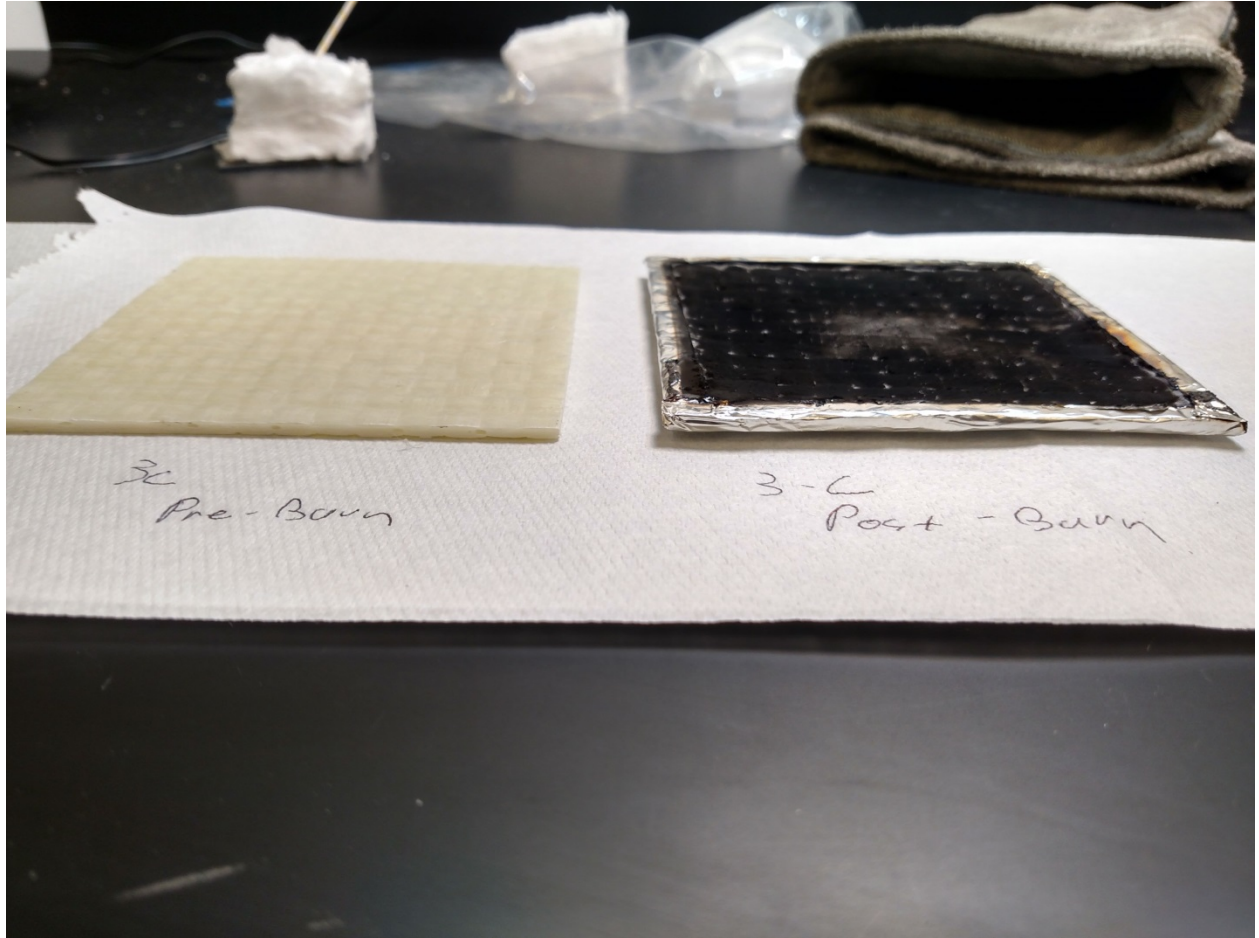


Figure 13-Pre and post burn comparison of sample 3C

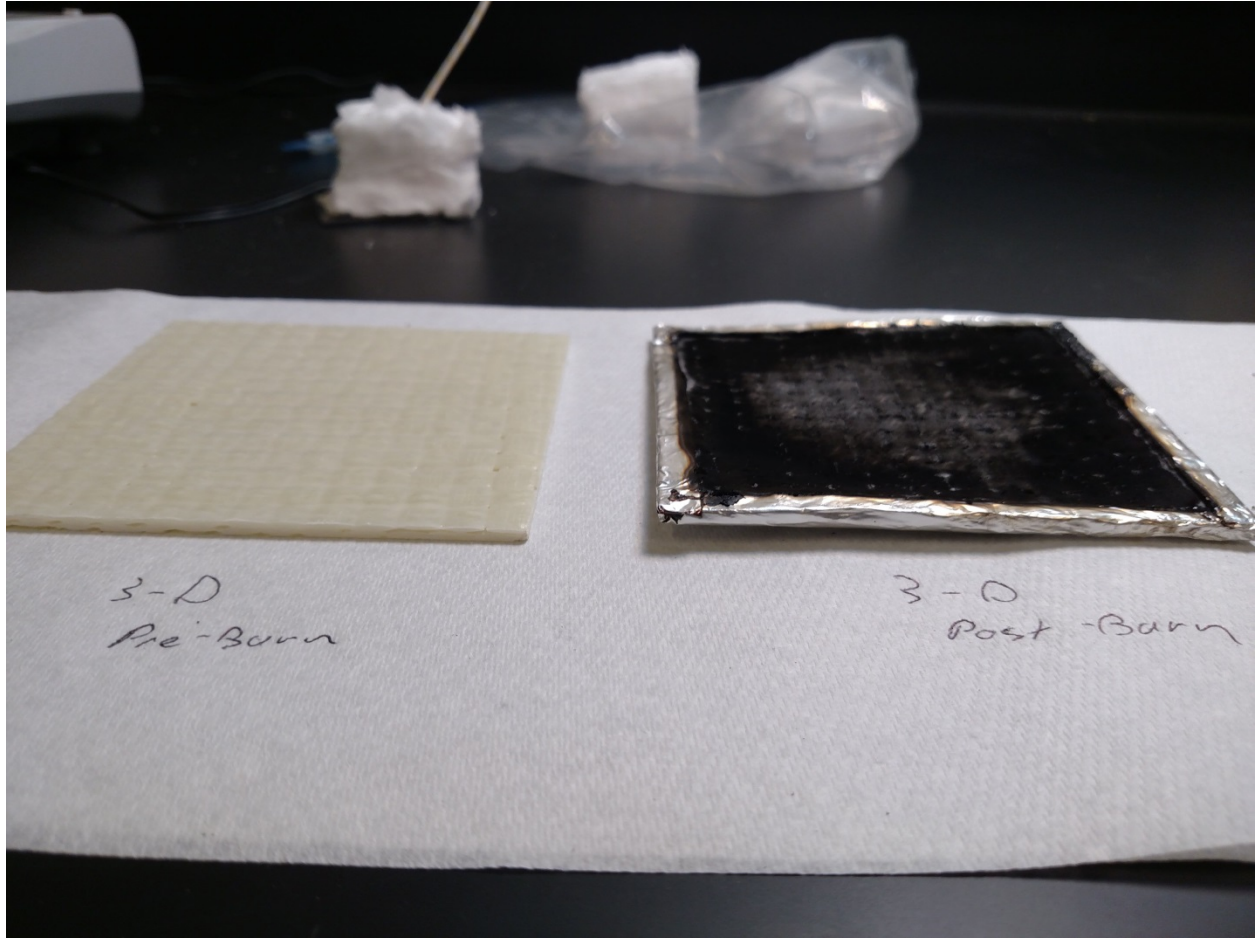


Figure 14-Pre and post burn comparison of sample 3D

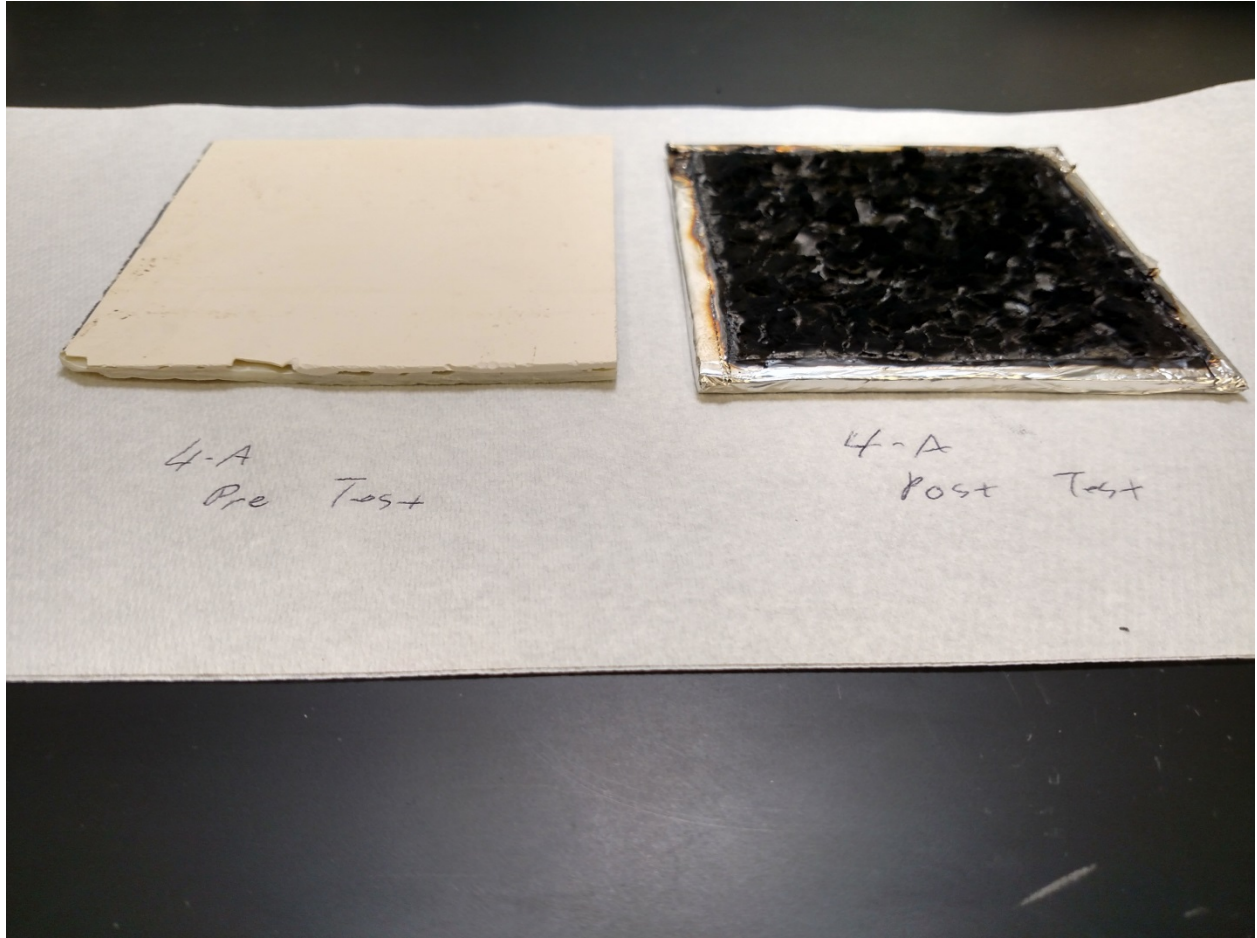


Figure 15-Pre and post burn comparison of sample 4A



Figure 16-Pre and post burn comparison of sample 4B

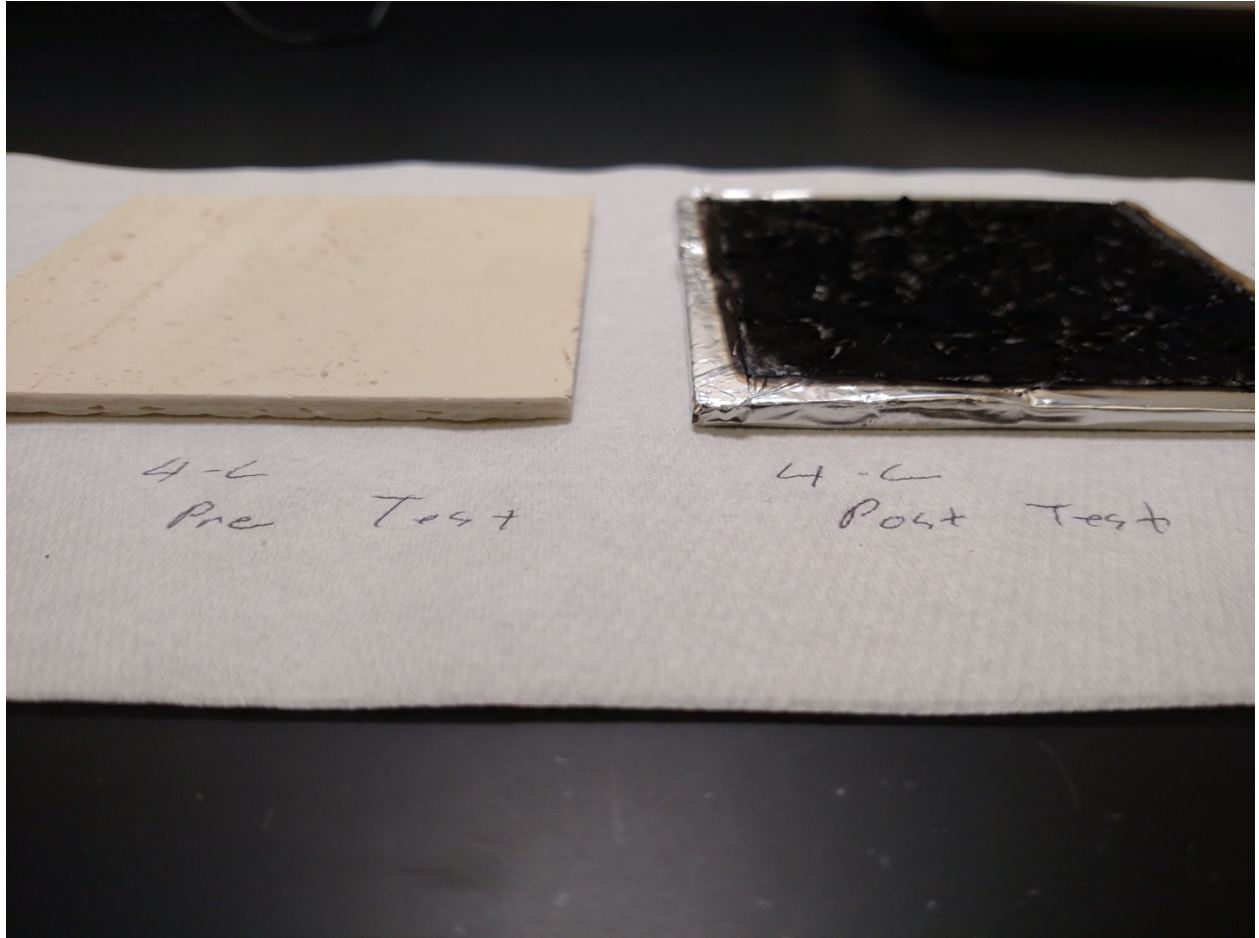


Figure 17-Pre and post burn comparison of sample 4C

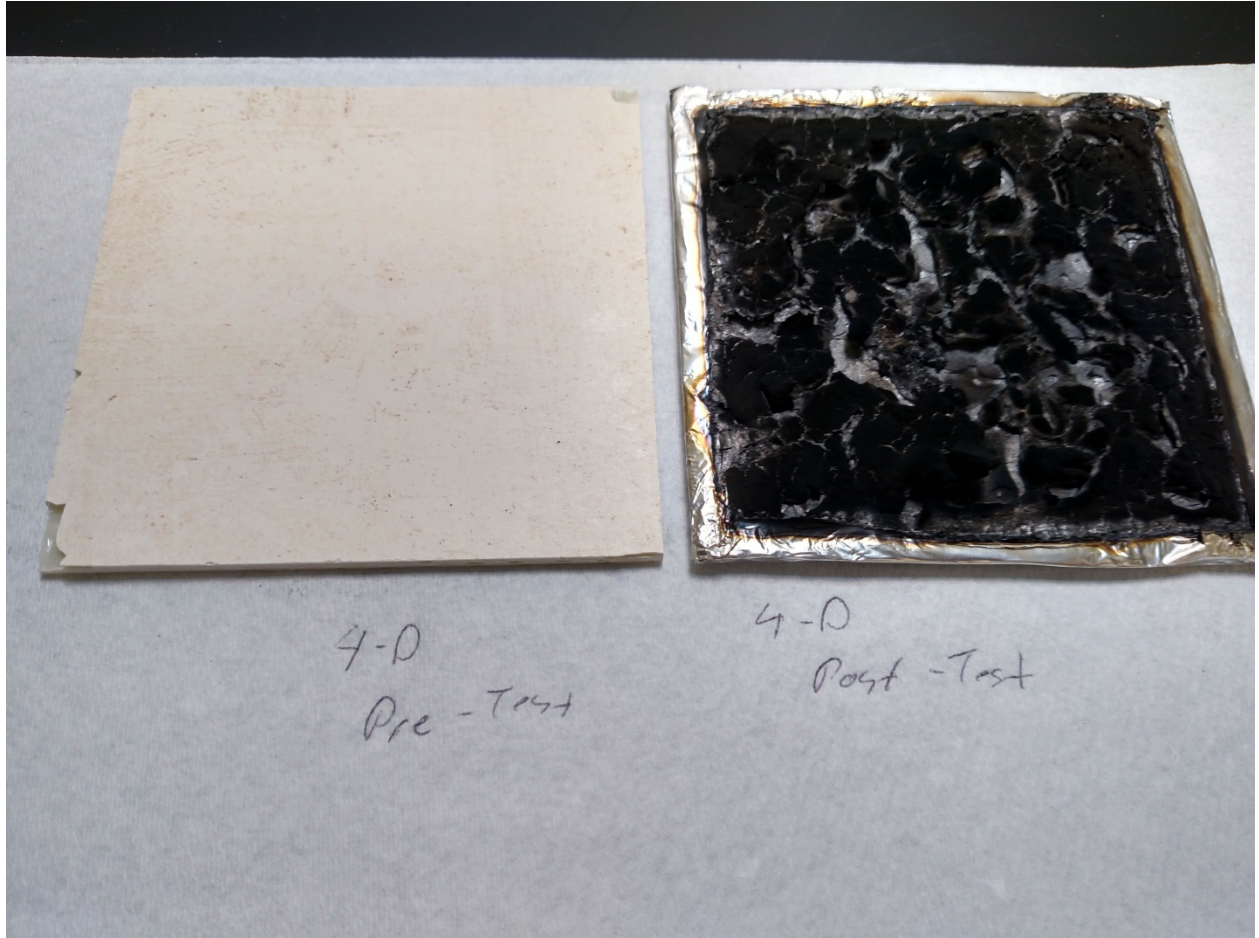


Figure 18-Pre and post burn comparison of sample 4D

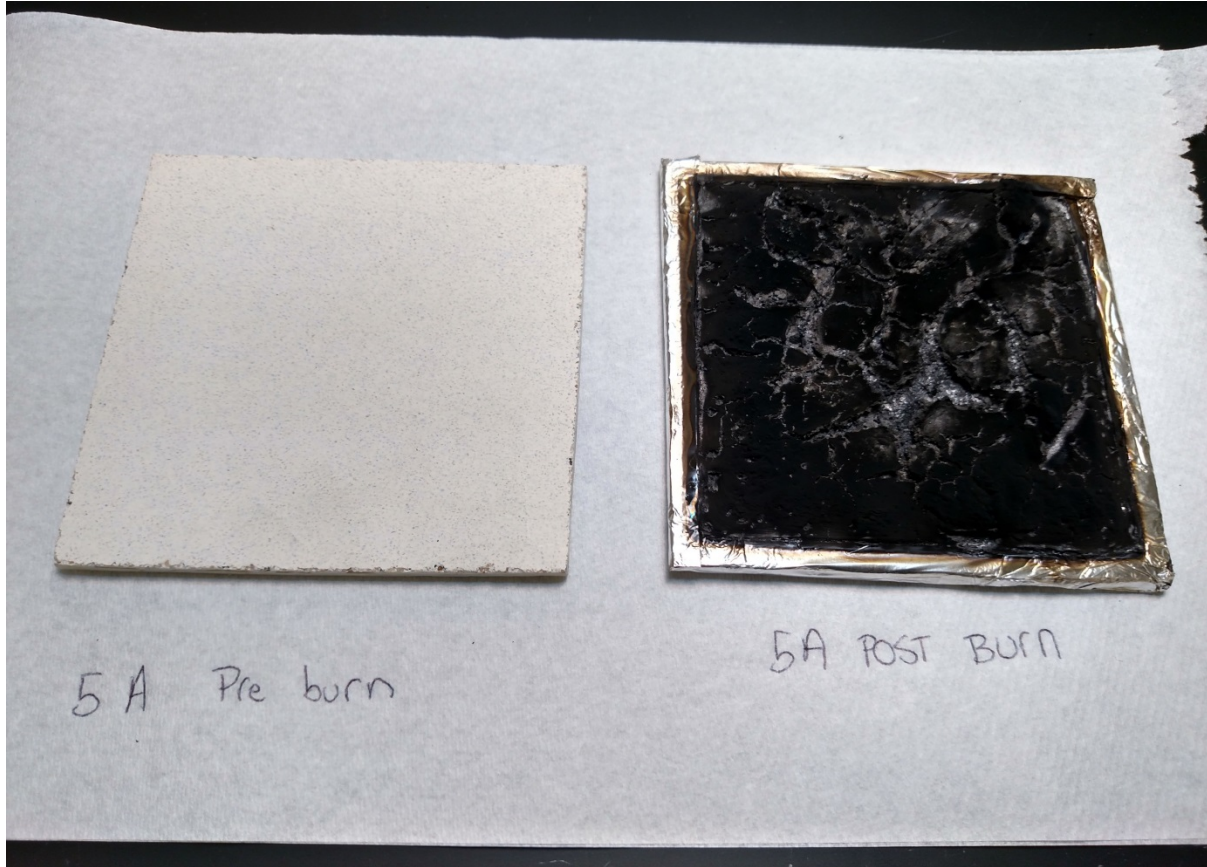


Figure 19-Pre and post burn comparison of sample 5A

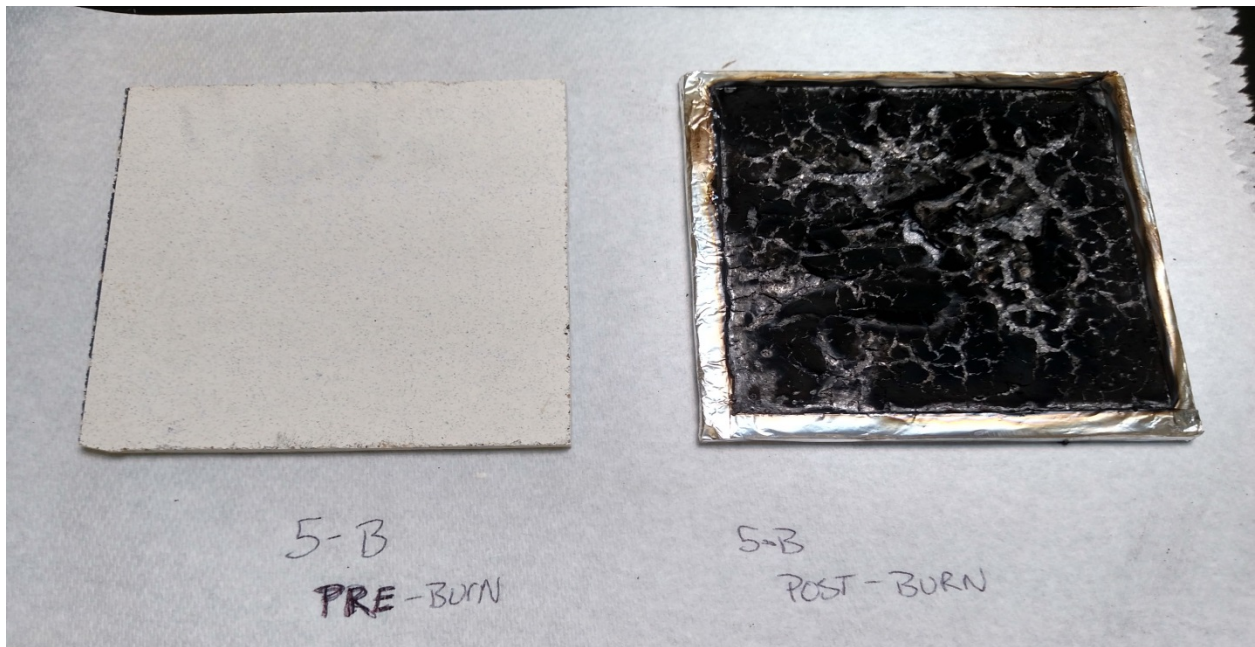


Figure 20-Pre and post burn comparison of sample 5B

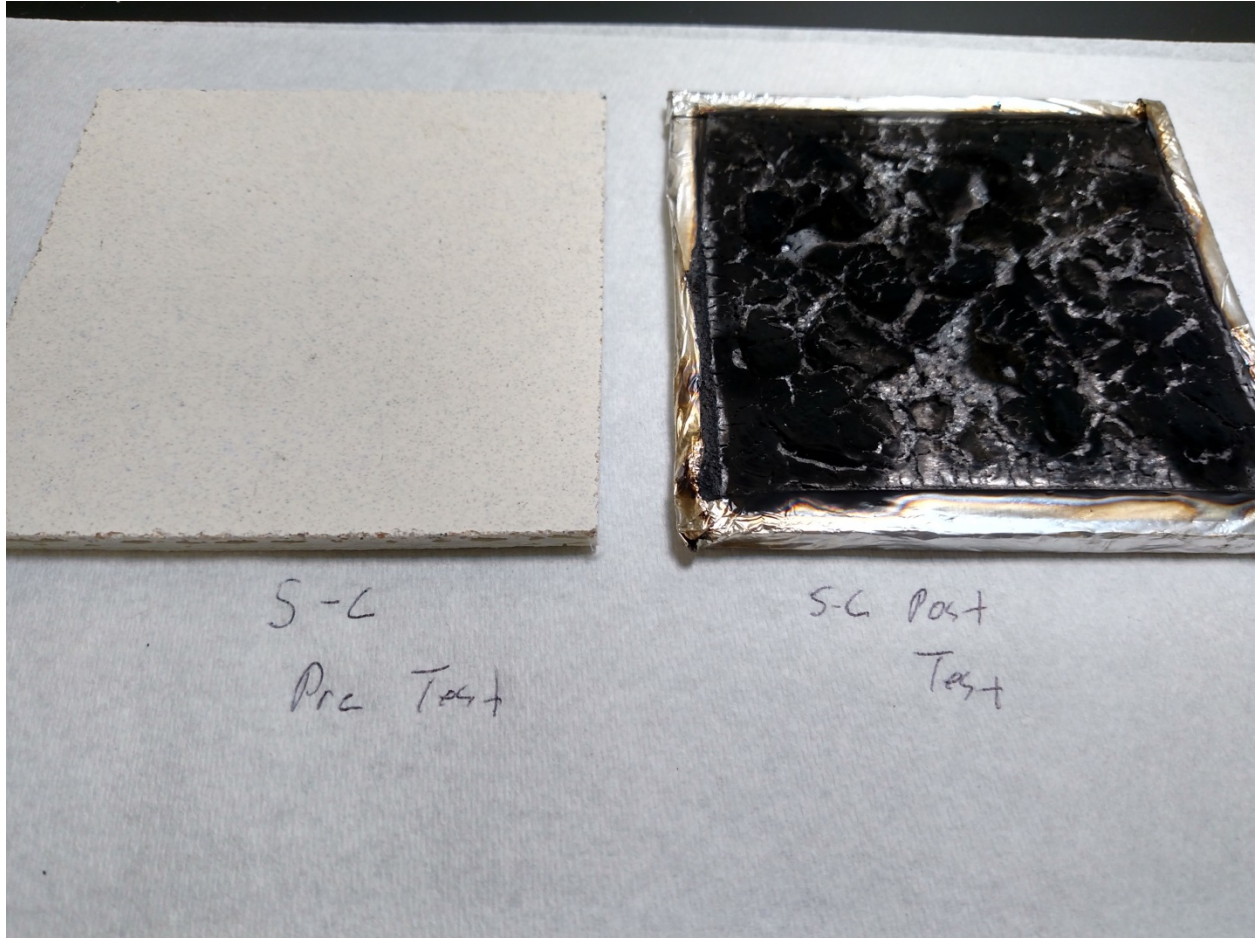


Figure 21-Pre and post burn comparison of sample 5C

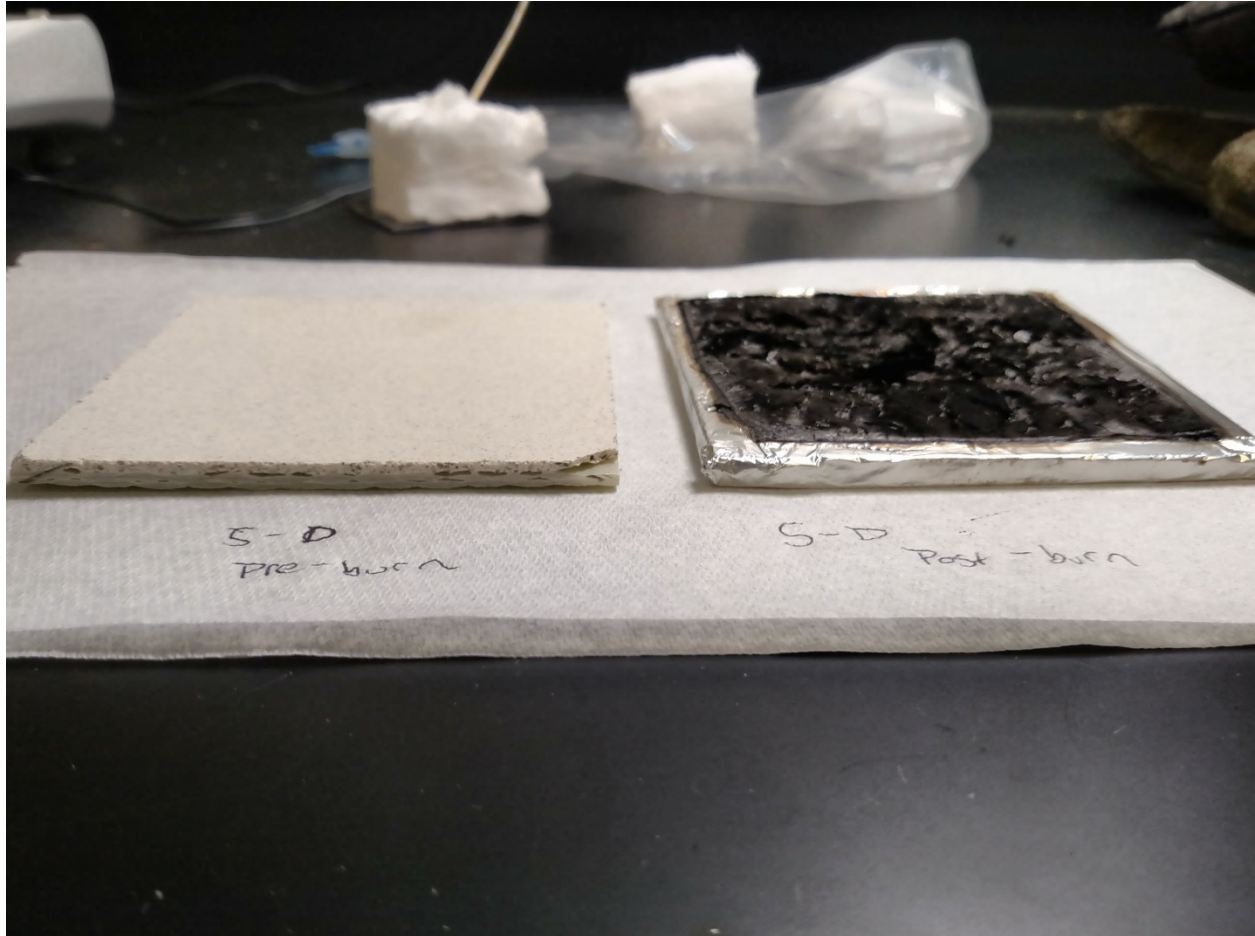


Figure 22-Pre and post burn comparison of sample 5D

Reproduction of Measurements

Direct Measurements

The cone calorimeter in WPI's Fire Protection Engineering Department in Gateway Park collected data by recording a series of voltages from several sensors. The purpose of this section is to explain how the VI, the engineering software used in raw data analysis converts recorded voltages to engineering units for further calculation and discussion. The voltages recorded by sensors have a linear relationship with the actual magnitudes (except temperature), which can be presented by the following equation:

$$E = (V - V_{base}) \times C + E_{base} \quad (C1)$$

In the equation above, E is the data in engineering units, V is the voltage, and the subscript means the magnitude of base-condition value. C in the equation is called the calibration factor, which is determined and generated during the process of calibration of the cone calorimeter. In most cases, it is considered that the 0 point is the base condition. However, sometimes the standard deviation at the 0 point is relatively big, and another point is chosen as base condition if it is available.

As mentioned above, the temperature doesn't fit the linear relationship. The reason is that the data recorded is not the voltage. It is recorded directly by engineering units in degrees Celsius. Therefore, to convert it into the necessary units needed for further calculation, it can be presented by following equation:

$$T(K) = T(^{\circ}C) + 273.15 \quad (C2)$$

Results and Comparison (based on experiment of PMMA):

Table 6- Summary of Calibration Factors

summary table of calibration factors			
main (%/V)	comp (%/V)	DPT (Pa/V)	O2 (1/V)
89.882054	37.659822	100.000000	0.029969
CO (ppm/V)	CO2 (1/V)	Mass (g/V)	Temp (K)
320.978507	0.010911	44.375905	273.150000

The table above shows the magnitudes and the units of the calibration factors of all the direct measurements. For beam intensities, the units are percentage per volt; for oxygen and carbon dioxide, the units are mole fraction per volt. The calibration of temperature is simply the transfer from degrees C to K. Therefore, the factor has units of K.

Oxygen Analyzer Reading

The oxygen analyzer recorded the oxygen mole fraction. The calibration factor was 0.029969 and the base-condition voltage was 0.014027 at 0 point.

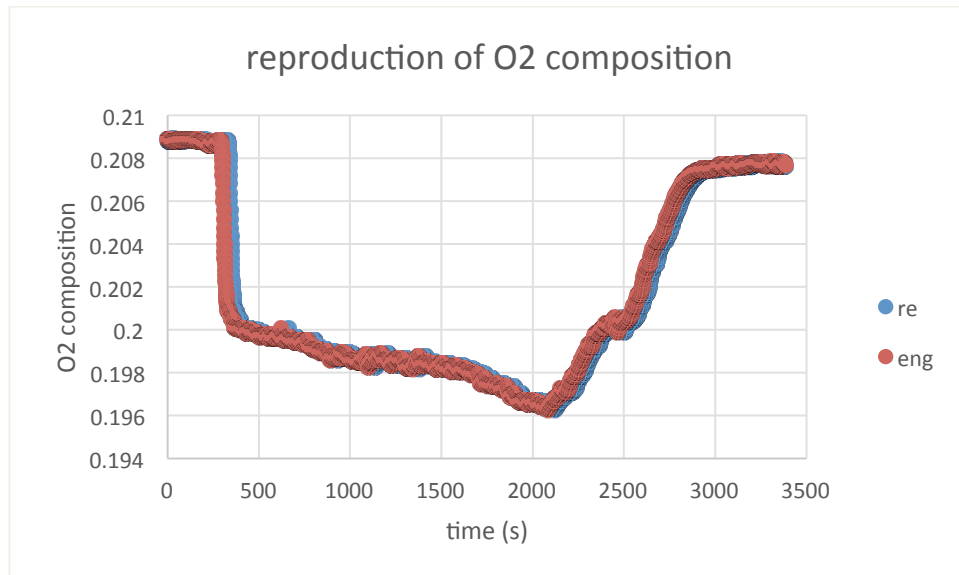


Figure 23-Reproduction and Comparison of Oxygen Analyzer Reading

Differential Pressure

The calibration factor was 100 and the base-condition voltage was 0.611932 at 0 point.

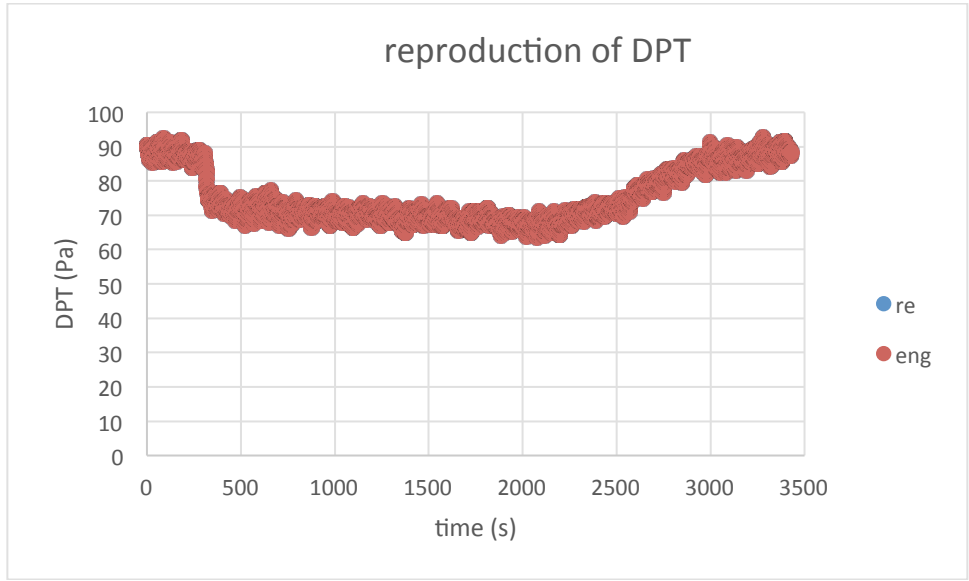


Figure 24-Reproduction and Comparison of Oxygen Analyzer Reading

The graph shown above is modified by 9-point average method to eliminate the noise.

Temperature

Temperatures were recorded at stack and at smoke tap. Only the reproduction of smoke temperature was shown.

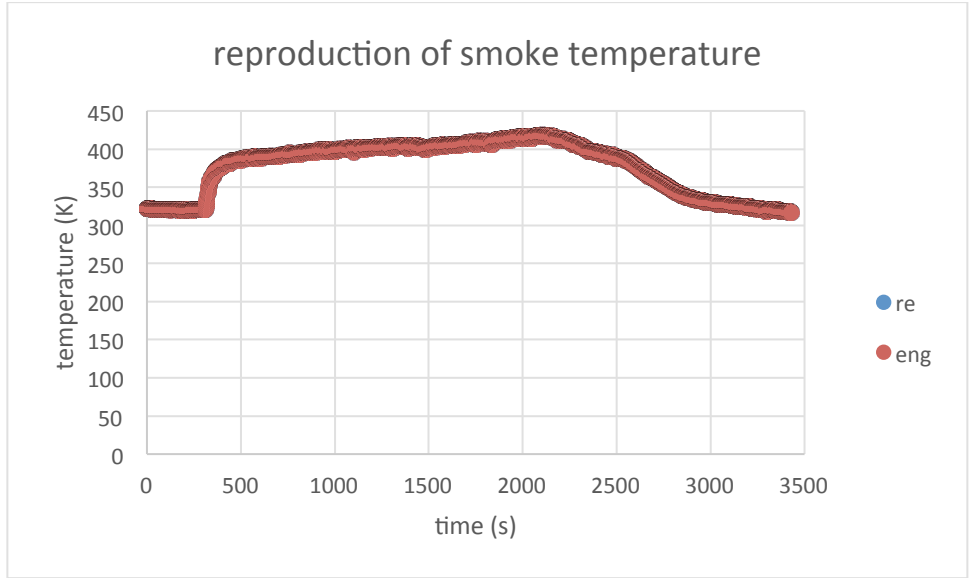


Figure 25-Smoke Reproduction and Comparison Temperature

Light Intensity

Two photo sensors measured the light intensity before the laser entered the smoke and after the laser passed through smoke. Those readings could be used to calculate the smoke obscuration. The calibration factors were 89.882054 and 37.659822, and the base-condition voltages were 0.002035 and 0.002511 at 0 point.

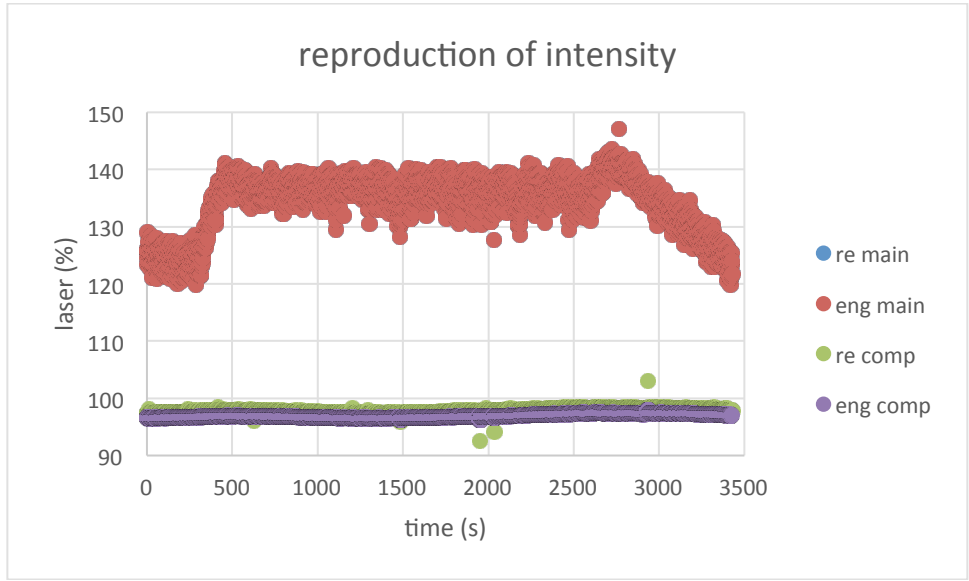


Figure 26-Reproduction and Comparison of Laser Readings

CO an CO₂ Readings

The compositions of carbon monoxide and carbon dioxide were measured in the cone calorimeter, where CO was measured in ppm and CO₂ was measured in mole fraction. The calibration factors were 320.978507 and 0.010911, and the base-condition voltages were -0.001337 and 0.008324 at 0 point.

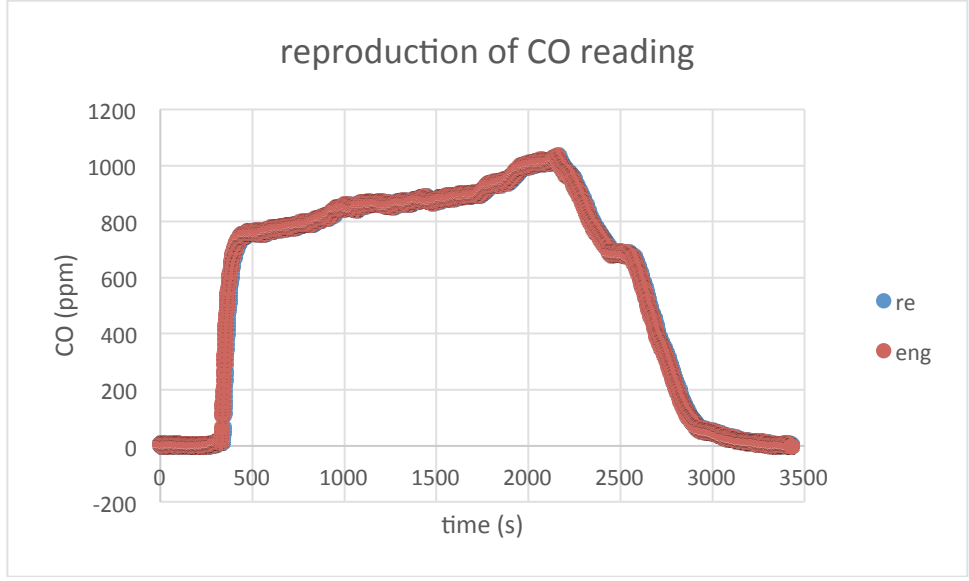


Figure 27-Reproduction and Comparison of Laser Readings

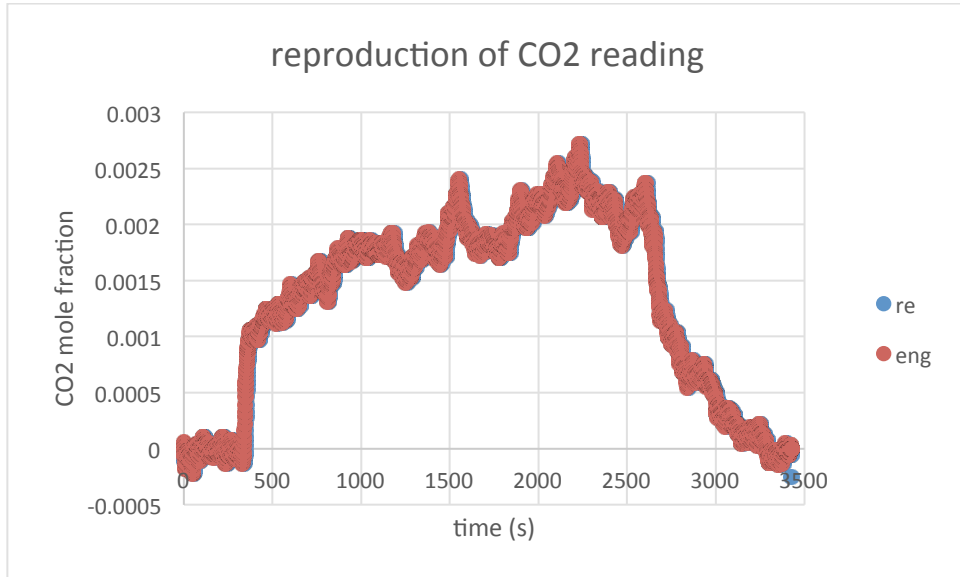


Figure 28-Reproduction and Comparison of CO and CO2 Readings

Fig.C6 is modified by 9-point average method.

Load Cell Measurement

The calibration factor is 44.375905 and the base-condition voltage is 1.156192 at 50 gram.

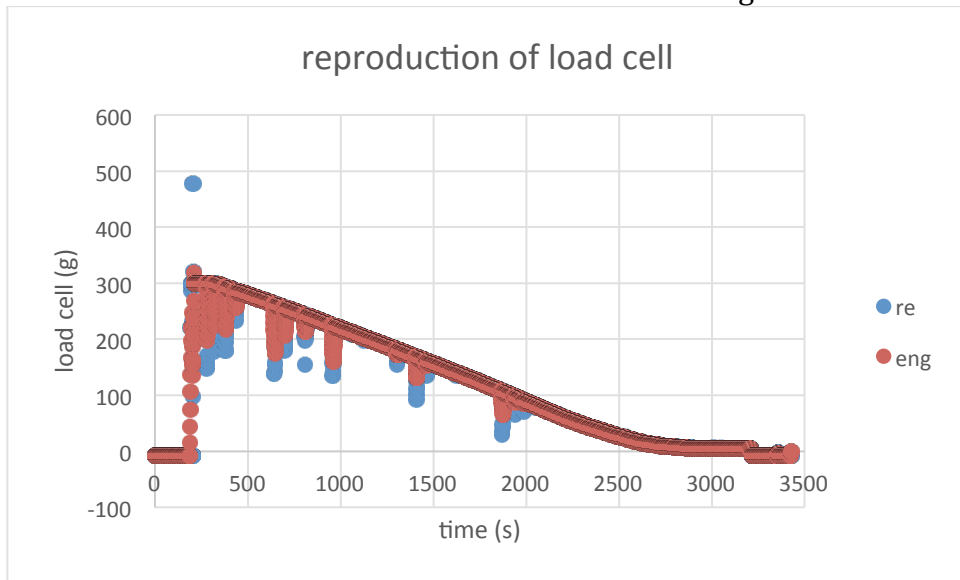


Figure 29-Reproduction and Comparison of Mass of Load Cell

Indirect Measurements

The last section of result reproduction provides an explanation of how the VI converts the voltages measured in the cone calorimeter into direct measurements in engineering units.

An explanation of how the software calculates the indirect measurements needed for further analysis is also provided.

All work was done by hand in order to prove that the procedure was understood. All the equations for converting raw data into indirect measurements are outlined in this section and results will be compared to those calculated directly by the VI to show the reliability of testing.

Mass loss rate

The mass of the specimen was recorded every second during the experiment. The mass loss rate was then calculated based on the mass recorded and was used in the calculation of specific extinction area and effective heat of combustion. The mass loss rate was calculated by the following equations:

$$-\left[\frac{dm}{dt}\right]_1 = \frac{25m_0 - 48m_1 + 36m_2 - 16m_3 + 3m_4}{12 \Delta t} \quad (C3)$$

$$-\left[\frac{dm}{dt}\right]_2 = \frac{3m_0 + 10m_1 - 18m_2 + 6m_3 - m_4}{12 \Delta t} \quad (C4)$$

$$-\left[\frac{dm}{dt}\right]_i = \frac{-m_{i-2} + 8m_{i-1} - 8m_{i+1} + m_{i+2}}{12 \Delta t} \quad (C5)$$

$$-\left[\frac{dm}{dt}\right]_{n-1} = \frac{-3m_n - 10m_{n-1} + 18m_{n-2} - 6m_{n-3} + m_{n-4}}{12 \Delta t} \quad (C6)$$

$$-\left[\frac{dm}{dt}\right]_n = \frac{-25m_n + 48m_{n-1} - 36m_{n-2} + 16m_{n-3} - 3m_{n-4}}{12 \Delta t} \quad (C7)$$

$-\left[\frac{dm}{dt}\right]_i$: the mass loss rate at i^{th} scan, (kg/s)

m_i : the mass at i^{th} scan, (kg)

There are four special cases: the first scan, the second scan, the penultimate scan, and the last scan. Those four trials have different equations for the calculation of the mass loss rate at the time from the general equation for the normal trials.

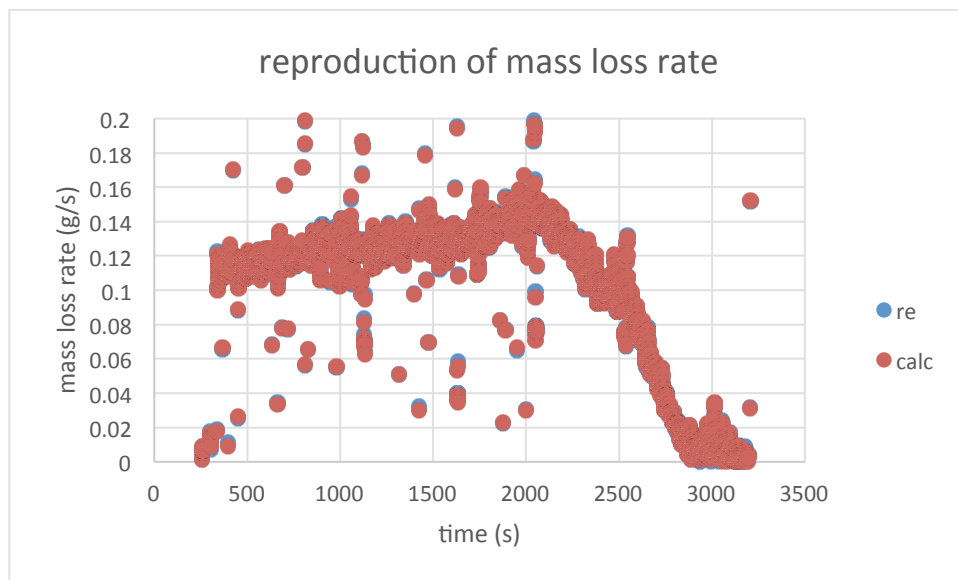


Figure 30-Reproduction and Comparison of Mass Loss Rate

Fig.C8 was modified by a 9-point average method to eliminate the noise. In addition, the data points were restricted to a range of 0 to 0.2 g/s, which could remove the invalid points.

Heat Release Rate and Effective Heat of Combustion

When analyzing the thermal properties of a specimen, the heat release rate and the effective heat of combustion are crucial criteria in the discussion. The cone calorimeter records temperature, pressure, and mole fraction of oxygen in the exhaust, and then the VI can generate what is needed for further discussion.

$$q'(t) = \left(\frac{\Delta h_c}{r}\right) (1.10)C \sqrt{\frac{\Delta P}{T_e}} \frac{(X_{O_2}^0 - X_{O_2}(t))}{1.105 - 1.5 X_{O_2}(t)} \quad (C8)$$

$q'(t)$: heat release rate at time t , (kW)

$\left(\frac{\Delta h_c}{r}\right)$: the value is specified for the material of the test specimen, (kJ/kg)

C : calibration constant for the oxygen consumption analysis, $(m \cdot kg \cdot K)^{0.5}$

T_e : absolute temperature at the orifice meter, (K)

ΔP : pressure drop through the orifice meter, (Pa)

X_{O_2} : oxygen analyzer reading, before delay time correction

$X_{O_2}^0$: oxygen analyzer reading

t : time, (s)

$$\Delta h_{c,eff} = \frac{\sum_i q'(t) \Delta t}{m_i - m_f} = \frac{q'(t)}{\left[\frac{dm}{dt}\right]} \quad (C9)$$

$\Delta h_{c,eff}$: effective heat of combustion, (kJ/kg)

$q'(t)$: heat release rate at time t , (kW)

m_i : initial mass of specimen, (kg)

m_f : final mass of specimen, (kg)

t : time, (s)

The above equations were used to perform the calculations and were compared to the results given by the VI

$$\frac{\Delta h_c}{r} = 13.1 \times 10^3 \text{ kJ/kg in the experiment of PMMA}$$

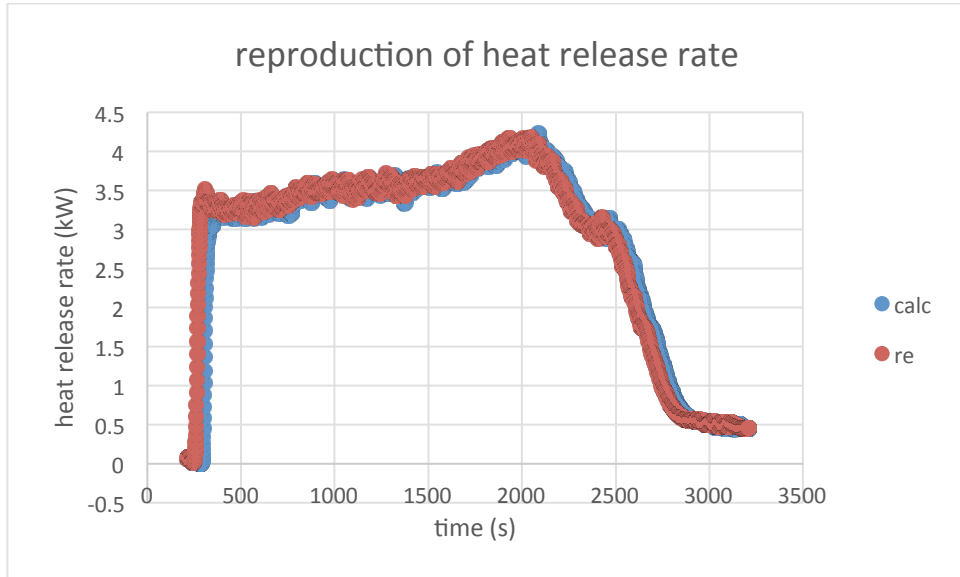


Figure 31-Reproduction and Comparison of Heat Release Rate

The same numbers were calculated as with the VI, but there was time delay of about 40 seconds. A possible reason for this case is that the time delay of the oxygen analyzer used is different from that used by the VI.

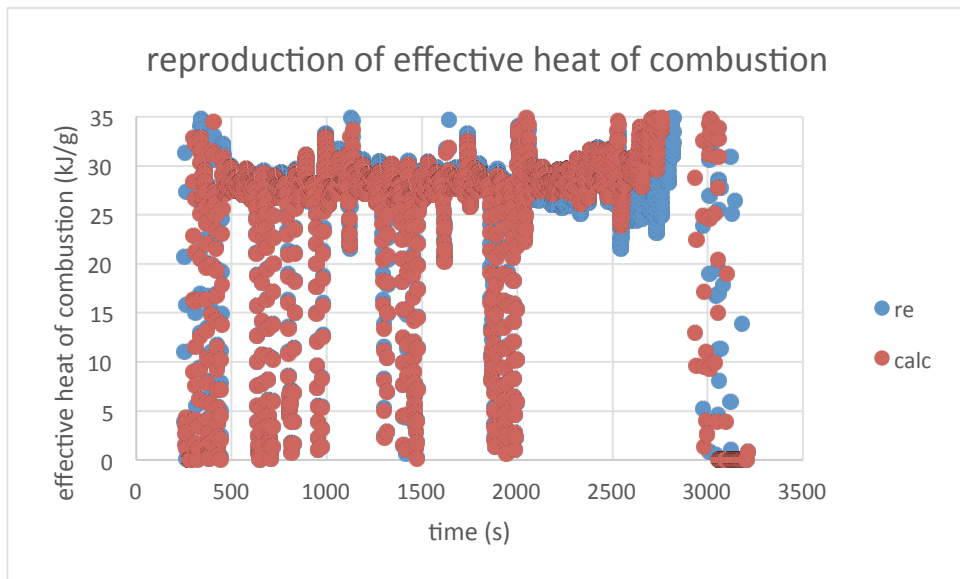


Figure 32-Reproduction and Comparison of Heat Release Rate

Two methods were used to modify Fig. C10. First, the numbers were calculated by a 9-point average method to eliminate the noise. Second, the data points were restricted to a range of 0 to 35 kJ/g, which can remove the invalid points caused by small mass loss rate. Basically,

the effective heat of combustion was around 30 kJ/g, which met the reference value of PMMA. The dramatic increase at the end was likely due to unstable mass loss.

Smoke Obscuration

The smoke developed index is an important standard of how a specimen performs during a fire. The smoke extinction coefficient and the specific extinction area (SEA) were calculated as the basic measurements of the smoke, and were then used for further calculation based on the following equations:

$$k = \left(\frac{1}{L}\right) \ln \frac{I_0}{I} \quad (C10)$$

k : smoke extinction coefficient, (m^{-1})

L : extinction beam path length, (m)

I : actual beam intensity, (cd)

I_0 : beam intensity with no smoke, (cd)

$$\varepsilon_f (avg) = \frac{\sum_i \dot{V}_i k_i \Delta t}{m_i - m_f} = \frac{\dot{V}_i k_i}{\left[\frac{dm}{dt}\right]} \quad (C11)$$

$\varepsilon_f (avg)$: specific extinction area of smoke, (m^2/kg)

\dot{V} : volume flow rate of exhaust, measured at the location of the laser photometer, (m^3/s)

k : smoke extinction coefficient, (m^{-1})

m_i : initial mass of specimen, (kg)

m_f : final mass of specimen, (kg)

t : time, (s)

The extinction beam path length is the length of laser tap, which is 0.11 meter.

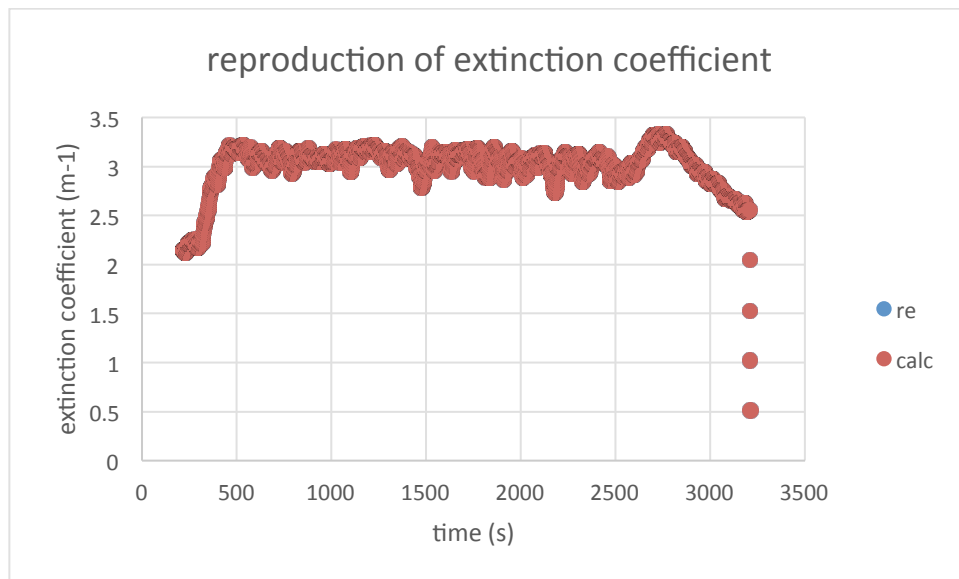


Figure 33-Reproduction and Comparison of Extinction Coefficient

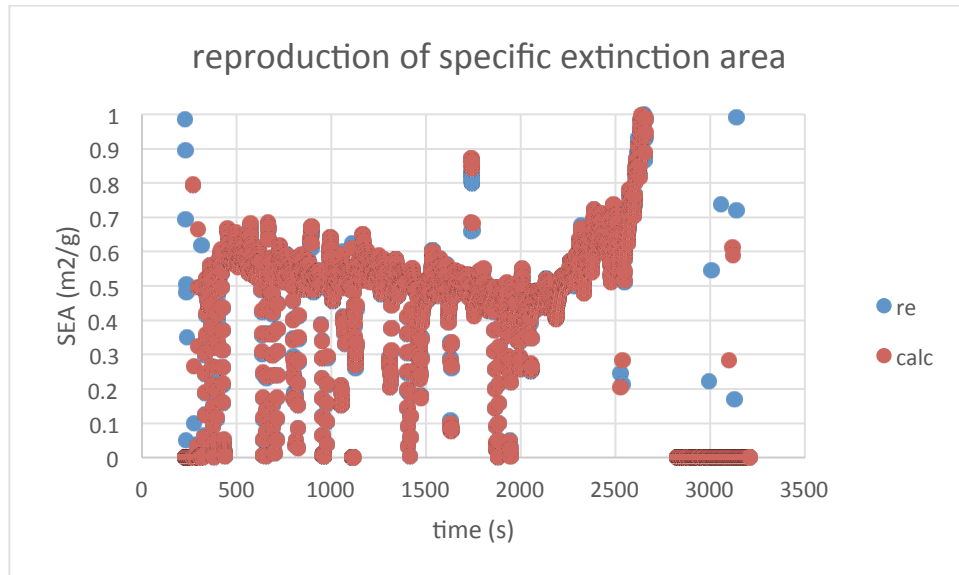


Figure 34-Reproduction and Comparison of Specific Extinction Area

Two methods were used to modify Fig.C12. First, the numbers were calculated by a 9-point average method to eliminate the noise. Second, the data points were restricted to a range of 0 to 1 m²/g, which could remove the invalid points caused by small mass loss rate. Generally, the SEA was below 1 m²/g (about 0.7), which was reasonable that a normal smoke would have a SEA in the range of 1-2 m²/g. The dramatic increase at the end was likely a result of unstable and infinitesimal mass loss rate.

Conclusion

All the graphs above show that the reproduced data has a good consistency with the data collected and calculated by the VI. Therefore, an understanding of how the cone calorimeter operates and how the data from the VI was calculated was achieved.

Description of Fires

Properties and flame shapes of specimens tested during initial apparatus familiarization experiments were recorded are listed below:

2C FRP a - "Hard to burn"

Properties:

- mass: 146.53 g
- area: 102.08 mm x 101.92 mm
- thickness: 9.35 g

- Smoking seen at shutter opening
- 309s: Blackening of surface
- 395s: Slight expansion of surface
- 442s :Ignition

Flame Shape:

- small fire, with little to no smoke visible
- low cone shape (barely classifiable as a cone), fragmentation of the flame
- “worms” formed on the surface

2C FRP b -“Also hard to burn”

Properties:

- mass: 146.99 g
- area: 101.77 mm x 101.85 mm
- thickness: 9.45 g

Similar style to the first sample.

- Smoking seen at shutter opening
- Blackening of surface
- Slight expansion of surface

Flame Shape:

- small fire, with little to no smoke visible
- low cone shape (barely classifiable as a cone), fragmentation of the flame
- “worms” formed on the surface

PMMA – “the perfect burn”

Properties:

- mass: 267.31 g
- area: 98.11mm x 100.31mm
- thickness: 23.11 mm
- 142s: Bubbling
- 596s: side hole flames
- 1646s: no central fire

Flame Shape:

- Large flame cone
- “Distinct gas burning layer”

Bath Tile FRP 1 – It’s like bath tile

Properties:

- mass: 53.21 g
- thickness: 3.98 mm
- area: 101.26mm x 100.60mm
- Surface cracking
- Surface charring
- Minute amounts of dark smoke
- “Aggressive Particulate Explosive Behavior”
- 410s: side smoke

- 483s: Fragmentation of the flame
- 504s: blue flames
- White decomposition in center of sample
- Fissure burning

Bath Tile FRP 2 – It's still like bath tile

Properties:

- mass: 50.58 g
- thickness: 3.9 mm
- area: 100.54 mm x 100.43 mm
- Surface cracking
- Surface charring
- Minute amounts of dark smoke
- Smoke igniting from holes of sample
- 470s: no more cone
- 470s: Fragmentation of the flame
- White decomposition in center of sample
- 716s: Fissure burning

Reliability

Two burns were conducted on two similar samples of bathroom tile at the same heat flux – 50 kW/m². The materials tested were almost identical in terms of mass, dimensions, and properties. The ignition times were almost the same at 141s and 143s, which showed that the two experiments acted similarly before the fire started. Four very crucial criteria of thermal performance are compared and plotted against time: heat release rate, mass loss rate, extinction coefficient, and specific extinction area.

Result and Comparison

Heat Release Rate

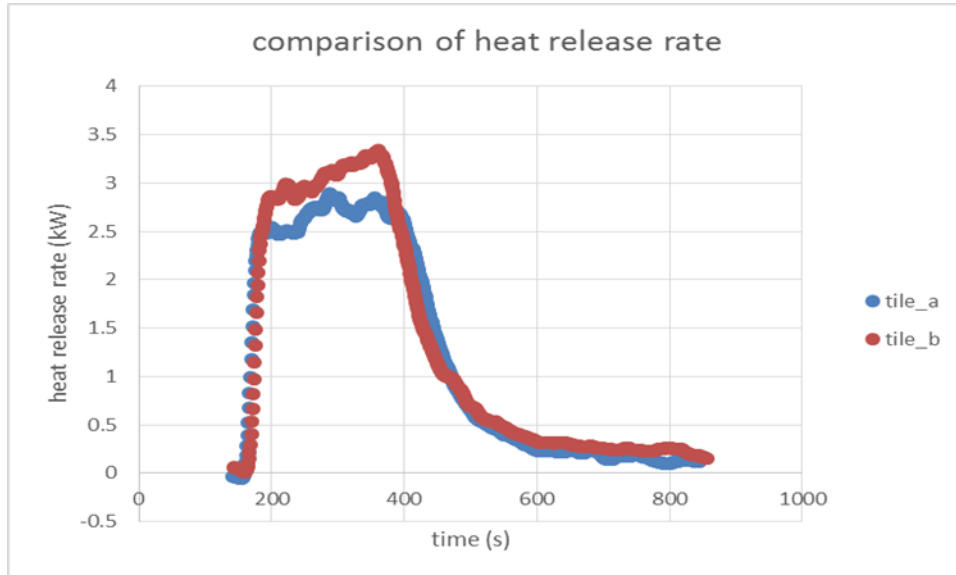


Figure 35-Comparison of Heat Release Rate of Tiles

Fig. C13 was modified by a 9-point average method to eliminate the noise. From these graphs, there is a strong correlation between the heat release rates of these two samples. The average heat release rate for Tile A was 141, and for Tile B it was 151 kW/m², with a max heat release rate of 338 and 396 kW/m². Total heat release for A and B was 95 and 103 MJ/m³, respectively.

Mass Loss Rate

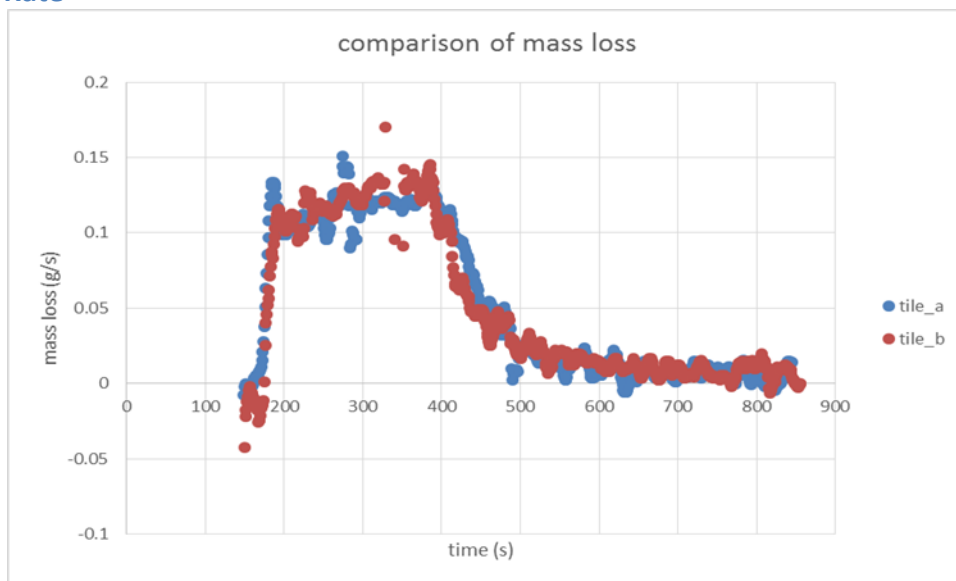


Figure 36-Comparison of Mass loss of Tiles

Two methods were used to modify Fig.11. The numbers were calculated by a 9-point average method to eliminate the noise. The data points were restricted to a range of 0 to 0.2 g/s, which removed the invalid points.

Again with these two samples, the peak heat release rates threw off any graphical representations made from the data. These fluctuations were due to the pump cycling on and off automatically throughout the duration of the test. The total mass lost was 32.8 grams (of 53.2 initially) for Tile A and 23.3 grams (of 50.6 initially), at an average rate of 0.105 and 0.096 g/s for tile A and tile B, respectively.

Extinction Coefficient

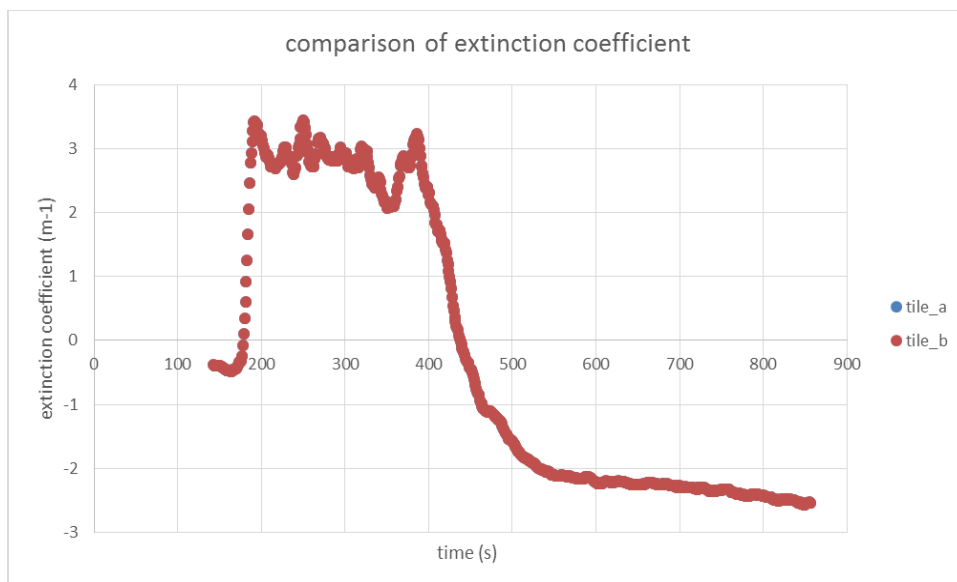


Figure 37-Comparison of Extinction Coefficient of Tiles

Fig. C15 was modified by a 9-point average method to eliminate the noise. The original data calculated by the VI was negative because of some calibration problems. However, the VI itself corrected the error by increasing all the points by about 2.8 m^{-1} to achieve the diagram above. The extinction coefficients after 430s were invalid, since they should never be negative.

Specific Extinction Area (SEA)

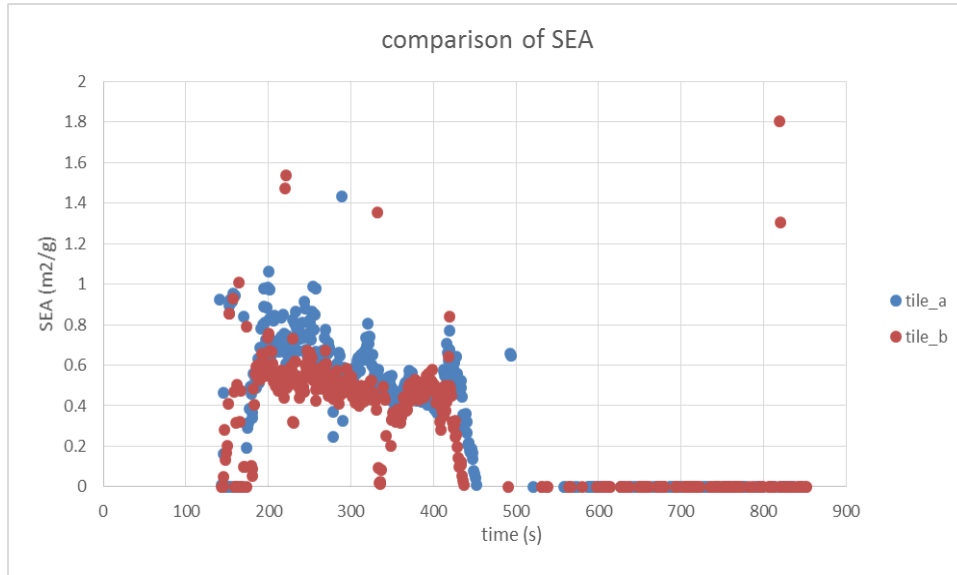


Figure 38-Comparison of Extinction Coefficient of Tiles

Two methods were used to modify Fig. C16. The numbers were calculated by a 9-point average method to eliminate the noise. the data points were restricted to a range of 0 m²/g to 2 m²/g, which removed the invalid points, since the extinction coefficients after 430s were negative.

As shown above, the two tests gave almost identical results of smoke performance. Both extinction coefficient and specific extinction area have similar trends and magnitudes, and the deviation is acceptable.

Conclusion

The work done in this section proves that there is an understanding of the cone calorimeter its data and the associated calculations done by the VI. Because of the reproducibility of the results it is evident the procedure is well understood. The tests for the Kreysler specimens will be reliable proven by the work done in this section.

Appendix D: Data Handling Strategy

As shown in the previous section, multiple experiments of the same sample are crucial to prove the accuracy and reliability of cone calorimeter tests. The consistency between separate experiments will be a strong evidence that the procedures are done correctly and the data is reliable. Therefore, for each specimen, three separate tests were performed. To make it clear, all the data collected will be shown in graphs. In this section, a description of the procedure of how the raw data collection by the VI was handled, including wiping off noises, modifying figures, and calculating averages.

Noise

The major factor that causes noise in the database is mass loss rate—since the mass of a specimen is not changing consecutively, there will be data unreasonable at some time points such as zero mass loss rate and infinite mass loss rate (or unreasonably large mass loss rate). Therefore, the modification of mass loss rate of wiping off those noises will be necessary, or the shape of the curve will be unclear. For instance, Fig. A1 shows the curve of the raw data of mass loss rate:

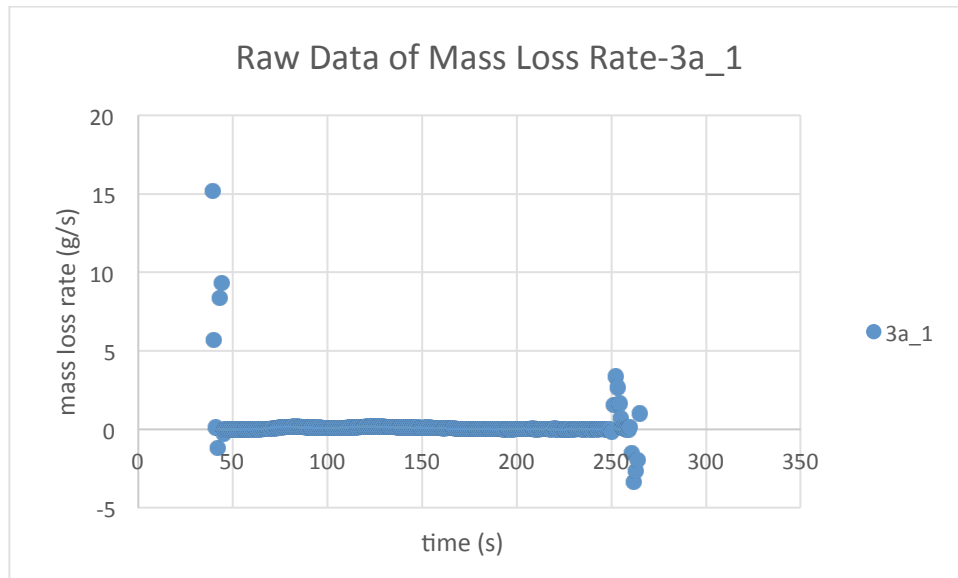


Figure 39-Raw Data of Mass Loss Rate of 3a_1

The strategy used to wipe off noises is to limit the magnitudes into a reasonable range. For mass loss rate, the range should be 0-0.5 g/s.

The low mass loss rate also causes noises in the graphs of Specific Extinction Area (SEA) and heat of combustion because mass loss rate is the dominant expression in the equations of SEA and heat of combustion. For example:

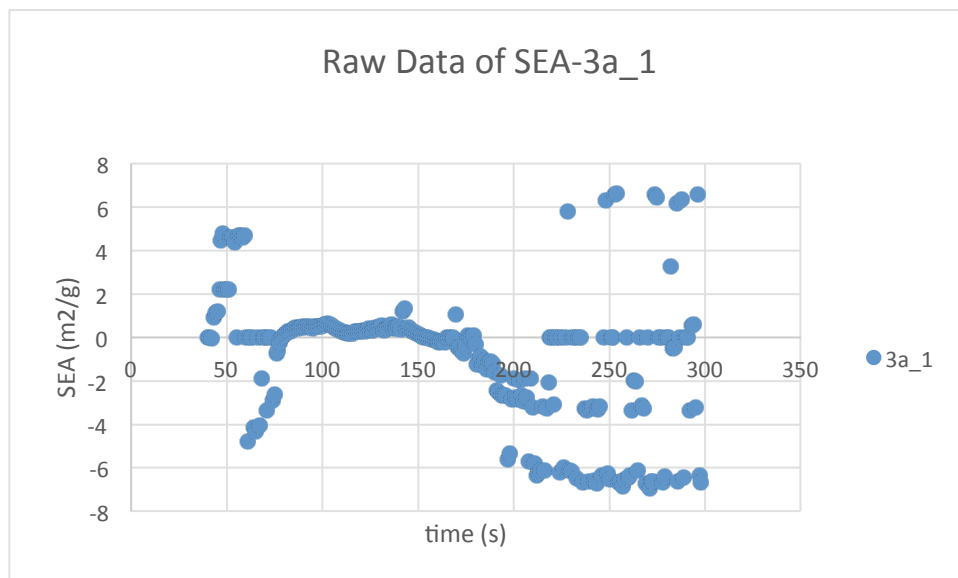


Figure 40-Raw Data of SEA of 3a_1

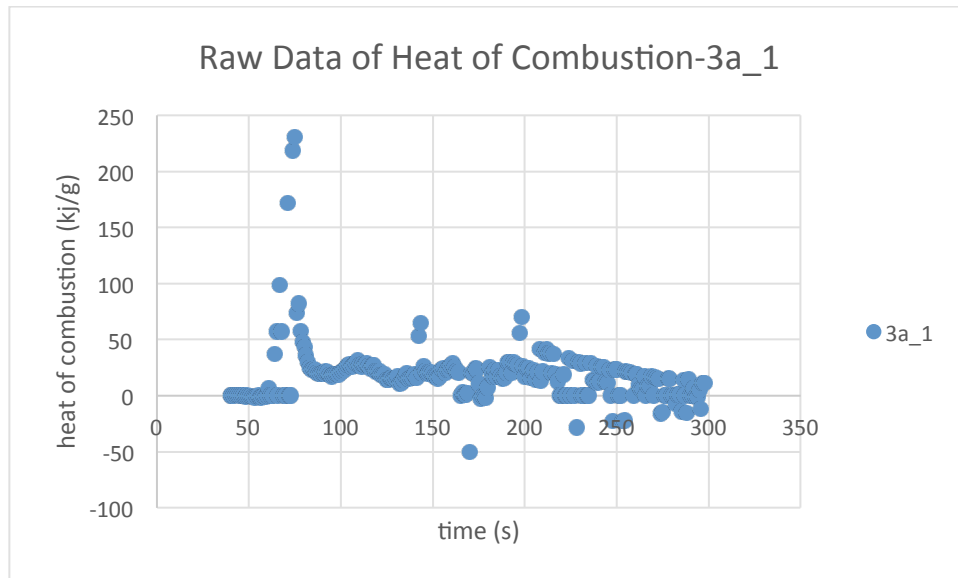


Figure 41-Raw Data of SEA of 3a_1

The range for SEA is 0-2 m²/g. (actually, 0.5-1 m²/g is a reasonable range for smoke generated by normal fiber reinforced polymer (FPR)). Smoke with SEA in the range of 1-2 m²/g will be very intense. The range for heat of combustion is 0-40 kJ/g.

9-Point Average

To make the curves smooth, a method called 9-point average is used to modify all the graphs. All the graphs of the first test of specimen 3a are shown below.

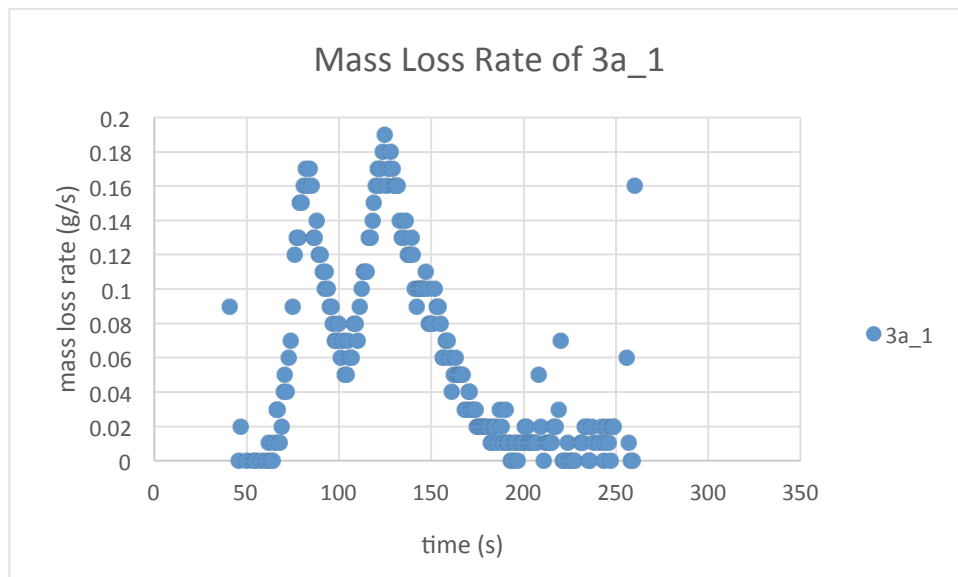


Figure 42-Mass Loss Rate of 3a_1

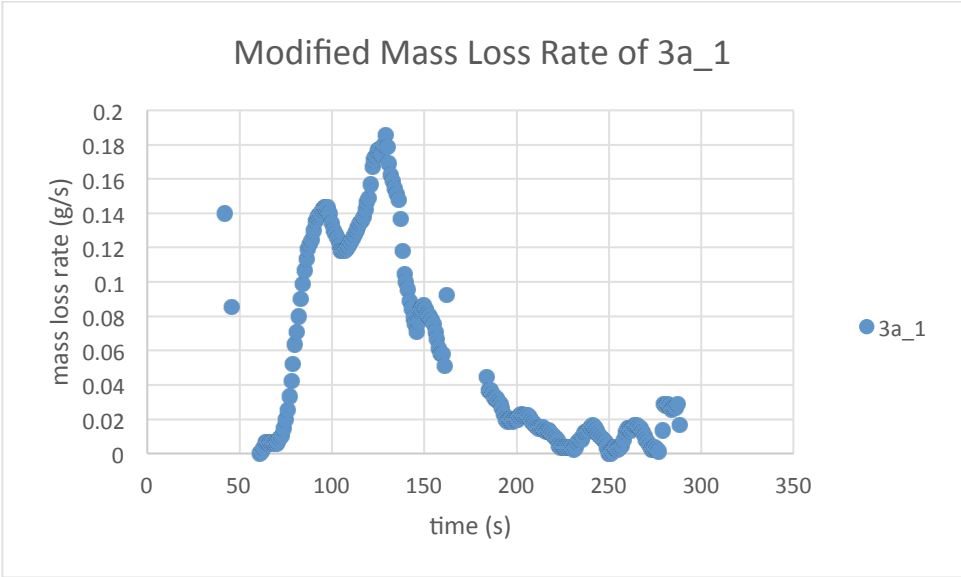


Figure 43-Modified Mass Loss Rate of 3a_1

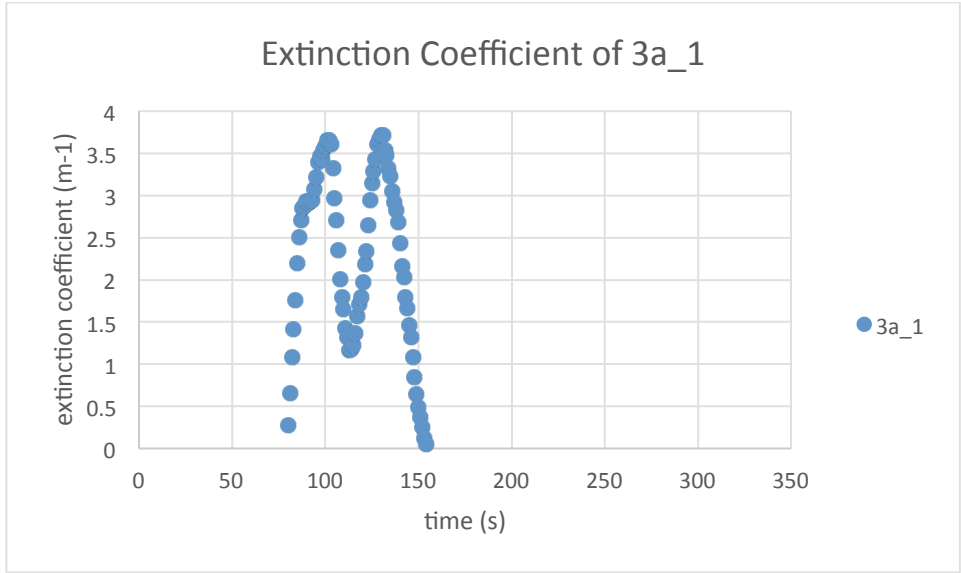


Figure 44-Extinction Coefficient of 3a_1

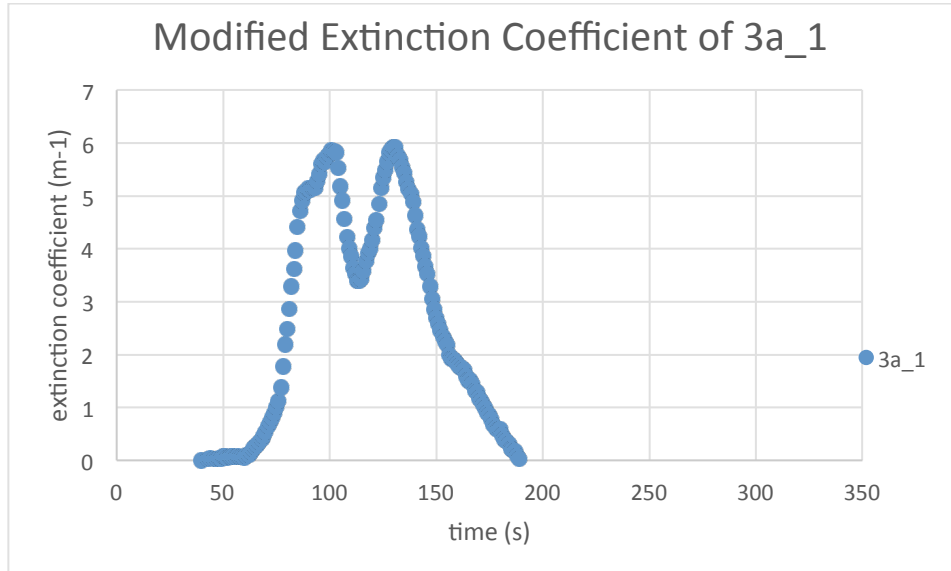


Figure 45-Modified Extinction Coefficient of 3a_1

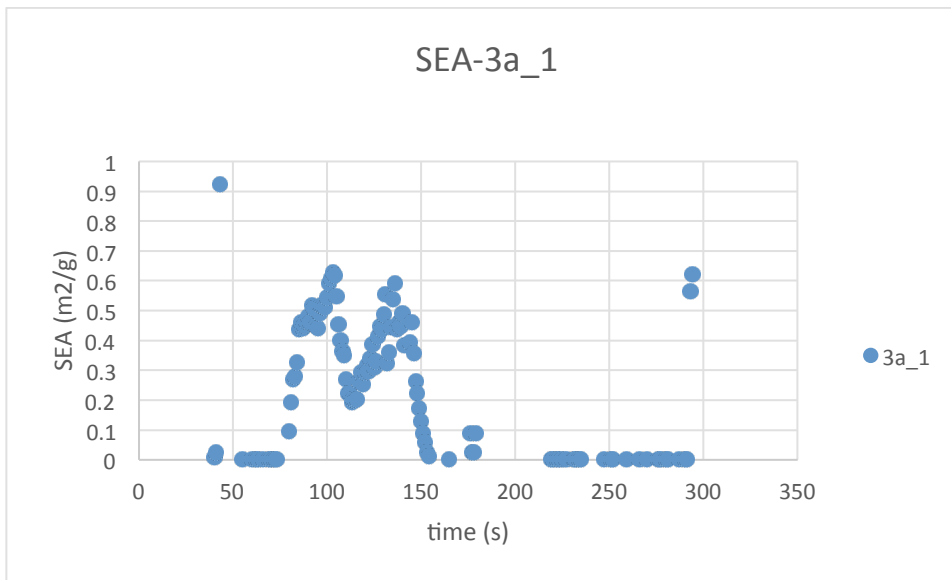


Figure 46-D8 SEA of 3a_1

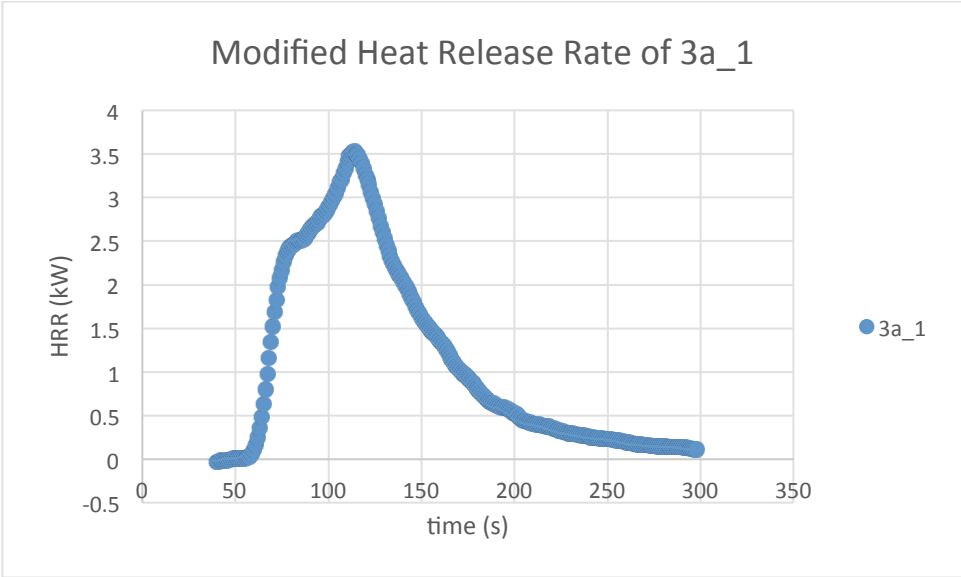


Figure 49-Modified Heat Release Rate of 3a_1

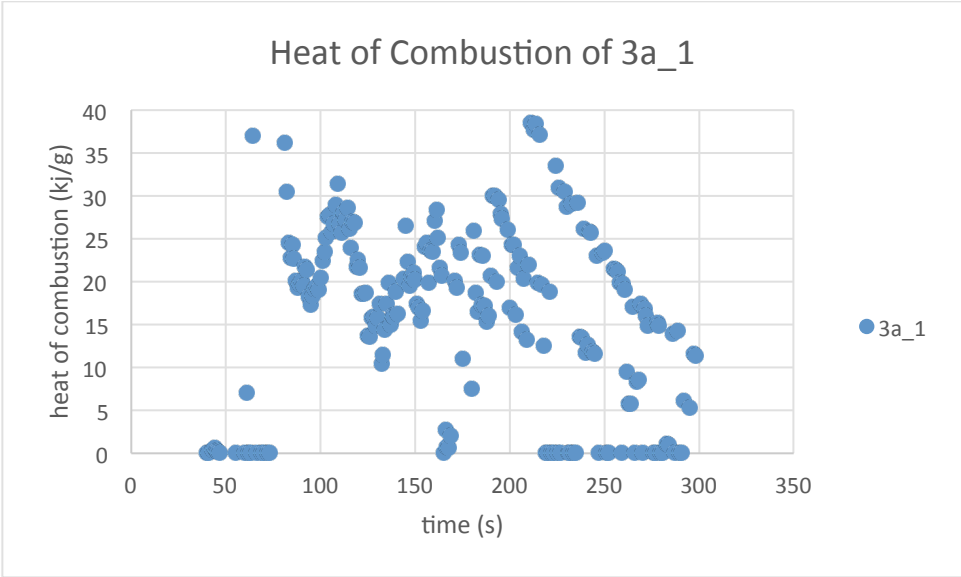


Figure 50-Heat of Combustion of 3a_1

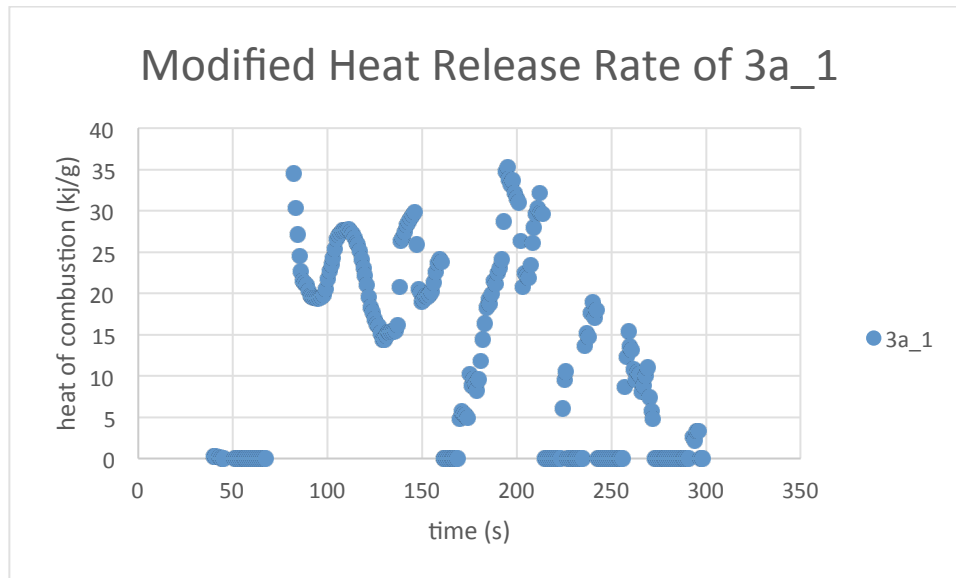


Figure 51-Modified Heat Release Rate of 3a_1

The modified graphs are clearer for viewers to identify shapes and trends of the curves, as well as the comparison between curves. Therefore, all the graphs shown will be modified by 9-point method.

Average—Wiping off Inconsistent Test

The comparisons between different specimens are required in order to decide the effects of ATH composition and different types of fire block. In the comparisons, the average data of three separate experiments is introduced and compared.

In most cases, the average is calculated by doing the average for all three tests. However, for the series 4 and series 5, the SEA data for the first experiment is not consistent with the second and third experiments, though the mass loss rate and extinction coefficient show good consistency. Since the SEA is calculated by dividing extinction coefficient by mass loss rate, the relatively small deviation of these two parameters can cause a relatively significant deviation of SEA. Therefore, the average was calculated for the SEA of these specimens only using the last two tests' data. All the SEA data calculated by averaging the two tests are listed below:

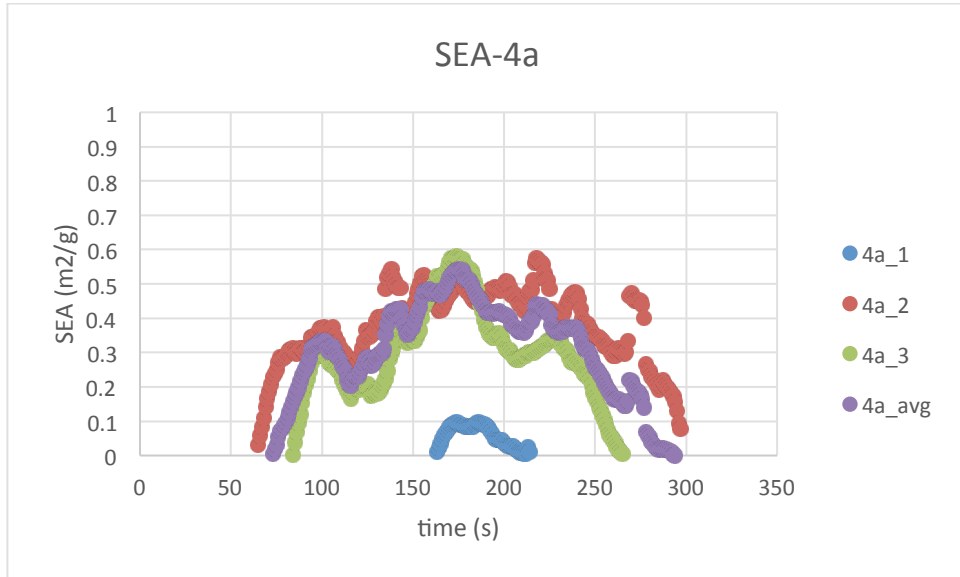


Figure 52-SEA of 4a

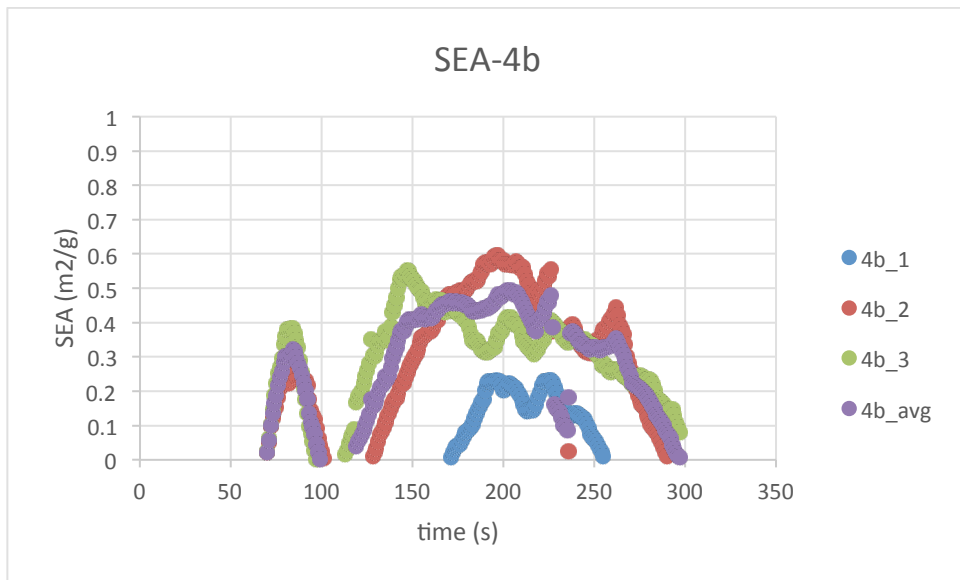


Figure 53-SEA of 4b

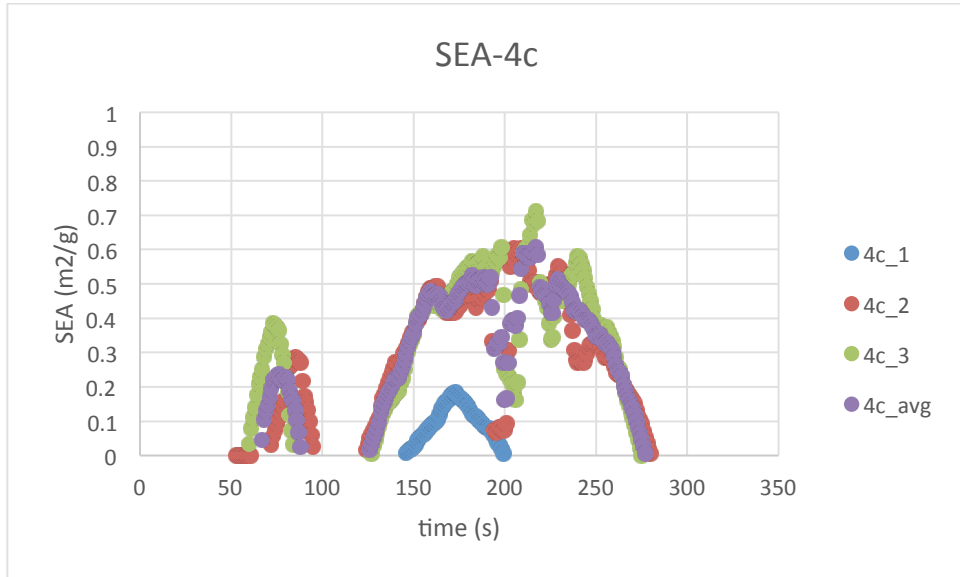


Figure 54-SEA of 4c

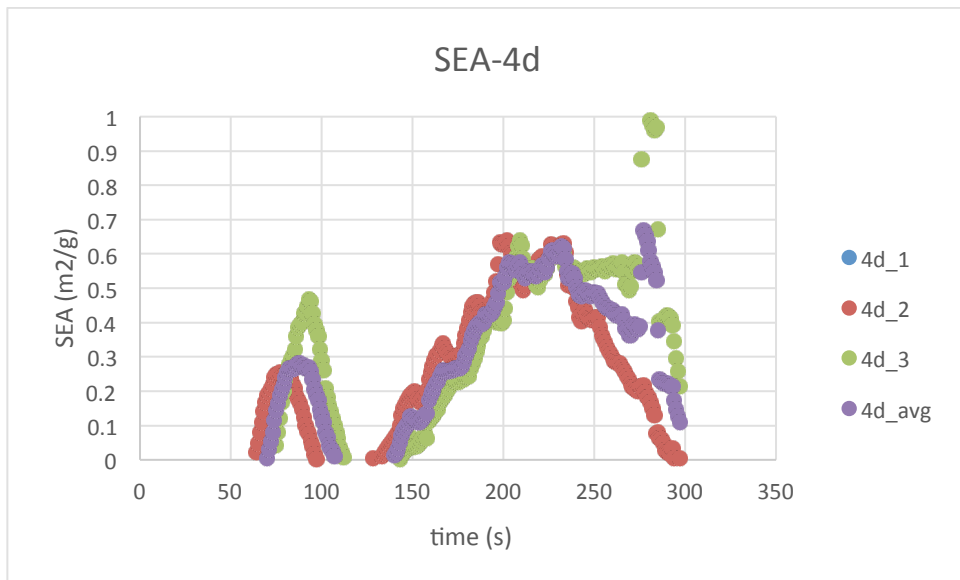


Figure 55-SEA of 4d

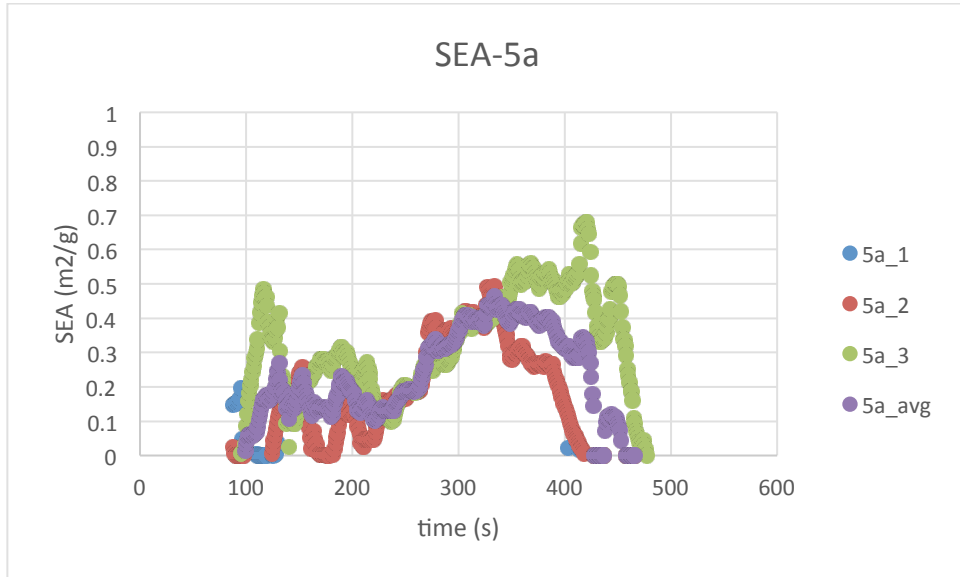


Figure 56-SEA of 5a

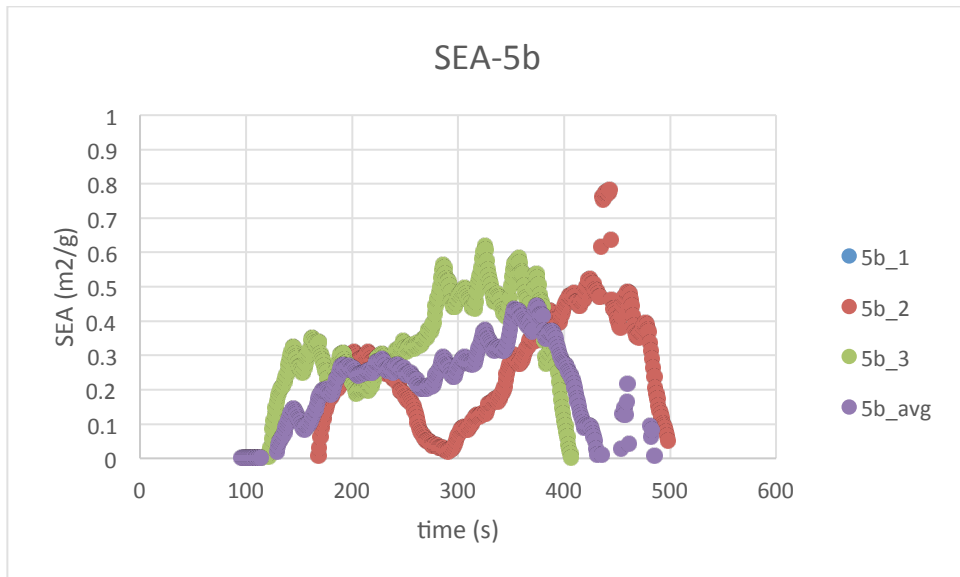


Figure 57-SEA of 5b

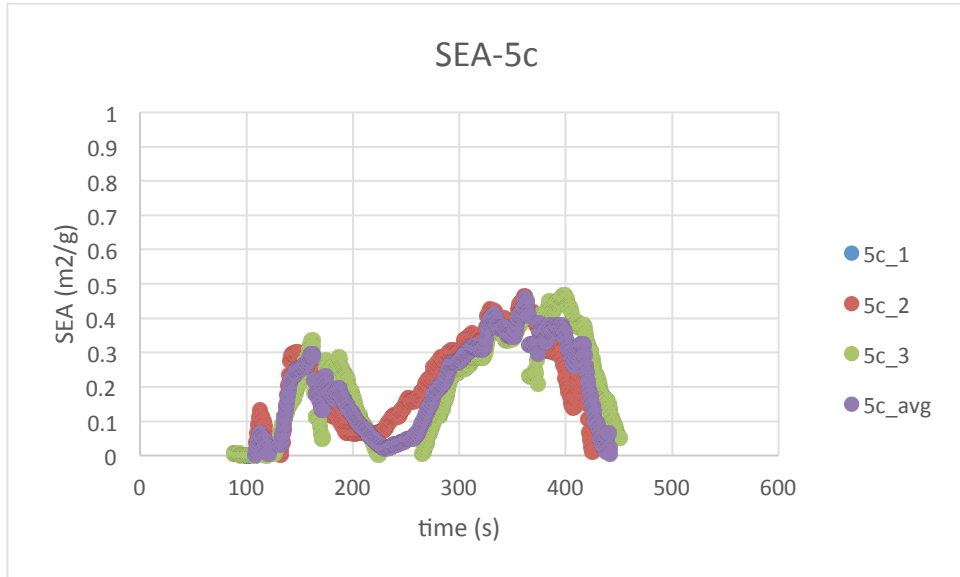


Figure 58-SEA of 5c

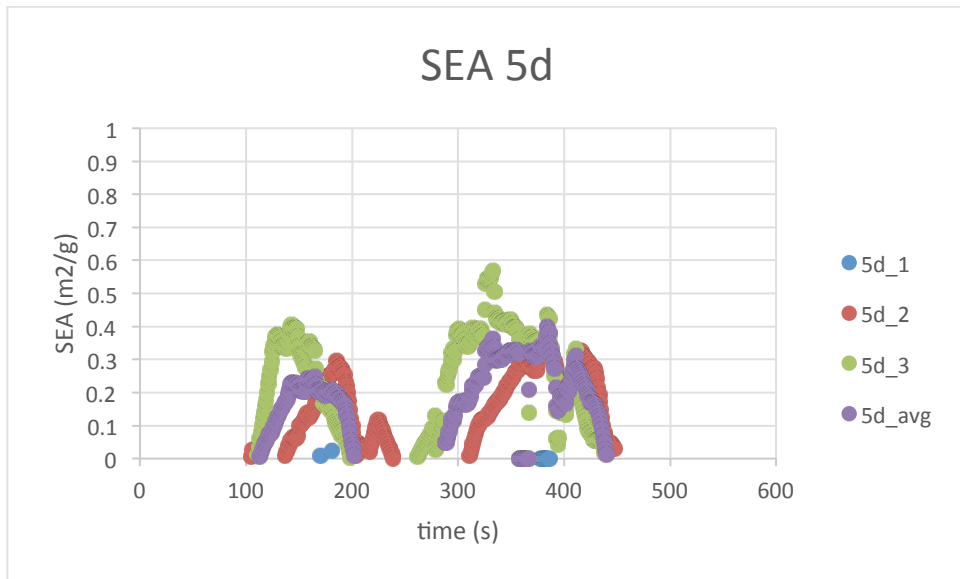


Figure 59-SEA of 5d

Appendix E: Data Summary

This section is the summary of the database of all the cone calorimeter experiments. All the data and graphs are handled in the method that has been described in previous sections. Mass loss rate, extinction coefficient, specific extinction area (SEA), heat release rate, and heat of combustion will be plotted and listed in this section. The first part is the summary for every single specimen. The second part of this section will show the comparisons between samples, including both in-series comparisons and cross-series comparisons.

Single Specimen

Series 3

3a

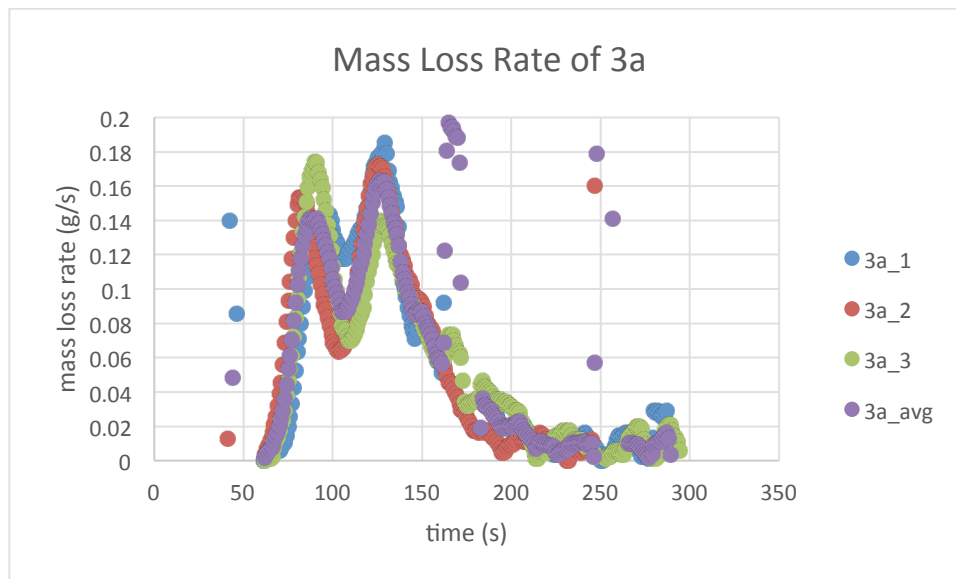


Figure 60-Mass Loss Rate of 3a

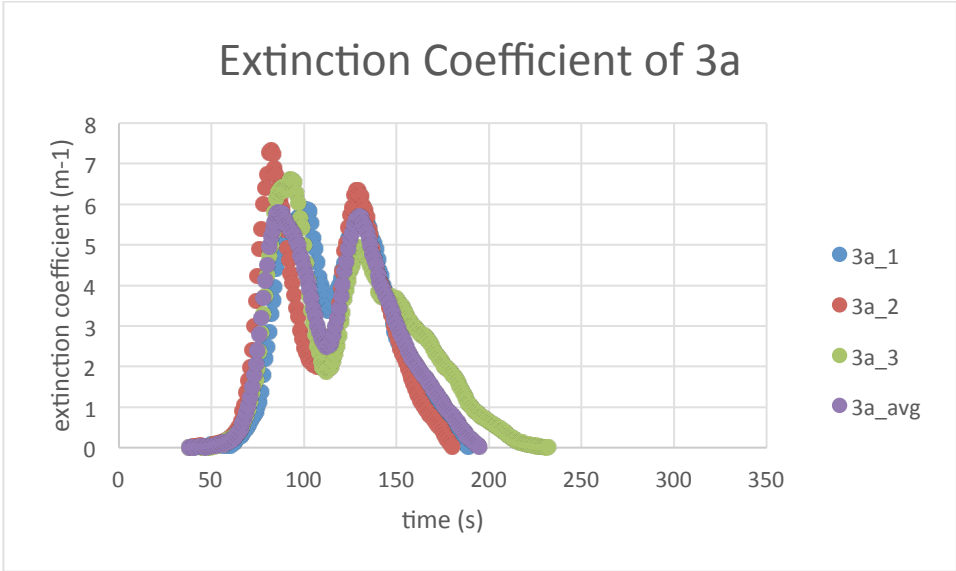


Figure 61-Extinction Coefficient of 3a

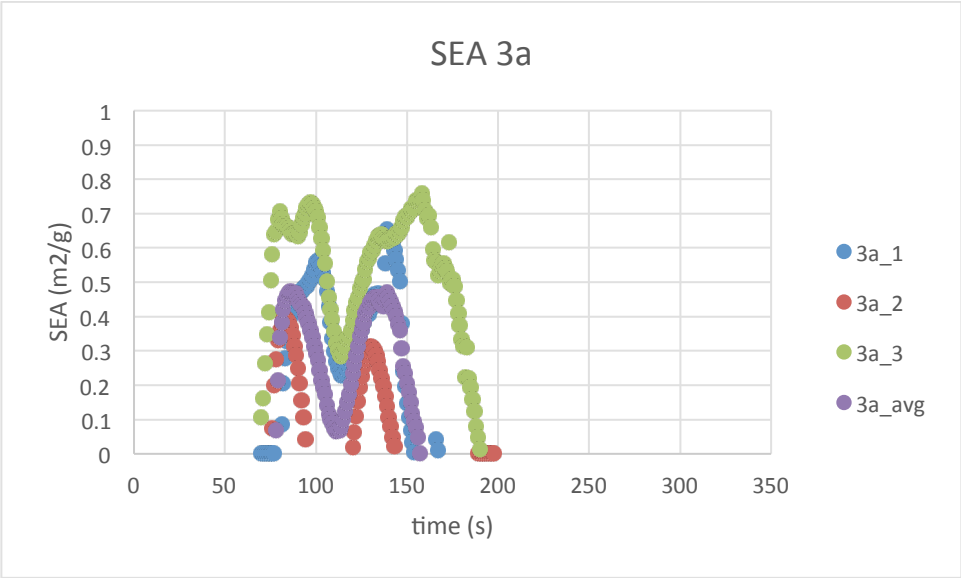


Figure 62-SEA of 3a

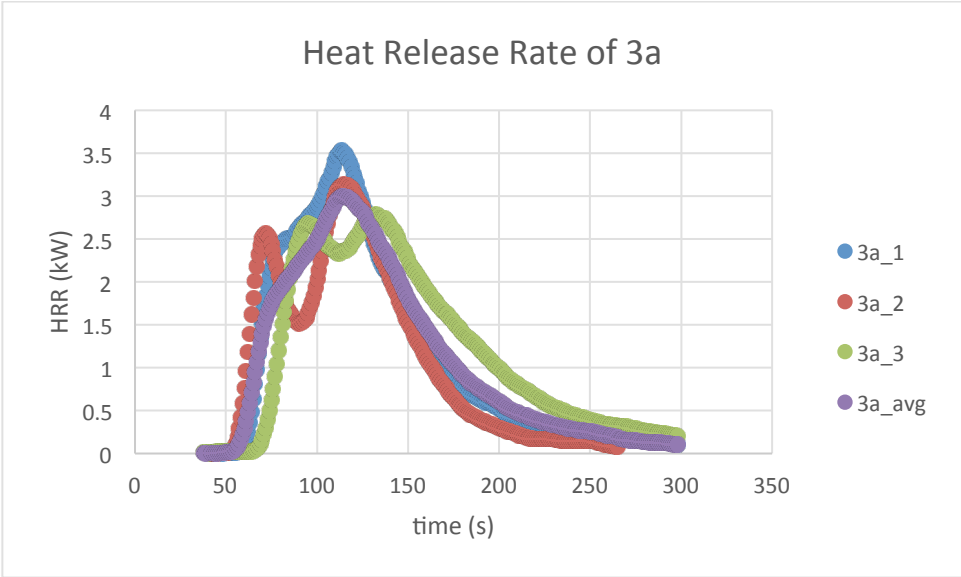


Figure 63-Heat Release Rate of 3a

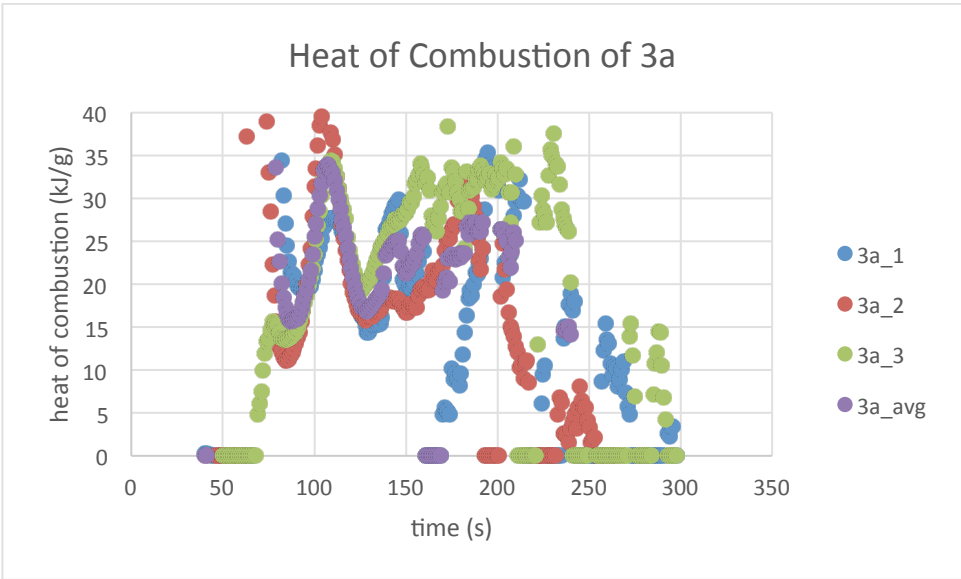


Figure 64-Heat of Combustion of 3a

3b

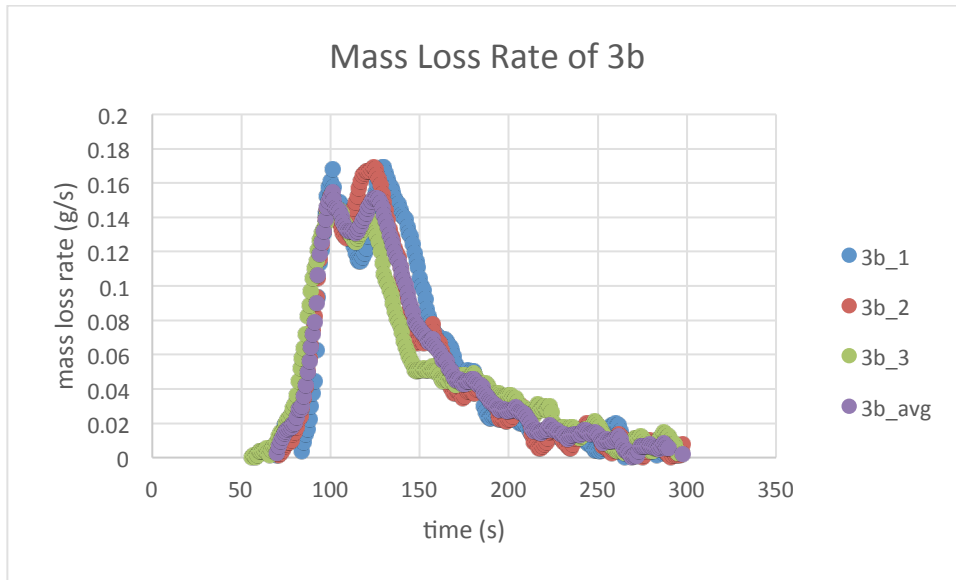


Figure 65-Mass Loss Rate of 3b

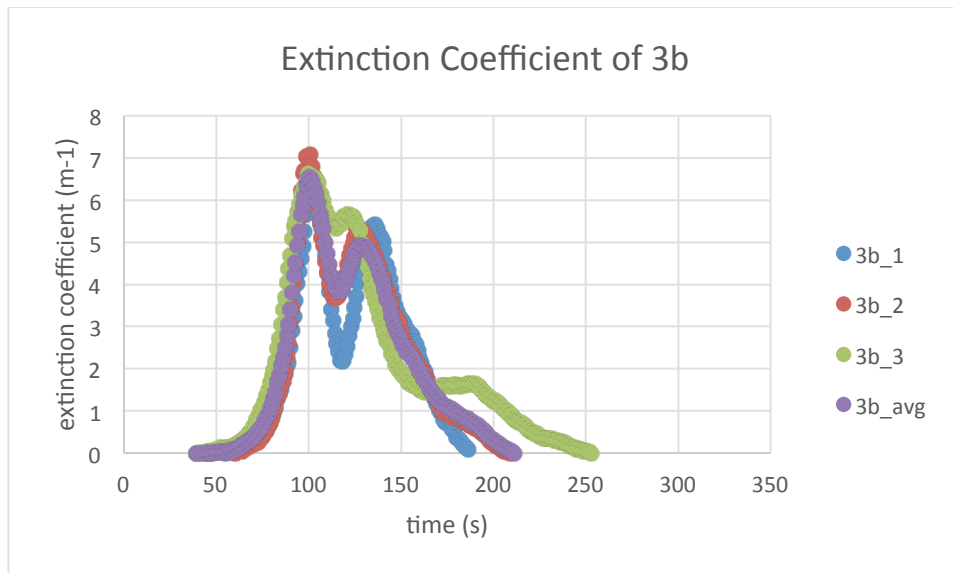


Figure 66-Extinction Coefficient of 3b

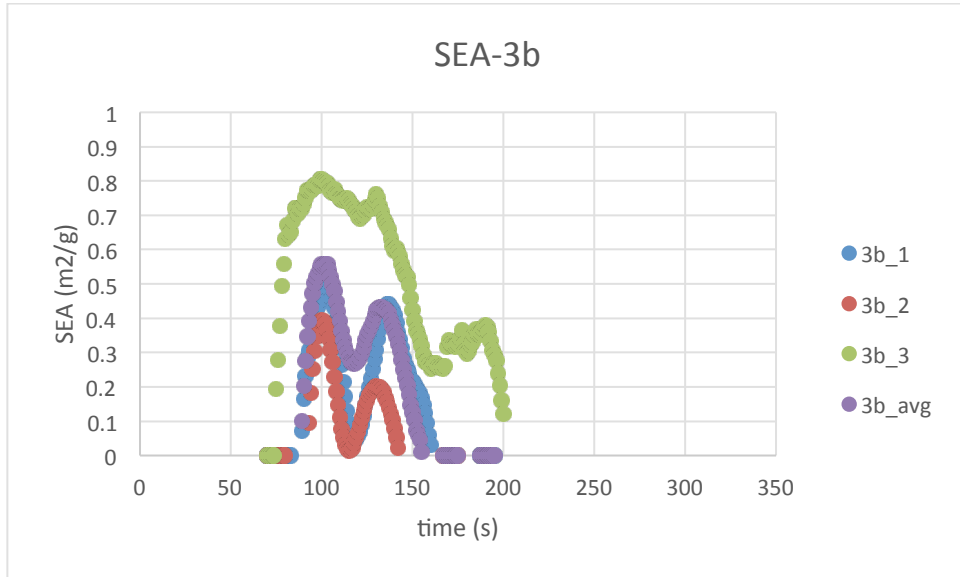


Figure 67-SEA of 3b

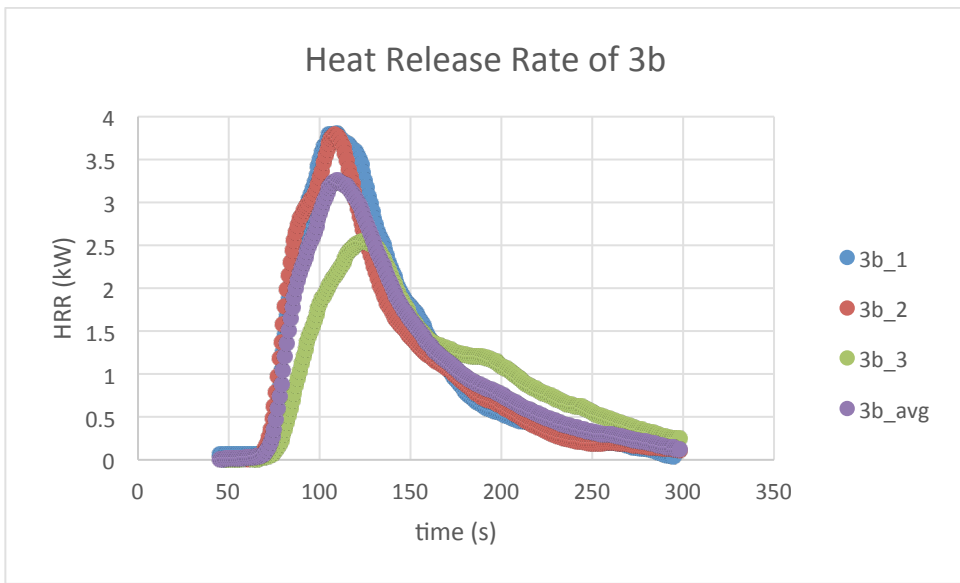


Figure 68-Heat Release Rate of 3b

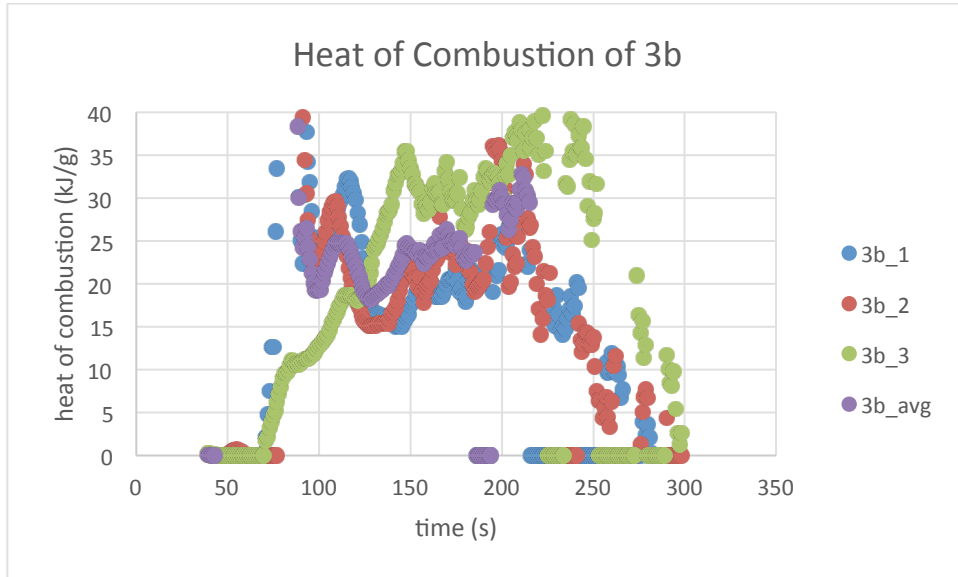


Figure 69-Heat of Combustion of 3b

3c

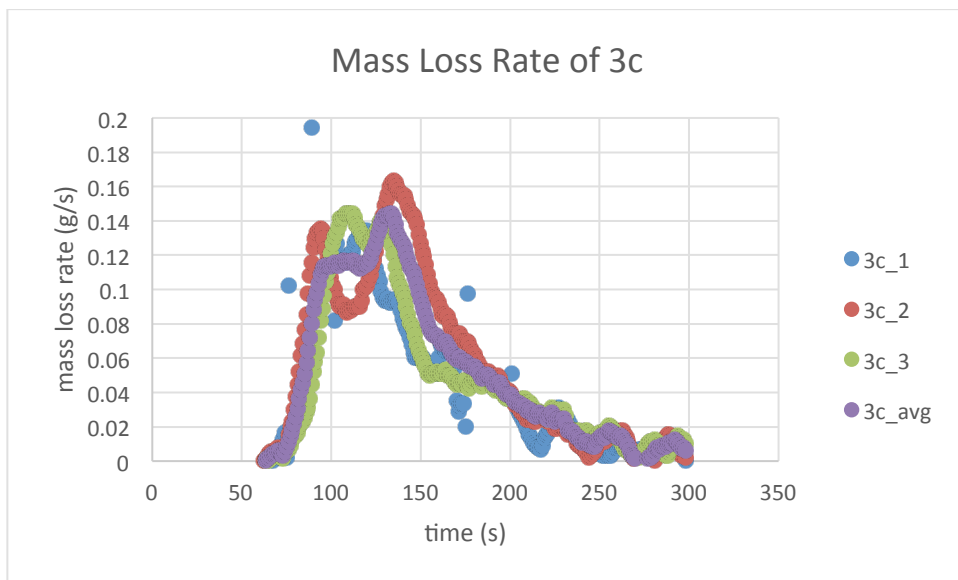


Figure 70-Mass Loss Rate of 3c

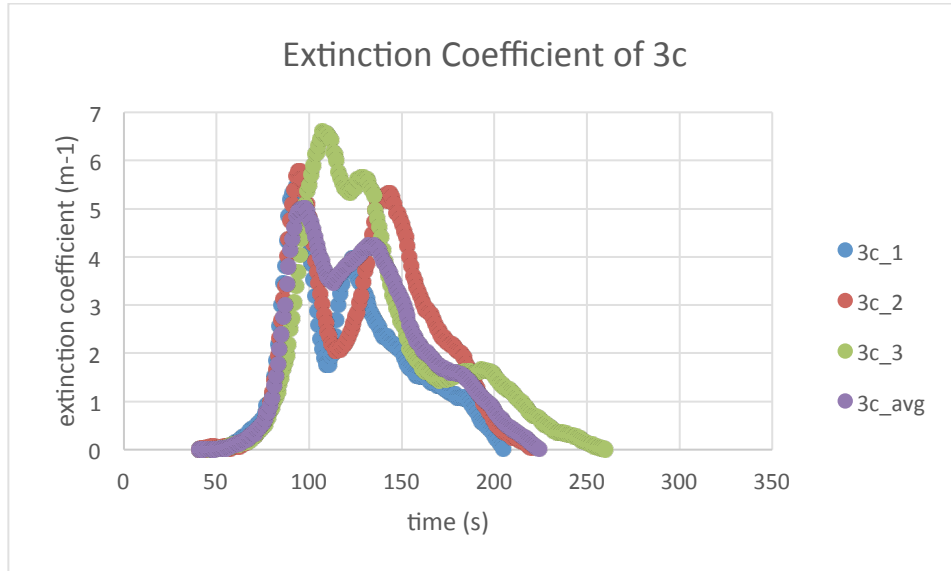


Figure 71-Extinction Coefficient of 3c

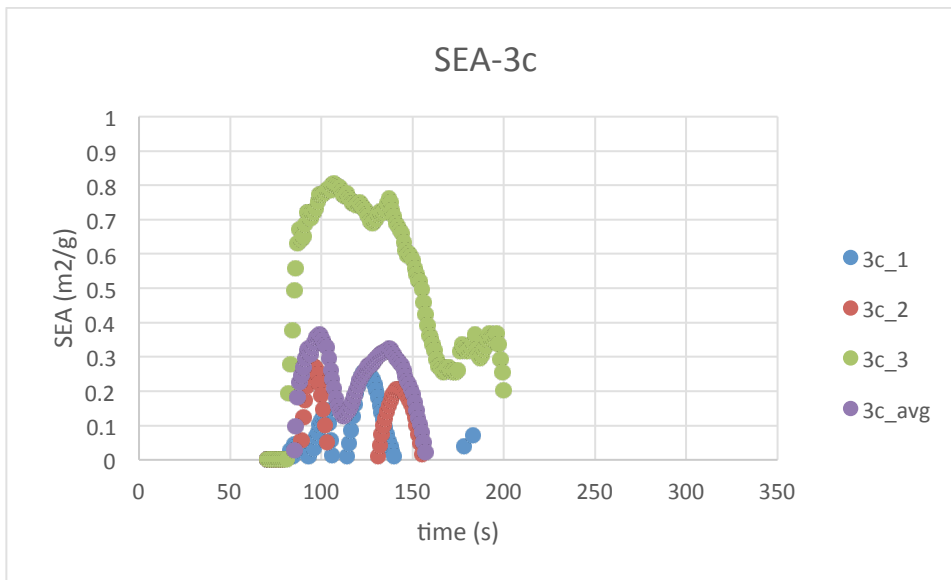


Figure 72-SEA of 3c

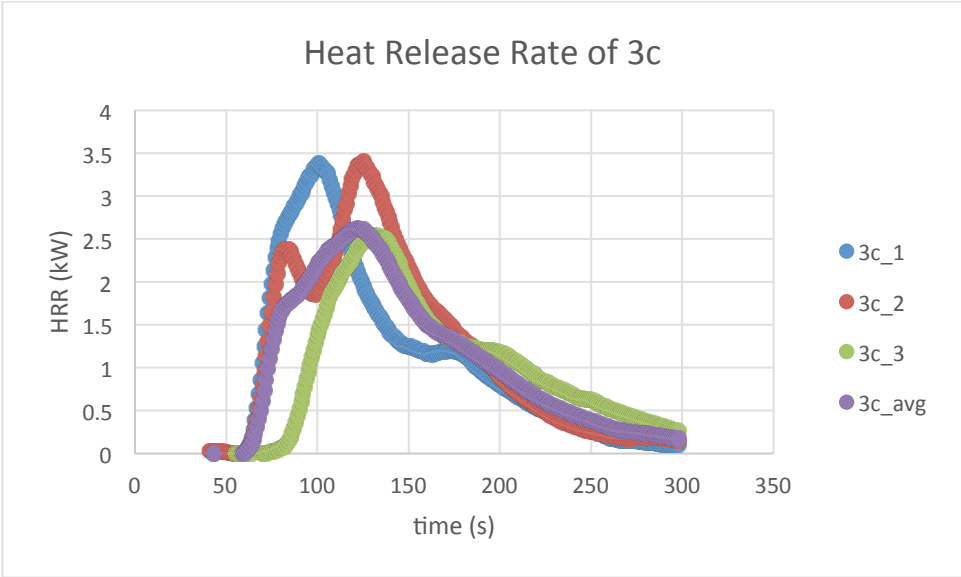


Figure 73-Heat Release Rate of 3c

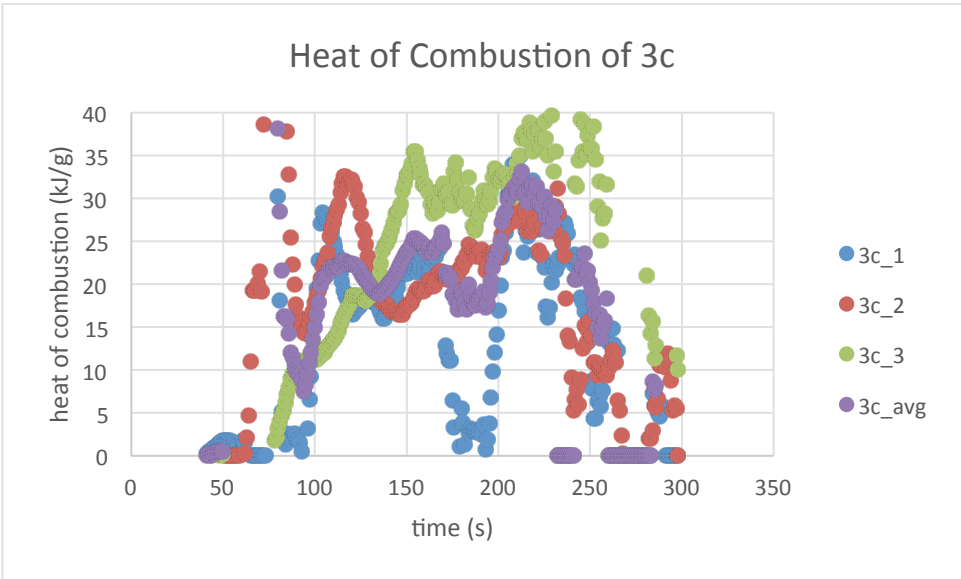


Figure 74-Heat of Combustion of 3c

3d

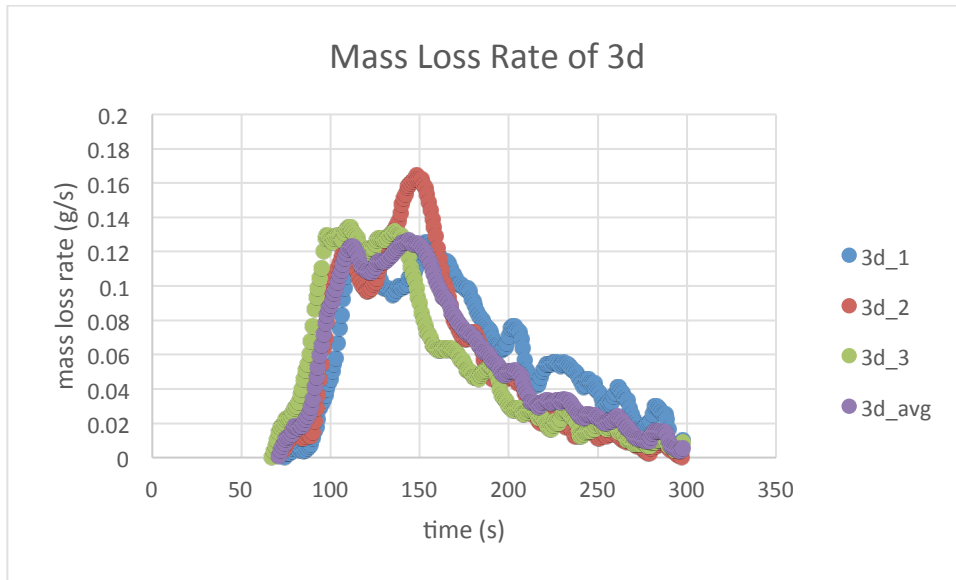


Figure 75-Mass Loss Rate of 3d

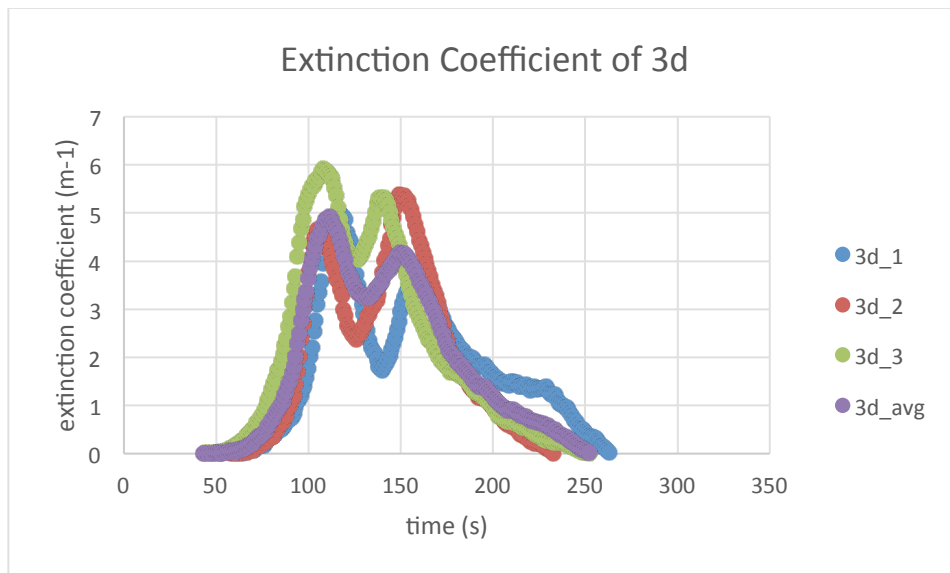


Figure 76-Extinction Coefficient of 3d

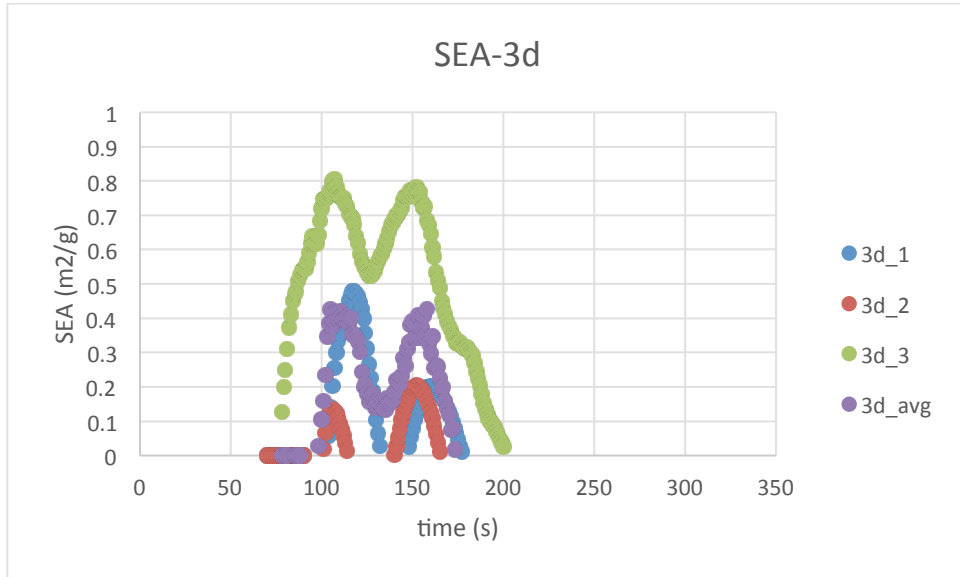


Figure 77-SEA of 3d

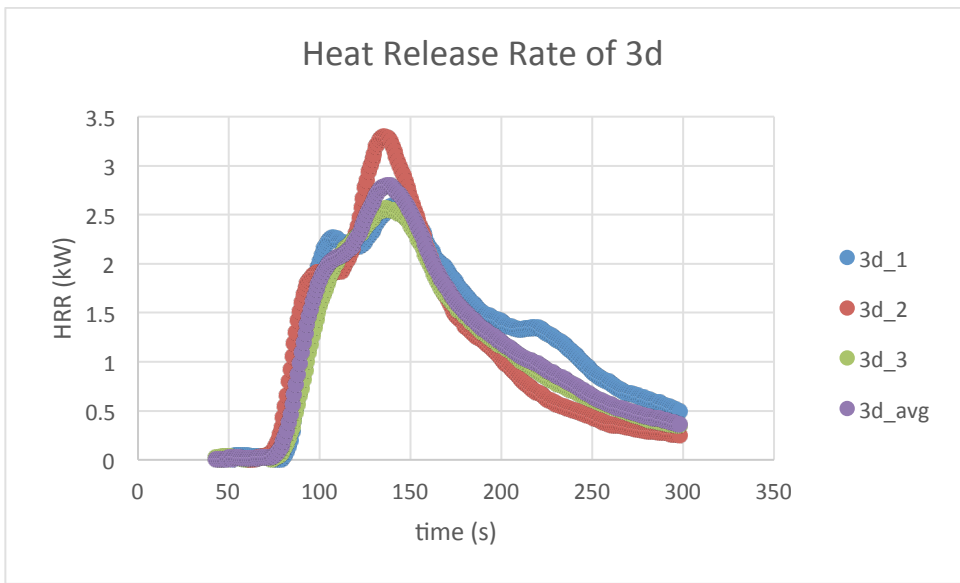


Figure 78-Heat Release Rate of 3d

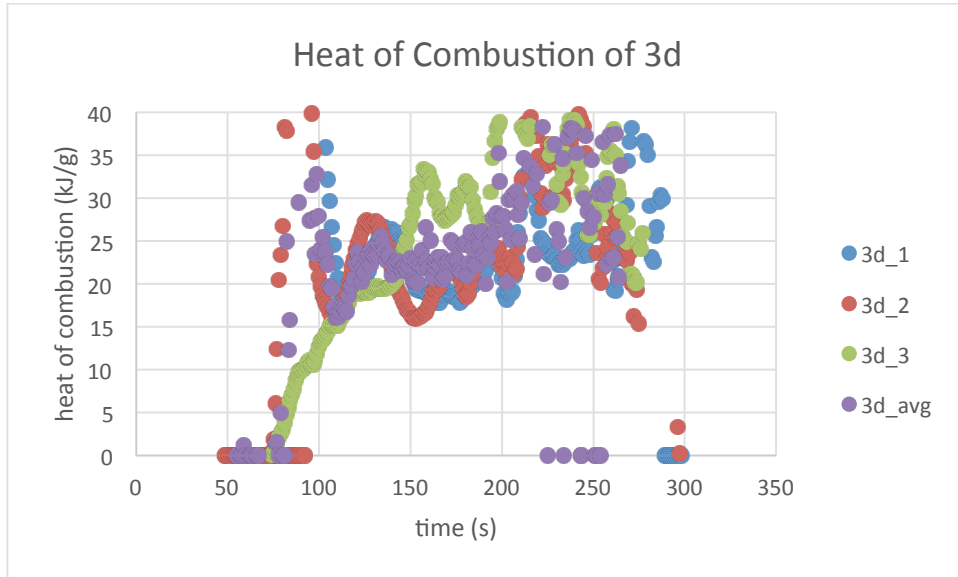


Figure 79-Heat of Combustion of 3d

Series 4

4a

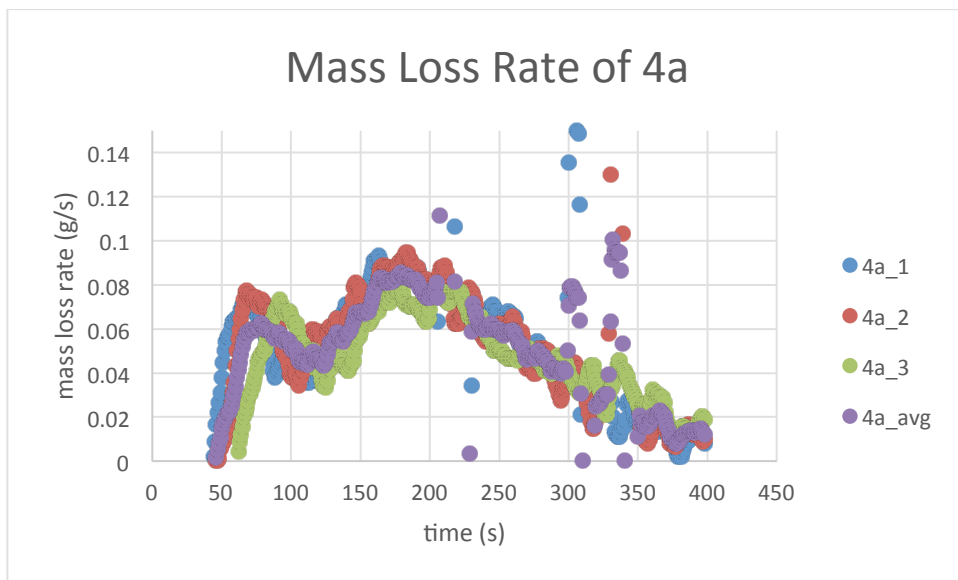


Figure 80-Mass Loss Rate of 4a

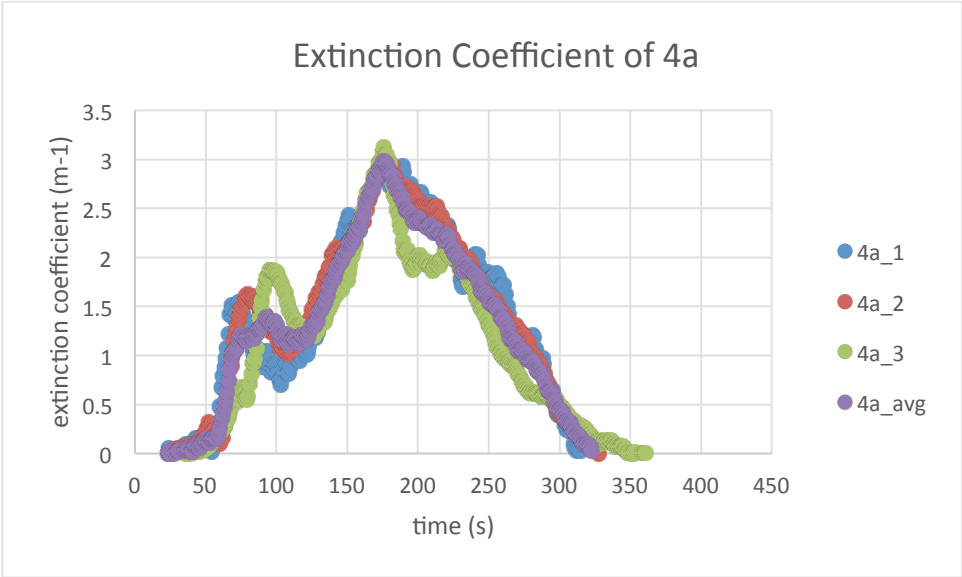


Figure 81-Extinction Coefficient of 4a

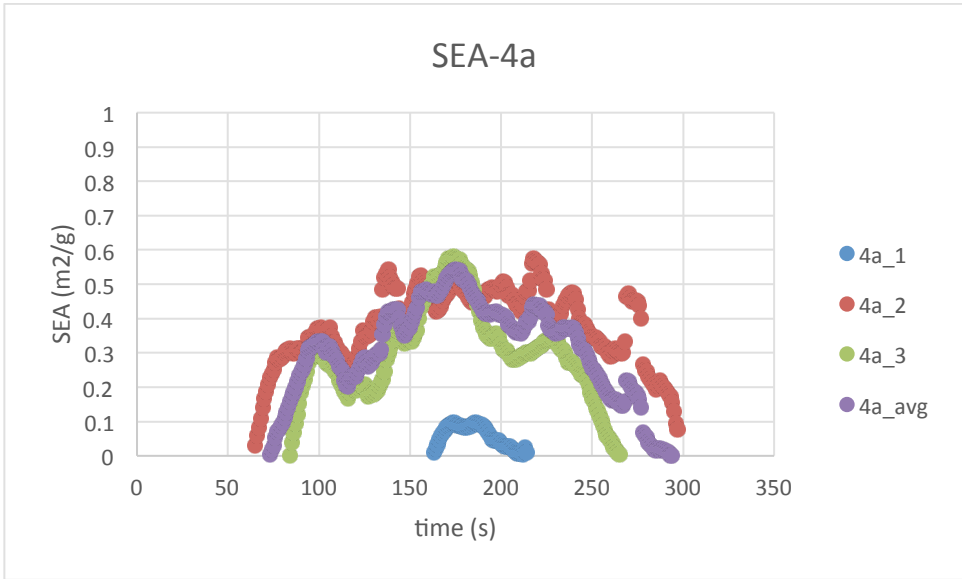


Figure 82- SEA of 4a

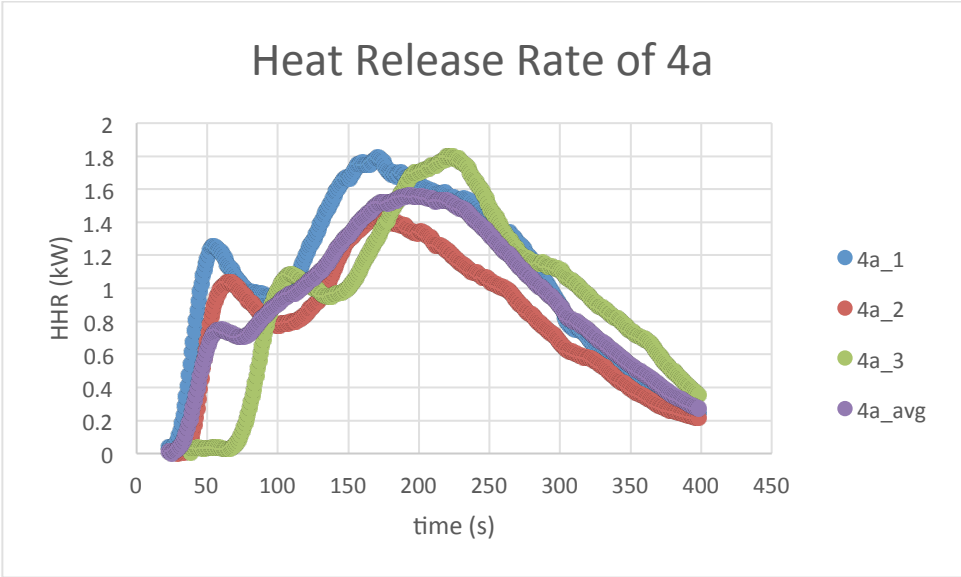


Figure 83-Heat Release Rate of 4a

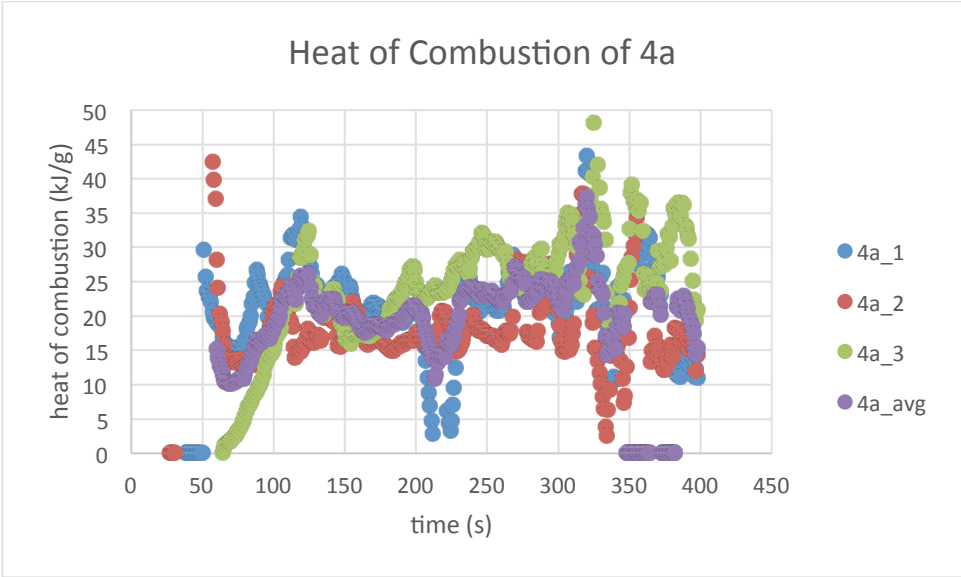


Figure 84-Heat of Combustion of 4a

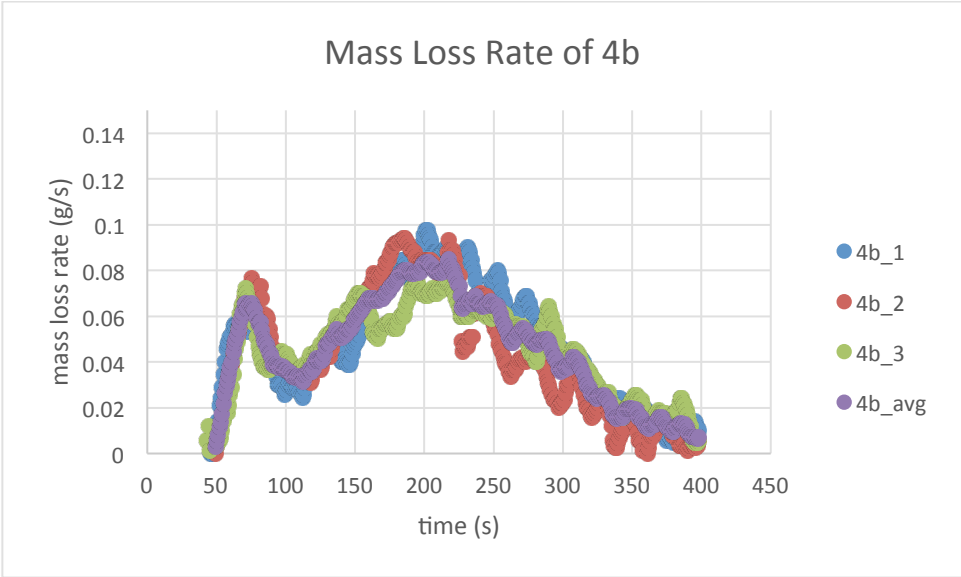


Figure 85-Mass Loss Rate of 4b

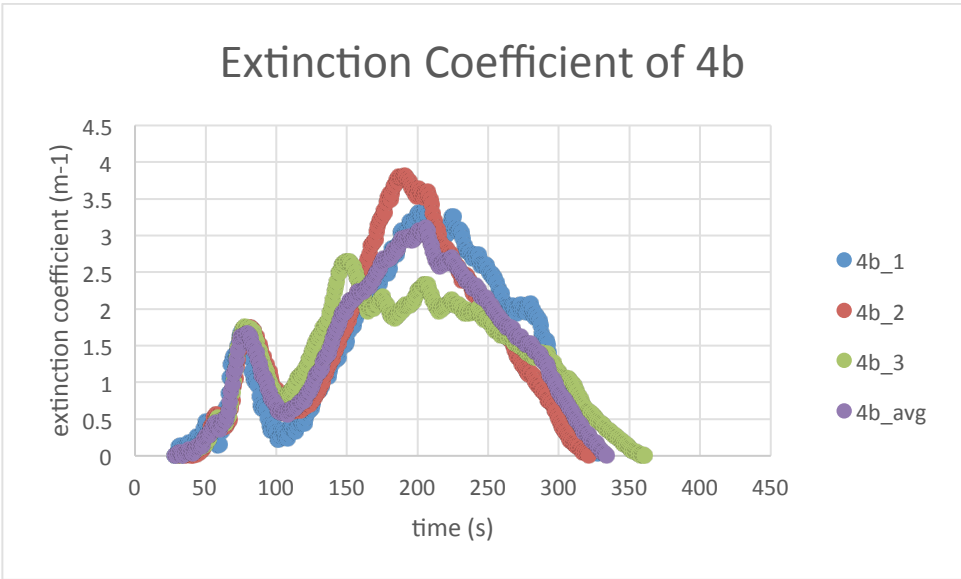


Figure 86-Extinction Coefficient of 4b

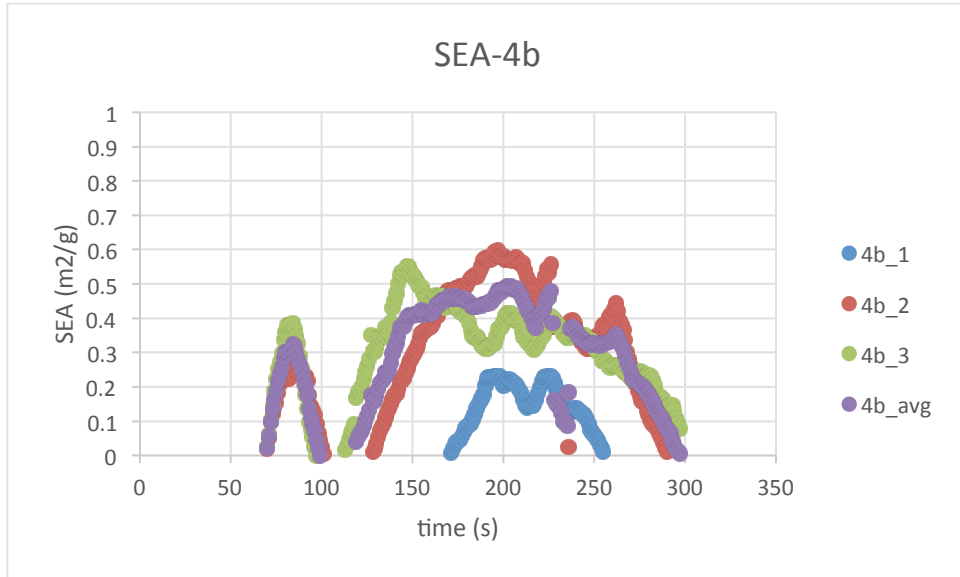


Figure 87-SEA of 4b

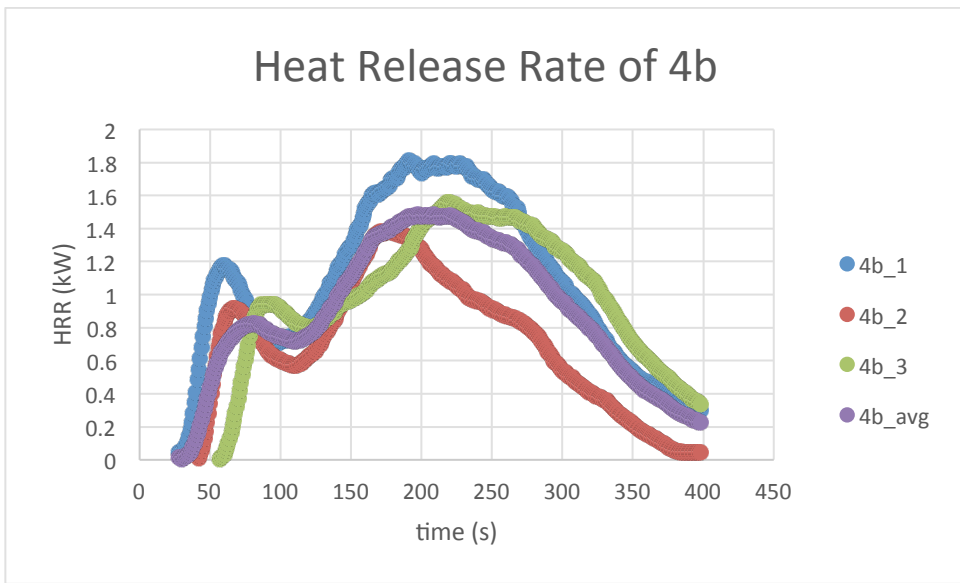


Figure 88-Heat Release Rate of 4b

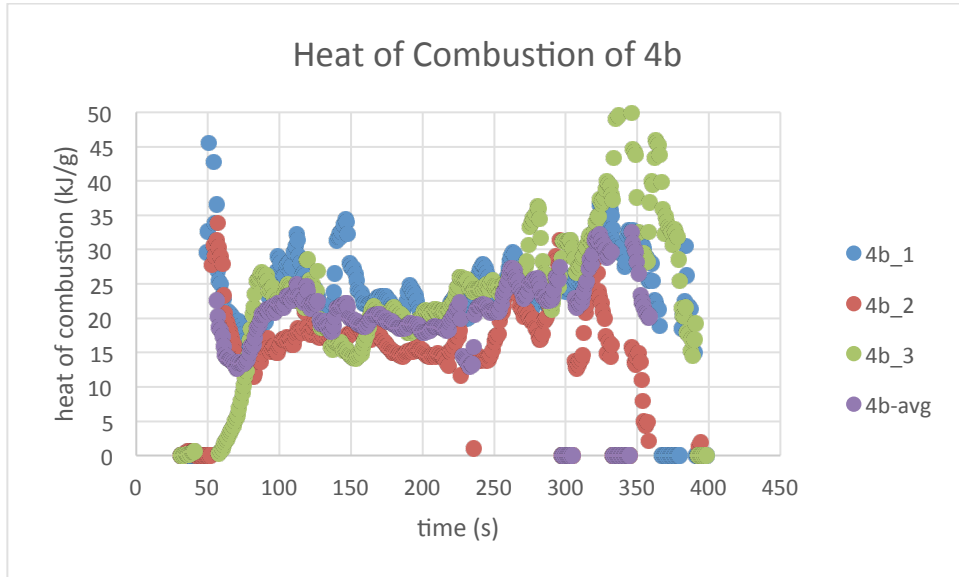


Figure 89-Heat of Combustion of 4b

4c

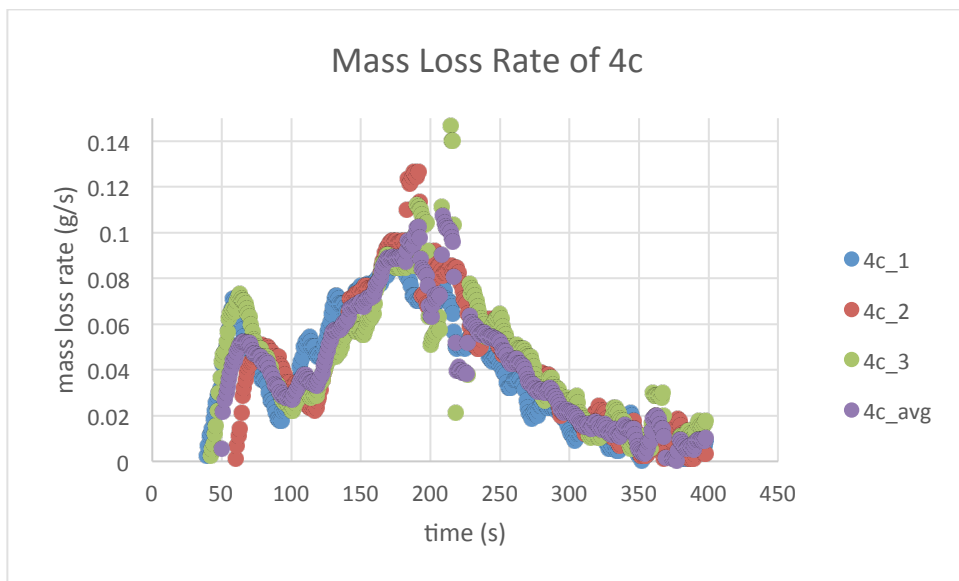


Figure 90-Mass Loss Rate of 4c

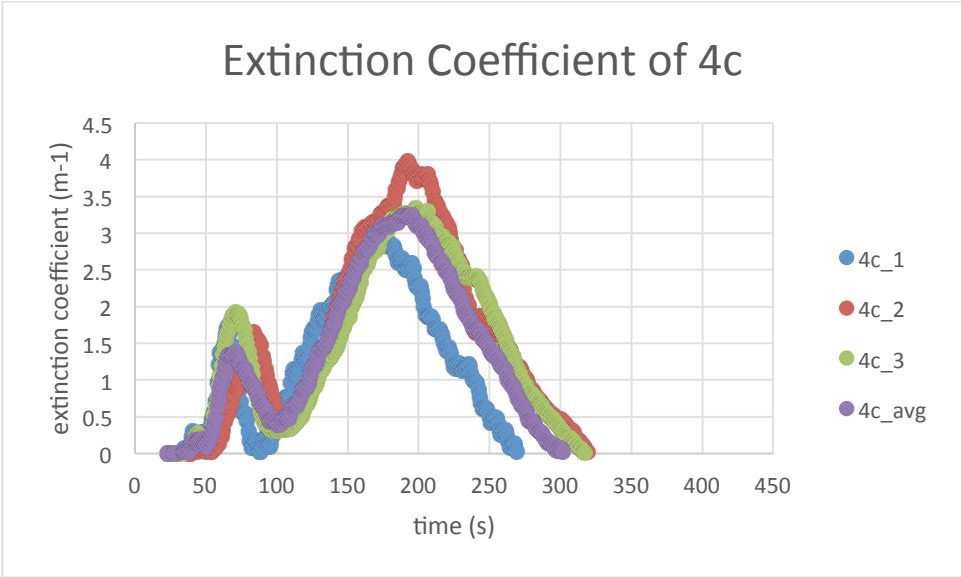


Figure 91-Extinction Coefficient of 4c

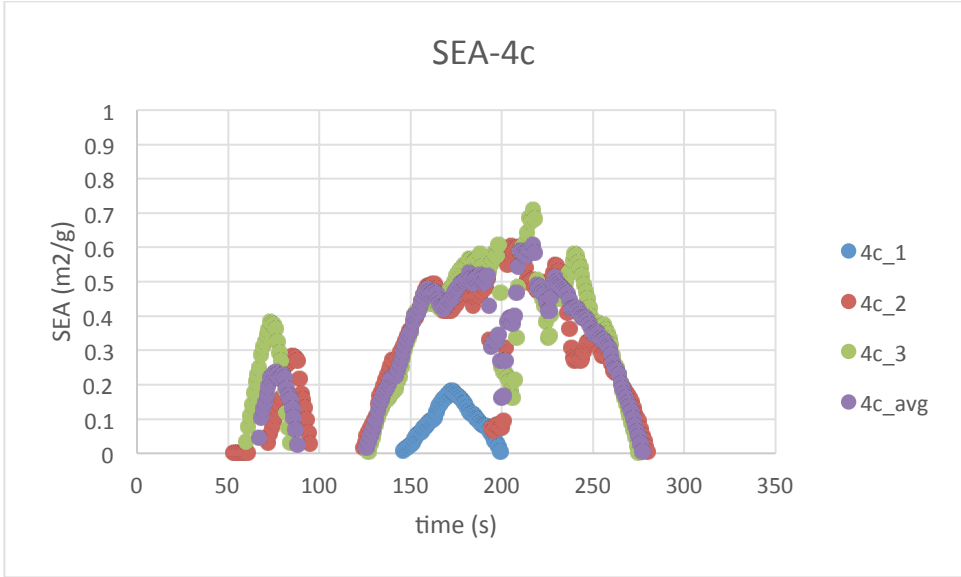


Figure 92-SEA of 4c

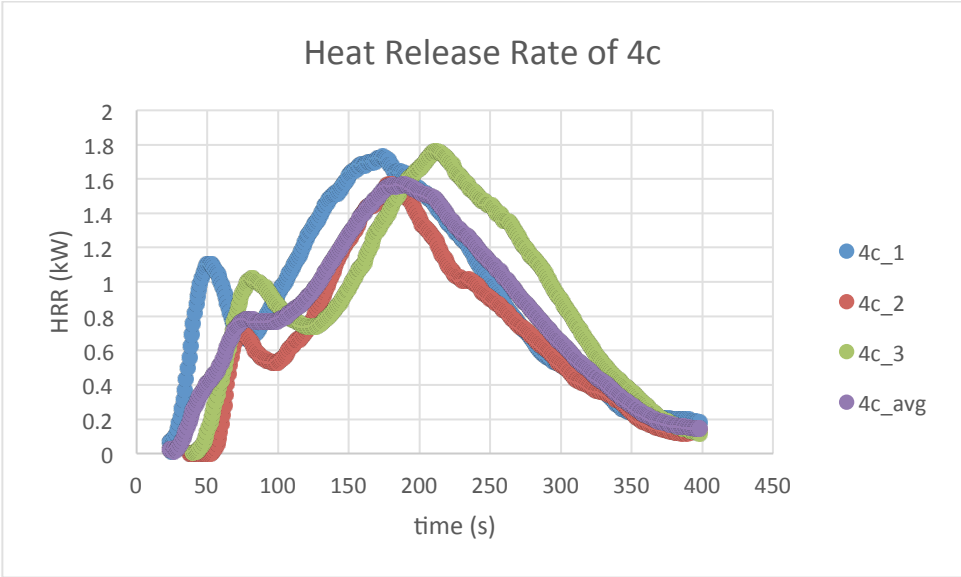


Figure 93-Heat Release Rate of 4c

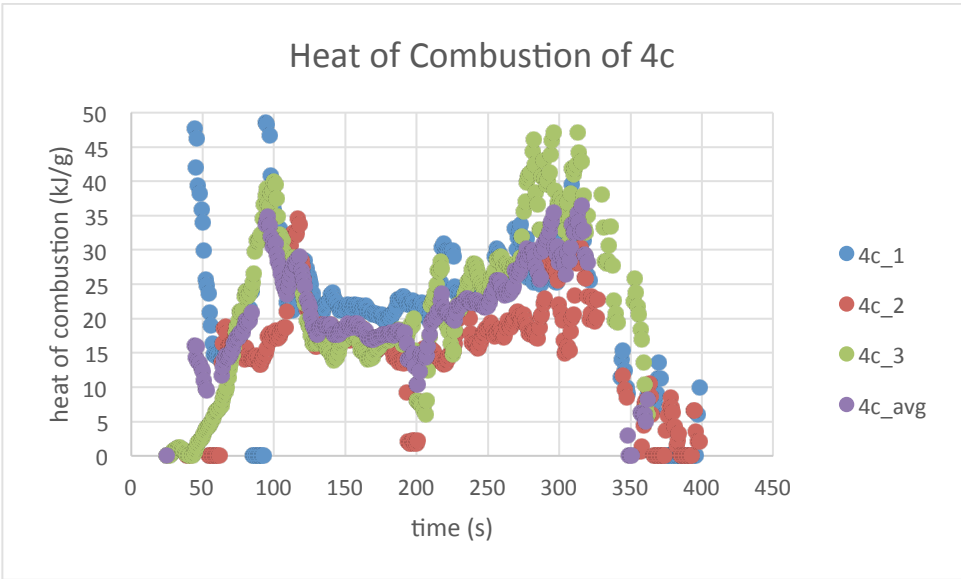


Figure 94-Heat of Combustion of 4c

4d

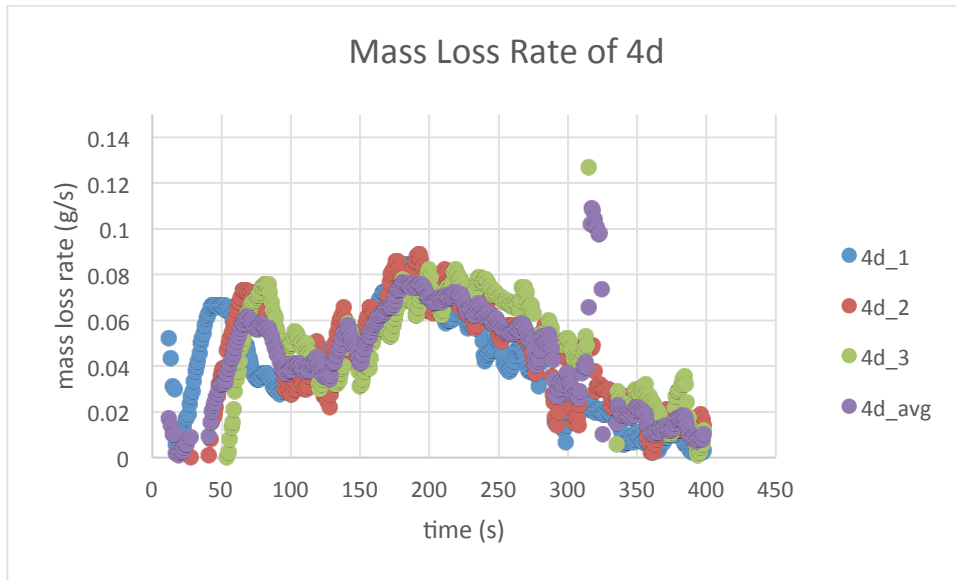


Figure 95-Mass Loss Rate of 4d

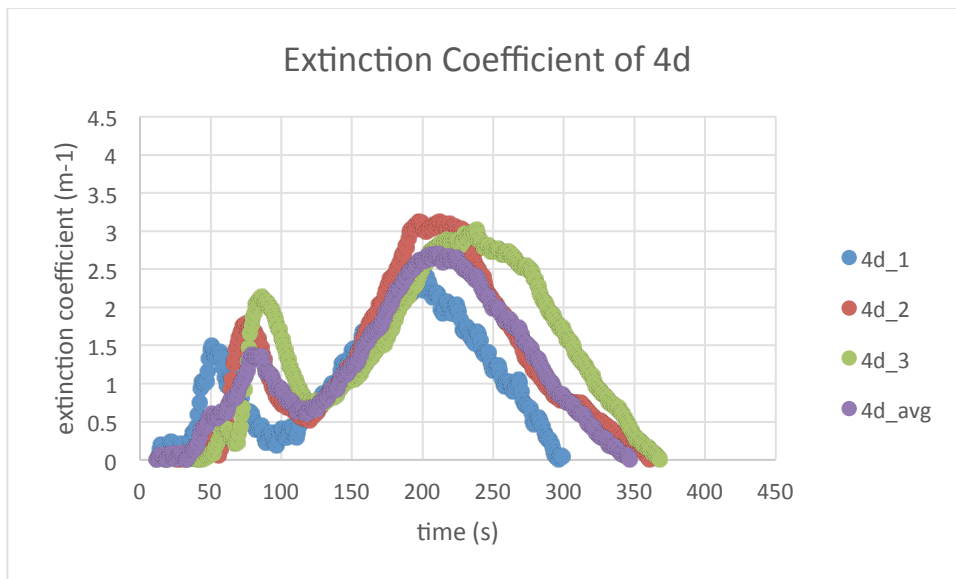


Figure 96-Extinction Coefficient of 4d

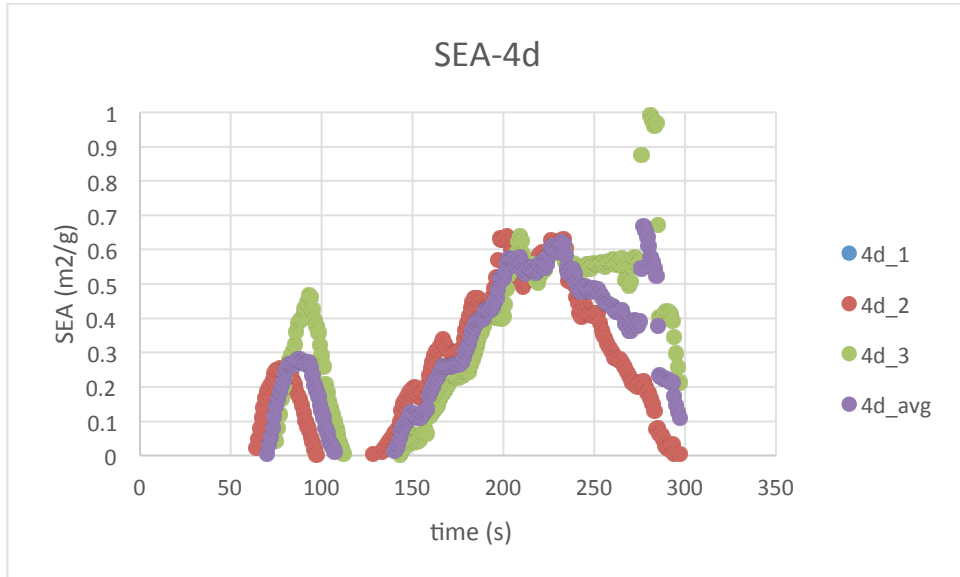


Figure 97-SEA of 4d

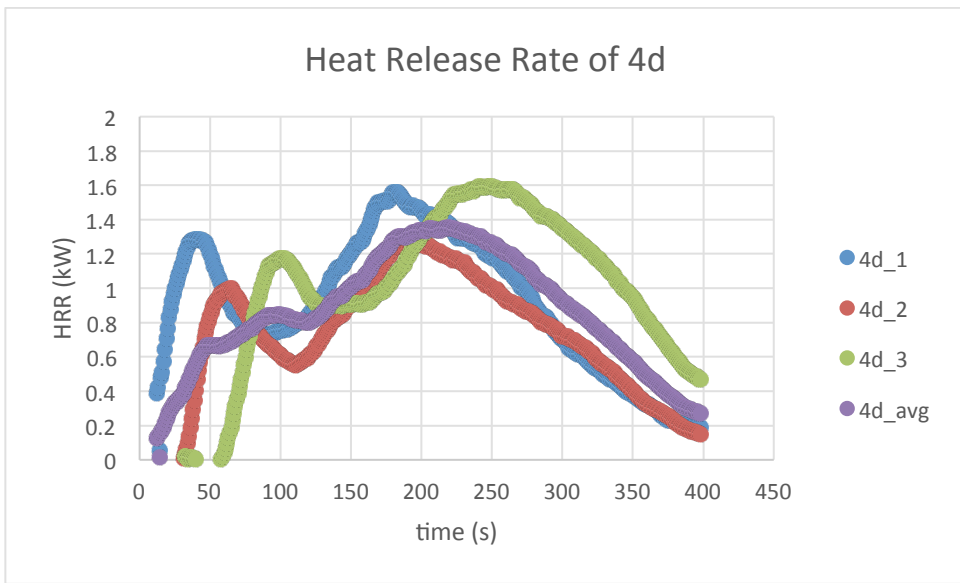


Figure 98-Heat Release Rate of 4d

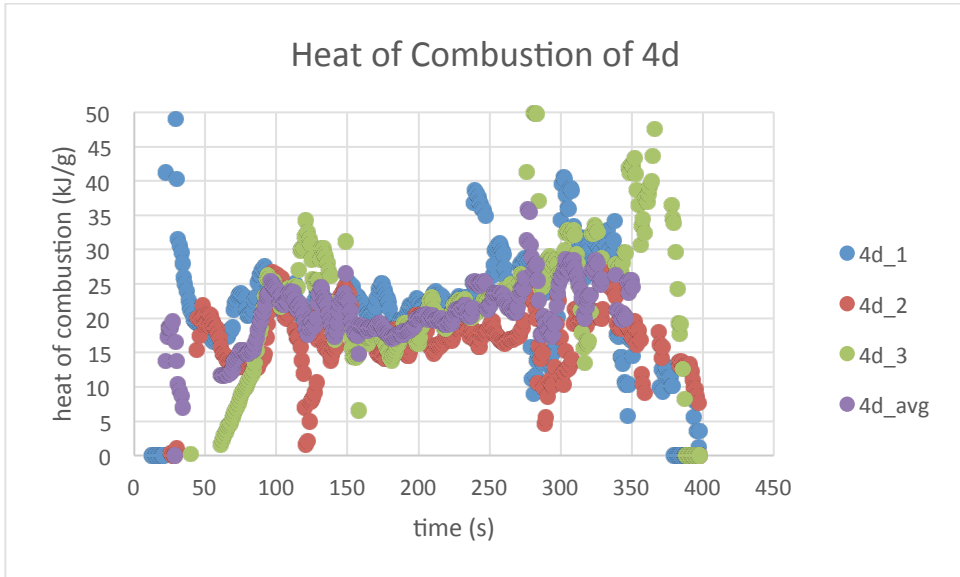


Figure 99-Heat of Combustion of 4d

Series 5

5a

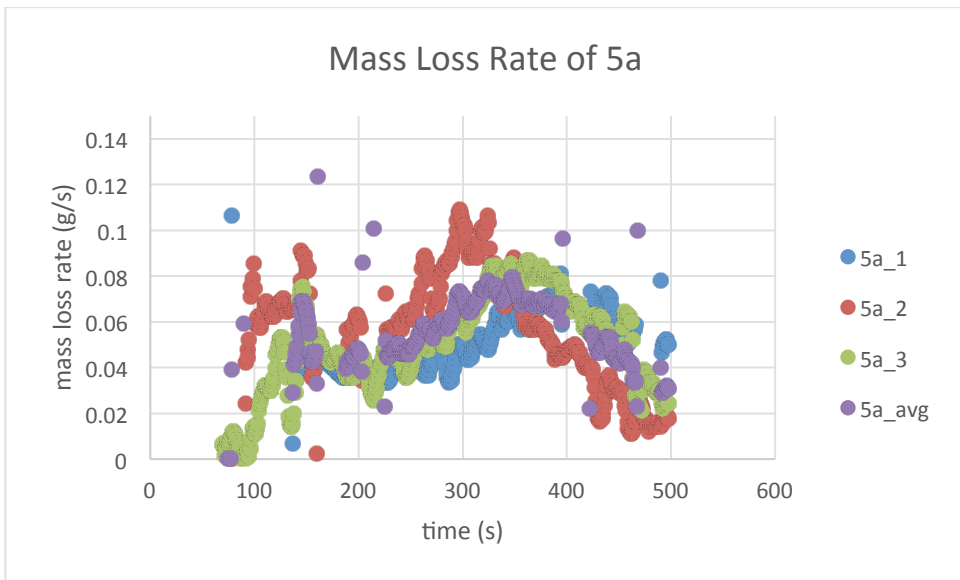


Figure 100-Mass Loss Rate of 5a

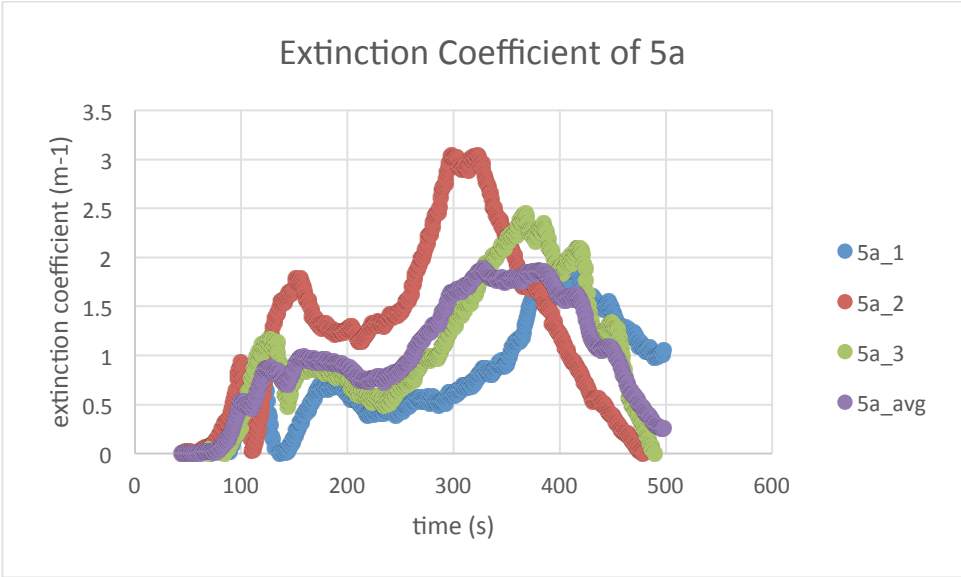


Figure 101-Extinction Coefficient of 5a

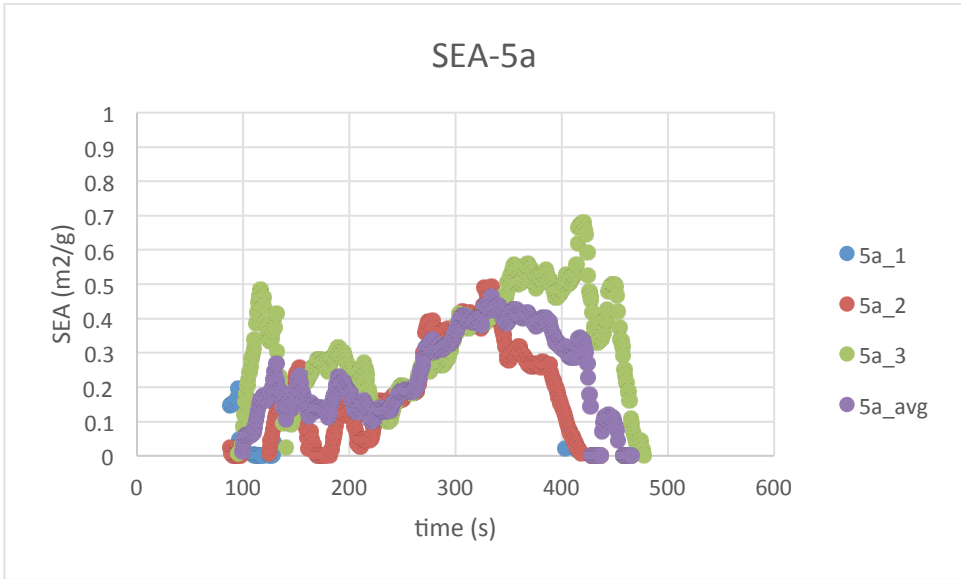


Figure 102-SEA of 5a

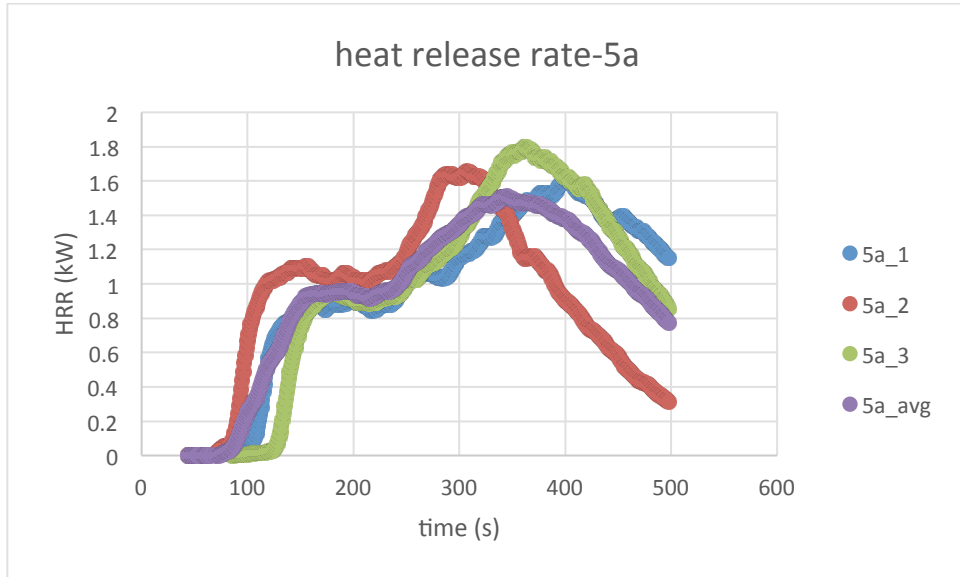


Figure 103-Heat Release Rate of 5a

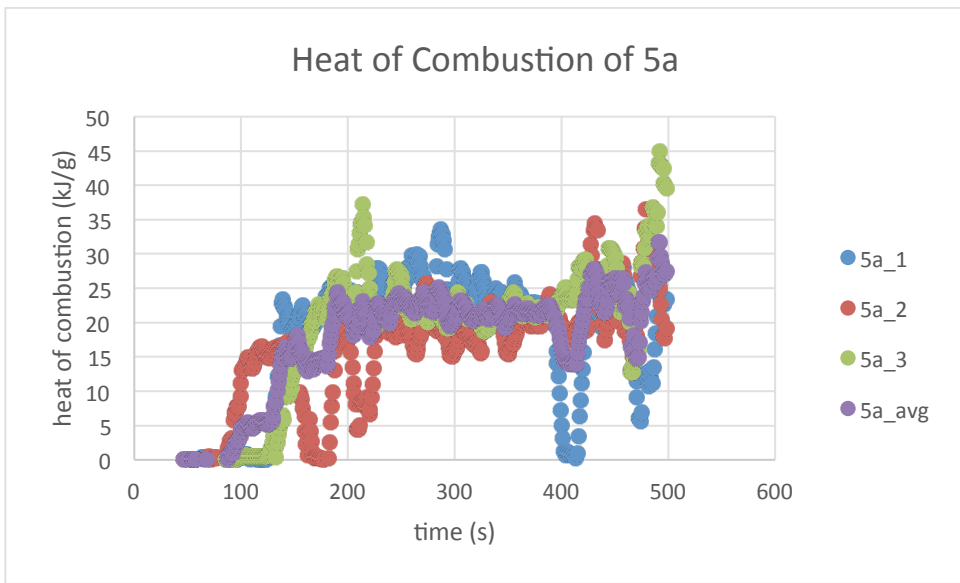


Figure 104-Heat of Combustion of 5a

5b

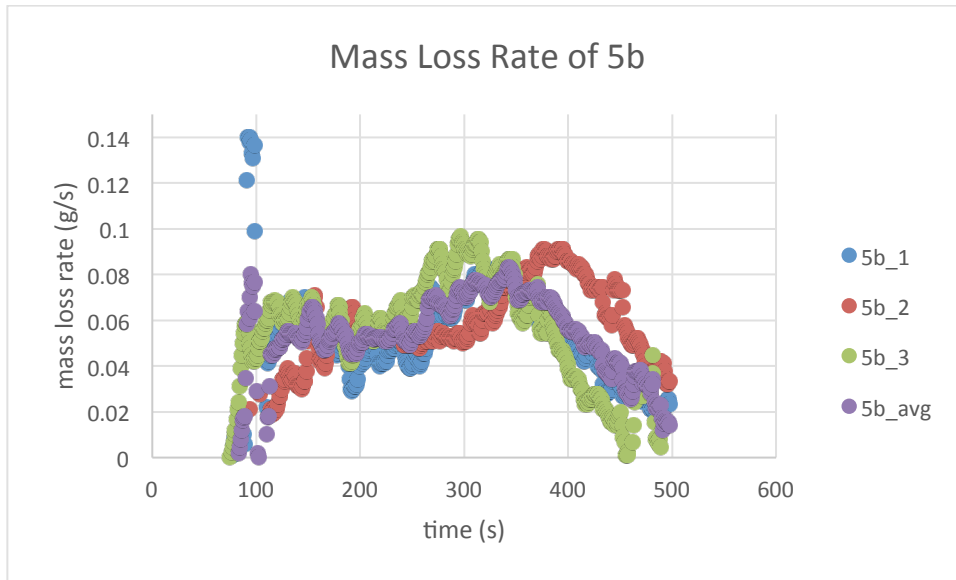


Figure 105-Mass Loss Rate of 5b

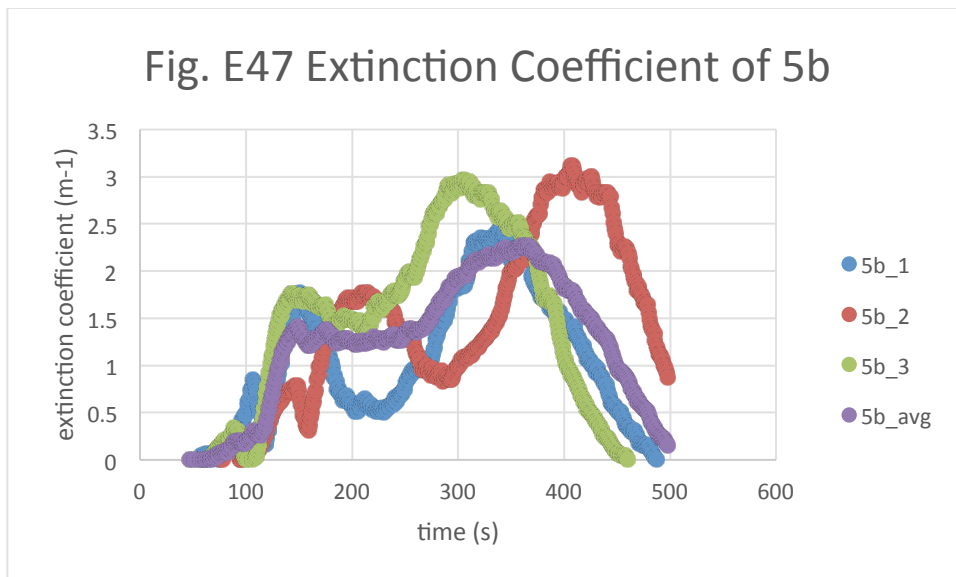


Figure 106-Fig. E47 Extinction Coefficient of 5b

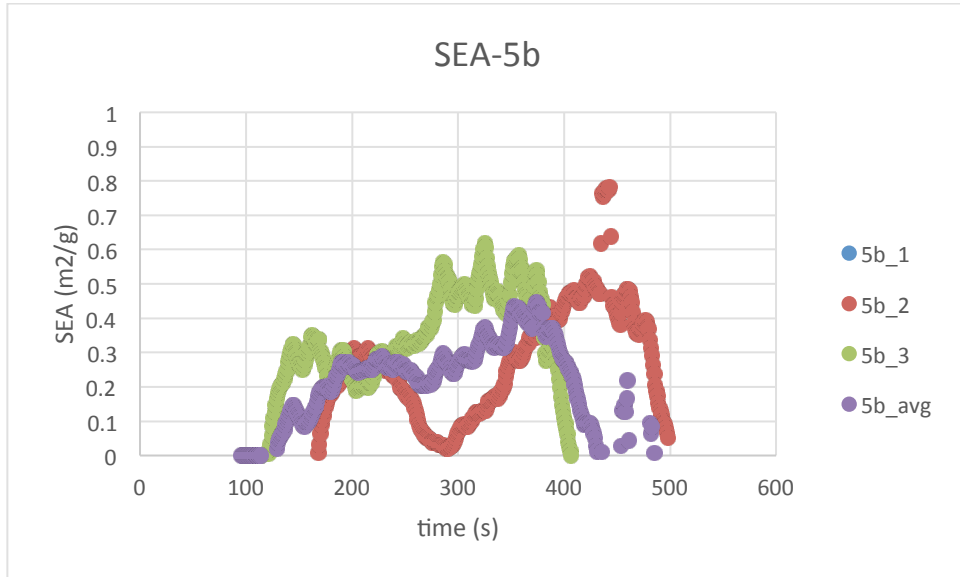


Figure 107-SEA of 5b

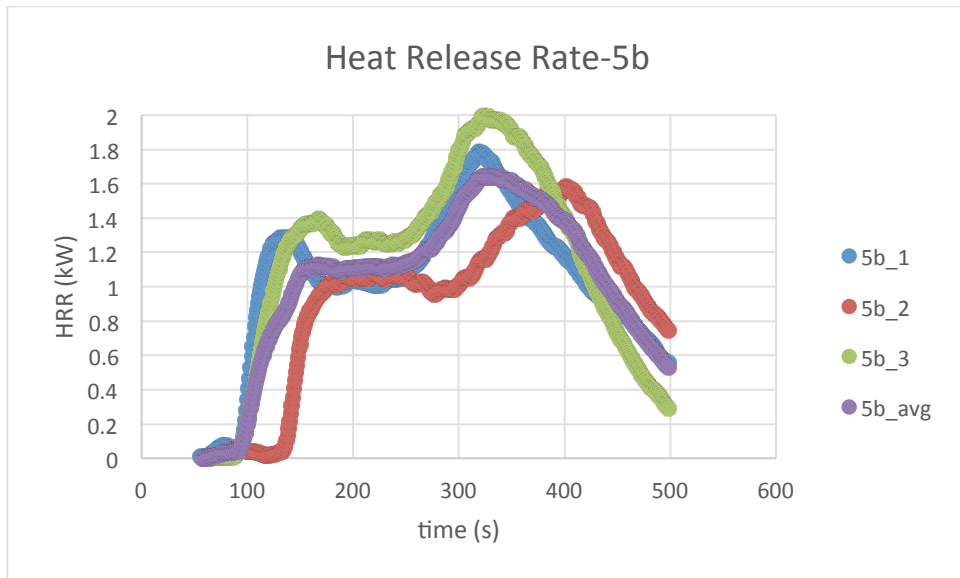


Figure 108-Heat Release Rate of 5b

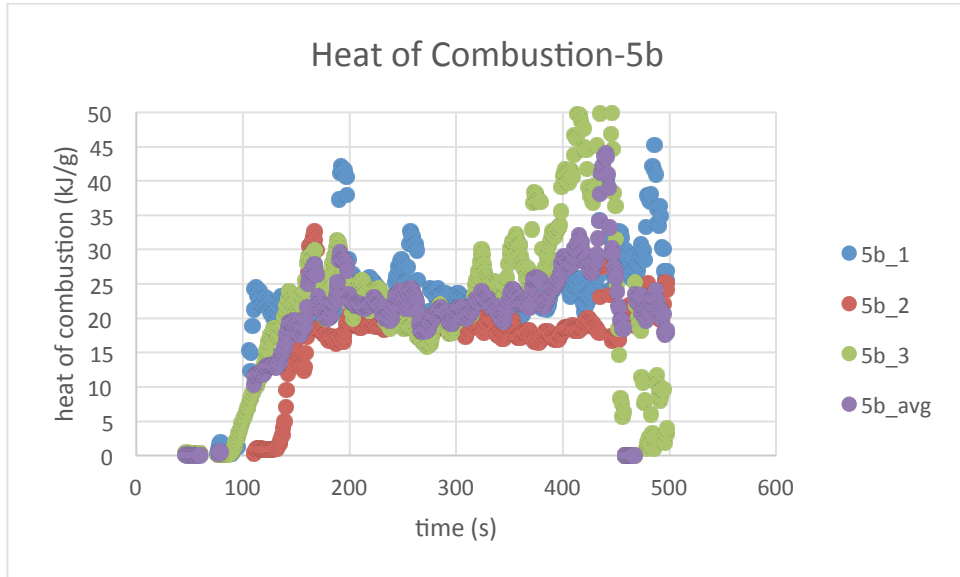


Figure 109-Heat of Combustion of 5b

5c

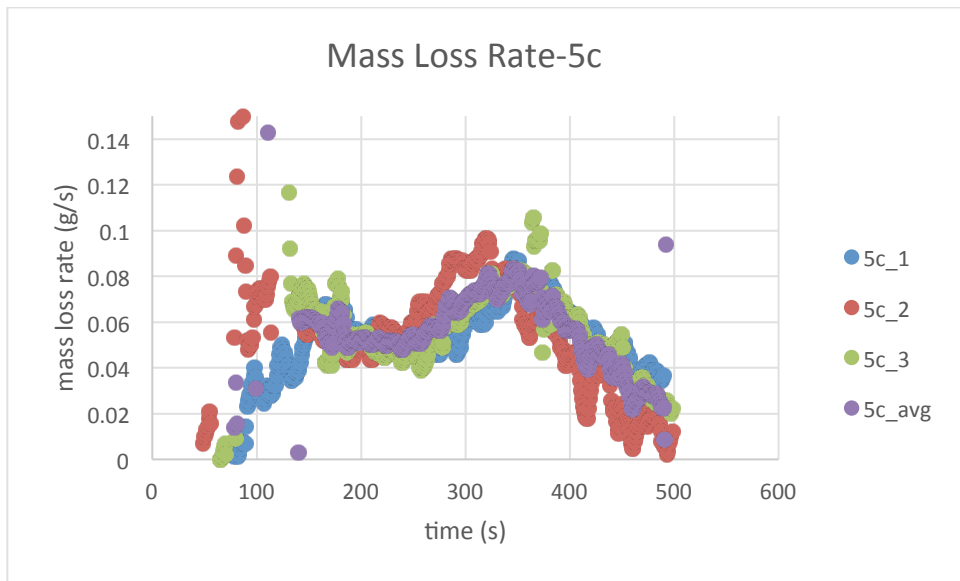


Figure 110-Mass Loss Rate of 5c

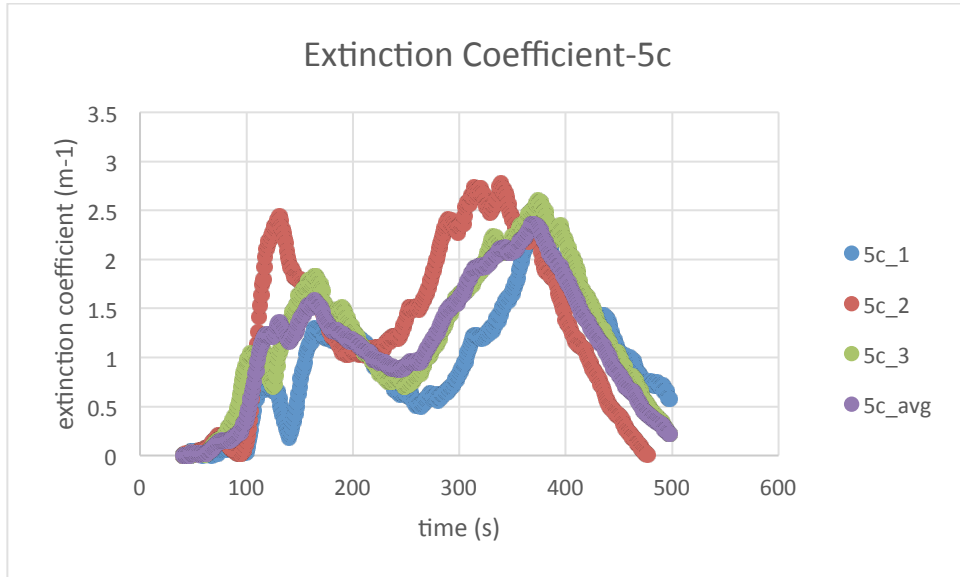


Figure 111-Extinction Coefficient of 5c

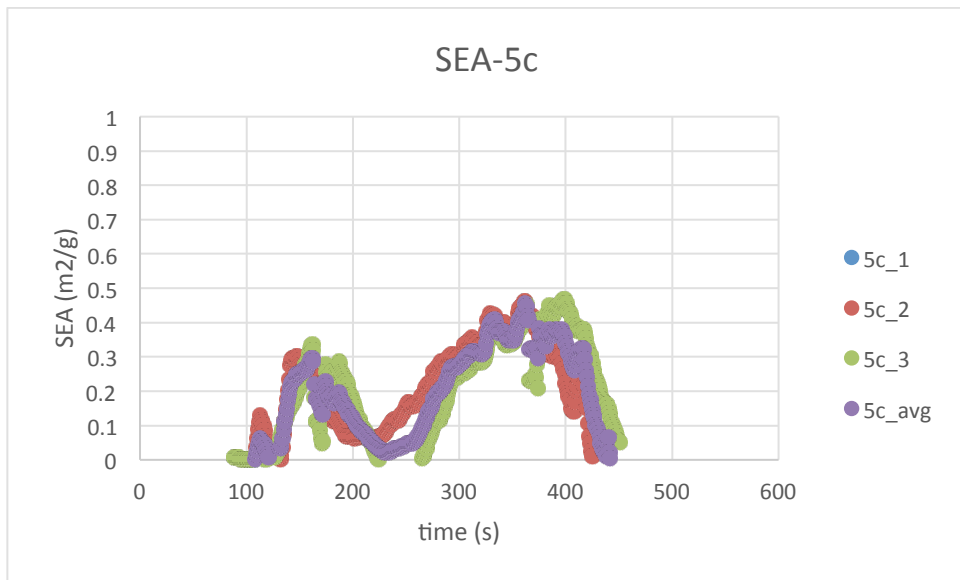


Figure 112-SEA of 5c

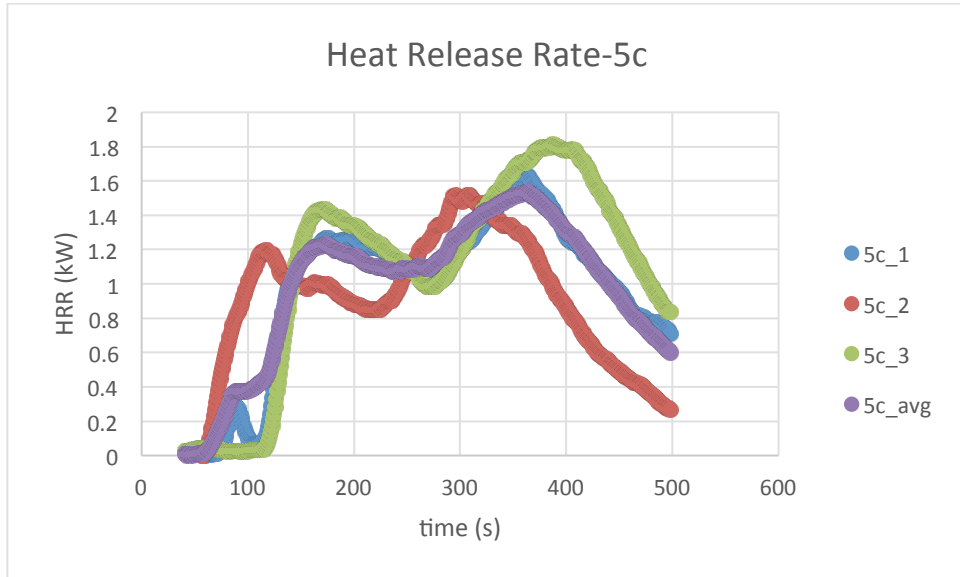


Figure 113-Heat Release Rate of 5c

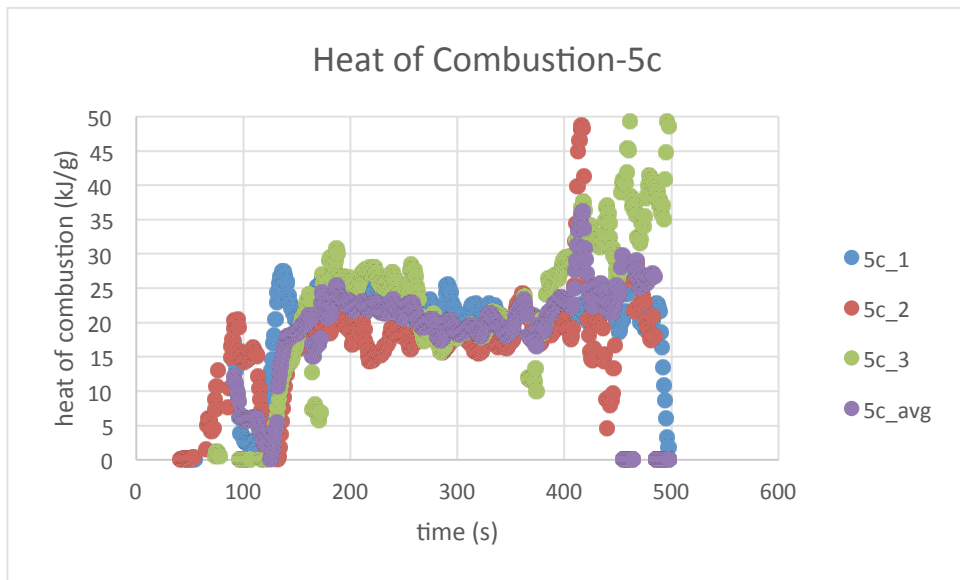


Figure 114-Heat of Combustion of 5c

5d

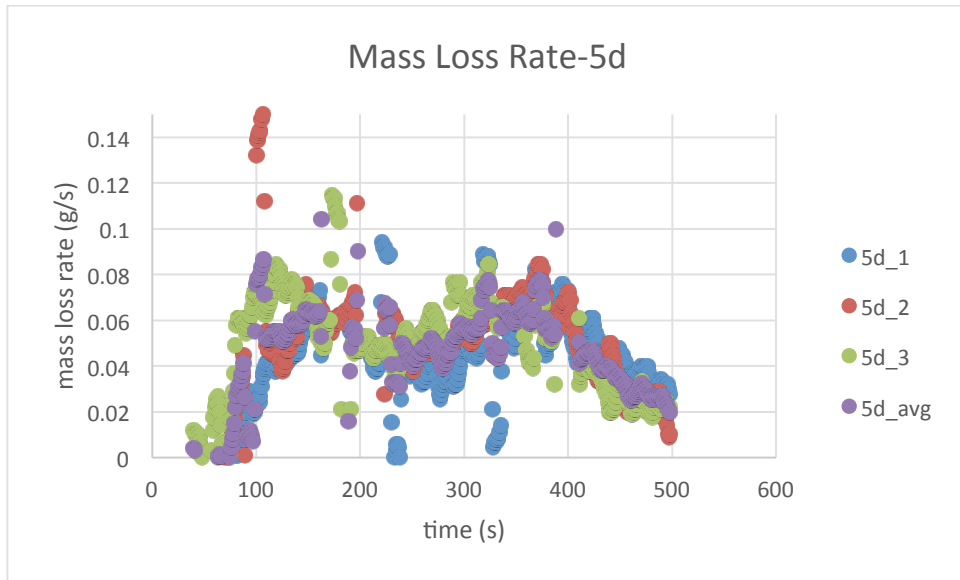


Figure 115-Mass Loss Rate of 5d

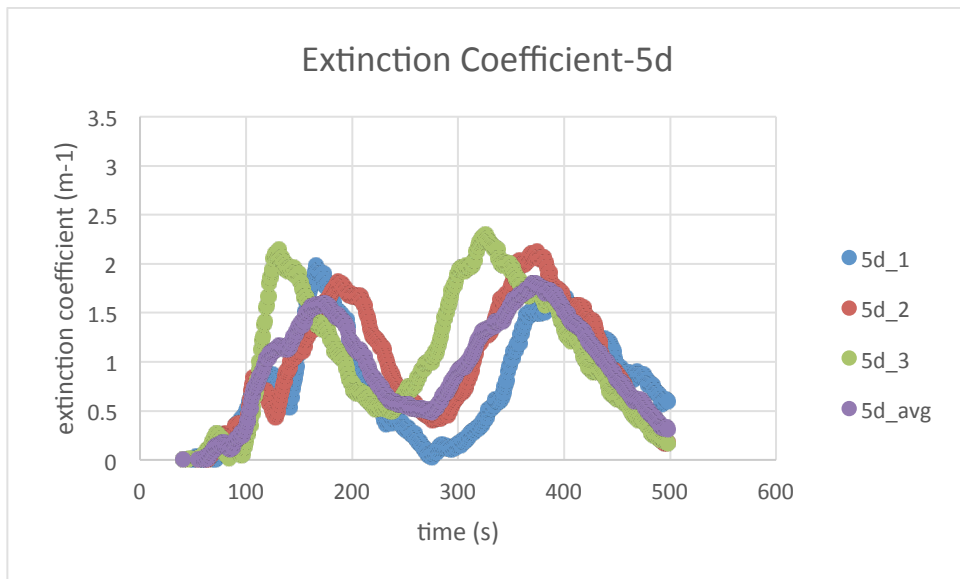


Figure 116-Extinction Coefficient of 5d

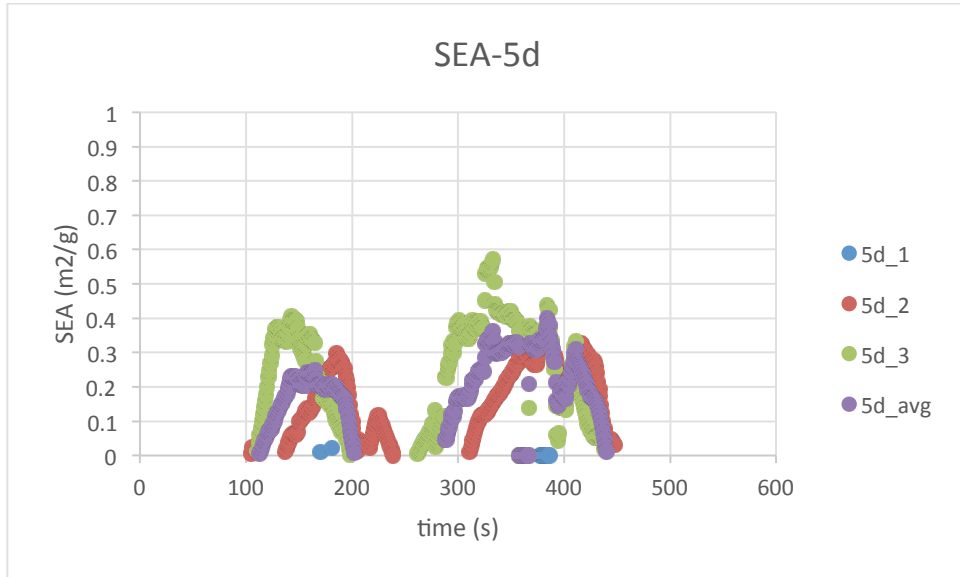


Figure 117-SEA of 5d

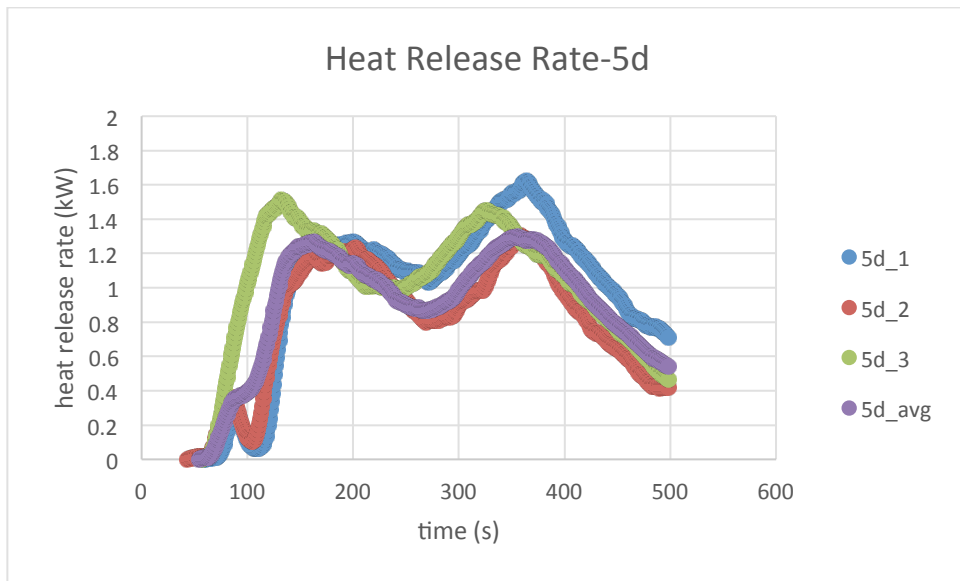


Figure 118-Heat Release Rate of 5d

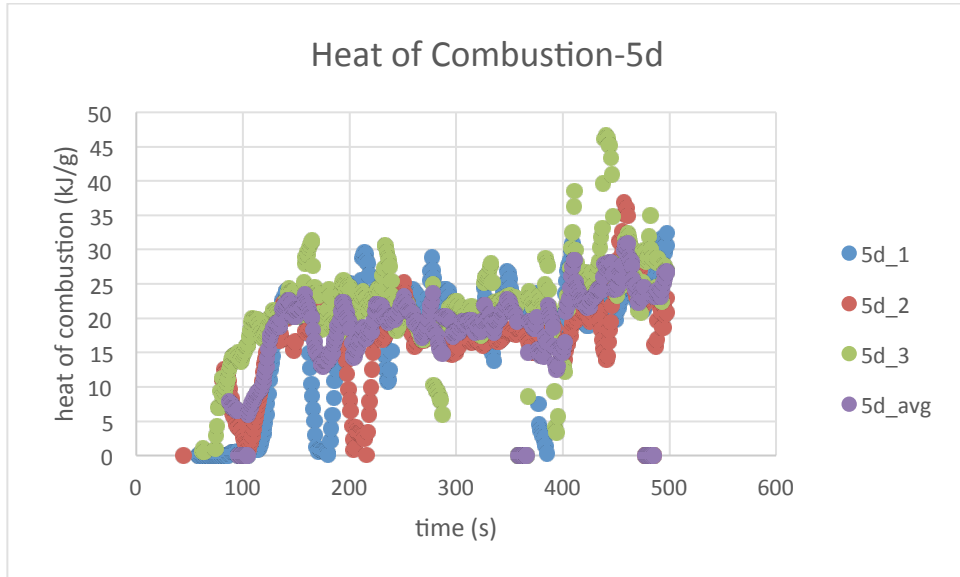


Figure 119-Heat of Combustion of 5d

Comparison

In-Series Comparison

Series 3

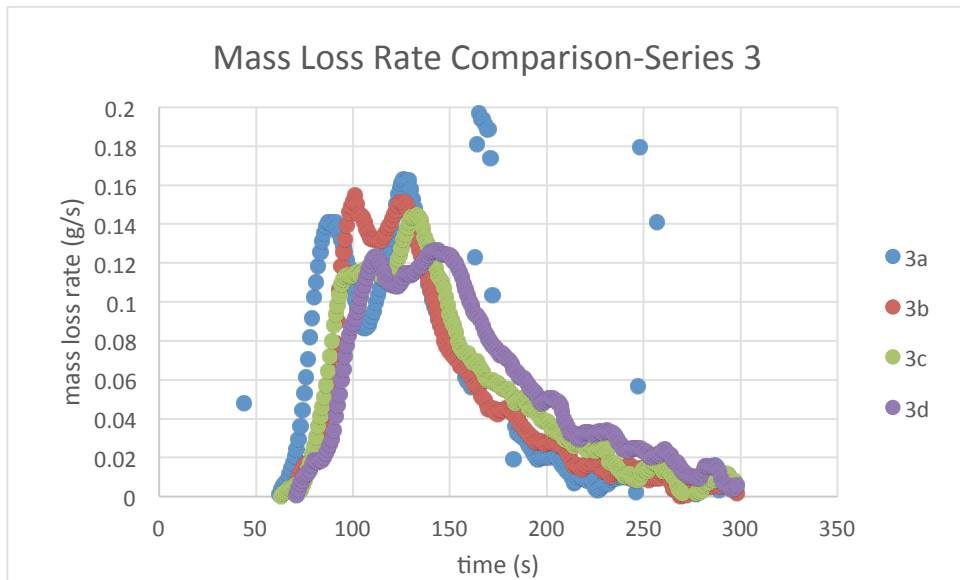


Figure 120-Mass Loss Rate Comparison of Series 3

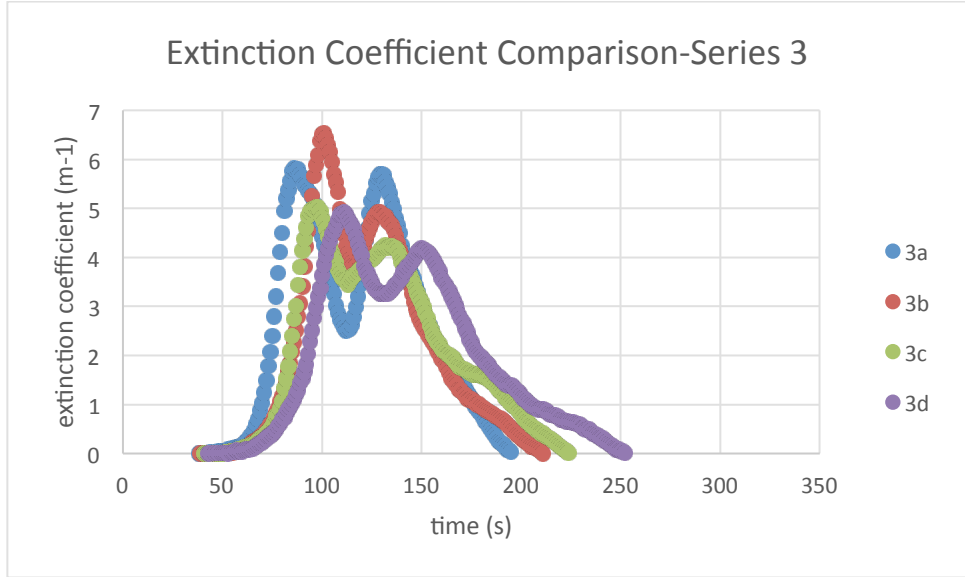


Figure 121-Extinction Coefficient Comparison of Series 3

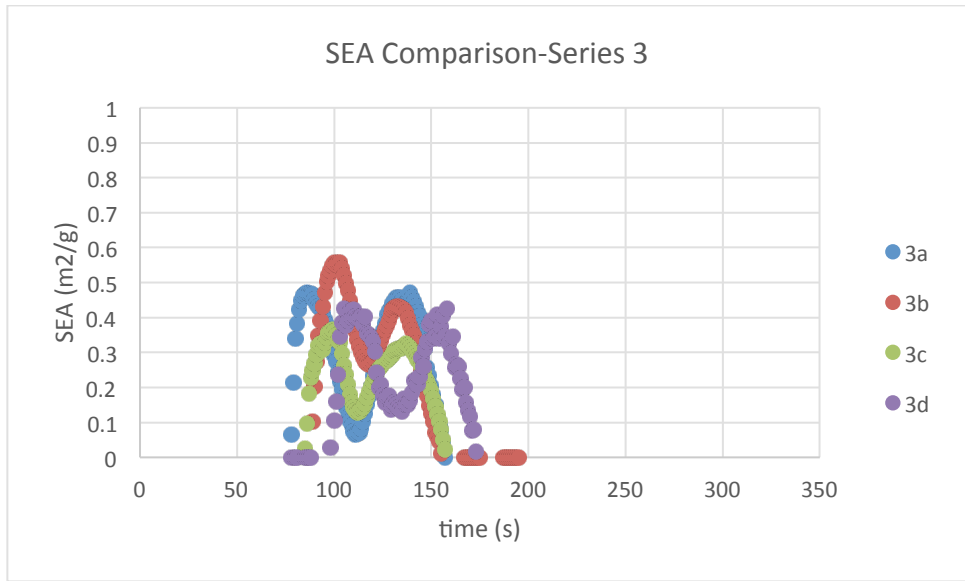


Figure 122-SEA Comparison of Series 3

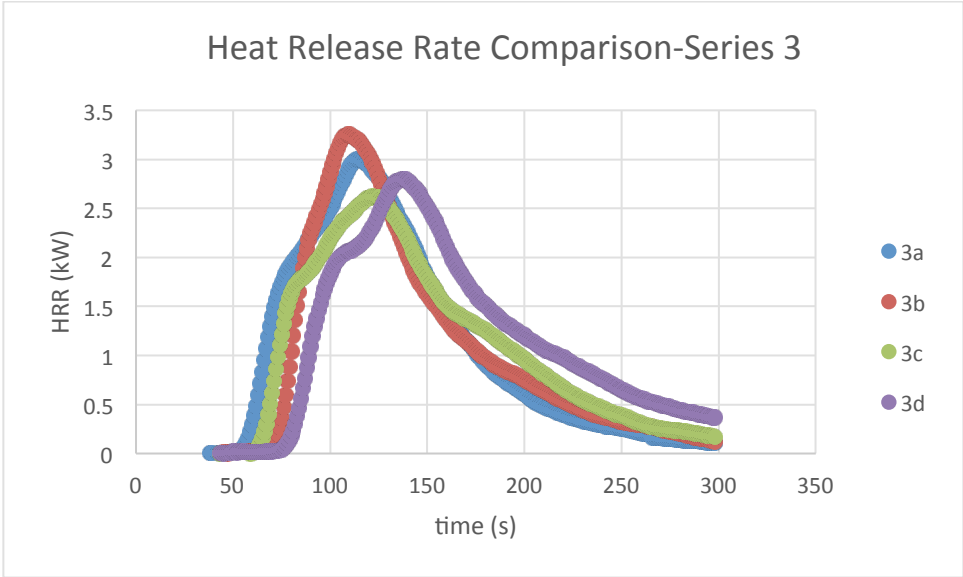


Figure 123-Heat Release Rate Comparison of Series 3

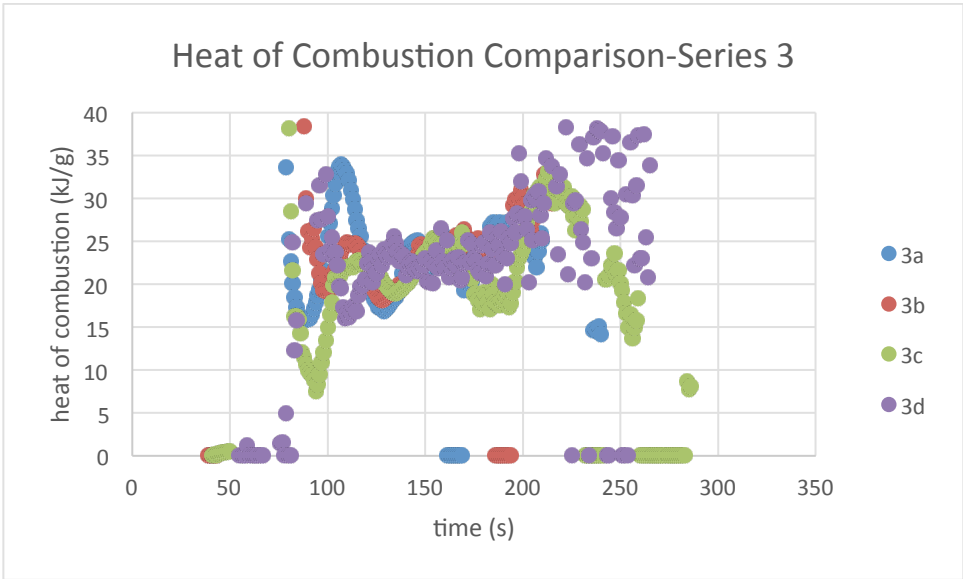


Figure 124-Heat of Combustion Comparison of Series 3

Series 4

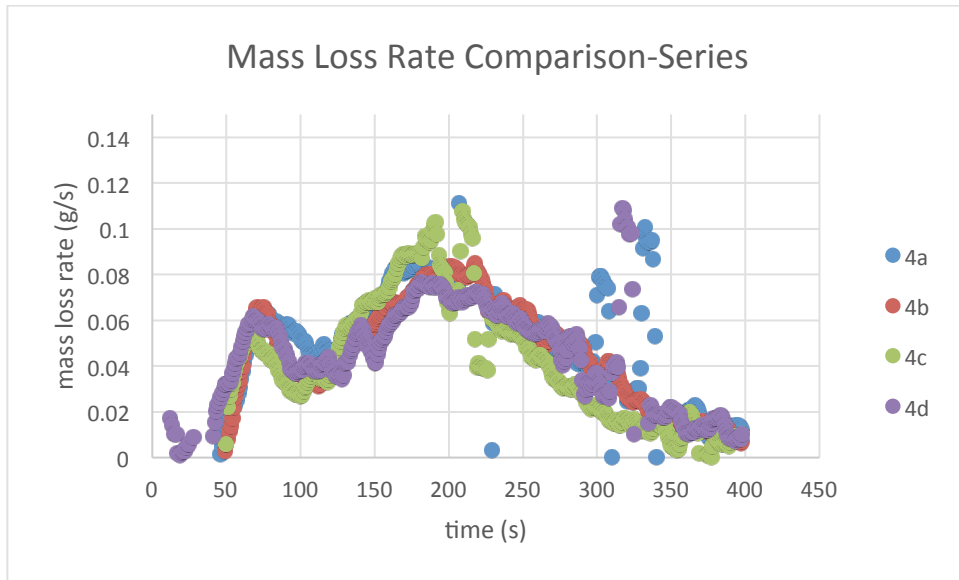


Figure 125-Mass Loss Rate Comparison of Series 4

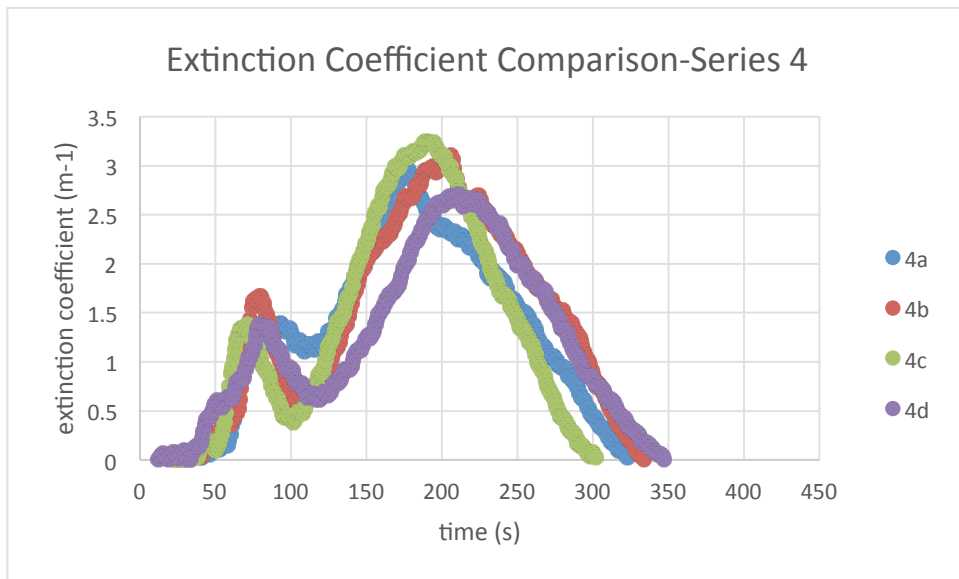


Figure 126-Extinction Coefficient Comparison of Series 4

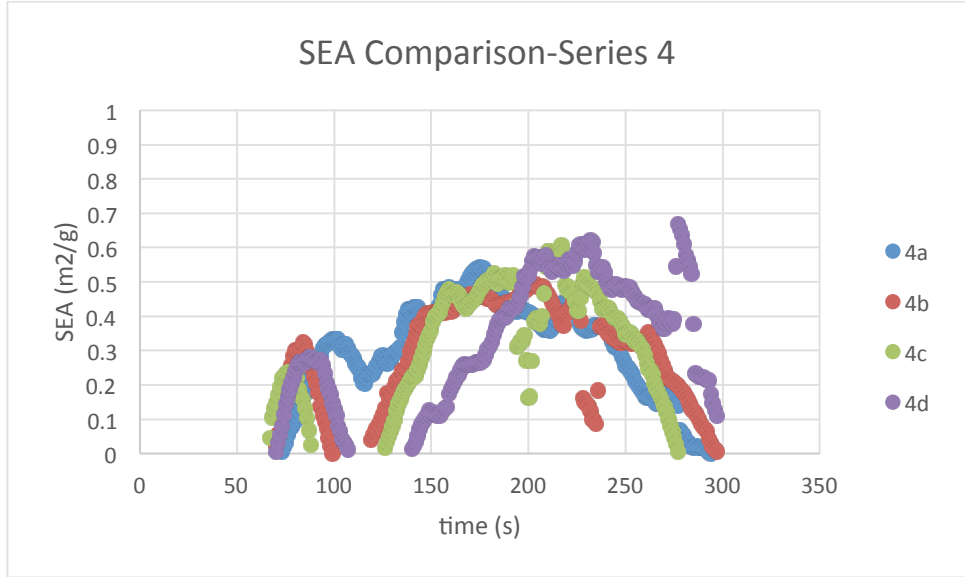


Figure 127-SEA Comparison of Series 4

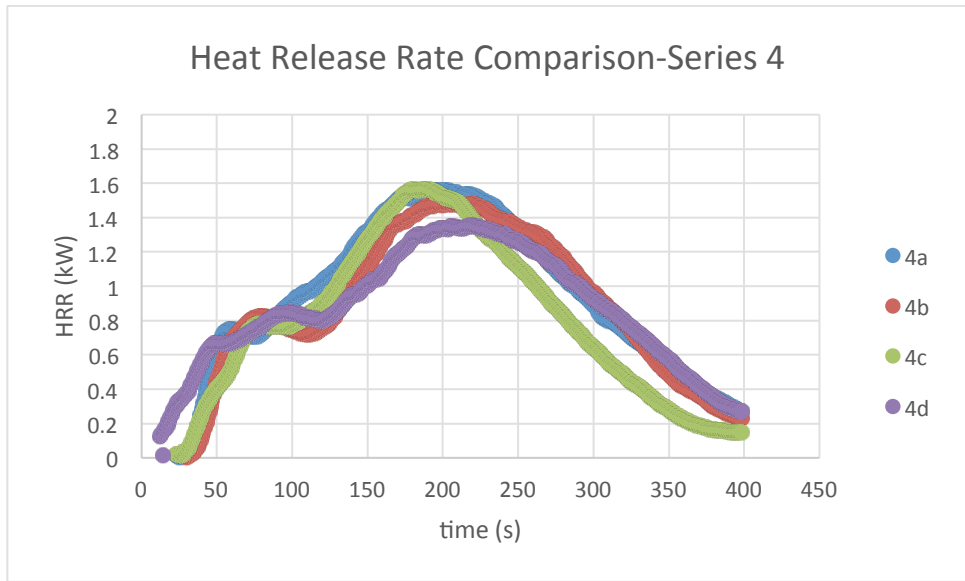


Figure 128-Heat Release Rate Comparison of Series 4

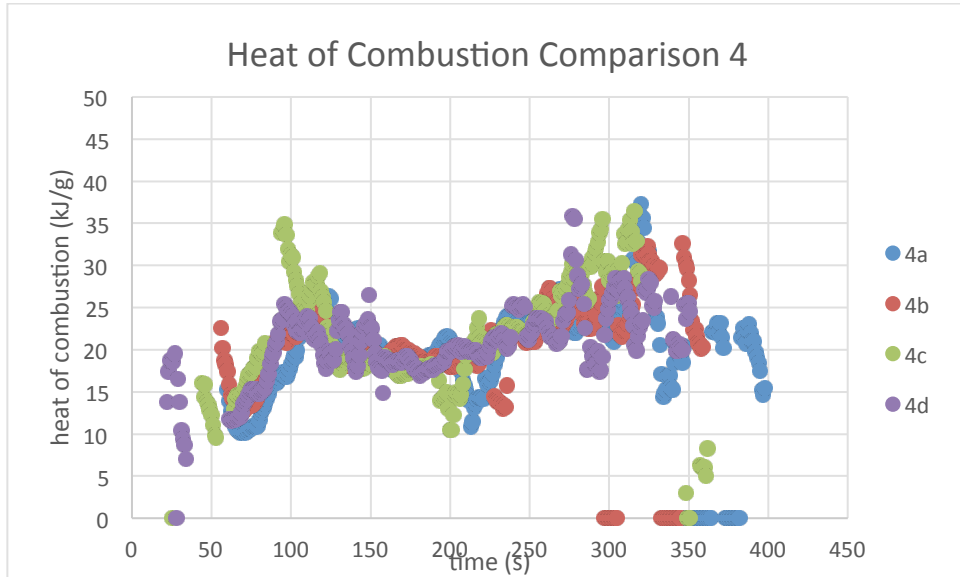


Figure 129-Heat of Combustion Comparison of Series 4

Series 5

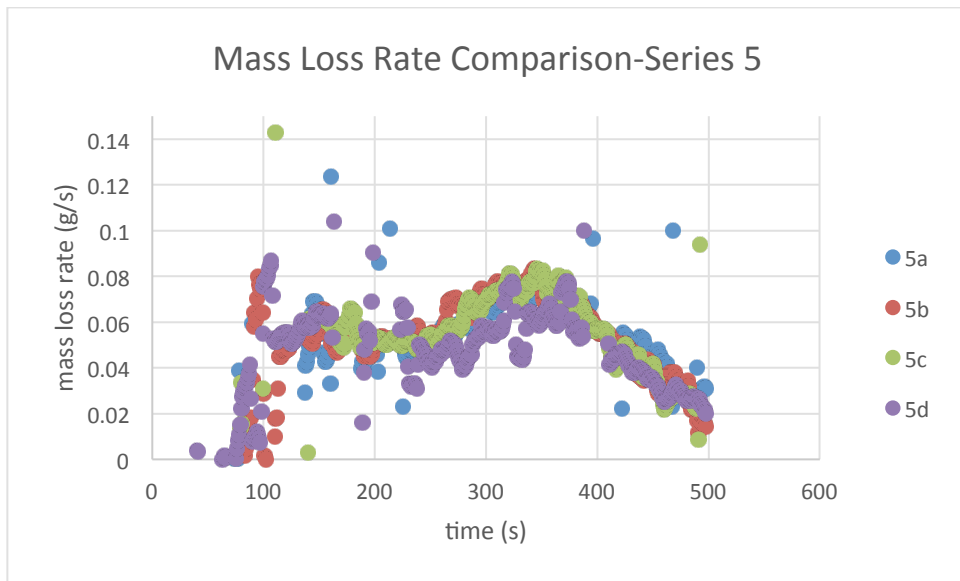


Figure 130-Mass Loss Rate Comparison of Series 5

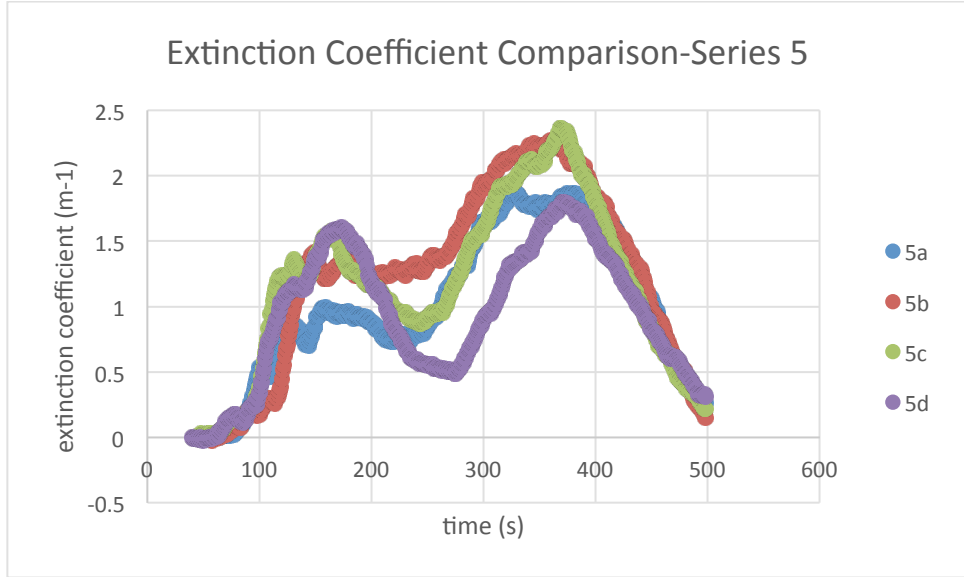


Figure 131-Extinction Coefficient Comparison of Series 5

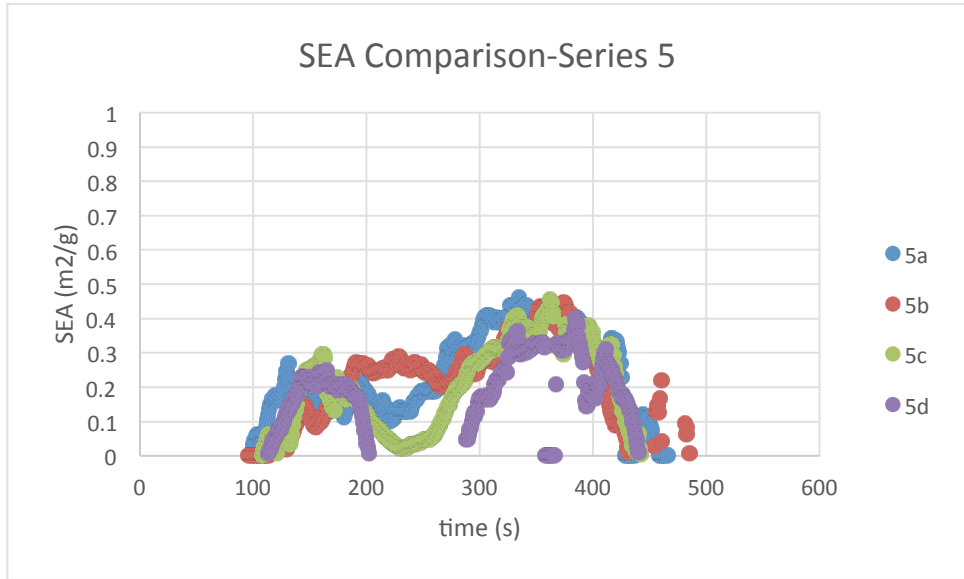


Figure 132-SEA Comparison of Series 5

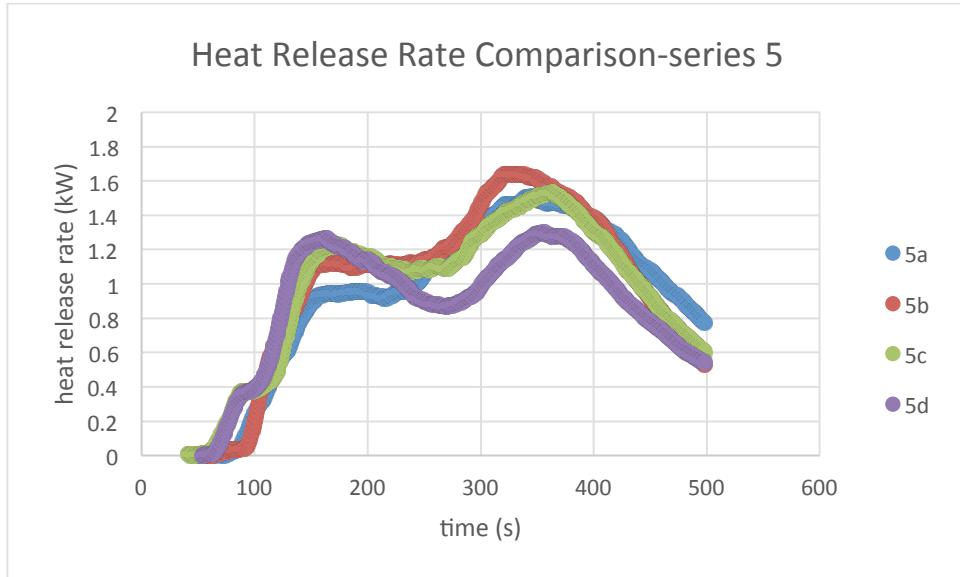


Figure 133-Heat Release Rate Comparison of Series 5

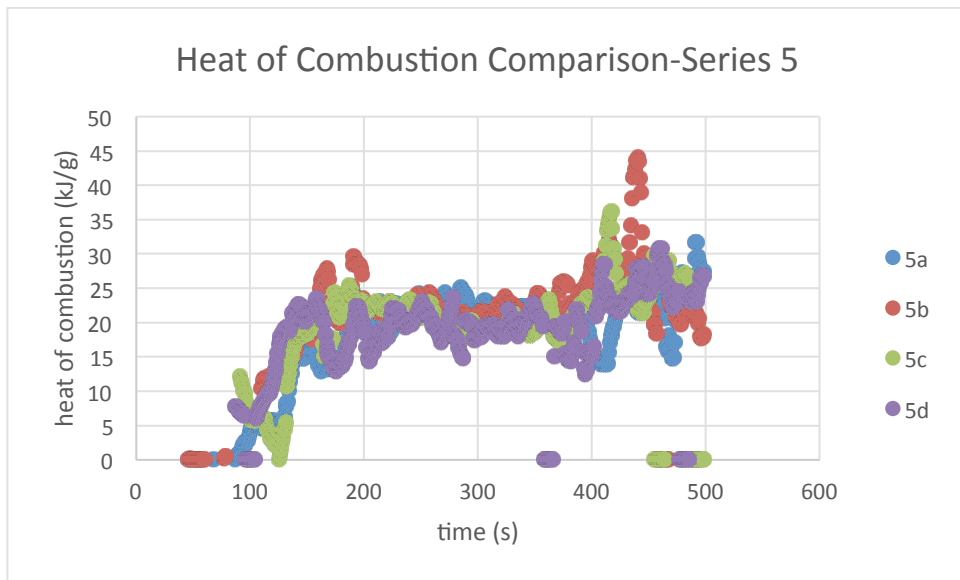


Figure 134-Heat of Combustion Comparison of Series 5

Cross-Series Comparison

Neat

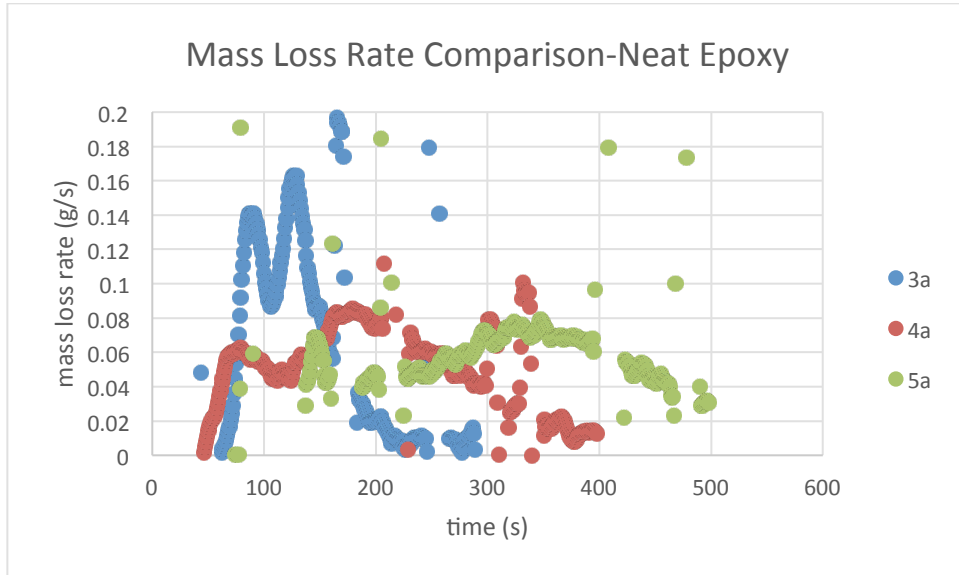


Figure 135-Mass Loss Rate Comparison of Neat Epoxy

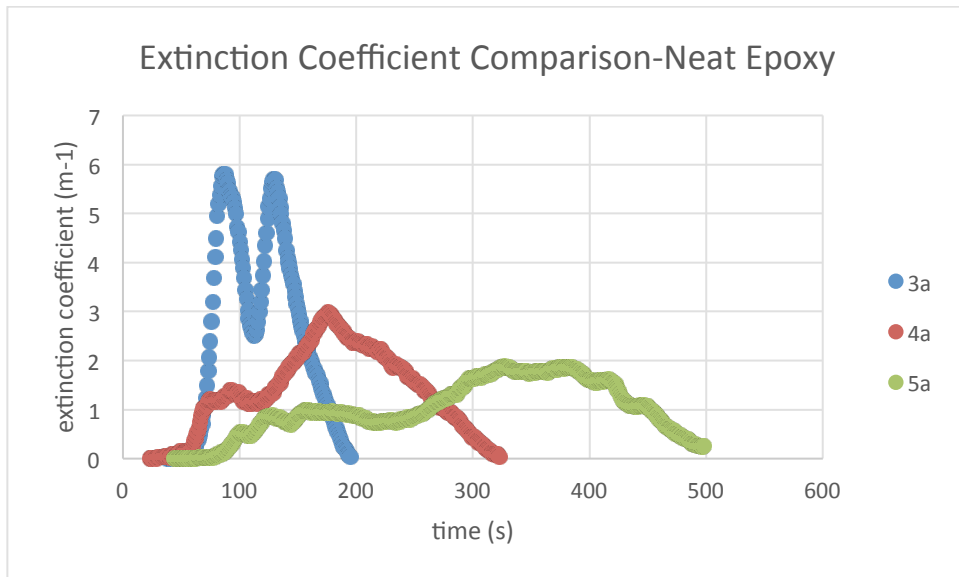


Figure 136-Extinction Coefficient Comparison of Neat Epoxy

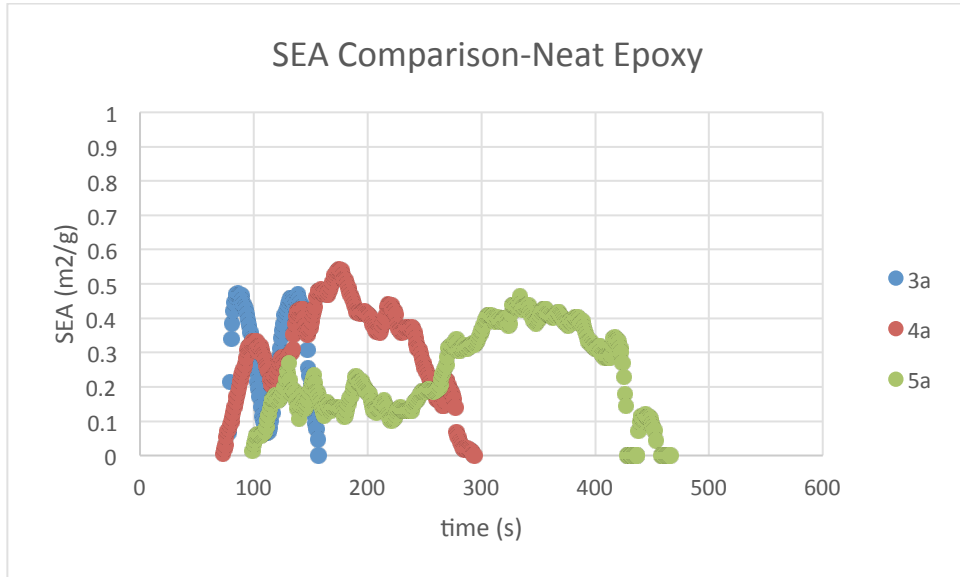


Figure 137-SEA Comparison of Neat Epoxy

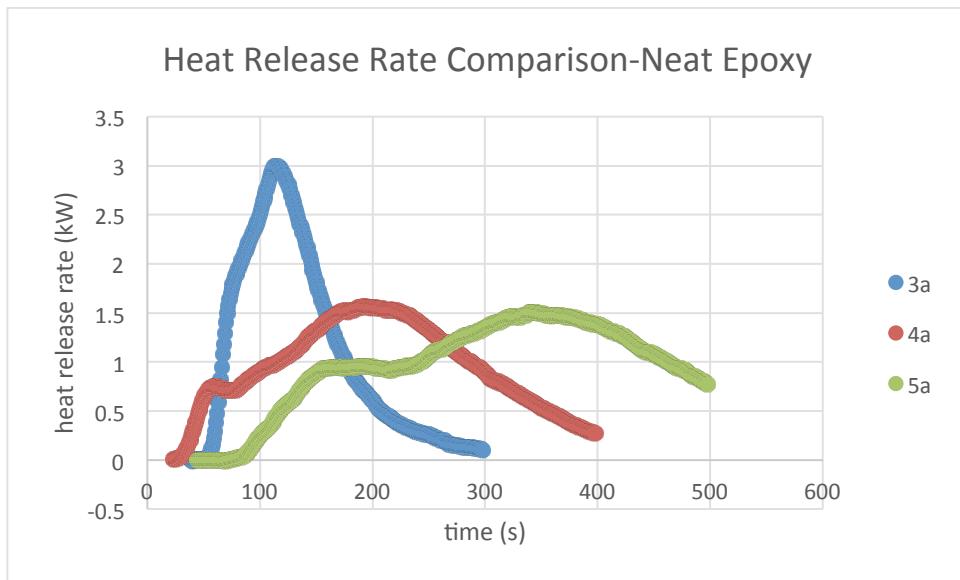


Figure 138-Heat Release Rate Comparison of Neat Epoxy

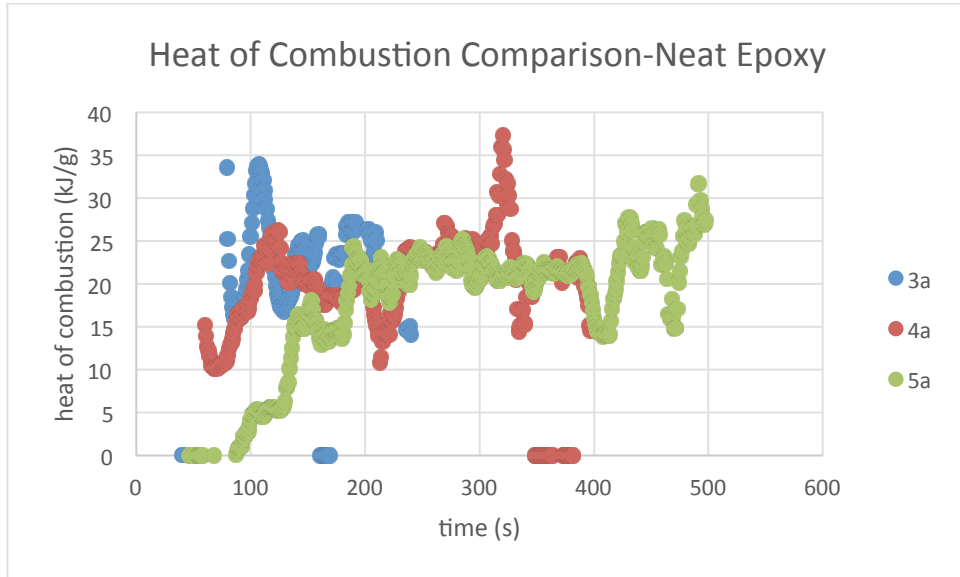


Figure 139-Heat of Combustion Comparison of Neat Epoxy

5% ATH

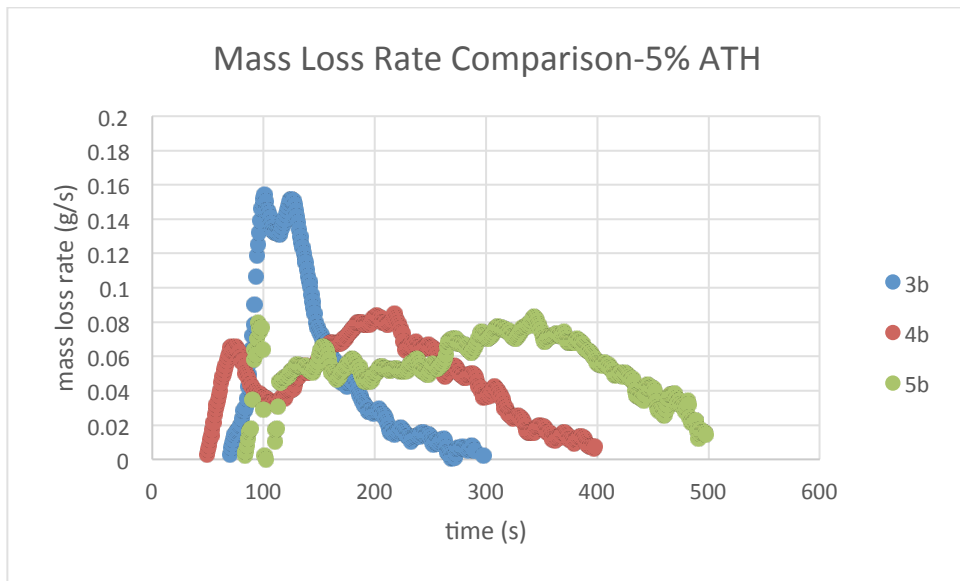


Figure 140-Mass Loss Rate Comparison 5% ATH

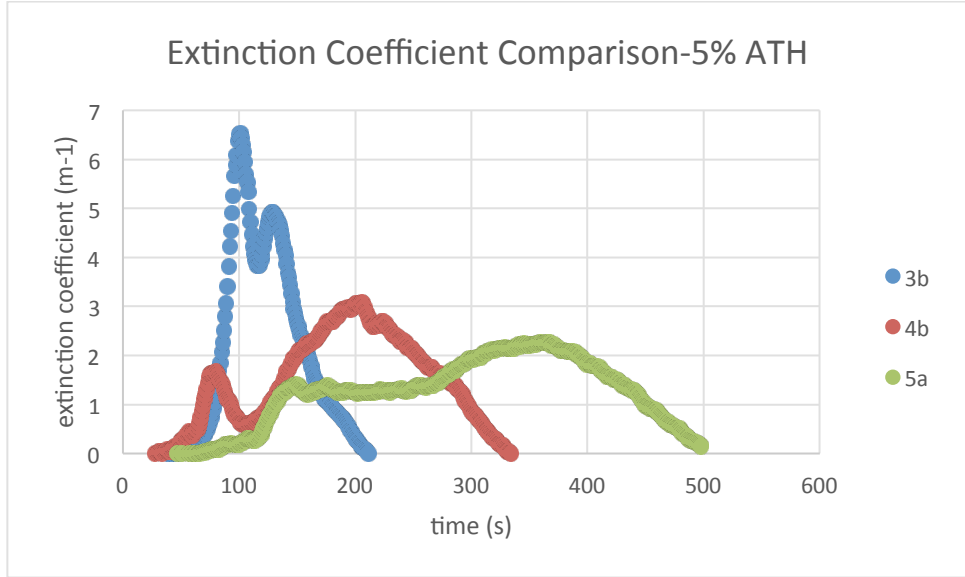


Figure 141-Extinction Coefficient Comparison 5% ATH

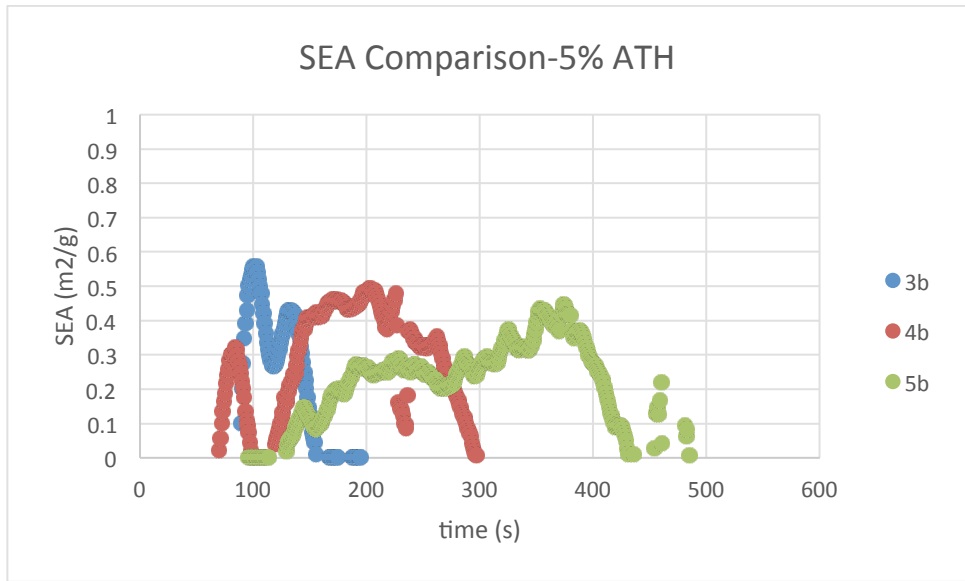


Figure 142-SEA Comparison 5% ATH

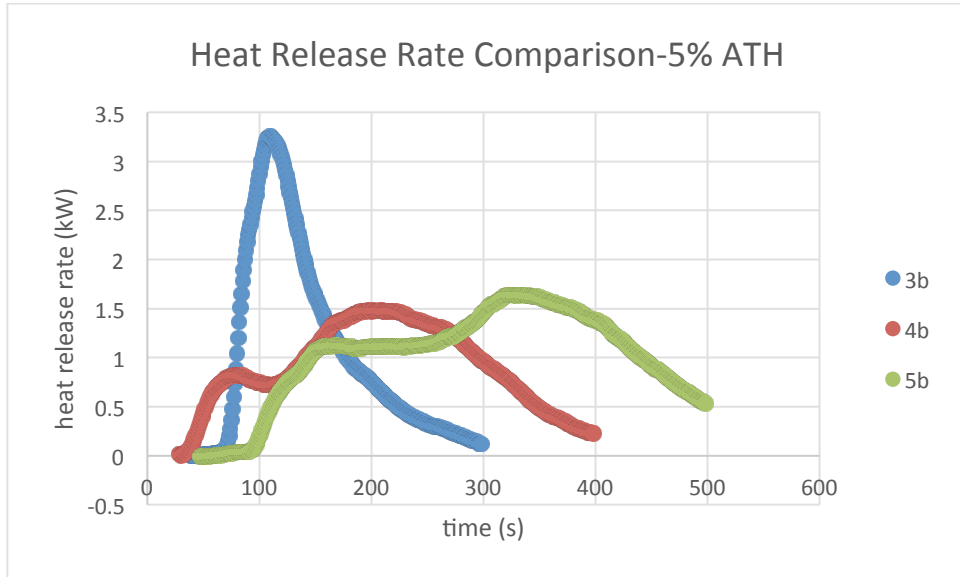


Figure 143-Heat Release Rate Comparison 5% ATH

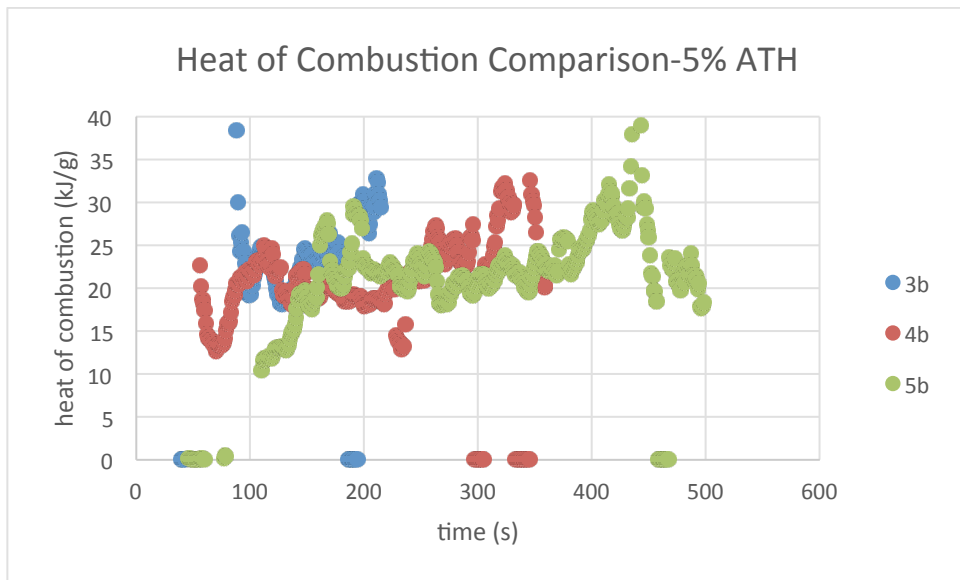


Figure 144-Heat of Combustion Comparison 5% ATH

10% ATH

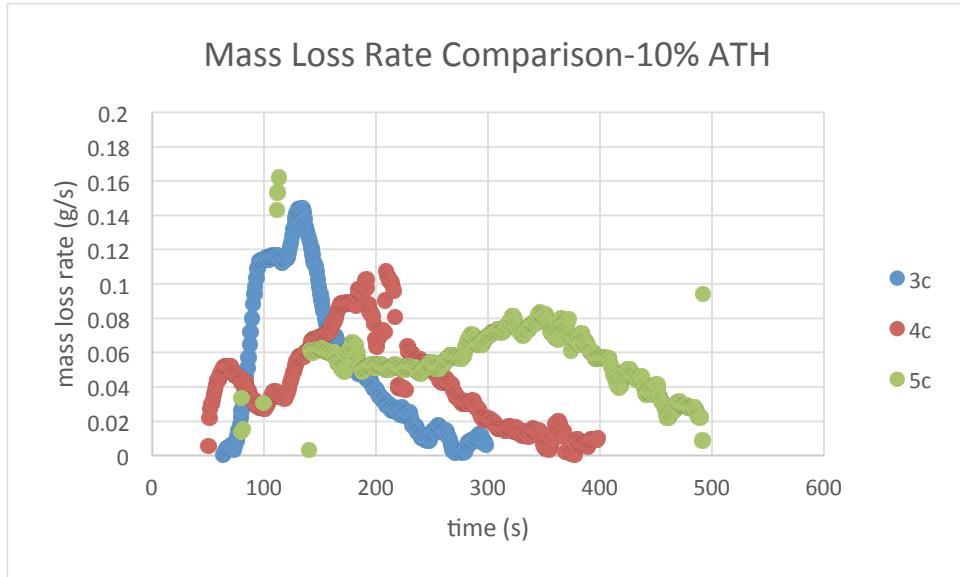


Figure 145-Mass Loss Rate Comparison 10% ATH

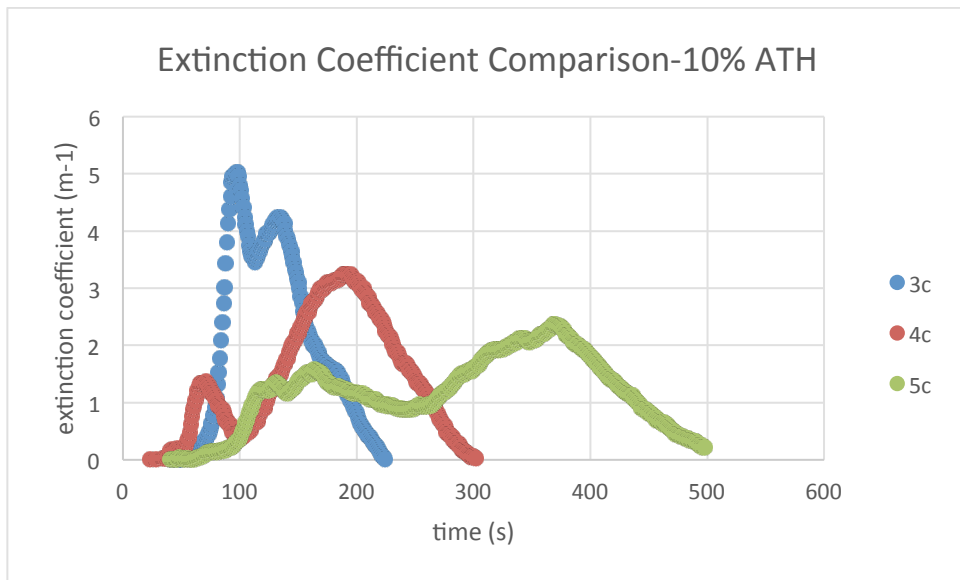


Figure 146-Extinction Coefficient Comparison 10% ATH

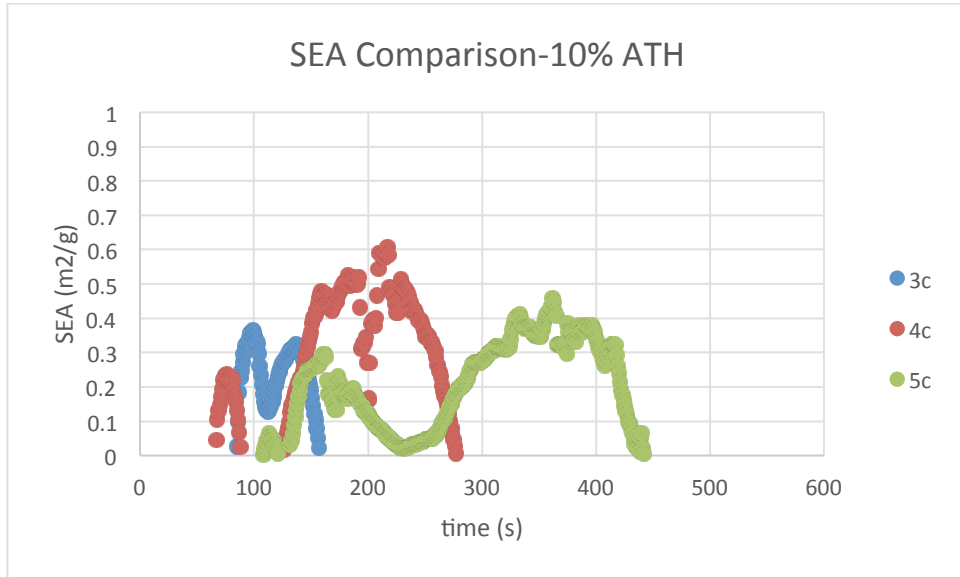


Figure 147-SEA Comparison 10% ATH

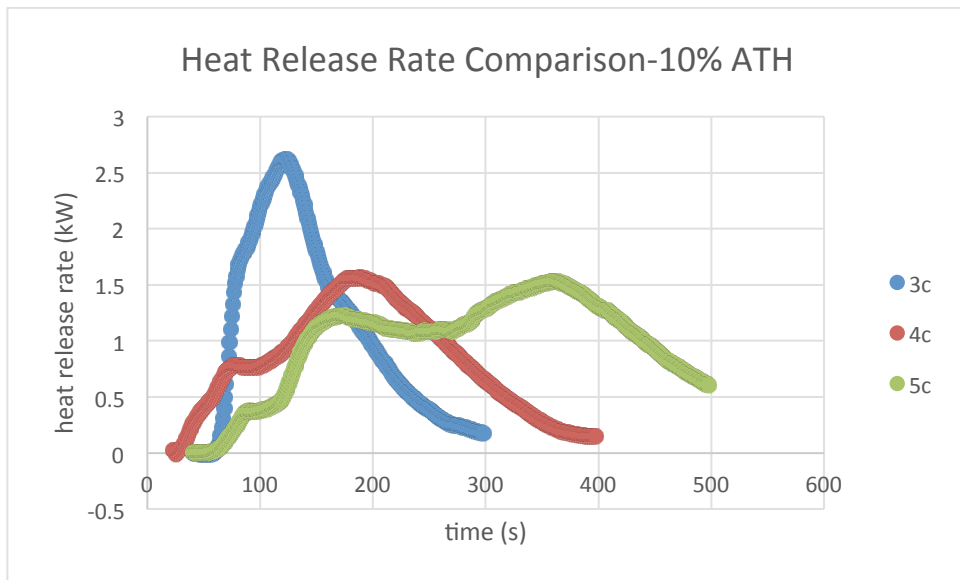


Figure 148-Heat Release Rate Comparison 10% ATH

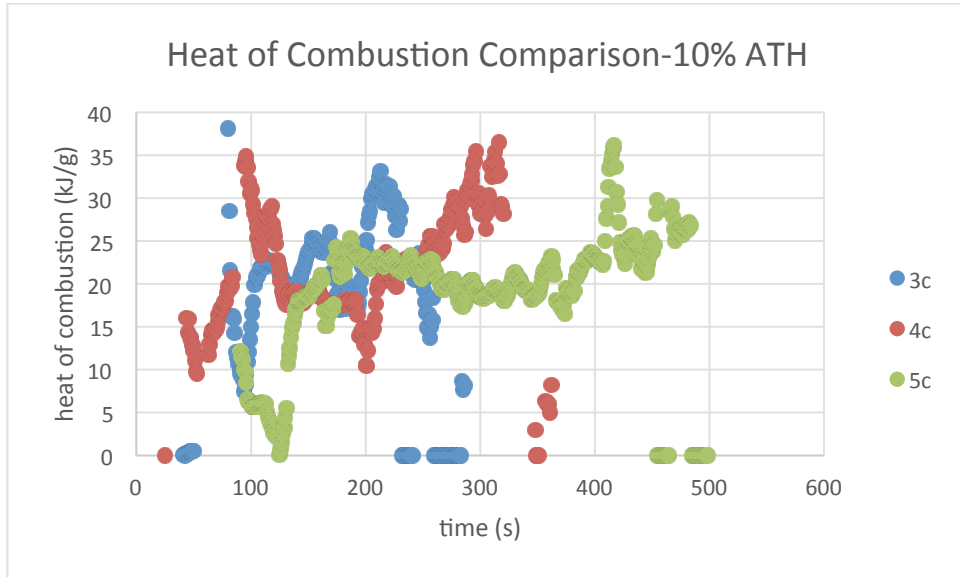


Figure 149-Heat of Combustion Comparison 10% ATH

20% ATH

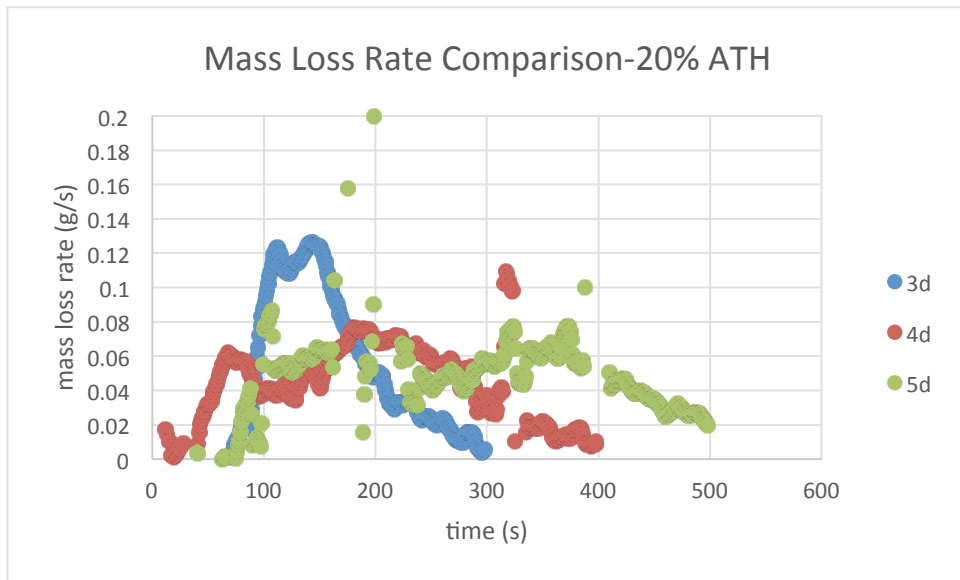


Figure 150-Mass Loss Rate Comparison 20% ATH

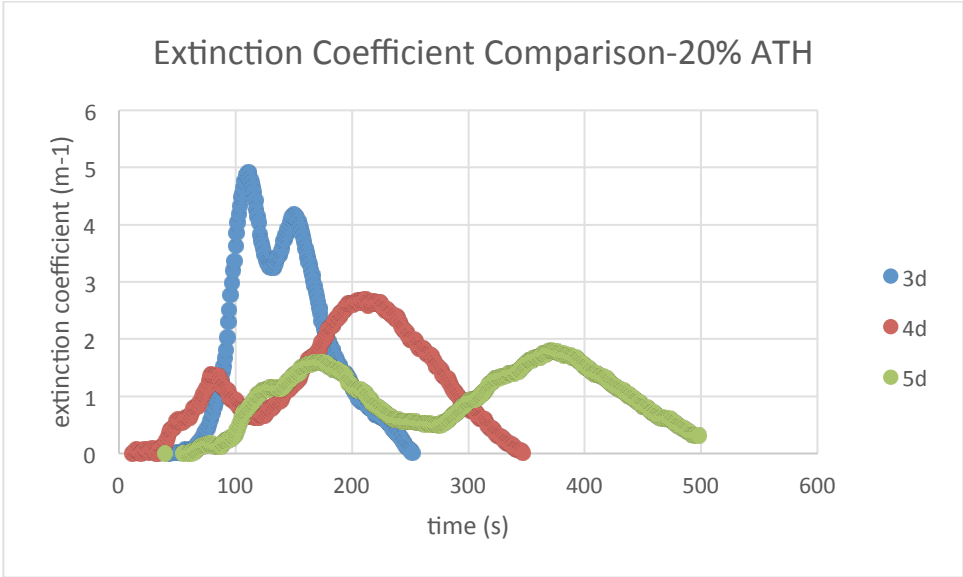


Figure 151-Extinction Coefficient Comparison 20% ATH

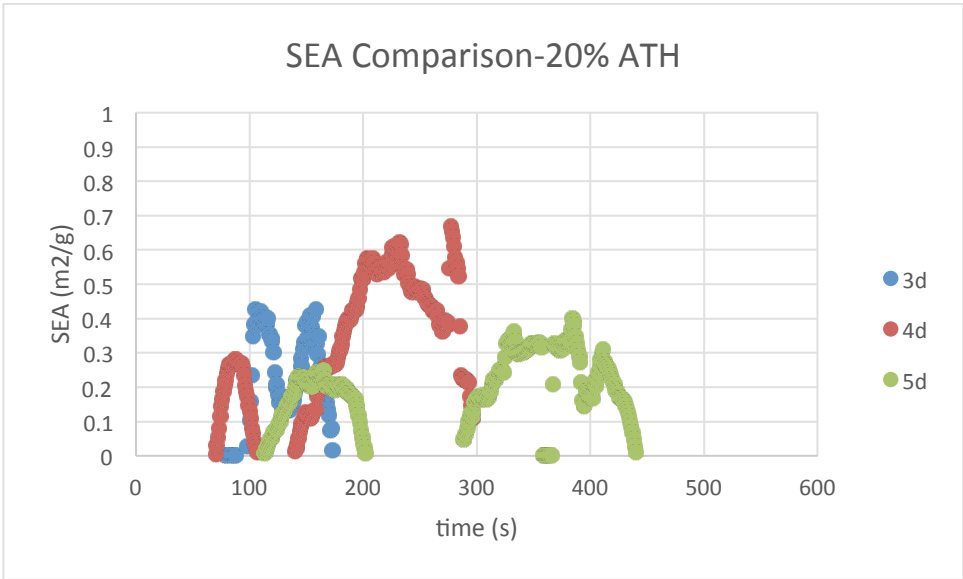


Figure 152-SEA Comparison 20% ATH

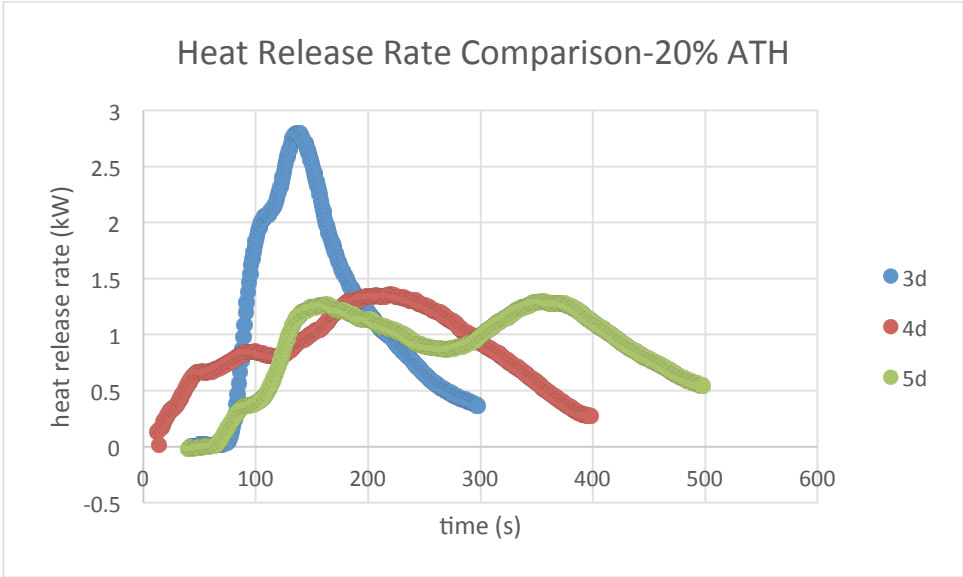


Figure 153-Heat Release Rate Comparison 20% ATH

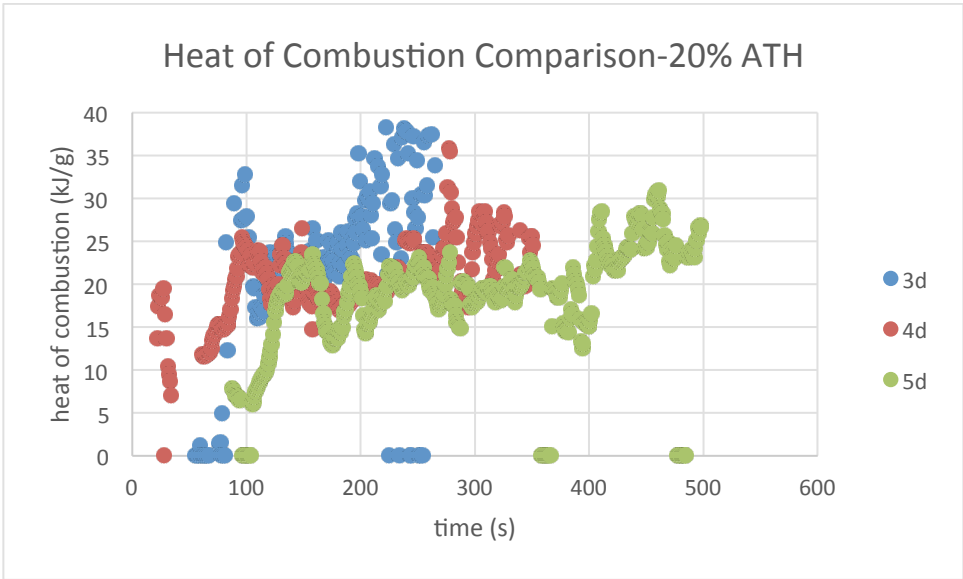


Figure 154-Heat of Combustion Comparison 20% ATH

Appendix F: Translation to Industry Standard Tests

According to the IBC, the fire performance of a FRP material should be determined by two importance numbers—Flame Spread Index (FSI) and Smoke Developed Index (SDI). FSI is a measure of material’s propensity to burn rapidly and spread flames, and SDI is a measure of the intensity of smoke a material emits as it burns. The IBC categorizes materials into three classes based on FSI and SDI.

Table 7- International Building Code Classes

	FSI	SDI
Class A	0-25	less than 450
Class B	26-75	less than 450
Class C	76-200	less than 450

Flammability Parameter

Flammability parameter, or called β parameter, is an analysis which uses the theoretical consideration of Mowrer and Williamson based on the concurrent flow flame spread model of Cleary and Quintiere. A flammability parameter with a positive value means an accelerating spread of flame, and a negative parameter means a decelerating spread. The parameter can be calculated based on direct and indirect measurements of cone calorimeter:

$$\beta = k_f \dot{Q} - \frac{t_f}{t_{bo}} - 1 \quad (F1)$$

In the Equation 1, t_f (s) is the time to ignition of the sample under the given incident heat flux (IHF), t_{bo} (s) is the burn duration and \dot{Q} (kW/m²) is the heat release rate per unit area (HRRPUA). The parameter k_f is related to the flame length or forward heating distance and is assigned to be 0.01 (m²/kW).

According to the work accomplished by 2014 cone MQP groups, the three different combinations of input needed for Equation 1 (peak HRRPUA and visual burn duration, average HRRPUA and visual burn duration, and average HRRPUA and burn duration based on total energy released) were studied. The results showed that the two combinations based on the average HRRPUA showed the most consistent outputs. Therefore, the average HRRPUA and visual burn duration were used to calculate the flammability parameter.

Table 8-Summary of Flammability Parameter Values of All Systems

	β		β		β		β
3a_1	-0.16	3b_1	0.31	3c_1	-0.10	3d_1	0.00
3a_2	0.27	3b_2	-0.04	3c_2	0.30	3d_2	0.10
3a_3	0.20	3b_3	0.15	3c_3	-0.07	3d_3	-0.06
4a_1	0.01	4b_1	-0.004	4c_1	-0.10	4d_1	-0.29
4a_2	-0.26	4b_2	-0.53	4c_2	-0.38	4d_2	-0.30
4a_3	-0.04	4b_3	-0.18	4c_3	-0.19	4d_3	-0.16
5a_1	-0.01	5b_1	-0.10	5c_1	-0.11	5d_1	-0.22
5a_2	-0.11	5b_2	-0.21	5c_2	-0.16	5d_2	-0.29
5a_3	-0.05	5b_3	0.05	5c_3	0.02	5d_3	-0.12

From Table.F3, all the samples without gelcoat (series 3) showed accelerating flame spread, and all the samples with gelcoat (series 4 & 5) showed decelerating flame spread. However, the specimens which had gelcoat with sand finish had relatively smaller magnitudes of β parameter compared with those that only had gelcoat coating. The results below show that the composition of ATH does not have a significant effect on the flame spread potential and gelcoat has a significant effect on it. In addition, the comparison of gelcoat (series 4) and gelcoat with sand (series 5) shows that adding sand to gelcoat does not significantly affect the flame spread potential.

Table 9-Summary of Average Flammability Parameter Values

ATH (%)	Glass and Epoxy	Glass and Epoxy with Gelcoat	Glass and Epoxy with Sand Gelcoat
0	0.10	-0.10	-0.06
5	0.14	-0.24	-0.09
10	0.04	-0.22	-0.08
20	0.02	-0.25	-0.21

ASTM E84 Screening Tool

Both FSI and SDI are supposed to be measured in the ASTM E84 standard test. Full-scale standard tests could not be performed in order to obtain the crucial numbers for Kreysler. Therefore, the FSI and SDI will be approximately calculated based on cone calorimeter data, using the method that was developed by 2014 MQP group.

Flame Spread Index (FSI)

In the standard tests, the FSI is calculated from the time integral of the flame extension by the following equations:

$$FSI = 0.515 \cdot A_T \quad A_T \leq 97.5 \quad (F2)$$

$$FSI = \frac{4900}{195 - A_T} \quad A_T > 97.5 \quad (F3)$$

A_T : time integral of the flame extension, (ft · min)

A screening tool developed by Acosta el was used to simulate flame extension. Two different versions of the tool were developed based on whether the FRP material had coating or not.

$$L_{f-coated} = \left(0.2322 \cdot \left(\frac{0.6\dot{Q}+88}{0.43} \right)^{0.6496} \right) - 4.5 \quad (F4)$$

$$L_{f-noncoated} = \left(0.1574 \cdot \left(\frac{0.6\dot{Q}+88}{0.43} \right)^{0.6496} \right) - 4.5 \quad (F5)$$

L_f : simulated flame extension, (ft)

\dot{Q} : heat release rate per unit area (HRRPUA), $\left(\frac{kW}{m^2} \right)$

The screening tool assumes zero flame extension before the time to ignition. Meanwhile, the time integral of flame extension is calculated only on the time interval from the time to ignition to the time of edge burning.

The cone calorimeter recorded data every second. Therefore, the time integral of flame extension is calculated as an approximation by summing the calculated flame extensions at every time point, which can be expressed by the following equation:

$$A_T = \sum L_f \Delta t \quad (F6)$$

In the equation above, the time interval will be one second and the heat flux at that second will be used.

Therefore, the first step to simulate the FSI in the standard test is to calculate flame extension based on the HRRPUA obtained by the cone calorimeter:

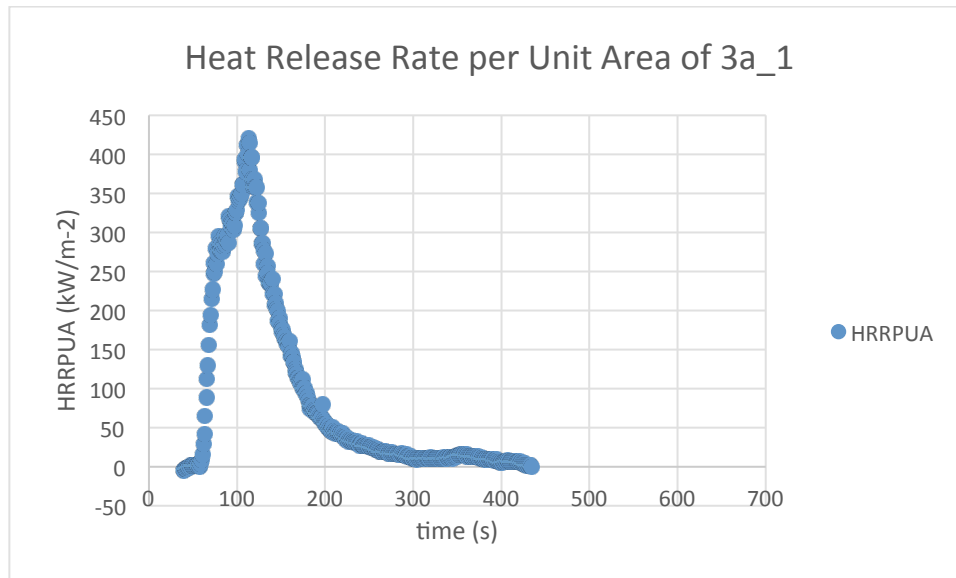


Figure 155-Heat Release Rate per Unit Area of 3a1

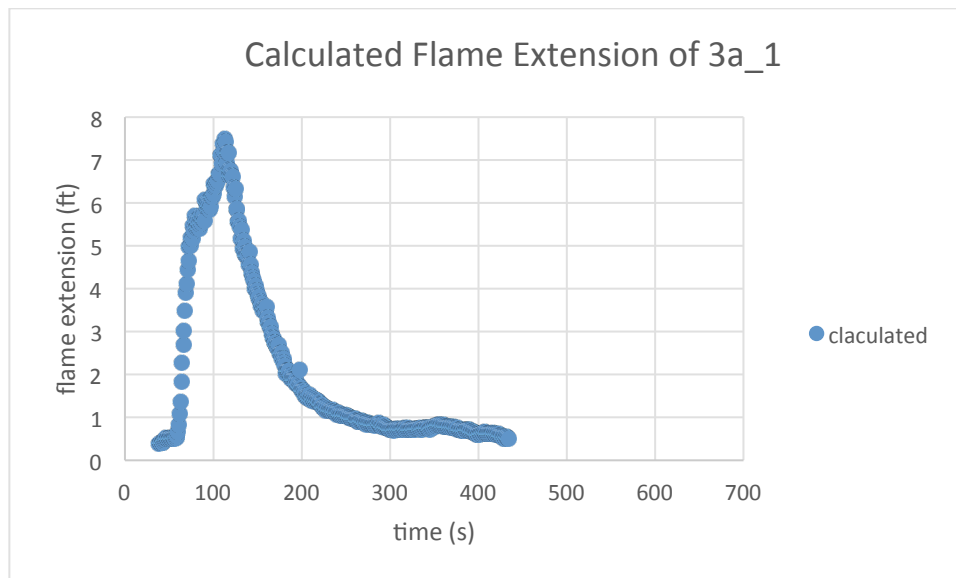


Figure 156-Calculated Flame Extension of 3a1

As shown above, the calculated flame extension has a similar shape as heat release rate per unit area because of the expression of the flame extension. The flame extension increases rapidly at the beginning of the fire and reaches its peak, and the peak appears before the time of edge burning. All the specimens in the 3 series have shown the same characteristic as 3a_1. However, FSI cannot be calculated simply by integrating the curve of the flame extension—an assumption has to be made that the flame extension is constant after the peak. The reason is that a flash fire can generate the same damage as a sustained fire because it is spreading to more material rather than burning out.

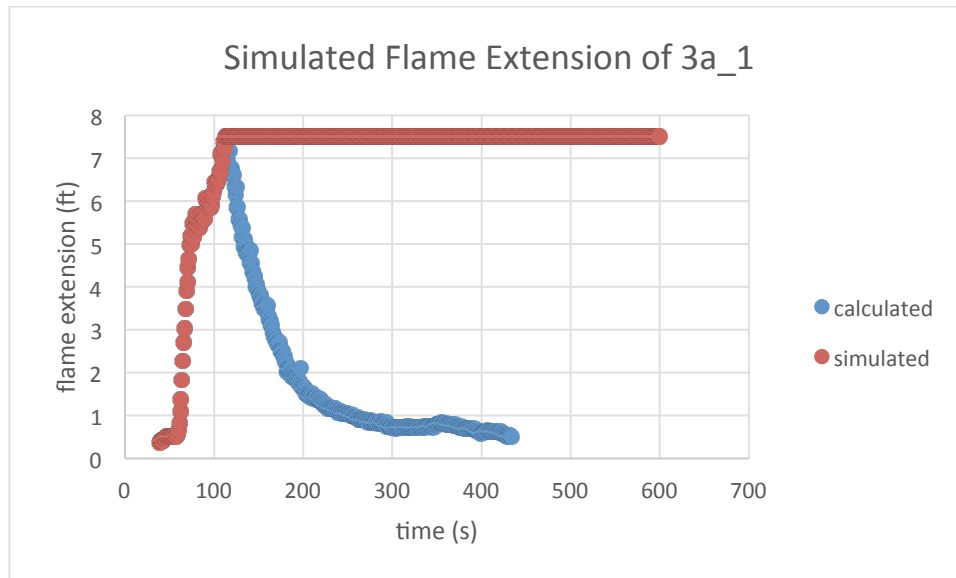


Figure 157-Simulated Flame Extension of 3a1

Therefore, the FSI will be the area under the red curve shown above instead of the blue one. However, for the specimens in the series 4 and 5, they have not only the first peak of flame extension before the time of edge burning but also have the second peak after that. Since edge burning creates invalid data for the standard test analysis, only the first peak was used to calculate the FSI.

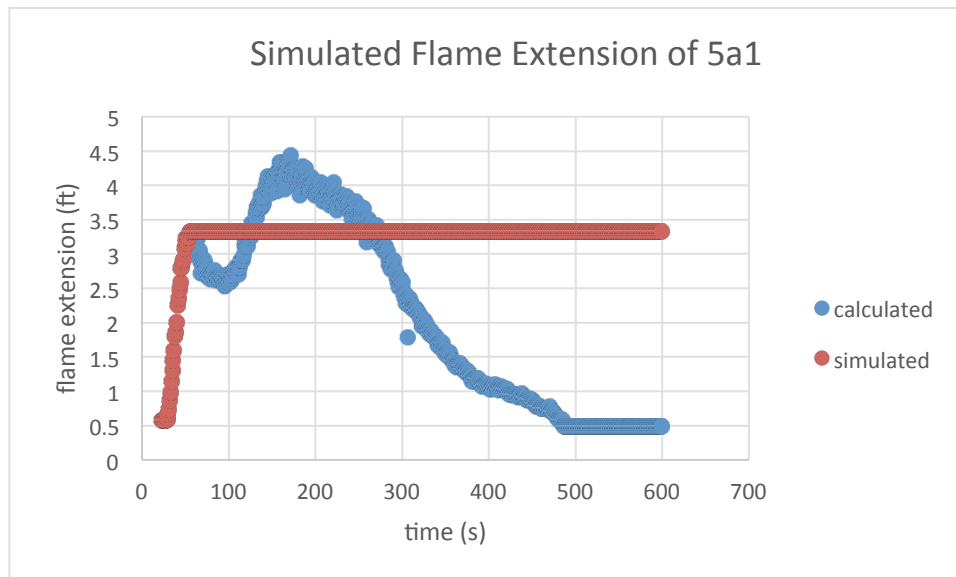


Figure 158-Simulated Flame Extension of 5a1

Again, the FSI will be the area under the red curve shown above instead of the blue one.

Smoke Developed Index (SDI)

The SDI is a ratio of the area under the curve of the light obscuration versus time of the sample being tested and a standard reference of red oak light obscuration. The following expressions were used to calculate the SDI:

$$SDI = \frac{(\int_0^{10 \text{ min}} (100 - T\%) dt)_{\text{specimen}}}{(\int_0^{10 \text{ min}} (100 - T\%) dt)_{\text{red oak}}} \times 100\% \quad (\text{F7})$$

$$T\% = \frac{100}{\exp\left(\frac{22.268 \cdot k}{0.645 \dot{Q} + 125.6}\right)} \quad (\text{F8})$$

k : extinction coefficient, (m^{-1})

\dot{Q} : heat release rate per unit area, ($\frac{kW}{m^2}$)

$T\%$: light transmission

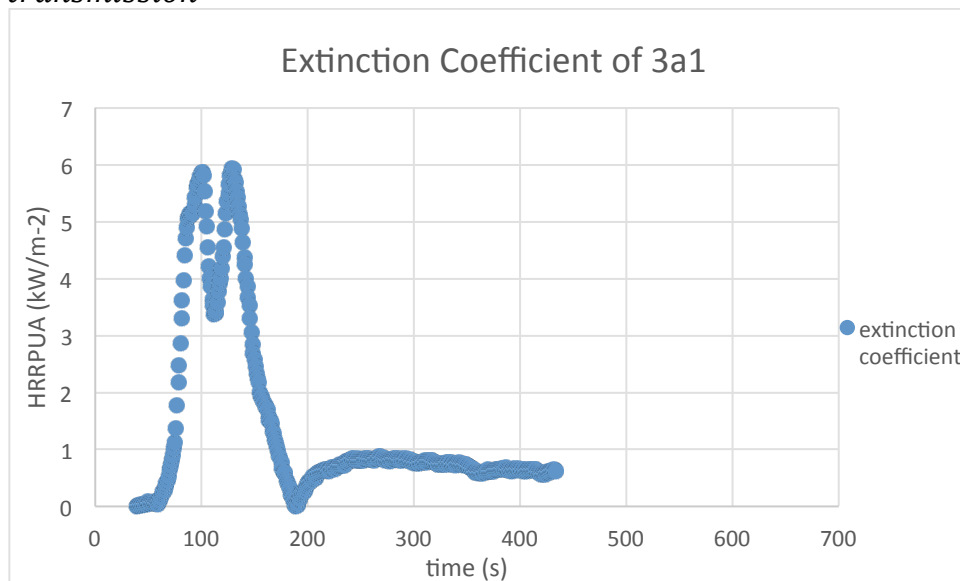


Figure 159- Extinction Coefficient of 3a1

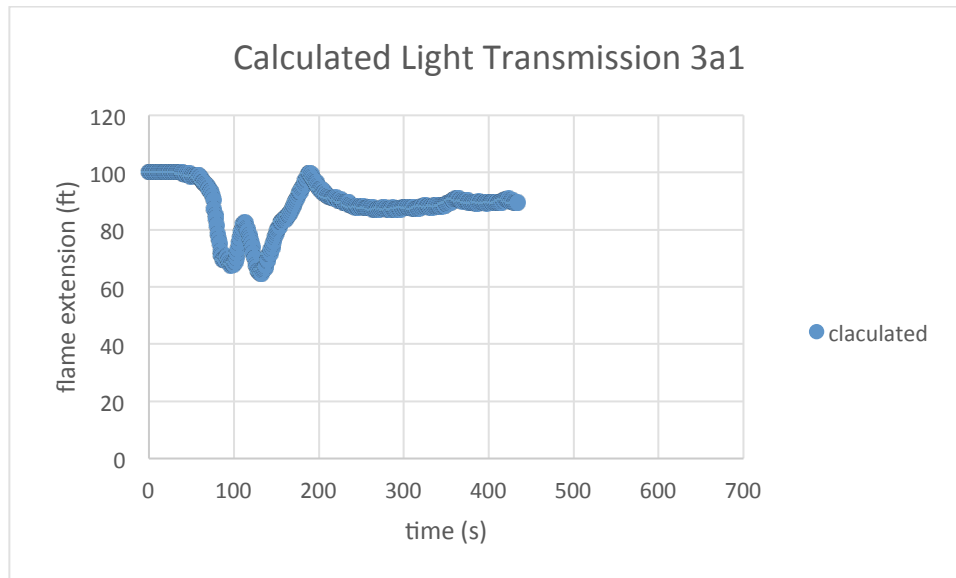


Figure 160-Calculated Light Transmission 3a1

As shown above, light transmission was calculated by the corresponding extinction coefficient and HRRPUA, shown in Fig.D1. Again, the time integral was approximated by summing the one-second time intervals.

$$SDI = \frac{\sum(100-T\%)\Delta t_{specimen}}{\sum(100-T\%)\Delta t_{red oak}} \times 100\% \quad (F9)$$

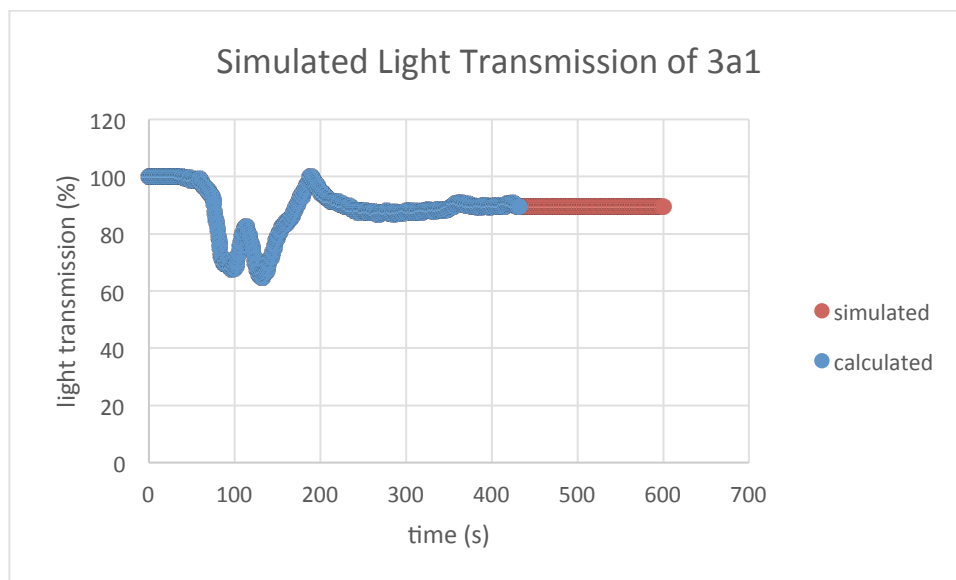


Figure 161-Simulated Light Transmission of 3a1

Shown above, the zero time point for the SDI simulation is the start of the test. Most specimens were not on fire for the necessary ten minutes. Since the shutter would be closed and clean air would be introduced into cone calorimeter after the time of flame out,

the smoke obscuration calculated would be inaccurate if raw data was used. Instead the light transmission was considered to be constant after time of flame out, which meant that the SDI calculated was larger than what it should be. Because the worst situation is being simulated the results provide an over expectation for the Kreysler samples. The values obtained from using the extended results were used to calculate the light transmission.

Special Considerations

Several special concerns are required to be explained carefully, including incident heat flux, definition of coating, time interval of FSI, time interval of SDI, and the reference of red oak.

Incident Heat Flux (IHF)

The flame length screening tool used in the simulation uses the heat release rate per unit area (HRRPUA) from the cone calorimeter at an IHF of 40 kW/m² for an input. However, all the tests operated on the cone calorimeter were at an IHF of 50 kW/m². According to the 2014 MQP group, simulations using HRRPUA from the cone calorimeter at an IHF of 50 kW/m² is a good approximation of that at an IHF of 40 kW/m².

Definition of Coating

Coated FRP for the FSI tool is defined as polymer concrete. Using this definition, series 5 specimens which have gelcoat and sand in the surface coating are the only samples that have a polymer concrete. All other series would be considered as uncoated except series 4 specimens can also be viewed as coated, or be viewed as a state between coated and uncoated. In this project, the samples were considered to be uncoated and the equation for uncoated FRPs was used.

The Reference of Red Oak

The light transmission through the red oak smoke is involved in the calculation of the SDI. When making comparisons to red oak, the results of a cone calorimeter test are referenced to make the necessary comparisons.

Result and Conclusion

Table 10 - Summary of the Prediction of Standard Tests of All Systems

	FSI	SDI		FSI	SDI		FSI	SDI		FSI	SDI
3a_1	34	386	3b_1	35	435	3c_1	33	370	3d_1	23	367
3a_2	27	344	3b_2	35	299	3c_2	25	327	3d_2	32	299
3a_3	27	246	3b_3	25	288	3c_3	25	286	3d_3	25	255
4a_1	16	380	4b_1	15	377	4c_1	15	359	4d_1	17	275
4a_2	14	388	4b_2	12	327	4c_2	10	311	4d_2	14	324
4a_3	13	260	4b_3	12	293	4c_3	13	299	4d_3	14	307
5a_1	26	218	5b_1	31	280	5c_1	31	264	5d_1	30	233
5a_2	29	332	5b_2	27	363	5c_2	31	354	5d_2	31	281
5a_3	26	303	5b_3	32	334	5c_3	32	324	5d_3	35	285

Table 11 - Summary of the Prediction of Standard Tests

	Glass and Epoxy			Glass and Epoxy with Gelcoat			Glass and Epoxy with Sand Gelcoat		
ATH (%)	FSI	SDI	class	FSI	SDI	class	FSI	SDI	class
0	30	325	B	15	345	A	27	320	B
5	32	340	B	14	335	A	31	325	B
10	28	330	B	13	325	A	32	315	B
20	27	310	B	15	305	A	32	285	B

As shown above, the samples in series 3 and 5 are in Class B; those in series 4 are in Class A. However, since the deviation of the FSI can reach 30% of its real value series 3 and 5 should be tested directly in standardized tests.

9.0 APPENDIX: G-PYRO

9.1. Inputs

The input file is used to set up all parameters as well as the desired outputs. An excel file front end is intended to assist the user in organizing data, but the DATA file that is ultimately created from the Excel file can also be edited. The DATA file will be referred to after a bare understanding of the Excel file is provided. The DATA file is simply a rewrite of the excel file into a .txt file that is then used by G-Pyro.

9.1.1. Editable sections

In the Excel file, 14 tabs correspond to different areas of information that can be edited, including solid properties, reactions, layering, and heating. Not all tabs are applicable to the types of simulations that are of interest. The only tabs that should be of concern are general, output, spros, rxns, layers, and qe. Some circumstances may require using other tabs, but this report will only focus on editing the previously listed tabs.

In the general tab, the overall process that G-Pyro runs and what is solved can be made TRUE or FALSE. The base conditions such as ambient temperature and pressure are inputted in this tab, but more often than not, they are left at 300 Kelvin, and atmospheric pressure.

The output tab lists the desired outputs that will be recorded throughout the simulation. There are two types of outputs that can be recorded, points and profiles. The point dump corresponds to an overall system value, or a value at a specific thickness recorded over the time of the simulation. Profile dumps can be more useful because they provide information for every cell and for every time, with which profiles of the sample can be made for different measurements. A list of types of output files is available in Table 1. Quantities Available for Dump of the G-Pyro User's Guide. Some particular profiles that will be used include, mass fraction, reaction rate, bulk density, and temperature.

The properties of the solid species is the next tab to edit. This tab is where all solid species are specified. Each species then has inherent properties that must be specified. Some properties are unimportant in the simulation that will be run, but the important ones include thermal conductivity (k), heat capacity (c), density (ρ), emissivity (ϵ), absorption (κ), and radiative thermal conductivity (γ).

The reactions tab follows the solid species tab and is used to input any reactions. Each reaction goes from species A to species B and has properties including the pre-exponential factor (Z), activation energy (E), heat of vaporization (ΔH_v), and order of reaction (n). The solid species provided in the previous tab should be used for the species of the reactions. Different kinetic models can also be selected, but the default n th order kinetic model will be used for all simulations of this report.

The second to last tab that can be edited is the layers tab. The main purpose of this section is to set up the physical geometry of the specimen that will be simulated. The program allows for multiple layers, varying thicknesses, and varying mass fractions. The parameters that will be changed are the number of layers, the thickness of the sample (z_1 , z_2), and mass fractions (Y_{i0}). Contact resistance (h_{crz}) should be altered if more than one layer is input. In order to maintain an insulated back face, the contact resistance of the last layer will be zero.

The final section to alter is the q_e tab, which includes information on the heating and other simulation parameters. The number of different cases can also be changed if multiple types of simulations will be made on the same specimen. The parameters that can be changed are the applied heat (q_e), the sample thickness (δ_0), number of cells ($n_{cell,z}$), duration of simulation (t_{stop}), and the linear heating rate (β). All cases will be done at an applied heat of 50 kW/m^2 , a thickness of 8mm, 81 cells, and a heating rate of 5 K/min. The duration of each simulation will be determined by looking at the mass loss rate and when it is essentially zero.

9.1.2. [Parameter Input](#)

All of the inputs are either from literature or from the desired settings of the simulation that would be run. The general tab is left as a default. The output file is set up so that the mass loss rate is generated as a point dump. The profiles that are generated are temperature, reaction rate of all reactions, mass fraction of all species, porosity, bulk density, and conversion. The specimen that will be simulated is Kreysler's samples of an epoxy with varying levels of ATH and glass. However, the material's properties of the Kreysler samples are not known exactly so properties of similar materials were found in Table 6 of Esther Kim's 2014 paper, Parameter Estimation for Comprehensive Pyrolysis Modeling: Guidance and Critical Observations. The Resin that is specified in her paper will represent the epoxy of Kreysler. The Additive represents ATH, and the glass represents glass. The solid properties used are tabulated below.

Species	ρ [kg/m ³]	k [W/m*K]	c [J/kg*K]	ϵ	κ [m ⁻¹]	γ [m]
Resin	1200	0.23	1400	0.84	10 ⁶	-
R_Residue	253	0.19	1900	0.90	10 ⁶	0.00348
Additive	2300	1.22	1200	0.81	10 ⁶	-
A_Residue	1558	0.24	1200	0.89	10 ⁶	0.00475
Glass	2600	0.18	400	0.88	10 ⁶	0.00769

Table 12-Solid Properties Input

The kinetic properties are also pulled from the same paper by Esther Kim. The properties for the reaction are tabulated below.

Reaction	n	Z [s ⁻¹]	E [J/mol]	ΔH_v [kJ/kg]
Resin -> R_Residue	1.3	3.2*10 ¹²	1.83*10 ⁵	2.5*10 ³
ATH -> A_Residue	5.0	1.6*10 ¹²	1.60*10 ⁵	3.76*10 ³

Table 13-Reaction Properties Input

The layers tab is then input. The x dimension is unimportant and left at ± 1 m. The z dimension for the specimen is set to 0.008 m unless specified otherwise in a later section. The contact resistance is left at zero because only a single layer is used. The mass fraction will change for the different levels of ATH and glass. The different layers are specified below

Case	z [m]	Y _{i0,1}	Y _{i0,2}	Y _{i0,3}	Y _{i0,4}
Epoxy_Neat	0.008	1.000	0.000	0.000	0.000
Epoxy_5%ATH	0.008	0.950	0.000	0.050	0.000
Epoxy_10%ATH	0.008	0.900	0.000	0.100	0.000
Epoxy_20%ATH	0.008	0.800	0.000	0.200	0.000

Table 14-Layer Property Input

The heating parameters were specified in an earlier section. The properties include an applied heat of 50 kW/m², a thickness of 8mm, 81 cells, and a heating rate of 5 K/min.

9.2. Epoxy and ATH systems

This section will be devoted to looking at systems with epoxy and ATH and no glass. The analysis is focused on the trends that are followed and not so much the quantitative results. Any comparisons that will be made will be found in Section 9.7. Analysis for 5%, 10%, and 20% ATH systems will be more limited than the epoxy due to the repetitive nature of the information. Only important notes will be stated for the previously mentioned sections.

9.3. Epoxy Neat

The Epoxy Neat specimen contains no ATH and will not have an output for the second reaction rate, or the mass fractions of ATH or ATH residue. Any profile graphed will be a comparison of the examined property and the thickness with multiple curves for different points in time.

9.3.1. Temperature Profile

The graph below shows the temperature across an 8mm sample at time steps of 400 seconds. The temperature starts at ~25 °C as shown by the t=0s line. The back face is insulated because the temperature levels out as it approaches 8mm when viewing the graph.

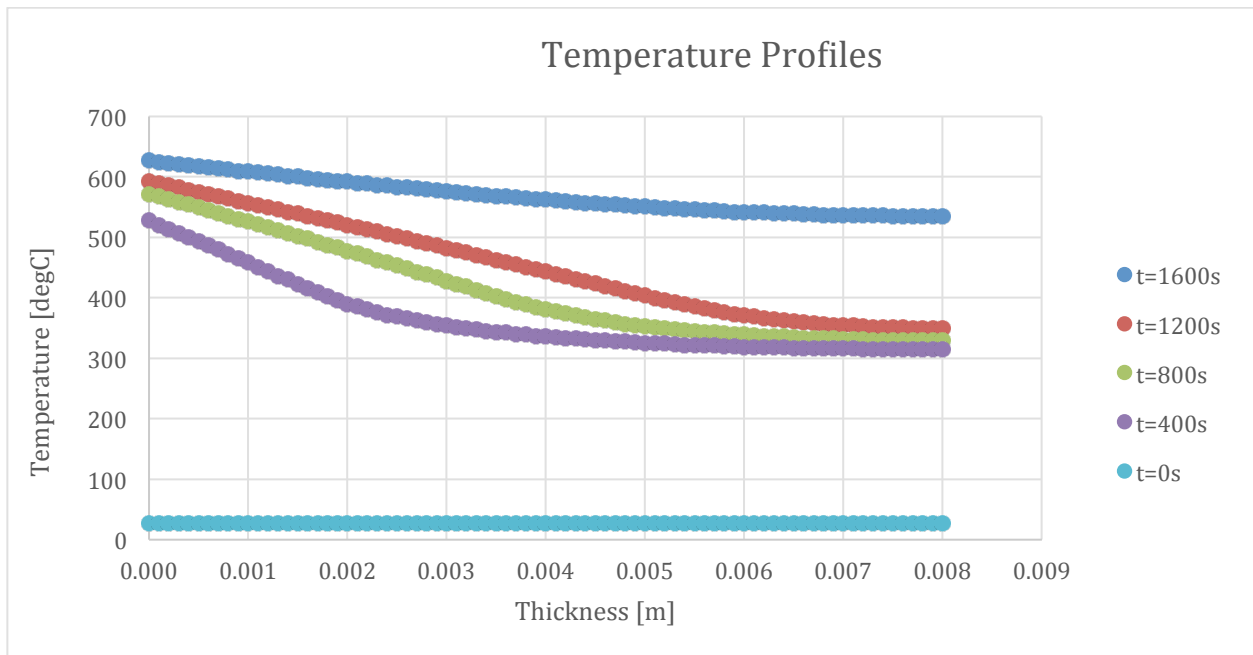


Figure 162-Temperature Profile for Epoxy Neat at 400 second intervals

9.3.2. Mass Loss Rate

The graph below shows the mass loss rate of a sample until mass loss goes to zero. In this case, the simulation ran for ~1600 seconds until the mass loss was zero. All other simulations for the Epoxy/ATH series were run for 1600 seconds in order to properly compare them later on.

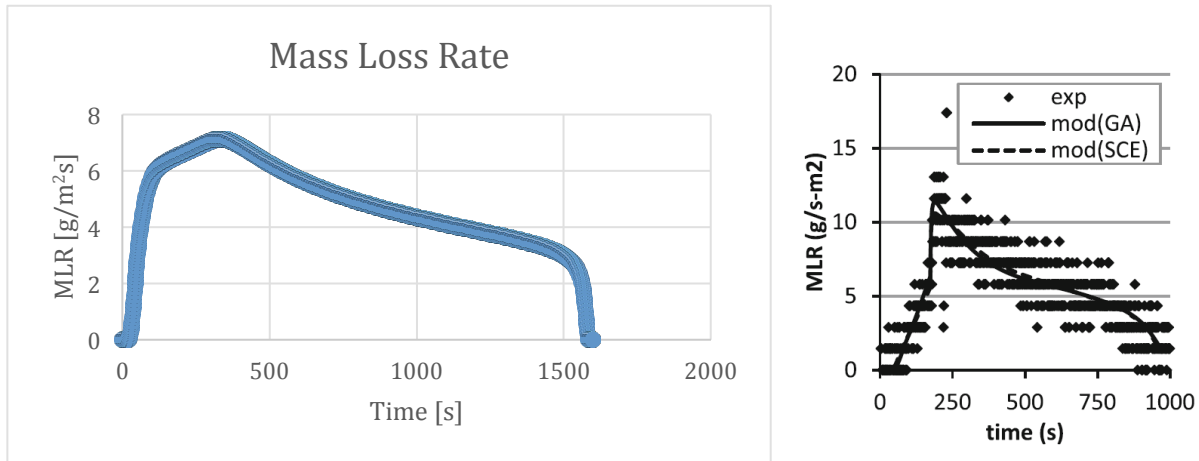


Figure 163-Mass Loss Rate curve of Epoxy Neat compared to FRP literature curve

The graph on the right resembles an FRP, which means there is likely ATH and glass included, but the important comparison is the similar shape of the two mass loss rate graphs, despite one containing glass and the other not. Another comparison will be made later on between a simulated FRP and the graph on the right.

9.3.3. Mass Fraction

The mass fraction of the resin is one at $t=0$ because it is pure resin, and then the three middle curves show that the reaction is creeping through the sample and occurring deeper and deeper as time continues.

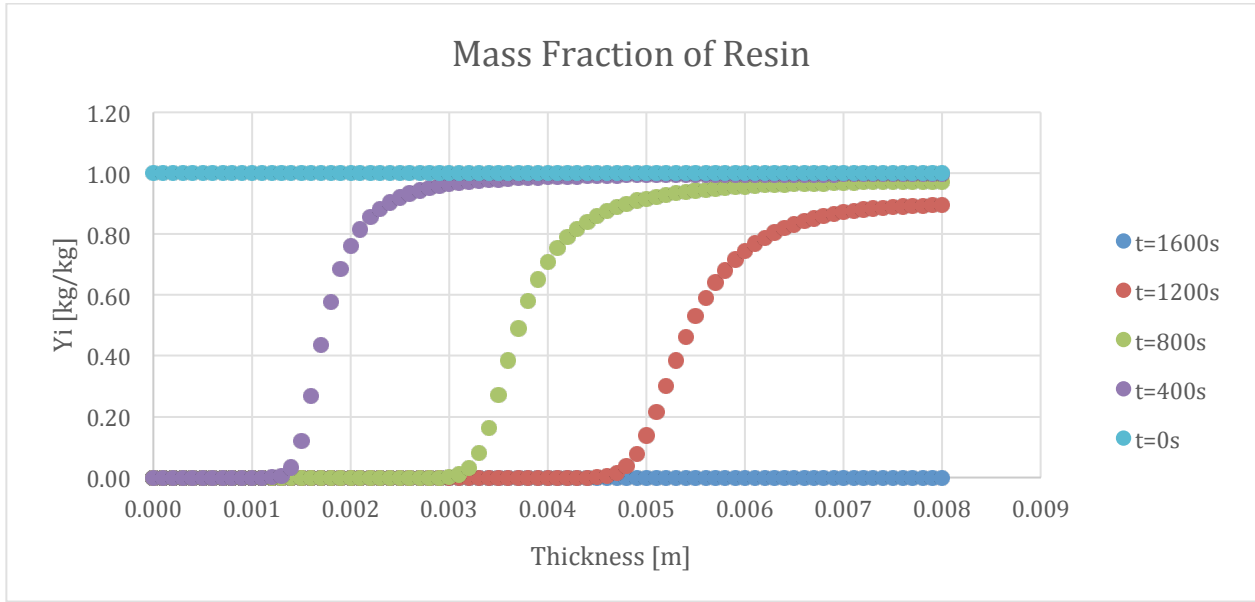


Figure 164-Mass Fraction of Resin for Epoxy Neat at 400 second intervals

The mass fraction of the residue should be the inverse of the above graph because there are only two solids in the system.

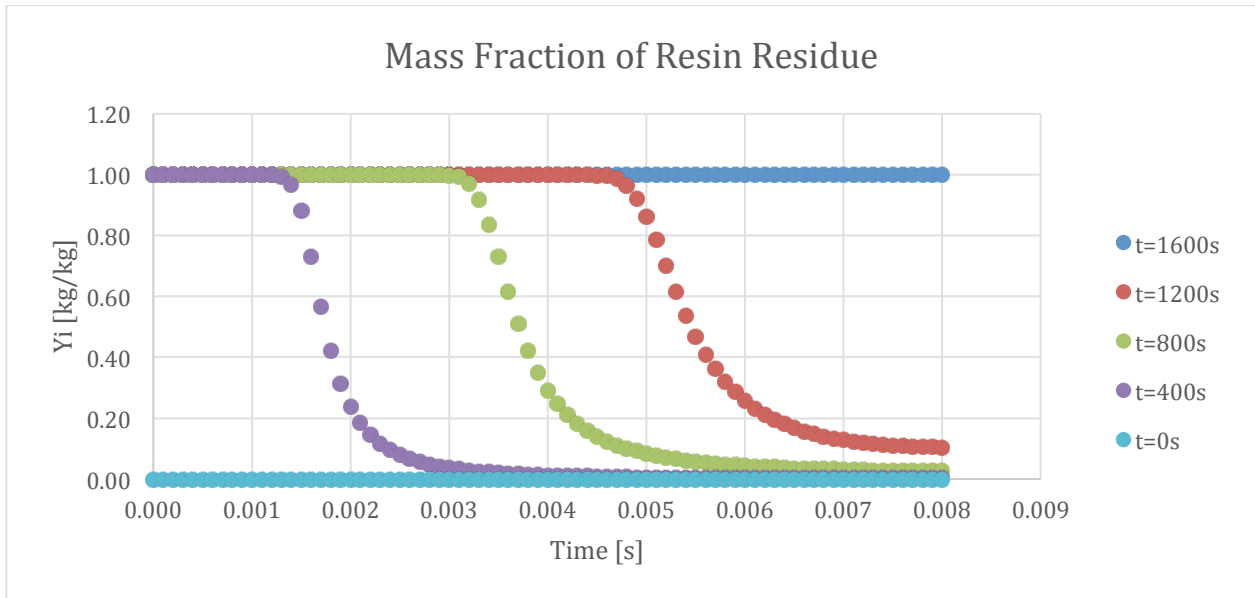


Figure 165-Mass Fraction of Resin Residue for Epoxy Neat at 400 second intervals

9.3.4. Conversion

Shown below is a graph of the conversion of a specimen. Initially none of the sample is converted, but as time passes more is converted until the maximum, which is ~80% conversion.

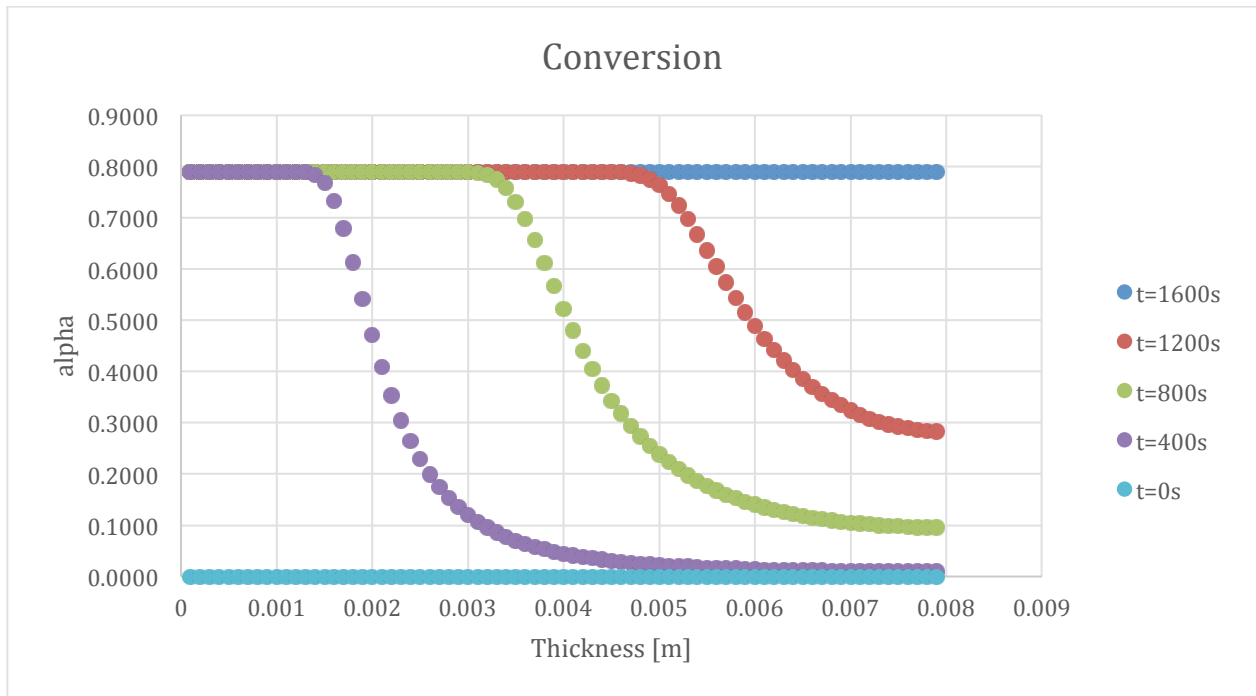


Figure 166-Conversion Profile for Epoxy Neat at 400 second intervals

The conversion was calculated from the “mass divided by the initial mass of the cell”, which was then divided by the initial mass again to achieve a value of 1 for the m/m_0 value. Then alpha was calculated by subtracting the value found previously from one.

9.3.5. [Reaction Rate](#)

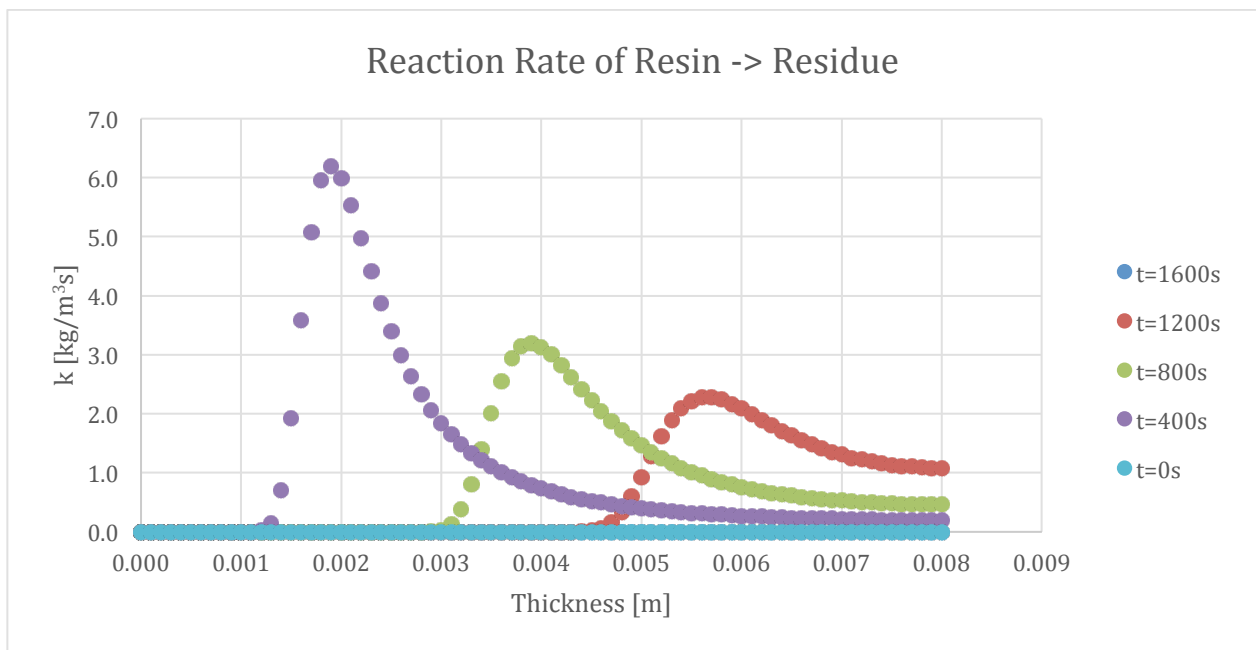


Figure 167-Reaction Rate of Resin to Resin Residue for Epoxy Neat at 400 second intervals

The graph seen above is the reaction rate of the first reaction. A comparison can be made between the conversion and the reaction rate. The reaction rate leads the conversion because only after reacting is a sample of the specimen 'converted'. The steepest tangent of the conversion can be found at the thickness where the reaction rate is the highest.

9.3.6. Density

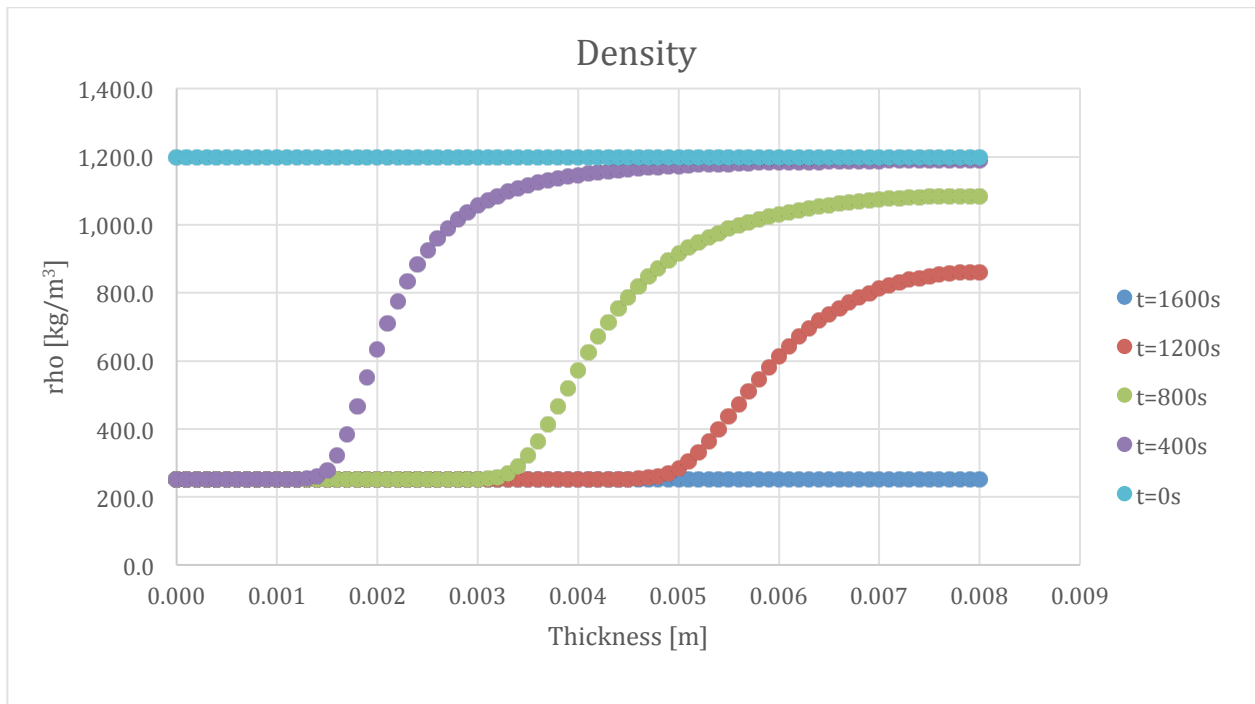


Figure 168-Density Profile for Epoxy Neat at 400 second intervals

The density of the resin is 1200 kg/m^3 which can be seen at $t=0\text{s}$, and the density of the residue is 253 kg/m^3 as seen at the surface levels of all times after $t=0\text{s}$, and entirely at $t=1600\text{s}$. The change in density is occurring during the reaction, which can be seen when comparing this graph to the graph of conversion.

9.3.7. Porosity

The graph below depicts the porosity through the sample. Initially the substance is assumed perfectly non-porous, but as time proceeds, the sample reaches maximum porosity at a value of 0.77. This is rational because as the material is burned there will be empty spaces, which correlates partially to the lower density.

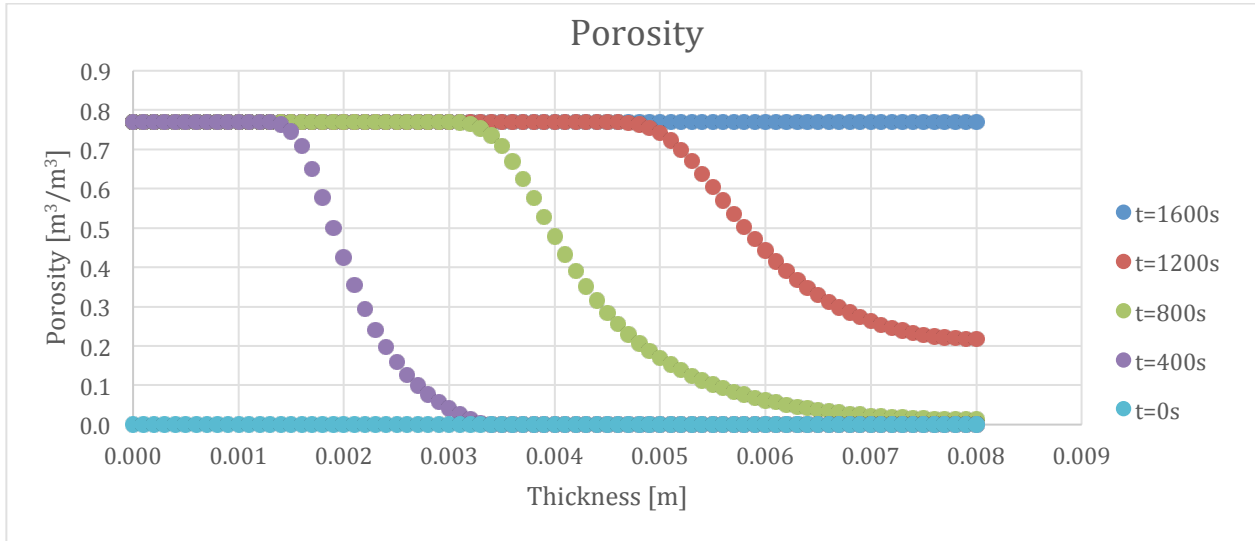


Figure 169-Porosity Profile for Epoxy Neat at 400 second intervals

9.4. Epoxy 5% ATH

This section shows the property outputs of Epoxy with 5% ATH. The analysis will be limited due to the fact that most trends were already explained in the Epoxy Neat section.

9.4.1. Temperature Profile

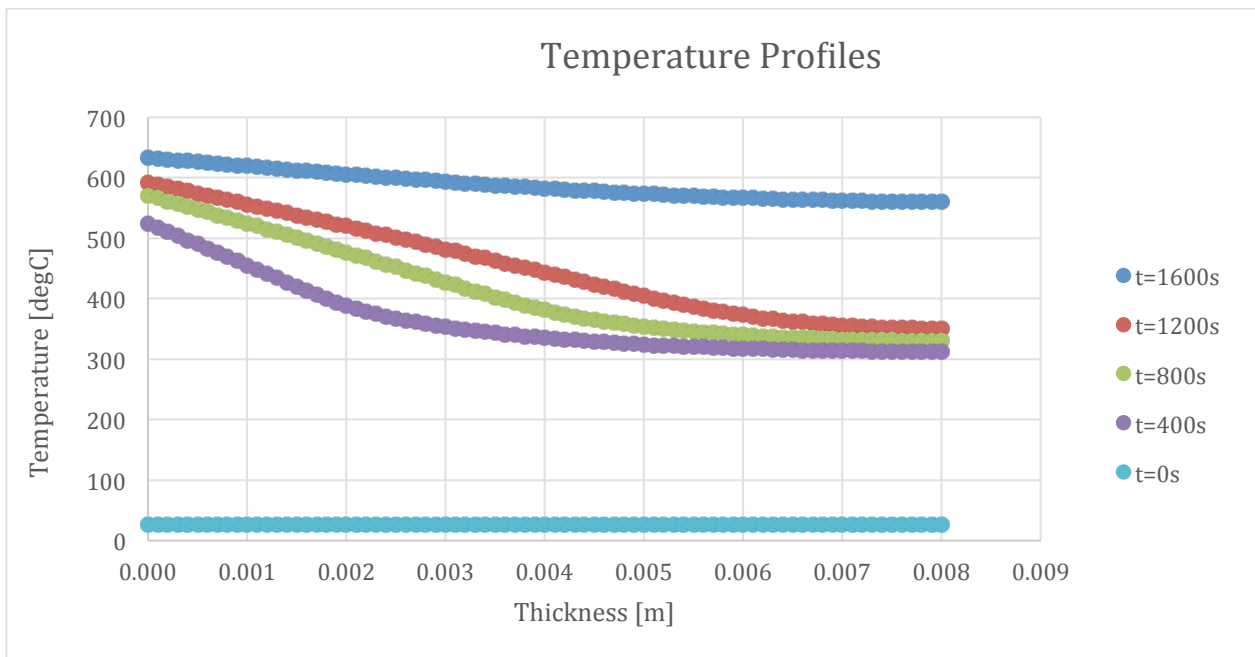


Figure 170-Temperature Profile for Epoxy with 5% ATH at 400 second intervals

9.4.2. Mass Loss Rate

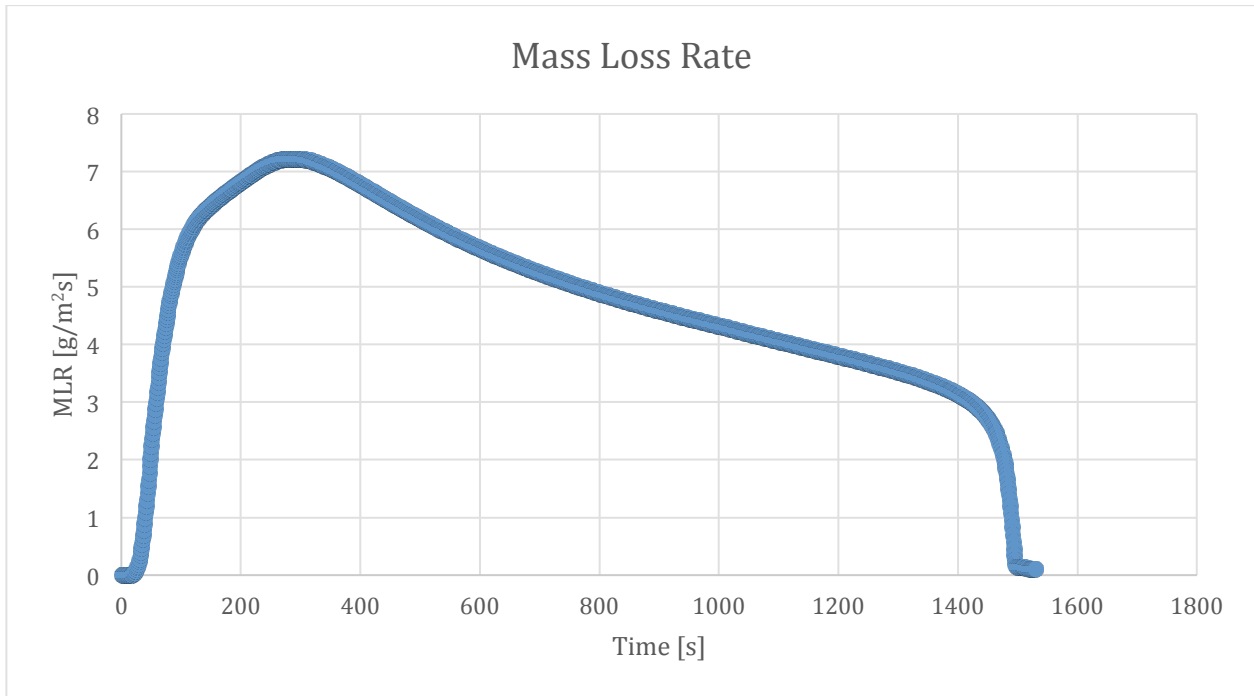


Figure 171-Mass Loss Rate curve for Epoxy with 5% ATH

9.4.3. Mass Fraction

The initial mass fraction is now 0.95 rather than 1.0, but all is consumed during the simulation.

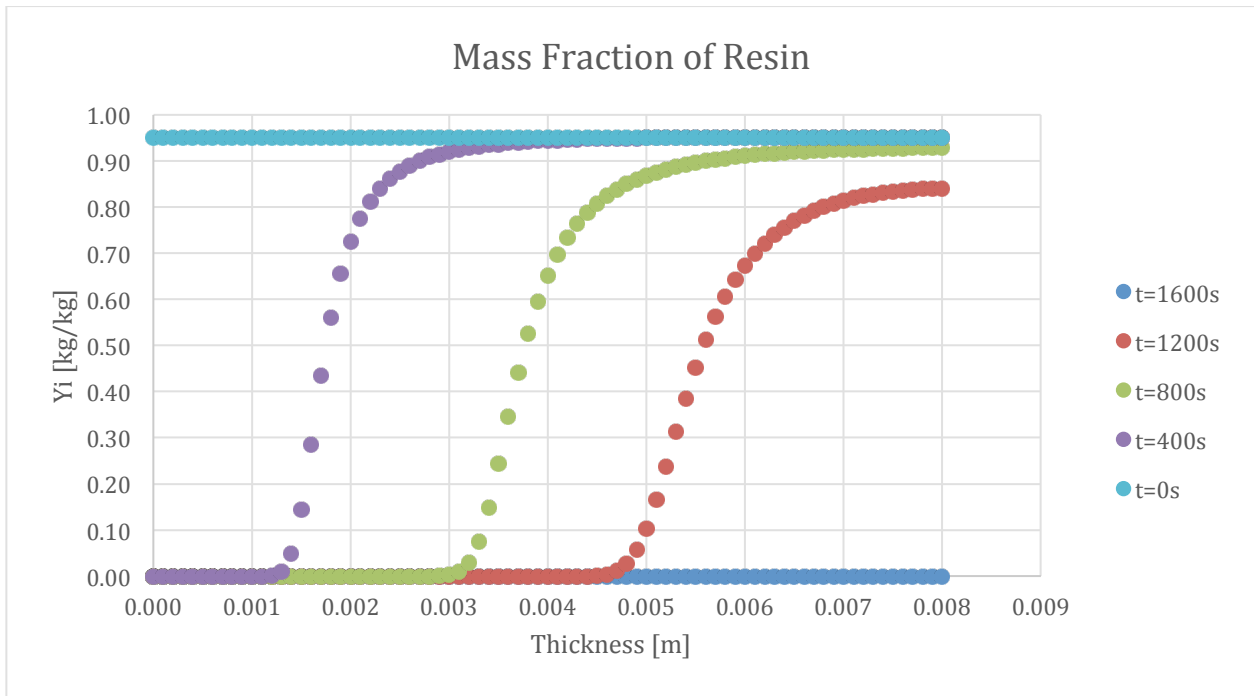


Figure 172-Mass Fraction Profile of Resin for Epoxy with 5% ATH at 400 second intervals

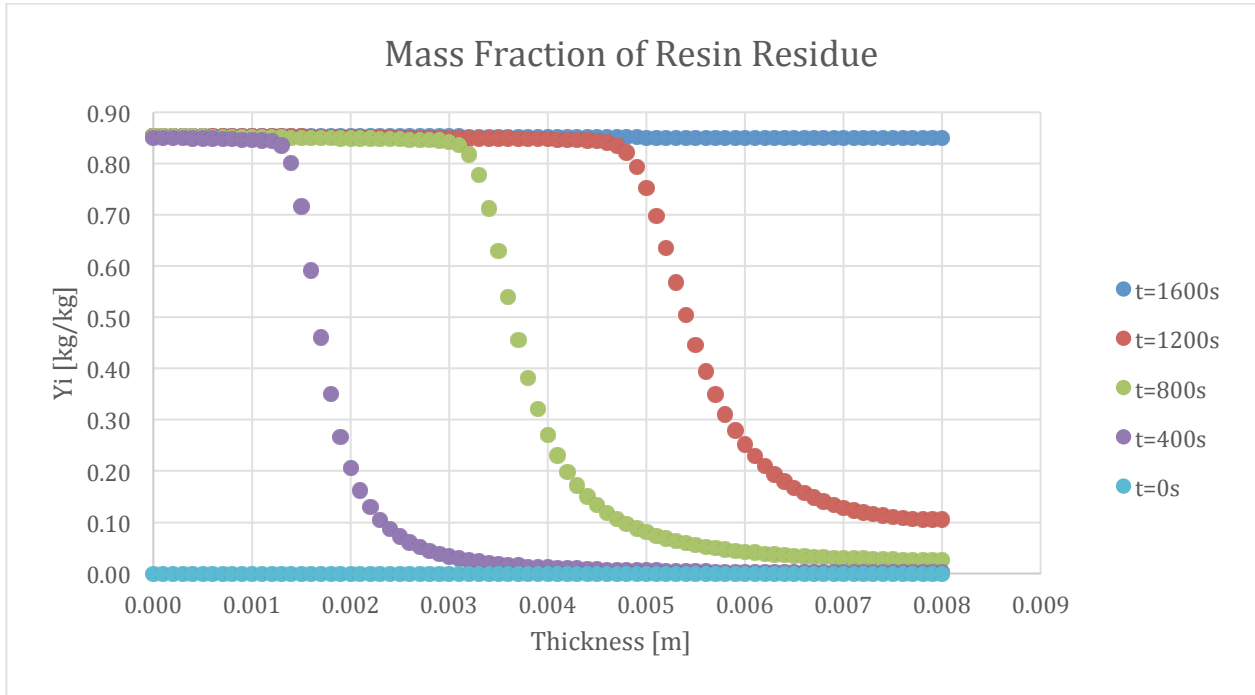


Figure 173-Mass Fraction Profile of Resin Residue for Epoxy with 5% ATH at 400 second intervals

The graph below seems to be varying a lot, but the scale is much smaller with a maximum of 5% initially. The wave form is a result of the burning of resin which increases the fraction of ATH at a specific thickness, where the crests can be seen.

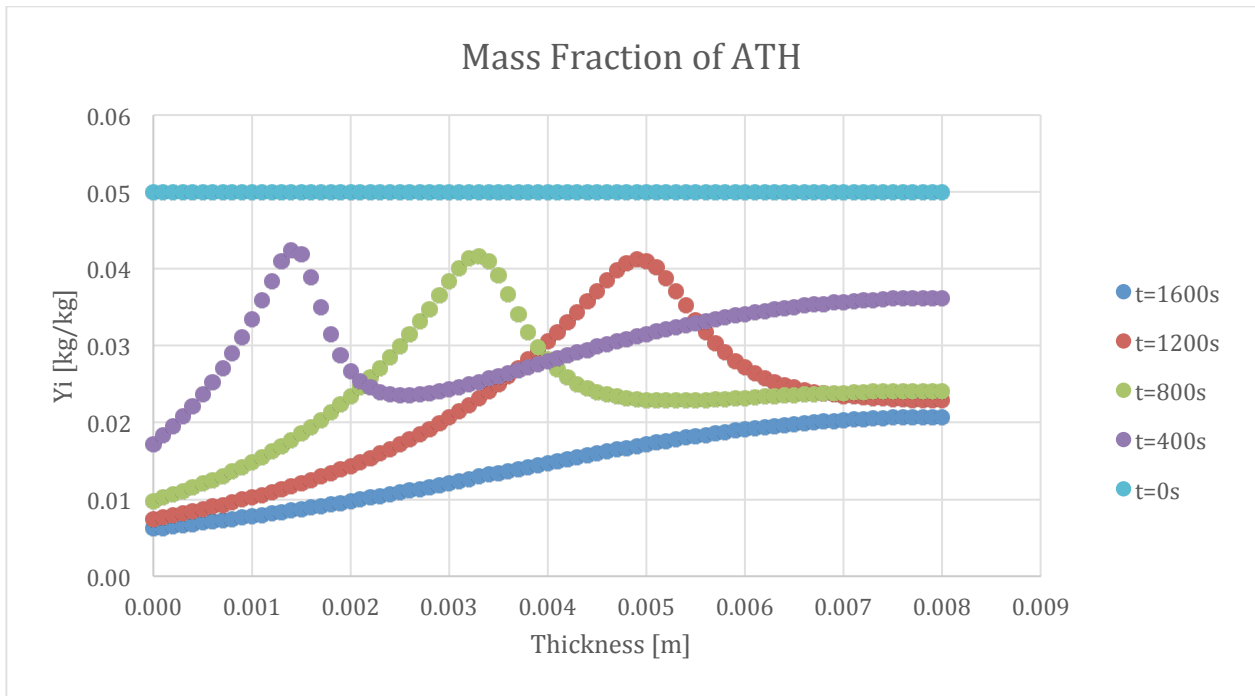


Figure 174-Mass Fraction Profile of ATH for Epoxy with 5% ATH at 400 second intervals

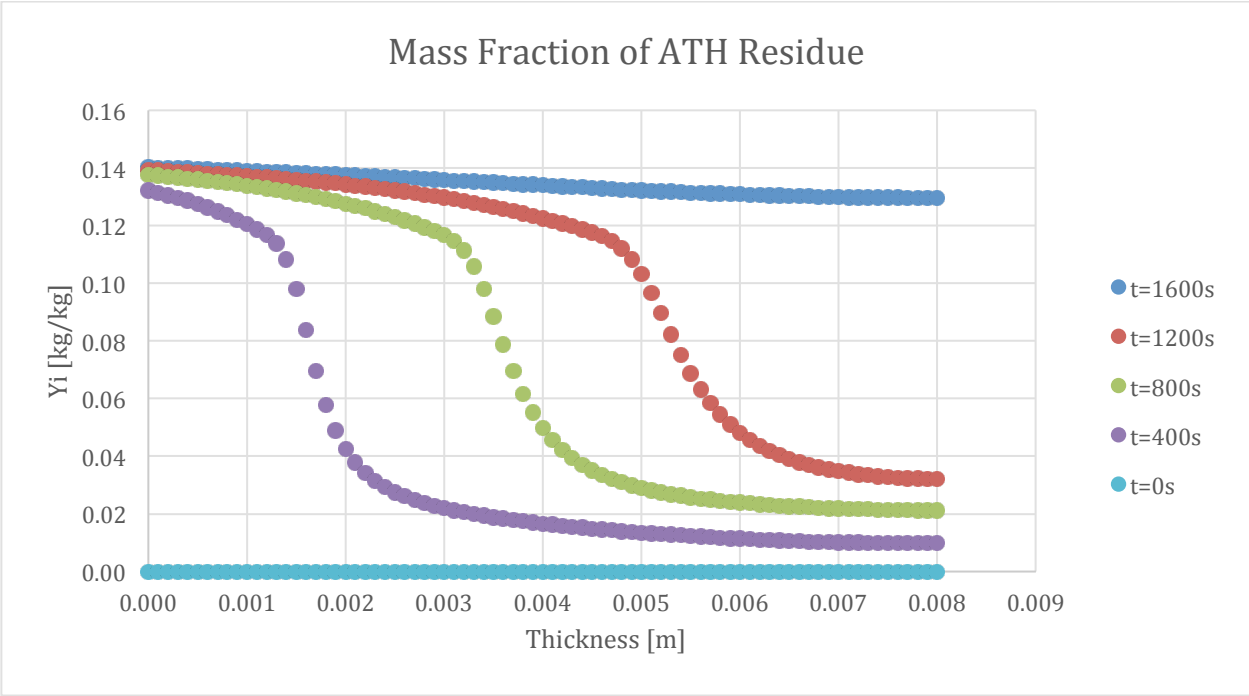


Figure 175-Mass Fraction Profile of ATH Residue for Epoxy with 5% ATH at 400 second intervals

9.4.4. Conversion

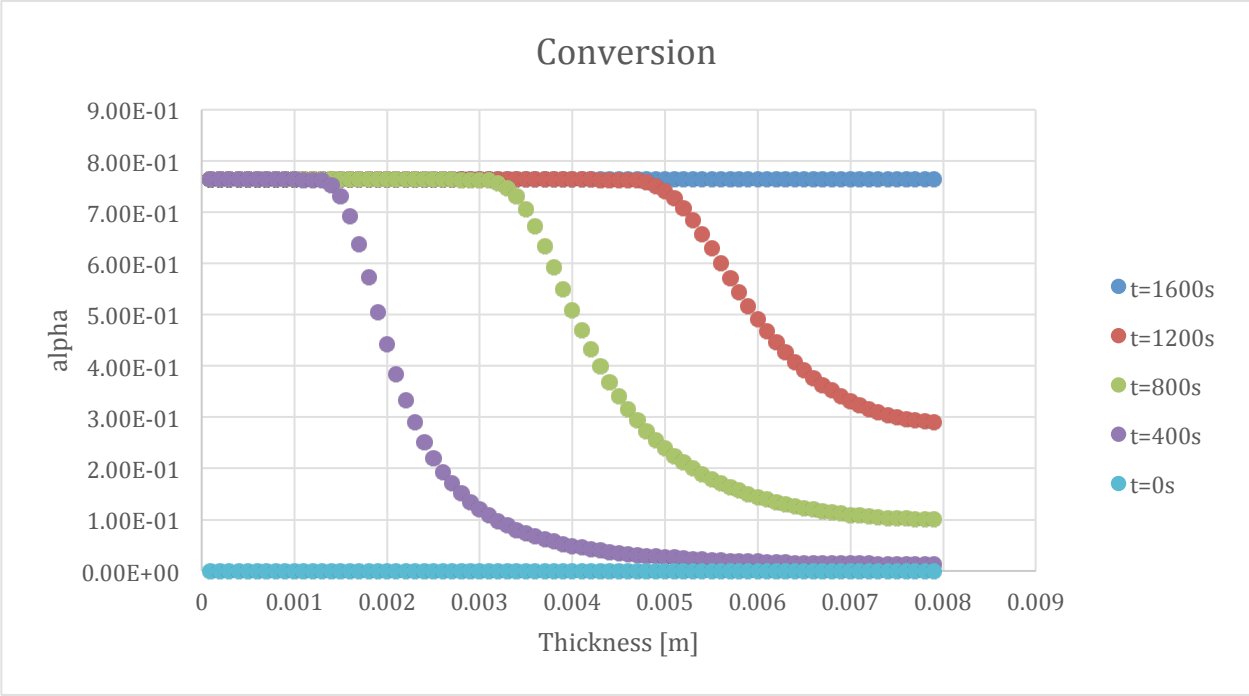


Figure 176-Conversion Profile for Epoxy with 5% ATH at 400 second intervals

9.4.5. Reaction Rate

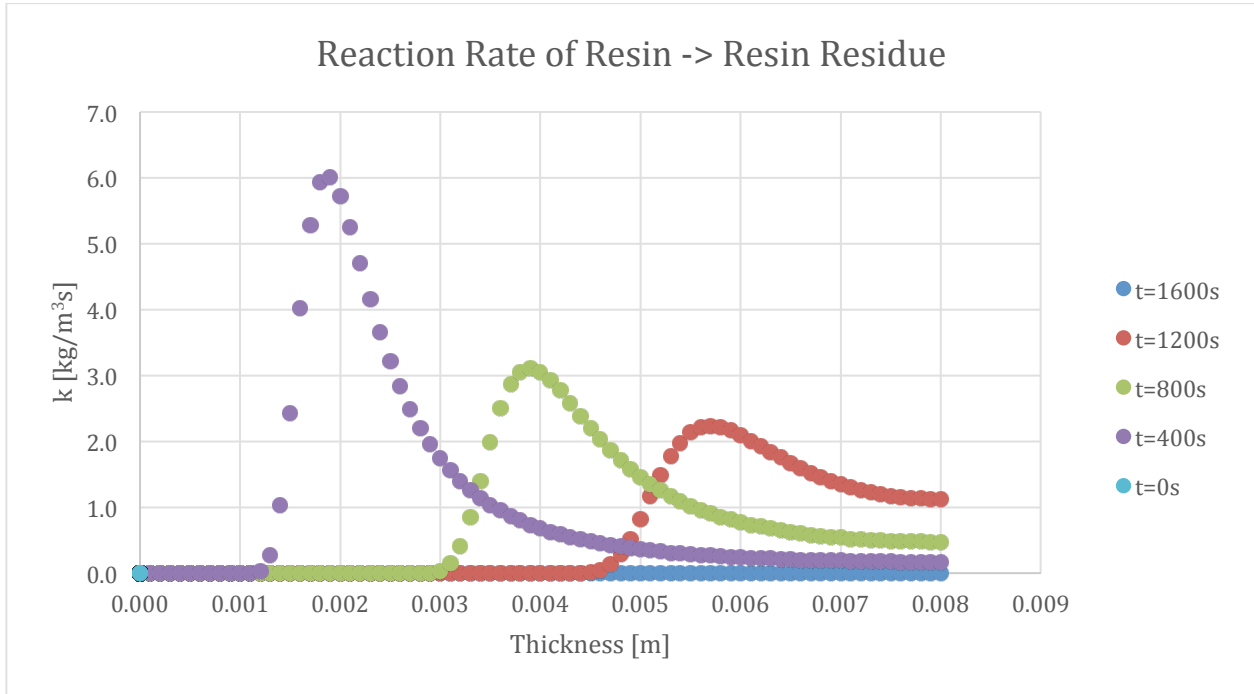


Figure 177-Reaction Rate Profile Resin to Resin Residue for Epoxy with 5% ATH at 400 second intervals

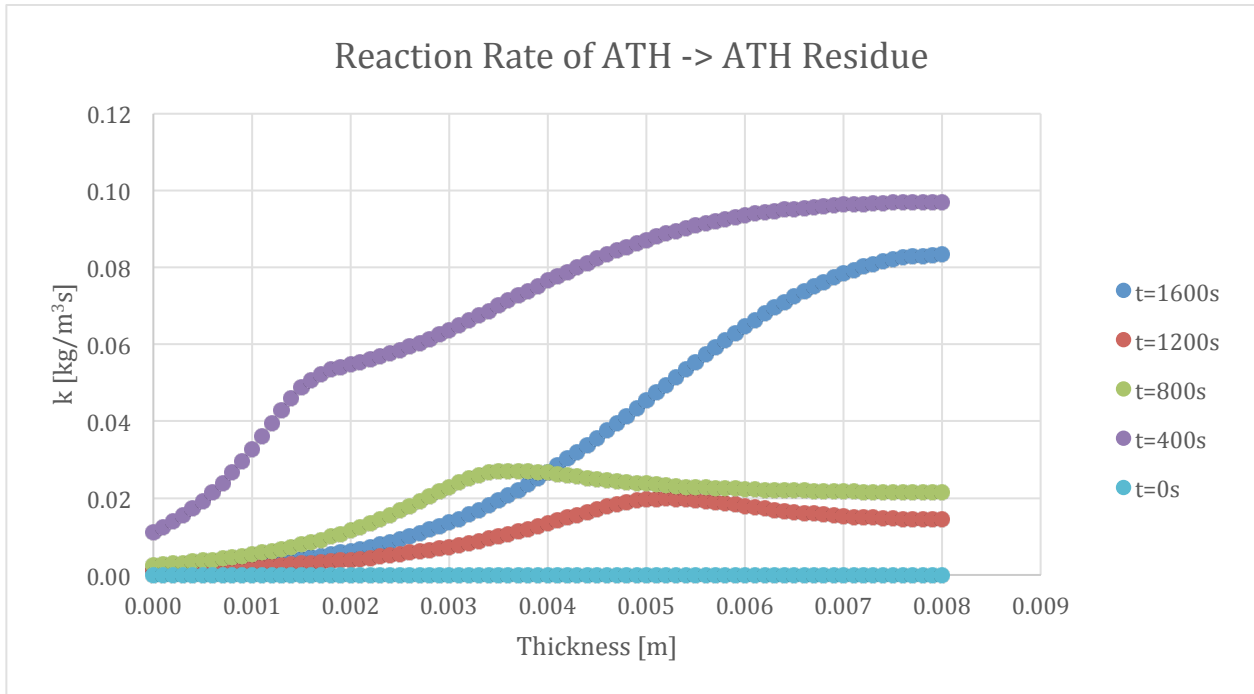


Figure 178-Reaction Rate Profile for ATH to ATH Residue for Epoxy with 5% ATH at 400 second intervals

9.4.6. Density

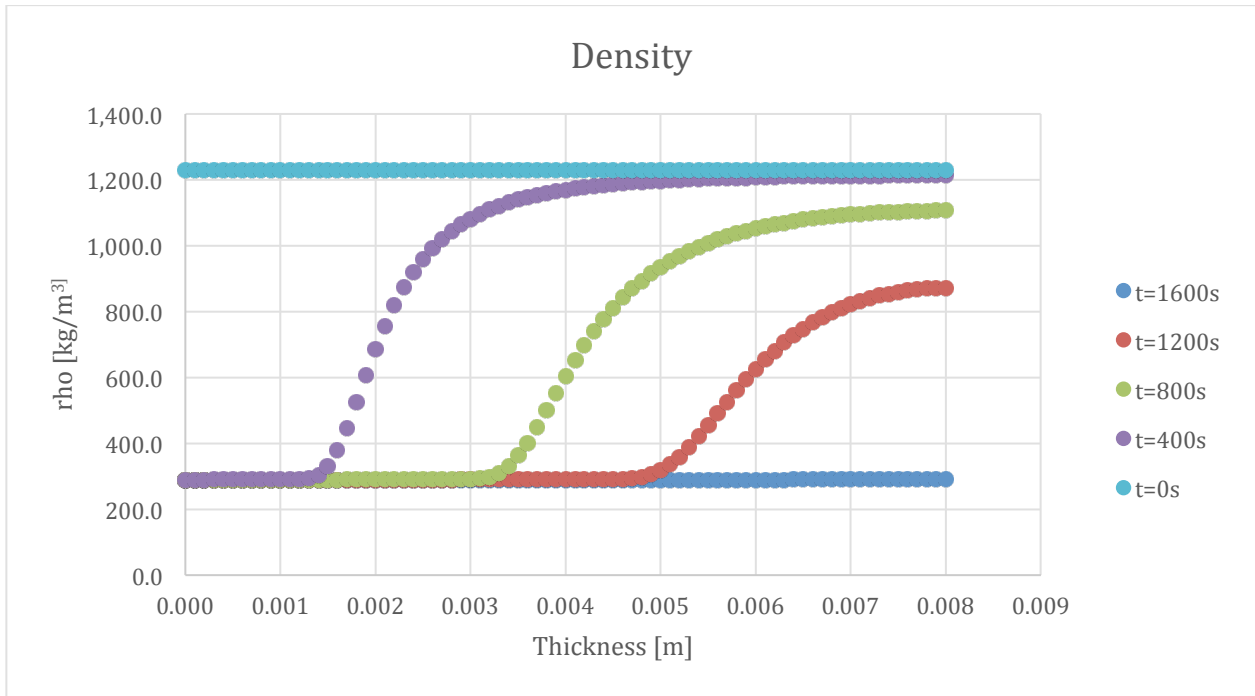


Figure 179-Density Profile for Epoxy with 5% ATH at 400 second intervals

9.4.7. Porosity

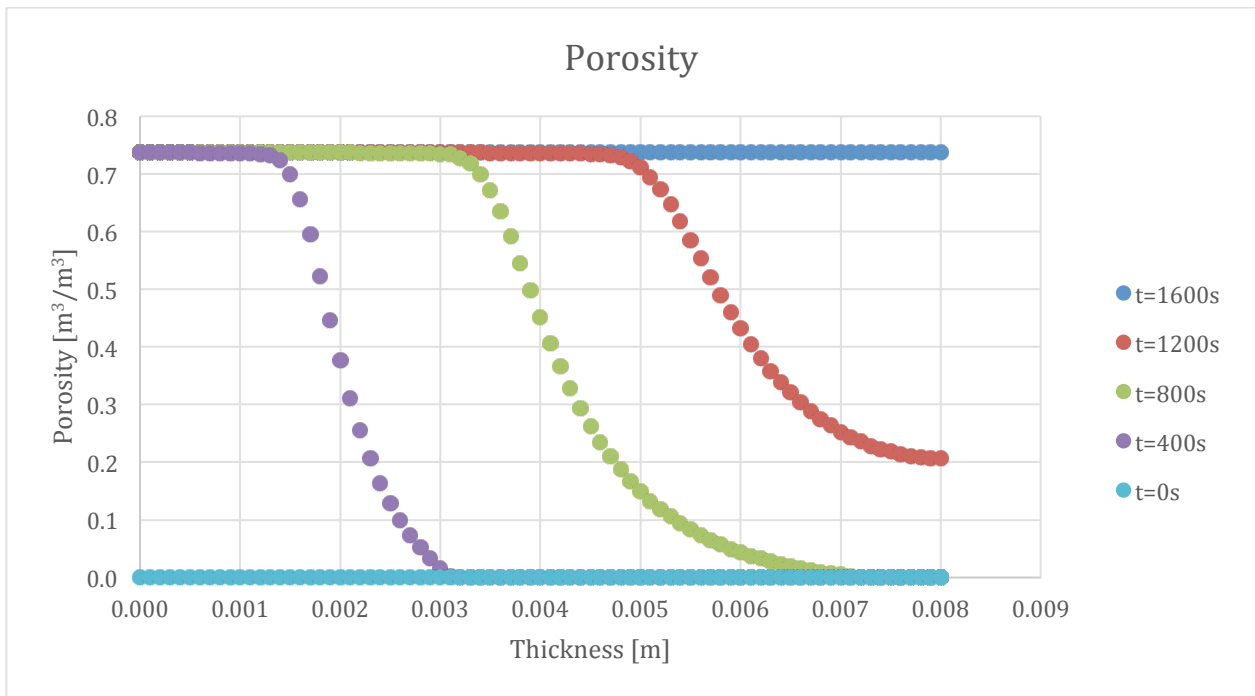


Figure 180-Porosity Profile for Epoxy with 5% ATH at 400 second intervals

9.5. Epoxy 10% ATH

This section shows the results of a simulation with Epoxy and 10% ATH. The results of this section follow the same trends as with Epoxy and 5% ATH.

9.5.1. Temperature Profile

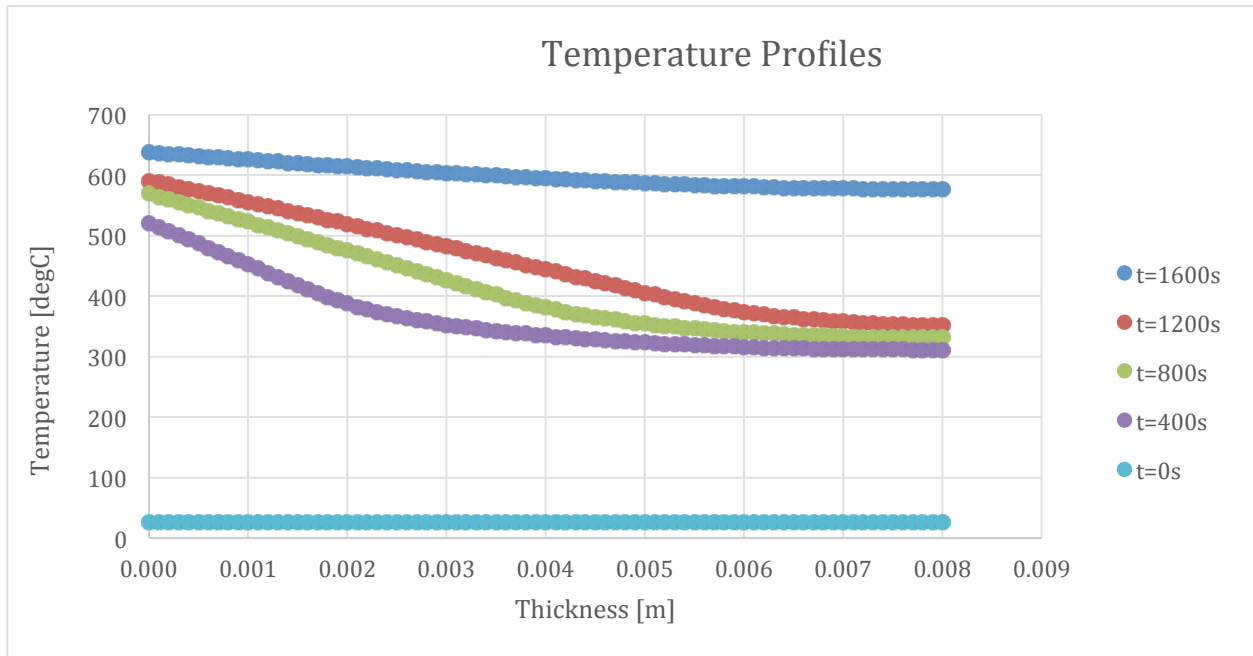


Figure 181-Temperature Profile for Epoxy with 10% ATH at 400 second intervals

9.5.2. Mass Loss Rate

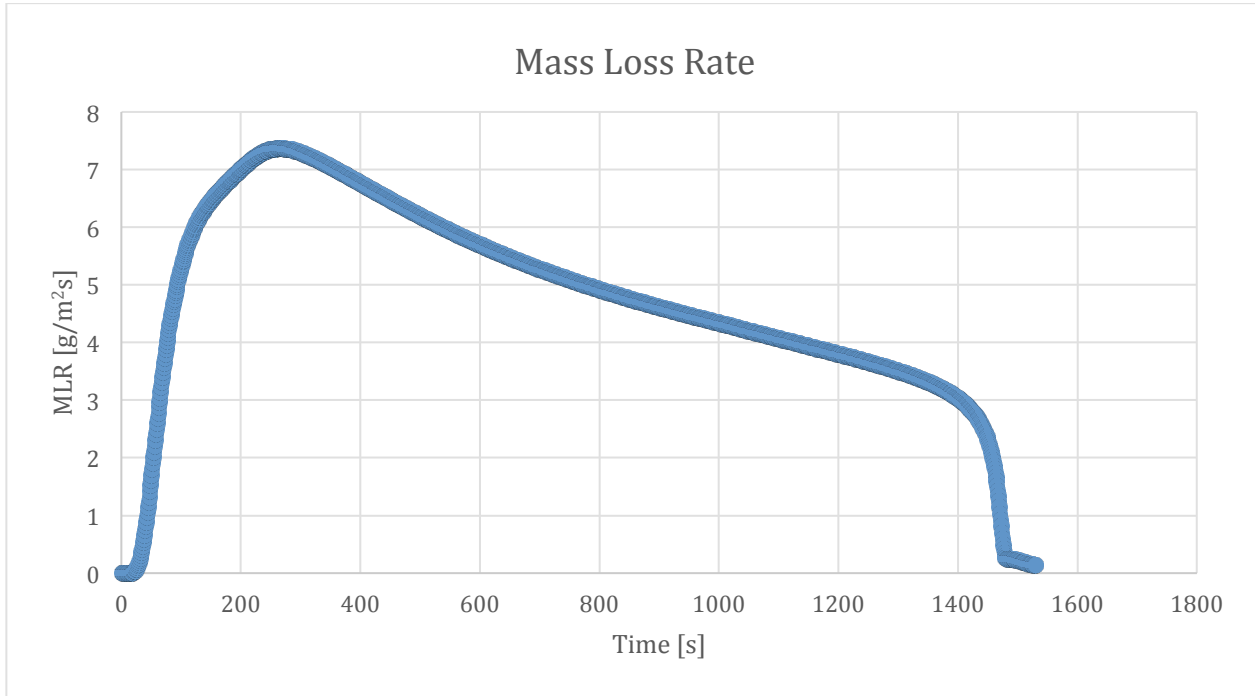


Figure 182-Mass Loss Rate curve for Epoxy with 10% ATH

9.5.3. Mass Fraction

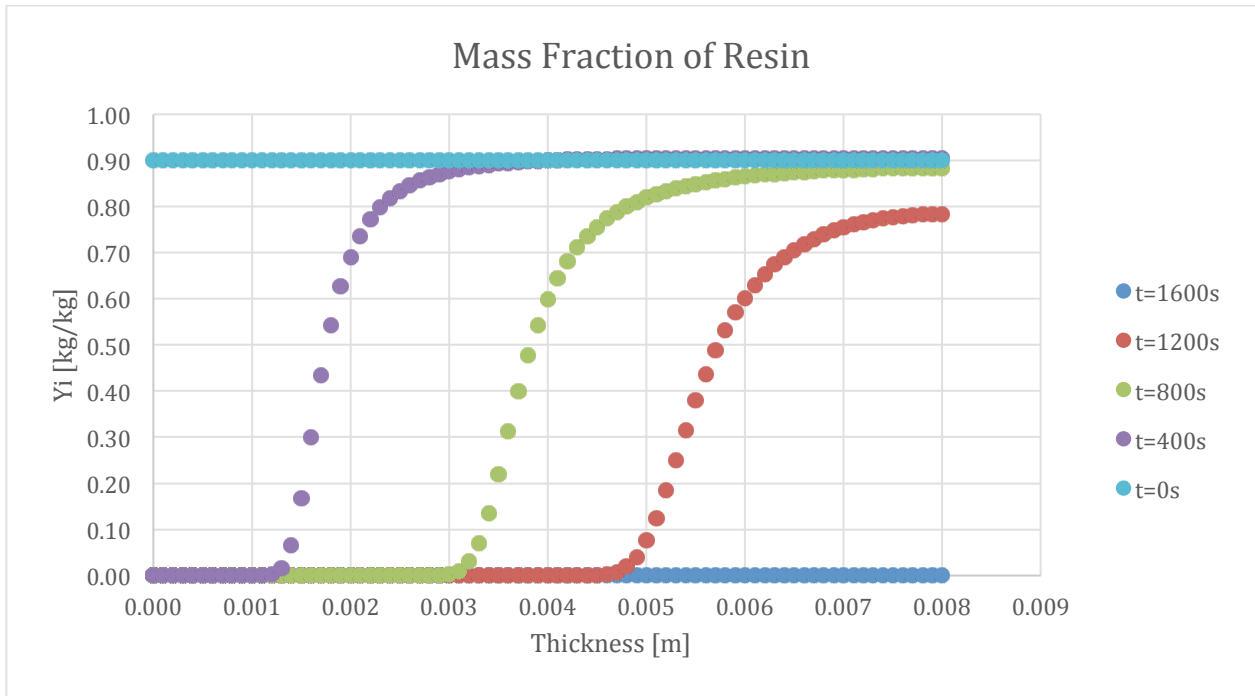


Figure 183-Mass Fraction Profile of Resin for Epoxy with 10% ATH at 400 second intervals

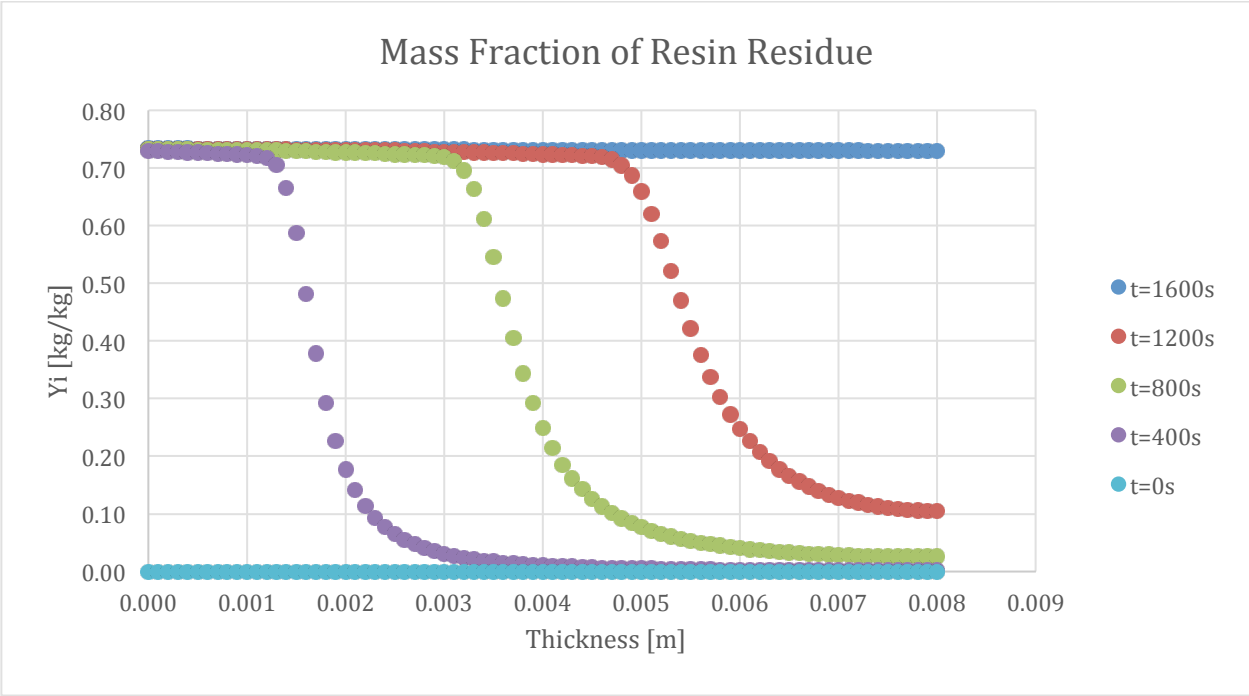


Figure 184-Mass Fraction Profile of Resin Residue for Epoxy with 10% ATH at 400 second intervals

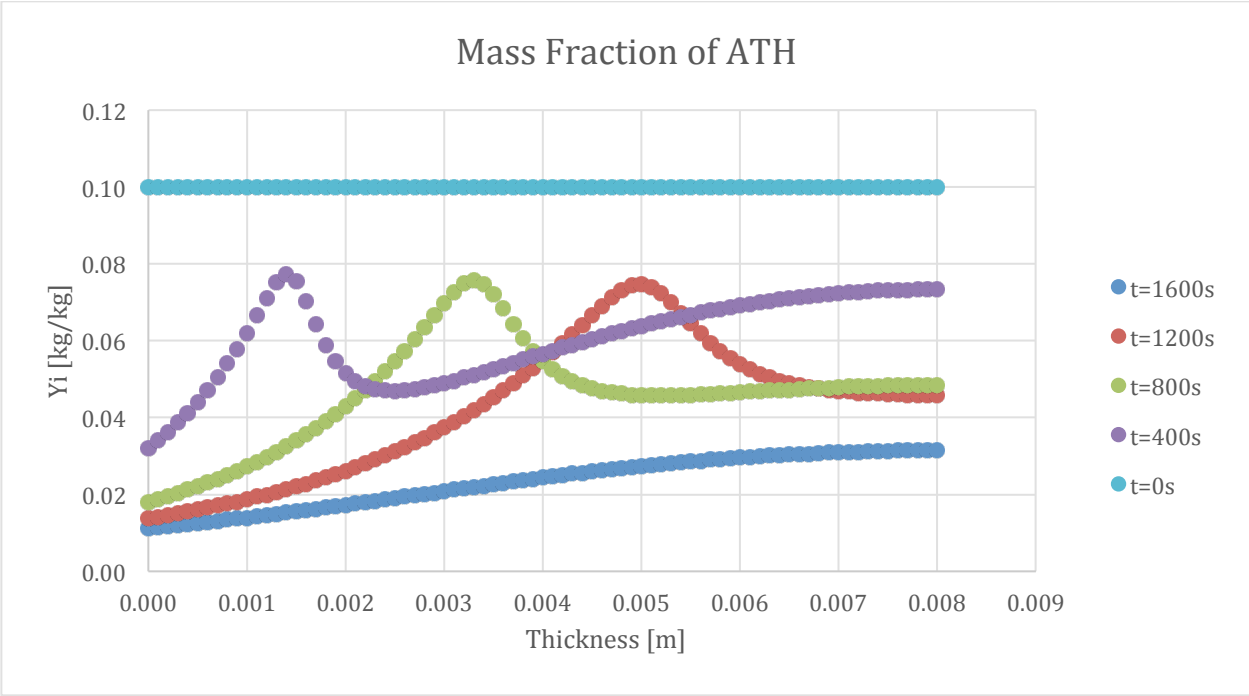


Figure 185-Mass Fraction Profile of ATH for Epoxy with 10% ATH at 400 second intervals

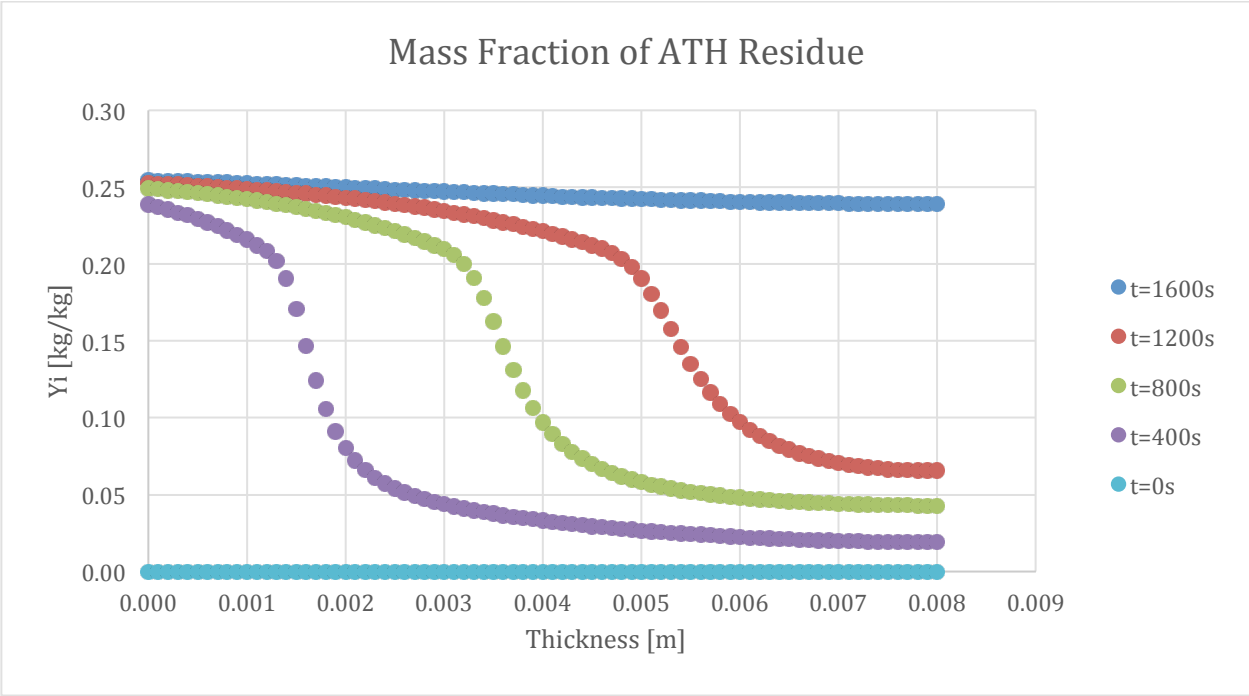


Figure 186-Mass Fraction Profile of ATH Residue for Epoxy with 10% ATH at 400 second intervals

9.5.4. Conversion

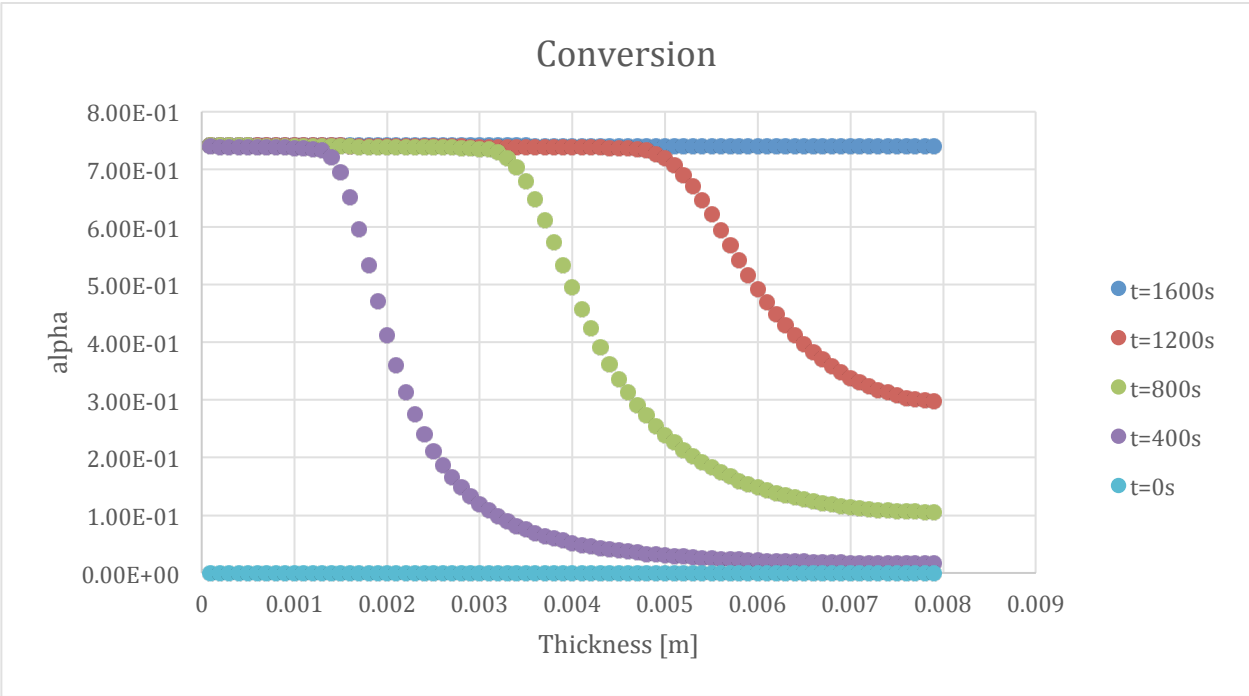


Figure 187-Converison Profile for Epoxy with 10% ATH at 400 second intervals

9.5.5. Reaction Rate

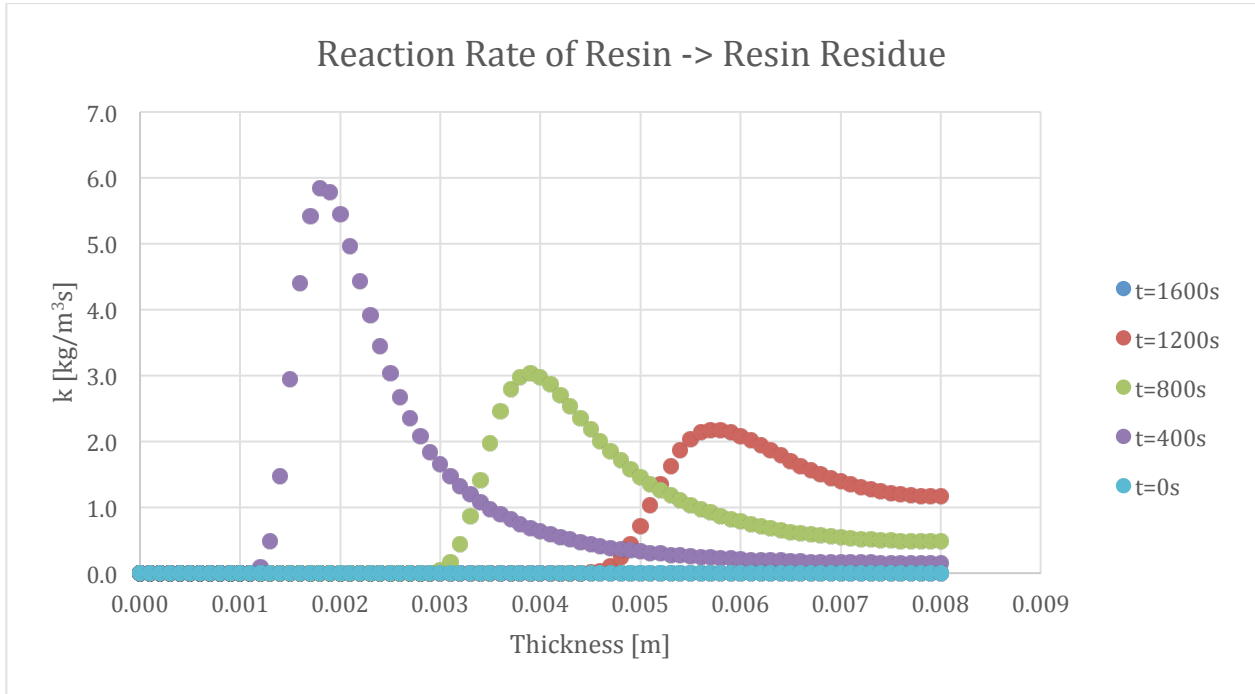


Figure 188-Reaction Rate Profile of Resin to Resin Residue for Epoxy with 10% ATH at 400 second intervals

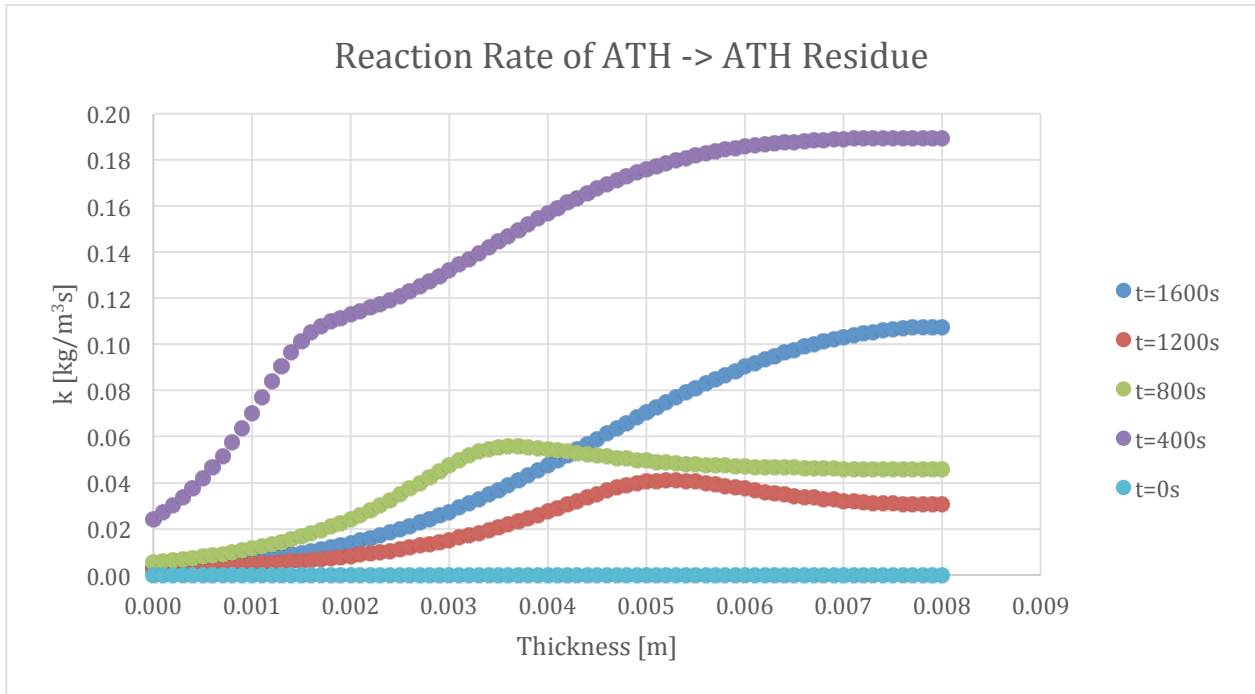


Figure 189-Reaction Rate Profile of ATH to ATH Residue for Epoxy with 10% ATH at 400 second intervals

9.5.6. Density

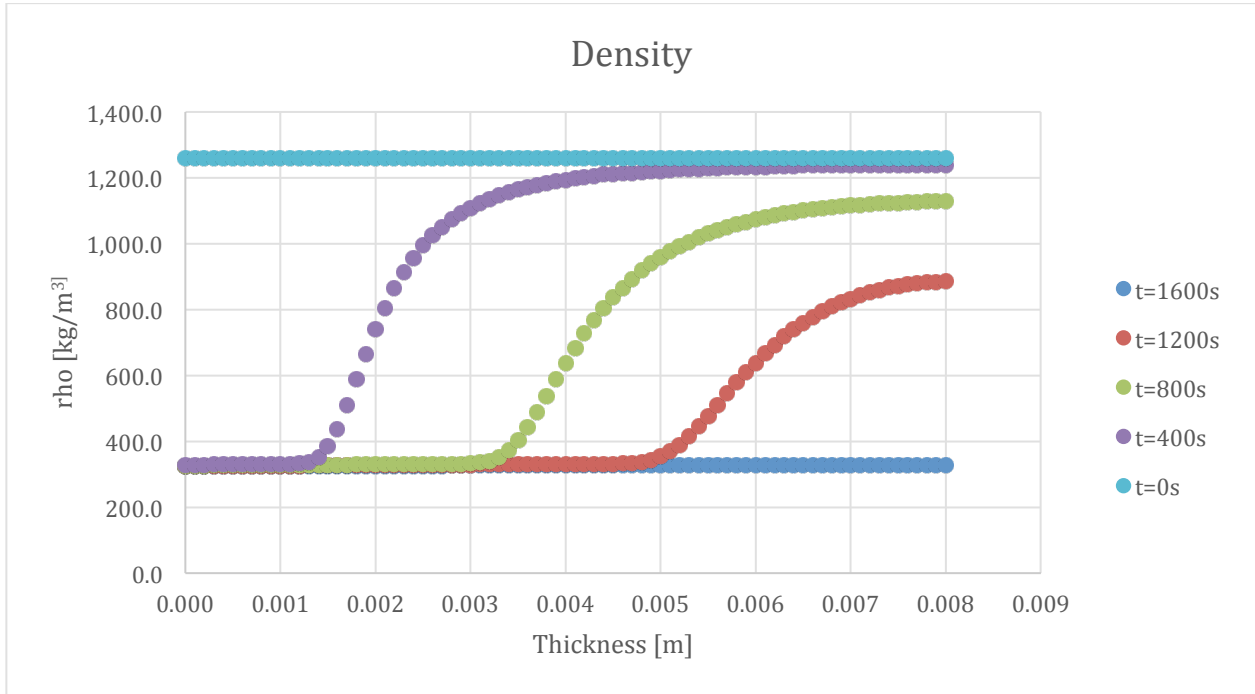


Figure 190-Density Profile for Epoxy with 10% ATH at 400 second intervals

9.5.7. Porosity

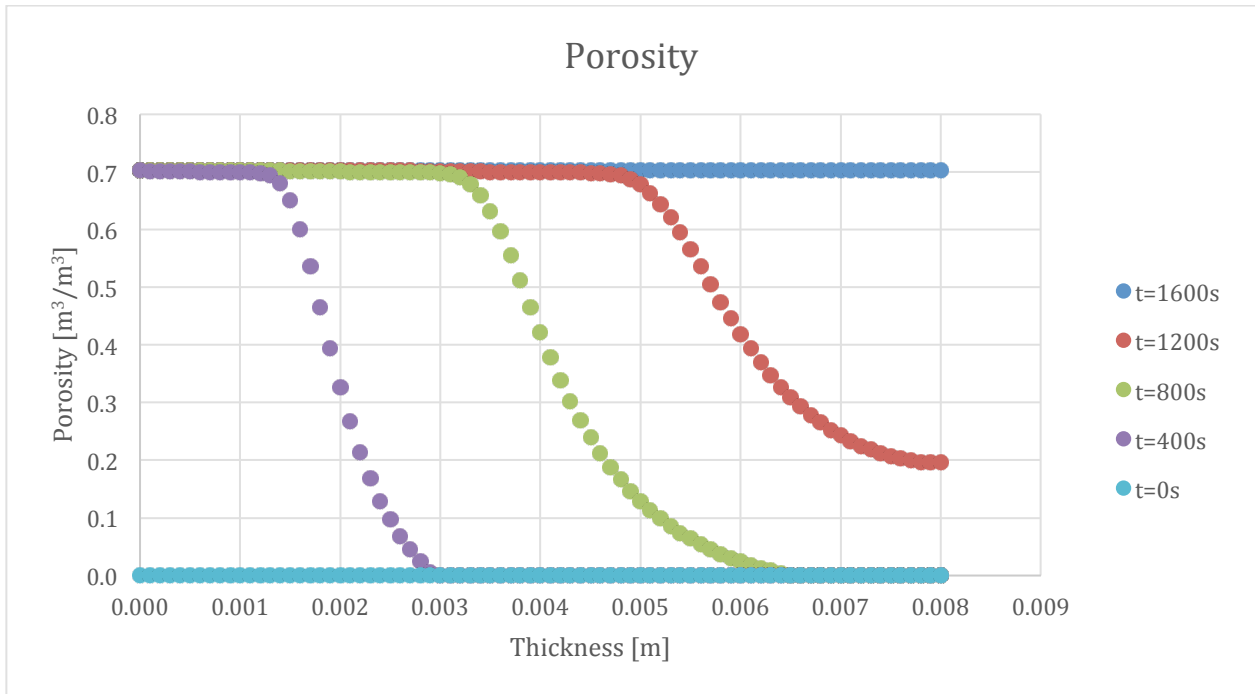


Figure 191-Porosity Profile for Epoxy with 10% ATH at 400 second intervals

9.6. Epoxy 20% ATH

The simulation with Epoxy and 20% ATH follows the same trends as the previous two sections.

9.6.1. Temperature Profile

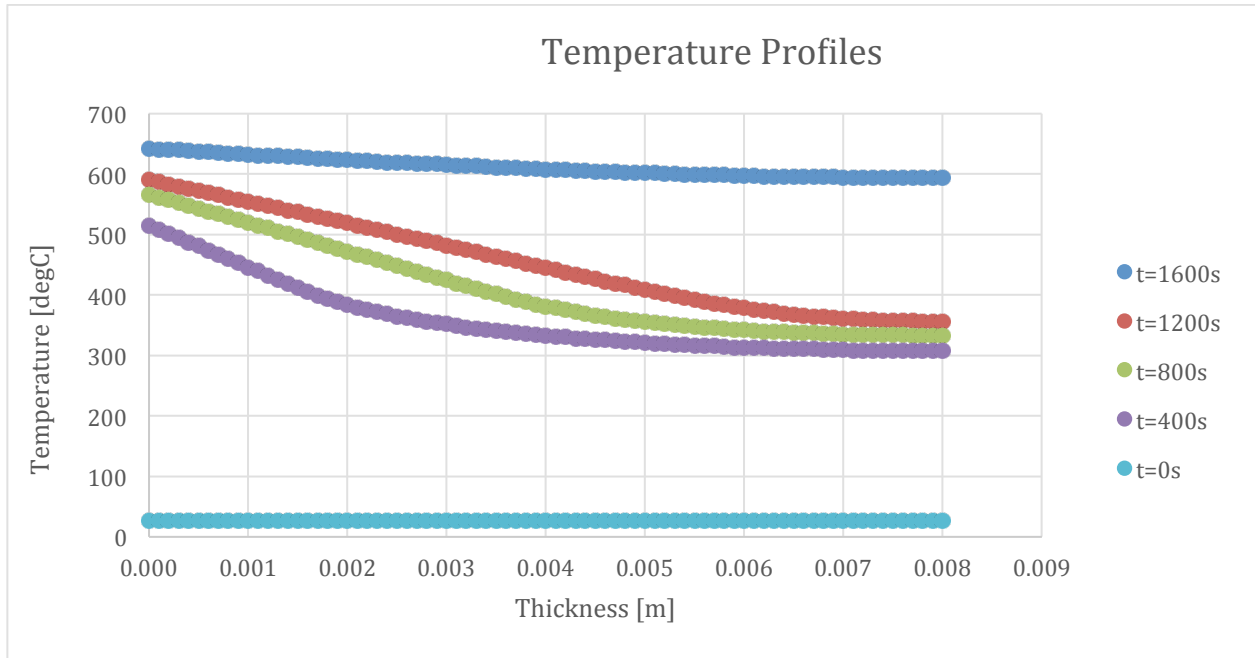


Figure 192-Temperature Profile for Epoxy with 20% ATH at 400 second intervals

9.6.2. Mass Loss Rate

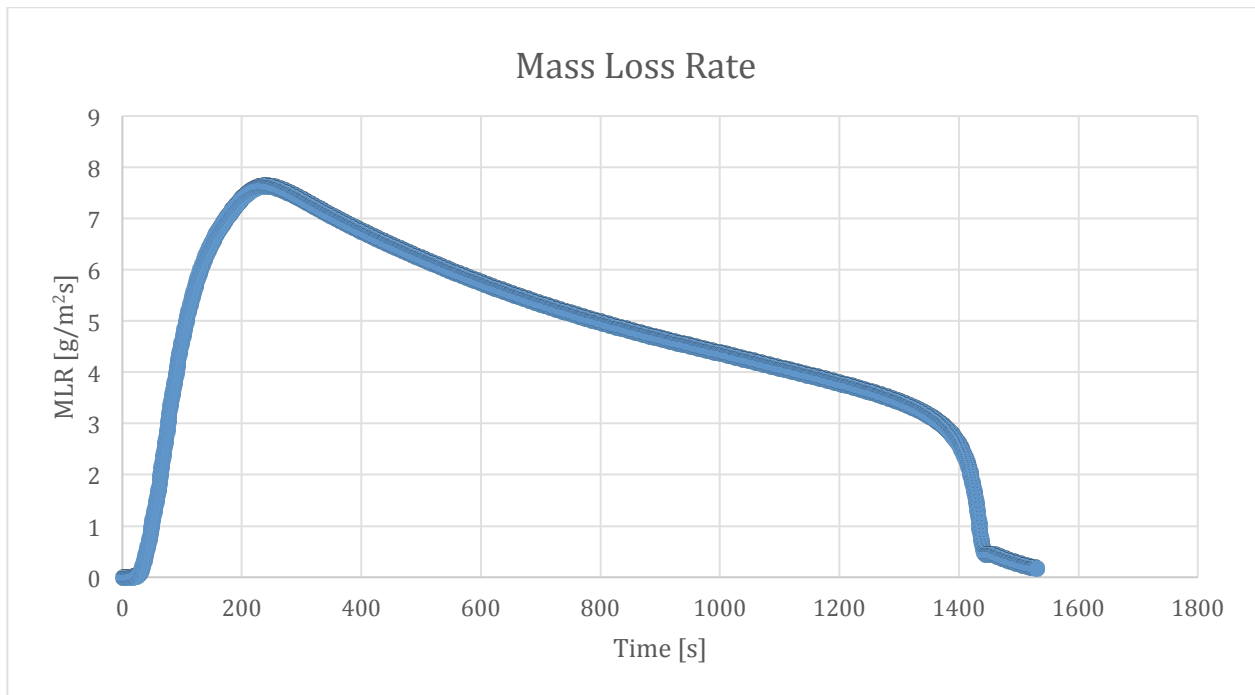


Figure 193-Mass Loss Rate curve for Epoxy with 20% ATH

9.6.3. Mass Fraction

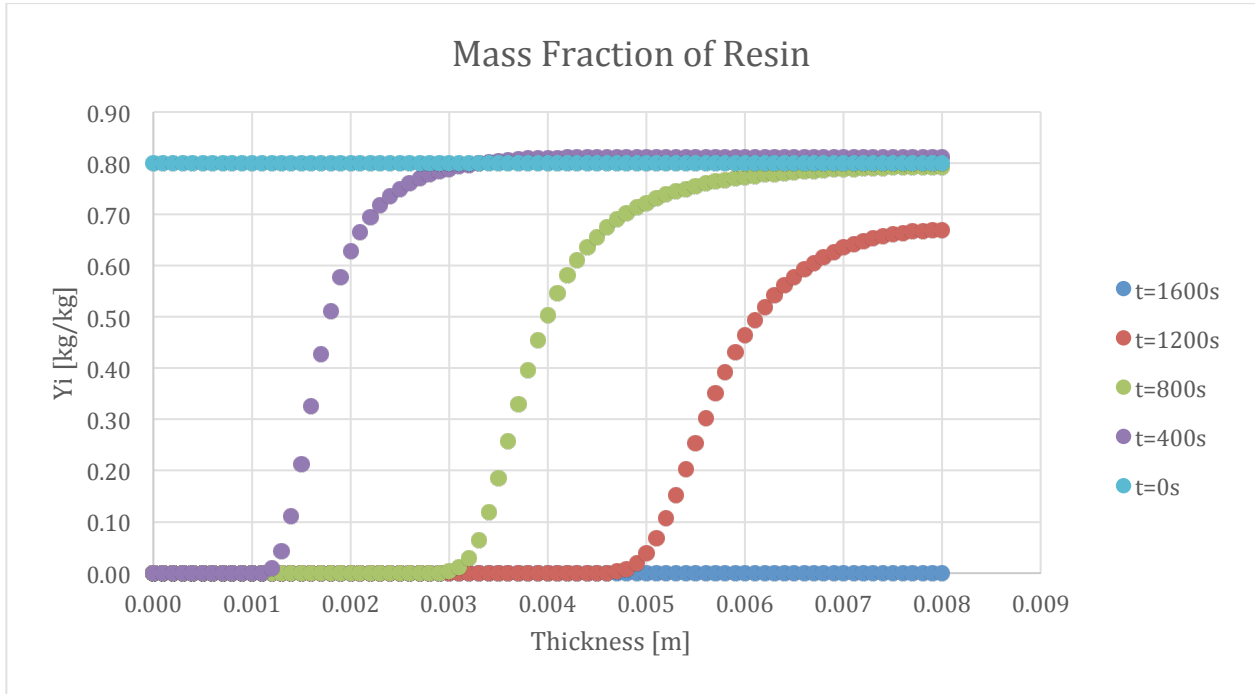


Figure 194-Mass Fraction Profile of Resin for Epoxy with 20% ATH at 400 second intervals

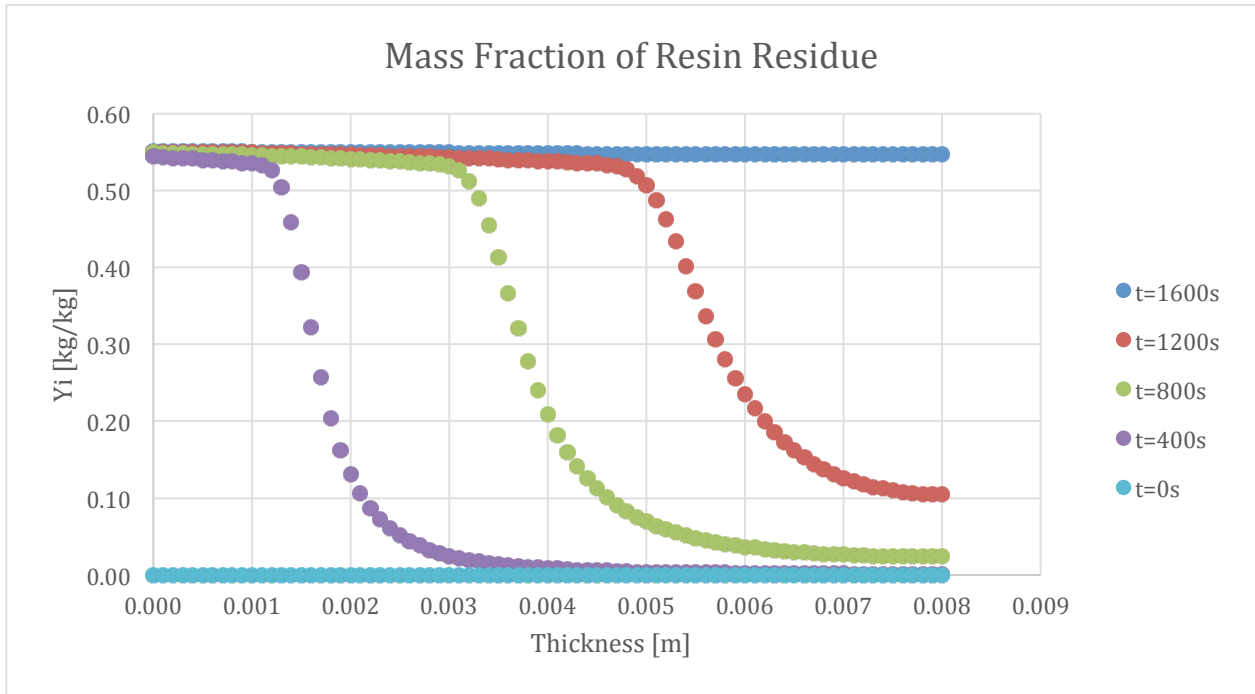


Figure 195-Mass Fraction Profile of Resin Residue for Epoxy with 20% ATH at 400 second intervals

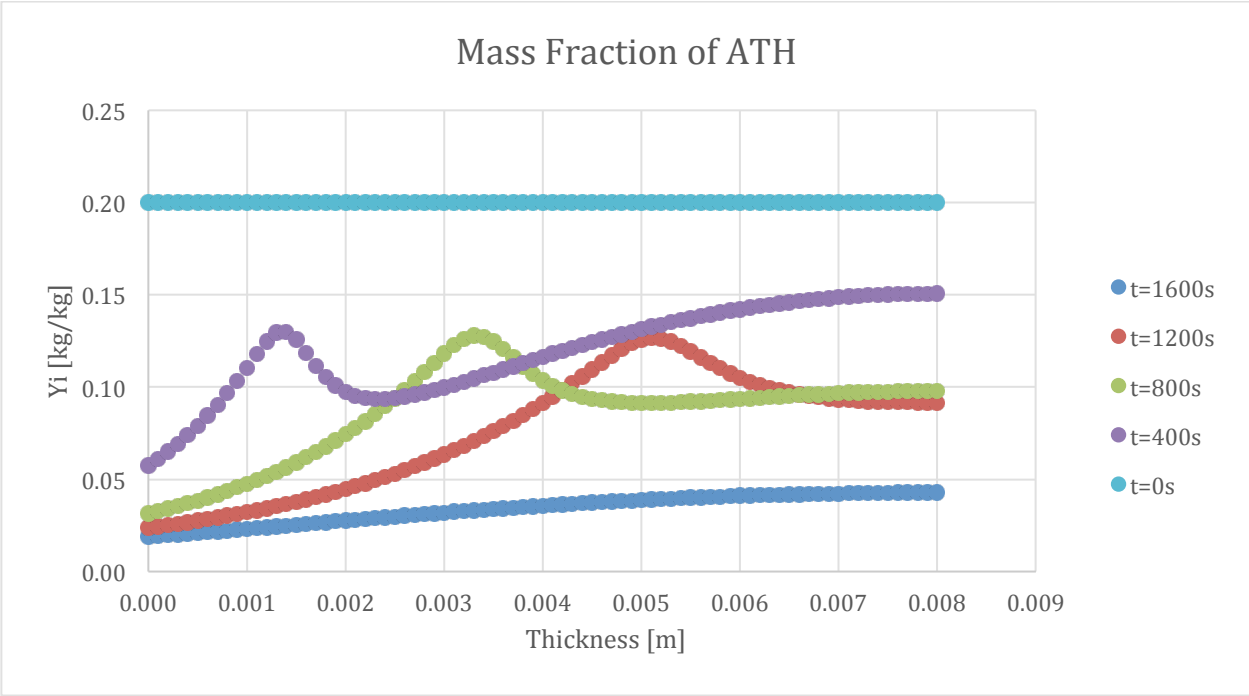


Figure 196-Mass Fraction Profile of ATH for Epoxy with 20% ATH at 400 second intervals

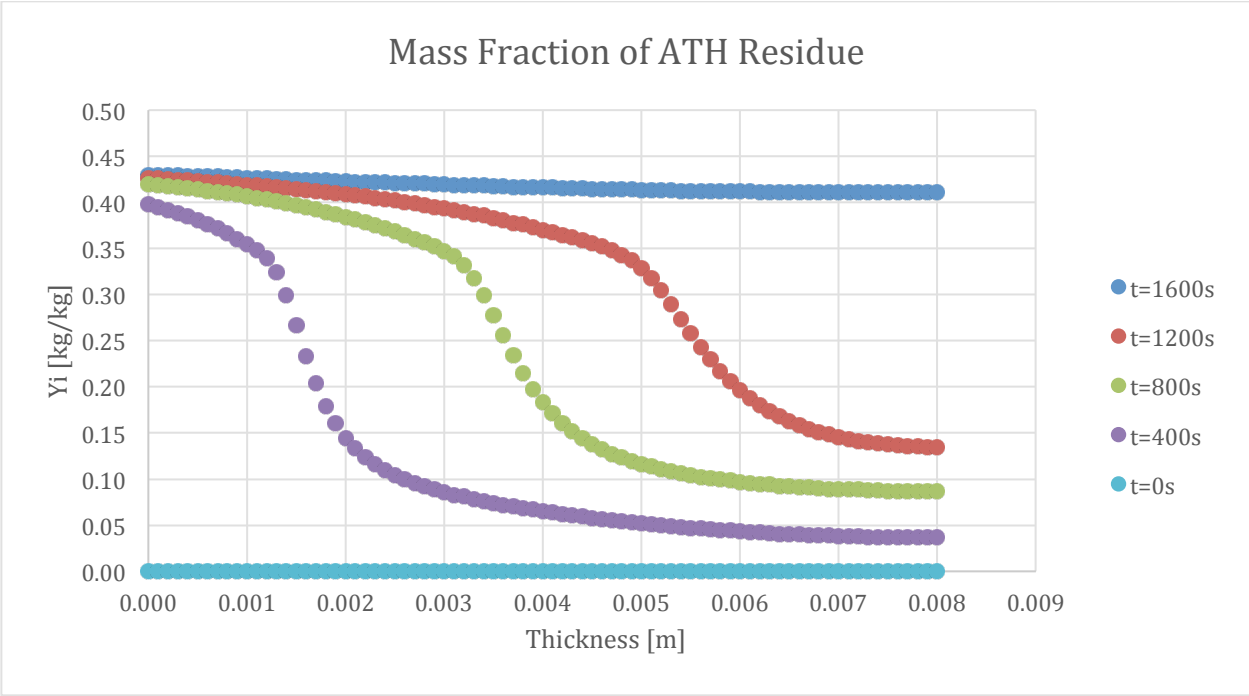


Figure 197-Mass Fraction Profile of ATH Residue for Epoxy with 20% ATH at 400 second intervals

9.6.4. Conversion

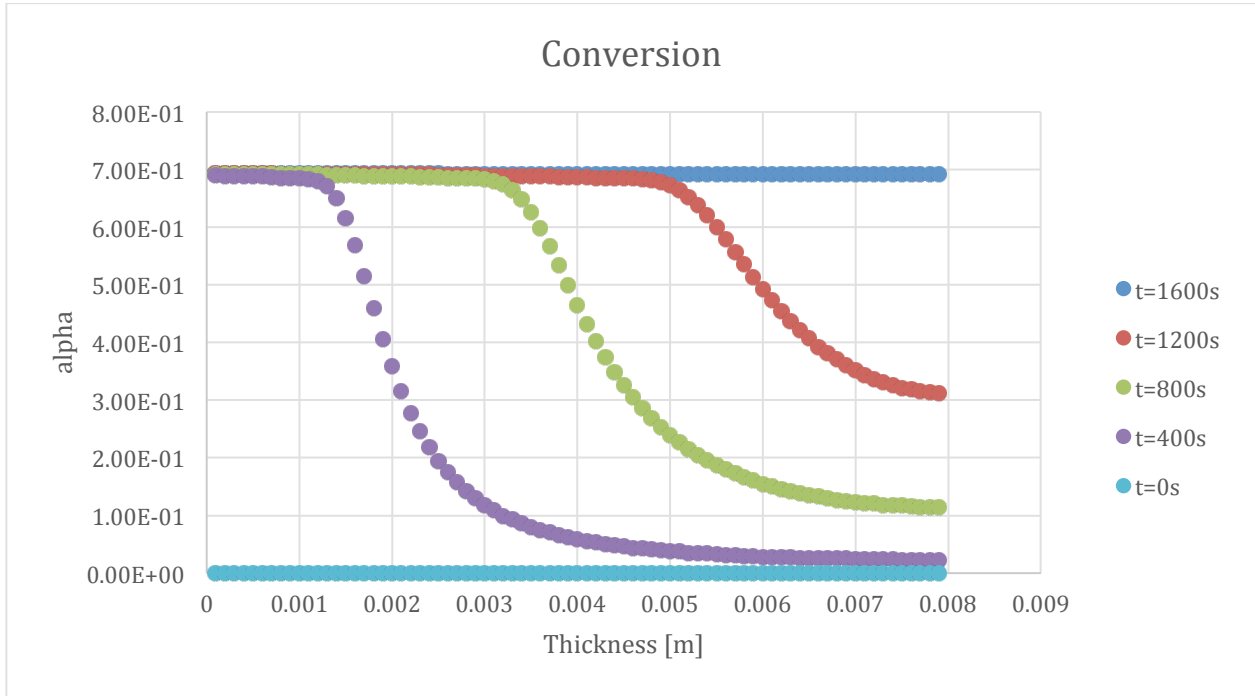


Figure 198-Conversion Profile for Epoxy with 20% ATH at 400 second intervals

9.6.5. Reaction Rate

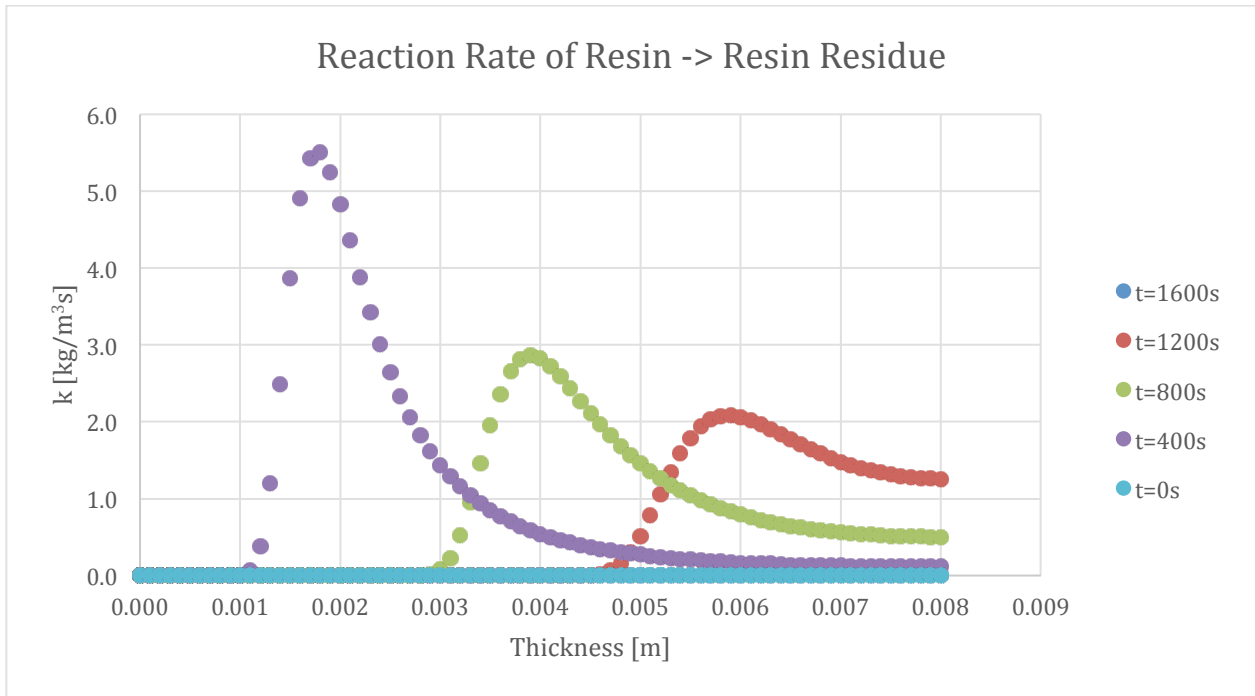


Figure 199-Reaction Rate Profile of Resin to Resin Residue for Epoxy with 20% ATH at 400 second intervals

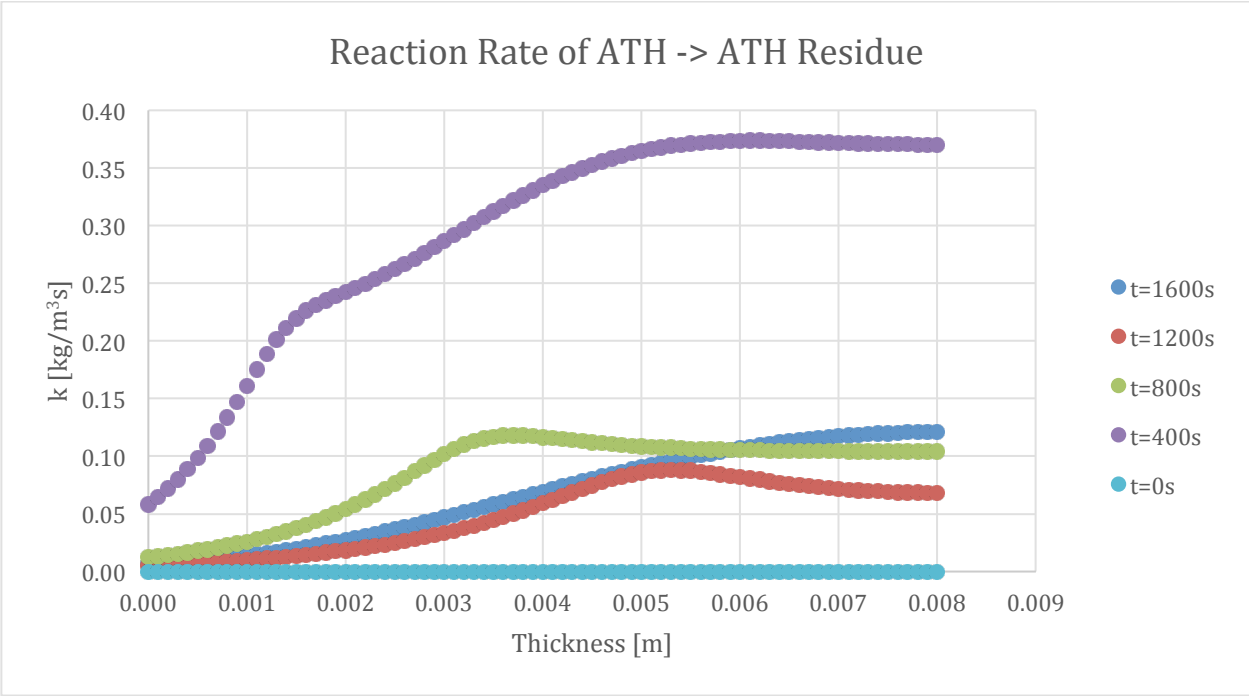


Figure 200-Reaction Rate Profile of ATH to ATH Residue for Epoxy with 20% ATH at 400 second intervals

9.6.6. Density

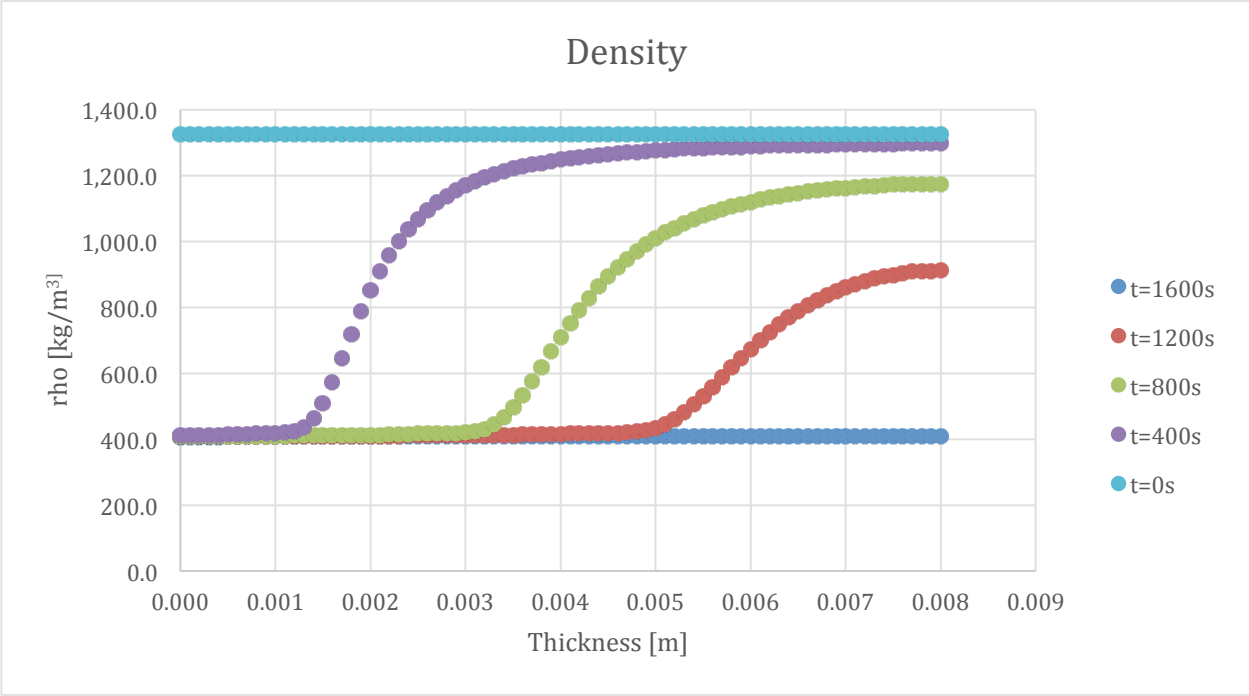


Figure 201-Density Profile for Epoxy with 20% ATH at 400 second intervals

9.6.7. Porosity

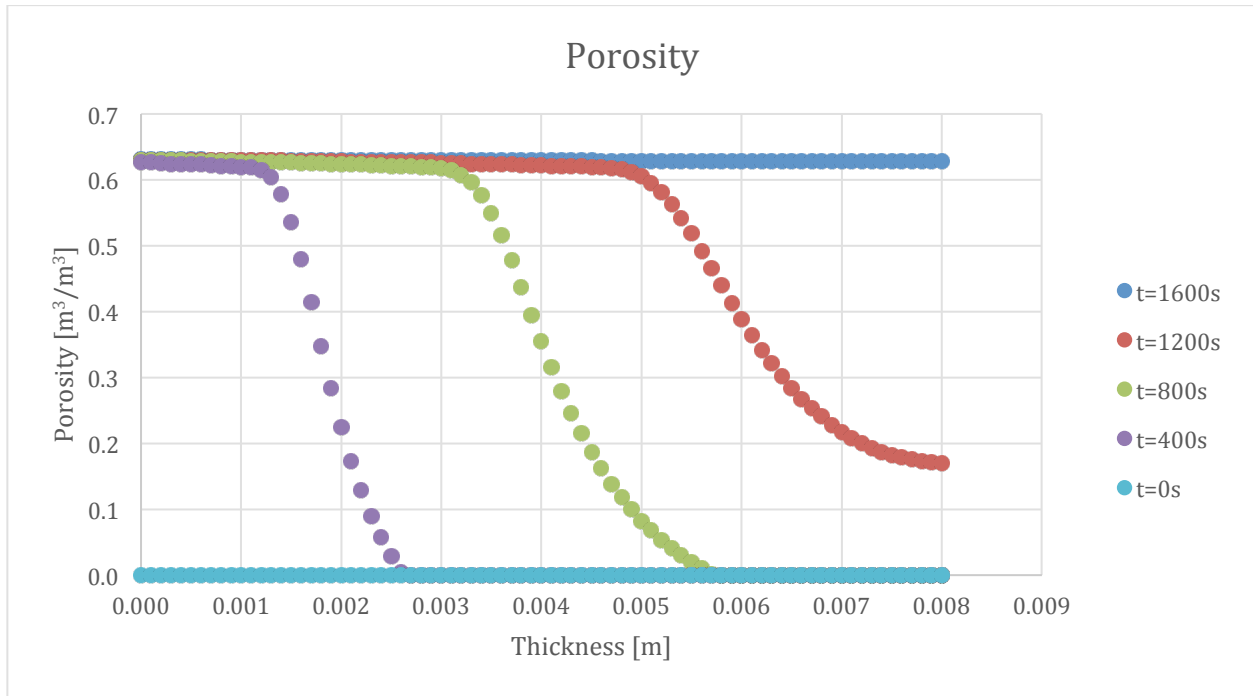


Figure 202-Porosity Profile for Epoxy with 20% ATH at 400 second intervals

9.7. Comparisons of Varied ATH

This section will be devoted to comparing the specimens with different levels of ATH for each property.

9.7.1. Mass Loss Rate

The mass loss rate of the 20% specimen peaks higher than the other systems, but is also does not burn as long or as soon. The graph likely has a higher peak because the ATH reaction will delay the resin reaction, but eventually they will both be burning. ATH is also more dense than Resin, so the more mass there is in the system, the higher the rate can be.

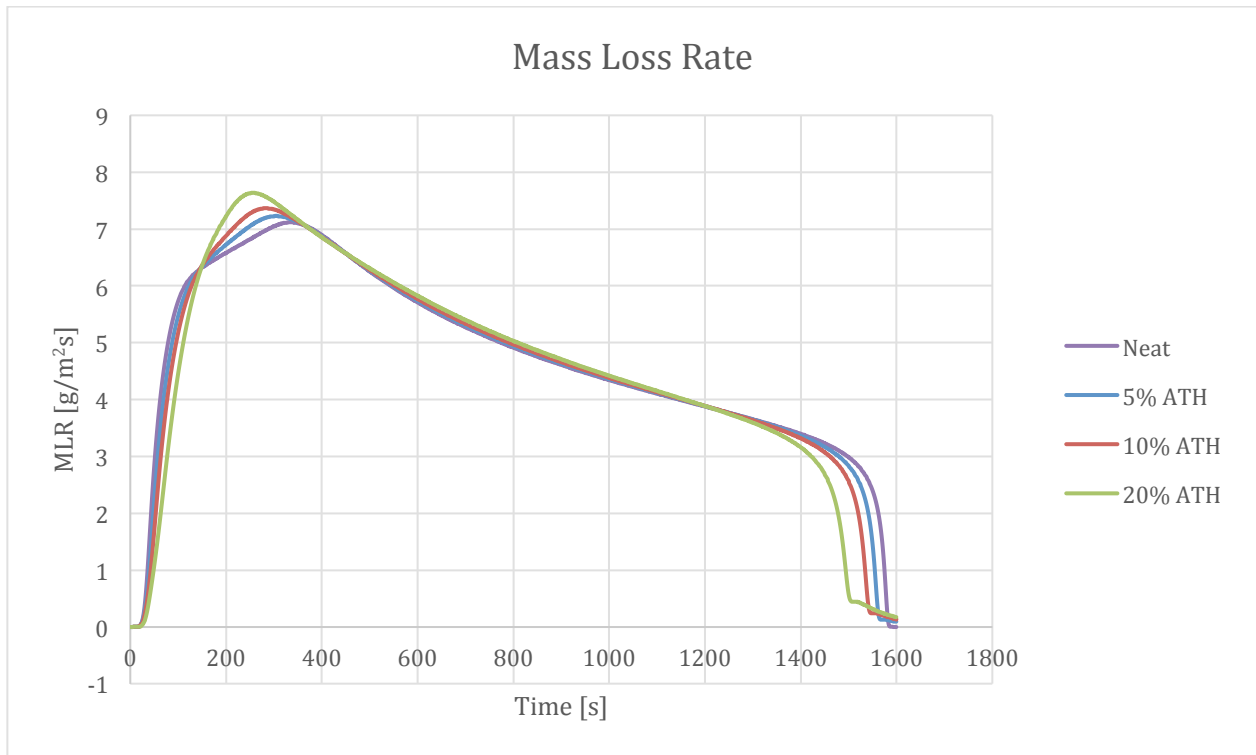


Figure 203-Comparison of Mass Loss Rate curves for varying levels of ATH

9.7.2. Reaction Rate 1

The figures below show the progression of the reaction from resin to residue at several time steps. The 0 and 1500 seconds are not included because the rate was zero for both. The 20% specimen had the lowest reaction rate for each of the times and reacted the least into the sample. This is due to the delay caused by the reaction of ATH.

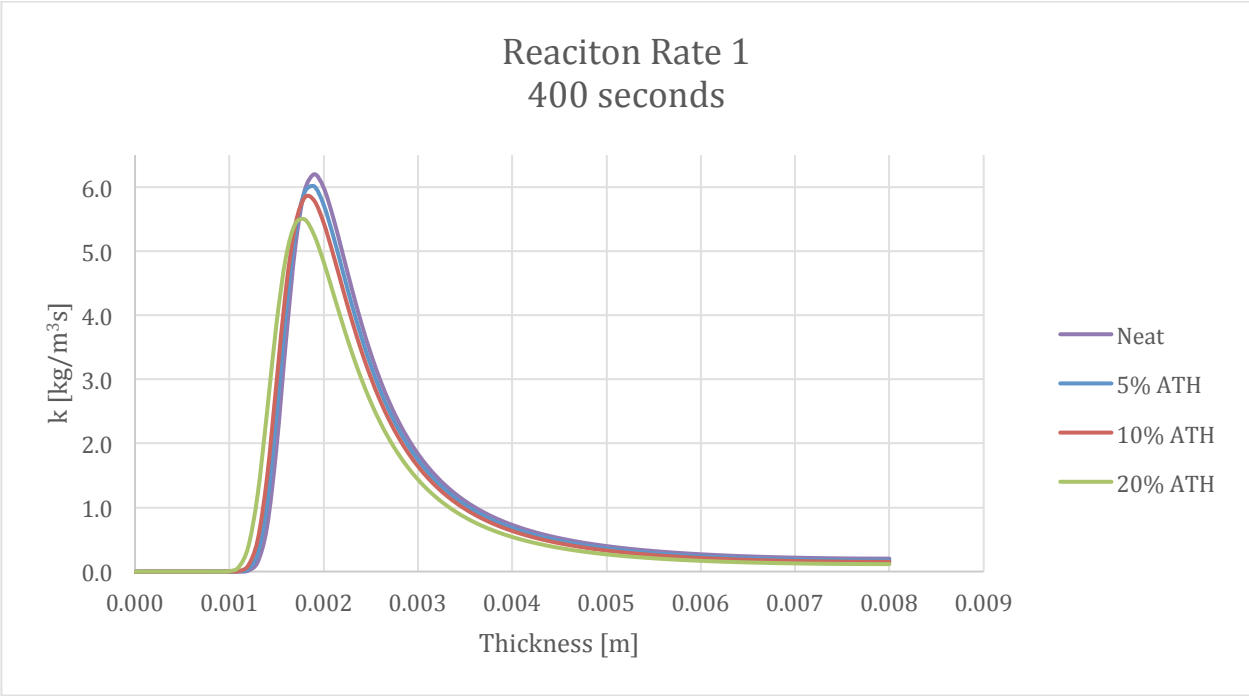


Figure 204a- Reaction Rate of Resin to Resin Residue with varying ATH at 400 seconds

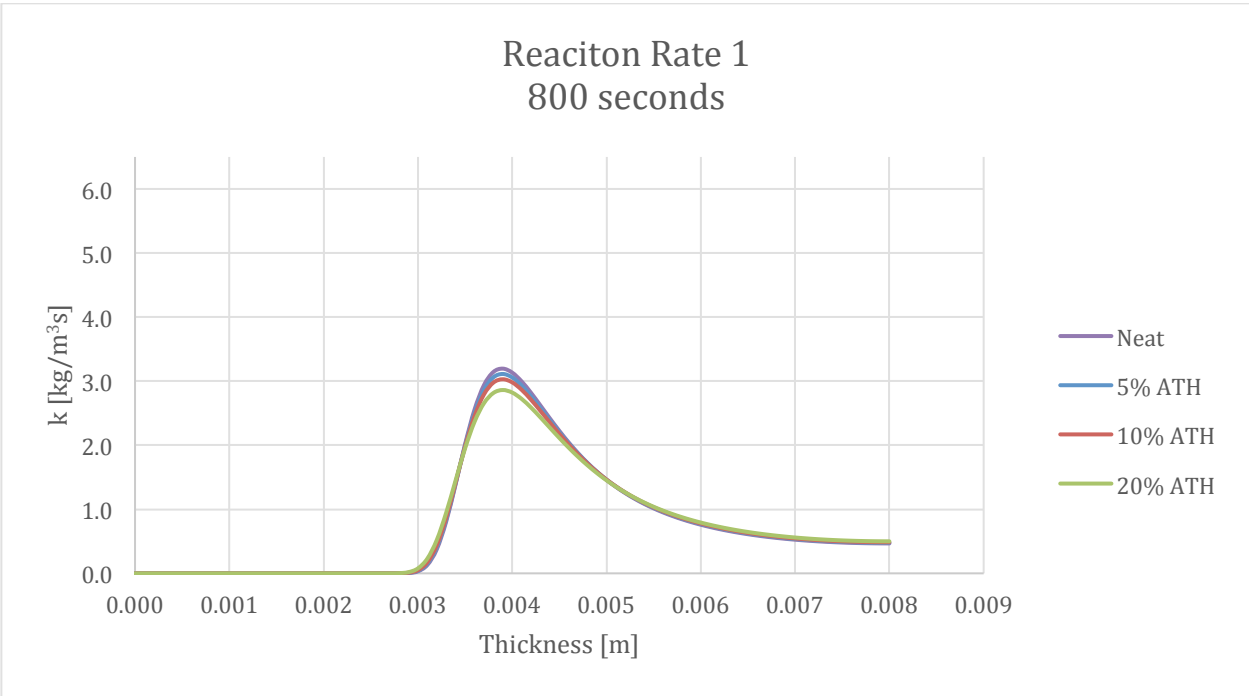


Figure 205-- Reaction Rate of Resin to Resin Residue with varying ATH at 800 seconds

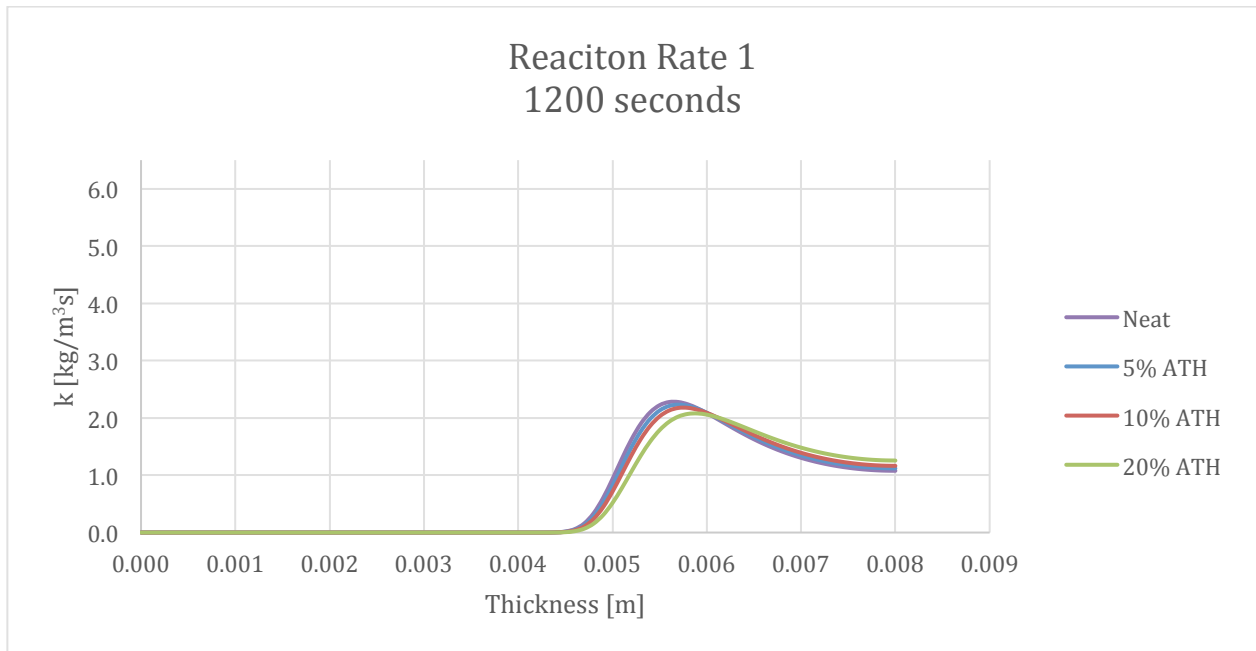


Figure 206--Reaction Rate of Resin to Resin Residue with varying ATH at 1200 seconds

9.7.3. Reaction Rate 2

The rate of the ATH reaction (maximum ~ 1.1) is much lower than the rate of the Resin reaction (maximum ~ 6.5). The rate of the ATH reaction is highest earlier in the simulation. However, the reaction spreads across the whole sample as shown in Figures Figure 208-Figure 211.

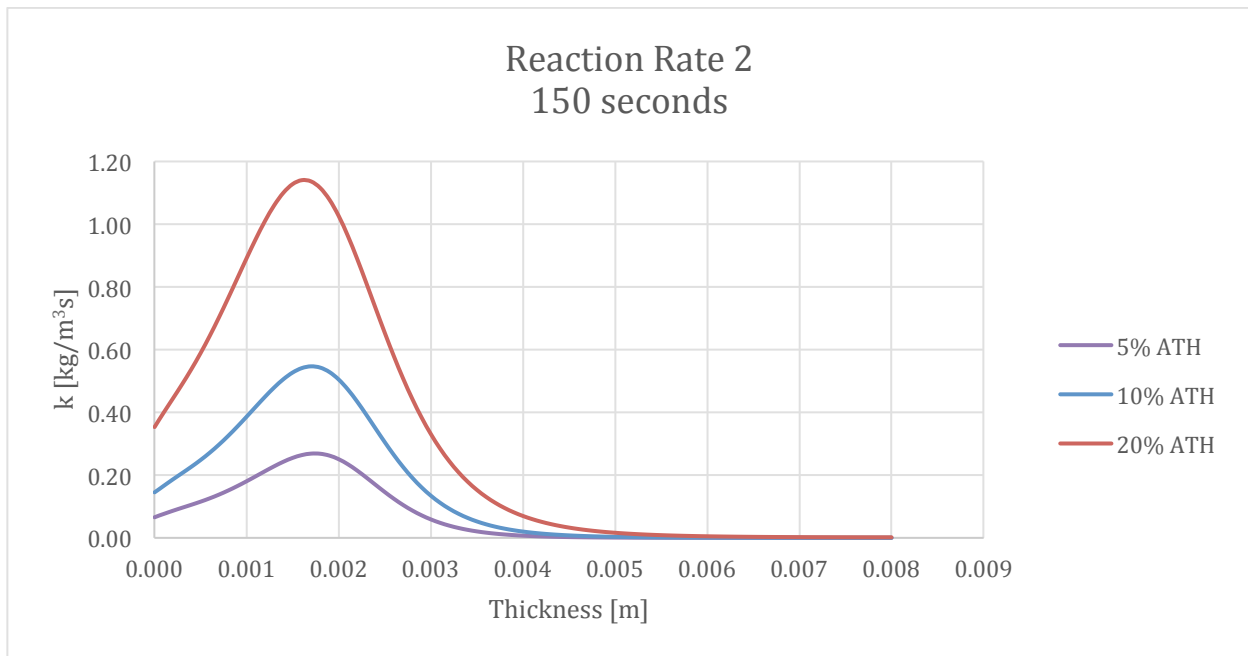


Figure 207--Reaction Rate of ATH to ATH Residue with varying ATH at 150 seconds

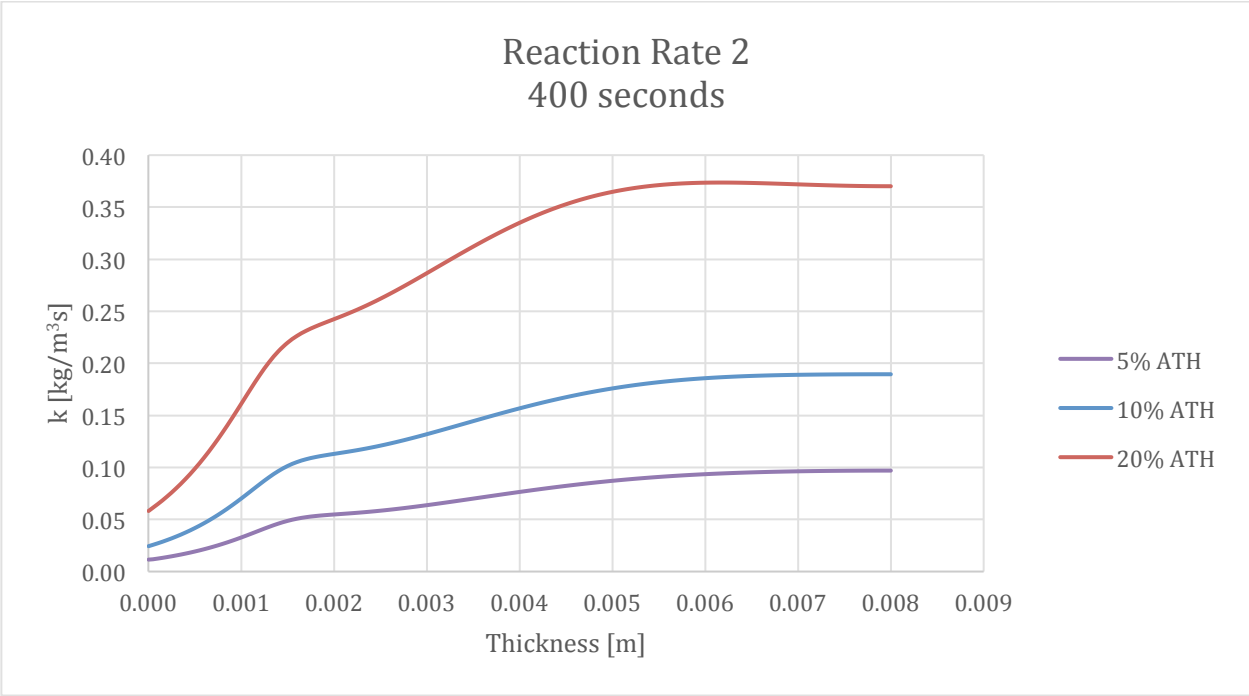


Figure 208-Reaction Rate of ATH to ATH Residue with varying ATH at 400 seconds

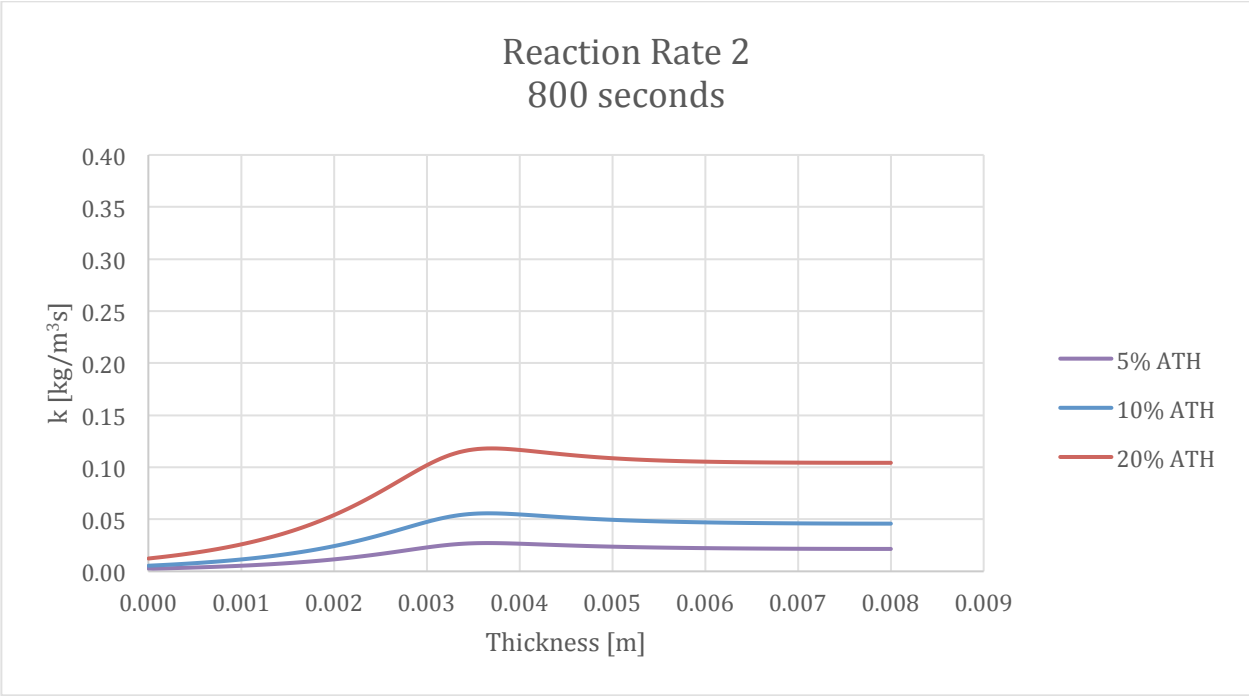


Figure 209-Reaction Rate of ATH to ATH Residue with varying ATH at 800 seconds

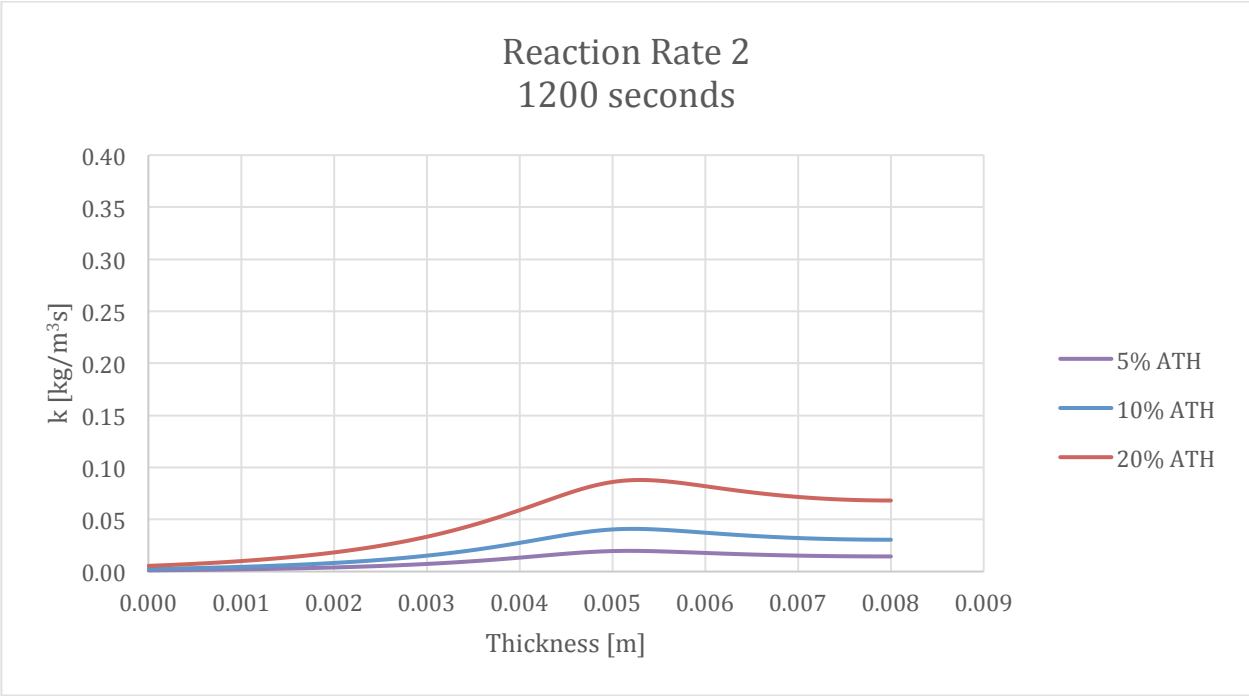


Figure 210-Reaction Rate of ATH to ATH Residue with varying ATH at 1200 seconds

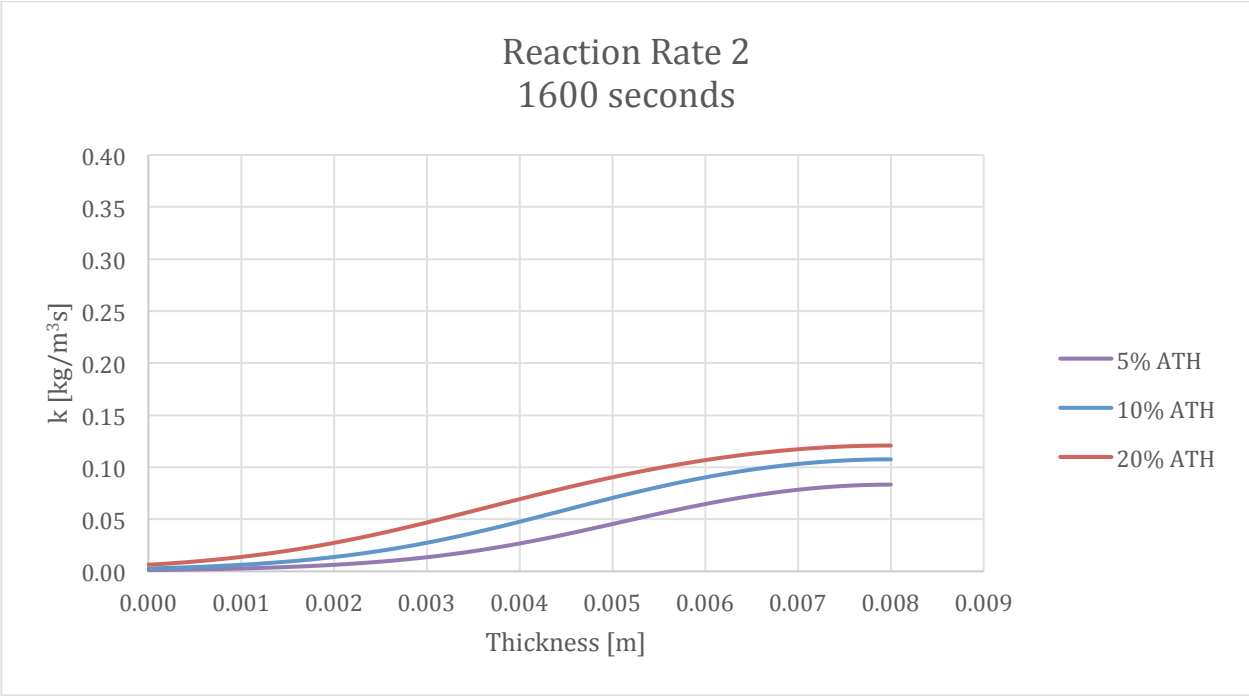


Figure 211-Reaction Rate of ATH to ATH Residue with varying ATH at 1600 seconds

In the previous four graphs, a small bump moves through the specimen with time. This seems to correlate to the position of the reaction of Resin in the specimen. Once the resin is burned the ATH then becomes the primary reactant, which likely causes the small bump in the graphs.

9.7.4. Conversion

The maximum conversion is affected by varying the amount of ATH. Most other properties have seen a delay due to ATH, but the conversion is lowered with increasing ATH.

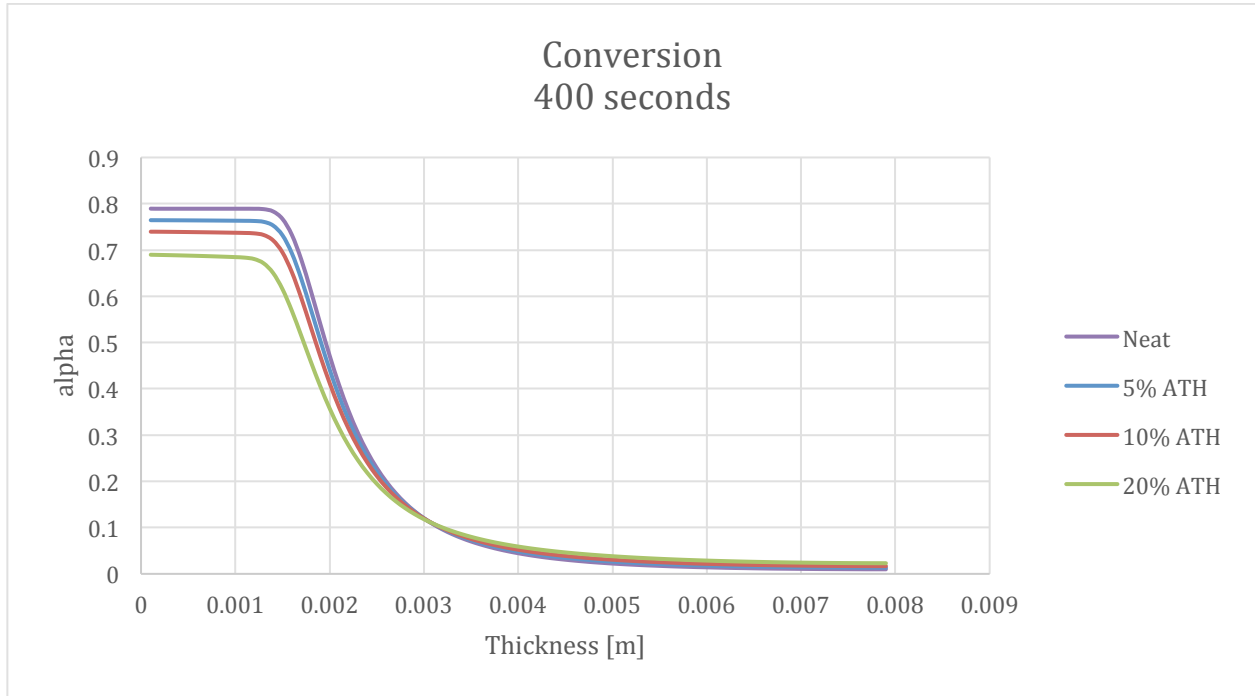


Figure 212-Conversion Profile at varying ATH at 400 seconds

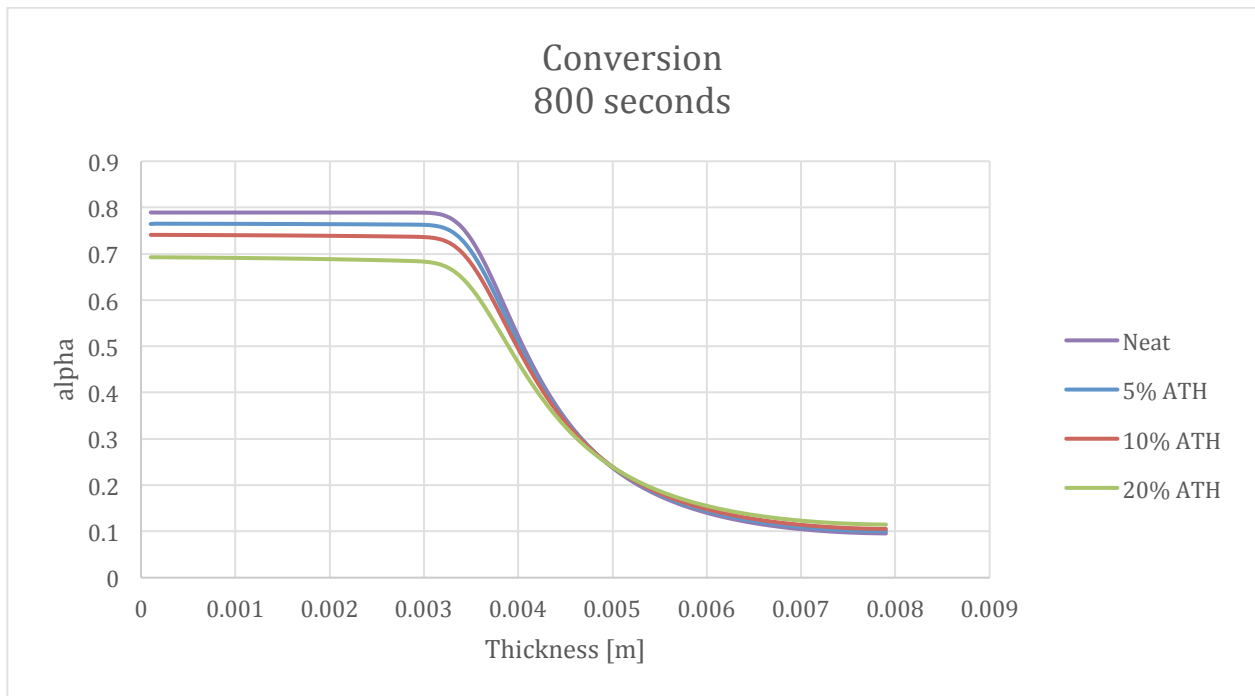


Figure 213-Conversion Profile at varying ATH at 800 seconds

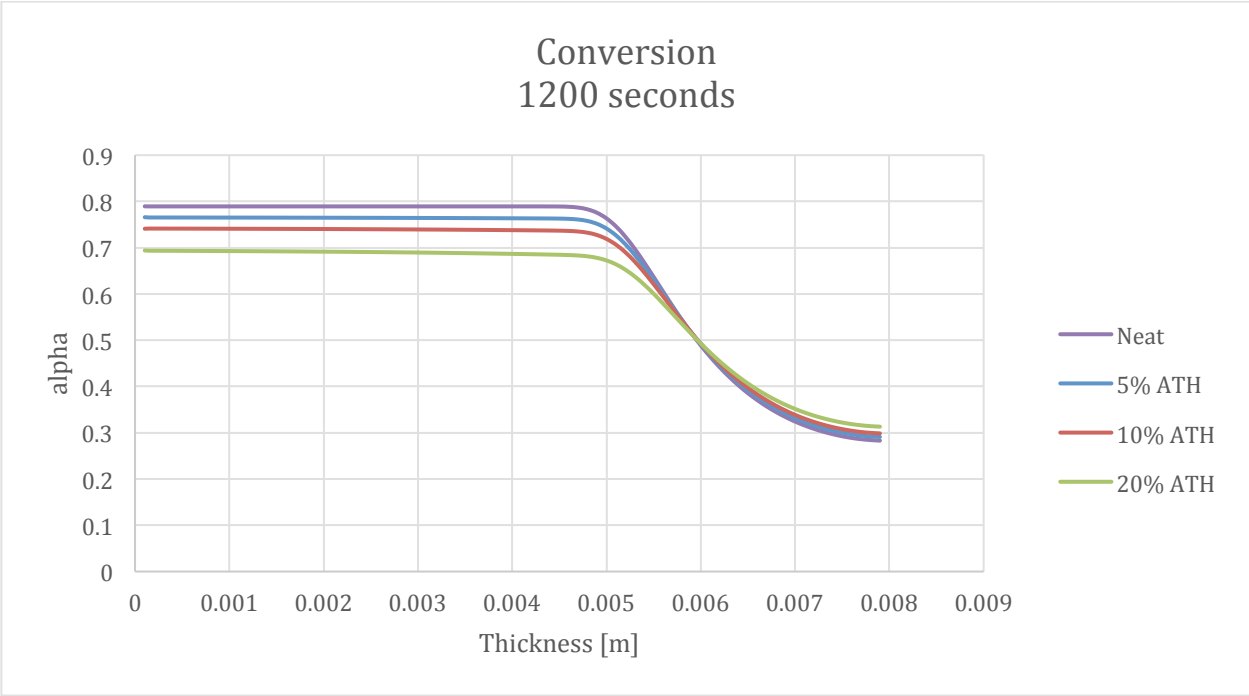


Figure 214-Conversion Profile at varying ATH at 1200 seconds

9.7.5. Density

The density is not altered much by varying levels of ATH either. The specimen is only denser when there is more ATH.

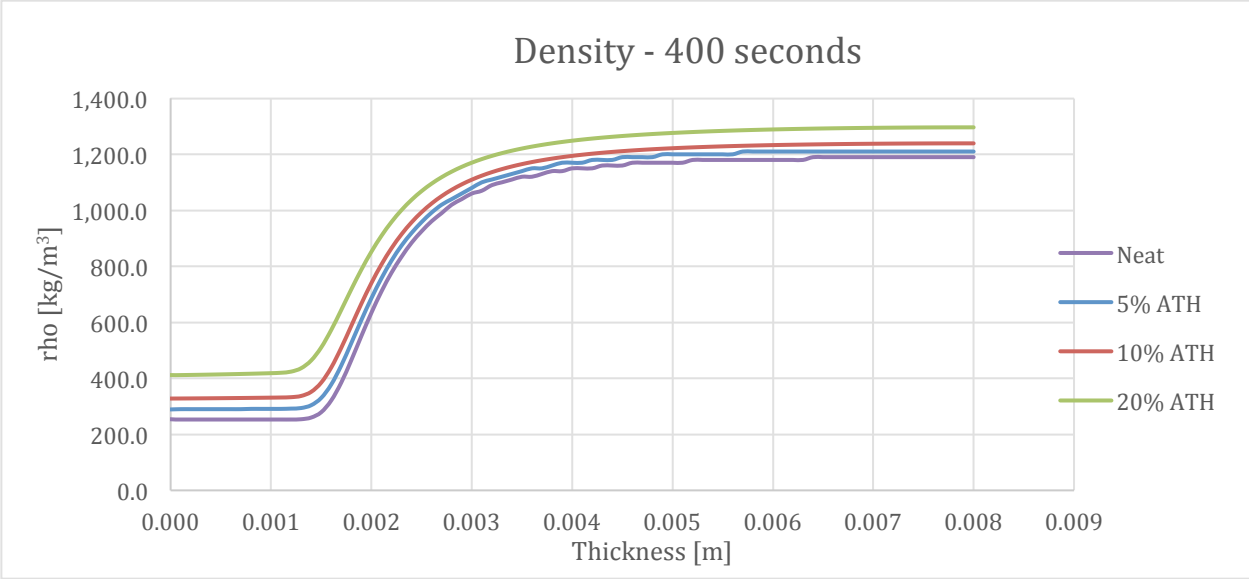


Figure 215-Density Profile at varying ATH at 400 seconds

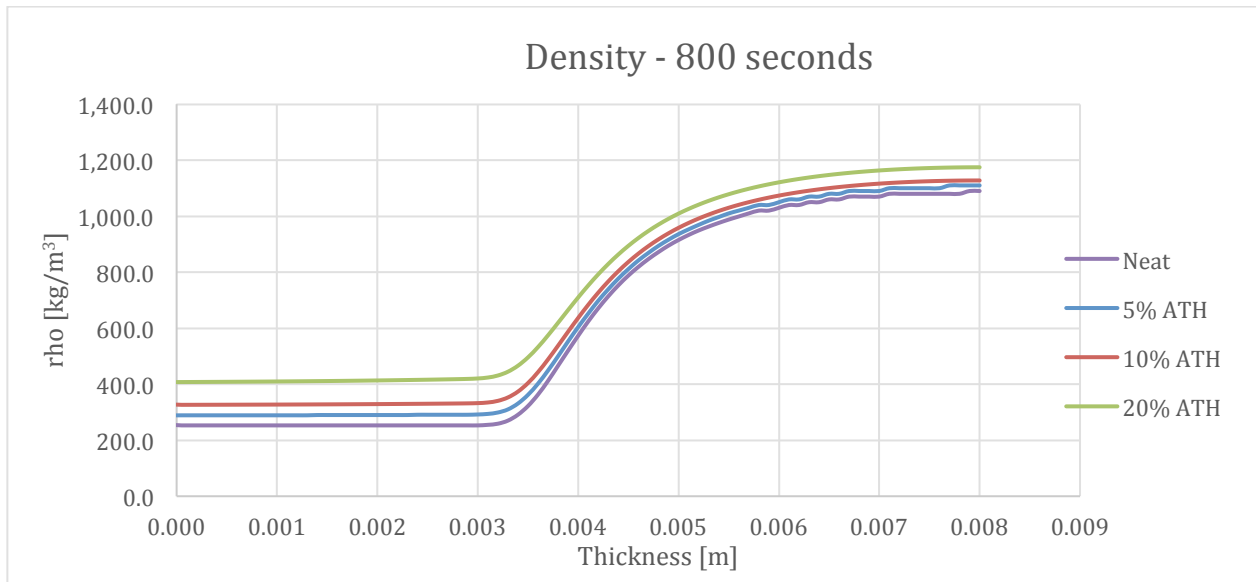


Figure 216--Density Profile at varying ATH at 800 seconds

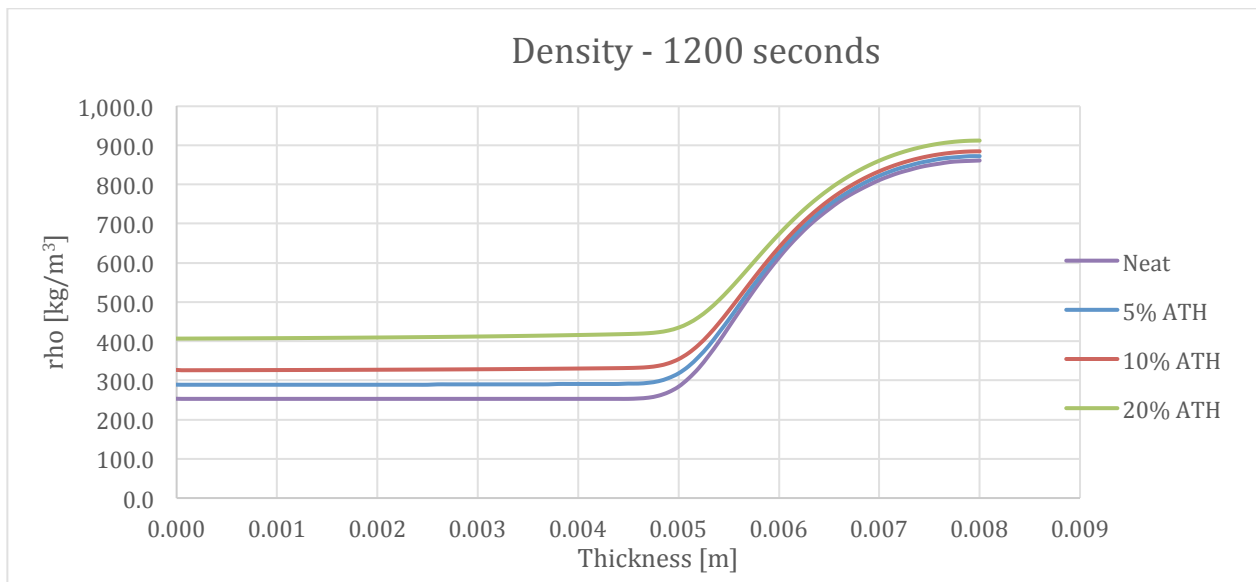


Figure 217--Density Profile at varying ATH at 1200 seconds

9.7.6. Porosity

Similar to the density, the porosity is only slightly affected by the variation in ATH. The porosity closely follows the reaction of the resin. The specimen remains non-porous for longer when there are higher levels of ATH.

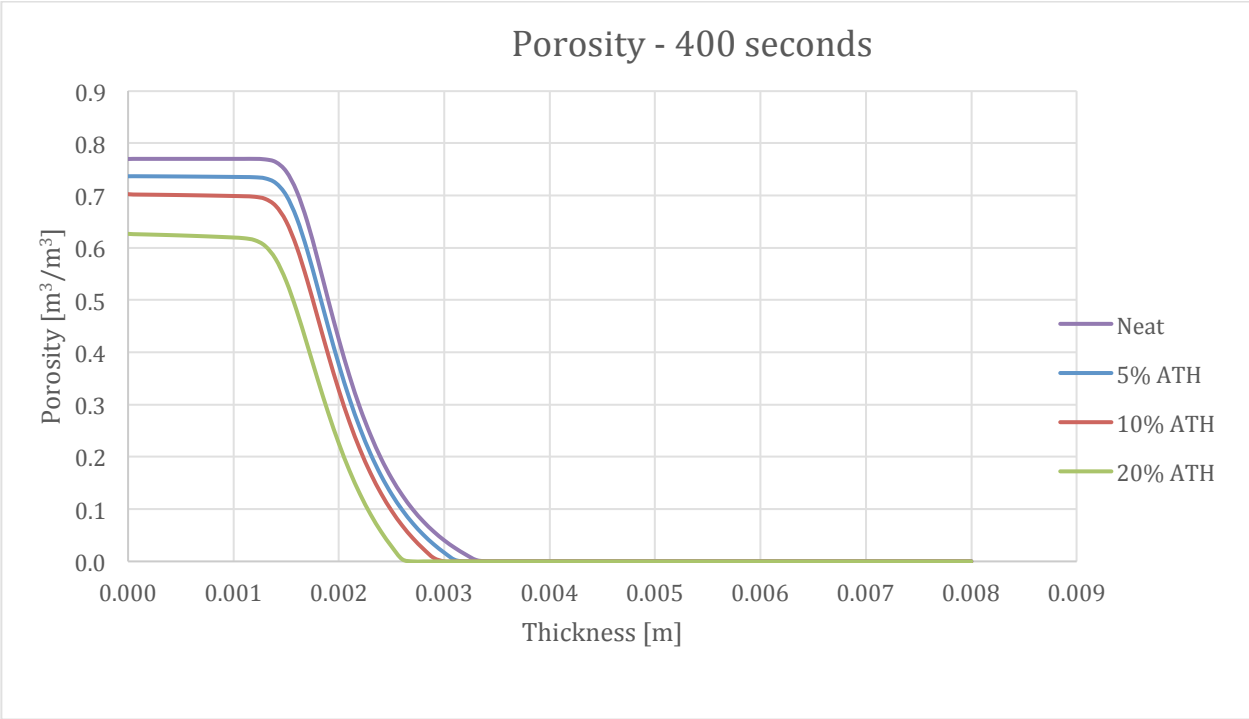


Figure 218--Porosity Profile at varying ATH at 400 seconds

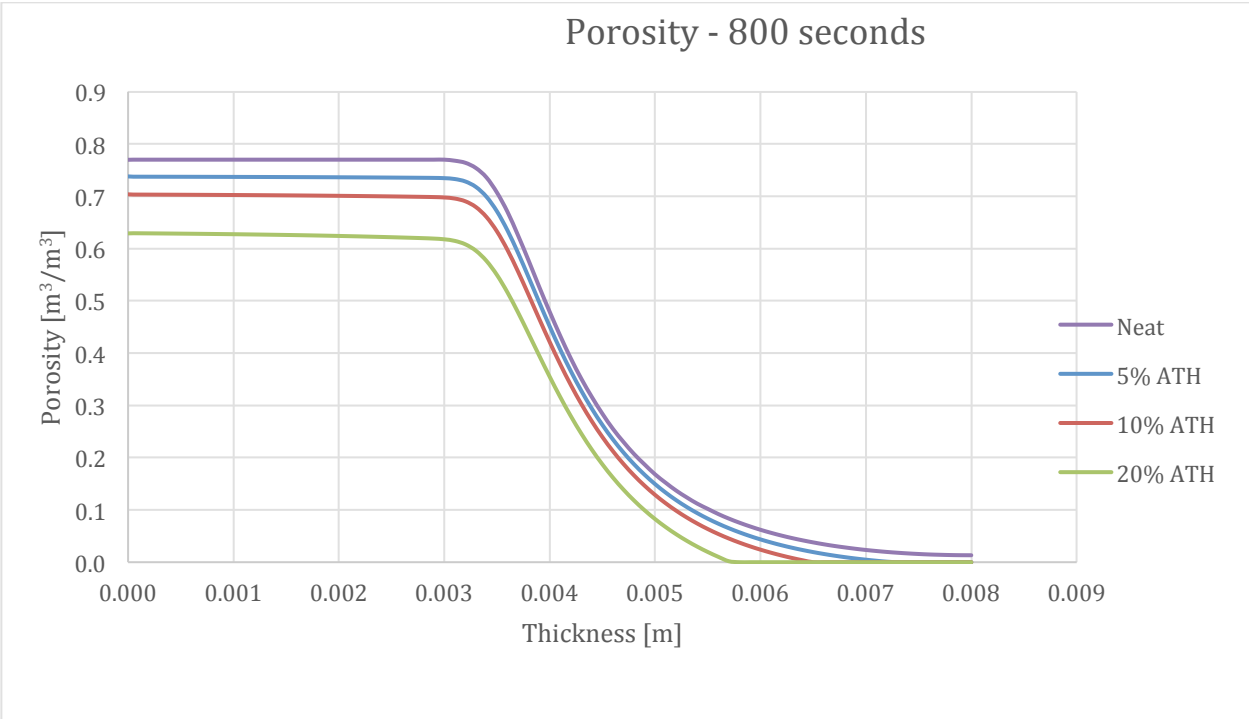


Figure 219-Porosity Profile at varying ATH at 800 seconds

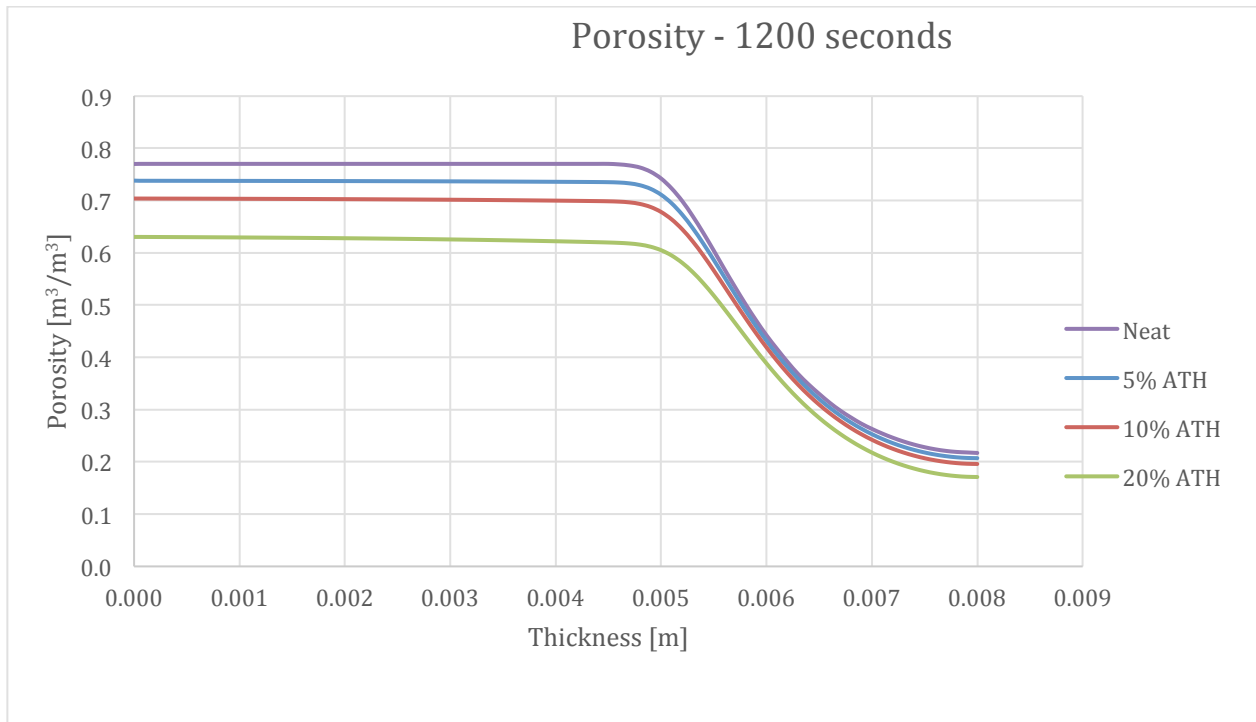


Figure 220-Porosity Profile at varying ATH at 1200 seconds

9.7.7. Temperature

Temperature is the most unaffected property with variations of ATH. The only time temperature affects the specimen is at the end when the increase in ATH makes the specimen hotter.

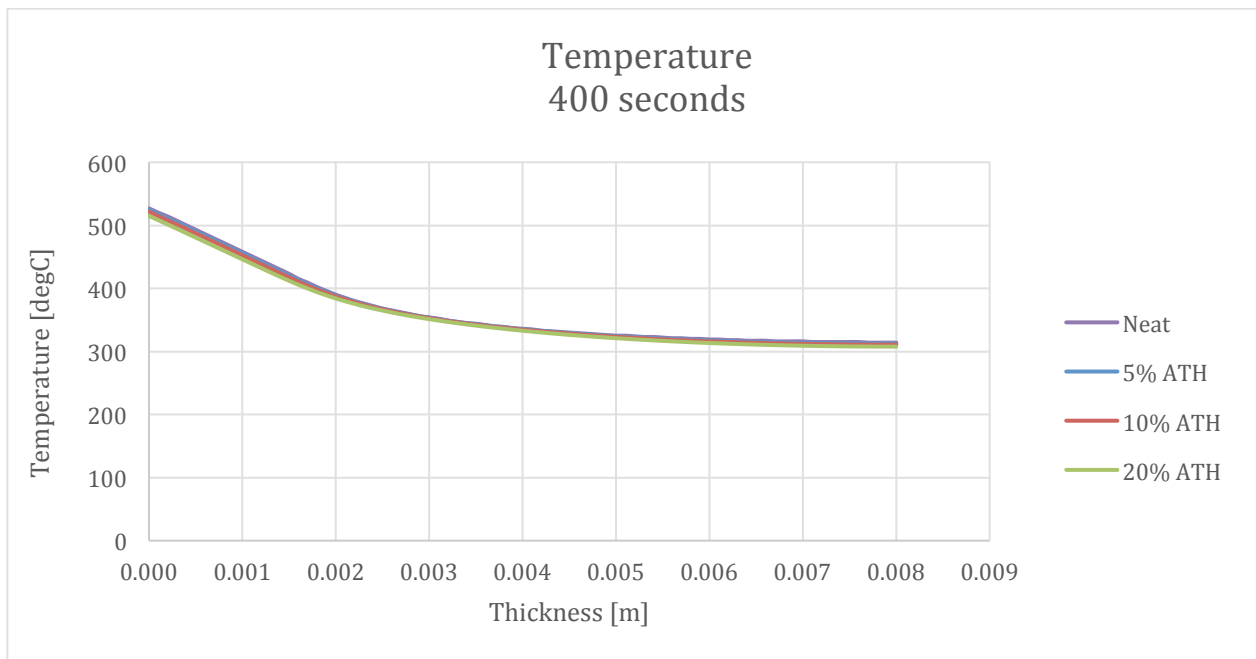


Figure 221-Temperature Profile at varying ATH at 400 seconds

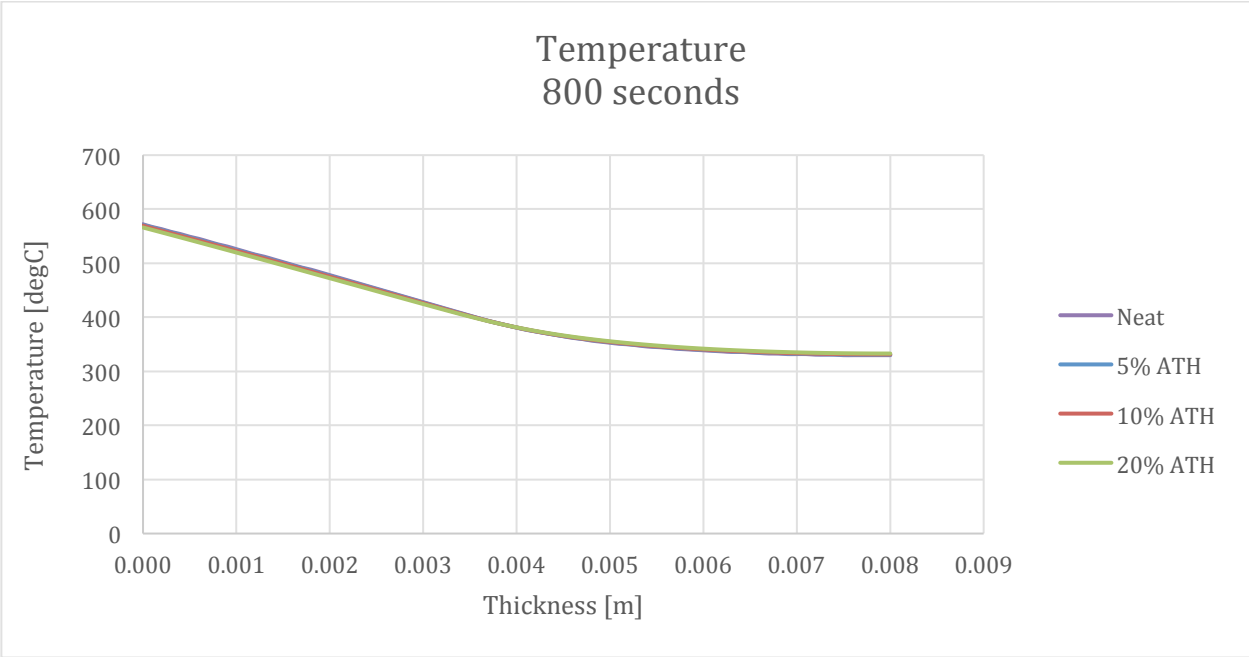


Figure 222-Temperature Profile at varying ATH at 800 seconds

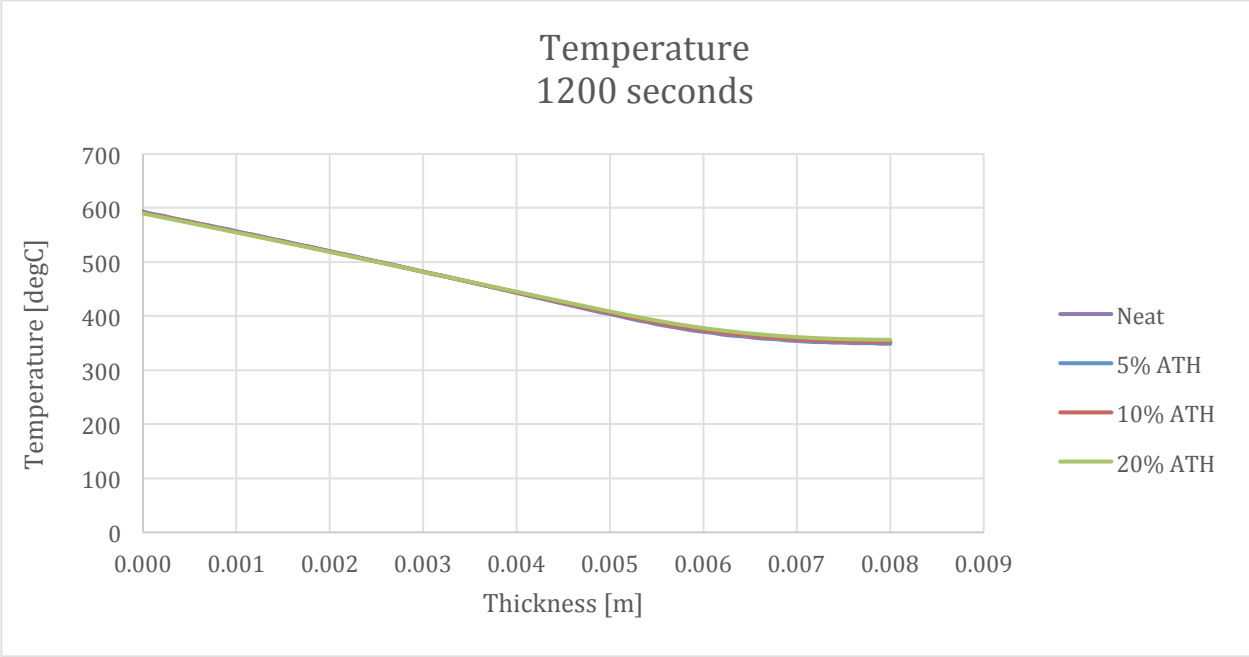


Figure 223-Temperature Profile at varying ATH at 1200 seconds

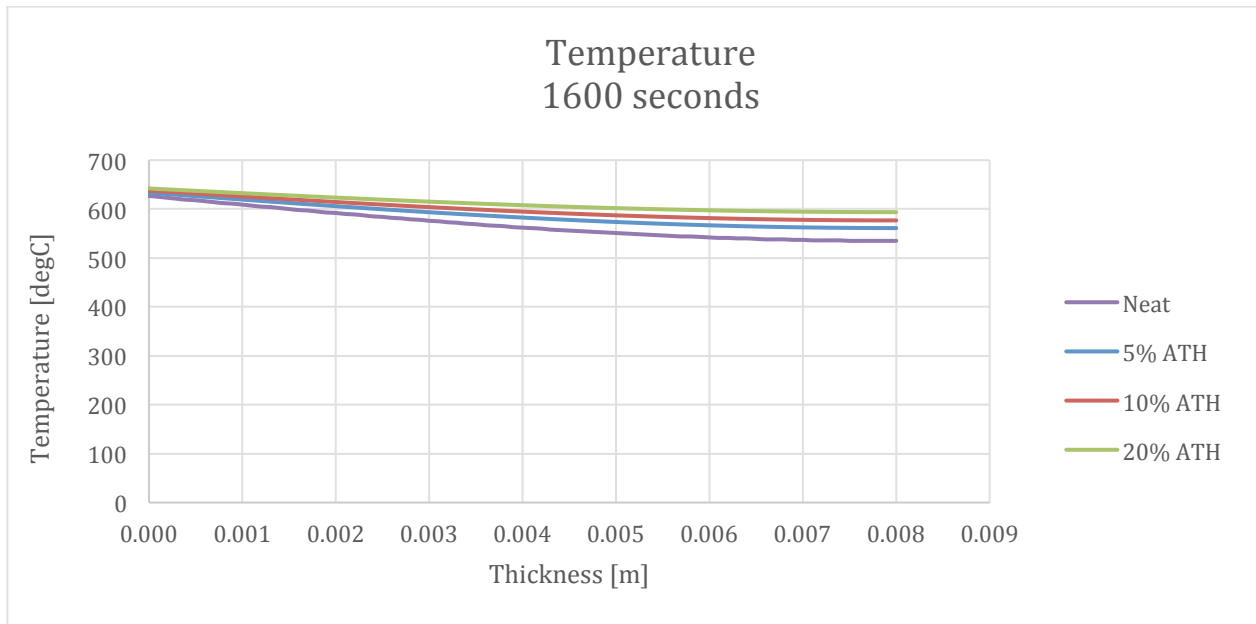


Figure 224-Temperature Profile at varying ATH at 1600 seconds

9.7.8. Mass Fraction at 400 Seconds

For all mass fractions, the variations in ATH mainly affect the overall fraction of each species. There are slightly effects in how quickly the mass fraction of a species is converted to another species, but it is minimal and has already been considered in previous sections.

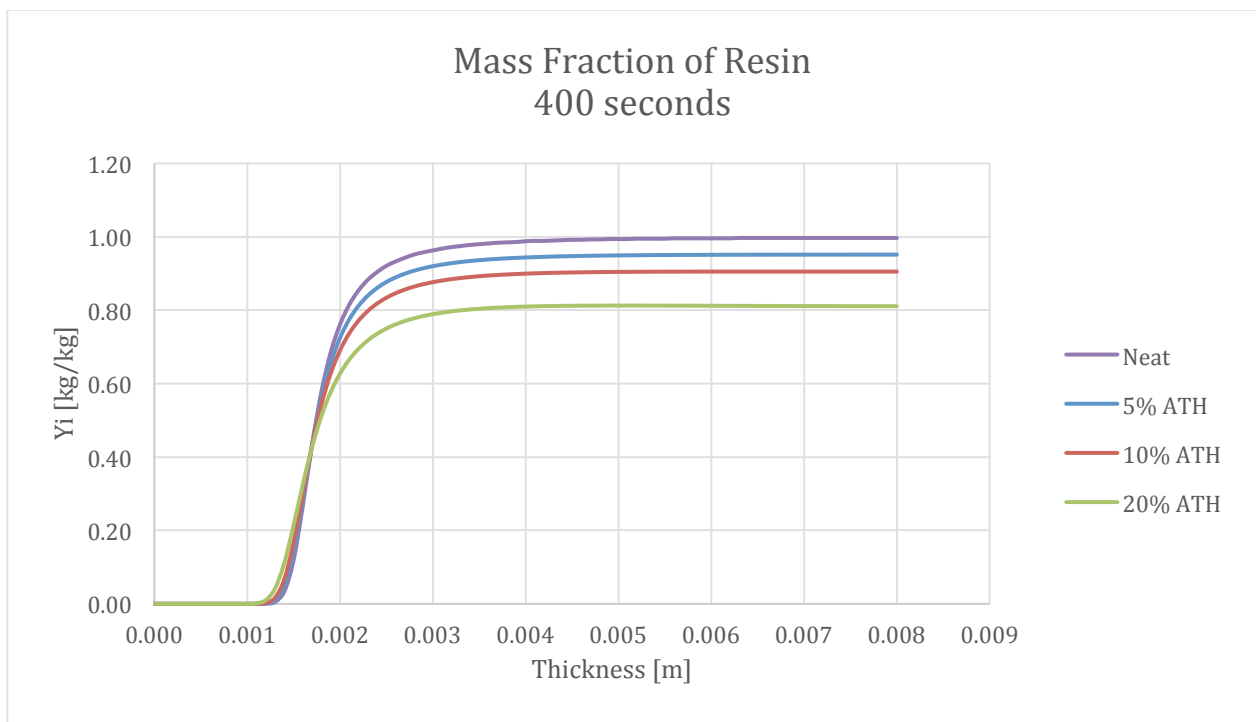


Figure 225-Mass Fraction Profile of Resin at 400 seconds

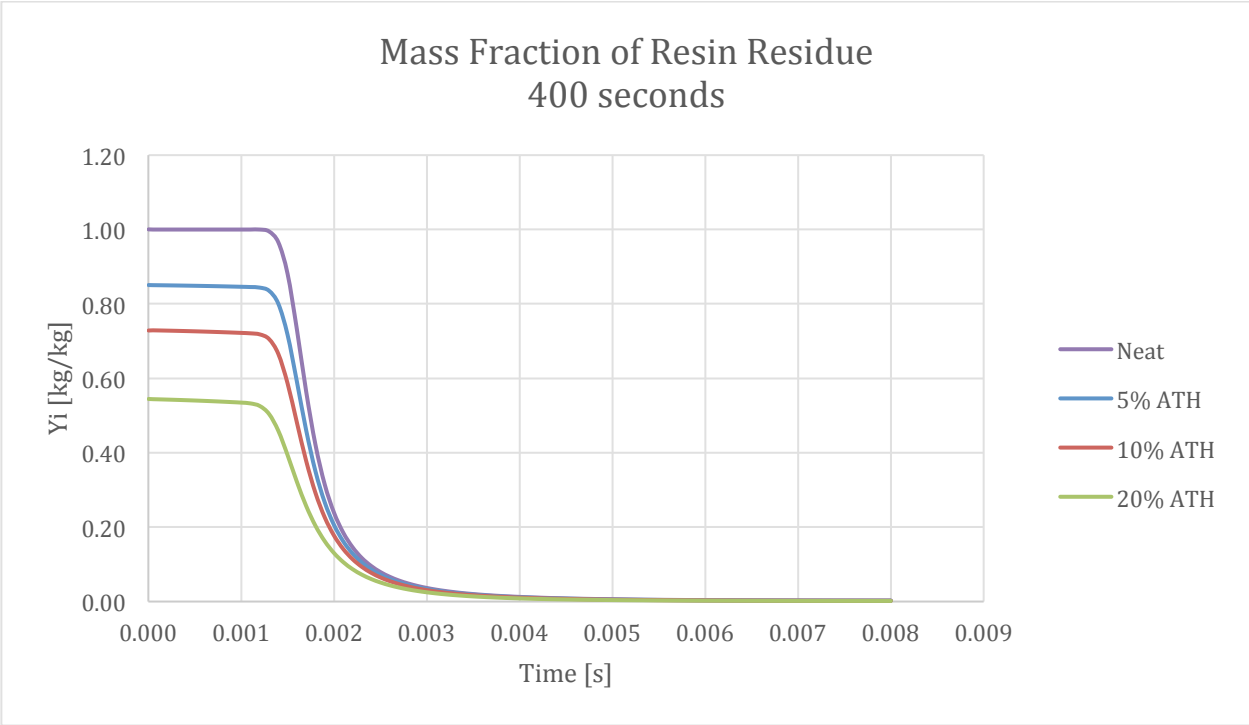


Figure 226-Mass Fraction Profile of Resin Residue at 400 seconds

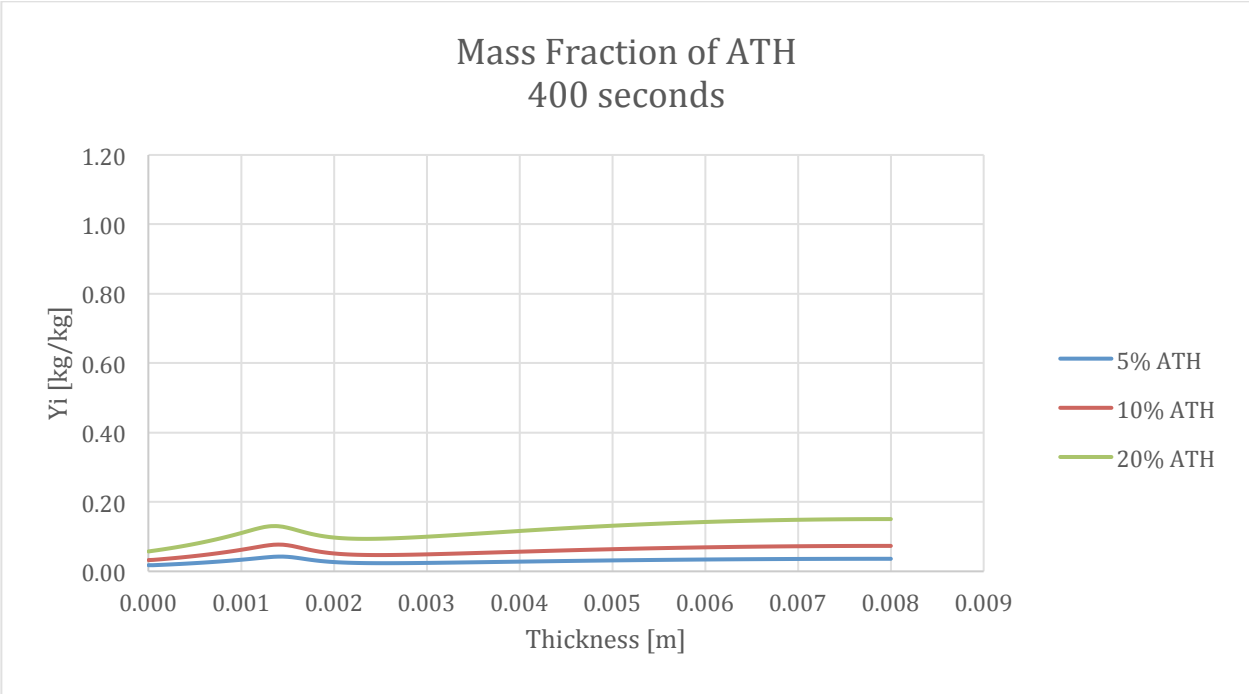


Figure 227-Mass Fraction Profile of ATH at 400 seconds

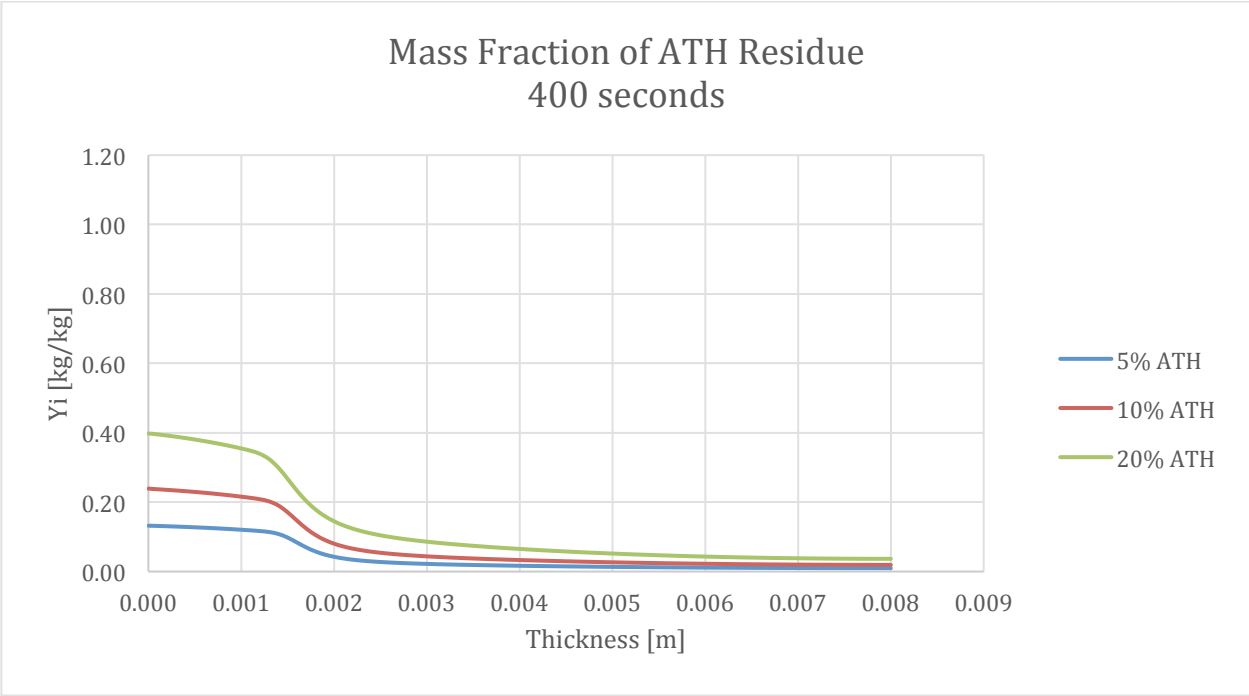


Figure 228-Mass Fraction Profile of ATH to ATH Residue at 400 seconds

9.7.9. Mass Fraction at 800 Seconds

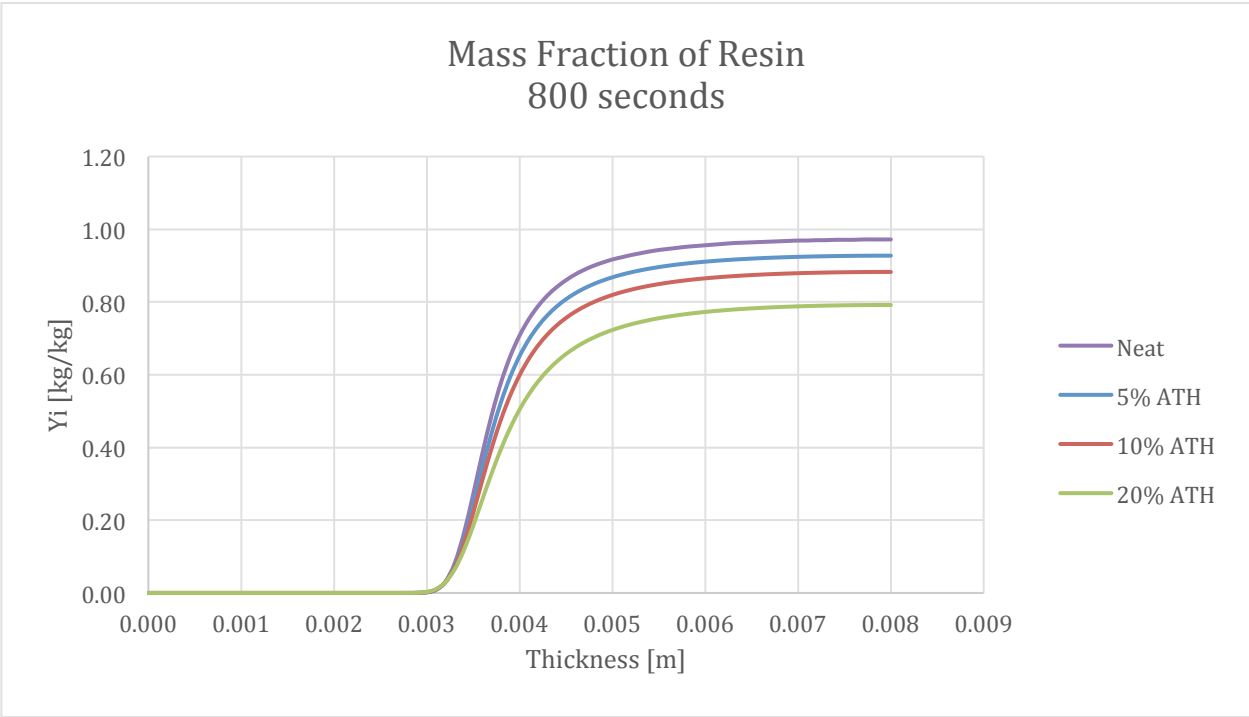


Figure 229-Mass Fraction Profile of Resin at 800 seconds

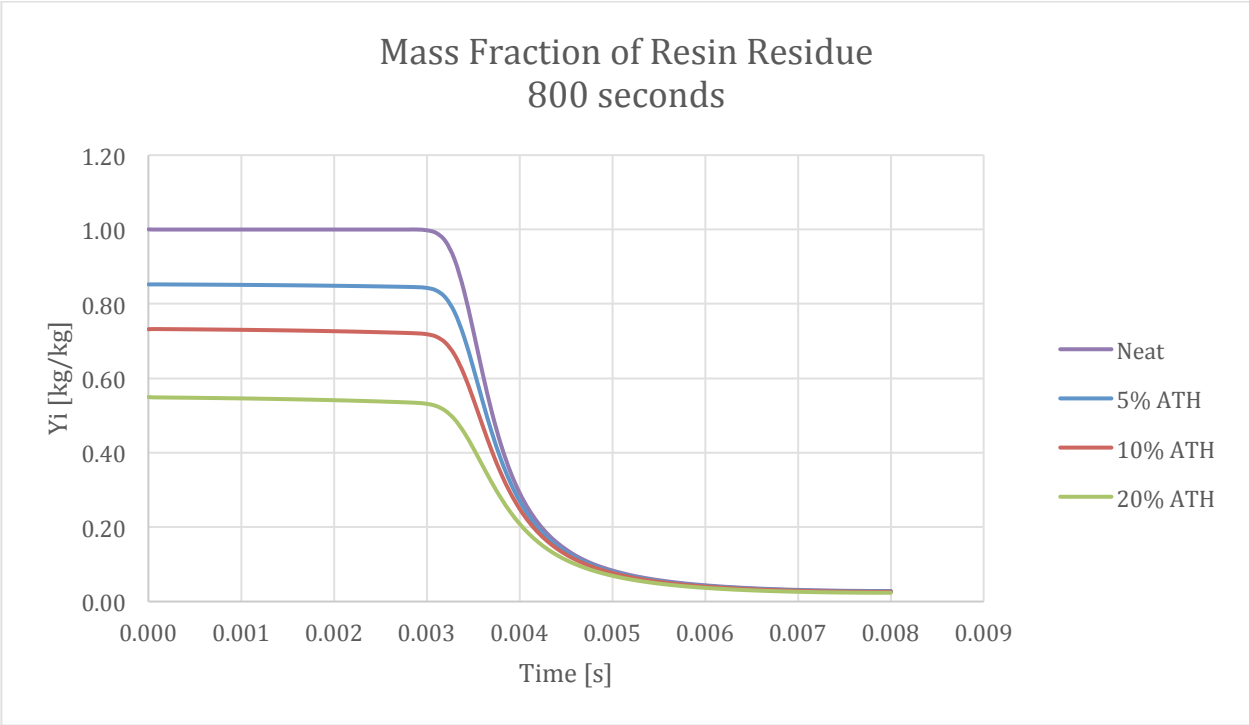


Figure 230-Mass Fraction Profile of Resin Residue at 800 seconds

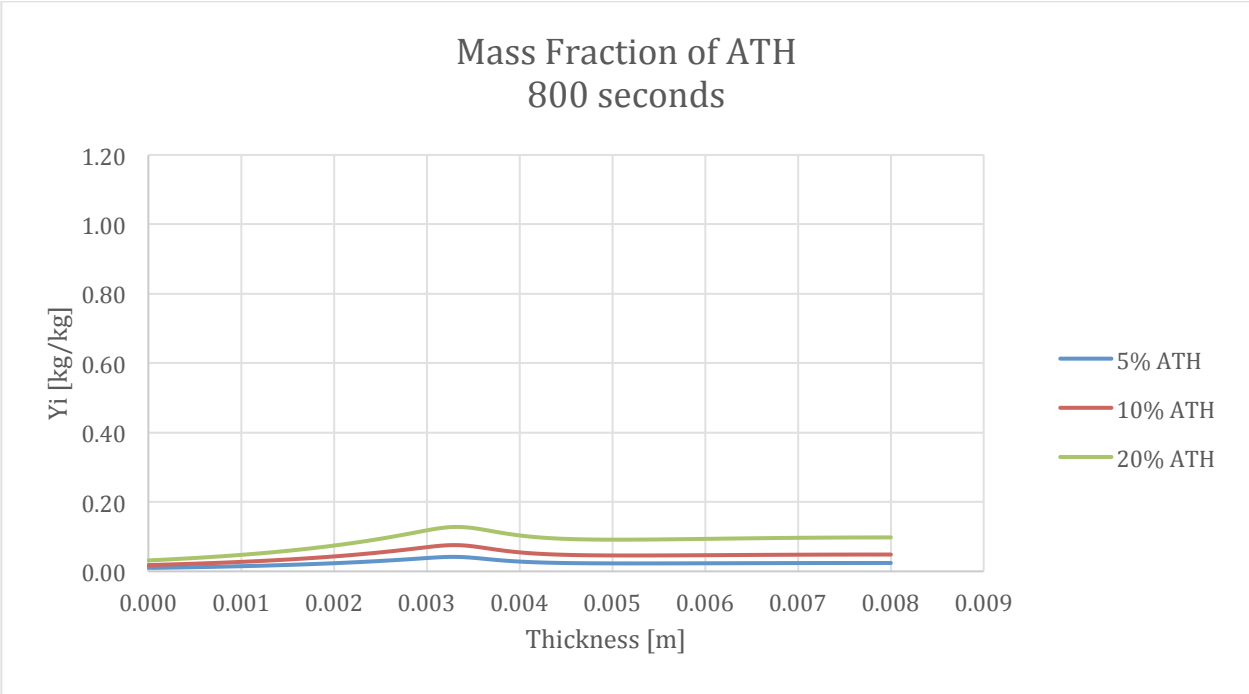


Figure 231-Mass Fraction Profile of ATH at 800 seconds

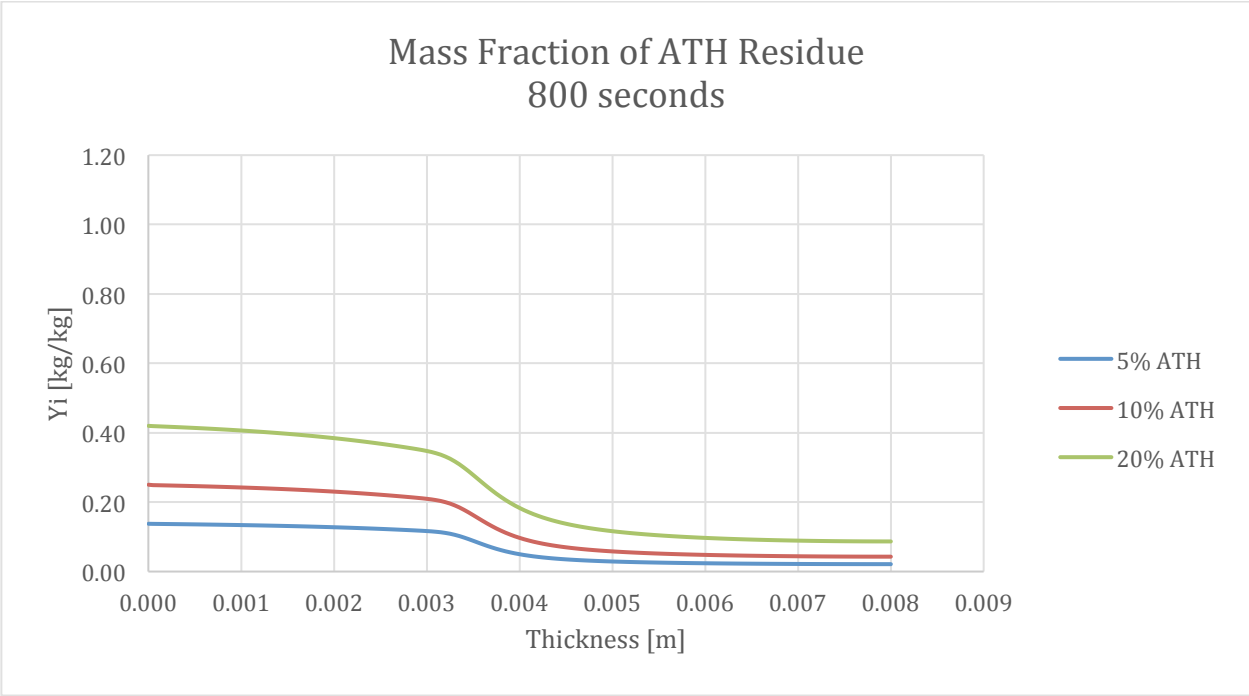


Figure 232-Mass Fraction Profile of ATH to ATH Residue at 800 seconds

9.7.10. Mass Fraction at 1200 Seconds

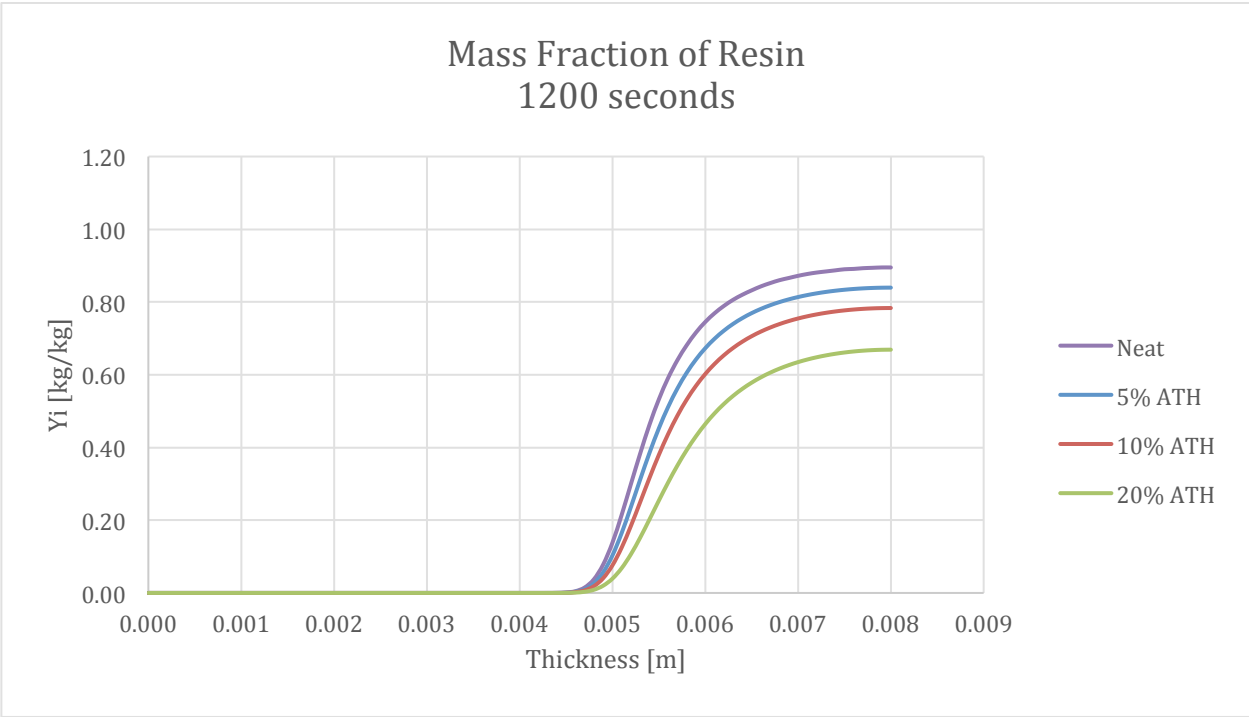


Figure 233-Mass Fraction Profile of Resin at 1200 seconds

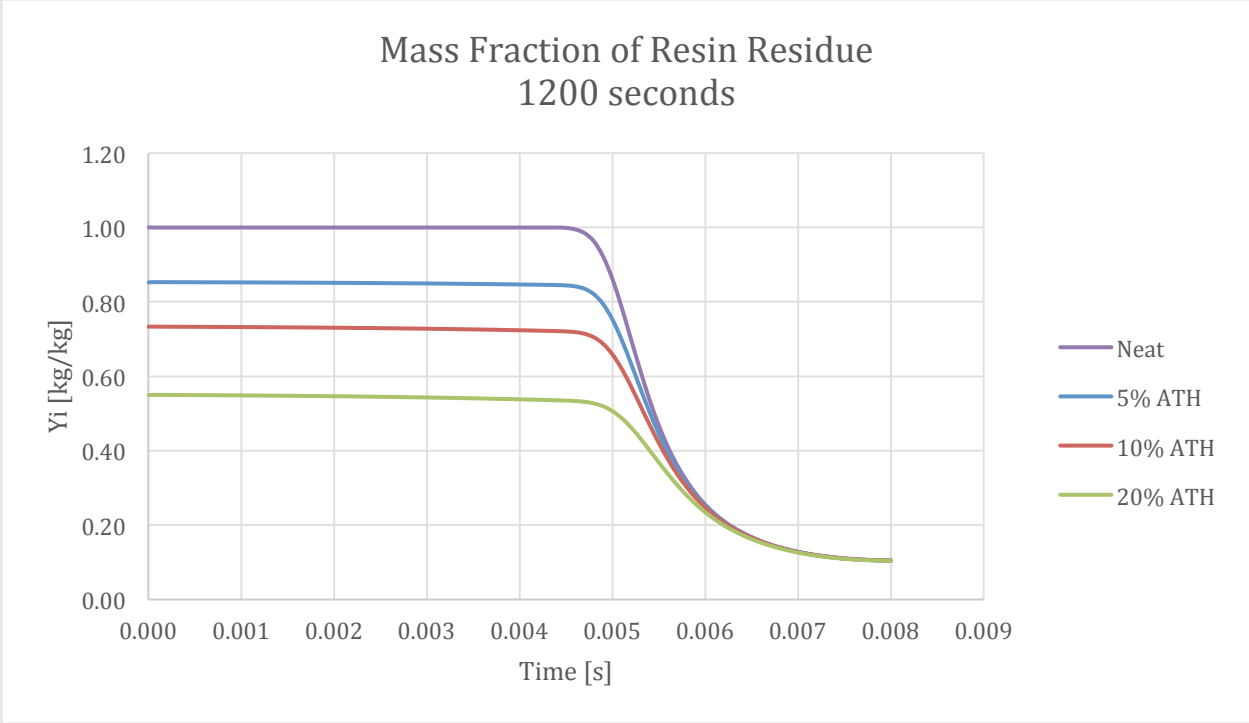


Figure 234-Mass Fraction Profile of Resin Residue at 1200 seconds

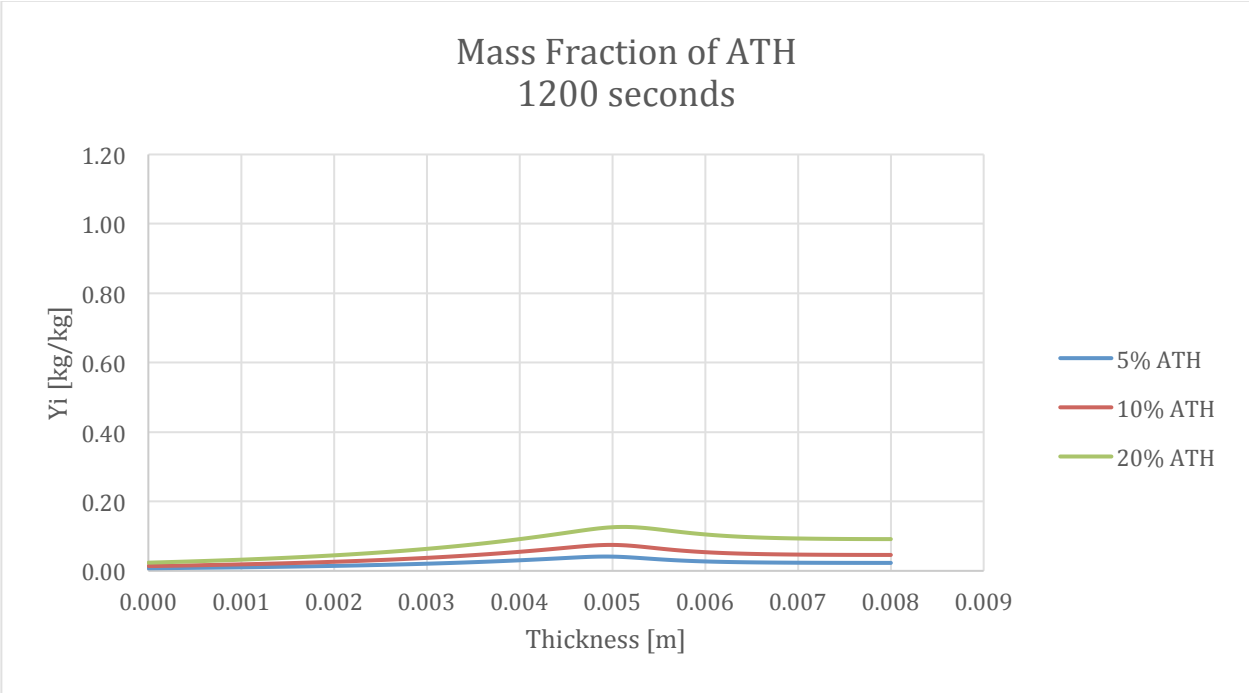


Figure 235-Mass Fraction Profile of ATH at 1200 seconds

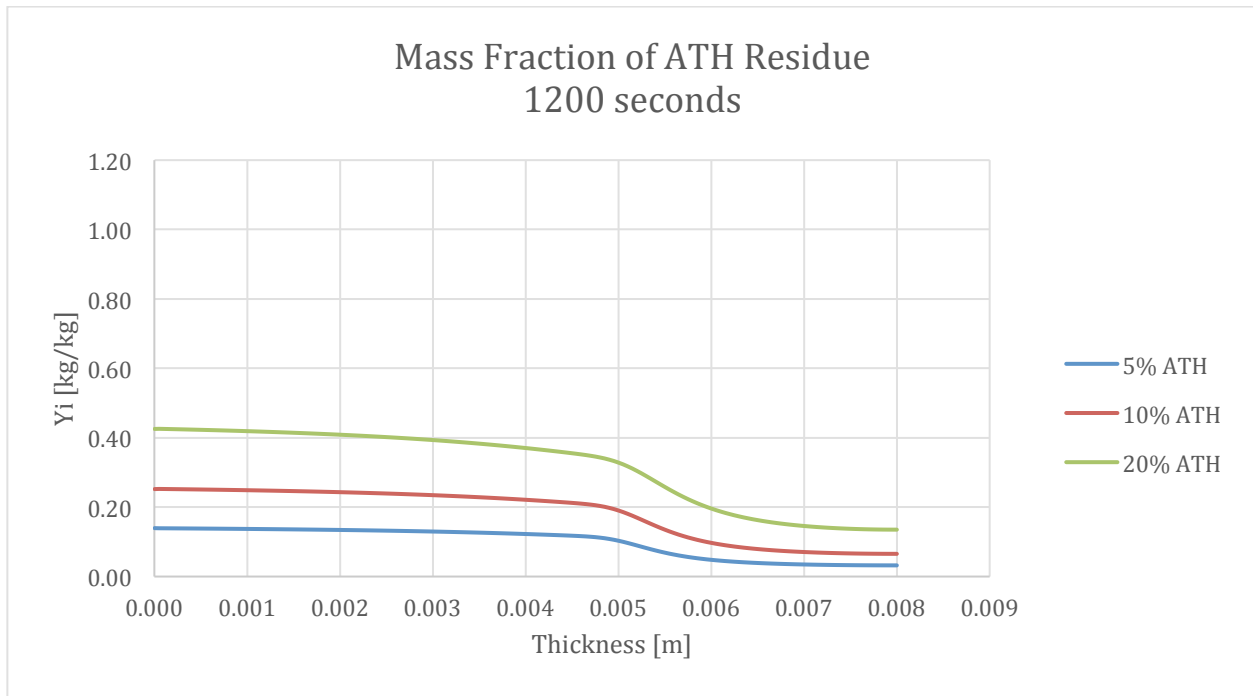


Figure 236-Mass Fraction Profile of ATH to ATH Residue at 1200 seconds

9.8. Illustrations of Simulated Samples

The figures in this section are illustrations that are meant to represent the samples that were simulated in the report analysis.

9.8.1. Validating G-Pyro

A 9 mm sample with 100 part resin and either 0 or 130 parts ATH with 50% glass. The gray and red represents the resin and ATH mixture, respectively, and the yellow represents the glass

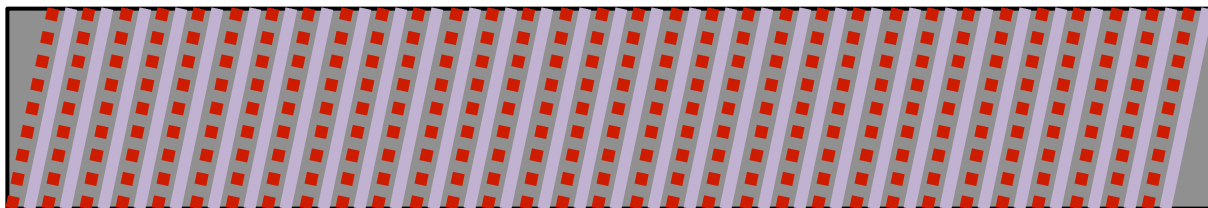


Figure 237-Illustration of 100:130 resin/ATH system with 50% glass

9.8.2. Varying ATH

A 9 mm sample with Varying compositions of ATH, and 50 wt% glass in all tests. The yellow represents the glass in the figure below, while the gray and red represents the resin and ATH

respectively. The notable change is the thinner red lines showing the use of less ATH in the system.

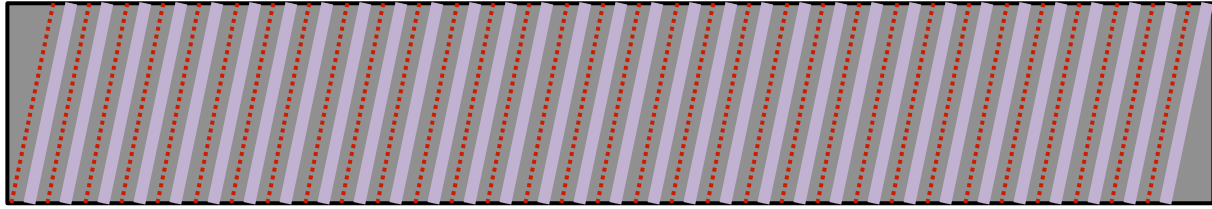


Figure 238-Illustration of varying levels of resin/ATH system with 50% glass

9.8.3. Varying Coating Thickness

A 9 mm sample of 100:130 resin:ATH with 50 wt% glass, with the addition of a coating of glass.

The glass coating, in dark yellow, varies in size during the analysis.

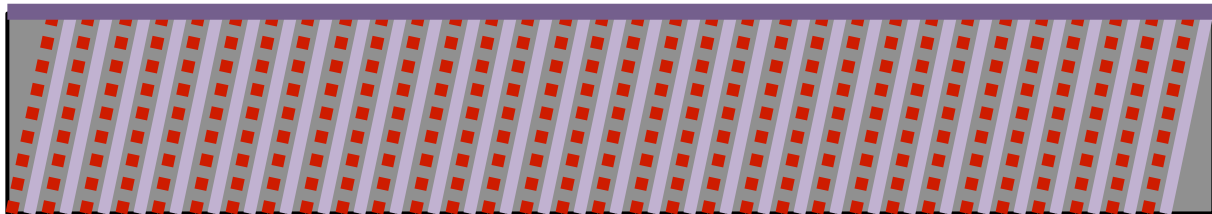


Figure 239-Illustration of 100:130 resin/ATH system with 50% glass and a coating with varied thickness

9.8.4. Varying Layering Style

A 9 mm sample with separated sections of pure resin/ATH, and glass. The layering shown below is determined set by seven 0.5 mm glass layers, filling the remaining 9 mm evenly with resin/ATH. The thicknesses of those layers were determined to be 0.785 mm, while the top and bottom layer were approximately half at 0.395 mm.

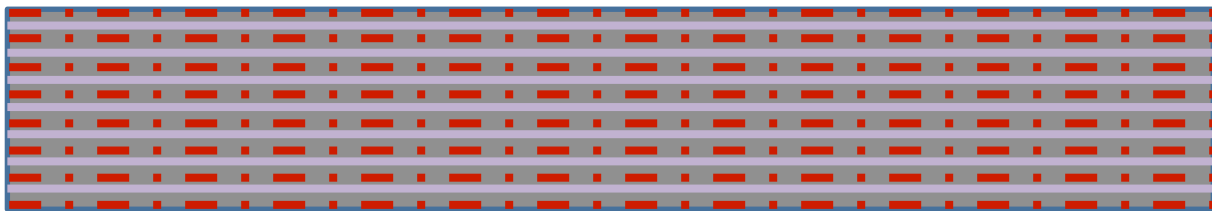


Figure 240-Illustration of 100:130 resin/ATH system with glass layering

9.9. Summary of testing

The table below lists all the tests that were performed throughout the course of this project. Not all of the tests were done to get results. Some of the tests were performed to gain a better

understanding of G-Pyro, or did not have all the necessary features turned on. The tests that produced results are highlighted at the bottom of the list.

- Char example (1 test)
 - This is from the samples provided by G-Pyro
 - Attempted multiple times to understand how to run the program
 - Slight changes made multiple times to determine what could be changed
- Modified Acrylic Series (4 tests)
 - Performed tests to evaluate the result getting procedure of G-Pyro
 - Performed at levels of 0, 5, 10, & 20% ATH.
 - Used preliminary properties
- Modified Acrylic FRP Series (4 tests)
 - Same as previous series but with added glass at a level of 50% ATH
- Industrial Standard Series (1 test)
 - Used “Industry Standards” highlighted in Esther Kim’s other work
 - 9 mm sample, with ~55% ATH and 30% glass
 - This was performed to see how the samples being tested compared to the “actual FRPs”
- Hybrid FRP 20% ATH (1 test)
 - The first step for using the hybrid material
 - This sample was compared to the Modified acrylic 20% to sight differences
- Layering tests (3 tests)
 - Layering was developed in this test to determine how easily a sample could be created
 - After a single tests there was a problem that was solved by altering the thermal contact between samples and making them nearly perfect
 - This test was done for 100:0 and 100:130 samples.
- Pure tests (2 tests)
 - These tests were done on 100:0 and 100:130 to compare how the layered sample looked to a sample without glass
- Mixed tests (2 tests)
 - These tests were done on 100:0 and 100:130 to compare how the layered sample looked to the non-layered FRP
- Industry Standard rho (1 test)
 - This test was performed in order to determine the inconsistencies that occurred because of porosity
 - This issue was solved by changing the inputs to get the initial density and solid density to be equal.
- Reradiation input testing (5 tests)
 - Tests done to learn how to use reradiation boundary condition

- Increased front face heat transfer coefficient test to see how reradiation compared to a simple increase in heating
- A front and back face reradiation with heating on the back face as well as the front because the inputs were unclear for the back face
- A front face heating with front and back reradiation
- A front face heating and reradiation and insulated back face which was the proper results
- Reradiation results for previous tests (6 tests) [final results]
 - The 100:0 and 100:130 samples were repeated with reradiation (2 tests)
 - The % ATH simulations were repeated with reradiation on (3 tests)
 - The layered sample was repeated with reradiation (1 test)
- Coating test with reradiation (3 tests) [final results]
 - Performed at 0.25, 0.5, and 1 mm thick coatings

9.10. Additional Results from Report Analysis

This section provides graphs for additional properties that were recorded during all the tests provided in the section on the results and analysis of G-Pyro. Each section will be broken up by the differences between the different simulations. Each simulation will be structured in the same order: MLR, bulk density, reaction rate (resin->resin residue), reaction rate (ATH->ATH residue), resin composition, resin residue composition, ATH composition, ATH residue composition, temperature, porosity, conversion, and glass composition.

9.10.1. Validity of G-Pyro

The first set of results were the simulation of 100:0 resin/ATH. This sample will be the baseline for all further simulation and will not be repeated but will be acknowledged.

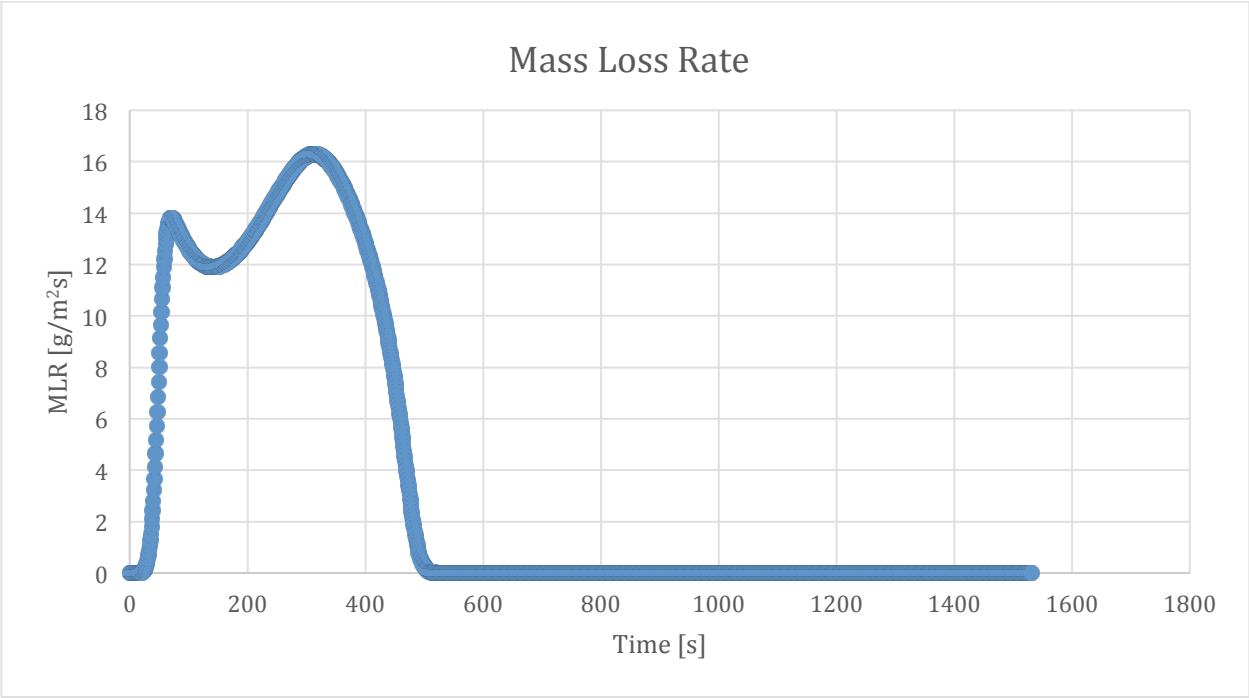


Figure 241-Mass loss rate curve for 100:0 resin/ATH sample and 50% glass

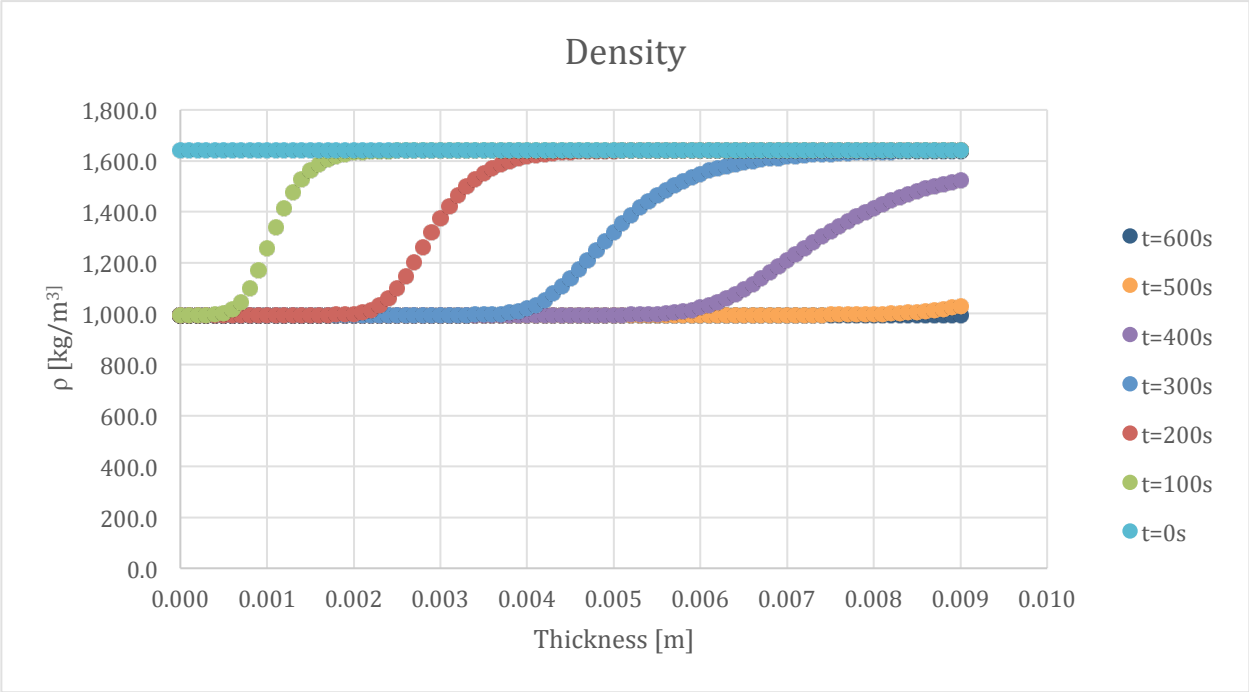


Figure 242-Density profile for 100:0 resin/ATH sample and 50% glass

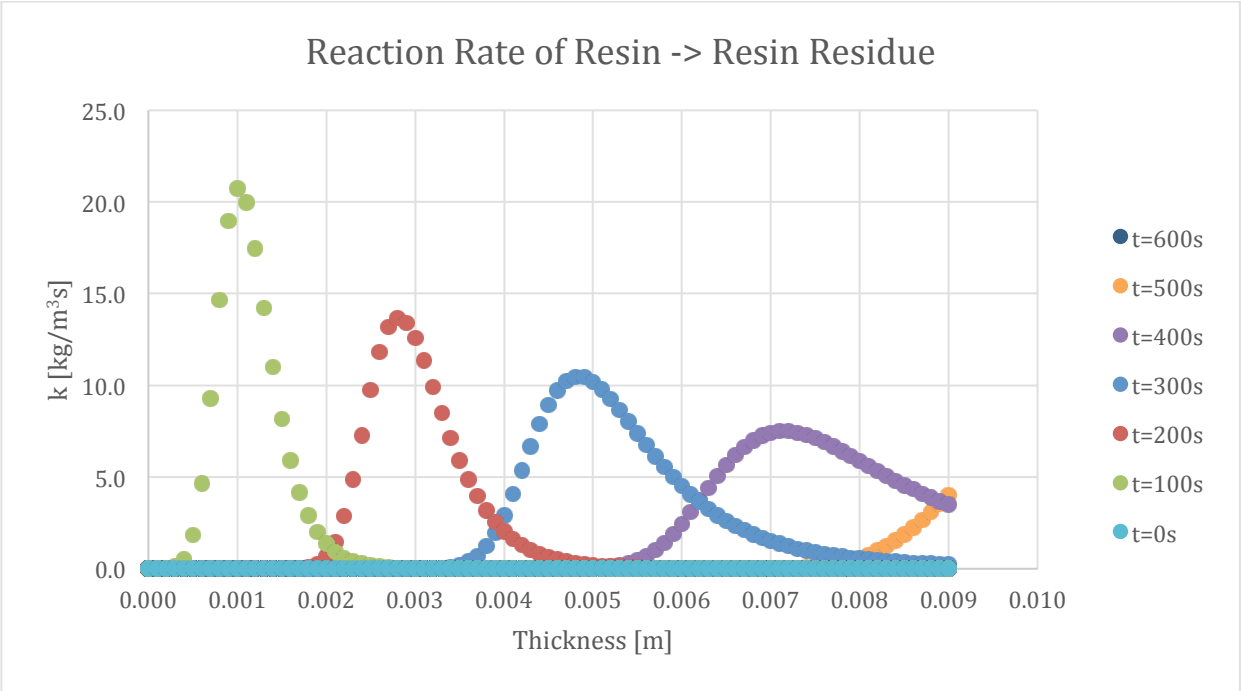


Figure 243-Reaction rate profile for Resin->Resin Residue in 100:0 resin/ATH sample and 50% glass

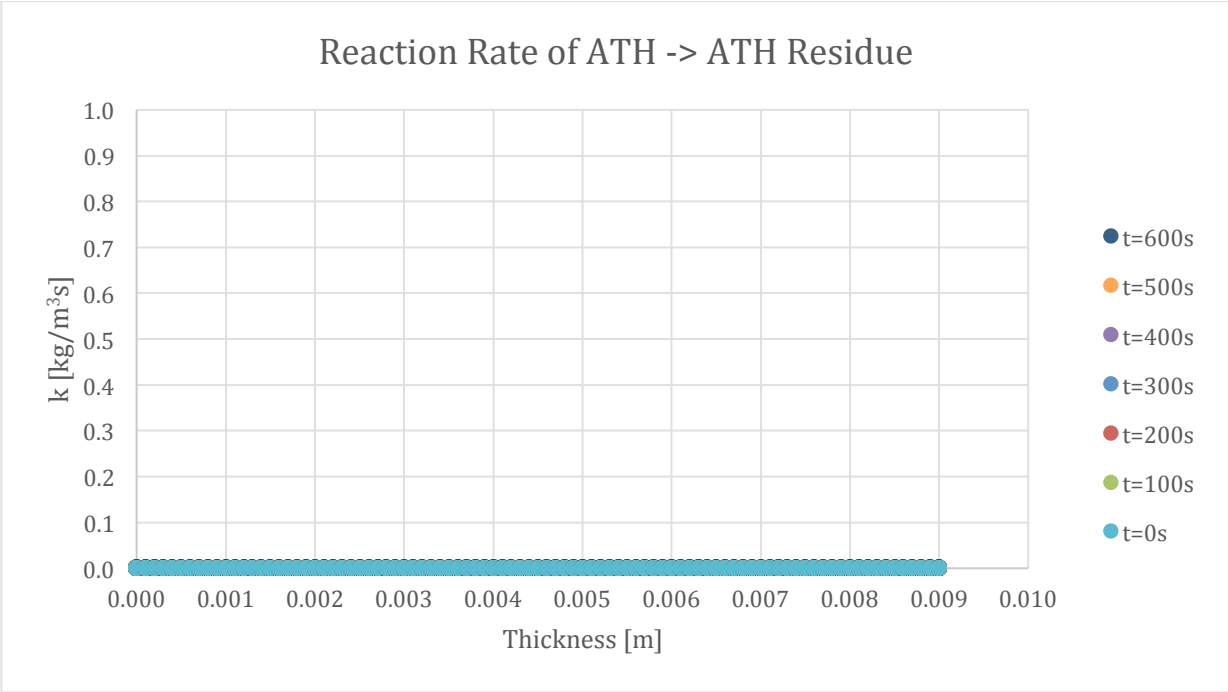


Figure 244-Reaction rate profile for ATH->ATH Residue in 100:0 resin/ATH sample and 50% glass

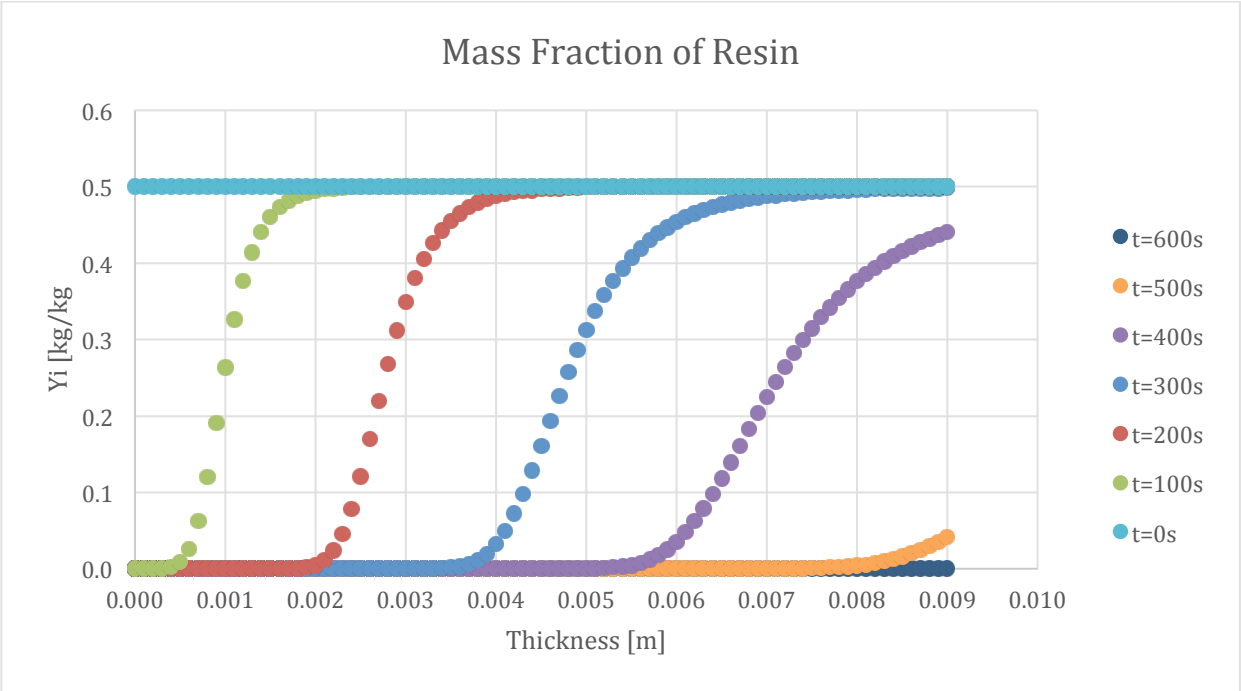


Figure 245-Mass fraction profile for Resin in 100:0 resin/ATH sample and 50% glass

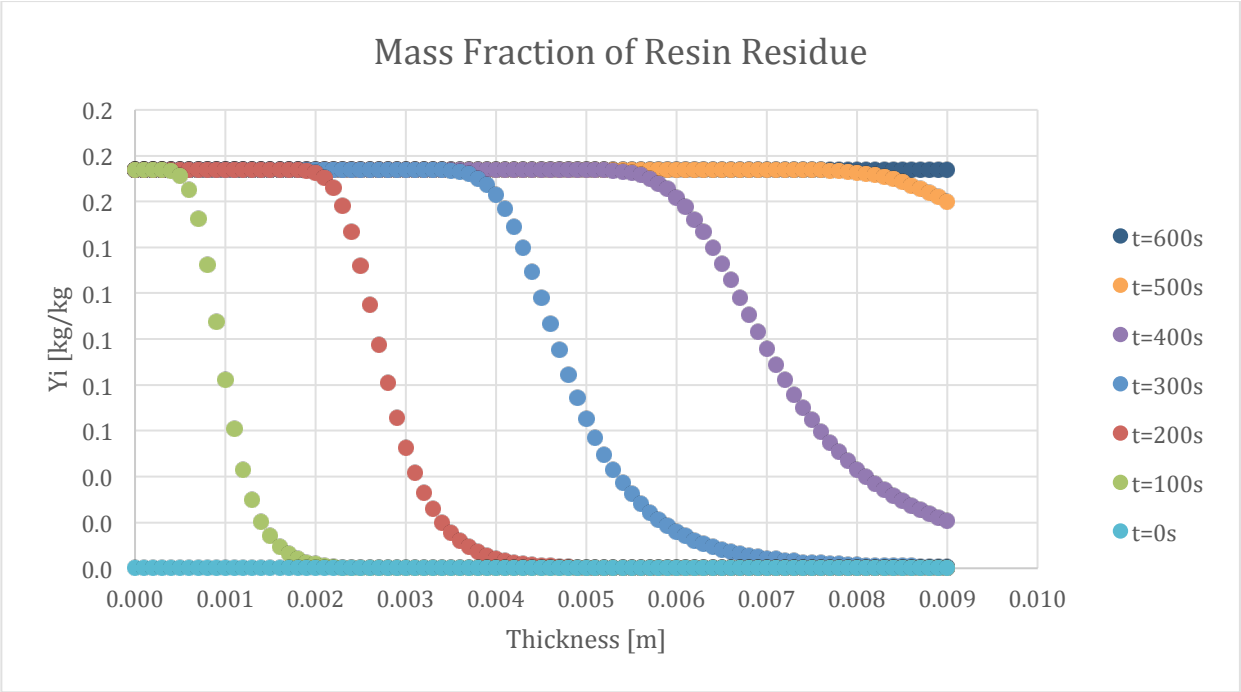


Figure 246-Mass fraction profile for Resin Residue in 100:0 resin/ATH sample and 50% glass

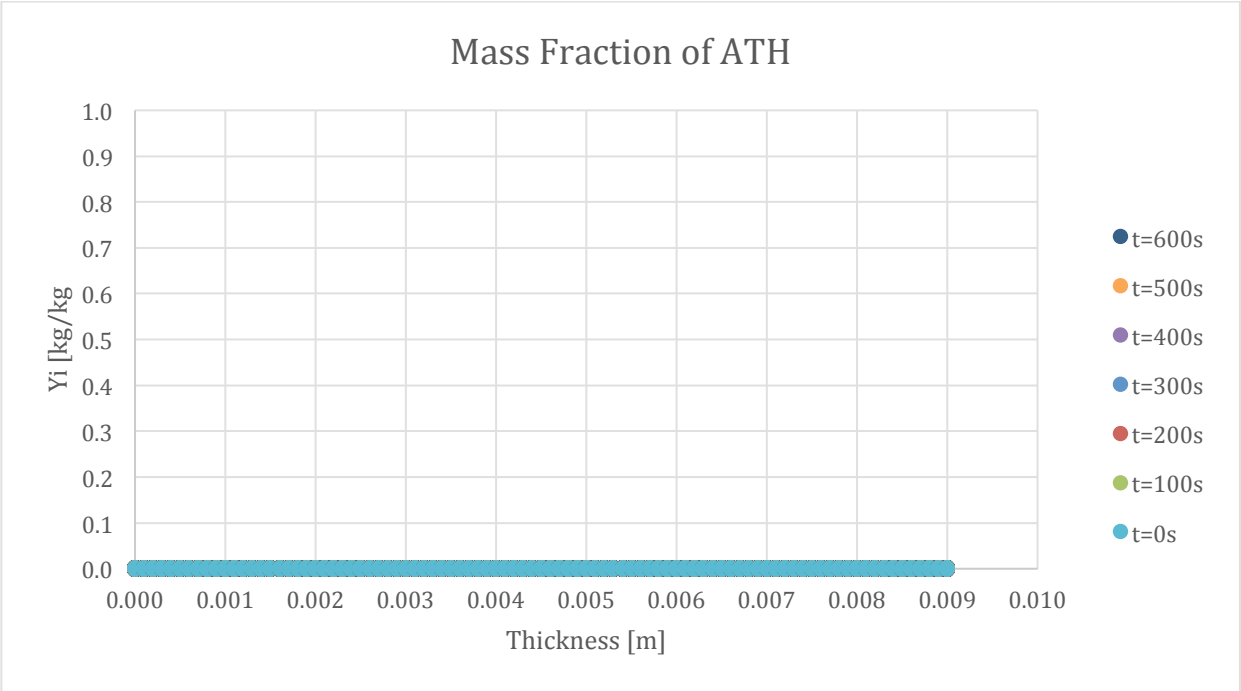


Figure 247-Mass fraction profile for ATH in 100:0 resin/ATH sample and 50% glass

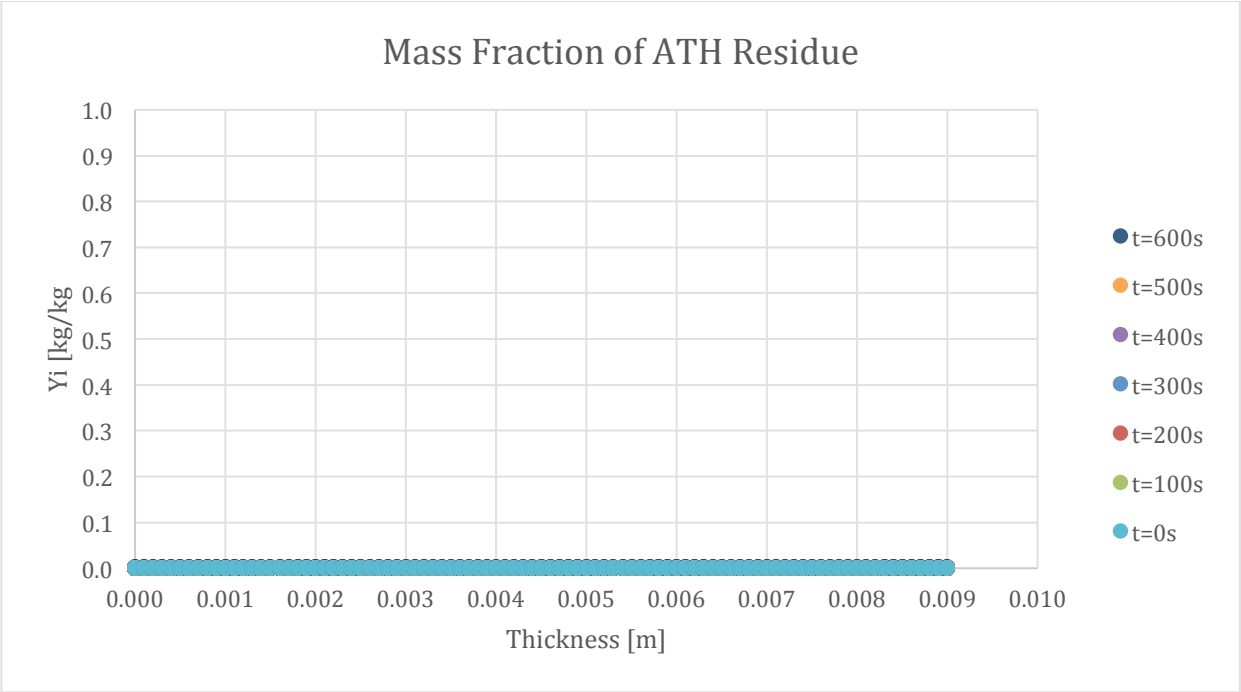


Figure 248-Mass fraction profile for ATH Residue in 100:0 resin/ATH sample and 50% glass

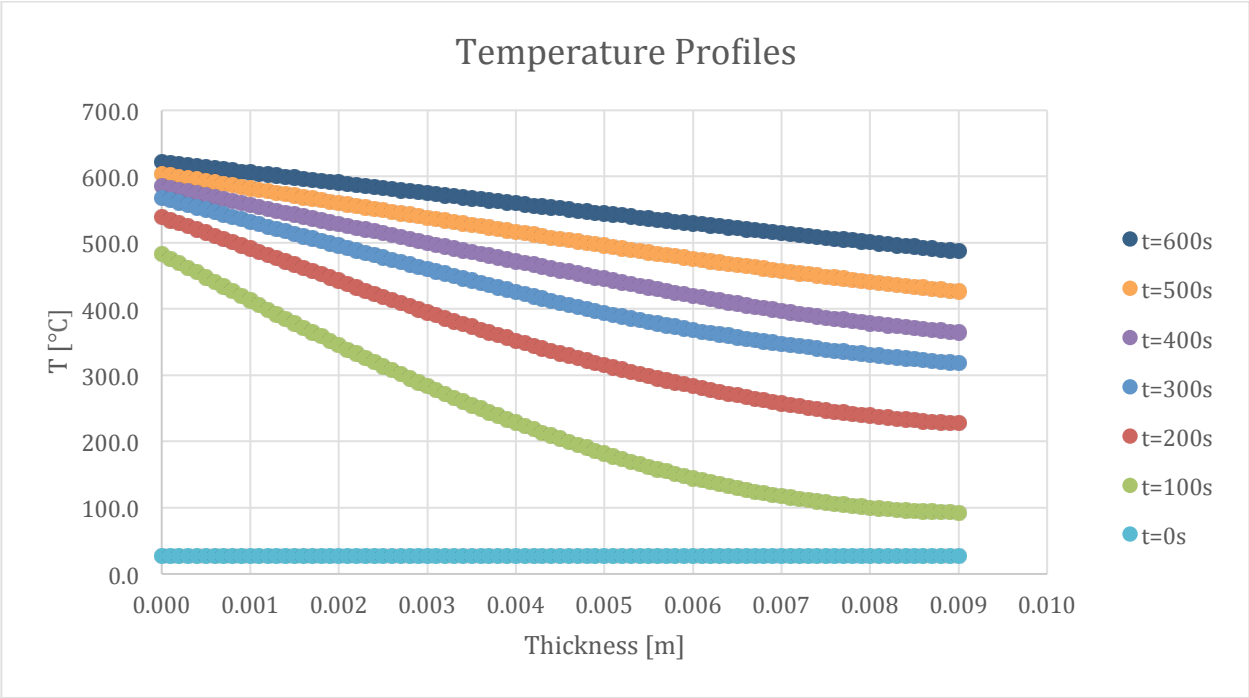


Figure 249-Temperature profile for ATH->ATH Residue in 100:0 resin/ATH sample and 50% glass

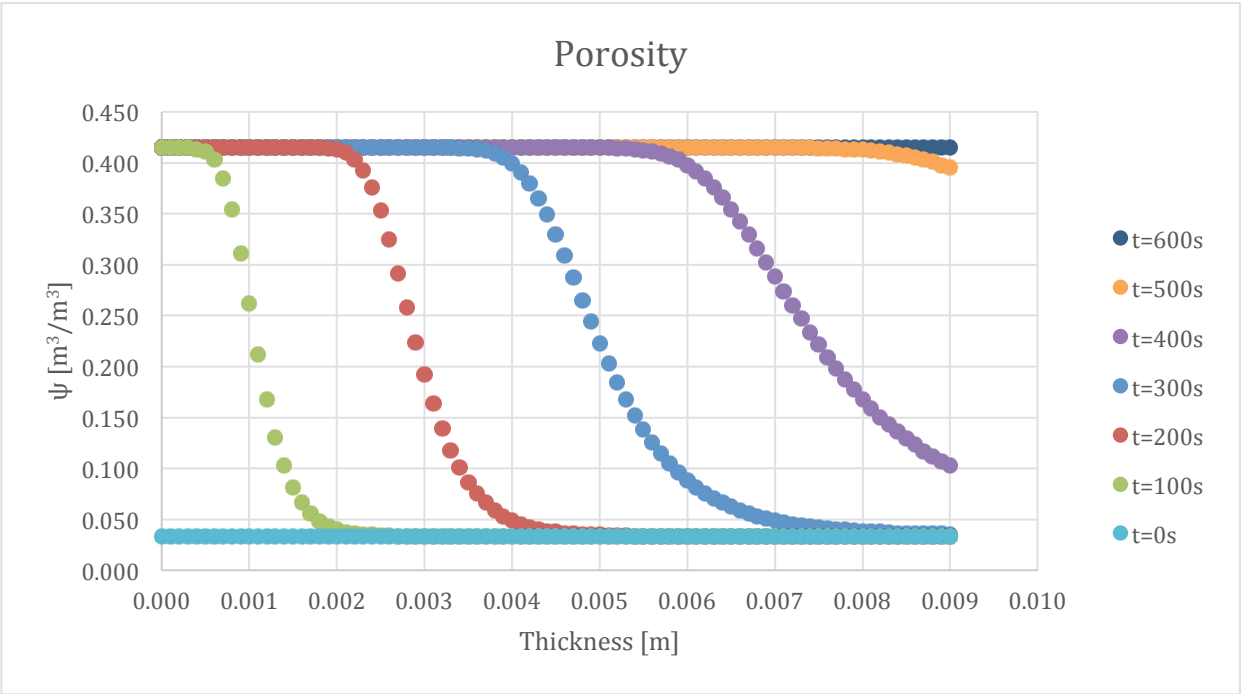


Figure 250-Porosity profile for ATH->ATH Residue in 100:0 resin/ATH sample and 50% glass

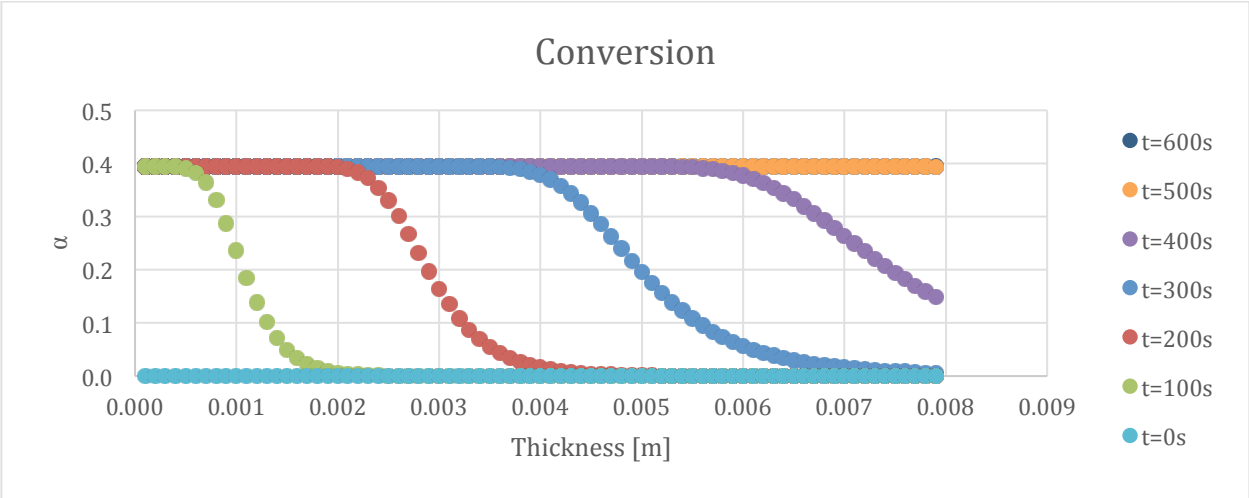


Figure 251-Conversion profile for ATH->ATH Residue in 100:0 resin/ATH sample and 50% glass

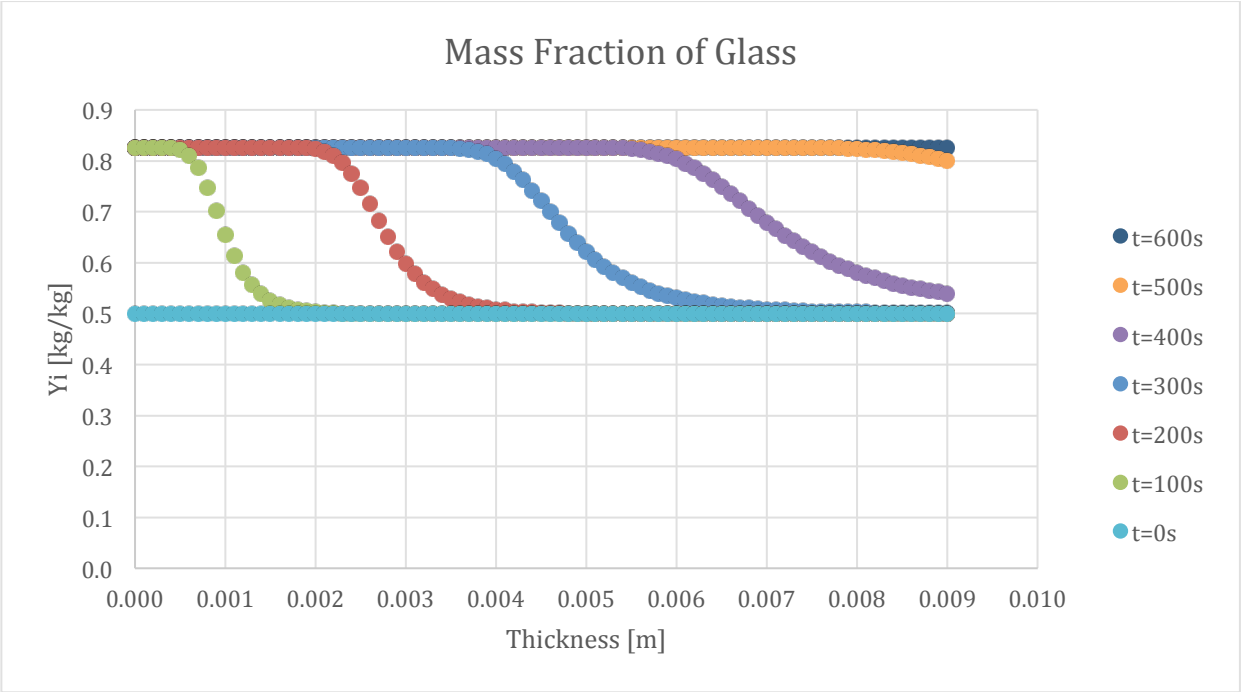


Figure 252-Mass fraction profile for Glass in 100:0 resin/ATH sample and 50% glass

The second set of results are from the simulation of 100:133 resin/ATH.

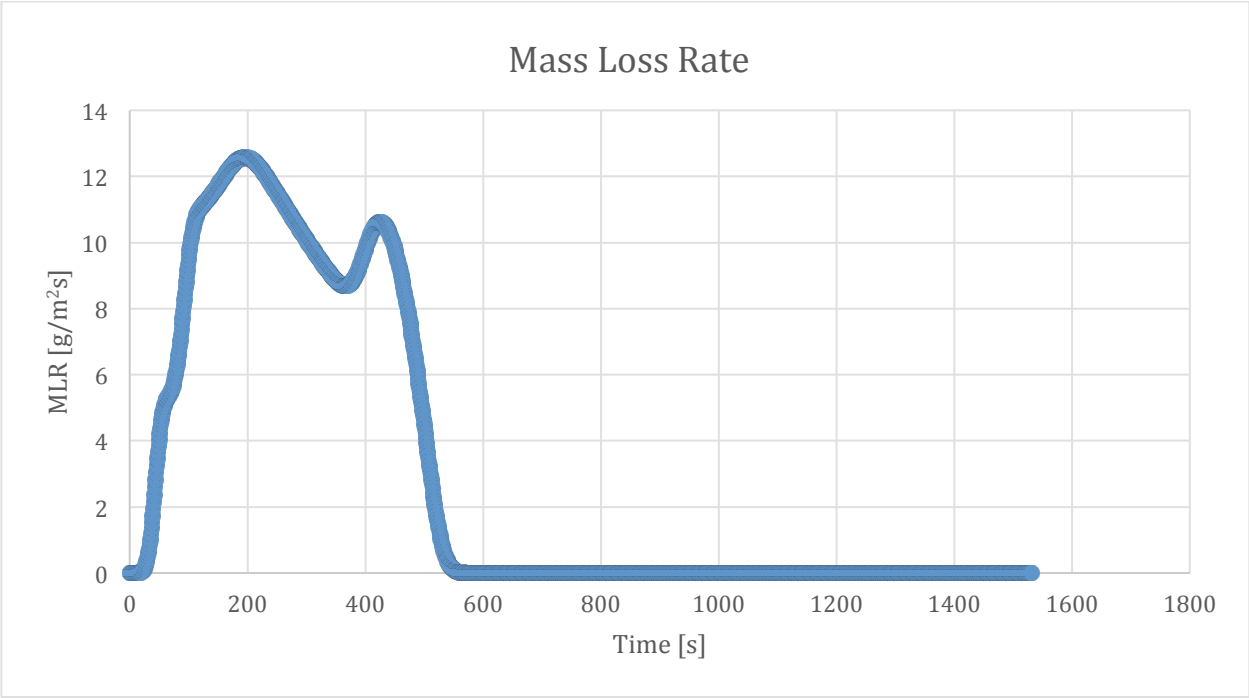


Figure 253-Mass loss rate curve for 100:130 resin/ATH sample and 50% glass

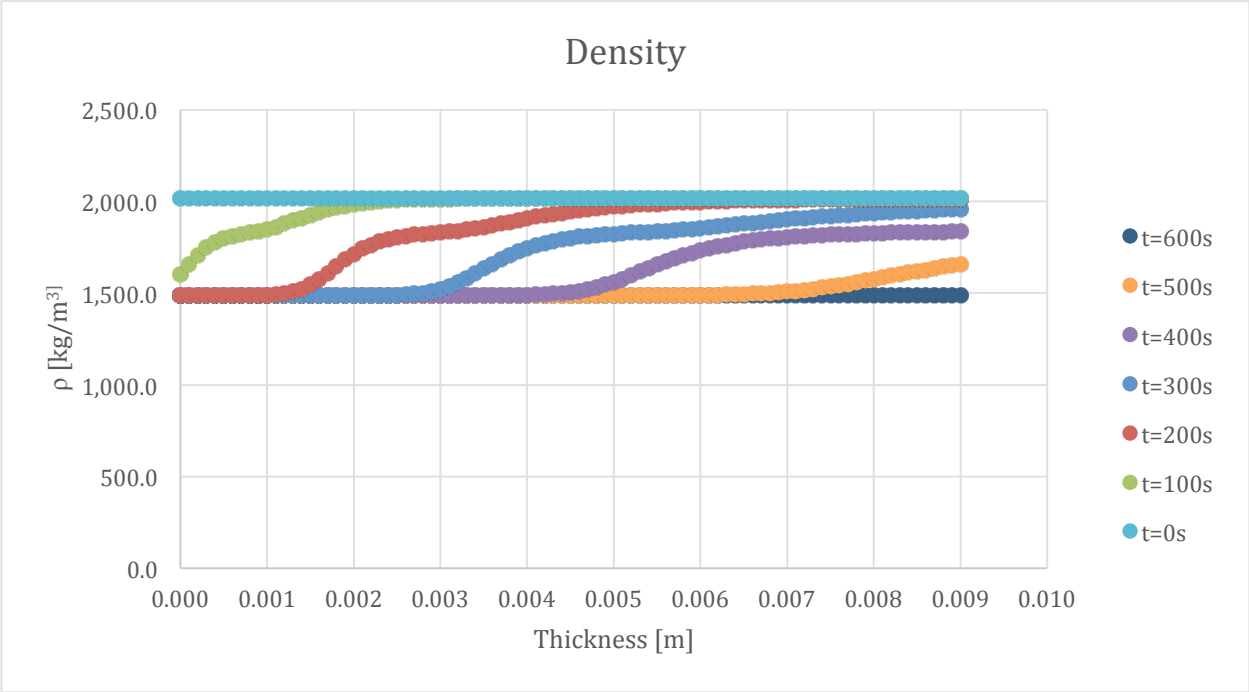


Figure 254-Density profile for 100:130 resin/ATH sample and 50% glass

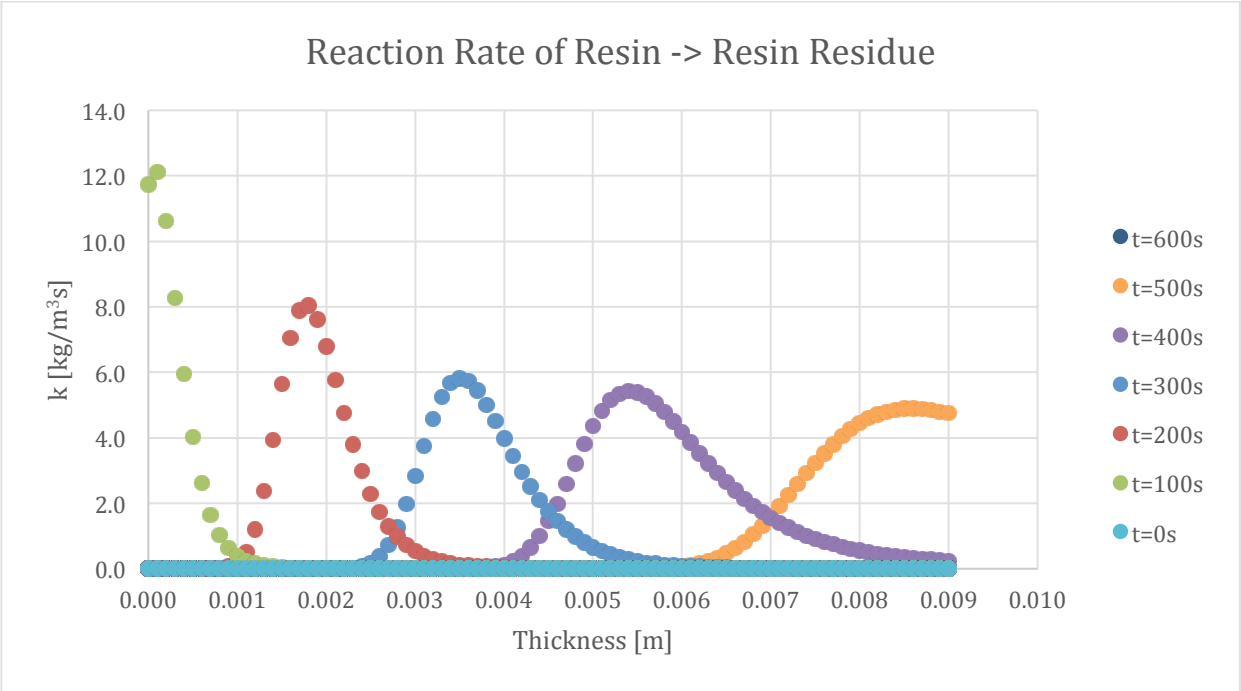


Figure 255-Reaction rate profile for Resin->Resin Residue in 100:130 resin/ATH sample and 50% glass

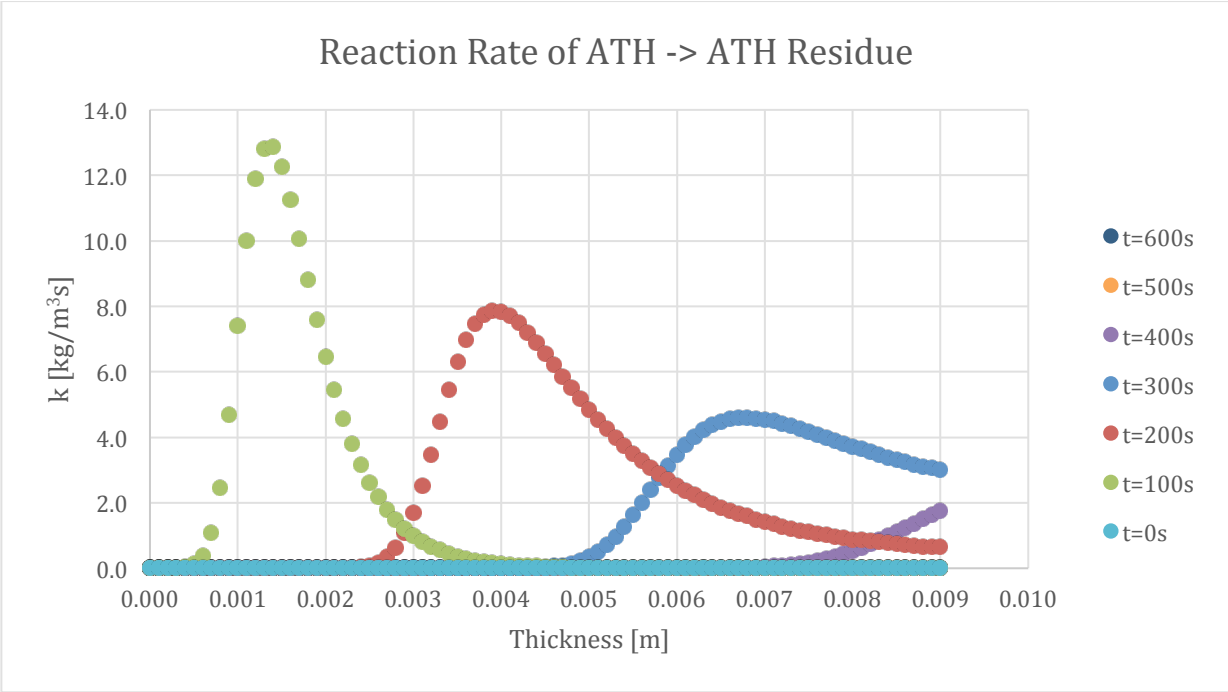


Figure 256-Reaction rate profile for ATH->ATH Residue in 100:1300 resin/ATH sample and 50% glass

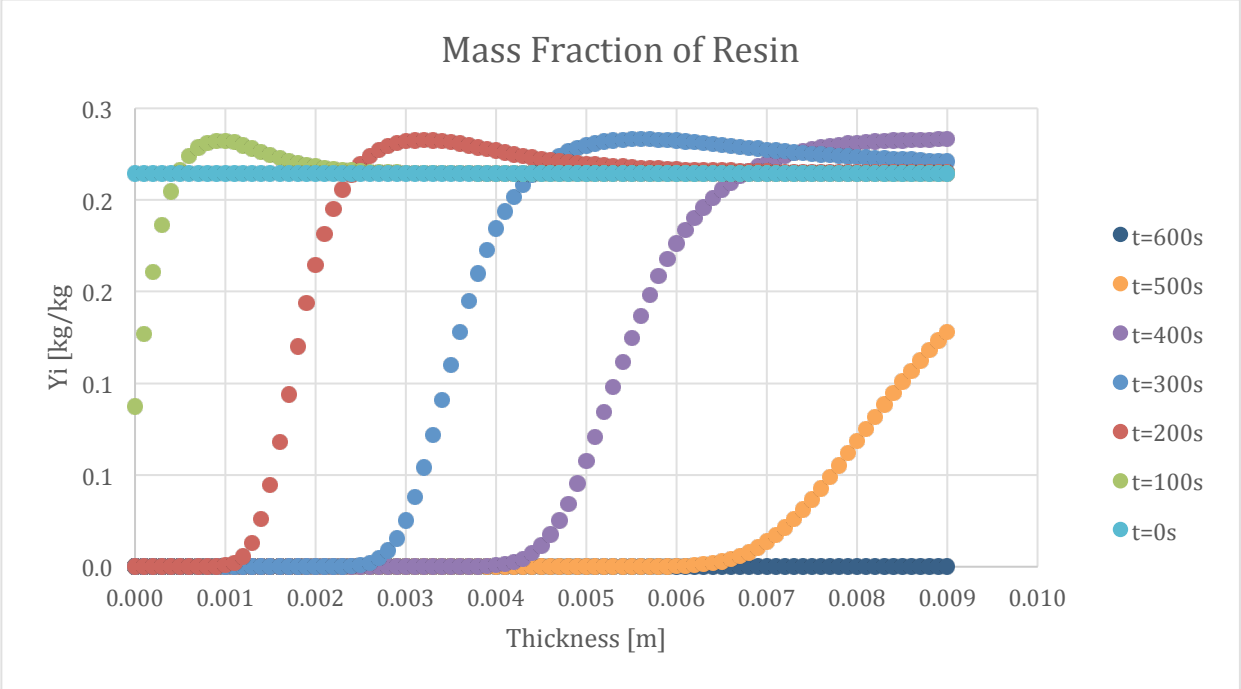


Figure 257-Mass fraction profile for Resin in 100:130 resin/ATH sample and 50% glass

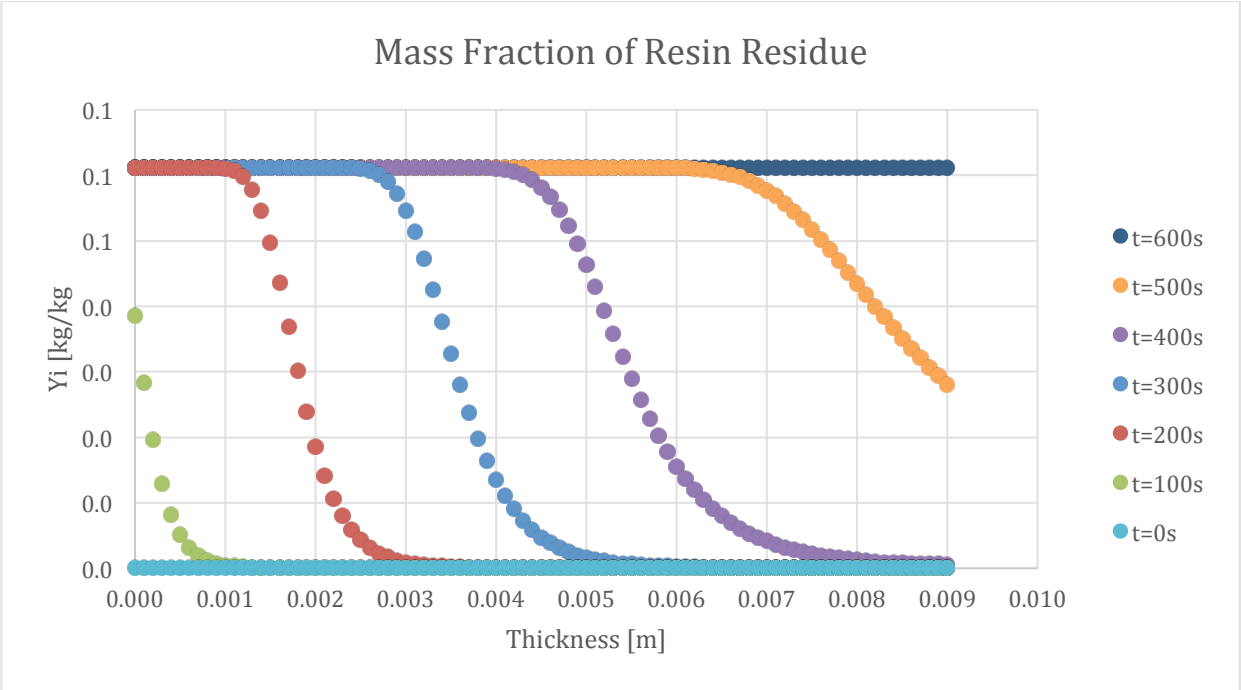


Figure 258-Mass fraction profile for Resin Residue in 100:130 resin/ATH sample and 50% glass

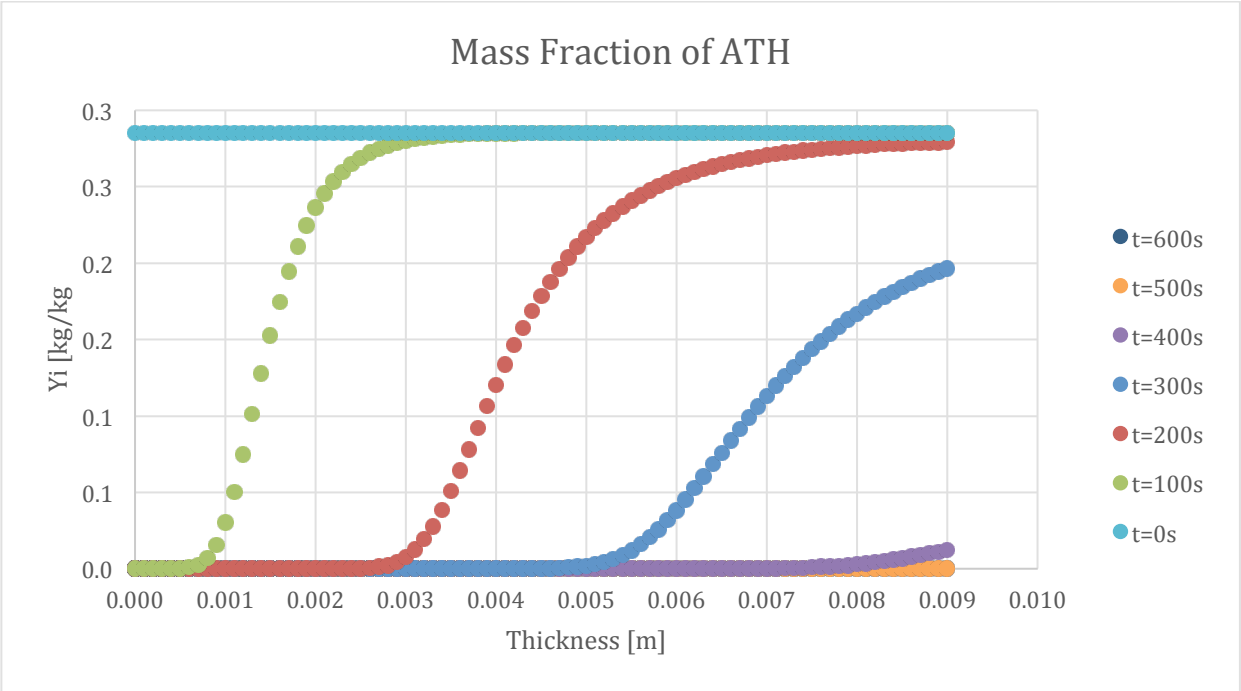


Figure 259-Mass fraction profile for ATH in 100:130 resin/ATH sample and 50% glass

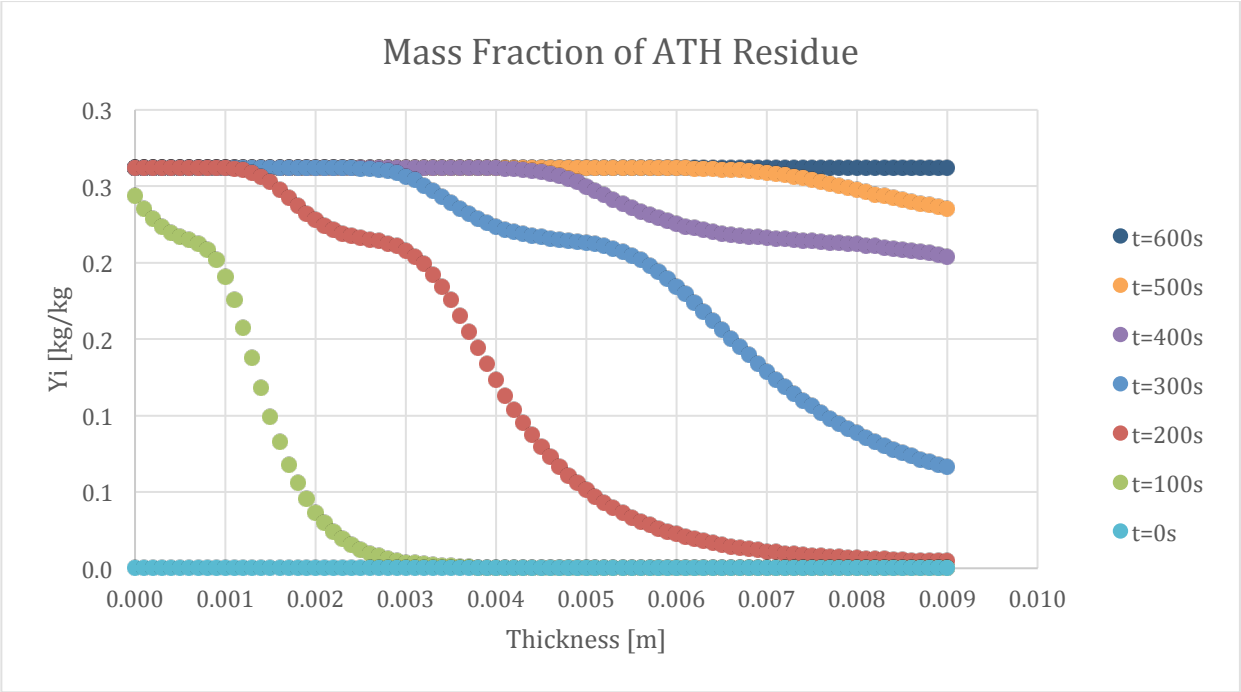


Figure 260-Mass fraction profile for ATH Residue in 100:130 resin/ATH sample and 50% glass

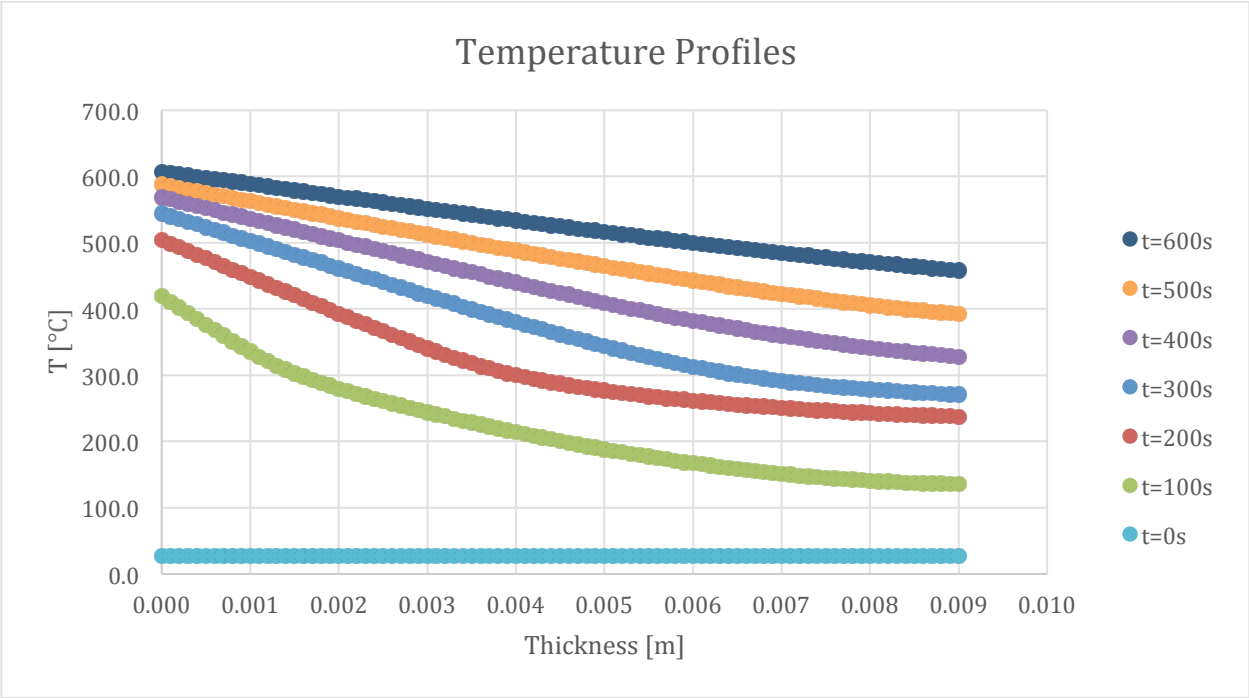


Figure 261-Temperature profile for 100:130 resin/ATH sample and 50% glass

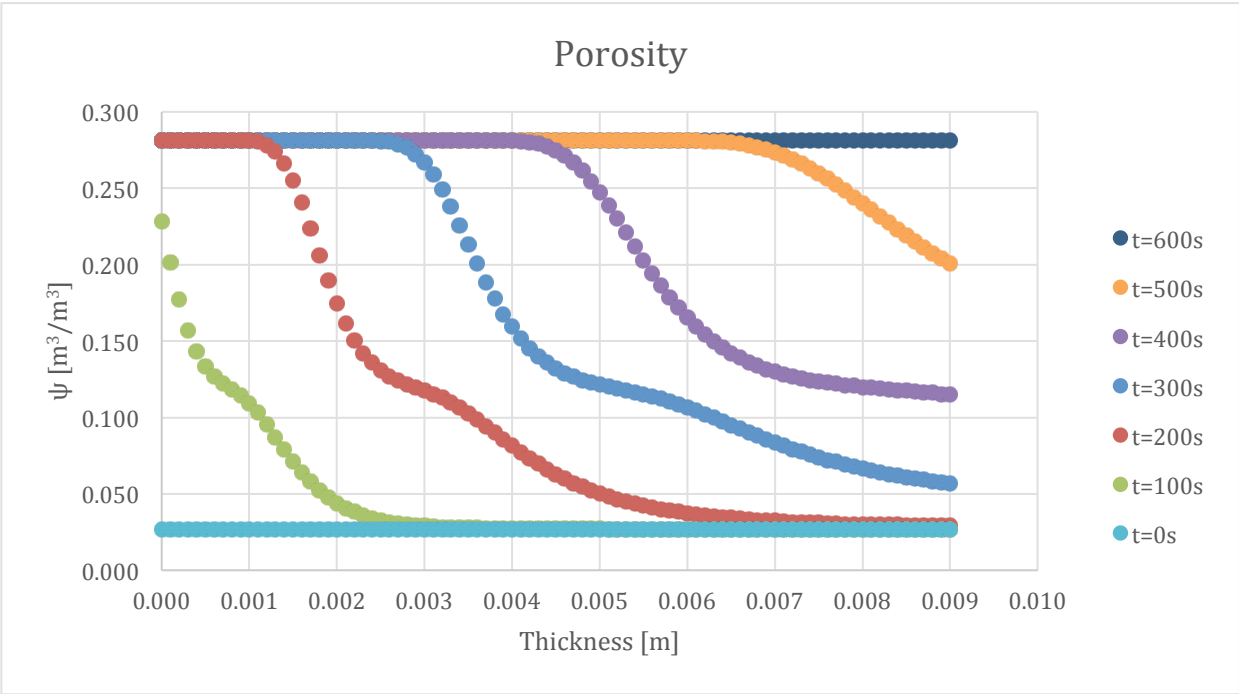


Figure 262-Porosity profile for 100:130 resin/ATH sample and 50% glass

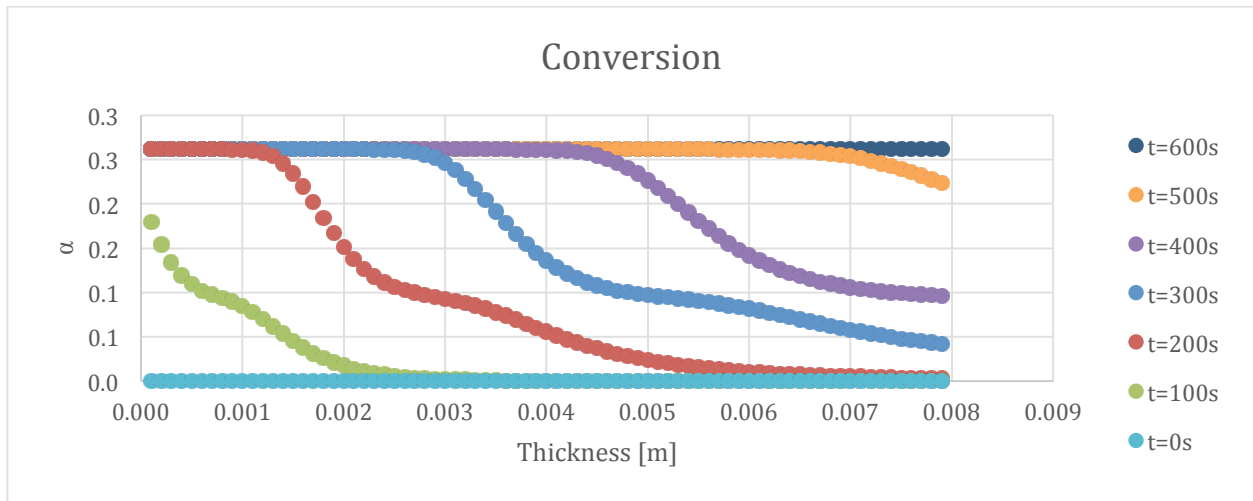


Figure 263-Conversion profile for 100:130 resin/ATH sample and 50% glass

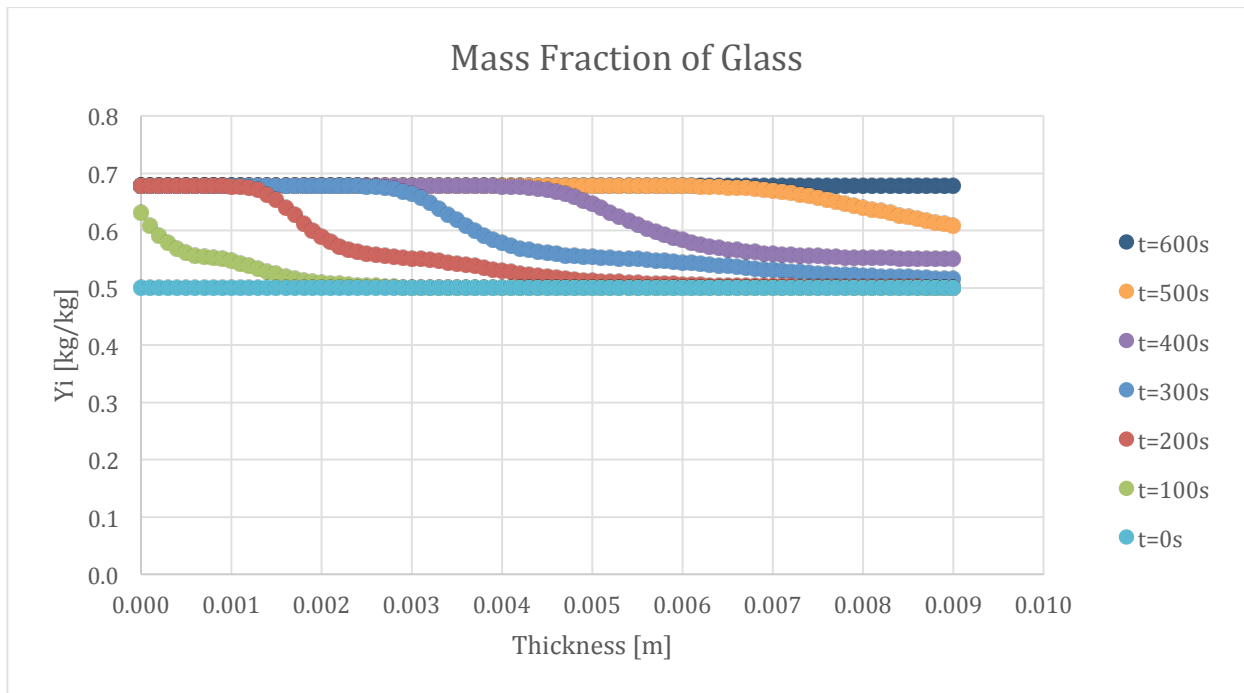


Figure 264-Mass fraction profile for Glass in 100:130 resin/ATH sample and 50% glass

9.10.2. Varying ATH

Four simulations were compiled in order to make a comparison when varying ATH. The baseline sample was used and can be referenced in the first section of graphs. The first set of graphs below shows the results of 5% ATH.



Figure 265-Mass loss rate curve for 5% ATH sample and 50% glass

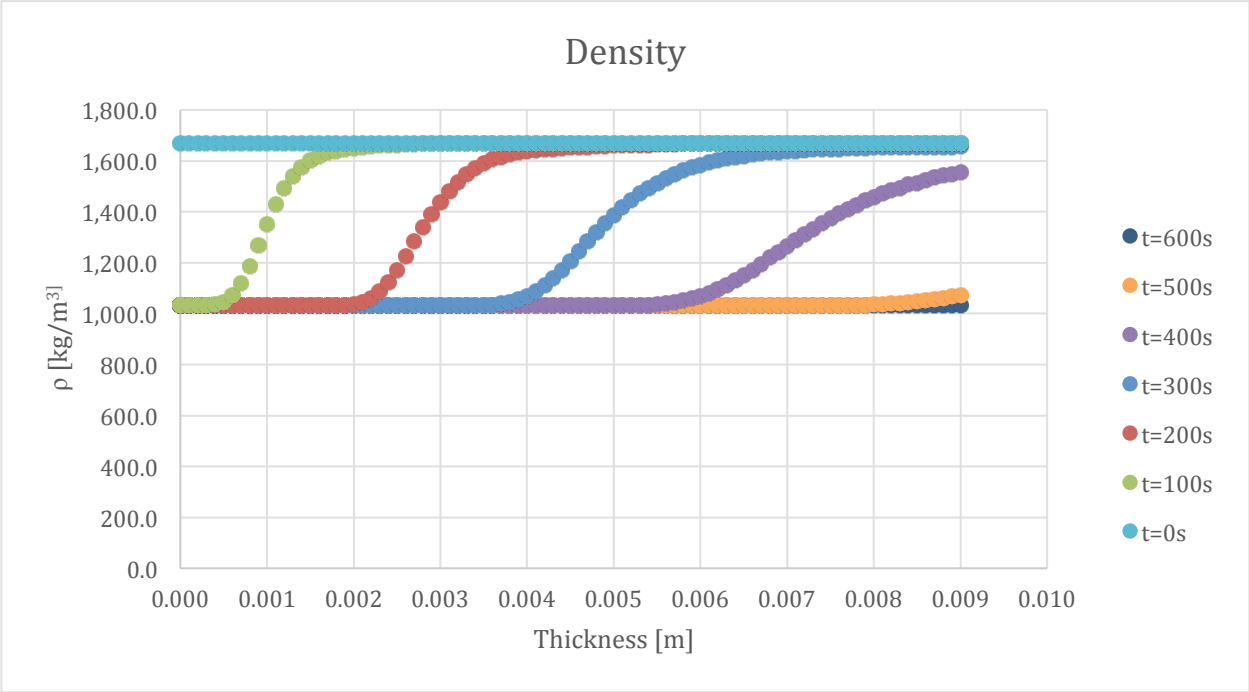


Figure 266-Density profile for 5% ATH sample and 50% glass

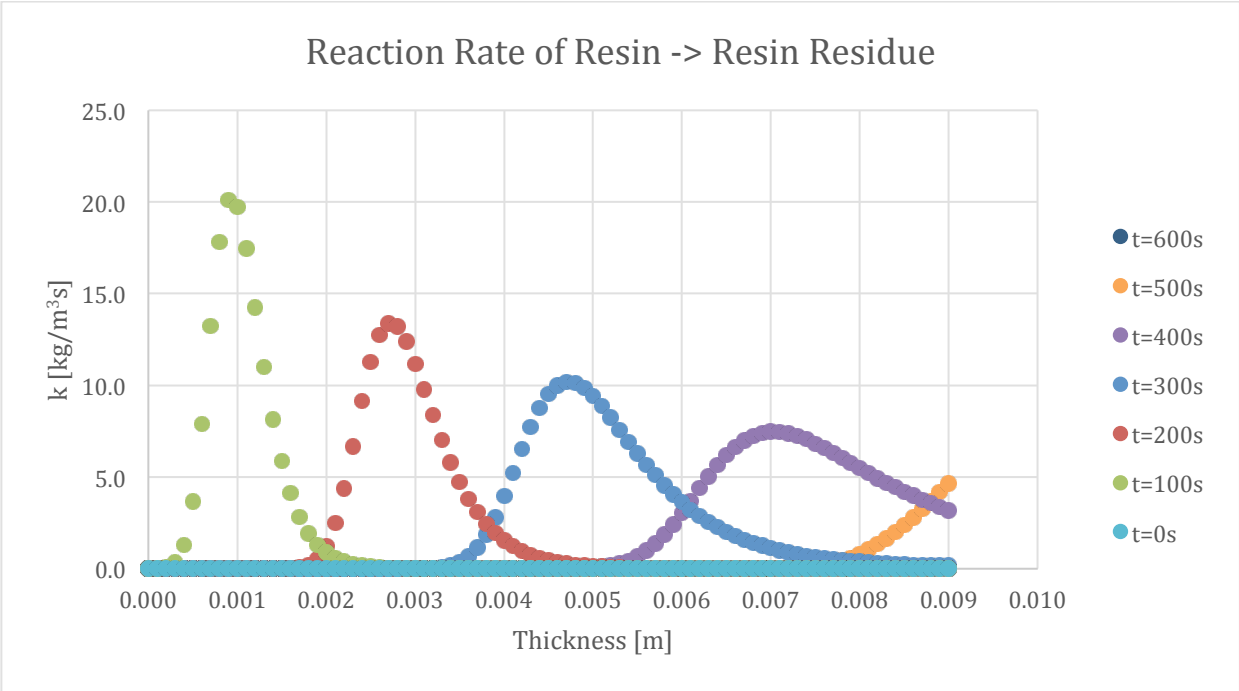


Figure 267-Reaction rate profile for Resin->Resin Residue in 5% ATH sample and 50% glass

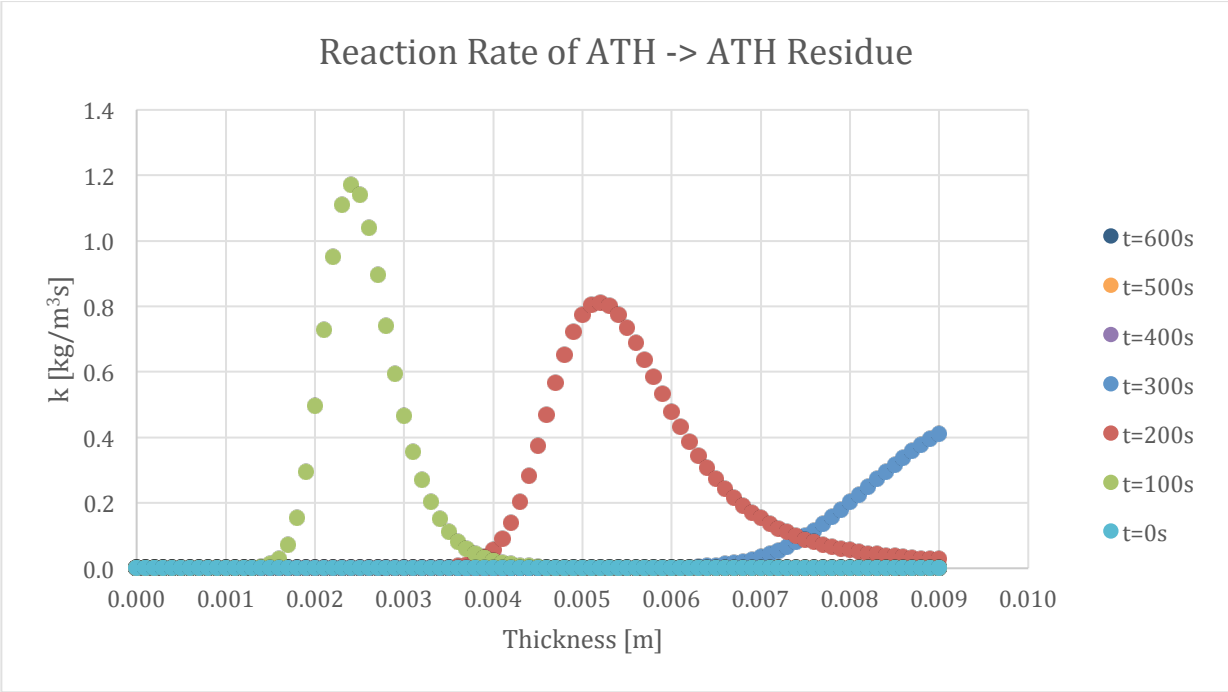


Figure 268-Reaction rate profile for ATH->ATH Residue in 5% ATH sample and 50% glass

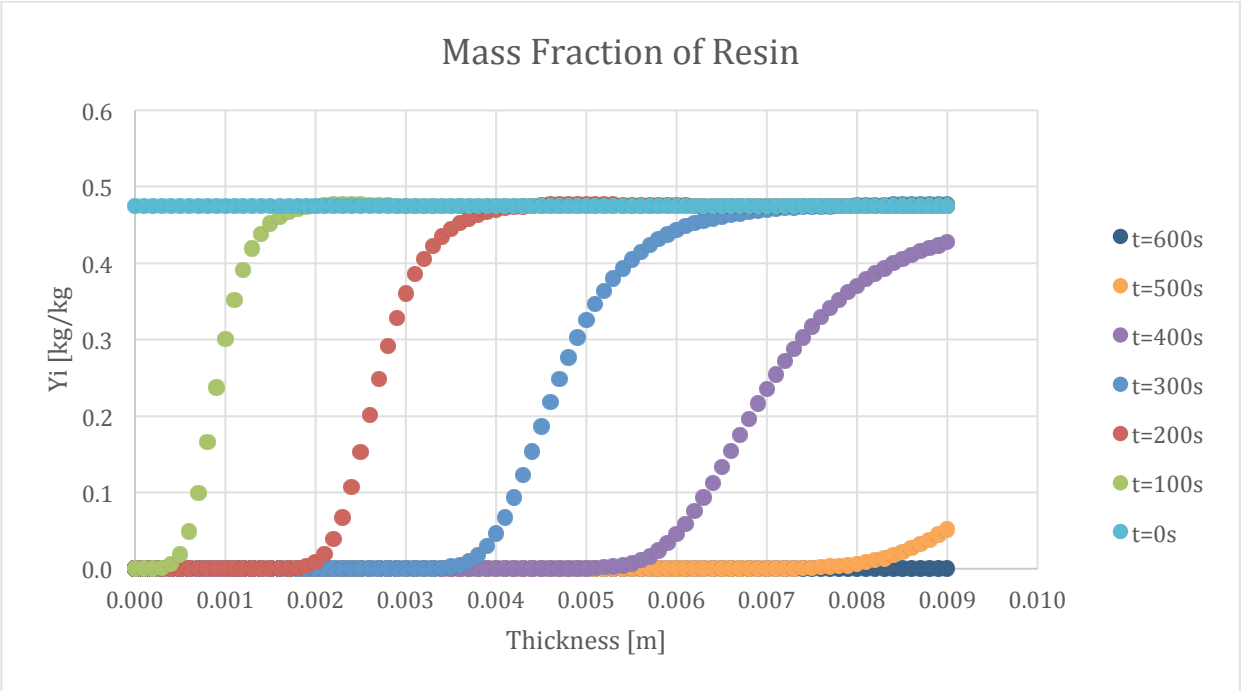


Figure 269-Mass fraction profile for Resin in 5% ATH sample and 50% glass

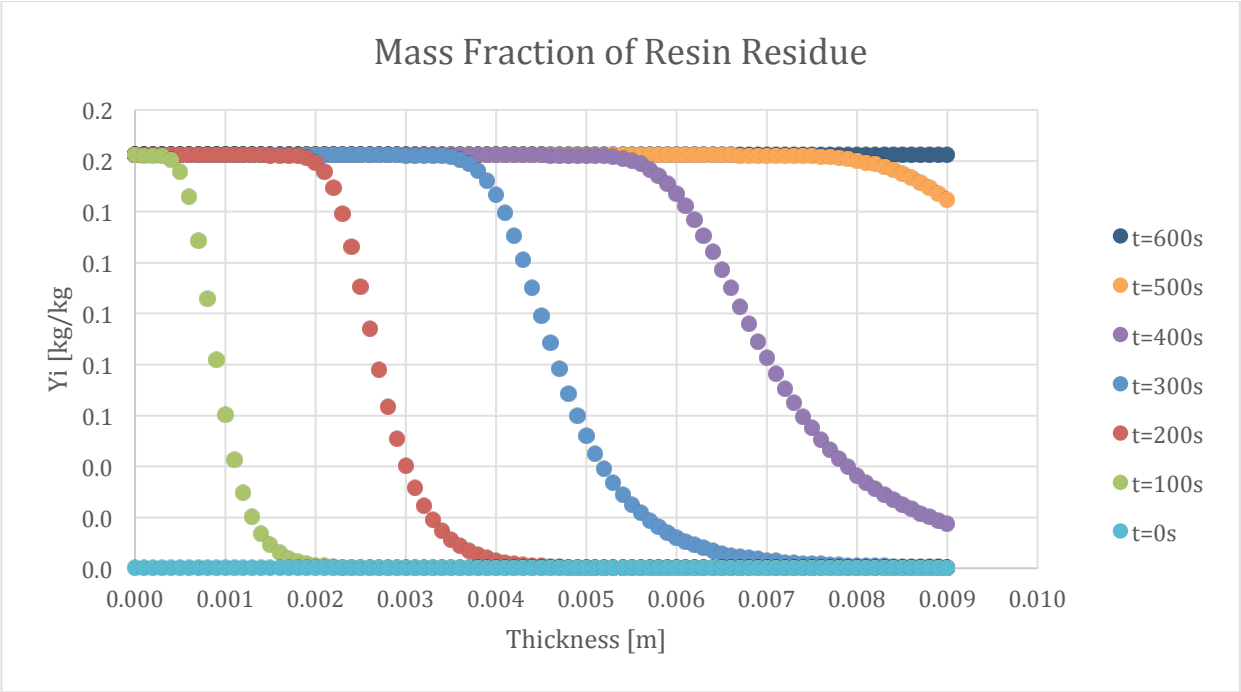


Figure 270-Mass fraction profile for Resin Residue in 5% ATH sample and 50% glass

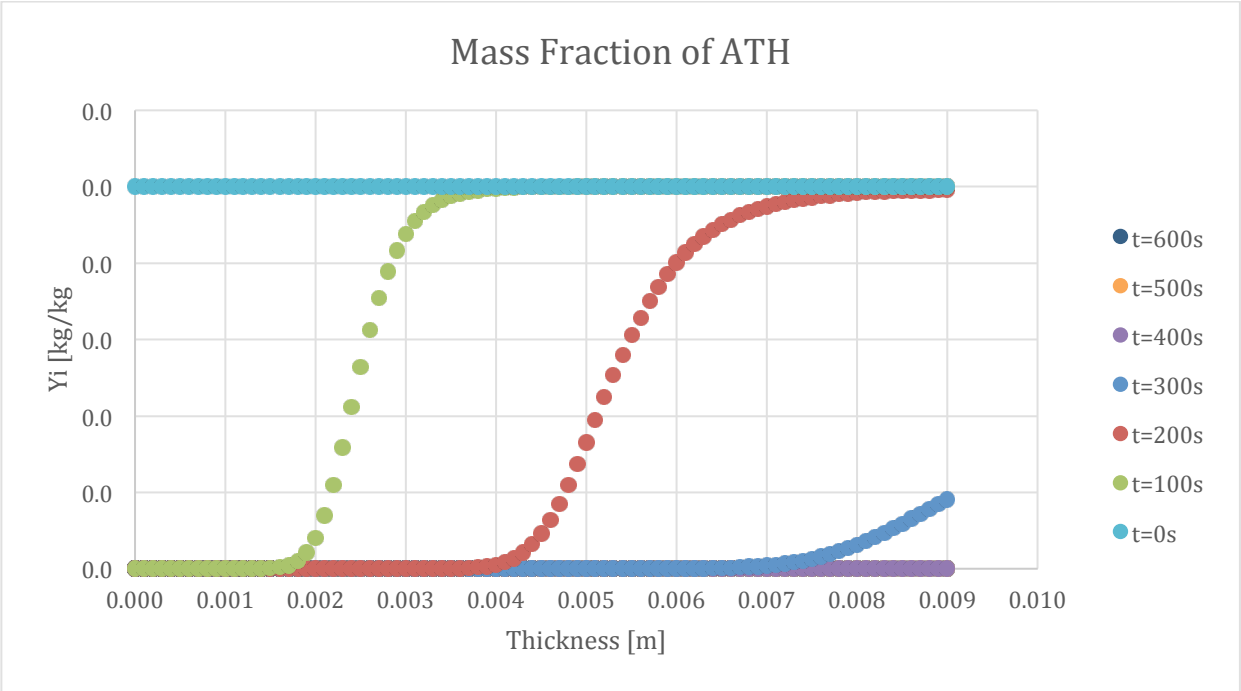


Figure 271-Mass fraction profile for ATH in 5% ATH sample and 50% glass

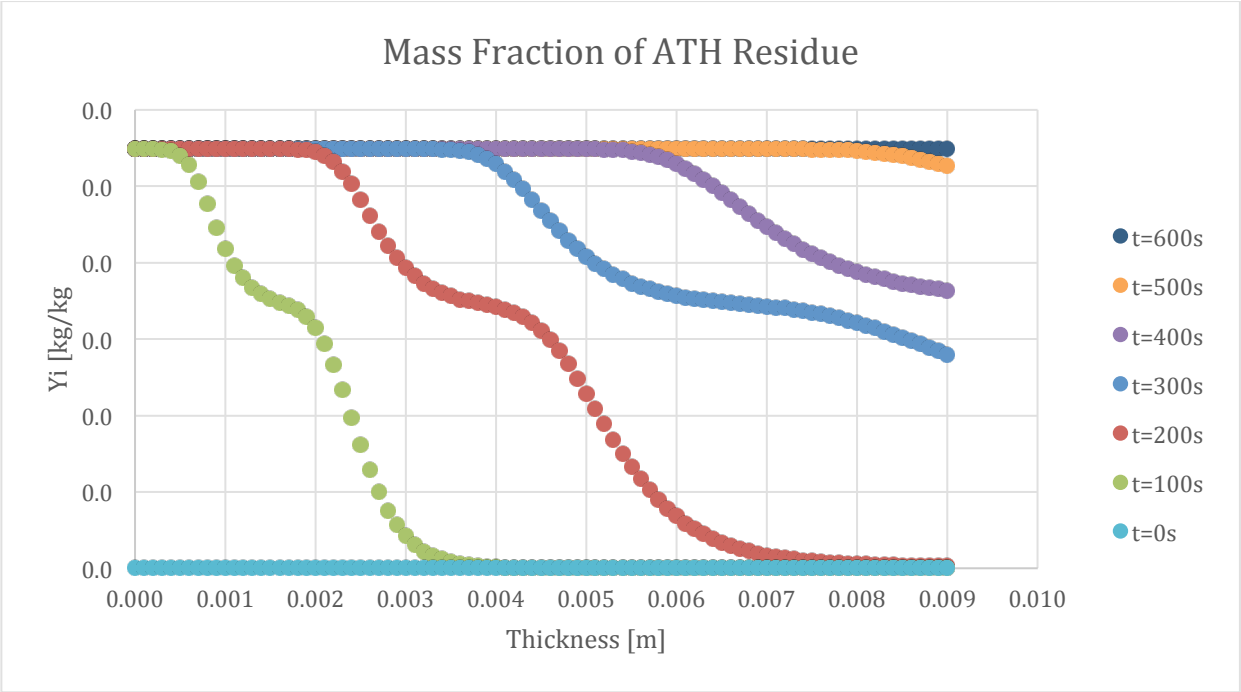


Figure 272-Mass fraction profile for ATH Residue in 5% ATH sample and 50% glass

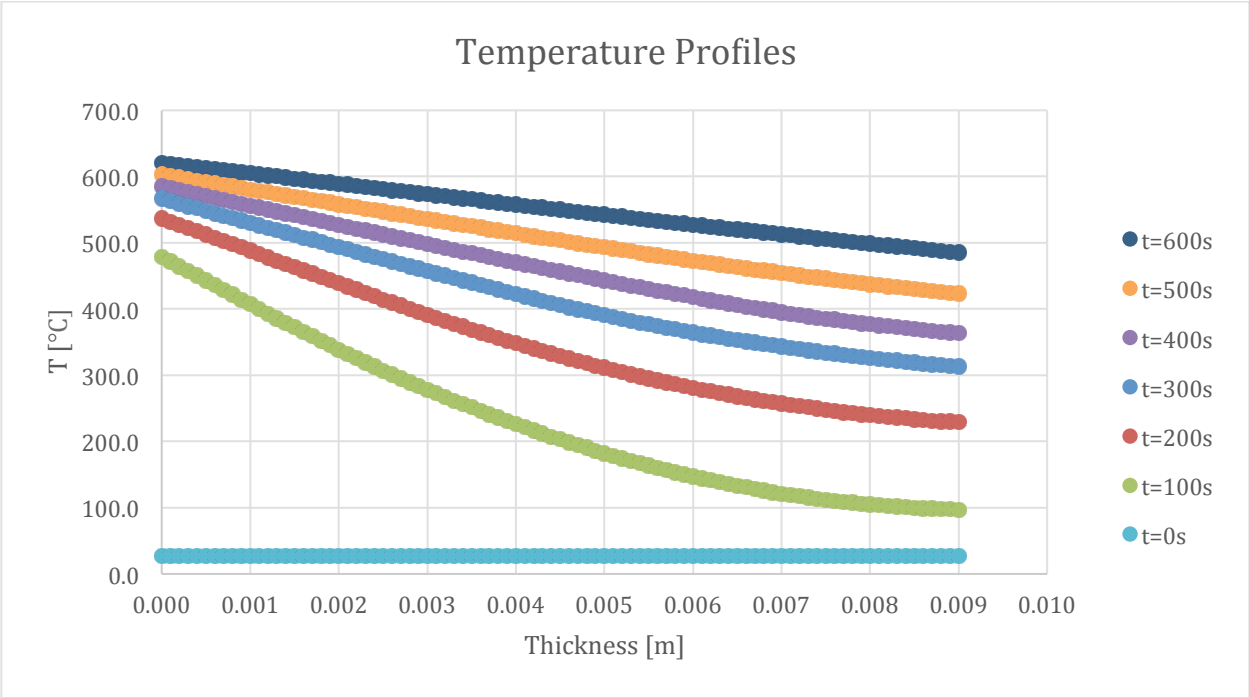


Figure 273-Temperature profile for 5% ATH sample and 50% glass

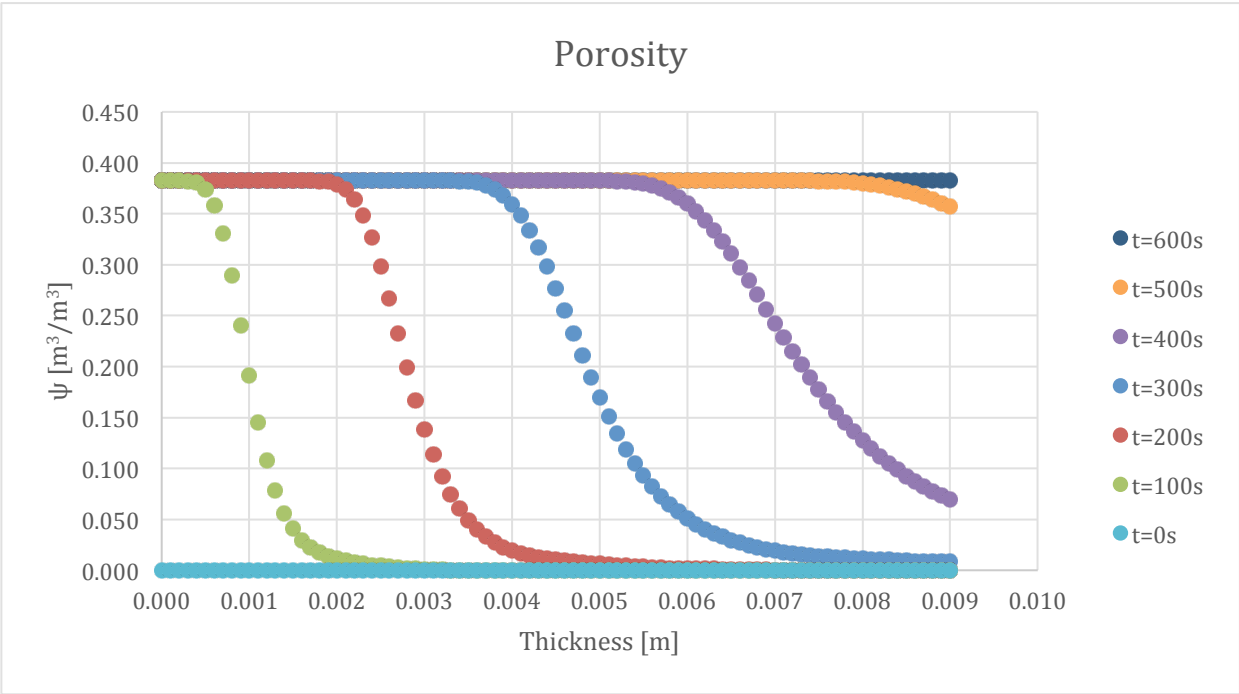


Figure 274-Porosity profile for 5% ATH sample and 50% glass

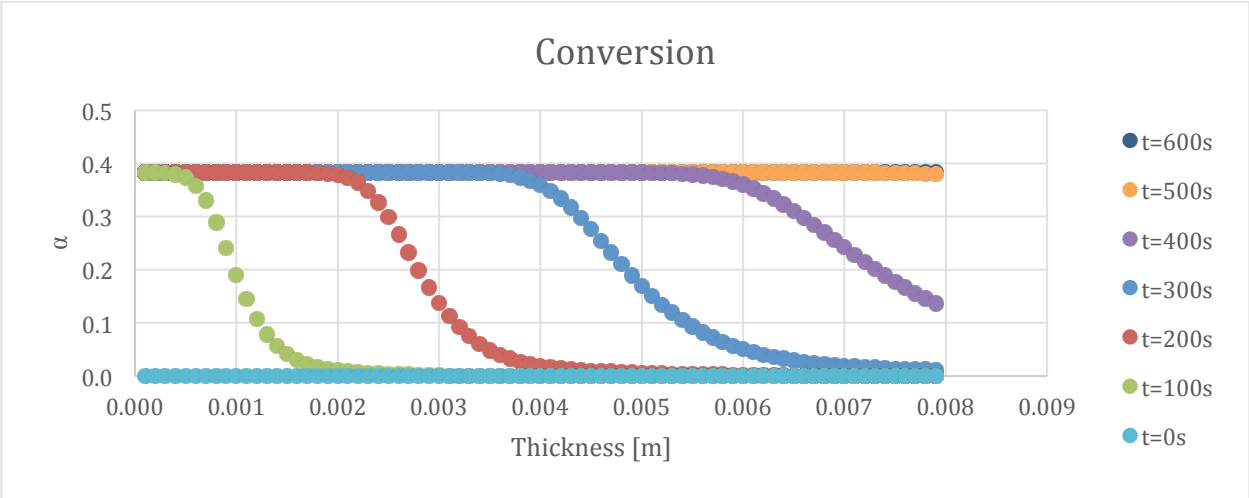


Figure 275-Conversion profile for 5% ATH sample and 50% glass

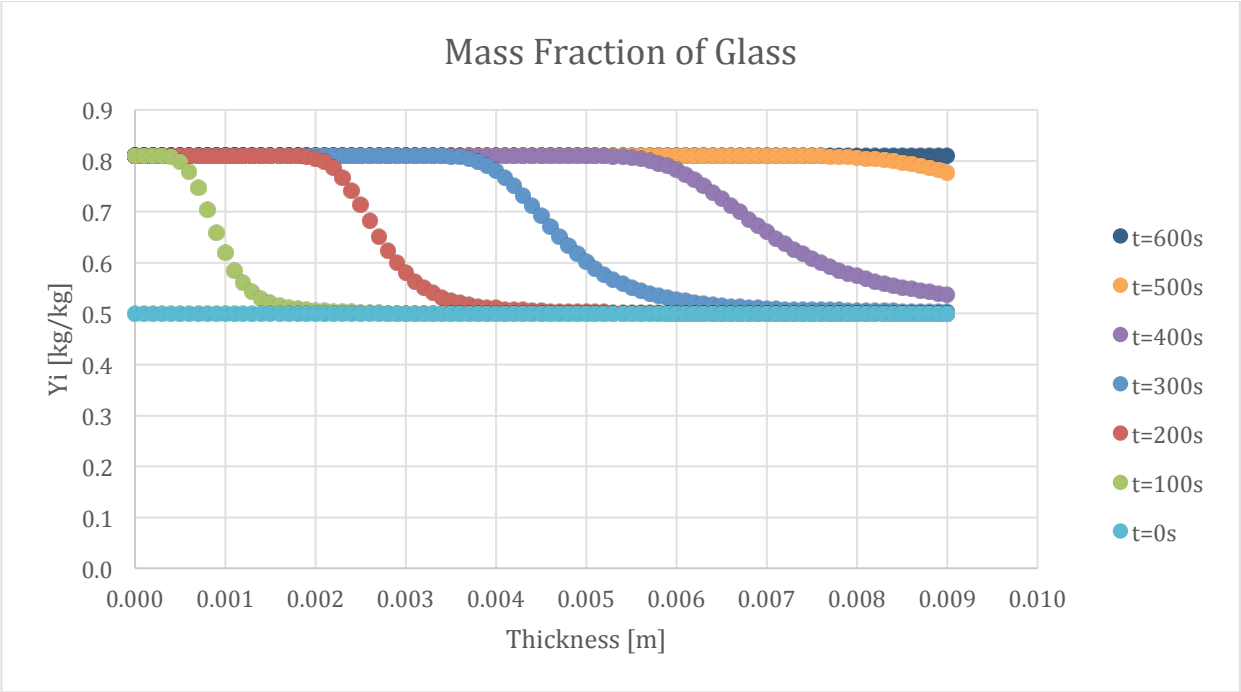


Figure 276-Mass fraction profile for Glass in 5% ATH sample and 50% glass

The following set of results are from the simulation of the 10% ATH sample.

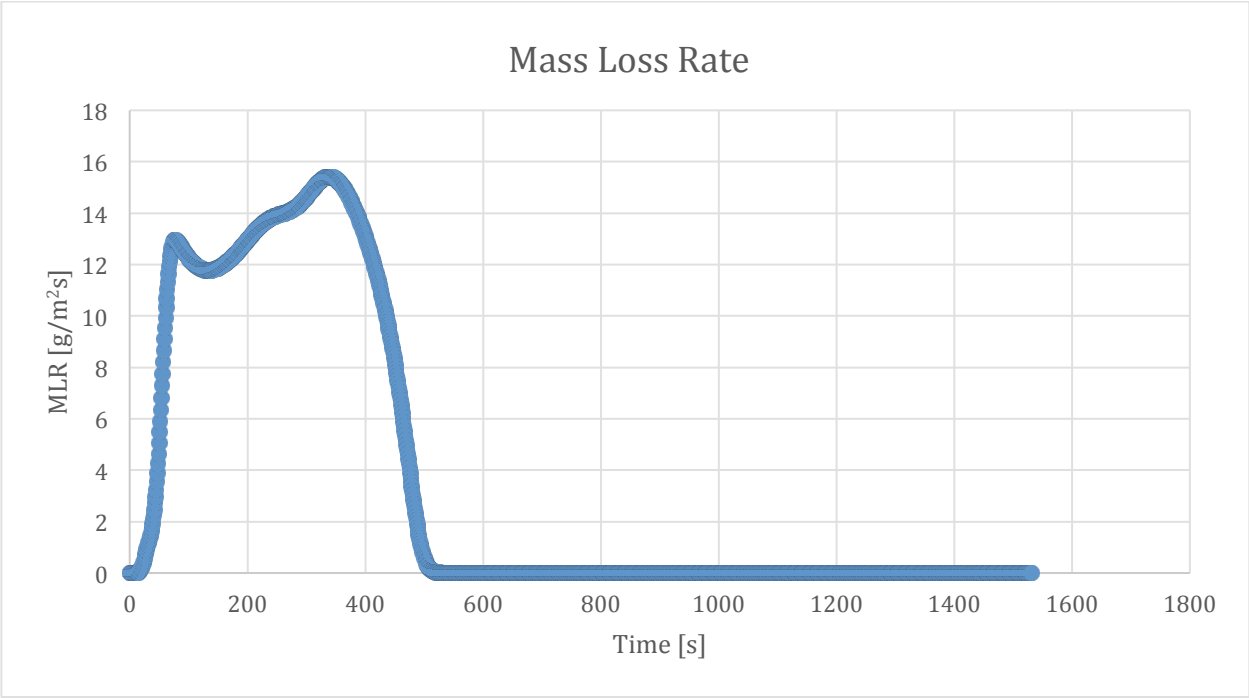


Figure 277-Mass loss rate curve for 10% ATH sample and 50% glass

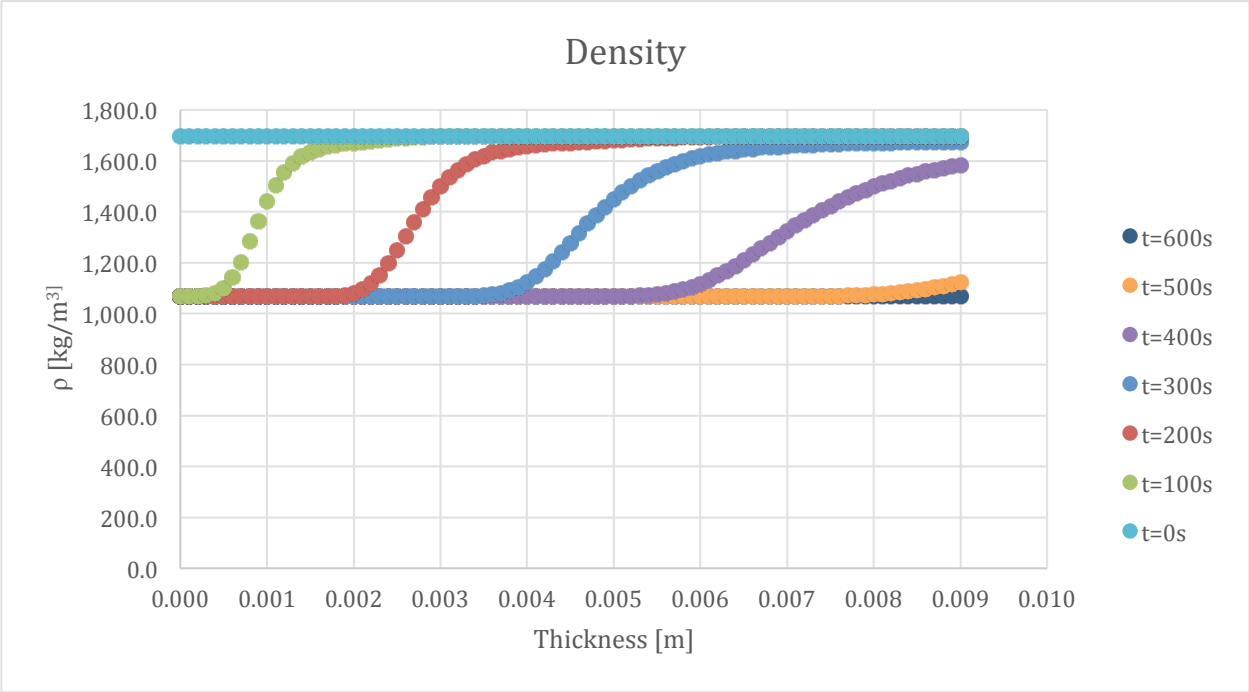


Figure 278-Density profile for 10% ATH sample and 50% glass

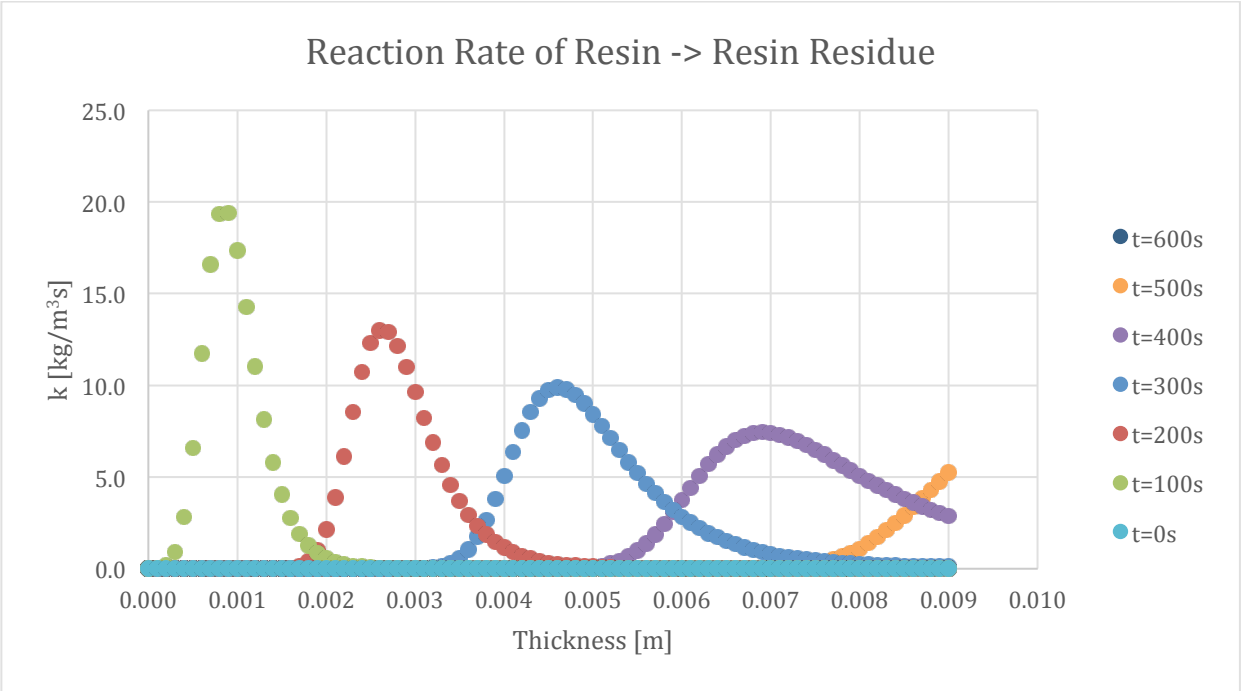


Figure 279-Reaction rate profile for Resin->Resin Residue in 10% ATH sample and 50% glass

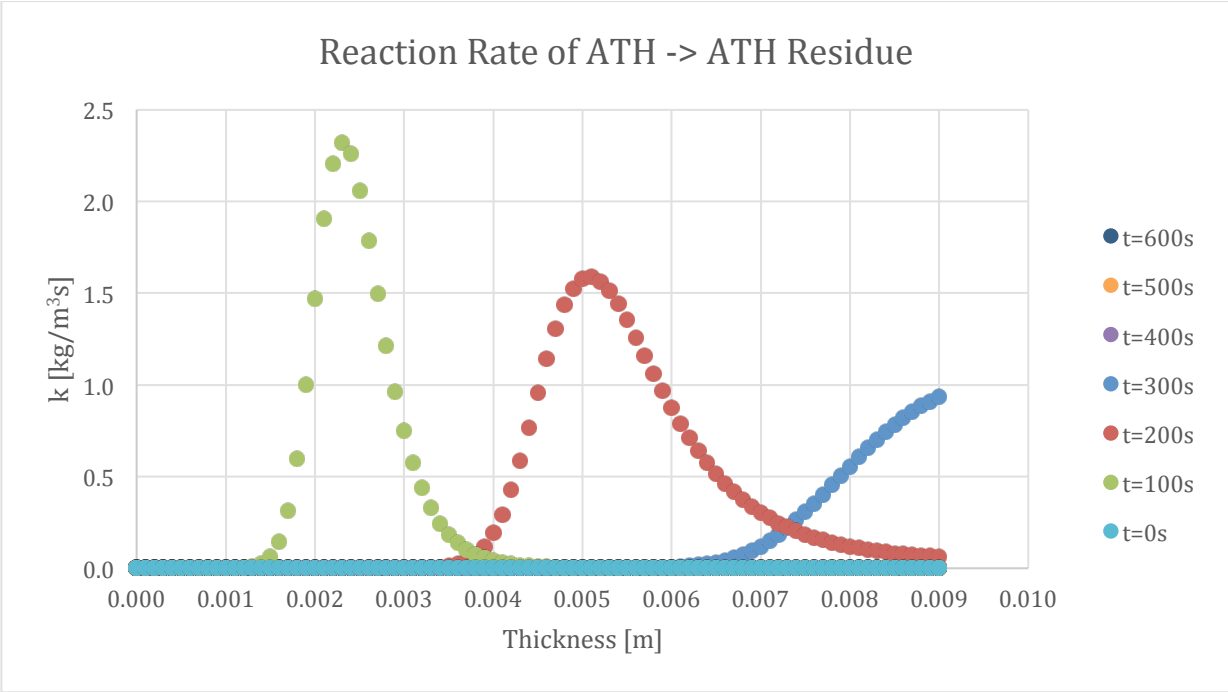


Figure 280-Reaction rate profile for ATH->ATH Residue in 10% ATH sample and 50% glass

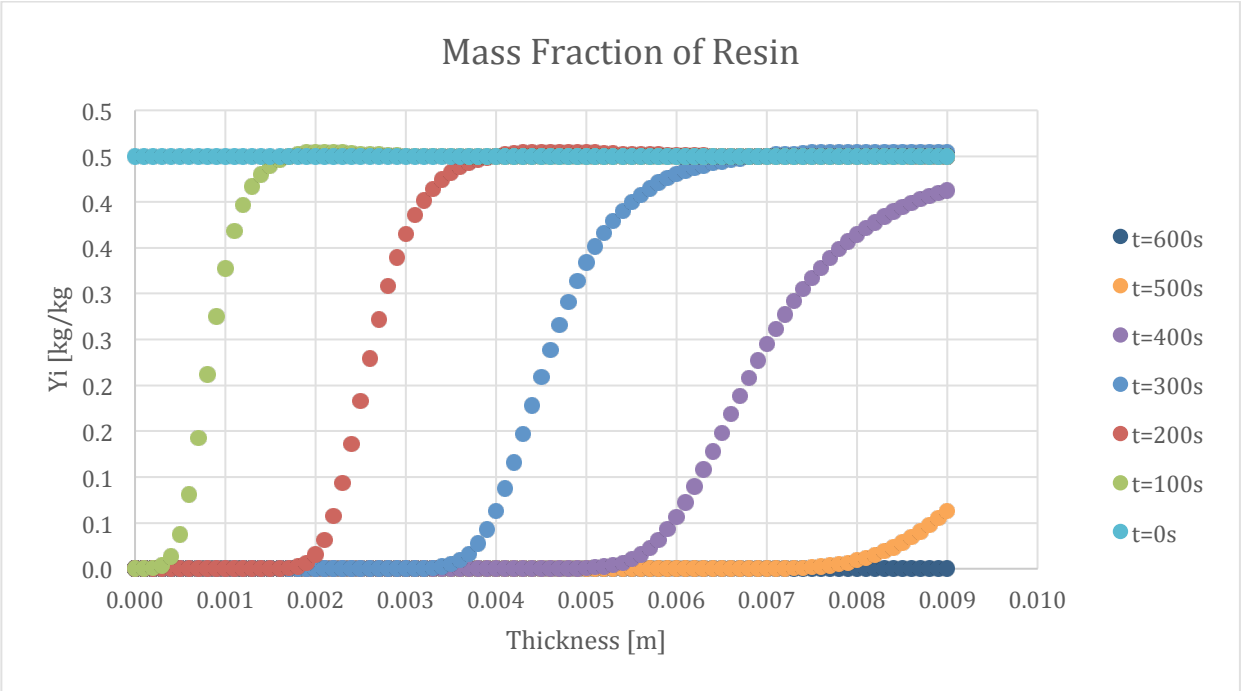


Figure 281-Mass fraction profile for Resin in 10% ATH sample and 50% glass

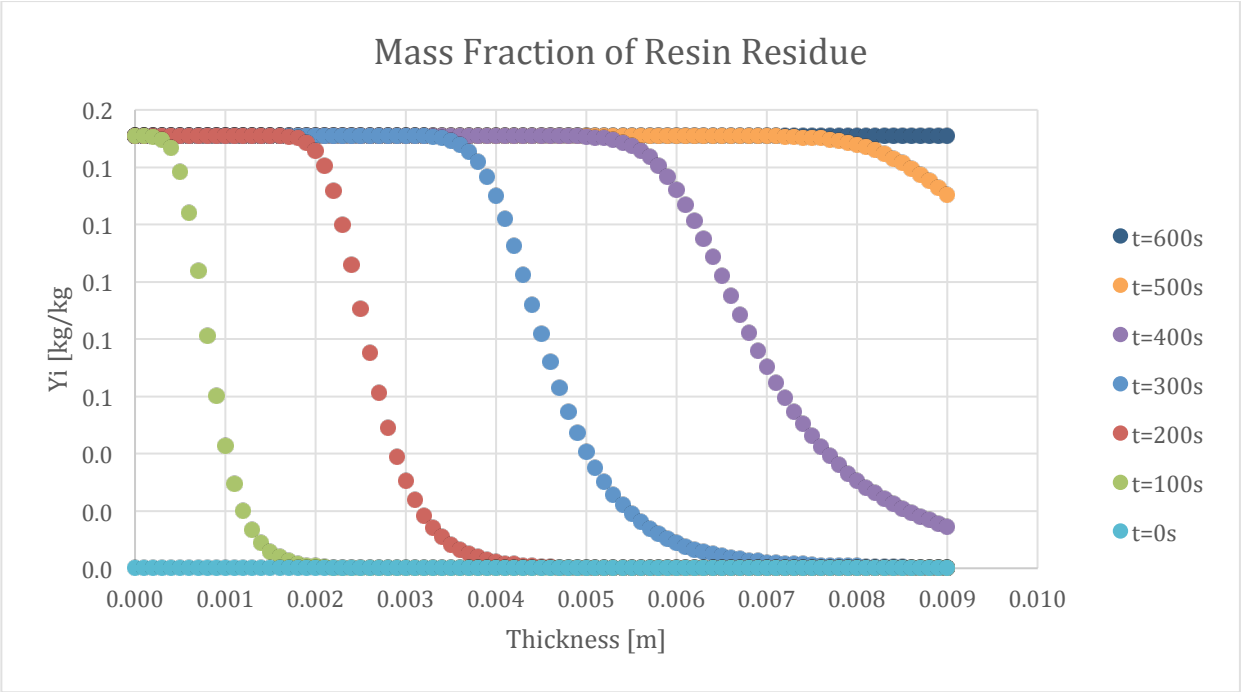


Figure 282-Mass fraction profile for Resin Residue in 10% ATH sample and 50% glass

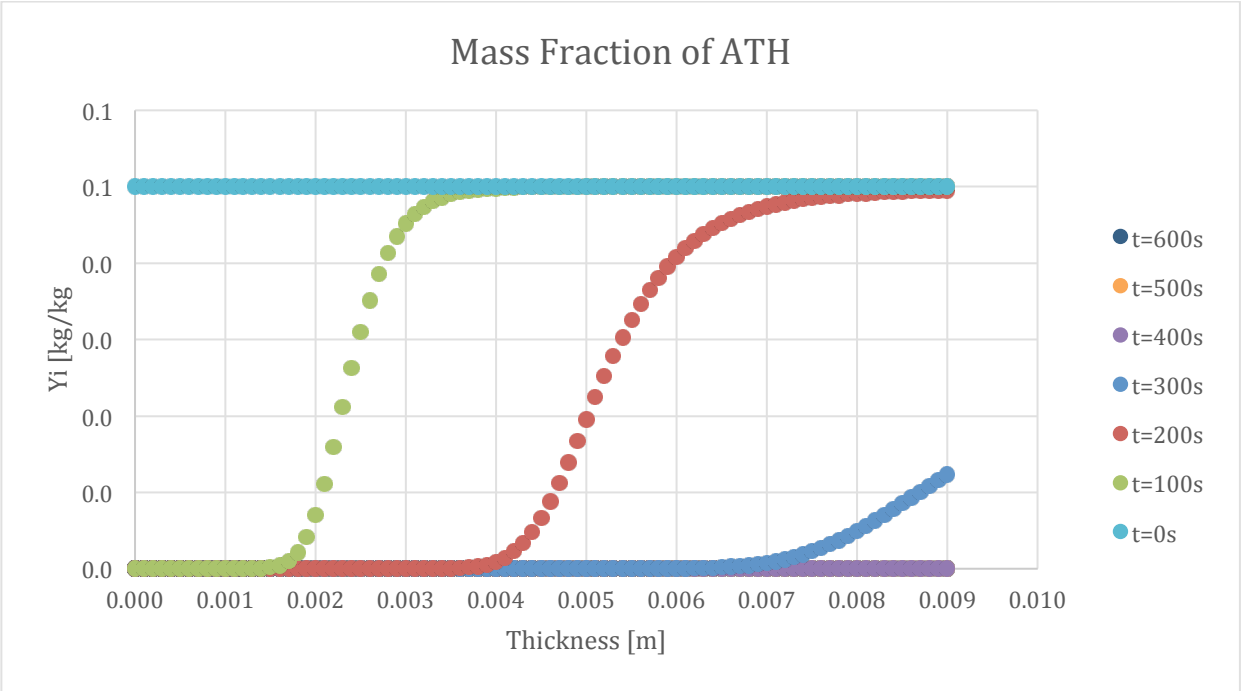


Figure 283-Mass fraction profile for ATH in 10% ATH sample and 50% glass

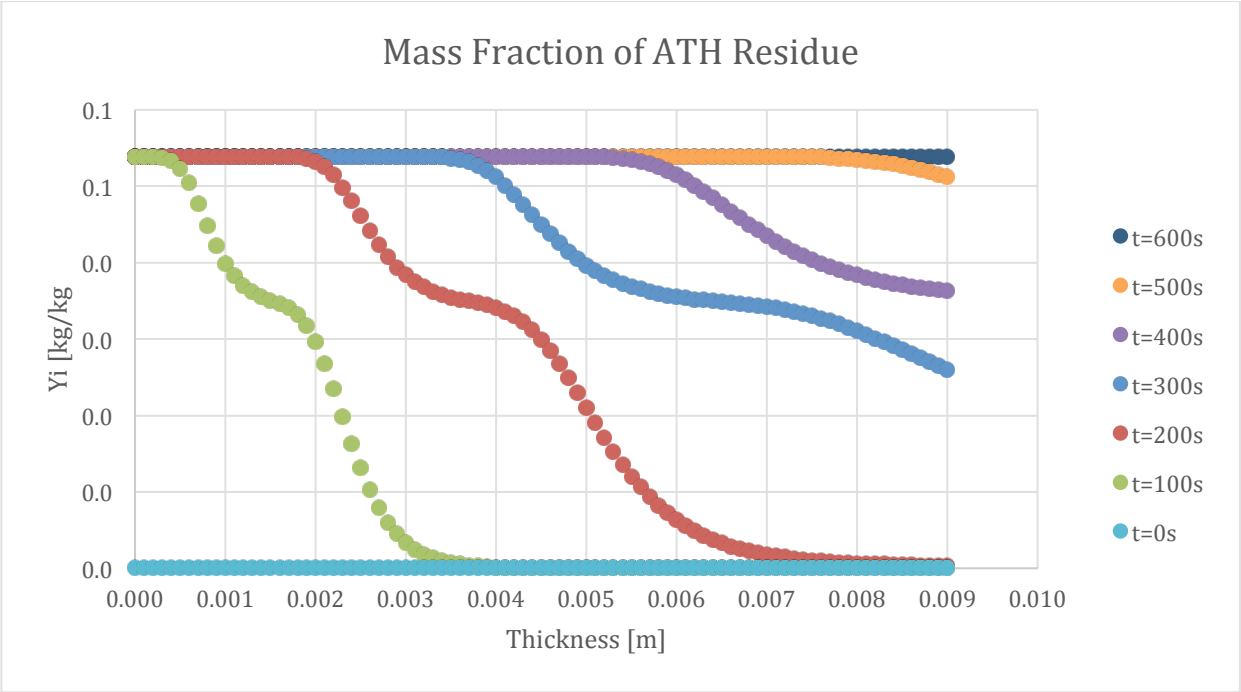


Figure 284-Mass fraction profile for ATH Residue in 10% ATH sample and 50% glass

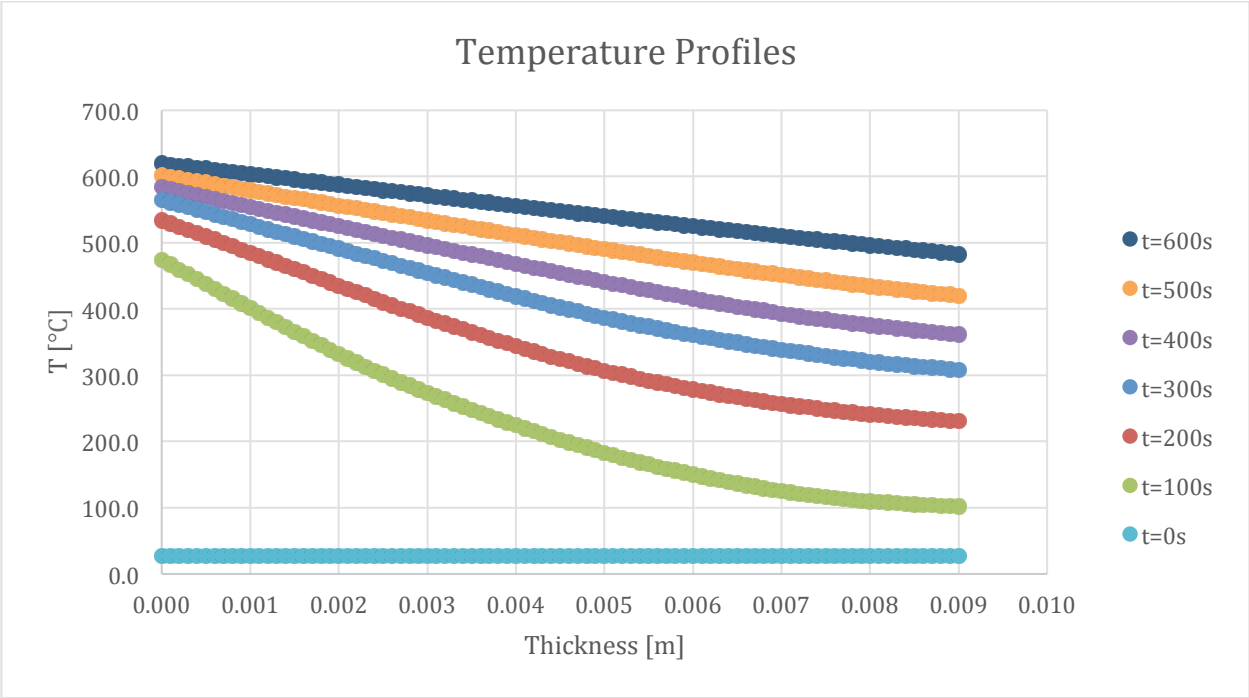


Figure 285-Temperature profile for 10% ATH sample and 50% glass

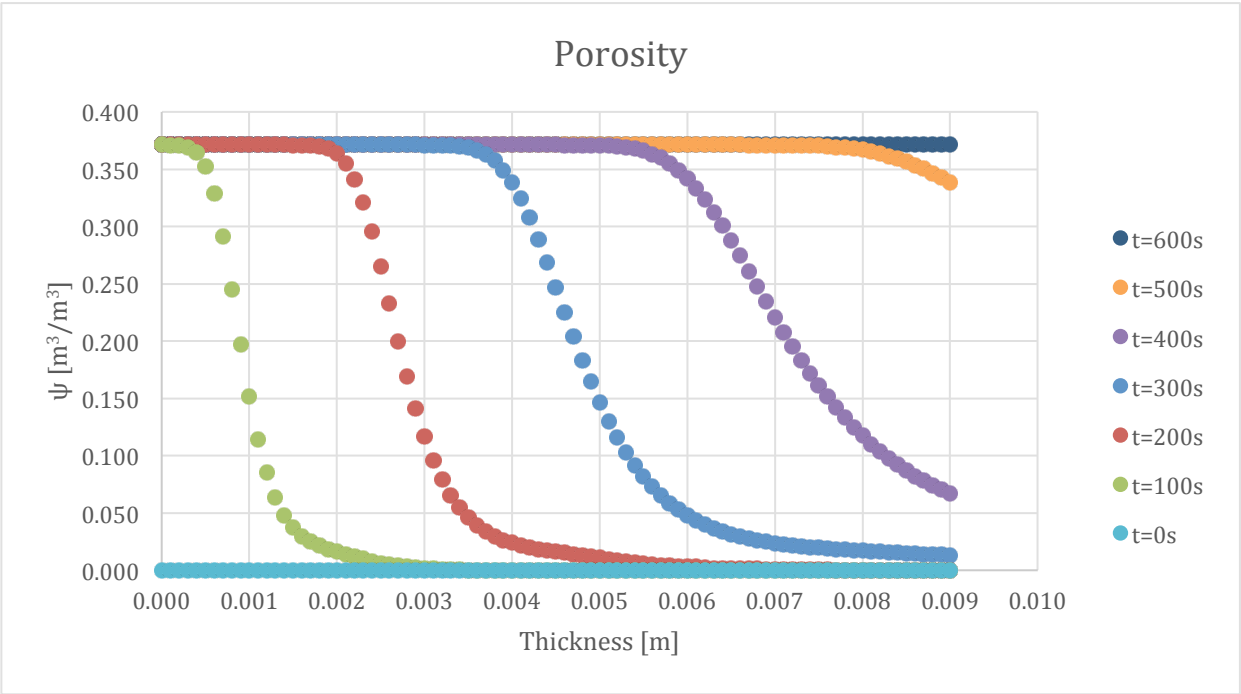


Figure 286-Porosity profile for 10% ATH sample and 50% glass

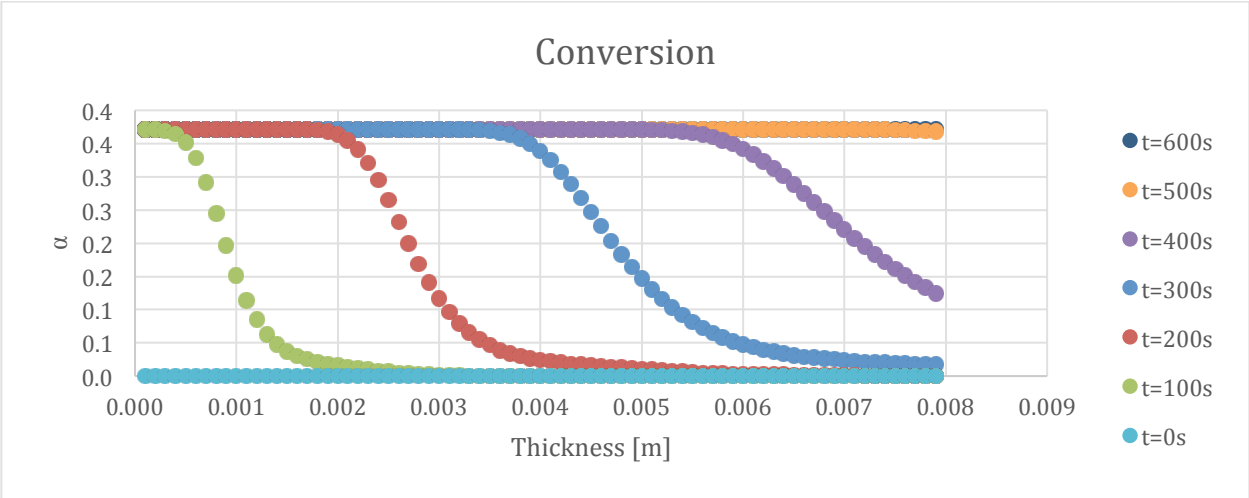


Figure 287-Conversion profile for 10% ATH sample and 50% glass

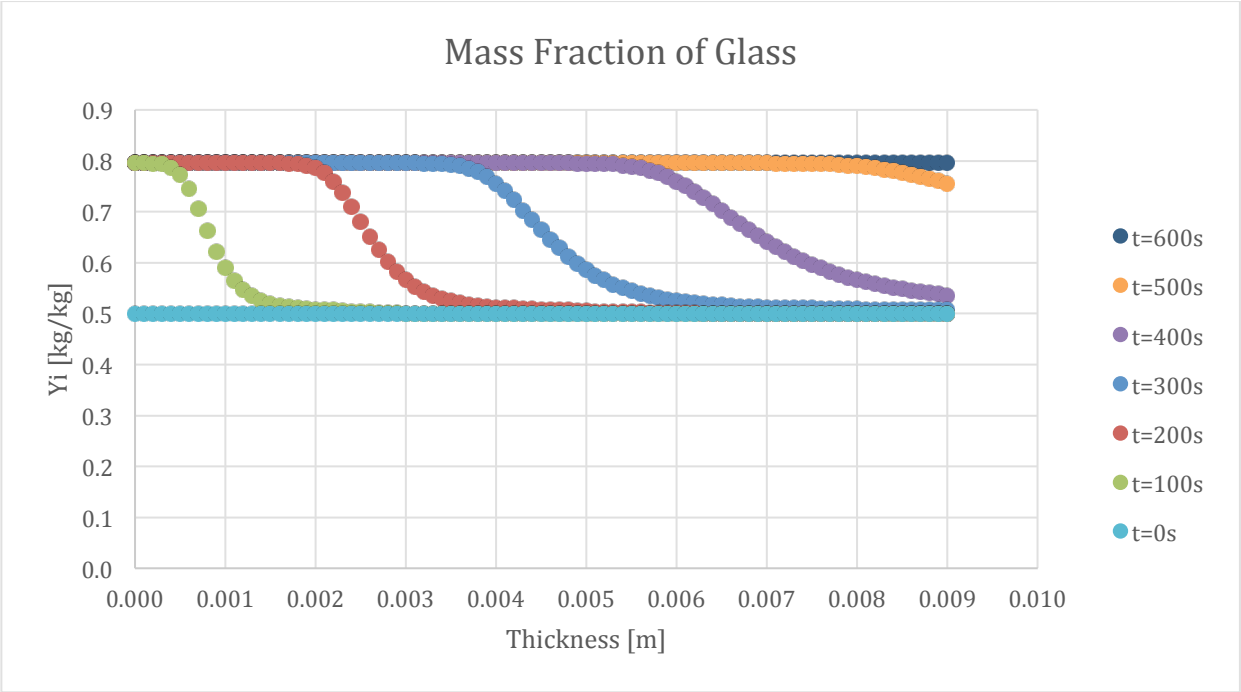


Figure 288-Mass fraction profile for Glass in 10% ATH sample and 50% glass

The following set of results are from the simulation of the 20% ATH sample.

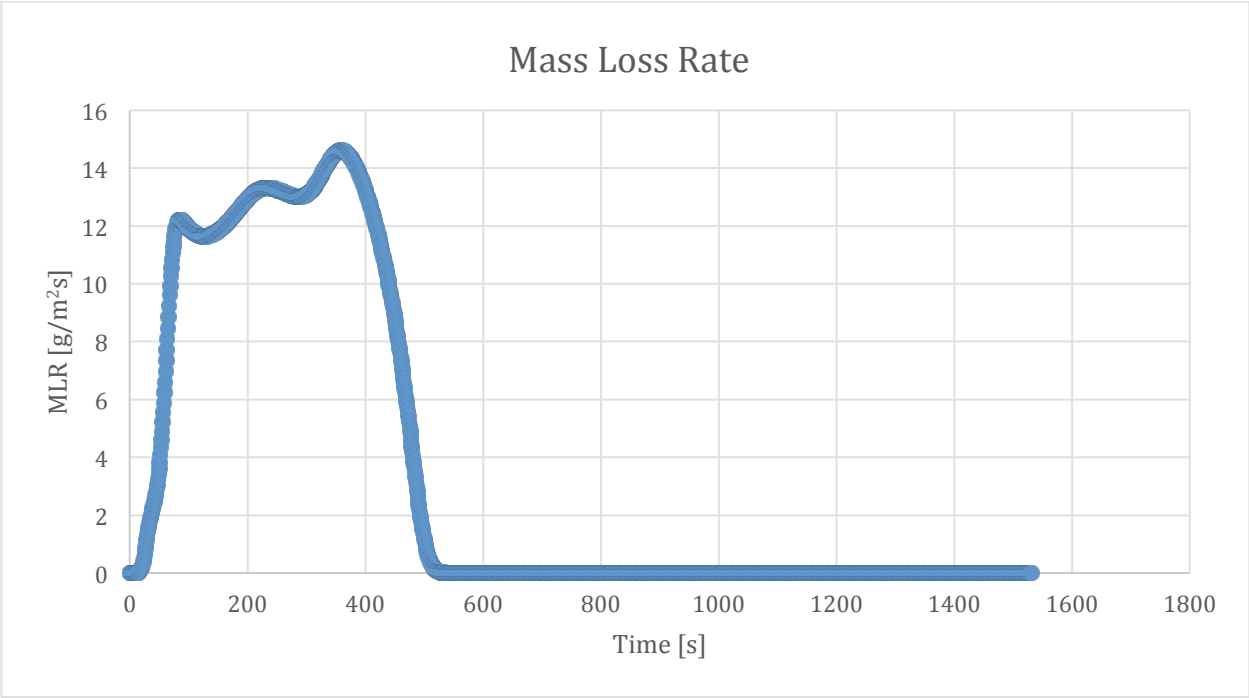


Figure 289-Mass loss rate curve for 20% ATH sample and 50% glass

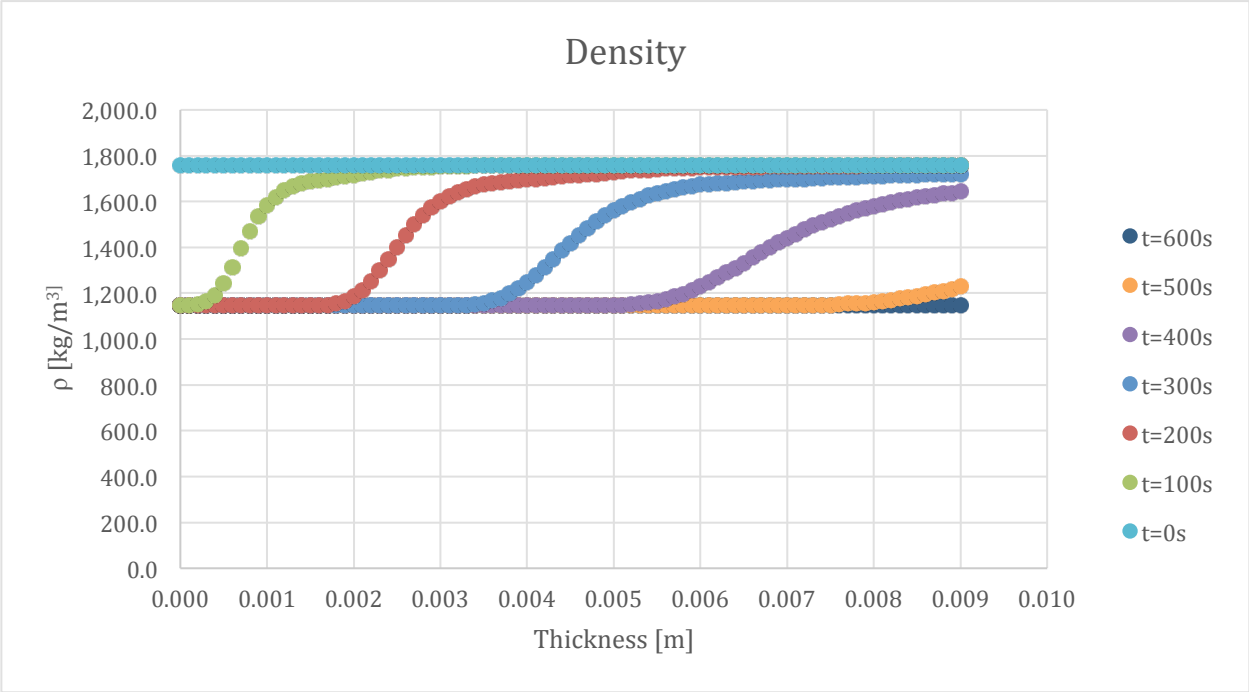


Figure 290-Density profile for 20% ATH sample and 50% glass

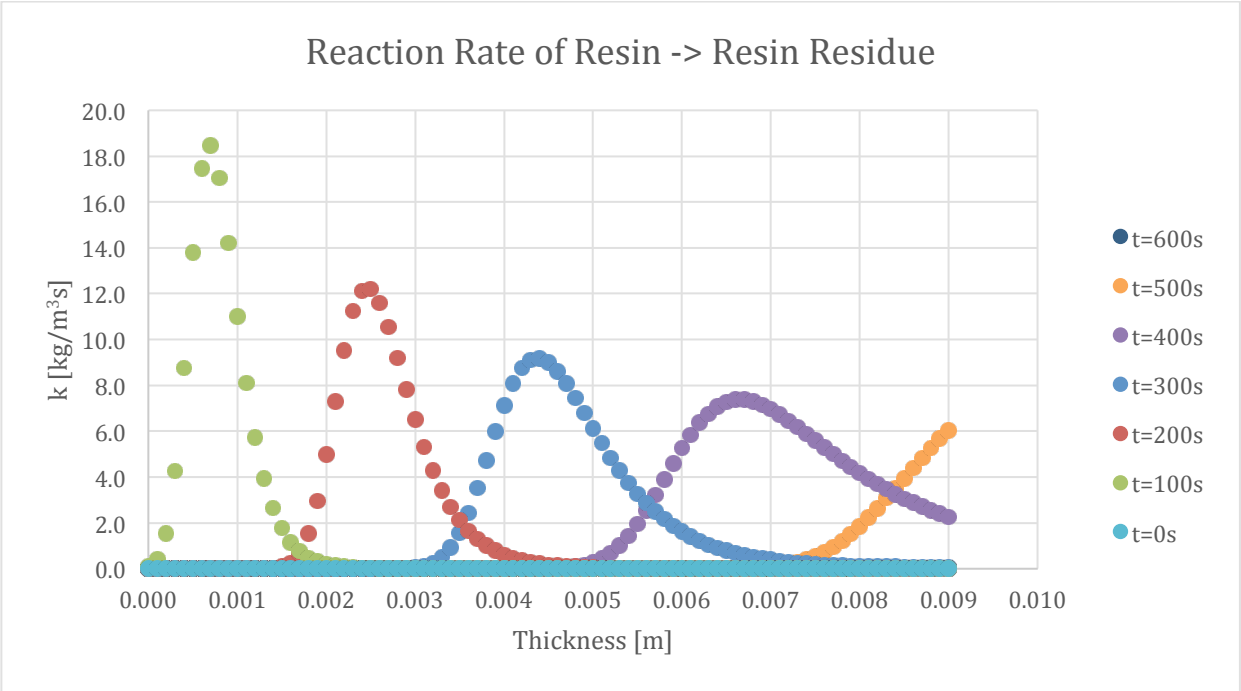


Figure 291-Reaction rate profile for Resin->Resin Residue in 20% ATH sample and 50% glass



Figure 292-Reaction rate profile for ATH->ATH Residue in 20% ATH sample and 50% glass

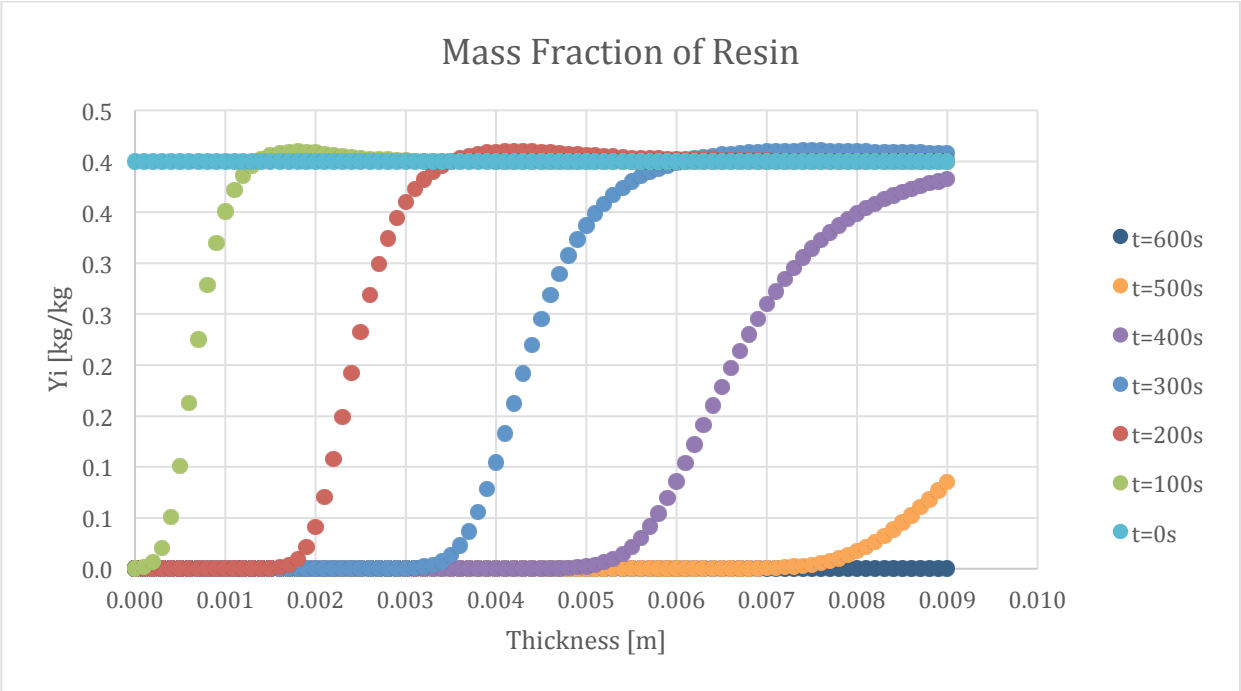


Figure 293-Mass fraction profile for Resin in 20% ATH sample and 50% glass

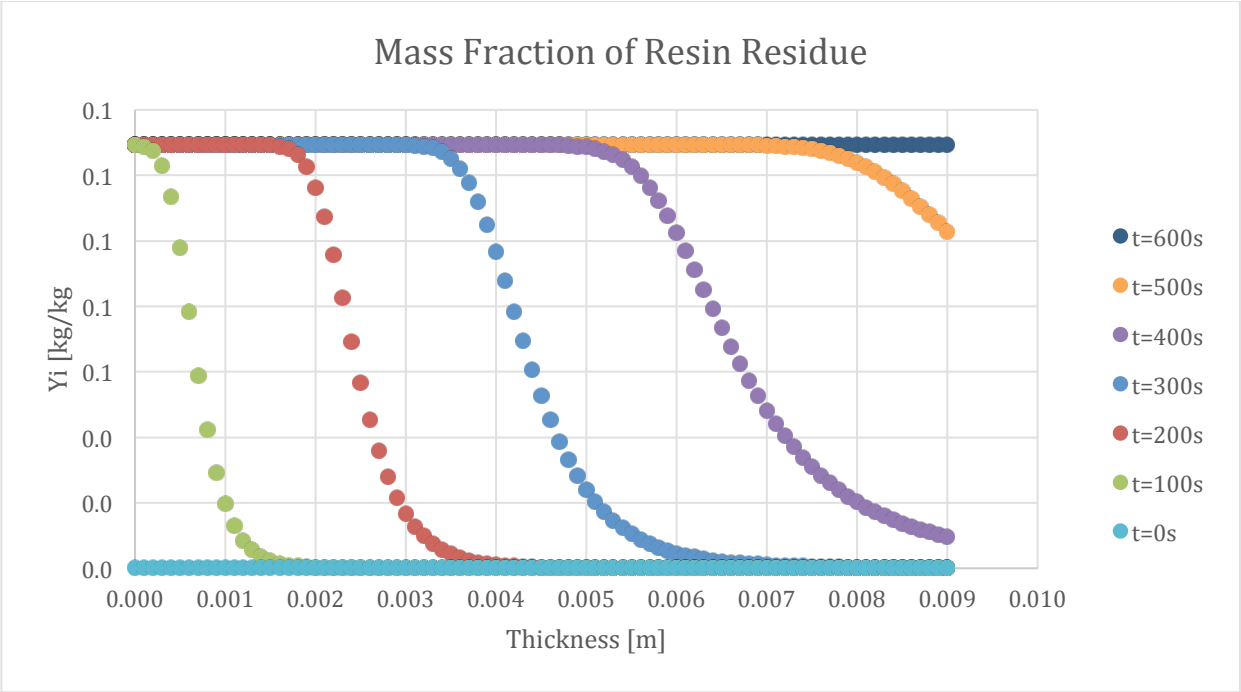


Figure 294-Mass fraction profile for Resin Residue in 20% ATH sample and 50% glass

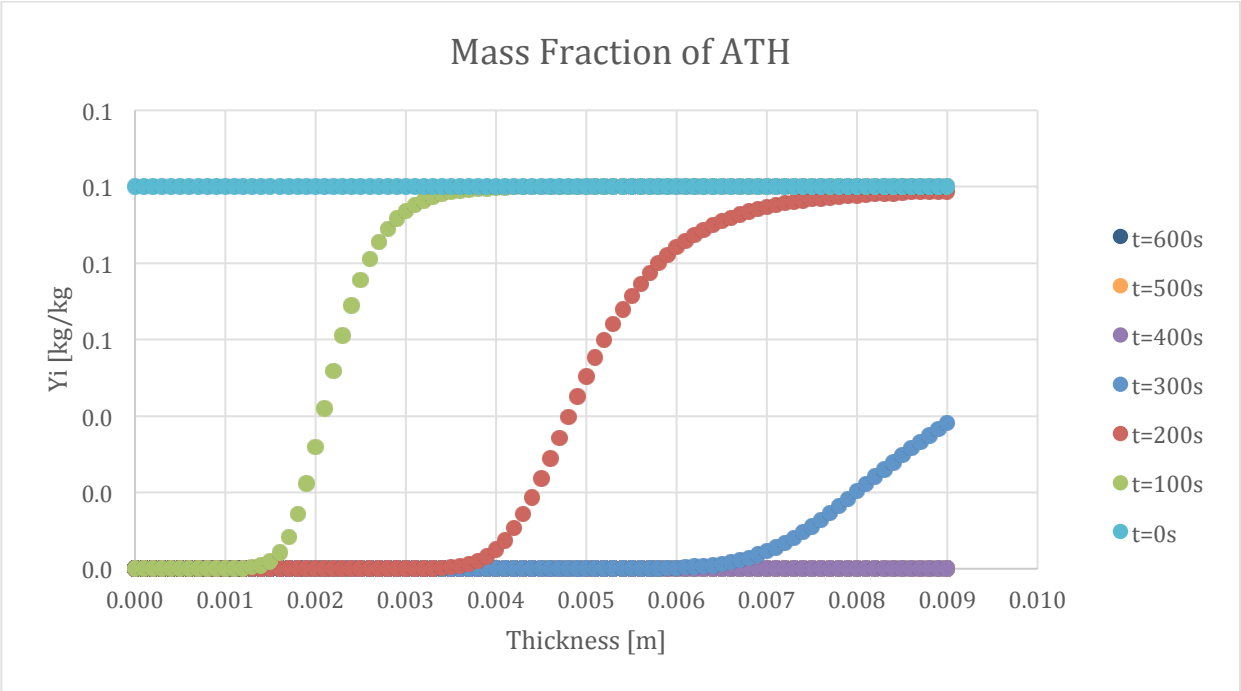


Figure 295-Mass fraction profile for ATH in 20% ATH sample and 50% glass

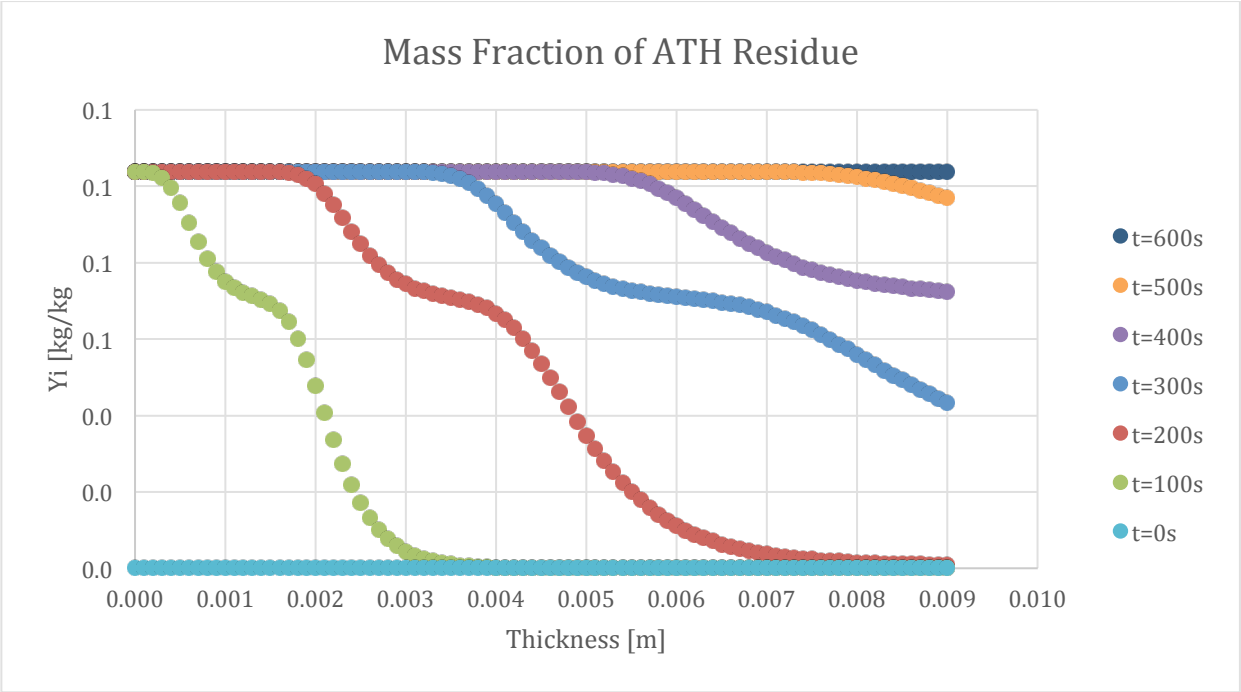


Figure 296-Mass fraction profile for ATH Residue in 20% ATH sample and 50% glass

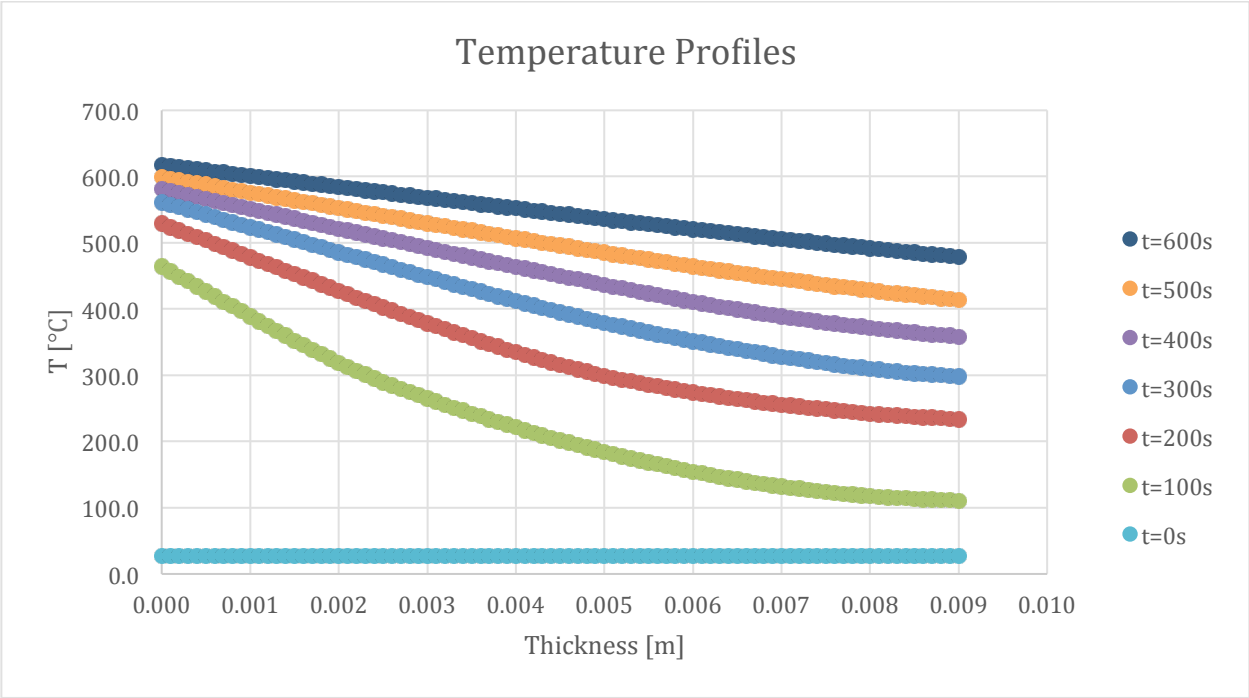


Figure 297-Temperature profile for 20% ATH sample and 50% glass

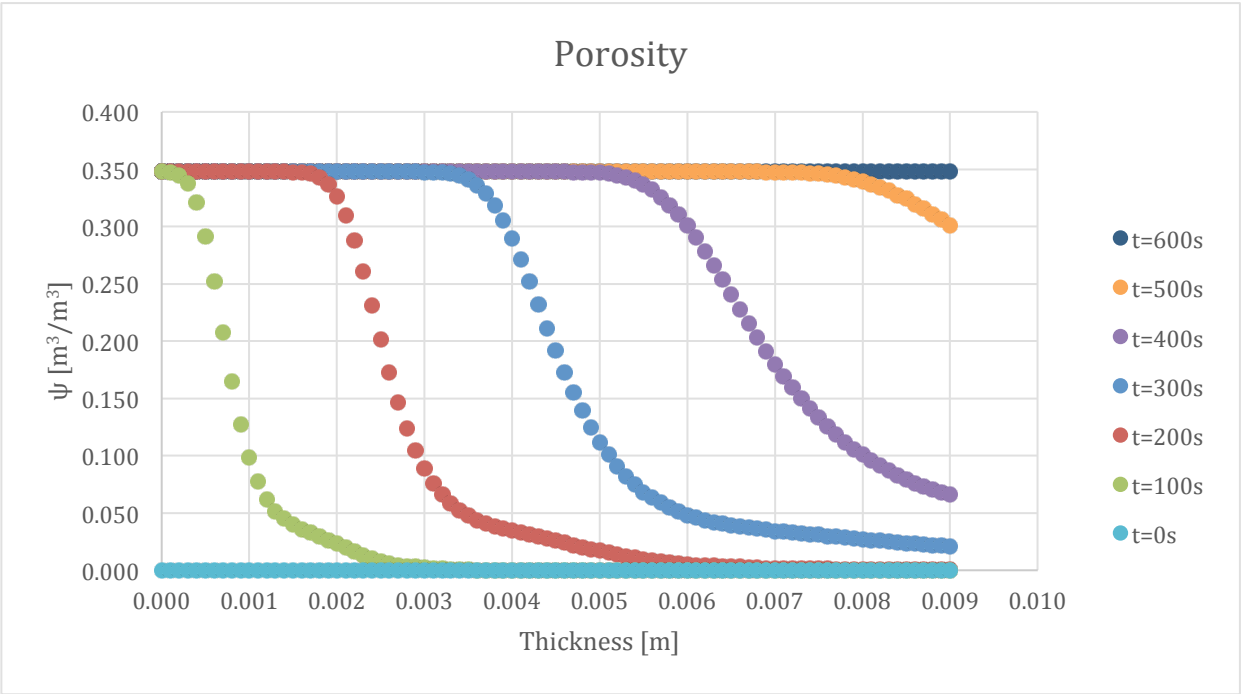


Figure 298-Porosity profile for 20% ATH sample and 50% glass

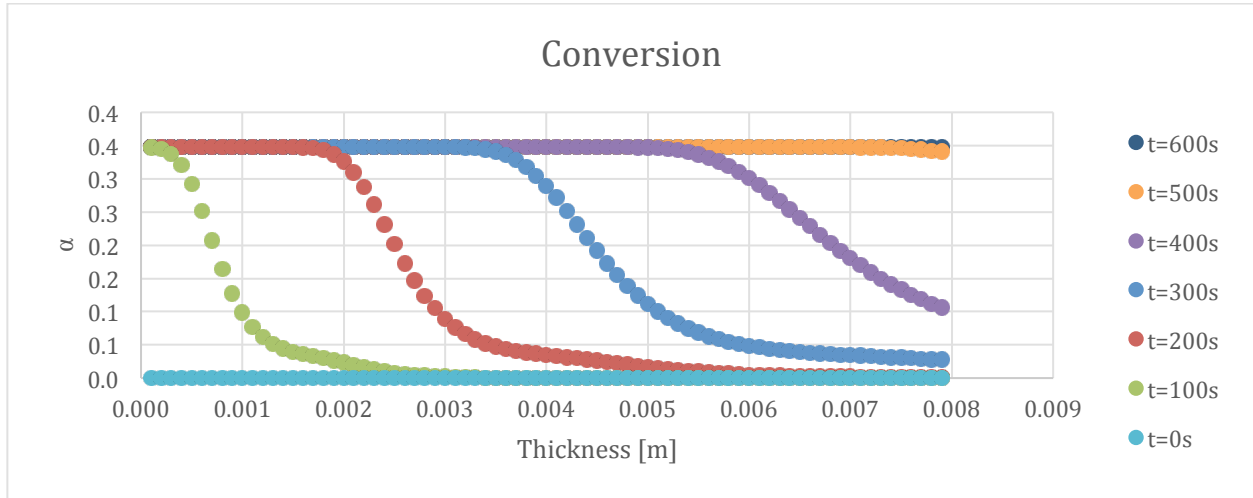


Figure 299-Conversion profile for 20% ATH sample and 50% glass

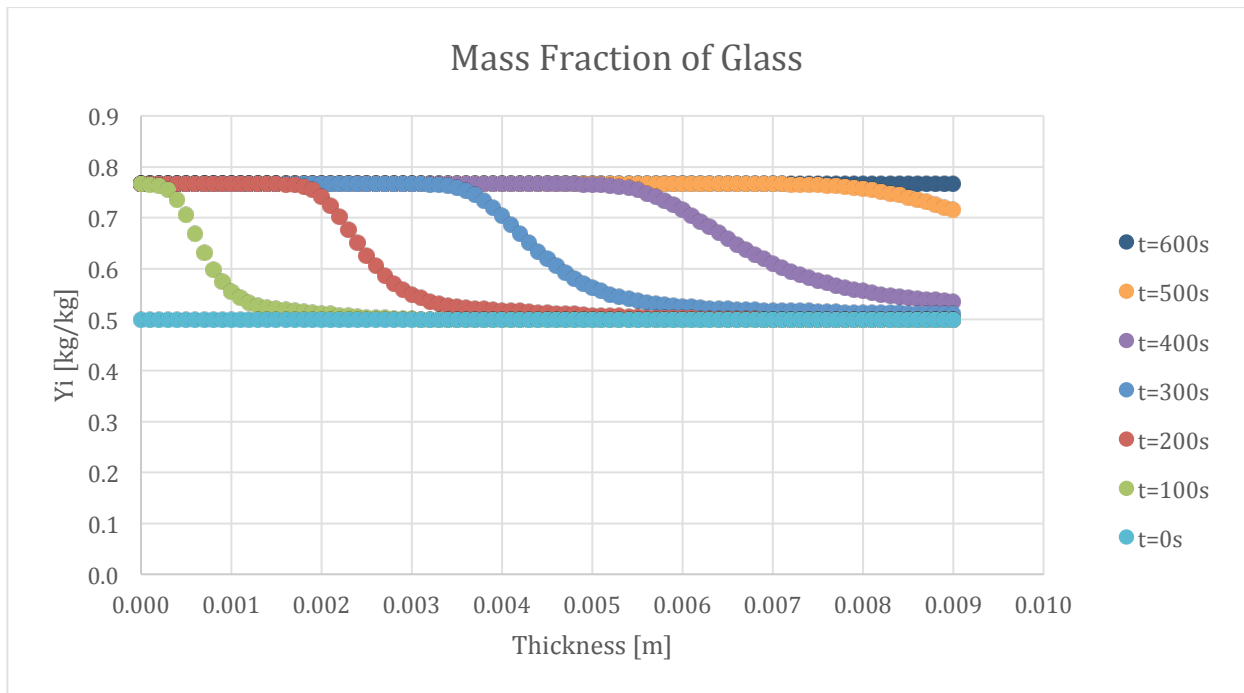


Figure 300-Mass fraction profile for Glass in 20% ATH sample and 50% glass

9.10.3. Varying Coating Thickness

The comparison of coating thickness was made between 4 different samples. The baseline sample was used and can be referenced in the first section of graphs. The set of results shown below are the results of the 0.25 mm coating sample.

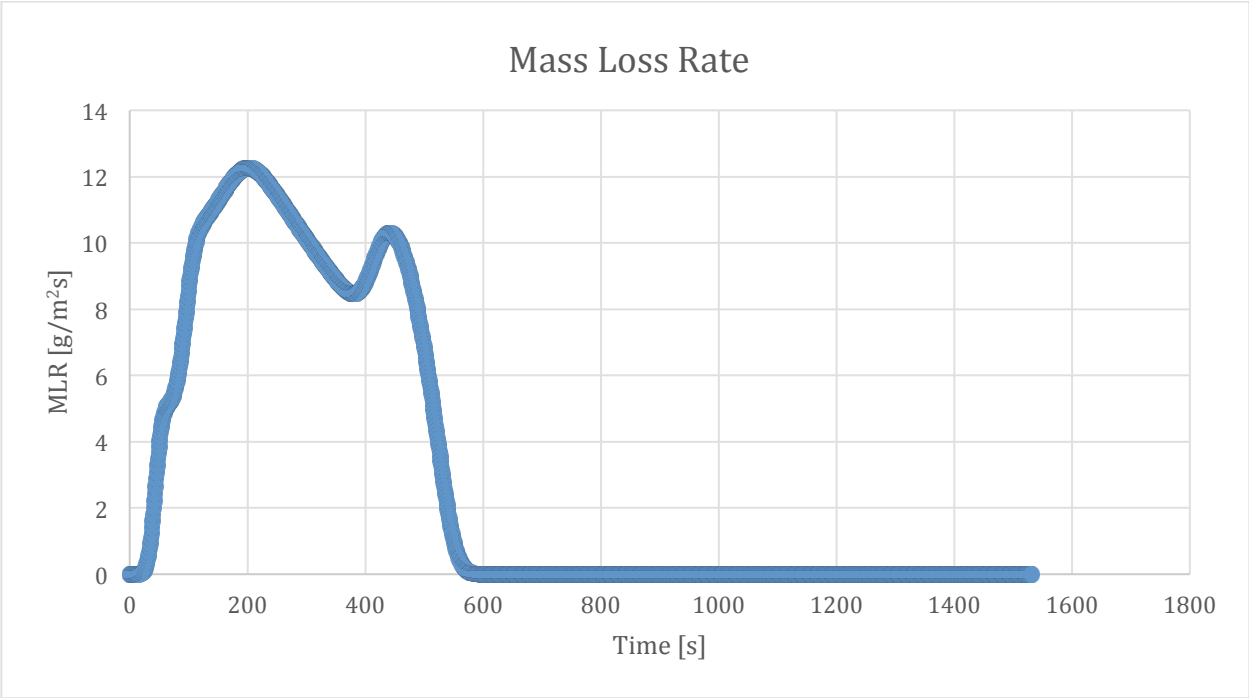


Figure 301-Mass loss rate curve for 100:130 resin/ATH sample and 50% glass with a 0.25mm coating

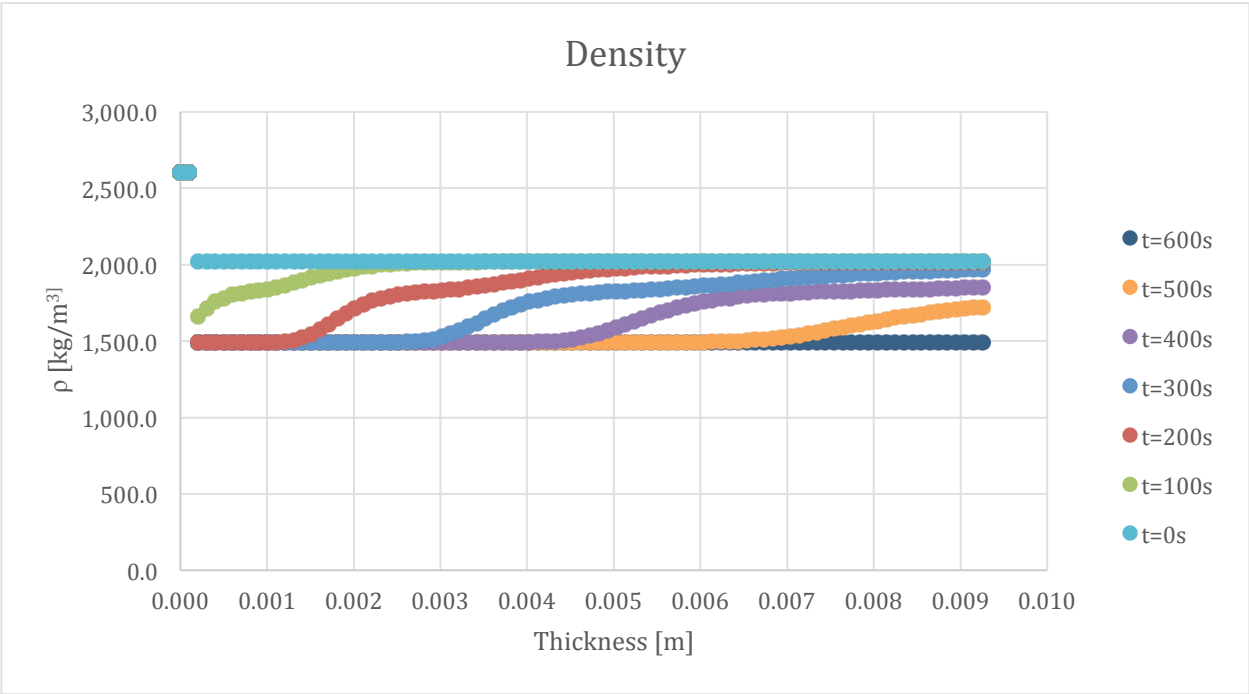


Figure 302-Density profile for 100:130 resin/ATH sample and 50% glass with a 0.25 mm coating

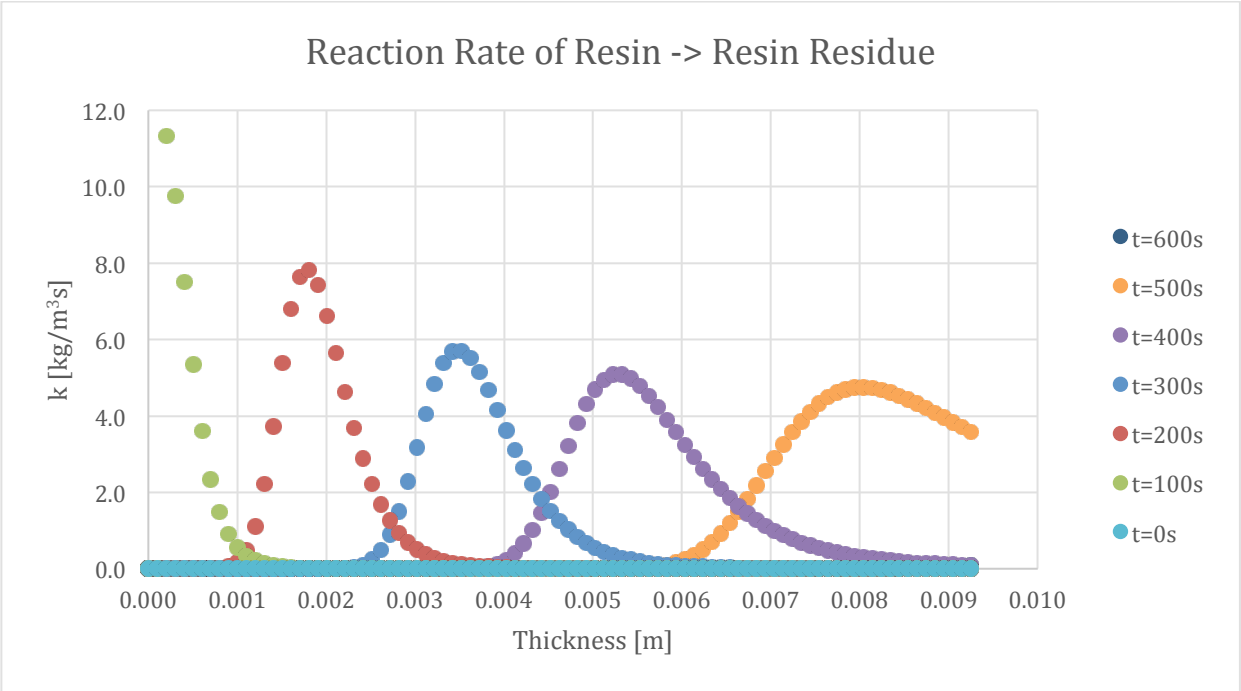


Figure 303-Reaction rate profile for Resin->Resin Residue in 100:130 resin/ATH sample and 50% glass with a 0.25 mm glass coating

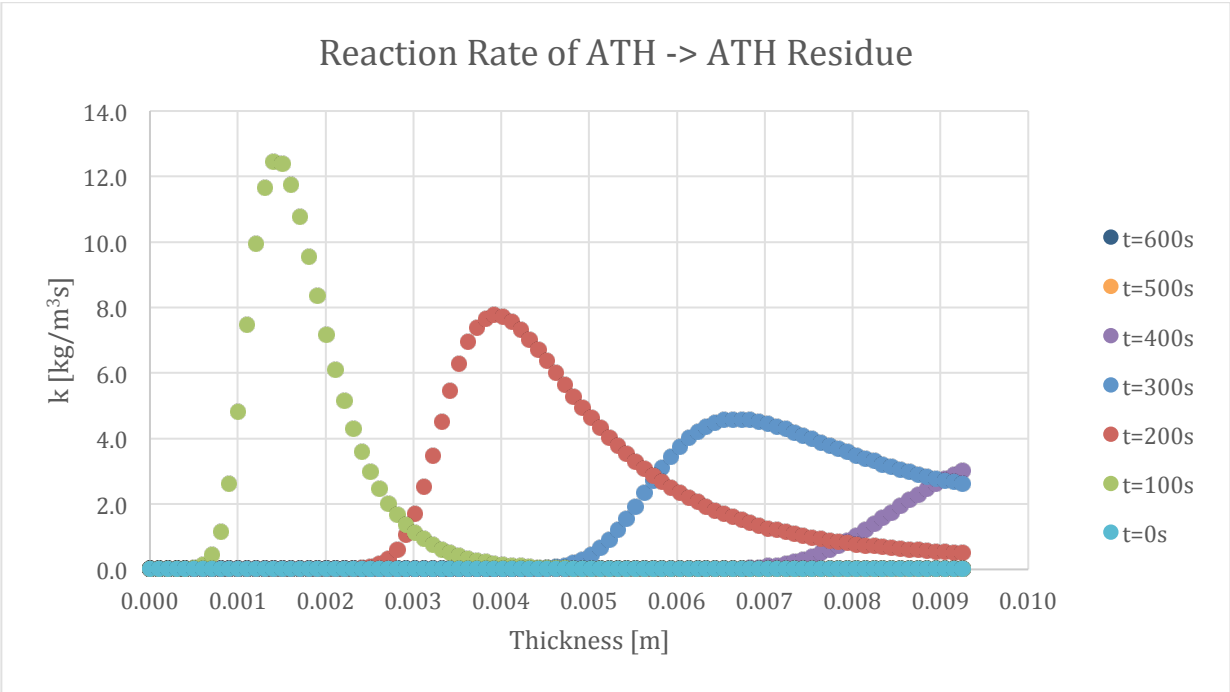


Figure 304-Reaction rate profile for ATH->ATH Residue in 100:130 resin/ATH sample and 50% glass with a 0.25 mm glass coating

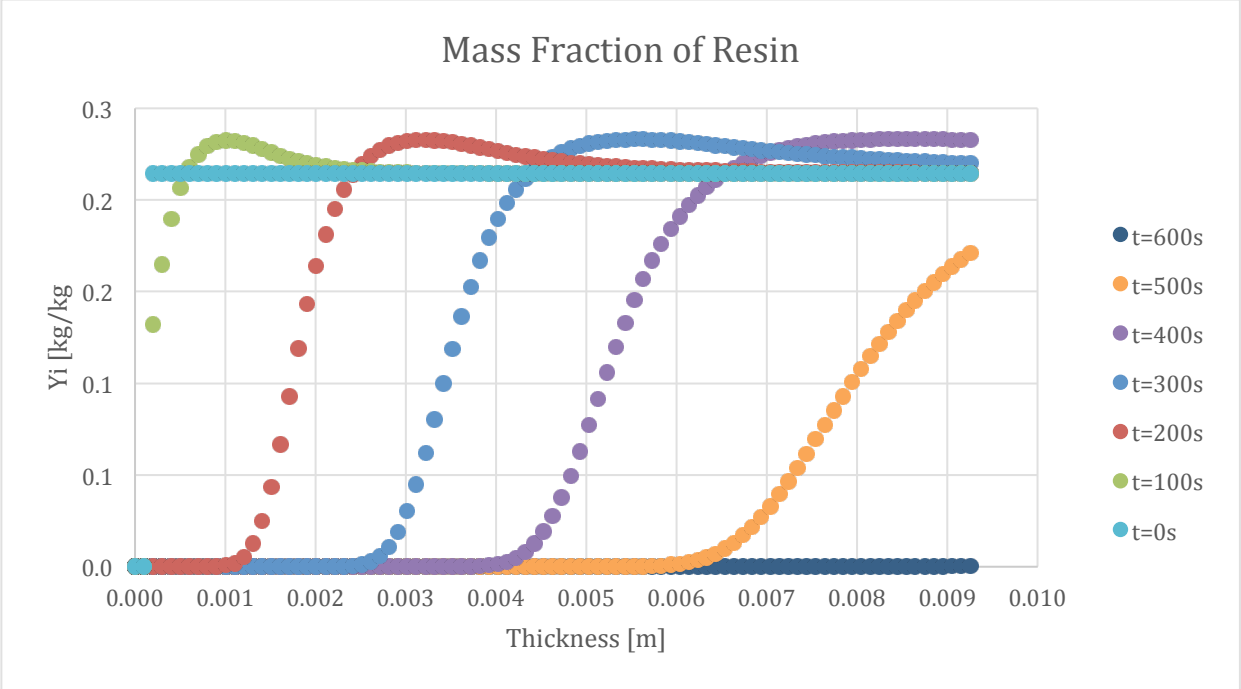


Figure 305-Mass fraction profile for Resin in 100:130 resin/ATH sample and 50% glass with a 0.25 mm glass coating

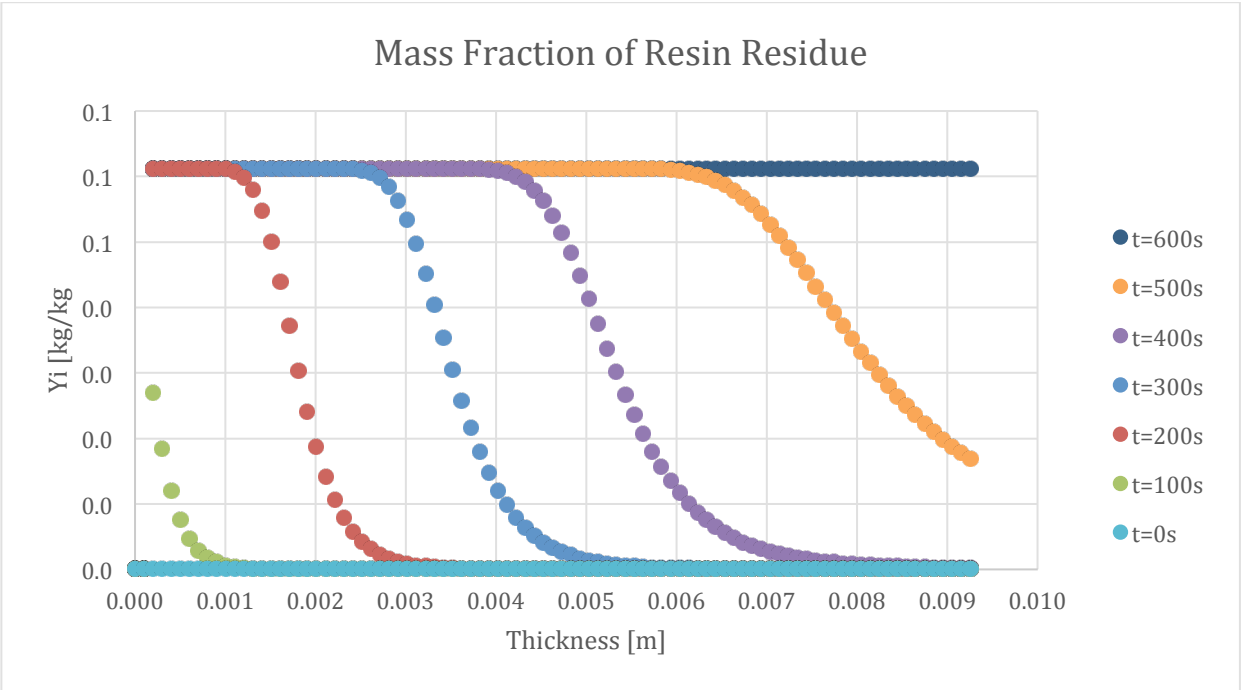


Figure 306-Mass fraction profile for Resin Residue in 100:130 resin/ATH sample and 50% glass with a 0.25 mm glass coating

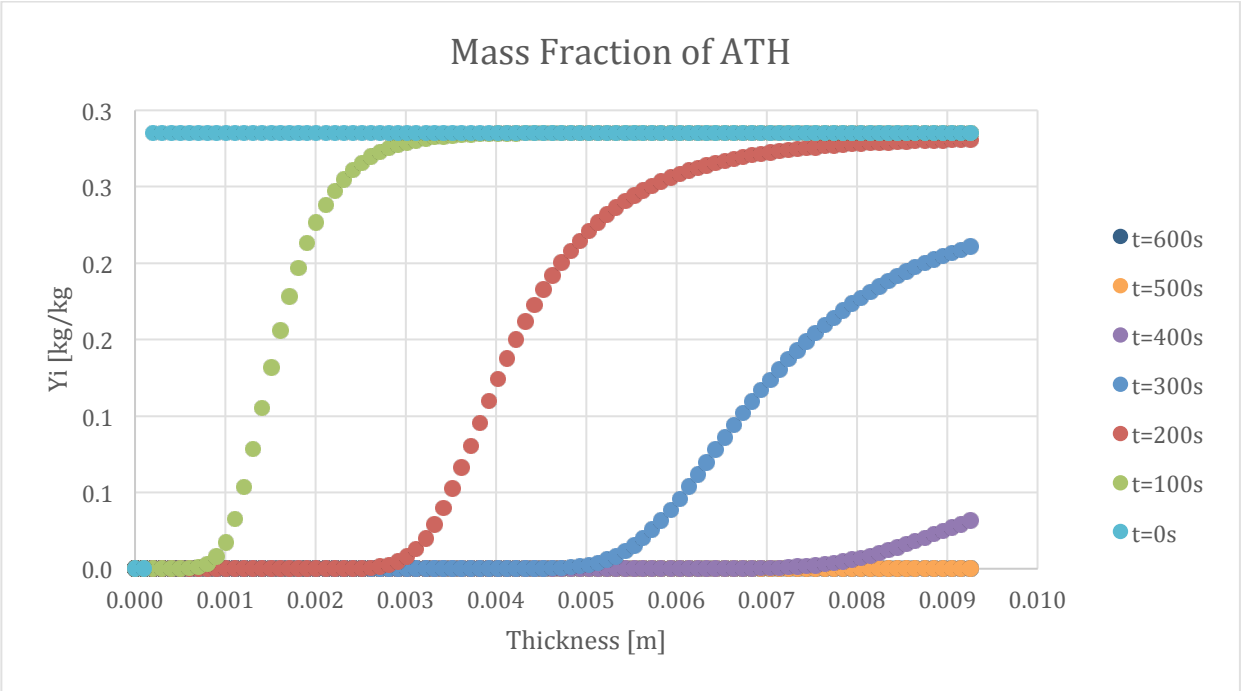


Figure 307-Mass fraction profile for ATH in 100:130 resin/ATH sample and 50% glass with a 0.25 mm glass coating

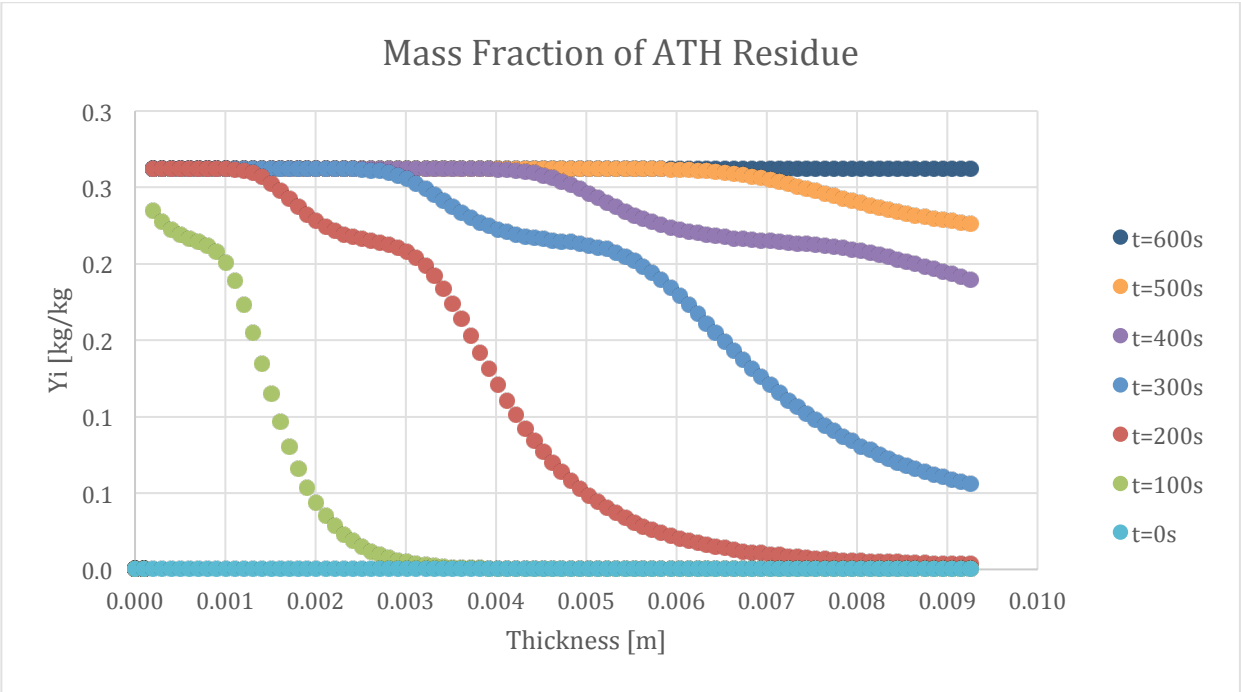


Figure 308-Mass fraction profile for ATH Residue in 100:130 resin/ATH sample and 50% glass with a 0.25 mm glass coating

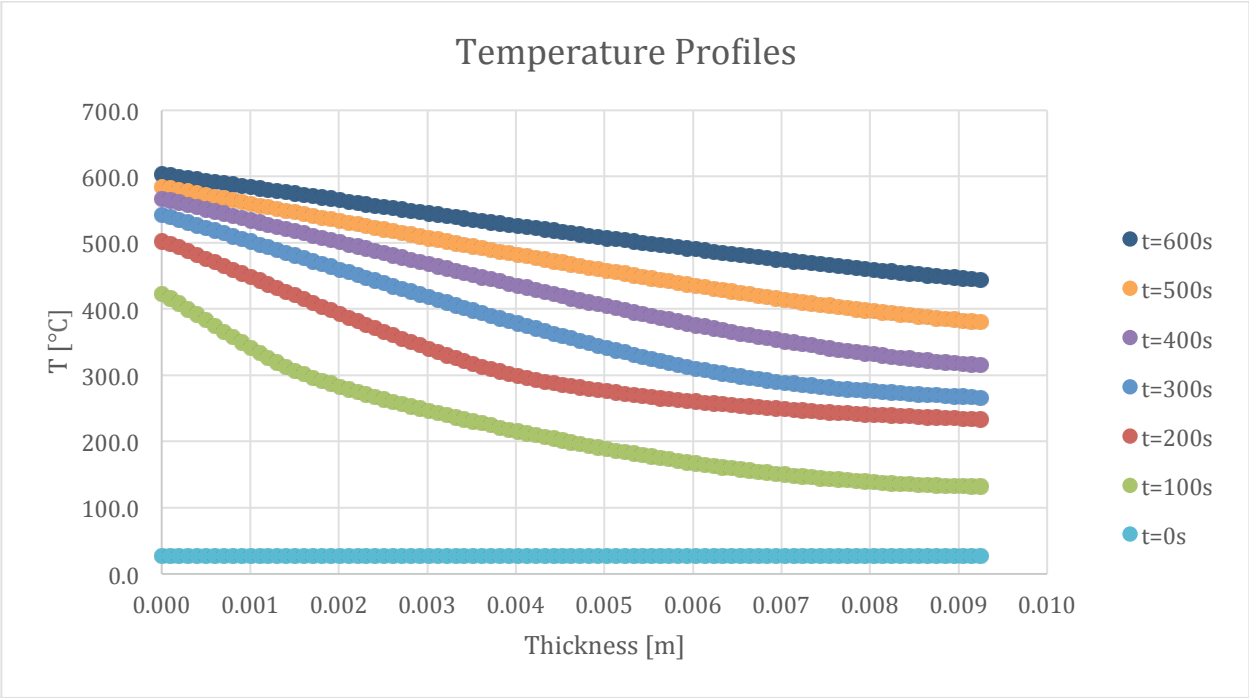


Figure 309-Temperature profile for 100:130 resin/ATH sample and 50% glass with a 0.25 mm coating

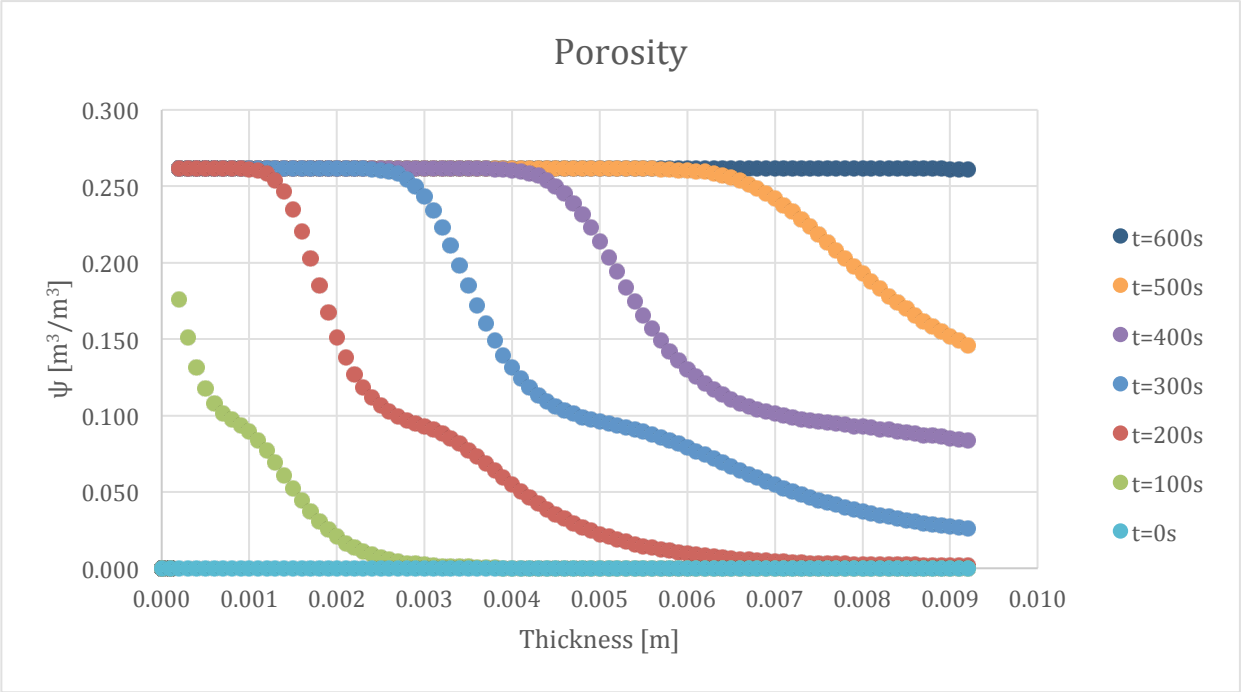


Figure 310-Porosity profile for 100:130 resin/ATH sample and 50% glass with a 0.25 mm coating

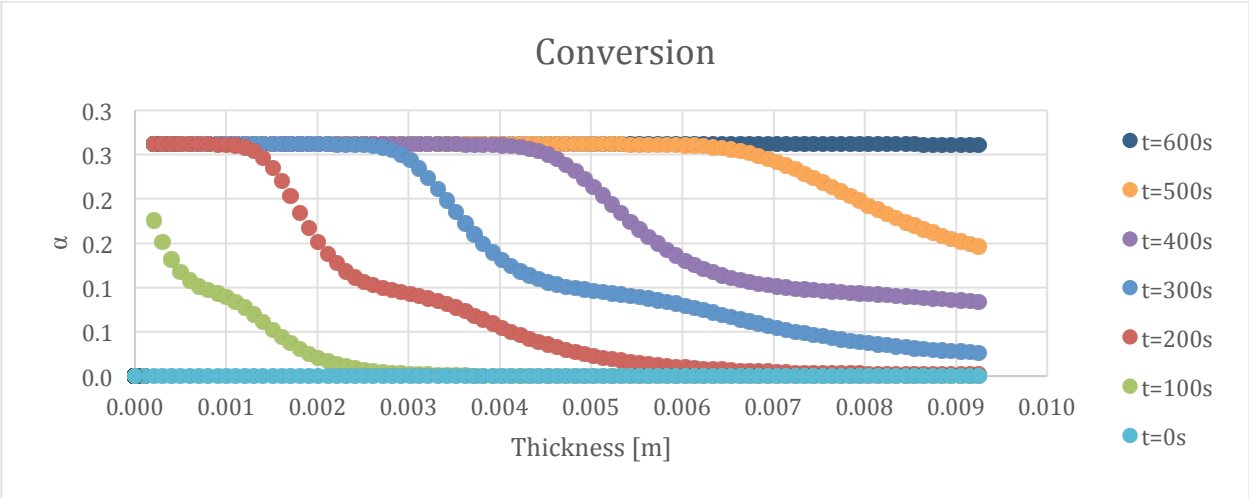


Figure 311-Conversion profile for 100:130 resin/ATH sample and 50% glass with a 0.25 mm coating

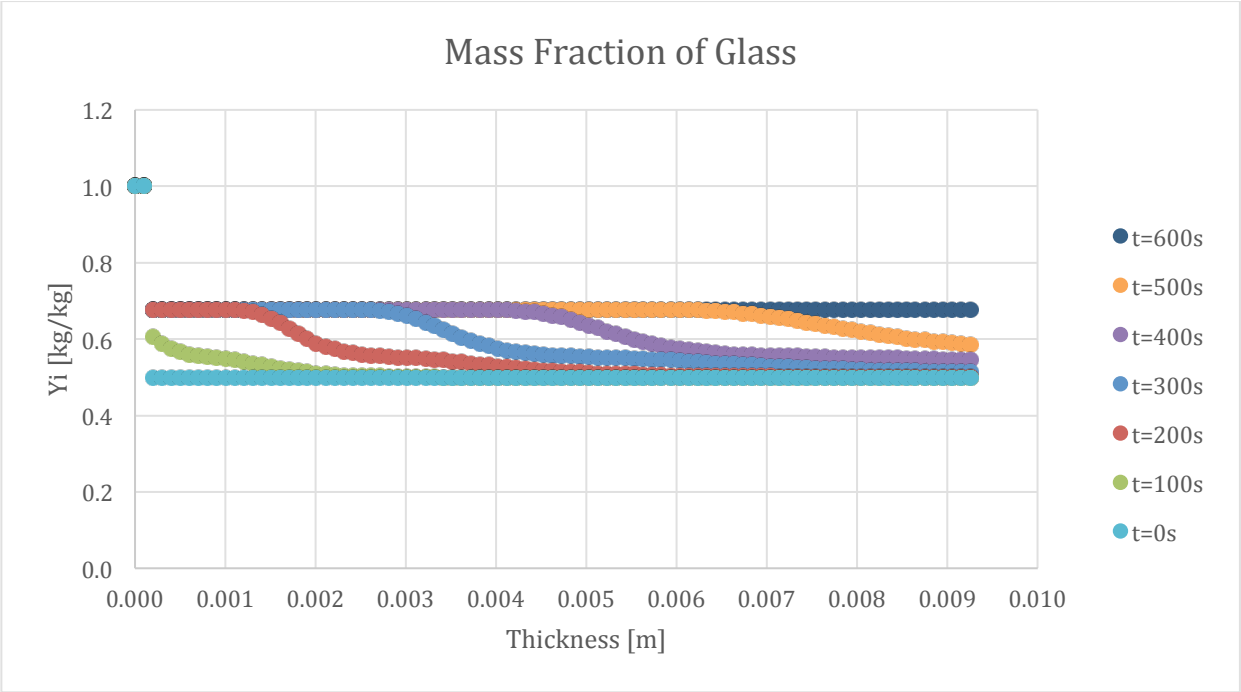


Figure 312-Mass fraction profile for Glass in 100:130 resin/ATH sample and 50% glass with a 0.25 mm glass coating

The following set of results are from the simulation of the 0.5 mm coating sample.

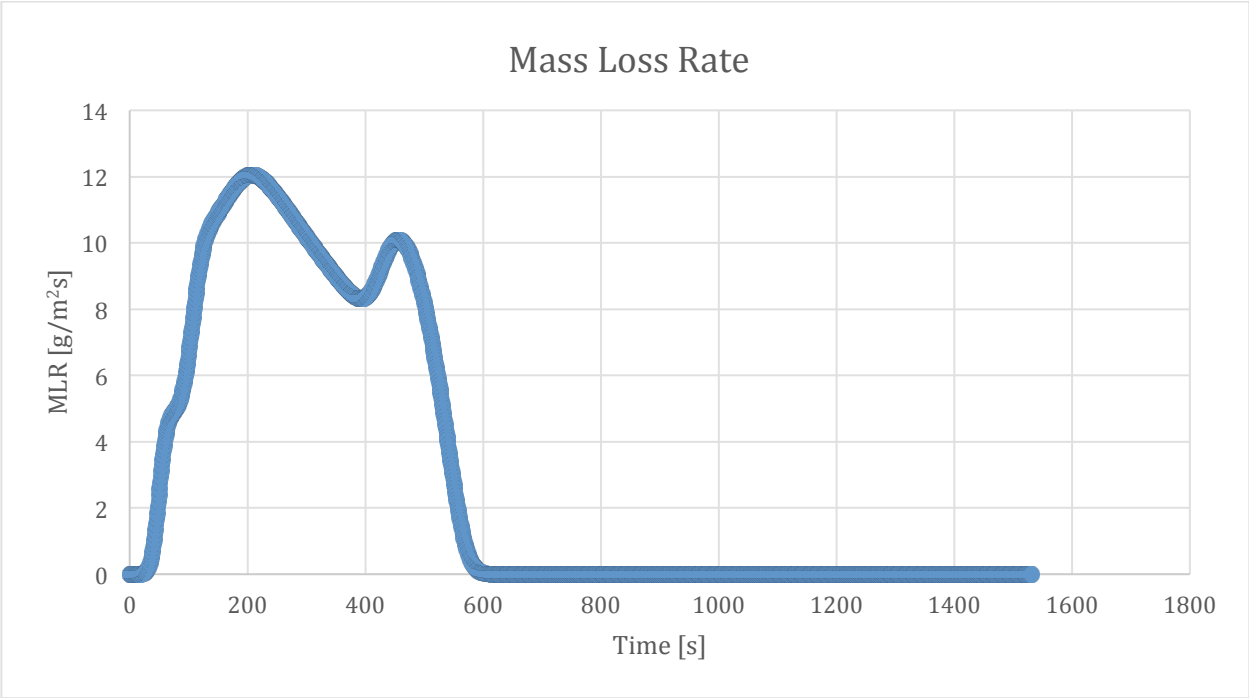


Figure 313-Mass loss rate curve for 100:130 resin/ATH sample and 50% glass with a 0.5 mm glass coating

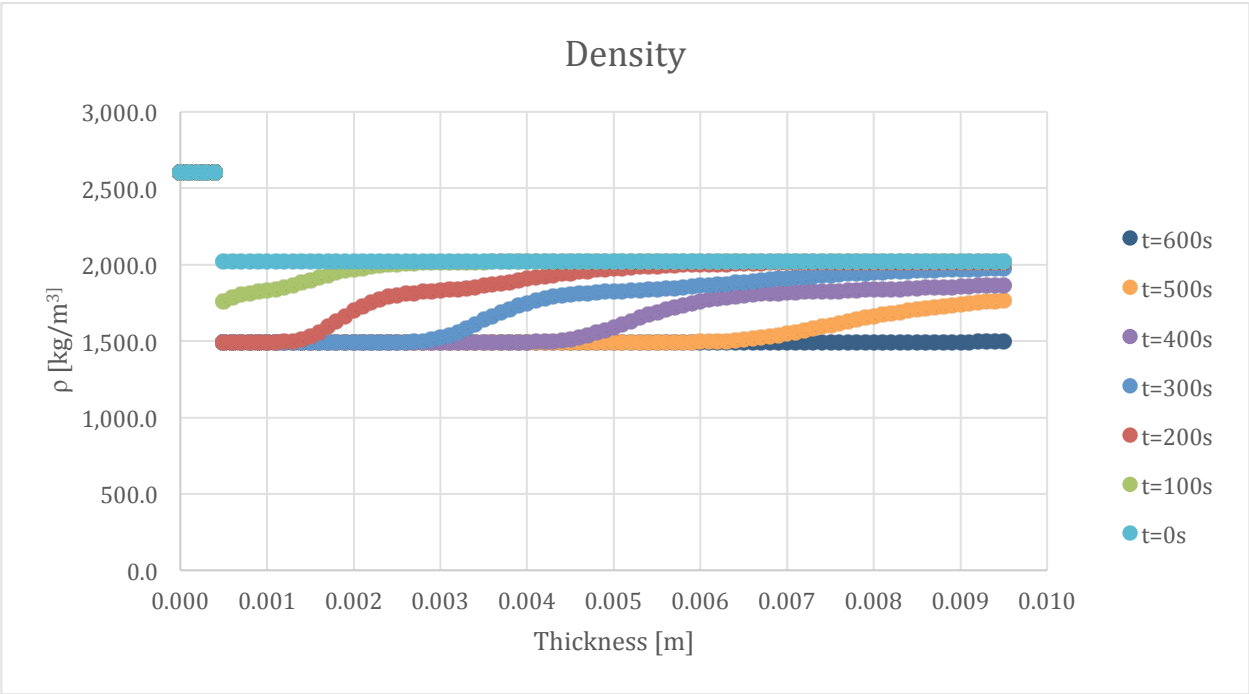


Figure 314-Density profile for 100:130 resin/ATH sample and 50% glass with a 0.5 mm coating

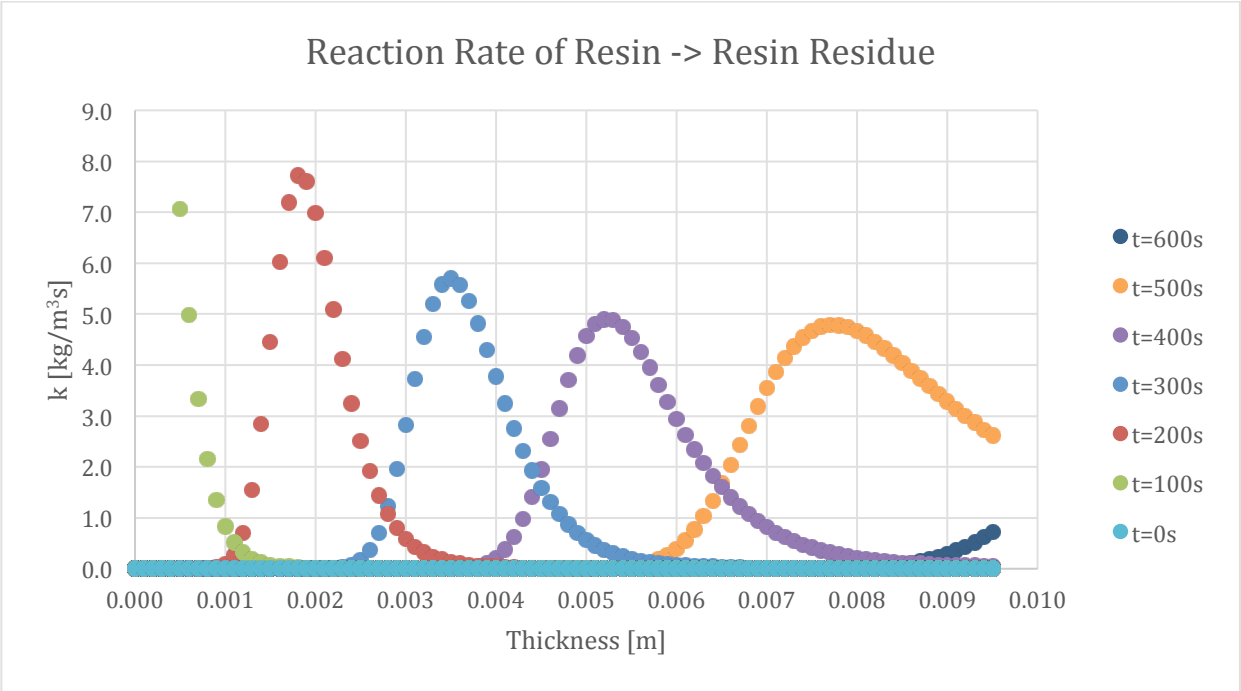


Figure 315-Reaction rate profile for Resin->Resin Residue in 100:130 resin/ATH sample and 50% glass with a 0.5 mm glass coating

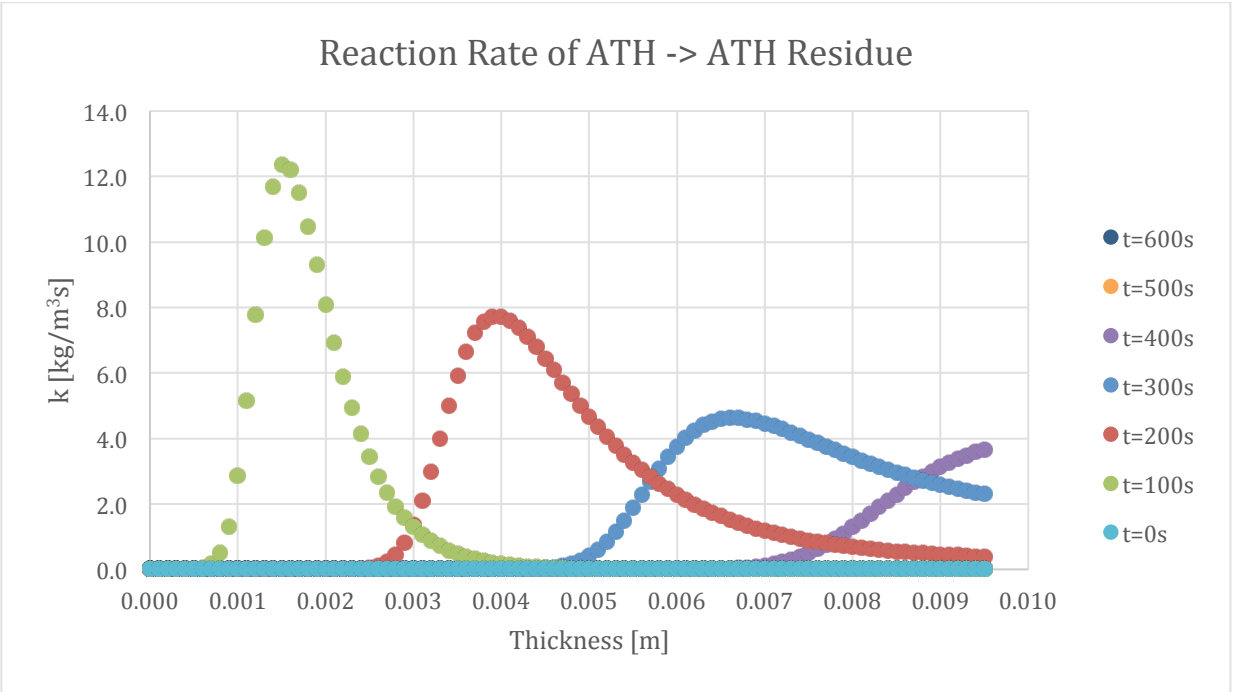


Figure 316-Reaction rate profile for ATH->ATH Residue in 100:130 resin/ATH sample and 50% glass with a 0.5 mm glass coating

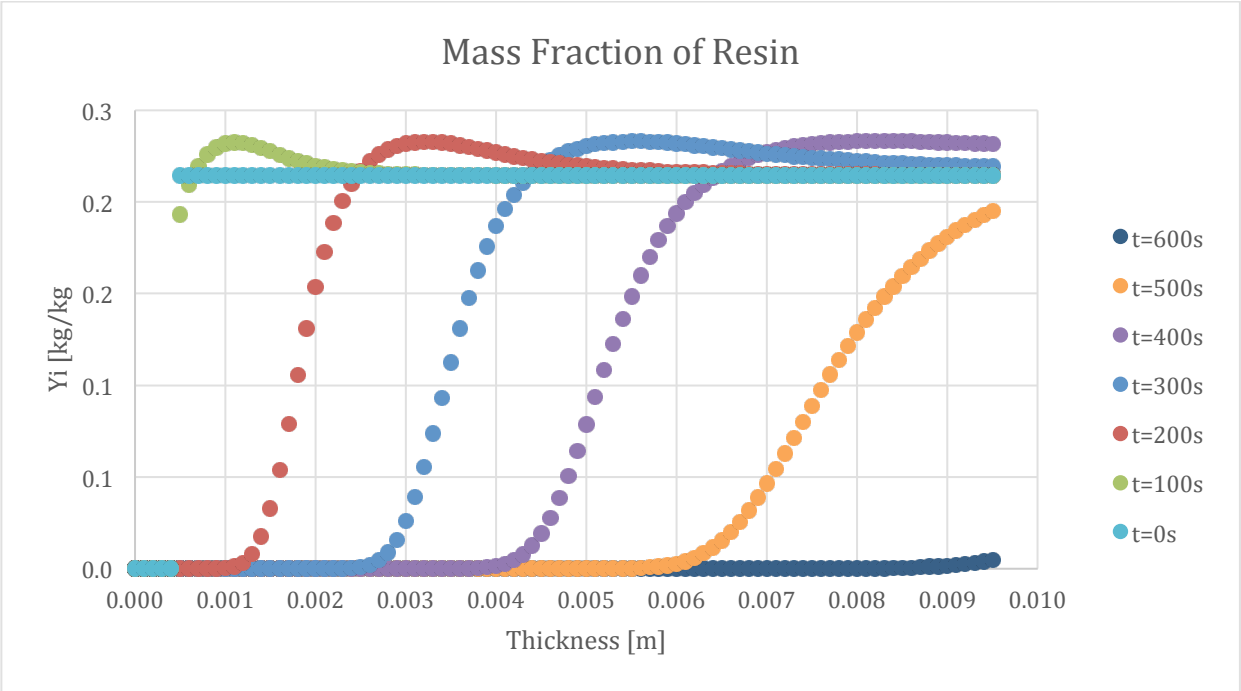


Figure 317-Mass fraction profile for Resin in 100:130 resin/ATH sample and 50% glass with a 0.5 mm glass coating

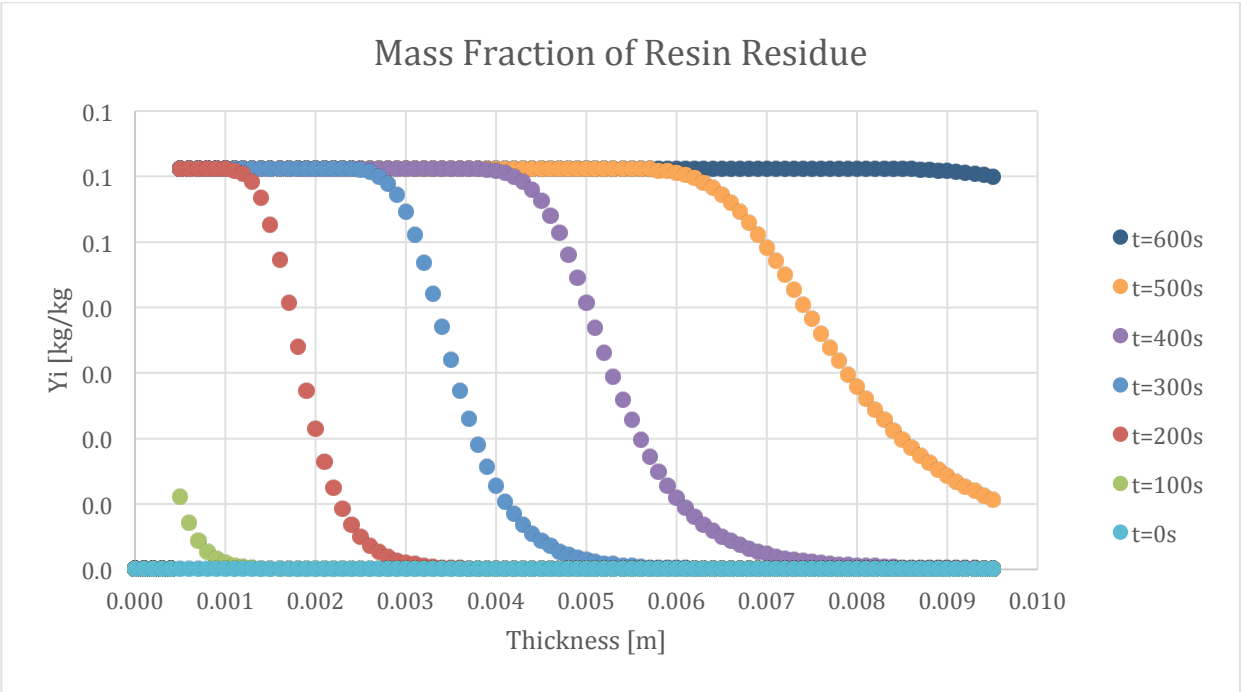


Figure 318-Mass fraction profile for Resin Residue in 100:130 resin/ATH sample and 50% glass with a 0.5 mm glass coating

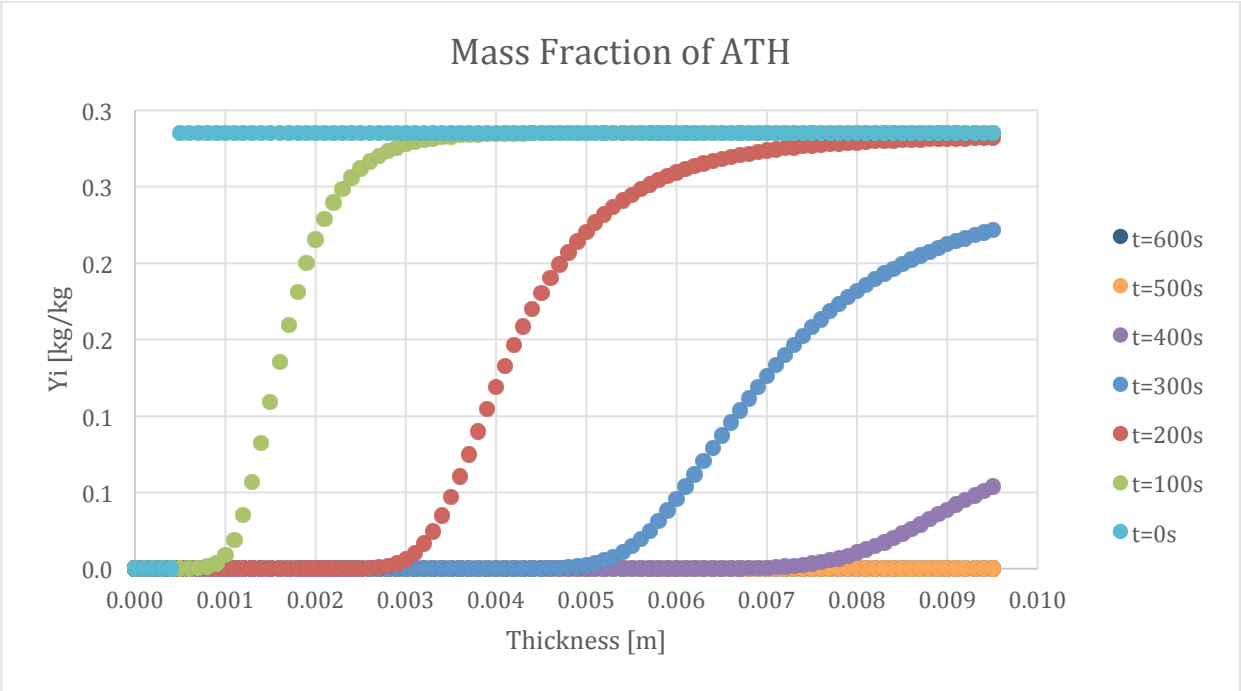


Figure 319-Mass fraction profile for ATH in 100:130 resin/ATH sample and 50% glass with a 0.5 mm glass coating

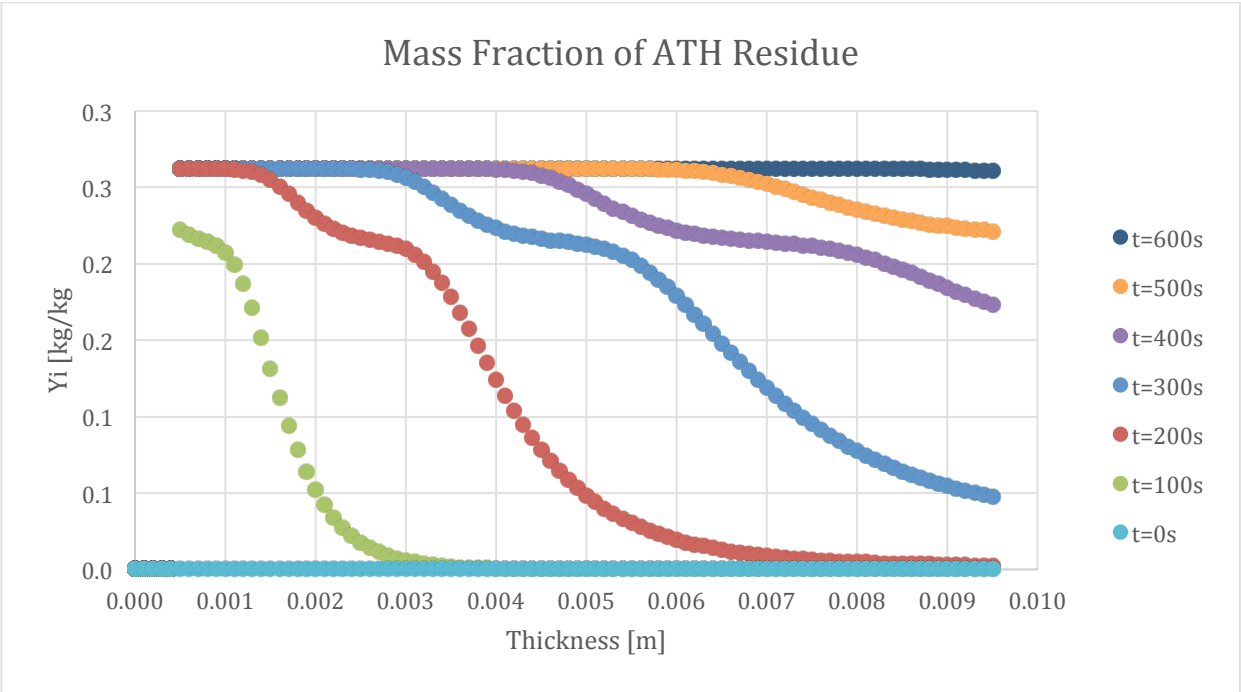


Figure 320-Mass fraction profile for ATH Residue in 100:130 resin/ATH sample and 50% glass with a 0.5 mm glass coating

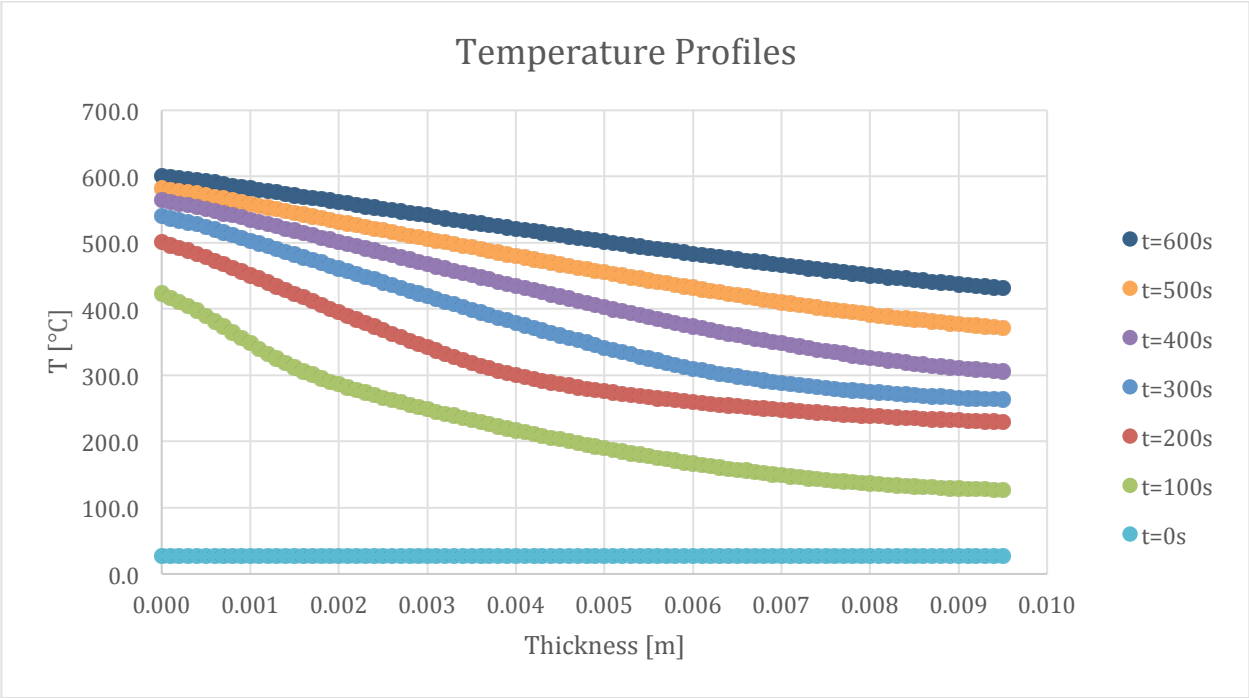


Figure 321-Temperature profile for 100:130 resin/ATH sample and 50% glass with a 0.5 mm coating

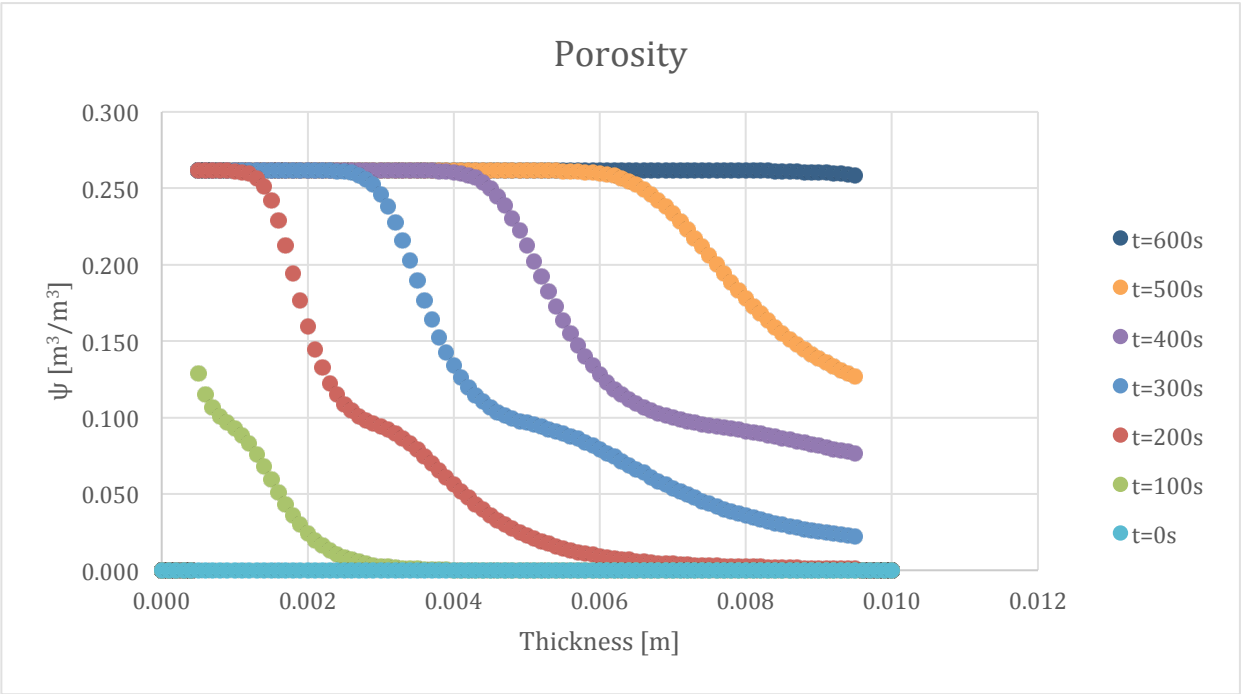


Figure 322-Porosity profile for 100:130 resin/ATH sample and 50% glass with a 0.5 mm coating

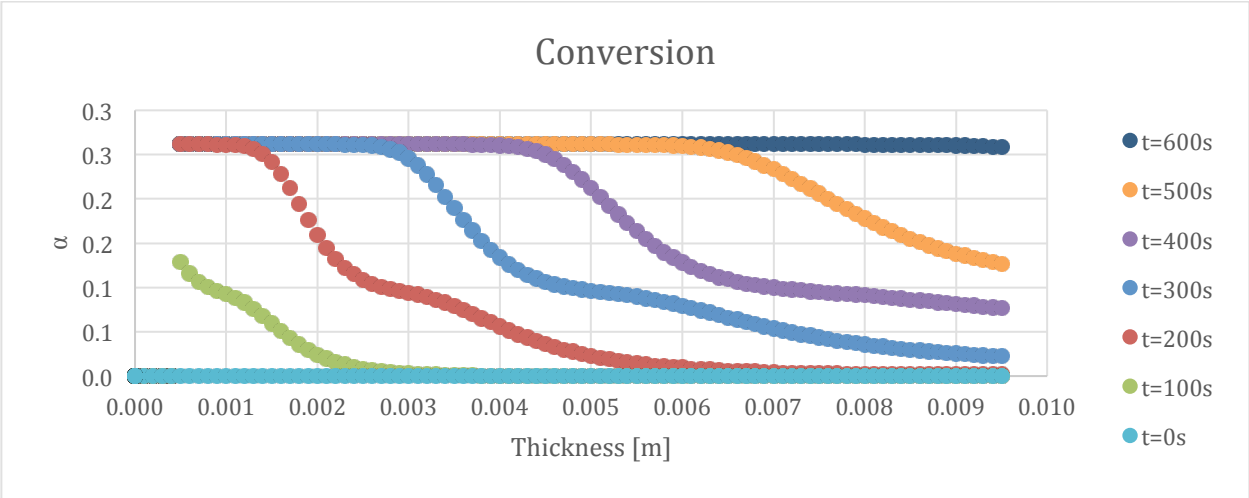


Figure 323-Conversion profile for 100:130 resin/ATH sample and 50% glass with a 0.5 mm coating

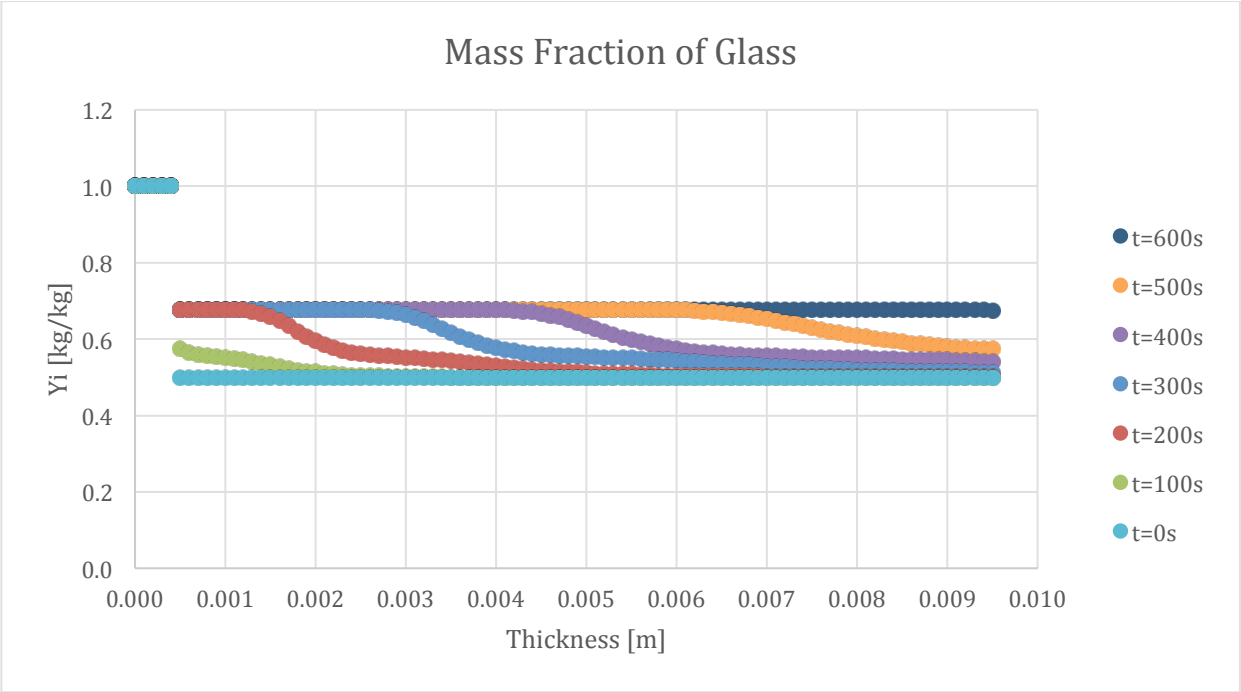


Figure 324-Mass fraction profile for Glass in 100:130 resin/ATH sample and 50% glass with a 0.5 mm glass coating

The following set of results are from the simulation of the 1 mm coating sample.

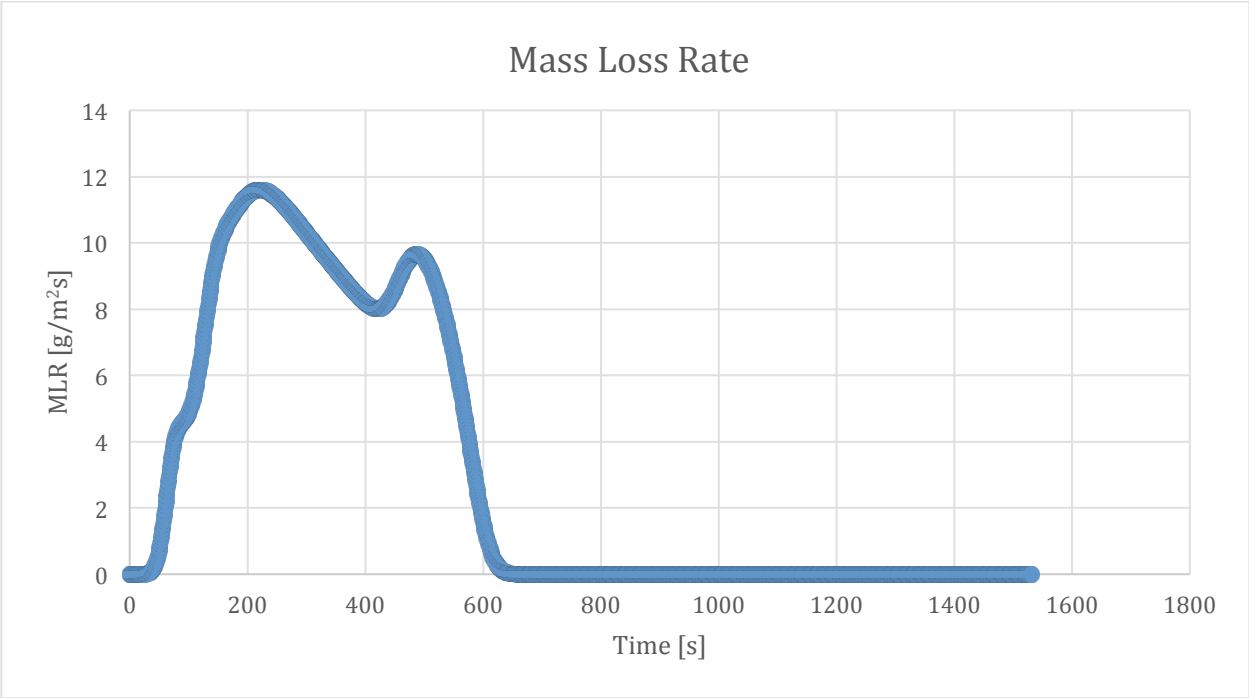


Figure 325-Mass loss rate curve for 100:130 resin/ATH sample and 50% glass with a 1 mm glass coating

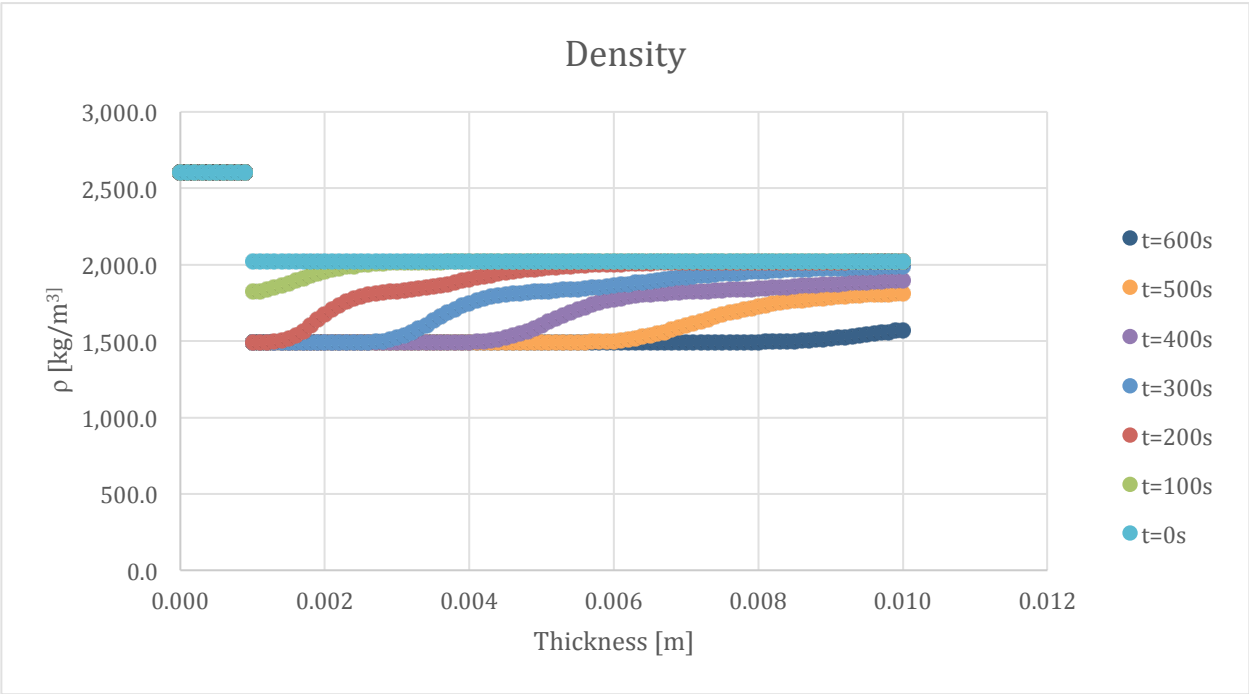


Figure 326-Density profile for 100:130 resin/ATH sample and 50% glass with a 1 mm coating

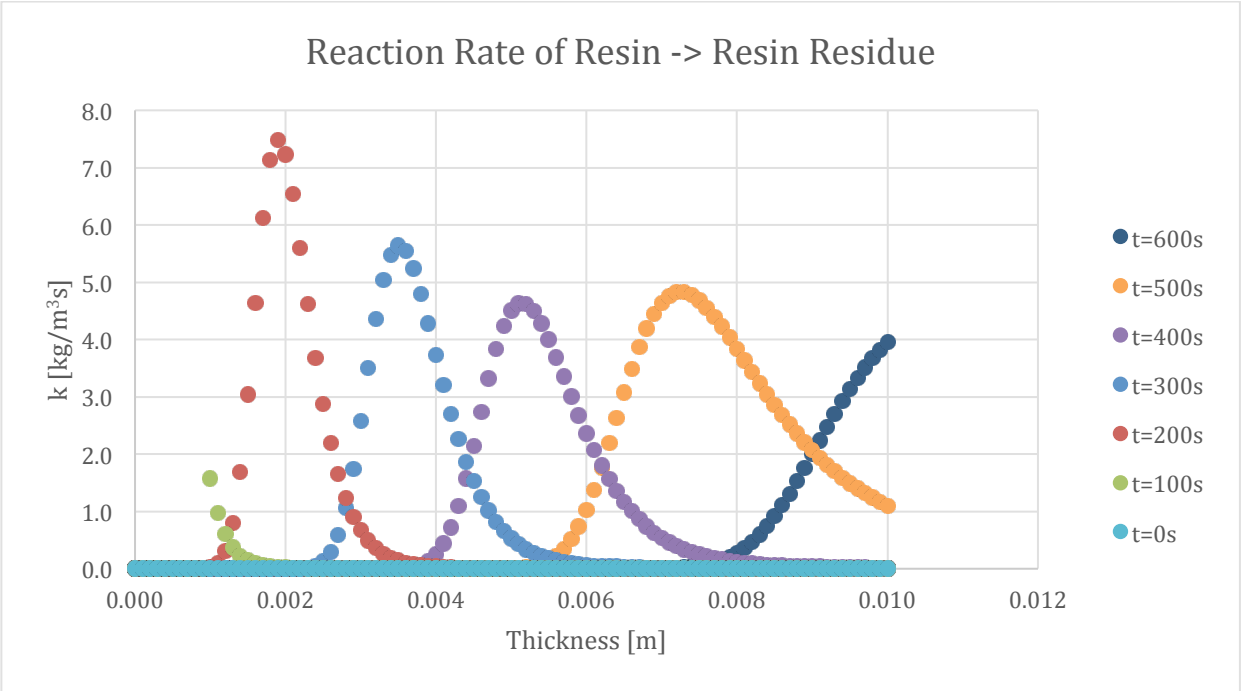


Figure 327-Reaction rate profile for Resin->Resin Residue in 100:130 resin/ATH sample and 50% glass with a 1 mm glass coating

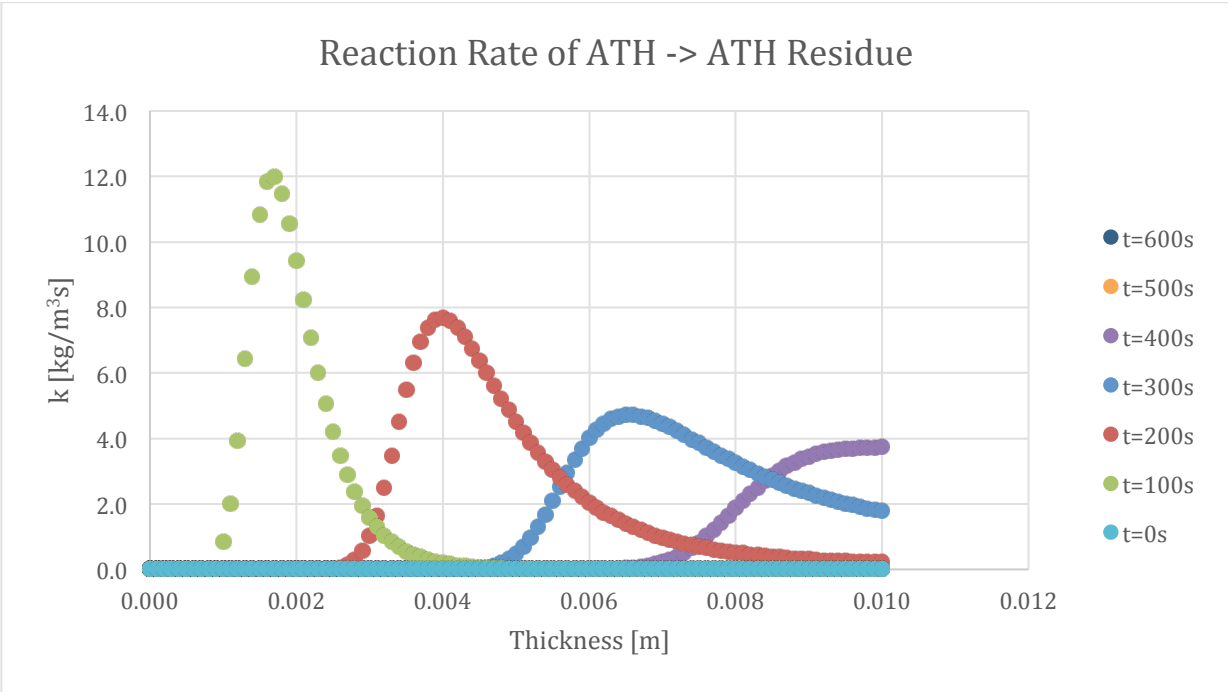


Figure 328-Reaction rate profile for ATH->ATH Residue in 100:130 resin/ATH sample and 50% glass with a 1 mm glass coating

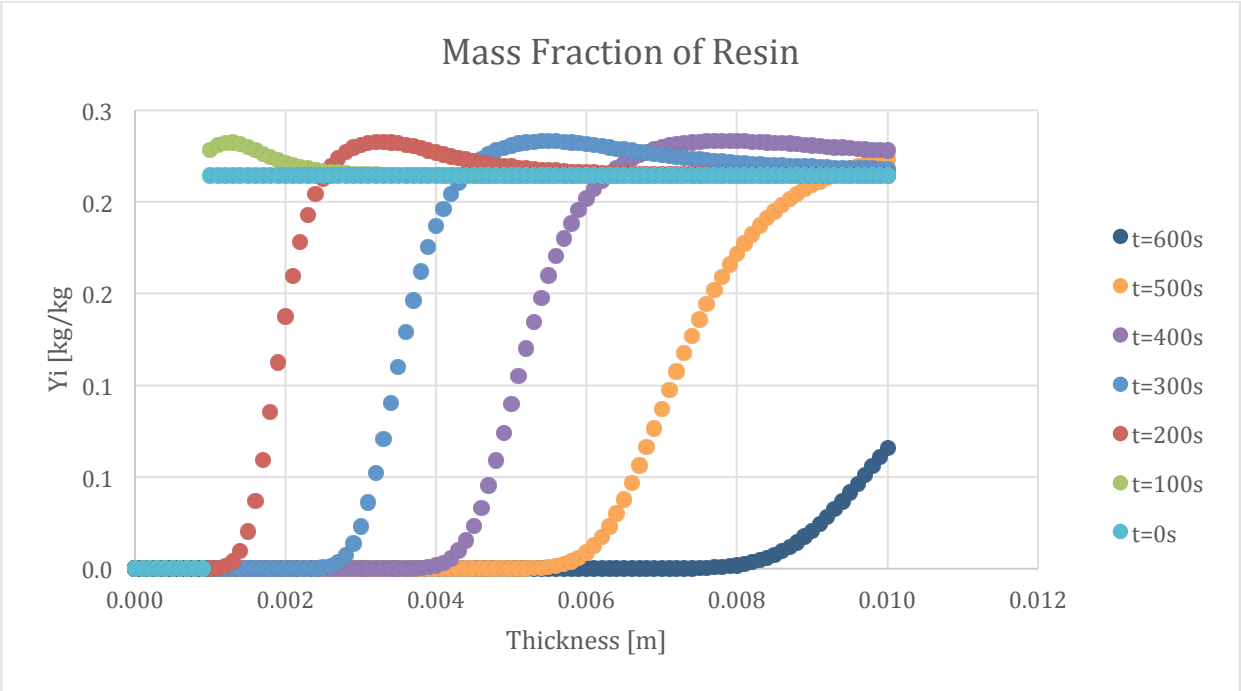


Figure 329-Mass fraction profile for Resin in 100:130 resin/ATH sample and 50% glass with a 1 mm glass coating

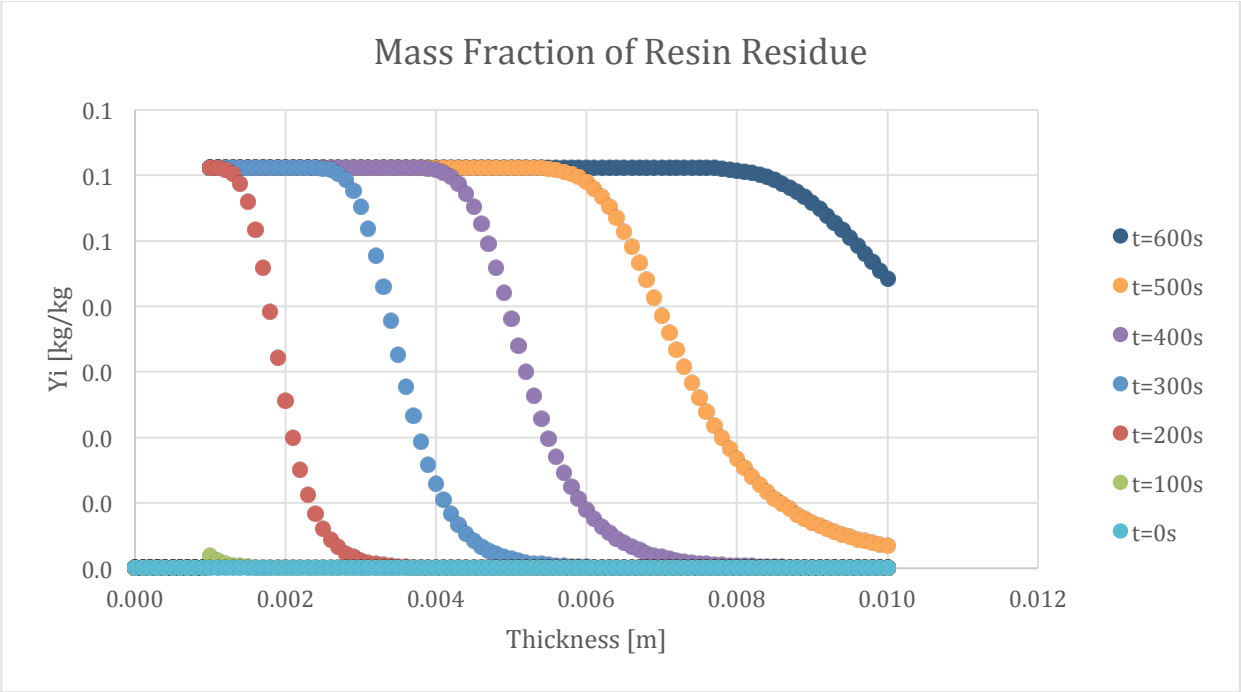


Figure 330-Mass fraction profile for Resin Residue in 100:130 resin/ATH sample and 50% glass with a 1 mm glass coating

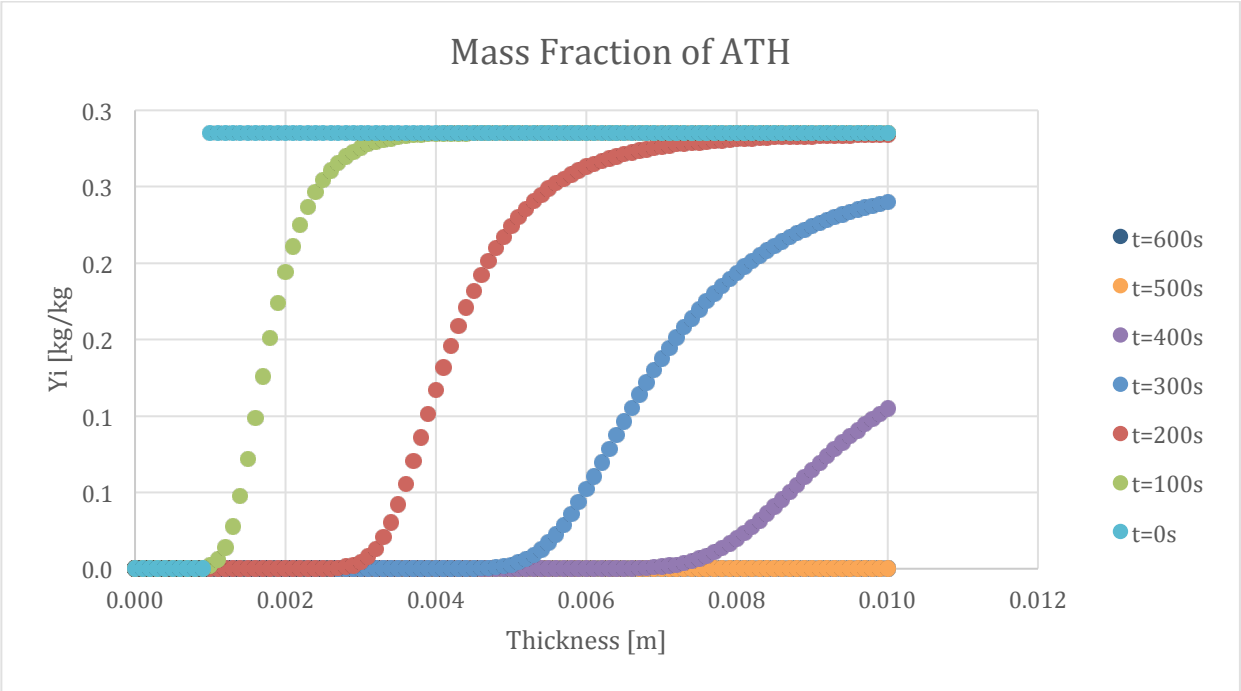


Figure 331-Mass fraction profile for ATH in 100:130 resin/ATH sample and 50% glass with a 1 mm glass coating

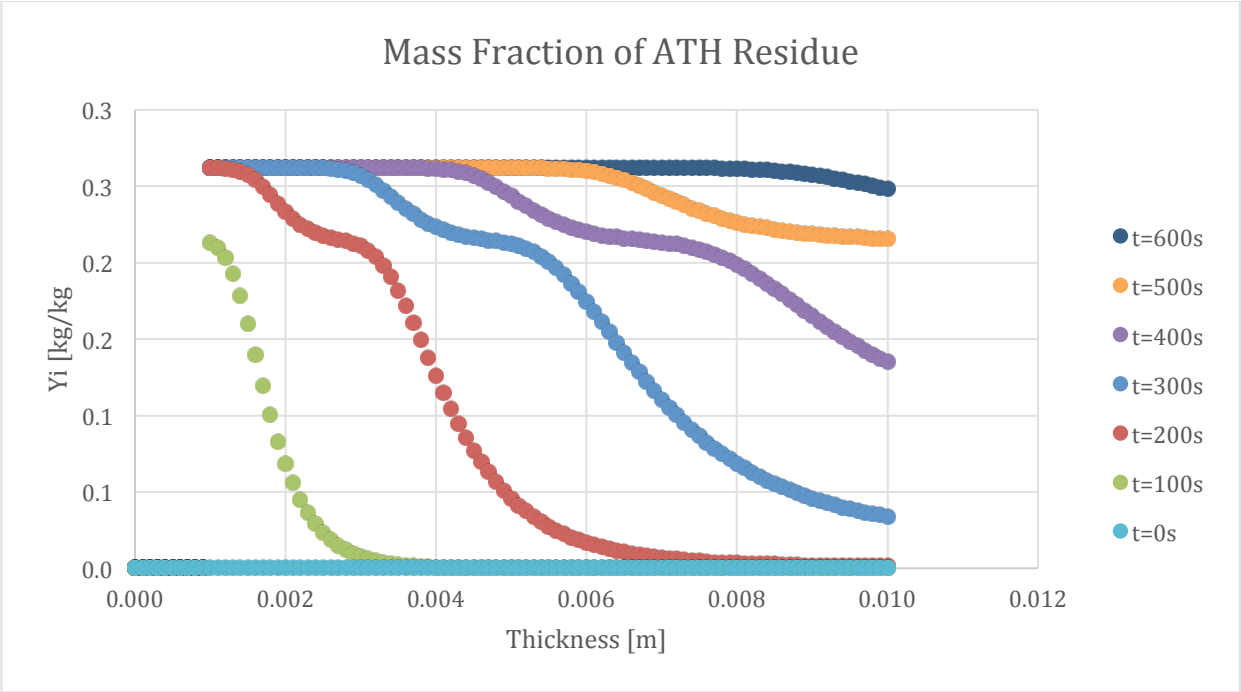


Figure 332-Mass fraction profile for ATH Residue in 100:130 resin/ATH sample and 50% glass with a 1 mm glass coating

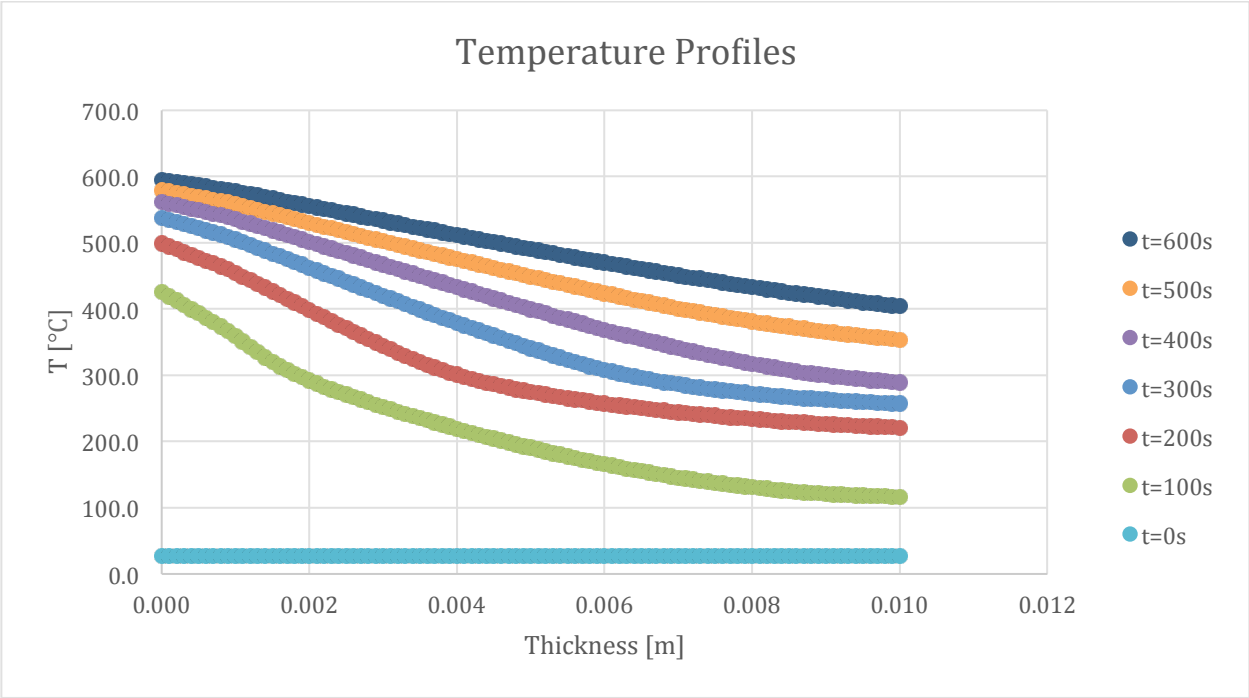


Figure 333-Temperature profile for 100:130 resin/ATH sample and 50% glass with a 1 mm coating

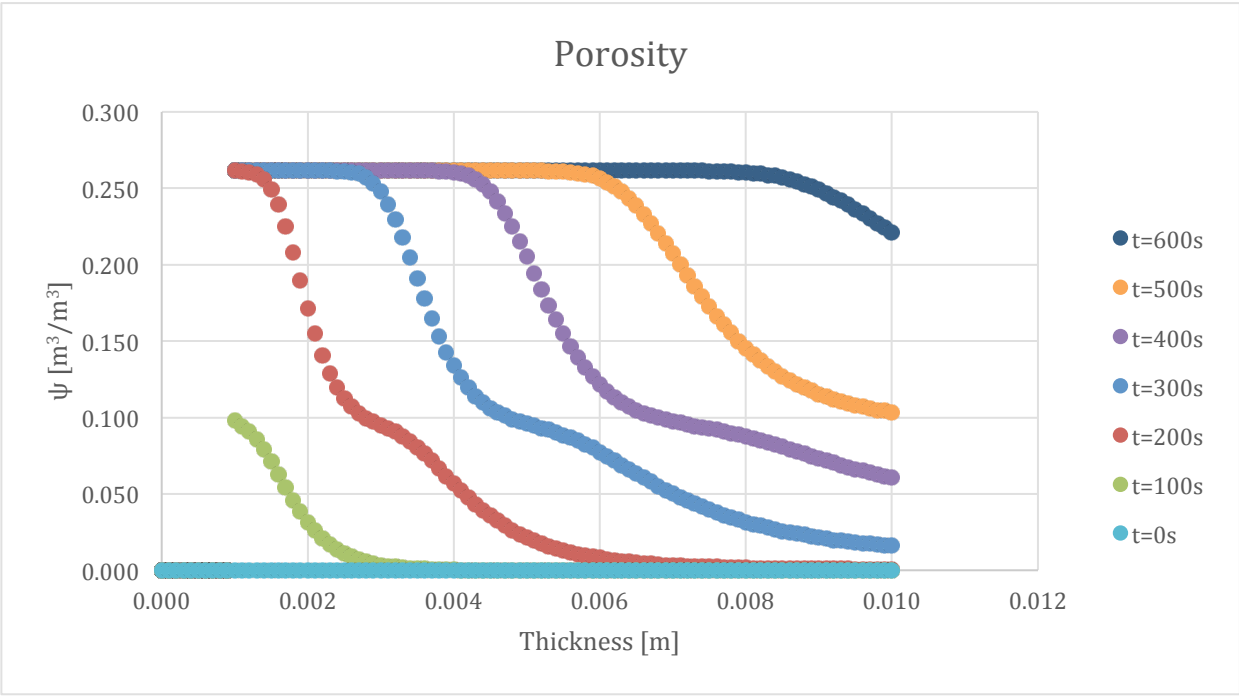


Figure 334-Porosity profile for 100:130 resin/ATH sample and 50% glass with a 1 mm coating

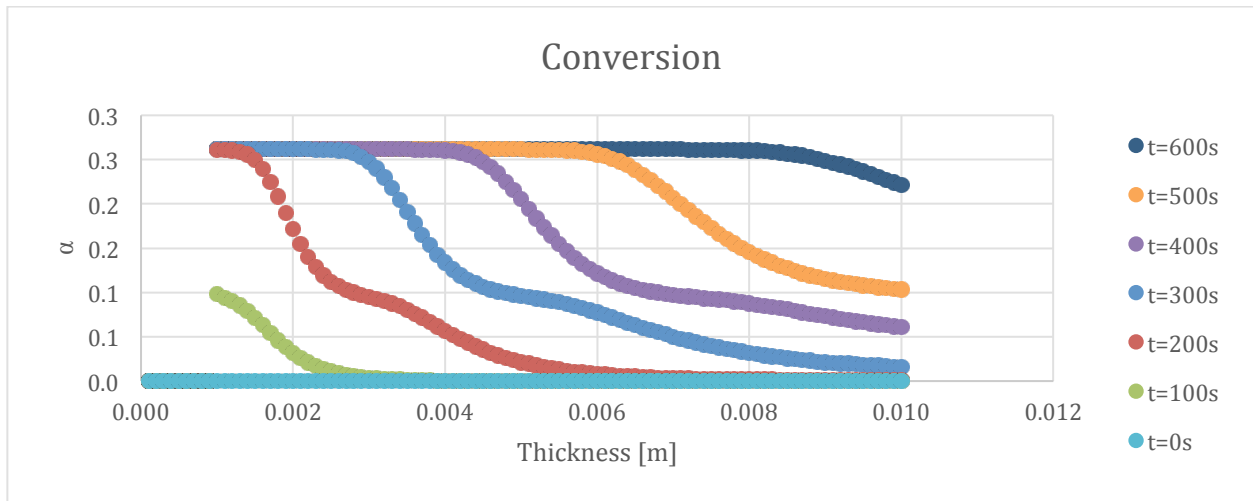


Figure 335-Conversion profile for 100:130 resin/ATH sample and 50% glass with a 1 mm coating

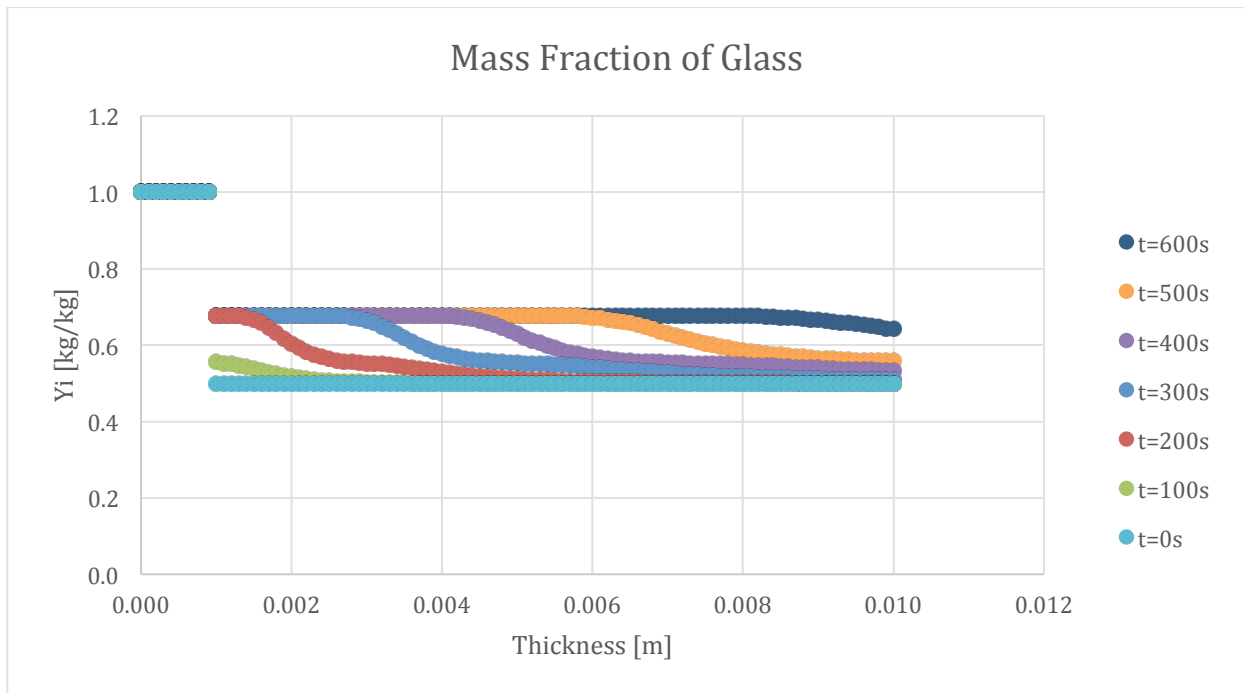


Figure 336-Mass fraction profile for Glass in 100:130 resin/ATH sample and 50% glass with a 1 mm glass coating

9.10.4. Varying Layering Style

A comparison was made between the baseline and the layered sample. The baseline sample was used and can be referenced in the first section of graphs. The results of the layered sample simulation are shown below.

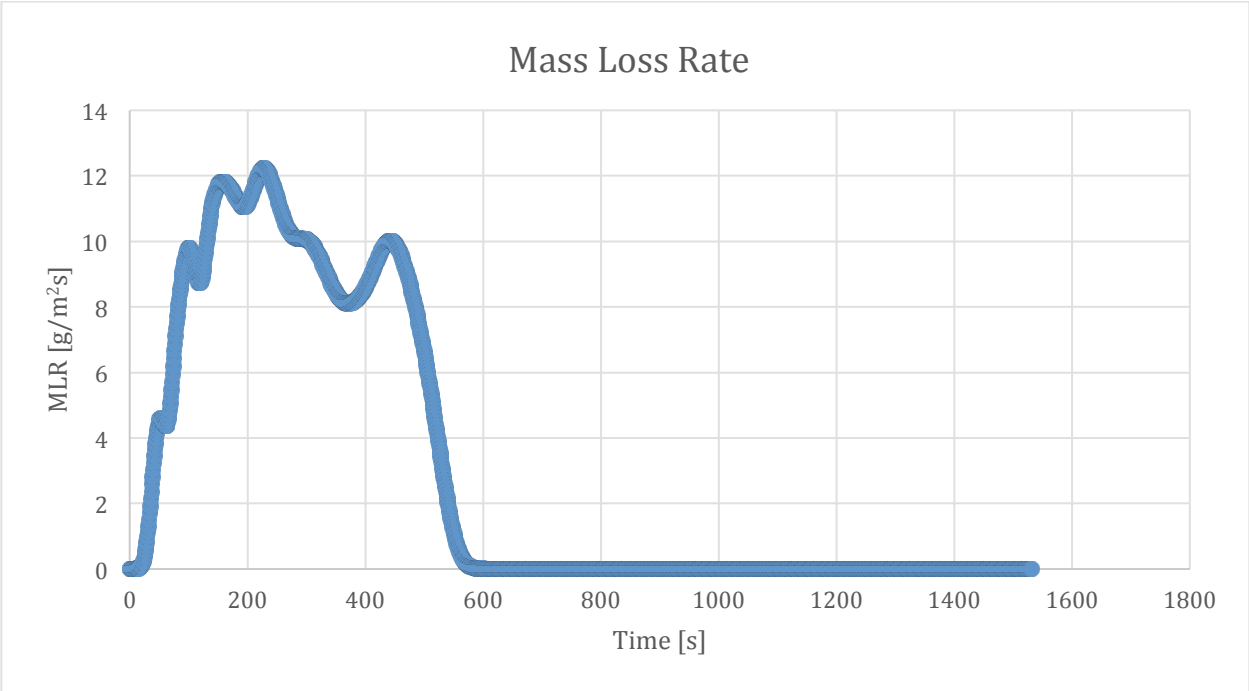


Figure 337-Mass loss rate curve for 100:130 resin/ATH sample with glass layering

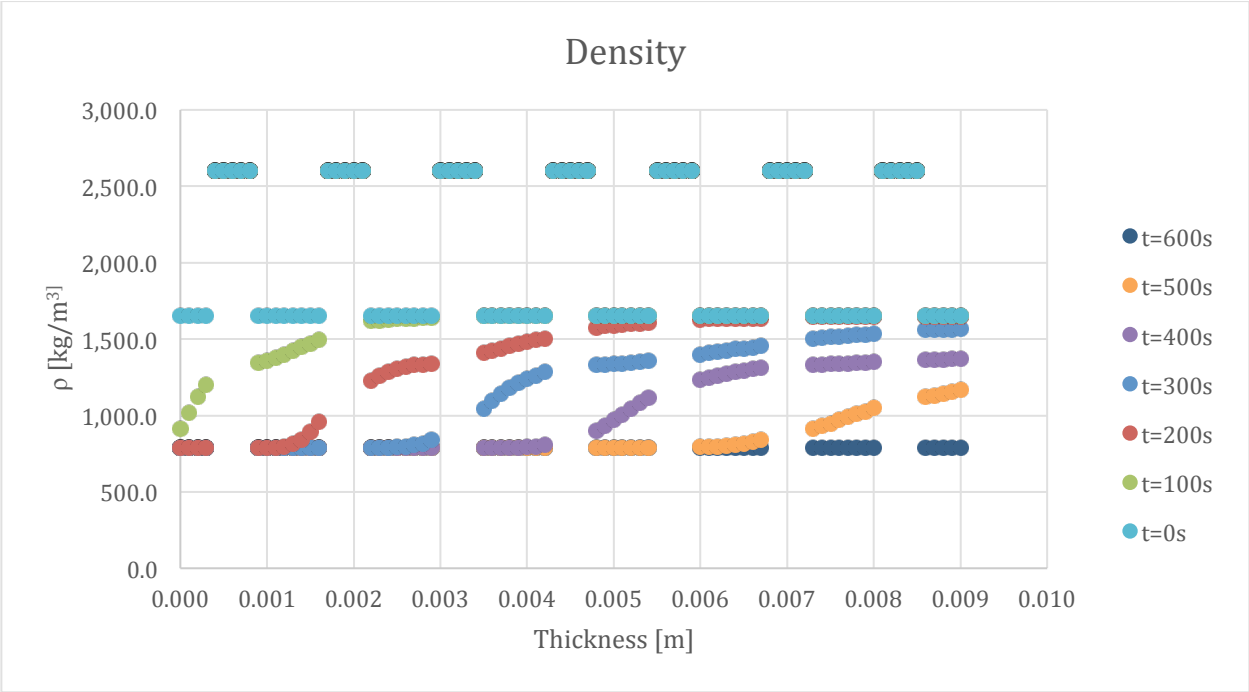


Figure 338-Density profile for 100:130 resin/ATH with glass layering

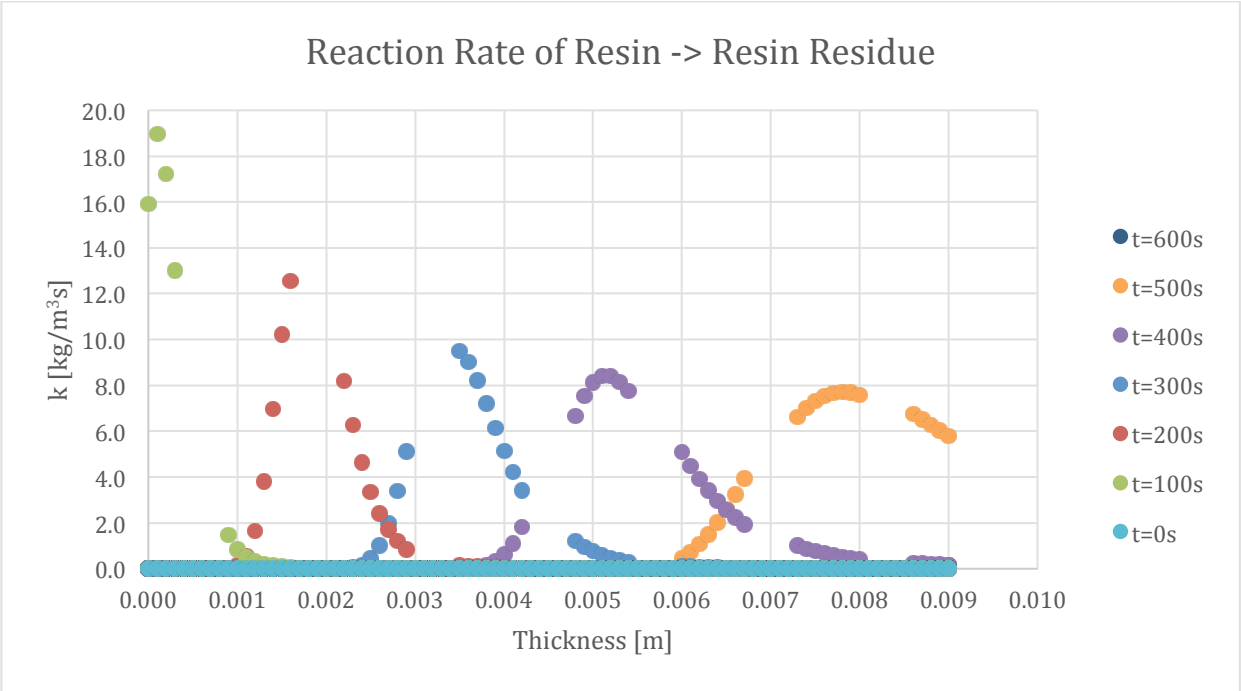


Figure 339-Reaction rate profile for Resin->Resin Residue in 100:130 resin/ATH sample with glass layering

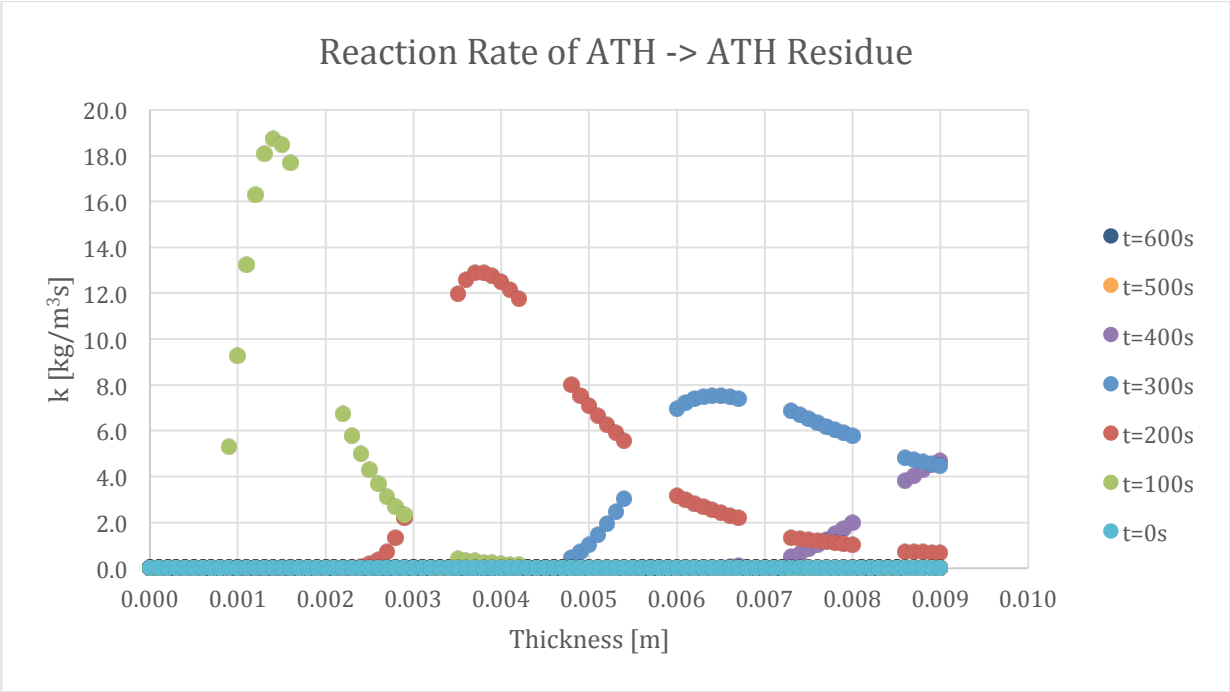


Figure 340-Reaction rate profile for ATH->ATH Residue in 100:130 resin/ATH sample with glass layering

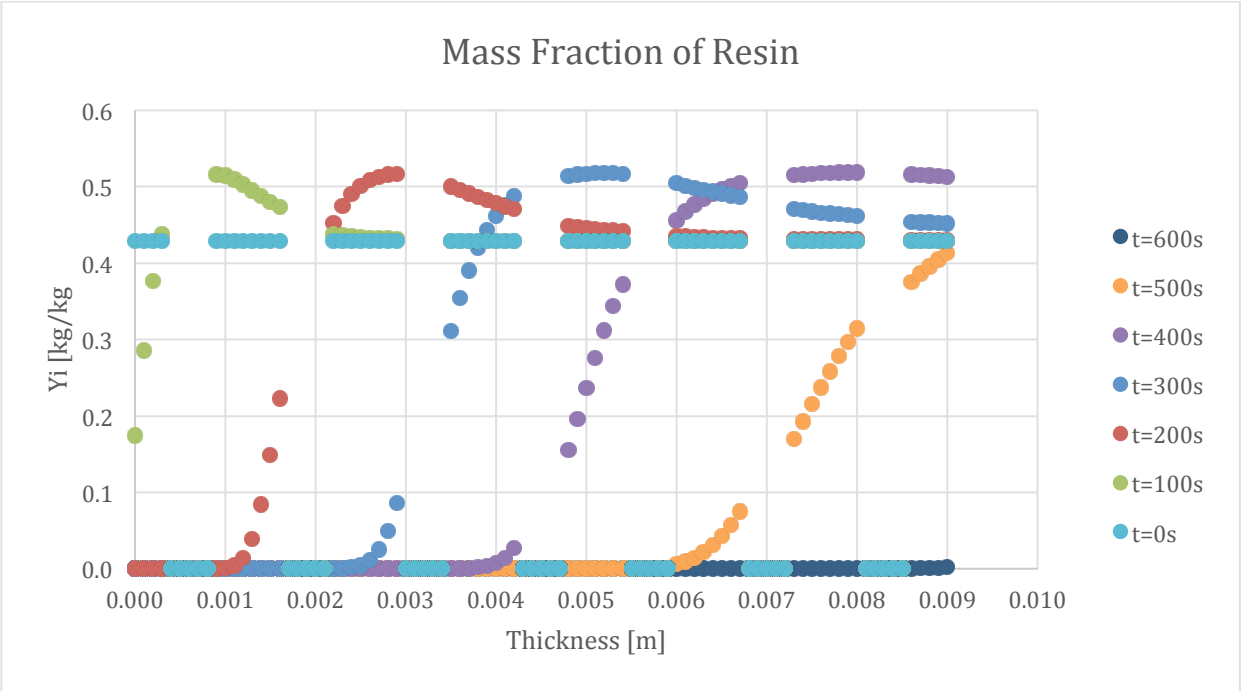


Figure 341-Mass fraction profile for Resin in 100:130 resin/ATH sample with glass layering

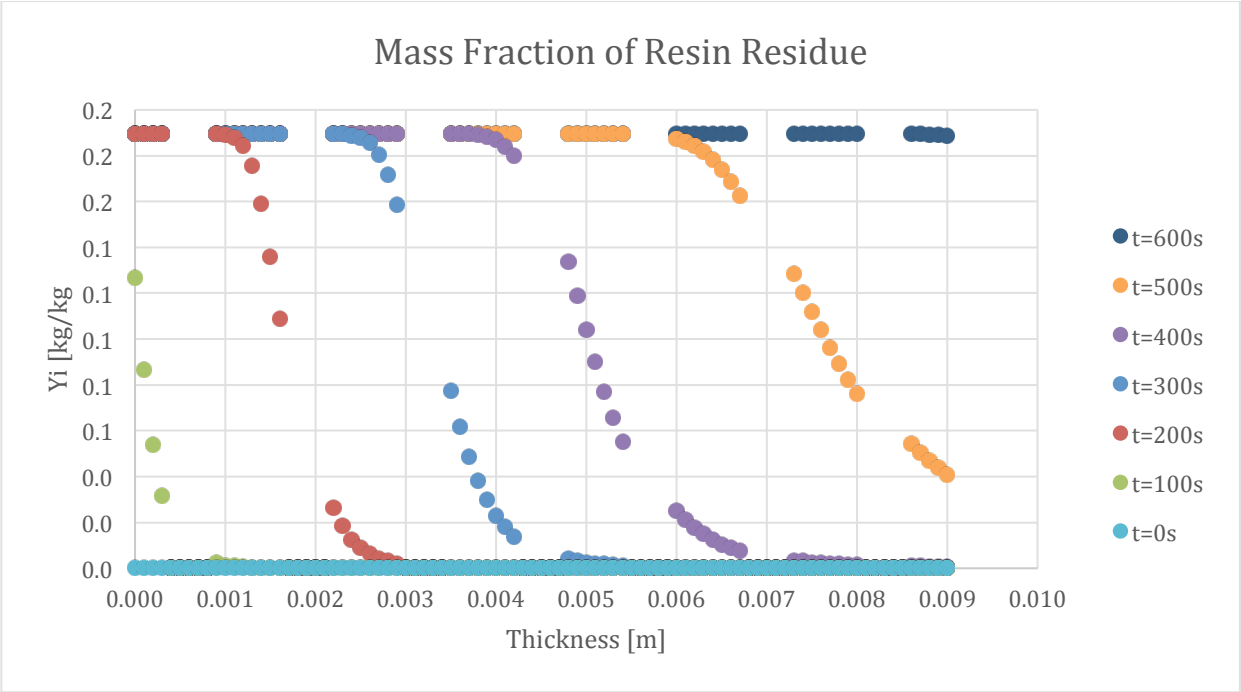


Figure 342-Mass fraction profile for Resin Residue in 100:130 resin/ATH sample with glass layering

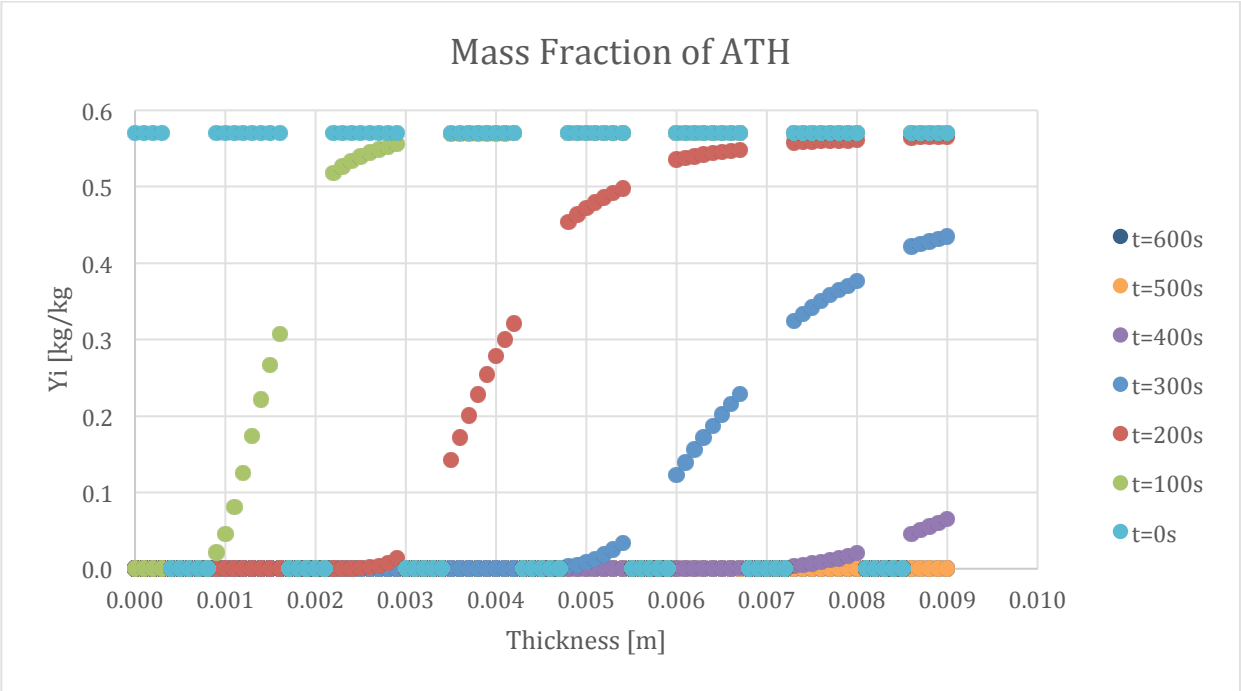


Figure 343-Mass fraction profile for ATH in 100:130 resin/ATH sample with glass layering

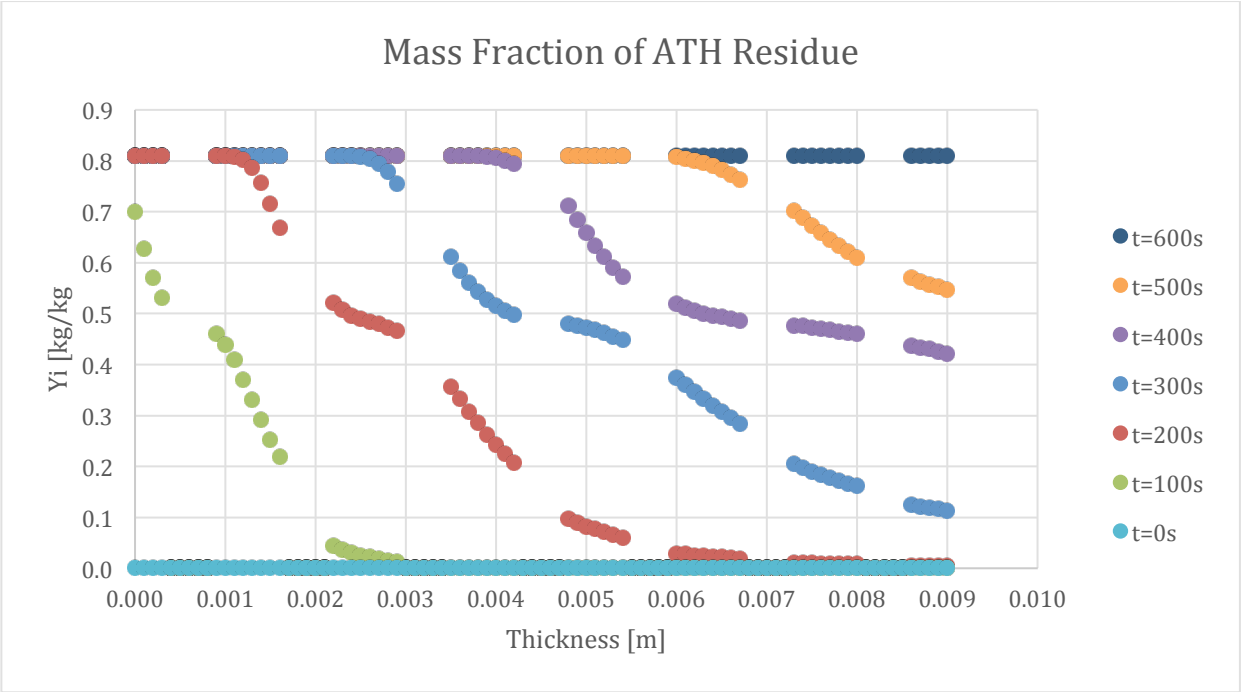


Figure 344-Mass fraction profile for ATH Residue in 100:130 resin/ATH sample with glass layering

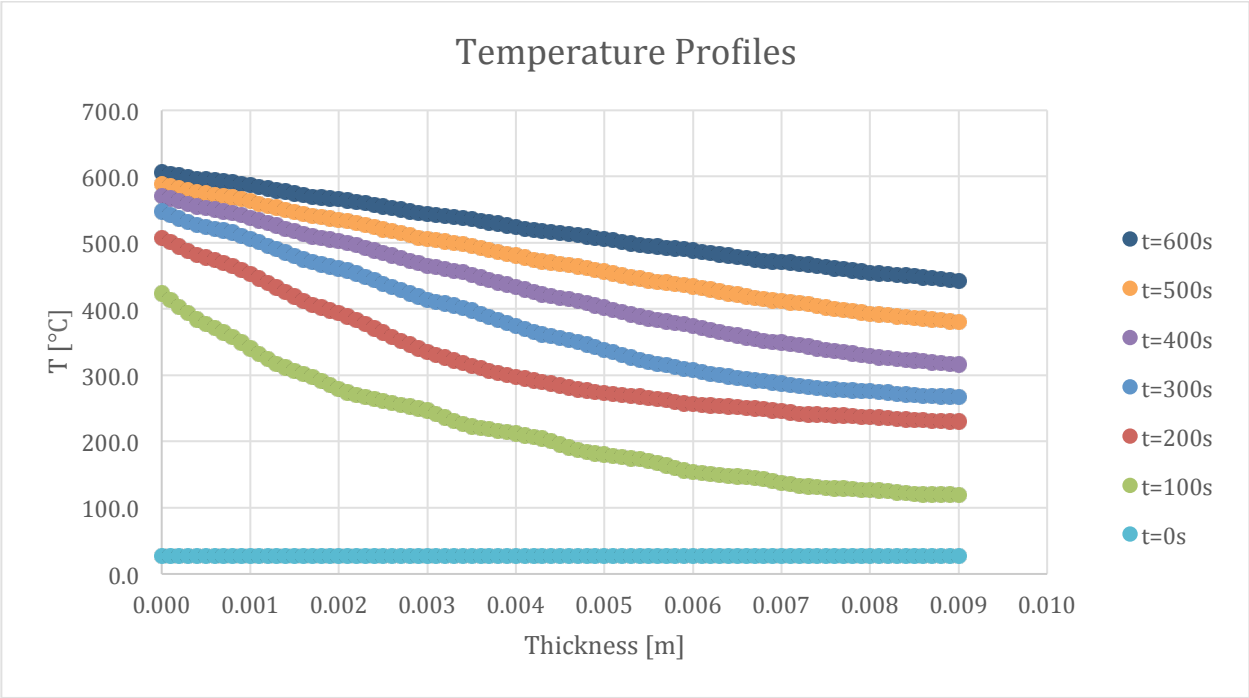


Figure 345-Temperature profile for 100:130 resin/ATH with glass layering

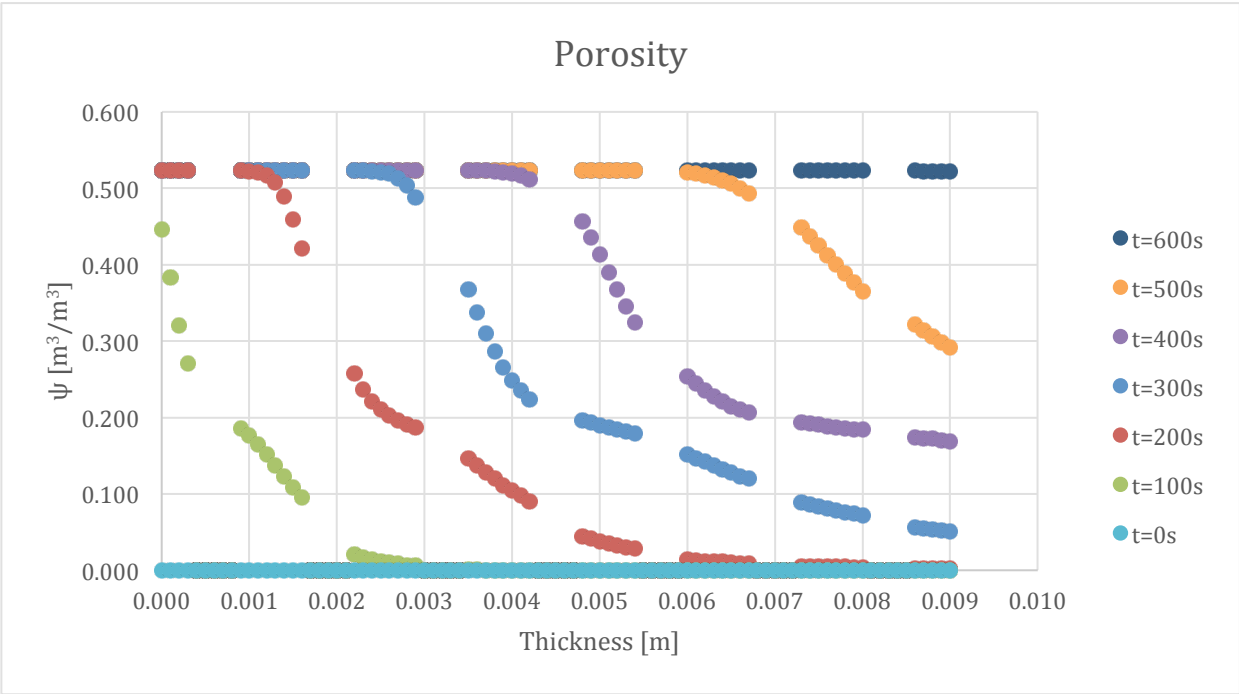


Figure 346-Porosity profile for 100:130 resin/ATH with glass layering

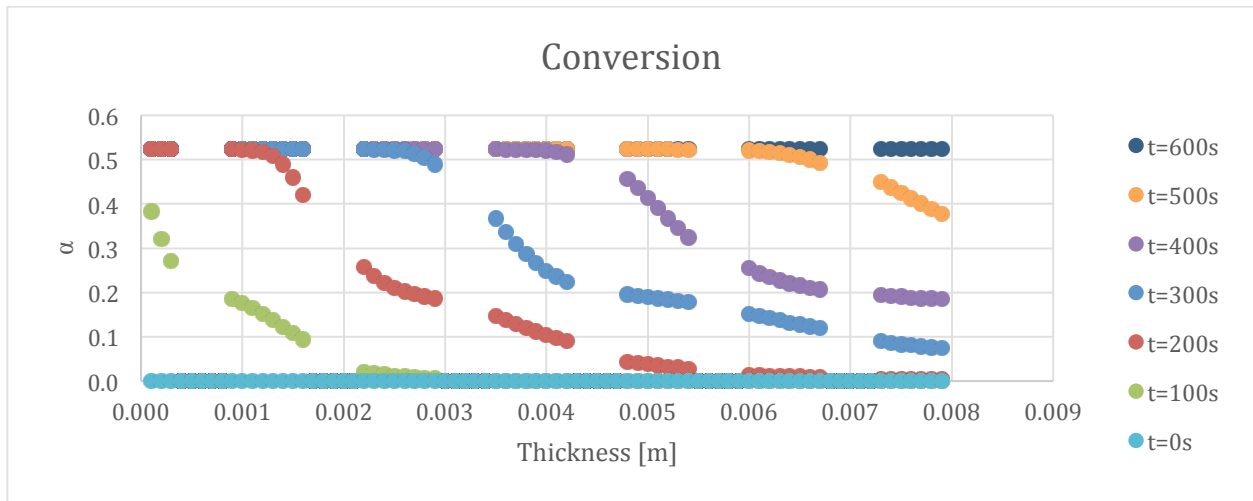


Figure 347-Conversion profile for 100:130 resin/ATH with glass layering

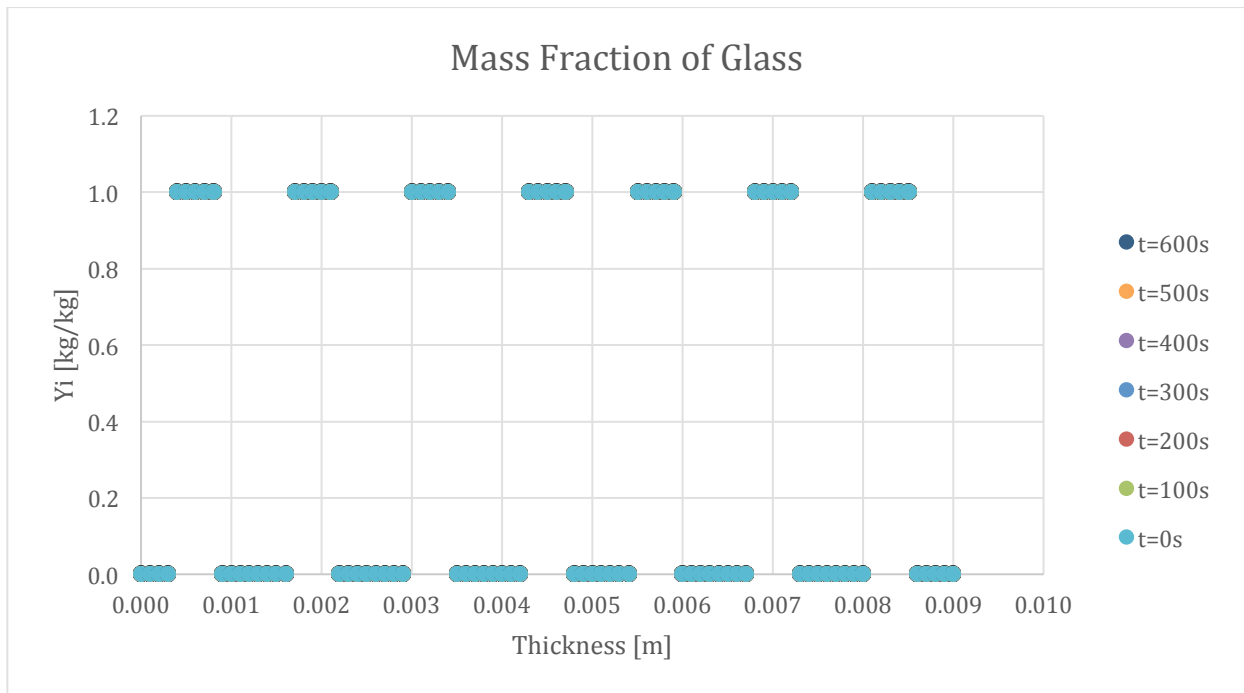


Figure 348-Mass fraction profile for Glass in 100:130 resin/ATH sample with glass layering

9.11. Input files

This section contains the input files for each simulation that produced the results

9.11.1. 100:0 FRP

&GPYRO_GENERAL

DT0 = 0.1,

TAMB = 300,
TREF = 300,
P0 = 101300,
GX = 0,
GZ = 0,
THERMAL_EQUILIBRIUM = .TRUE.,
VHLC = 0,
HCV = 1000000,
NU_A = 2,
NU_B = 1,
NU_C = 0.5,
NTDMA_ITERATIONS = 1000,
NSSPECIESITERNS = 1,
NCONTINUITYITERNS = 1,
ALPHA = 1,
TMPTOL = 0.0001,
HTOL = 0.00000001,
YITOL = 0.0001,
PTOL = 0.0001,
YJTOL = 0.0001,
HGTOL = 0.1,
EXPLICIT_T = .FALSE.,
SOLVE_GAS_YJ = .TRUE.,
SOLVE_GAS_ENERGY = .FALSE.,
SOLVE_PRESSURE = .FALSE.,
SOLVE_POROSITY = .FALSE.,
PROPERTY_LINTERP = .FALSE.,
USE_TOFH_NEWTON = .TRUE.,
SHYI_CORRECTION = .TRUE.,
NCOEFF_UPDATE_SKIP = 1,
FDSMODE = .FALSE.,
CONVENTIONAL_RXN_ORDER = .FALSE.,
TWOD = .FALSE.,
USE_BC_PATCHES = .TRUE.,
NOCONSUMPTION = .FALSE.,
EPS = 0.0000000001,
GAS_DIFFUSION = .FALSE.,
FRONT_GAS_DIFFUSION = .FALSE.,
BLOWING = .FALSE.,
MINIMUM_CONDUCTIVITY = 0,
CONSTANT_DHVOL = .TRUE.,
FULL_QSG = .FALSE.,
GASES_PRODUCED_AT_TSOLID = .FALSE.,
/

&GPYRO_OUTPUT

CASENAME = '100_0 Mixed True',
DUMP_ENERGY_BALANCE = .FALSE.,
N_POINT_QUANTITIES = 1,
N_PROFILE_QUANTITIES = 11,
N_SMOKEVIEW_QUANTITIES = 0,
DUMP_EVERYTHING = .FALSE.,
DTDUMP_GA = 1,
DTDUMP_POINT = 1,
DTDUMP_PROFILE = 1,
DTDUMP_SMOKEVIEW = 1,
TMP_REDUCED_DTDUMP = 5000,
REDUCED_DTDUMP = 0.0001,
DTMIN_KILL = 0.0000001,
POINT_QUANTITY(1) = 'MLR',
POINT_QUANTITY_INDEX(1) = 0,
POINT_Z(1) = 0,
POINT_X(1) = 0,
PROFILE_QUANTITY(1) = 'BULK_DENSITY',
PROFILE_QUANTITY_INDEX(1) = 0,
PROFILE_TYPE(1) = 'z',
PROFILE_LOCATION(1) = 0,
PROFILE_ISKIP(1) = 1,
PROFILE_QUANTITY(2) = 'REACTION_RATE_K',
PROFILE_QUANTITY_INDEX(2) = 1,
PROFILE_TYPE(2) = 'z',
PROFILE_LOCATION(2) = 0,
PROFILE_ISKIP(2) = 1,
PROFILE_QUANTITY(3) = 'REACTION_RATE_K',
PROFILE_QUANTITY_INDEX(3) = 2,
PROFILE_TYPE(3) = 'z',
PROFILE_LOCATION(3) = 0,
PROFILE_ISKIP(3) = 1,
PROFILE_QUANTITY(4) = 'YI',
PROFILE_QUANTITY_INDEX(4) = 1,
PROFILE_TYPE(4) = 'z',
PROFILE_LOCATION(4) = 0,
PROFILE_ISKIP(4) = 1,
PROFILE_QUANTITY(5) = 'YI',
PROFILE_QUANTITY_INDEX(5) = 2,
PROFILE_TYPE(5) = 'z',
PROFILE_LOCATION(5) = 0,
PROFILE_ISKIP(5) = 1,
PROFILE_QUANTITY(6) = 'YI',
PROFILE_QUANTITY_INDEX(6) = 3,
PROFILE_TYPE(6) = 'z',
PROFILE_LOCATION(6) = 0,

PROFILE_ISKIP(6) = 1,
PROFILE_QUANTITY(7) = 'YI',
PROFILE_QUANTITY_INDEX(7) = 4,
PROFILE_TYPE(7) = 'z',
PROFILE_LOCATION(7) = 0,
PROFILE_ISKIP(7) = 1,
PROFILE_QUANTITY(8) = 'TEMPERATURE',
PROFILE_QUANTITY_INDEX(8) = 0,
PROFILE_TYPE(8) = 'z',
PROFILE_LOCATION(8) = 0,
PROFILE_ISKIP(8) = 1,
PROFILE_QUANTITY(9) = 'POROSITY',
PROFILE_QUANTITY_INDEX(9) = 0,
PROFILE_TYPE(9) = 'z',
PROFILE_LOCATION(9) = 0,
PROFILE_ISKIP(9) = 1,
PROFILE_QUANTITY(10) = 'M/M0',
PROFILE_QUANTITY_INDEX(10) = 0,
PROFILE_TYPE(10) = 'z',
PROFILE_LOCATION(10) = 0,
PROFILE_ISKIP(10) = 1,
PROFILE_QUANTITY(11) = 'YI',
PROFILE_QUANTITY_INDEX(11) = 5,
PROFILE_TYPE(11) = 'z',
PROFILE_LOCATION(11) = 0,
PROFILE_ISKIP(11) = 1,
/

&GPYRO_SPROPS

NSSPEC = 5,
NAME(1) = 'Hetron',
K0Z(1) = 0.23,
NKZ(1) = 0,
R0(1) = 1200,
NR(1) = 0,
C0(1) = 1400,
NC(1) = 0,
EMIS(1) = 0.84,
KAPPA(1) = 1000000,
TMELT(1) = 3000,
DHMELT(1) = 0,
SIGMA2MELT(1) = 0,
GAMMA(1) = 0,
PERMZ(1) = 1D-10,
RS0(1) = 1250,
PORE_DIAMETER(1) = 0.0005,

KOX(1) = 0.2,
NKX(1) = 0,
PERMX(1) = 1D-10,
NAME(2) = 'Hetrn_residue',
KOZ(2) = 0.19,
NKZ(2) = 0,
R0(2) = 253,
NR(2) = 0,
C0(2) = 1900,
NC(2) = 0,
EMIS(2) = 0.90,
KAPPA(2) = 1000000,
TMELT(2) = 3000,
DHMELT(2) = 0,
SIGMA2MELT(2) = 0,
GAMMA(2) = 0.00348,
PERMZ(2) = 1D-10,
RS0(2) = 300,
PORE_DIAMETER(2) = 0.0005,
KOX(2) = 0.2,
NKX(2) = 0,
PERMX(2) = 1D-10,
NAME(3) = 'ATH',
KOZ(3) = 1.220,
NKZ(3) = 0,
R0(3) = 2300,
NR(3) = 0,
C0(3) = 1200,
NC(3) = 0,
EMIS(3) = 0.81,
KAPPA(3) = 1000000,
TMELT(3) = 3000,
DHMELT(3) = 0,
SIGMA2MELT(3) = 0,
GAMMA(3) = 0.000,
PERMZ(3) = 1D-10,
RS0(3) = 2350,
PORE_DIAMETER(3) = 0.0005,
KOX(3) = 0.2,
NKX(3) = 0,
PERMX(3) = 1D-10,
NAME(4) = 'ATH_residue',
KOZ(4) = 0.240,
NKZ(4) = 0.0,
R0(4) = 1558,
NR(4) = 0.0,

C0(4) = 1200,
NC(4) = 0.0,
EMIS(4) = 0.89,
KAPPA(4) = 1000000,
TMELT(4) = 3000,
DHMELT(4) = 0,
SIGMA2MELT(4) = 0,
GAMMA(4) = 0.00475,
PERMZ(4) = 1D-10,
RS0(4) = 1600,
PORE_DIAMETER(4) = 0.0005,
K0X(4) = 0.2,
NKX(4) = 0,
PERMX(4) = 1D-10,
NAME(5) = 'glass',
K0Z(5) = 0.18,
NKZ(5) = 0.59,
R0(5) = 2600,
NR(5) = 0.0,
C0(5) = 400,
NC(5) = 0.53,
EMIS(5) = 0.88,
KAPPA(5) = 1D6,
TMELT(5) = 3000,
DHMELT(5) = 0,
SIGMA2MELT(5) = 0,
GAMMA(5) = 0.00769,
PERMZ(5) = 1D-10,
RS0(5) = 2650,
PORE_DIAMETER(5) = 0.0005,
K0X(5) = 0.2,
NKX(5) = 0,
PERMX(5) = 1D-10,
/

&GPYRO_LAYERS

NLAYERS = 1,
X1(1) = -1,
X2(1) = 1,
Z1(1) = 0,
Z2(1) = 0.009,
NZCELLS_PER_LAYER(1) = 381,
NXCELLS_PER_LAYER(1) = 1,
HCRZ(1) = 0,
HCRX(1) = 0,
TINITIAL(1) = 300,

```
SOLVE_POROSITY_IN_LAYER(1) = .FALSE.,  
YI0(1,1) = 0.5,  
YI0(1,2) = 0,  
YI0(1,3) = 0,  
YI0(1,4) = 0,  
YI0(1,5) = 0.50,  
/
```

```
&GPYRO_RXNS  
NRXNS = 2,  
CFROM(1) = 'Hetron',  
CTO(1) = 'Hetron_residue',  
Z(1) = 5000000000000000,  
E(1) = 195,  
DHS(1) = 0,  
DHV(1) = 172000,  
CHI(1) = 1,  
ORDER(1) = 1.125,  
ORDERO2(1) = 0,  
IKINETICMODEL(1) = 0,  
IO2TYPE(1) = 0,  
M(1) = 0,  
KCAT(1) = 0,  
ICAT(1) = 0,  
CFROM(2) = 'ATH',  
CTO(2) = 'ATH_residue',  
Z(2) = 2500000000000000,  
E(2) = 140.1,  
DHS(2) = 0,  
DHV(2) = 1000000,  
CHI(2) = 1,  
ORDER(2) = 1.24,  
ORDERO2(2) = 0,  
IKINETICMODEL(2) = 0,  
IO2TYPE(2) = 0,  
M(2) = 0,  
KCAT(2) = 0,  
ICAT(2) = 0,  
/
```

```
&GPYRO_HGRXNS  
NHGRXNS = 0,  
/
```

```
&GPYRO_GPROPS  
NGSPEC = 1,
```



```
IBG = 1,  
IO2 = 2,  
CPG = 1000,  
NAME(1) = 'pyrolysate' ,  
YJ0(1) = 1 ,  
M(1) = 44 ,  
SIGMA(1) = 5.061 ,  
EPSOK(1) = 254 ,  
B(1) = 0 ,  
TONSET(1) = 653 ,  
TSPAN(1) = 50 ,  
/  

```

```
&GPYRO_GYIELDS  
GYIELDS(1,1) = 1,  
GYIELDS(1,2) = 1,  
/  

```

```
&GPYRO_HGYIELDS  
/  

```

```
&GPYRO_SEBCPATCH  
NSEBCPATCH = 2,  
T(1) = 0,  
X1(1) = -1,  
X2(1) = 1,  
Z1(1) = 0,  
Z2(1) = 0,  
QE(1) = 50000,  
HC(1) = 10,  
TINF(1) = 300,  
RERADIATION(1) = .TRUE.,  
TFIXED(1) = -1,  
T(2) = 0,  
X1(2) = -1,  
X2(2) = 1,  
Z1(2) = 0.009,  
Z2(2) = 0.009,  
QE(2) = 0,  
HC(2) = 10,  
TINF(2) = 300,  
RERADIATION(2) = .FALSE.,  
TFIXED(2) = -1,  
/  

```

```
&GPYRO_GMBCPATCH
```

NGMBCPATCH = 0,
/

&GPYRO_GSBCPATCH
NGSBCPATCH = 0,
/

&GPYRO_GEBCPATCH
NGEBCPATCH = 0,
/

&GPYRO_QE
NQE = 1,
QE(1) = 50000,
HCO(1) = 10,
NHC(1) = 0,
DELTA0(1) = 0.009,
NCELL(1) = 91,
L(1) = 0.01,
NBC(1) = 1,
TIG(1) = 10000,
QFL(1) = 0,
TSTOP(1) = 1600,
MIG(1) = 3,
TMPIG(1) = 350,
ZEROD(1) = .FALSE.,
BETA(1) = 5,
YJINF(1,1) = 1,
/

&GA_GENINPUT NGEN = 100,
NINDIV = 200,
MAXCOPIES = 4,
LINUX = .TRUE.,
SIMULATED_EXPERIMENTAL_DATA = .FALSE.,
RESTART = .FALSE.,
FITMIN = 0,
FITCLIP = 0,
FITEXPONENT = 2,
WHOLEGENEFRAC = 0.3,
BRUTE_FORCE = .FALSE.,
KILL_NONCONVERGED_SOLNS = .TRUE.,
/

&GA_PHI
NPHI = 0,
/

&GA_VARS
NGENE = 0,
/
[9.11.2. 100:130 FRP](#)

&GPYRO_GENERAL
DT0 = 0.1,
TAMB = 300,
TREF = 300,
P0 = 101300,
GX = 0,
GZ = 0,
THERMAL_EQUILIBRIUM = .TRUE.,
VHLC = 0,
HCV = 1000000,
NU_A = 2,
NU_B = 1,
NU_C = 0.5,
NTDMA_ITERATIONS = 1000,
NSSPECIESITERNS = 1,
NCONTINUITYITERNS = 1,
ALPHA = 1,
TMPTOL = 0.0001,
HTOL = 0.00000001,
YITOL = 0.0001,
PTOL = 0.0001,
YJTOL = 0.0001,
HGTOL = 0.1,
EXPLICIT_T = .FALSE.,
SOLVE_GAS_YJ = .TRUE.,
SOLVE_GAS_ENERGY = .FALSE.,
SOLVE_PRESSURE = .FALSE.,
SOLVE_POROSITY = .FALSE.,
PROPERTY_LINTERP = .FALSE.,
USE_TOFH_NEWTON = .TRUE.,
SHYI_CORRECTION = .TRUE.,
NCOEFF_UPDATE_SKIP = 1,
FDSMODE = .FALSE.,
CONVENTIONAL_RXN_ORDER = .FALSE.,
TWOOD = .FALSE.,
USE_BC_PATCHES = .TRUE.,
NOCONSUMPTION = .FALSE.,
EPS = 0.0000000001,
GAS_DIFFUSION = .FALSE.,
FRONT_GAS_DIFFUSION = .FALSE.,

BLOWING = .FALSE.,
MINIMUM_CONDUCTIVITY = 0,
CONSTANT_DHVOL = .TRUE.,
FULL_QSG = .FALSE.,
GASES_PRODUCED_AT_TSOLID = .FALSE.,
/

&GPYRO_OUTPUT

CASENAME = '100.113 Mixed True',
DUMP_ENERGY_BALANCE = .FALSE.,
N_POINT_QUANTITIES = 1,
N_PROFILE_QUANTITIES = 11,
N_SMOKEVIEW_QUANTITIES = 0,
DUMP_EVERYTHING = .FALSE.,
DTDUMP_GA = 1,
DTDUMP_POINT = 1,
DTDUMP_PROFILE = 1,
DTDUMP_SMOKEVIEW = 1,
TMP_REDUCED_DTDUMP = 5000,
REDUCED_DTDUMP = 0.0001,
DTMIN_KILL = 0.0000001,
POINT_QUANTITY(1) = 'MLR',
POINT_QUANTITY_INDEX(1) = 0,
POINT_Z(1) = 0,
POINT_X(1) = 0,
PROFILE_QUANTITY(1) = 'BULK_DENSITY',
PROFILE_QUANTITY_INDEX(1) = 0,
PROFILE_TYPE(1) = 'z',
PROFILE_LOCATION(1) = 0,
PROFILE_ISKIP(1) = 1,
PROFILE_QUANTITY(2) = 'REACTION_RATE_K',
PROFILE_QUANTITY_INDEX(2) = 1,
PROFILE_TYPE(2) = 'z',
PROFILE_LOCATION(2) = 0,
PROFILE_ISKIP(2) = 1,
PROFILE_QUANTITY(3) = 'REACTION_RATE_K',
PROFILE_QUANTITY_INDEX(3) = 2,
PROFILE_TYPE(3) = 'z',
PROFILE_LOCATION(3) = 0,
PROFILE_ISKIP(3) = 1,
PROFILE_QUANTITY(4) = 'YI',
PROFILE_QUANTITY_INDEX(4) = 1,
PROFILE_TYPE(4) = 'z',
PROFILE_LOCATION(4) = 0,
PROFILE_ISKIP(4) = 1,
PROFILE_QUANTITY(5) = 'YI',

PROFILE_QUANTITY_INDEX(5) = 2,
PROFILE_TYPE(5) = 'z',
PROFILE_LOCATION(5) = 0,
PROFILE_ISKIP(5) = 1,
PROFILE_QUANTITY(6) = 'YI',
PROFILE_QUANTITY_INDEX(6) = 3,
PROFILE_TYPE(6) = 'z',
PROFILE_LOCATION(6) = 0,
PROFILE_ISKIP(6) = 1,
PROFILE_QUANTITY(7) = 'YI',
PROFILE_QUANTITY_INDEX(7) = 4,
PROFILE_TYPE(7) = 'z',
PROFILE_LOCATION(7) = 0,
PROFILE_ISKIP(7) = 1,
PROFILE_QUANTITY(8) = 'TEMPERATURE',
PROFILE_QUANTITY_INDEX(8) = 0,
PROFILE_TYPE(8) = 'z',
PROFILE_LOCATION(8) = 0,
PROFILE_ISKIP(8) = 1,
PROFILE_QUANTITY(9) = 'POROSITY',
PROFILE_QUANTITY_INDEX(9) = 0,
PROFILE_TYPE(9) = 'z',
PROFILE_LOCATION(9) = 0,
PROFILE_ISKIP(9) = 1,
PROFILE_QUANTITY(10) = 'M/M0',
PROFILE_QUANTITY_INDEX(10) = 0,
PROFILE_TYPE(10) = 'z',
PROFILE_LOCATION(10) = 0,
PROFILE_ISKIP(10) = 1,
PROFILE_QUANTITY(11) = 'YI',
PROFILE_QUANTITY_INDEX(11) = 5,
PROFILE_TYPE(11) = 'z',
PROFILE_LOCATION(11) = 0,
PROFILE_ISKIP(11) = 1,
/
/

&GPYRO_SPROPS

NSSPEC = 5,
NAME(1) = 'Hetron',
K0Z(1) = 0.23,
NKZ(1) = 0,
R0(1) = 1200,
NR(1) = 0,
C0(1) = 1400,
NC(1) = 0,
EMIS(1) = 0.84,

KAPPA(1) = 1000000,
TMELT(1) = 3000,
DHMELT(1) = 0,
SIGMA2MELT(1) = 0,
GAMMA(1) = 0,
PERMZ(1) = 1D-10,
RS0(1) = 1250,
PORE_DIAMETER(1) = 0.0005,
K0X(1) = 0.2,
NKX(1) = 0,
PERMX(1) = 1D-10,
NAME(2) = 'Hetron_residue',
K0Z(2) = 0.19,
NKZ(2) = 0,
R0(2) = 253,
NR(2) = 0,
C0(2) = 1900,
NC(2) = 0,
EMIS(2) = 0.90,
KAPPA(2) = 1000000,
TMELT(2) = 3000,
DHMELT(2) = 0,
SIGMA2MELT(2) = 0,
GAMMA(2) = 0.00348,
PERMZ(2) = 1D-10,
RS0(2) = 300,
PORE_DIAMETER(2) = 0.0005,
K0X(2) = 0.2,
NKX(2) = 0,
PERMX(2) = 1D-10,
NAME(3) = 'ATH',
K0Z(3) = 1.220,
NKZ(3) = 0,
R0(3) = 2300,
NR(3) = 0,
C0(3) = 1200,
NC(3) = 0,
EMIS(3) = 0.81,
KAPPA(3) = 1000000,
TMELT(3) = 3000,
DHMELT(3) = 0,
SIGMA2MELT(3) = 0,
GAMMA(3) = 0.000,
PERMZ(3) = 1D-10,
RS0(3) = 2350,
PORE_DIAMETER(3) = 0.0005,

KOX(3) = 0.2,
NKX(3) = 0,
PERMX(3) = 1D-10,
NAME(4) = 'ATH_residue',
K0Z(4) = 0.240,
NKZ(4) = 0.0,
R0(4) = 1558,
NR(4) = 0.0,
C0(4) = 1200,
NC(4) = 0.0,
EMIS(4) = 0.89,
KAPPA(4) = 1000000,
TMELT(4) = 3000,
DHMELT(4) = 0,
SIGMA2MELT(4) = 0,
GAMMA(4) = 0.00475,
PERMZ(4) = 1D-10,
RS0(4) = 1600,
PORE_DIAMETER(4) = 0.0005,
KOX(4) = 0.2,
NKX(4) = 0,
PERMX(4) = 1D-10,
NAME(5) = 'glass',
K0Z(5) = 0.18,
NKZ(5) = 0.59,
R0(5) = 2600,
NR(5) = 0.0,
C0(5) = 400,
NC(5) = 0.53,
EMIS(5) = 0.88,
KAPPA(5) = 1D6,
TMELT(5) = 3000,
DHMELT(5) = 0,
SIGMA2MELT(5) = 0,
GAMMA(5) = 0.00769,
PERMZ(5) = 1D-10,
RS0(5) = 2650,
PORE_DIAMETER(5) = 0.0005,
KOX(5) = 0.2,
NKX(5) = 0,
PERMX(5) = 1D-10,
/

&GPYRO_LAYERS
NLAYERS = 1,
X1(1) = -1,

X2(1) = 1,
Z1(1) = 0,
Z2(1) = 0.009,
NZCELLS_PER_LAYER(1) = 381,
NXCELLS_PER_LAYER(1) = 1,
HCRZ(1) = 0,
HCRX(1) = 0,
TINITIAL(1) = 300,
SOLVE_POROSITY_IN_LAYER(1) = .FALSE.,
YI0(1,1) = 0.2145,
YI0(1,2) = 0,
YI0(1,3) = 0.2855,
YI0(1,4) = 0,
YI0(1,5) = 0.50,
/

&GPYRO_RXNS
NRXNS = 2,
CFROM(1) = 'Hetron',
CTO(1) = 'Hetron_residue',
Z(1) = 5000000000000000,
E(1) = 195,
DHS(1) = 0,
DHV(1) = 172000,
CHI(1) = 1,
ORDER(1) = 1.125,
ORDERO2(1) = 0,
IKINETICMODEL(1) = 0,
IO2TYPE(1) = 0,
M(1) = 0,
KCAT(1) = 0,
ICAT(1) = 0,
CFROM(2) = 'ATH',
CTO(2) = 'ATH_residue',
Z(2) = 2500000000000000,
E(2) = 140.1,
DHS(2) = 0,
DHV(2) = 1000000,
CHI(2) = 1,
ORDER(2) = 1.24,
ORDERO2(2) = 0,
IKINETICMODEL(2) = 0,
IO2TYPE(2) = 0,
M(2) = 0,
KCAT(2) = 0,
ICAT(2) = 0,

/

&GPYRO_HGRXNS

NHGRXNS = 0,

/

&GPYRO_GPROPS

NGSPEC = 1,

IBG = 1,

IO2 = 2,

CPG = 1000,

NAME(1) = 'pyrolysate',

YJ0(1) = 1,

M(1) = 44,

SIGMA(1) = 5.061,

EPSOK(1) = 254,

B(1) = 0,

TONSET(1) = 653,

TSPAN(1) = 50,

/

&GPYRO_GYIELDS

GYIELDS(1,1) = 1,

GYIELDS(1,2) = 1,

/

&GPYRO_HGYIELDS

/

&GPYRO_SEBCPATCH

NSEBCPATCH = 2,

T(1) = 0,

X1(1) = -1,

X2(1) = 1,

Z1(1) = 0,

Z2(1) = 0,

QE(1) = 50000,

HC(1) = 10,

TINF(1) = 300,

RERADIATION(1) = .TRUE.,

TFIXED(1) = -1,

T(2) = 0,

X1(2) = -1,

X2(2) = 1,

Z1(2) = 0.009,

Z2(2) = 0.009,

```
QE(2) = 0,  
HC(2) = 10,  
TINF(2) = 300,  
RERADIATION(2) = .FALSE.,  
TFIXED(2) = -1,  
/  

```

```
&GPYRO_GMBCPATCH  
NGMBCPATCH = 0,  
/  

```

```
&GPYRO_GSBCPATCH  
NGSBCPATCH = 0,  
/  

```

```
&GPYRO_GEBCPATCH  
NGEBCPATCH = 0,  
/  

```

```
&GPYRO_QE  
NQE = 1,  
QE(1) = 50000,  
HCO(1) = 10,  
NHC(1) = 0,  
DELTA0(1) = 0.009,  
NCELL(1) = 91,  
L(1) = 0.01,  
NBC(1) = 1,  
TIG(1) = 10000,  
QFL(1) = 0,  
TSTOP(1) = 1600,  
MIG(1) = 3,  
TMPIG(1) = 350,  
ZEROD(1) = .FALSE.,  
BETA(1) = 5,  
YJINF(1,1) = 1,  
/  

```

```
&GA_GENINPUT NGEN = 100,  
NINDIV = 200,  
MAXCOPIES = 4,  
LINUX = .TRUE.,  
SIMULATED_EXPERIMENTAL_DATA = .FALSE.,  
RESTART = .FALSE.,  
FITMIN = 0,  
FITCLIP = 0,
```

```
FITEXPONENT = 2,  
WHOLEGENEFRAC = 0.3,  
BRUTE_FORCE = .FALSE.,  
KILL_NONCONVERGED_SOLNS = .TRUE.,  
/  
&GA_PHI  
NPHI = 0,  
/
```

```
&GA_VARS  
NGENE = 0,  
/
```

9.11.3. 5% ATH FRP

```
&GPYRO_GENERAL  
DT0 = 0.1,  
TAMB = 300,  
TREF = 300,  
P0 = 101300,  
GX = 0,  
GZ = 0,  
THERMAL_EQUILIBRIUM = .TRUE.,  
VHLC = 0,  
HCV = 1000000,  
NU_A = 2,  
NU_B = 1,  
NU_C = 0.5,  
NTDMA_ITERATIONS = 1000,  
NSSPECIESITERNS = 1,  
NCONTINUITYITERNS = 1,  
ALPHA = 1,  
TMPTOL = 0.0001,  
HTOL = 0.00000001,  
YITOL = 0.0001,  
PTOL = 0.0001,  
YJTOL = 0.0001,  
HGTOL = 0.1,  
EXPLICIT_T = .FALSE.,  
SOLVE_GAS_YJ = .TRUE.,  
SOLVE_GAS_ENERGY = .FALSE.,  
SOLVE_PRESSURE = .FALSE.,  
SOLVE_POROSITY = .FALSE.,  
PROPERTY_LINTERP = .FALSE.,  
USE_TOFH_NEWTON = .TRUE.,  
SHYI_CORRECTION = .TRUE.,  
NCOEFF_UPDATE_SKIP = 1,
```

```
FDSMODE = .FALSE.,
CONVENTIONAL_RXN_ORDER = .FALSE.,
TWOD = .FALSE.,
USE_BC_PATCHES = .TRUE.,
NOCONSUMPTION = .FALSE.,
EPS = 0.0000000001,
GAS_DIFFUSION = .FALSE.,
FRONT_GAS_DIFFUSION = .FALSE.,
BLOWING = .FALSE.,
MINIMUM_CONDUCTIVITY = 0,
CONSTANT_DHVOL = .TRUE.,
FULL_QSG = .FALSE.,
GASES_PRODUCED_AT_TSOLID = .FALSE.,
/
```

```
&GPYRO_OUTPUT
CASENAME = 'Hy_5ATH V2',
DUMP_ENERGY_BALANCE = .FALSE.,
N_POINT_QUANTITIES = 1,
N_PROFILE_QUANTITIES = 11,
N_SMOKEVIEW_QUANTITIES = 0,
DUMP_EVERYTHING = .FALSE.,
DTDUMP_GA = 1,
DTDUMP_POINT = 1,
DTDUMP_PROFILE = 1,
DTDUMP_SMOKEVIEW = 1,
TMP_REDUCED_DTDUMP = 5000,
REDUCED_DTDUMP = 0.0001,
DTMIN_KILL = 0.0000001,
POINT_QUANTITY(1) = 'MLR',
POINT_QUANTITY_INDEX(1) = 0,
POINT_Z(1) = 0,
POINT_X(1) = 0,
PROFILE_QUANTITY(1) = 'BULK_DENSITY',
PROFILE_QUANTITY_INDEX(1) = 0,
PROFILE_TYPE(1) = 'z',
PROFILE_LOCATION(1) = 0,
PROFILE_ISKIP(1) = 1,
PROFILE_QUANTITY(2) = 'REACTION_RATE_K',
PROFILE_QUANTITY_INDEX(2) = 1,
PROFILE_TYPE(2) = 'z',
PROFILE_LOCATION(2) = 0,
PROFILE_ISKIP(2) = 1,
PROFILE_QUANTITY(3) = 'REACTION_RATE_K',
PROFILE_QUANTITY_INDEX(3) = 2,
PROFILE_TYPE(3) = 'z',
```

PROFILE_LOCATION(3) = 0,
PROFILE_ISKIP(3) = 1,
PROFILE_QUANTITY(4) = 'YI',
PROFILE_QUANTITY_INDEX(4) = 1,
PROFILE_TYPE(4) = 'z',
PROFILE_LOCATION(4) = 0,
PROFILE_ISKIP(4) = 1,
PROFILE_QUANTITY(5) = 'YI',
PROFILE_QUANTITY_INDEX(5) = 2,
PROFILE_TYPE(5) = 'z',
PROFILE_LOCATION(5) = 0,
PROFILE_ISKIP(5) = 1,
PROFILE_QUANTITY(6) = 'YI',
PROFILE_QUANTITY_INDEX(6) = 3,
PROFILE_TYPE(6) = 'z',
PROFILE_LOCATION(6) = 0,
PROFILE_ISKIP(6) = 1,
PROFILE_QUANTITY(7) = 'YI',
PROFILE_QUANTITY_INDEX(7) = 4,
PROFILE_TYPE(7) = 'z',
PROFILE_LOCATION(7) = 0,
PROFILE_ISKIP(7) = 1,
PROFILE_QUANTITY(8) = 'TEMPERATURE',
PROFILE_QUANTITY_INDEX(8) = 0,
PROFILE_TYPE(8) = 'z',
PROFILE_LOCATION(8) = 0,
PROFILE_ISKIP(8) = 1,
PROFILE_QUANTITY(9) = 'POROSITY',
PROFILE_QUANTITY_INDEX(9) = 0,
PROFILE_TYPE(9) = 'z',
PROFILE_LOCATION(9) = 0,
PROFILE_ISKIP(9) = 1,
PROFILE_QUANTITY(10) = 'M/M0',
PROFILE_QUANTITY_INDEX(10) = 0,
PROFILE_TYPE(10) = 'z',
PROFILE_LOCATION(10) = 0,
PROFILE_ISKIP(10) = 1,
PROFILE_QUANTITY(11) = 'YI',
PROFILE_QUANTITY_INDEX(11) = 5,
PROFILE_TYPE(11) = 'z',
PROFILE_LOCATION(11) = 0,
PROFILE_ISKIP(11) = 1,
/

&GPYRO_SPROPS
NSSPEC = 5,

NAME(1) = 'Hetron',
K0Z(1) = 0.23,
NKZ(1) = 0,
R0(1) = 1200,
NR(1) = 0,
C0(1) = 1400,
NC(1) = 0,
EMIS(1) = 0.84,
KAPPA(1) = 1000000,
TMELT(1) = 3000,
DHMELT(1) = 0,
SIGMA2MELT(1) = 0,
GAMMA(1) = 0,
PERMZ(1) = 1D-10,
RS0(1) = 1200,
PORE_DIAMETER(1) = 0.0005,
K0X(1) = 0.2,
NKX(1) = 0,
PERMX(1) = 1D-10,
NAME(2) = 'Hetron_residue',
K0Z(2) = 0.19,
NKZ(2) = 0,
R0(2) = 253,
NR(2) = 0,
C0(2) = 1900,
NC(2) = 0,
EMIS(2) = 0.90,
KAPPA(2) = 1000000,
TMELT(2) = 3000,
DHMELT(2) = 0,
SIGMA2MELT(2) = 0,
GAMMA(2) = 0.00348,
PERMZ(2) = 1D-10,
RS0(2) = 253,
PORE_DIAMETER(2) = 0.0005,
K0X(2) = 0.2,
NKX(2) = 0,
PERMX(2) = 1D-10,
NAME(3) = 'ATH',
K0Z(3) = 1.220,
NKZ(3) = 0,
R0(3) = 2300,
NR(3) = 0,
C0(3) = 1200,
NC(3) = 0,
EMIS(3) = 0.81,

KAPPA(3) = 1000000,
TMELT(3) = 3000,
DHMELT(3) = 0,
SIGMA2MELT(3) = 0,
GAMMA(3) = 0.000,
PERMZ(3) = 1D-10,
RS0(3) = 2300,
PORE_DIAMETER(3) = 0.0005,
K0X(3) = 0.2,
NKX(3) = 0,
PERMX(3) = 1D-10,
NAME(4) = 'ATH_residue',
K0Z(4) = 0.240,
NKZ(4) = 0.0,
R0(4) = 1558,
NR(4) = 0.0,
C0(4) = 1200,
NC(4) = 0.0,
EMIS(4) = 0.89,
KAPPA(4) = 1000000,
TMELT(4) = 3000,
DHMELT(4) = 0,
SIGMA2MELT(4) = 0,
GAMMA(4) = 0.00475,
PERMZ(4) = 1D-10,
RS0(4) = 1558,
PORE_DIAMETER(4) = 0.0005,
K0X(4) = 0.2,
NKX(4) = 0,
PERMX(4) = 1D-10,
NAME(5) = 'glass',
K0Z(5) = 0.18,
NKZ(5) = 0.59,
R0(5) = 2600,
NR(5) = 0.0,
C0(5) = 400,
NC(5) = 0.53,
EMIS(5) = 0.88,
KAPPA(5) = 1D6,
TMELT(5) = 3000,
DHMELT(5) = 0,
SIGMA2MELT(5) = 0,
GAMMA(5) = 0.00769,
PERMZ(5) = 1D-10,
RS0(5) = 2600,
PORE_DIAMETER(5) = 0.0005,

CHI(2) = 1 ,
ORDER(2) = 1.24 ,
ORDERO2(2) = 0 ,
IKINETICMODEL(2) = 0 ,
IO2TYPE(2) = 0 ,
M(2) = 0 ,
KCAT(2) = 0 ,
ICAT(2) = 0 ,
/

&GPYRO_HGRXNS
NHGRXNS = 0,
/

&GPYRO_GPROPS
NGSPEC = 1,
IBG = 1,
IO2 = 2,
CPG = 1000,
NAME(1) = 'pyrolysate' ,
YJ0(1) = 1 ,
M(1) = 44 ,
SIGMA(1) = 5.061 ,
EPSOK(1) = 254 ,
B(1) = 0 ,
TONSET(1) = 653 ,
TSPAN(1) = 50 ,
/

&GPYRO_GYIELDS
GYIELDS(1,1) = 1,
GYIELDS(1,2) = 1,
/

&GPYRO_HGYIELDS
/

&GPYRO_SEBCPATCH
NSEBCPATCH = 2,
T(1) = 0,
X1(1) = -1,
X2(1) = 1,
Z1(1) = 0,
Z2(1) = 0,
QE(1) = 50000,
HC(1) = 10,

```
TINF(1) = 300,  
RERADIATION(1) = .TRUE.,  
TFIXED(1) = -1,  
T(2) = 0,  
X1(2) = -1,  
X2(2) = 1,  
Z1(2) = 0.009,  
Z2(2) = 0.009,  
QE(2) = 0,  
HC(2) = 10,  
TINF(2) = 300,  
RERADIATION(2) = .FALSE.,  
TFIXED(2) = -1,  
/  

```

```
&GPYRO_GMBCPATCH  
NGMBCPATCH = 0,  
/  

```

```
&GPYRO_GSBCPATCH  
NGSBCPATCH = 0,  
/  

```

```
&GPYRO_GEBCPATCH  
NGEBCPATCH = 0,  
/  

```

```
&GPYRO_QE  
NQE = 1,  
QE(1) = 50000,  
HCO(1) = 10,  
NHC(1) = 0,  
DELTA0(1) = 0.009,  
NCELL(1) = 91,  
L(1) = 0.01,  
NBC(1) = 1,  
TIG(1) = 10000,  
QFL(1) = 0,  
TSTOP(1) = 1600,  
MIG(1) = 3,  
TMPIG(1) = 350,  
ZEROD(1) = .FALSE.,  
BETA(1) = 5,  
YJINF(1,1) = 1,  
/  

```

```
&GA_GENINPUT NGEN = 100,  
NINDIV = 200,  
MAXCOPIES = 4,  
LINUX = .TRUE.,  
SIMULATED_EXPERIMENTAL_DATA = .FALSE.,  
RESTART = .FALSE.,  
FITMIN = 0,  
FITCLIP = 0,  
FITEXPONENT = 2,  
WHOLEGENEFAC = 0.3,  
BRUTE_FORCE = .FALSE.,  
KILL_NONCONVERGED_SOLNS = .TRUE.,  
/  
&GA_PHI  
NPHI = 0,  
/  
  
&GA_VARS  
NGENE = 0,  
/  
9.11.4. 10% ATH FRP
```

```
&GPYRO_GENERAL  
DT0 = 0.1,  
TAMB = 300,  
TREF = 300,  
P0 = 101300,  
GX = 0,  
GZ = 0,  
THERMAL_EQUILIBRIUM = .TRUE.,  
VHLC = 0,  
HCV = 1000000,  
NU_A = 2,  
NU_B = 1,  
NU_C = 0.5,  
NTDMA_ITERATIONS = 1000,  
NSSPECIESITERNS = 1,  
NCONTINUITYITERNS = 1,  
ALPHA = 1,  
TMPTOL = 0.0001,  
HTOL = 0.00000001,  
YITOL = 0.0001,  
PTOL = 0.0001,  
YJTOL = 0.0001,  
HGTOL = 0.1,  
EXPLICIT_T = .FALSE.,
```

```
SOLVE_GAS_YJ = .TRUE.,
SOLVE_GAS_ENERGY = .FALSE.,
SOLVE_PRESSURE = .FALSE.,
SOLVE_POROSITY = .FALSE.,
PROPERTY_LINTERP = .FALSE.,
USE_TOFH_NEWTON = .TRUE.,
SHYI_CORRECTION = .TRUE.,
NCOEFF_UPDATE_SKIP = 1,
FDSMODE = .FALSE.,
CONVENTIONAL_RXN_ORDER = .FALSE.,
TWOD = .FALSE.,
USE_BC_PATCHES = .TRUE.,
NOCONSUMPTION = .FALSE.,
EPS = 0.0000000001,
GAS_DIFFUSION = .FALSE.,
FRONT_GAS_DIFFUSION = .FALSE.,
BLOWING = .FALSE.,
MINIMUM_CONDUCTIVITY = 0,
CONSTANT_DHVOL = .TRUE.,
FULL_QSG = .FALSE.,
GASES_PRODUCED_AT_TSOLID = .FALSE.,
/
```

```
&GPYRO_OUTPUT
CASENAME = 'Hy_10ATH V2',
DUMP_ENERGY_BALANCE = .FALSE.,
N_POINT_QUANTITIES = 1,
N_PROFILE_QUANTITIES = 11,
N_SMOKEVIEW_QUANTITIES = 0,
DUMP_EVERYTHING = .FALSE.,
DTDUMP_GA = 1,
DTDUMP_POINT = 1,
DTDUMP_PROFILE = 1,
DTDUMP_SMOKEVIEW = 1,
TMP_REDUCED_DTDUMP = 5000,
REDUCED_DTDUMP = 0.0001,
DTMIN_KILL = 0.0000001,
POINT_QUANTITY(1) = 'MLR',
POINT_QUANTITY_INDEX(1) = 0,
POINT_Z(1) = 0,
POINT_X(1) = 0,
PROFILE_QUANTITY(1) = 'BULK_DENSITY',
PROFILE_QUANTITY_INDEX(1) = 0,
PROFILE_TYPE(1) = 'z',
PROFILE_LOCATION(1) = 0,
PROFILE_ISKIP(1) = 1,
```

PROFILE_QUANTITY(2) = 'REACTION_RATE_K',
PROFILE_QUANTITY_INDEX(2) = 1,
PROFILE_TYPE(2) = 'z',
PROFILE_LOCATION(2) = 0,
PROFILE_ISKIP(2) = 1,
PROFILE_QUANTITY(3) = 'REACTION_RATE_K',
PROFILE_QUANTITY_INDEX(3) = 2,
PROFILE_TYPE(3) = 'z',
PROFILE_LOCATION(3) = 0,
PROFILE_ISKIP(3) = 1,
PROFILE_QUANTITY(4) = 'YI',
PROFILE_QUANTITY_INDEX(4) = 1,
PROFILE_TYPE(4) = 'z',
PROFILE_LOCATION(4) = 0,
PROFILE_ISKIP(4) = 1,
PROFILE_QUANTITY(5) = 'YI',
PROFILE_QUANTITY_INDEX(5) = 2,
PROFILE_TYPE(5) = 'z',
PROFILE_LOCATION(5) = 0,
PROFILE_ISKIP(5) = 1,
PROFILE_QUANTITY(6) = 'YI',
PROFILE_QUANTITY_INDEX(6) = 3,
PROFILE_TYPE(6) = 'z',
PROFILE_LOCATION(6) = 0,
PROFILE_ISKIP(6) = 1,
PROFILE_QUANTITY(7) = 'YI',
PROFILE_QUANTITY_INDEX(7) = 4,
PROFILE_TYPE(7) = 'z',
PROFILE_LOCATION(7) = 0,
PROFILE_ISKIP(7) = 1,
PROFILE_QUANTITY(8) = 'TEMPERATURE',
PROFILE_QUANTITY_INDEX(8) = 0,
PROFILE_TYPE(8) = 'z',
PROFILE_LOCATION(8) = 0,
PROFILE_ISKIP(8) = 1,
PROFILE_QUANTITY(9) = 'POROSITY',
PROFILE_QUANTITY_INDEX(9) = 0,
PROFILE_TYPE(9) = 'z',
PROFILE_LOCATION(9) = 0,
PROFILE_ISKIP(9) = 1,
PROFILE_QUANTITY(10) = 'M/M0',
PROFILE_QUANTITY_INDEX(10) = 0,
PROFILE_TYPE(10) = 'z',
PROFILE_LOCATION(10) = 0,
PROFILE_ISKIP(10) = 1,
PROFILE_QUANTITY(11) = 'YI',

PROFILE_QUANTITY_INDEX(11) = 5,
PROFILE_TYPE(11) = 'z',
PROFILE_LOCATION(11) = 0,
PROFILE_ISKIP(11) = 1,
/

&GPYRO_SPROPS

NSSPEC = 5,
NAME(1) = 'Hetron',
K0Z(1) = 0.23,
NKZ(1) = 0,
R0(1) = 1200,
NR(1) = 0,
C0(1) = 1400,
NC(1) = 0,
EMIS(1) = 0.84,
KAPPA(1) = 1000000,
TMELT(1) = 3000,
DHMELT(1) = 0,
SIGMA2MELT(1) = 0,
GAMMA(1) = 0,
PERMZ(1) = 1D-10,
RS0(1) = 1200,
PORE_DIAMETER(1) = 0.0005,
K0X(1) = 0.2,
NKX(1) = 0,
PERMX(1) = 1D-10,
NAME(2) = 'Hetron_residue',
K0Z(2) = 0.19,
NKZ(2) = 0,
R0(2) = 253,
NR(2) = 0,
C0(2) = 1900,
NC(2) = 0,
EMIS(2) = 0.90,
KAPPA(2) = 1000000,
TMELT(2) = 3000,
DHMELT(2) = 0,
SIGMA2MELT(2) = 0,
GAMMA(2) = 0.00348,
PERMZ(2) = 1D-10,
RS0(2) = 253,
PORE_DIAMETER(2) = 0.0005,
K0X(2) = 0.2,
NKX(2) = 0,
PERMX(2) = 1D-10,

NAME(3) = 'ATH',
K0Z(3) = 1.220,
NKZ(3) = 0,
R0(3) = 2300,
NR(3) = 0,
C0(3) = 1200,
NC(3) = 0,
EMIS(3) = 0.81,
KAPPA(3) = 1000000,
TMELT(3) = 3000,
DHMELT(3) = 0,
SIGMA2MELT(3) = 0,
GAMMA(3) = 0.000,
PERMZ(3) = 1D-10,
RS0(3) = 2300,
PORE_DIAMETER(3) = 0.0005,
K0X(3) = 0.2,
NKX(3) = 0,
PERMX(3) = 1D-10,
NAME(4) = 'ATH_residue',
K0Z(4) = 0.240,
NKZ(4) = 0.0,
R0(4) = 1558,
NR(4) = 0.0,
C0(4) = 1200,
NC(4) = 0.0,
EMIS(4) = 0.89,
KAPPA(4) = 1000000,
TMELT(4) = 3000,
DHMELT(4) = 0,
SIGMA2MELT(4) = 0,
GAMMA(4) = 0.00475,
PERMZ(4) = 1D-10,
RS0(4) = 1558,
PORE_DIAMETER(4) = 0.0005,
K0X(4) = 0.2,
NKX(4) = 0,
PERMX(4) = 1D-10,
NAME(5) = 'glass',
K0Z(5) = 0.18,
NKZ(5) = 0.59,
R0(5) = 2600,
NR(5) = 0.0,
C0(5) = 400,
NC(5) = 0.53,
EMIS(5) = 0.88,

KCAT(1) = 0 ,
ICAT(1) = 0 ,
CFROM(2) = 'ATH' ,
CTO(2) = 'ATH_residue' ,
Z(2) = 250000000000 ,
E(2) = 140.1 ,
DHS(2) = 0 ,
DHV(2) = 1000000 ,
CHI(2) = 1 ,
ORDER(2) = 1.24 ,
ORDERO2(2) = 0 ,
IKINETICMODEL(2) = 0 ,
IO2TYPE(2) = 0 ,
M(2) = 0 ,
KCAT(2) = 0 ,
ICAT(2) = 0 ,
/

&GPYRO_HGRXNS
NHGRXNS = 0,
/

&GPYRO_GPROPS
NGSPEC = 1,
IBG = 1,
IO2 = 2,
CPG = 1000,
NAME(1) = 'pyrolysate' ,
YJ0(1) = 1 ,
M(1) = 44 ,
SIGMA(1) = 5.061 ,
EPSOK(1) = 254 ,
B(1) = 0 ,
TONSET(1) = 653 ,
TSPAN(1) = 50 ,
/

&GPYRO_GYIELDS
GYIELDS(1,1) = 1,
GYIELDS(1,2) = 1,
/

&GPYRO_HGYIELDS
/

&GPYRO_SEBCPATCH

```
NSEBCPATCH = 2,  
T(1) = 0,  
X1(1) = -1,  
X2(1) = 1,  
Z1(1) = 0,  
Z2(1) = 0,  
QE(1) = 50000,  
HC(1) = 10,  
TINF(1) = 300,  
RERADIATION(1) = .TRUE.,  
TFIXED(1) = -1,  
T(2) = 0,  
X1(2) = -1,  
X2(2) = 1,  
Z1(2) = 0.009,  
Z2(2) = 0.009,  
QE(2) = 0,  
HC(2) = 10,  
TINF(2) = 300,  
RERADIATION(2) = .FALSE.,  
TFIXED(2) = -1,  
/  
  
&GPYRO_GMBCPATCH  
NGMBCPATCH = 0,  
/  
  
&GPYRO_GSBCPATCH  
NGSBCPATCH = 0,  
/  
  
&GPYRO_GEBCPATCH  
NGEBCPATCH = 0,  
/  
  
&GPYRO_QE  
NQE = 1,  
QE(1) = 50000,  
HC0(1) = 10,  
NHC(1) = 0,  
DELTA0(1) = 0.009,  
NCELL(1) = 91,  
L(1) = 0.01,  
NBC(1) = 1,  
TIG(1) = 10000,  
QFL(1) = 0,
```

TSTOP(1) = 1600,
MIG(1) = 3,
TMPIG(1) = 350,
ZEROD(1) = .FALSE.,
BETA(1) = 5,
YJINF(1,1) = 1,
/

&GA_GENINPUT NGEN = 100,
NINDIV = 200,
MAXCOPIES = 4,
LINUX = .TRUE.,
SIMULATED_EXPERIMENTAL_DATA = .FALSE.,
RESTART = .FALSE.,
FITMIN = 0,
FITCLIP = 0,
FITEXPONENT = 2,
WHOLEGENEFAC = 0.3,
BRUTE_FORCE = .FALSE.,
KILL_NONCONVERGED_SOLNS = .TRUE.,
/
&GA_PHI
NPHI = 0,
/

&GA_VARS
NGENE = 0,
/

9.11.5. 20% ATH FRP

&GPYRO_GENERAL
DT0 = 0.1,
TAMB = 300,
TREF = 300,
P0 = 101300,
GX = 0,
GZ = 0,
THERMAL_EQUILIBRIUM = .TRUE.,
VHLC = 0,
HCV = 1000000,
NU_A = 2,
NU_B = 1,
NU_C = 0.5,
NTDMA_ITERATIONS = 1000,
NSSPECIESITERNS = 1,
NCONTINUITYITERNS = 1,

ALPHA = 1,
TMPTOL = 0.0001,
HTOL = 0.00000001,
YITOL = 0.0001,
PTOL = 0.0001,
YJTOL = 0.0001,
HGTOL = 0.1,
EXPLICIT_T = .FALSE.,
SOLVE_GAS_YJ = .TRUE.,
SOLVE_GAS_ENERGY = .FALSE.,
SOLVE_PRESSURE = .FALSE.,
SOLVE_POROSITY = .FALSE.,
PROPERTY_LINTERP = .FALSE.,
USE_TOFH_NEWTON = .TRUE.,
SHYI_CORRECTION = .TRUE.,
NCOEFF_UPDATE_SKIP = 1,
FDSMODE = .FALSE.,
CONVENTIONAL_RXN_ORDER = .FALSE.,
TWO_D = .FALSE.,
USE_BC_PATCHES = .TRUE.,
NOCONSUMPTION = .FALSE.,
EPS = 0.0000000001,
GAS_DIFFUSION = .FALSE.,
FRONT_GAS_DIFFUSION = .FALSE.,
BLOWING = .FALSE.,
MINIMUM_CONDUCTIVITY = 0,
CONSTANT_DHVOL = .TRUE.,
FULL_QSG = .FALSE.,
GASES_PRODUCED_AT_TSOLID = .FALSE.,
/

&GPYRO_OUTPUT
CASENAME = 'Hy_20ATH V2',
DUMP_ENERGY_BALANCE = .FALSE.,
N_POINT_QUANTITIES = 1,
N_PROFILE_QUANTITIES = 11,
N_SMOKEVIEW_QUANTITIES = 0,
DUMP_EVERYTHING = .FALSE.,
DTDUMP_GA = 1,
DTDUMP_POINT = 1,
DTDUMP_PROFILE = 1,
DTDUMP_SMOKEVIEW = 1,
TMP_REDUCED_DTDUMP = 5000,
REDUCED_DTDUMP = 0.0001,
DTMIN_KILL = 0.0000001,
POINT_QUANTITY(1) = 'MLR',

POINT_QUANTITY_INDEX(1) = 0,
POINT_Z(1) = 0,
POINT_X(1) = 0,
PROFILE_QUANTITY(1) = 'BULK_DENSITY',
PROFILE_QUANTITY_INDEX(1) = 0,
PROFILE_TYPE(1) = 'z',
PROFILE_LOCATION(1) = 0,
PROFILE_ISKIP(1) = 1,
PROFILE_QUANTITY(2) = 'REACTION_RATE_K',
PROFILE_QUANTITY_INDEX(2) = 1,
PROFILE_TYPE(2) = 'z',
PROFILE_LOCATION(2) = 0,
PROFILE_ISKIP(2) = 1,
PROFILE_QUANTITY(3) = 'REACTION_RATE_K',
PROFILE_QUANTITY_INDEX(3) = 2,
PROFILE_TYPE(3) = 'z',
PROFILE_LOCATION(3) = 0,
PROFILE_ISKIP(3) = 1,
PROFILE_QUANTITY(4) = 'YI',
PROFILE_QUANTITY_INDEX(4) = 1,
PROFILE_TYPE(4) = 'z',
PROFILE_LOCATION(4) = 0,
PROFILE_ISKIP(4) = 1,
PROFILE_QUANTITY(5) = 'YI',
PROFILE_QUANTITY_INDEX(5) = 2,
PROFILE_TYPE(5) = 'z',
PROFILE_LOCATION(5) = 0,
PROFILE_ISKIP(5) = 1,
PROFILE_QUANTITY(6) = 'YI',
PROFILE_QUANTITY_INDEX(6) = 3,
PROFILE_TYPE(6) = 'z',
PROFILE_LOCATION(6) = 0,
PROFILE_ISKIP(6) = 1,
PROFILE_QUANTITY(7) = 'YI',
PROFILE_QUANTITY_INDEX(7) = 4,
PROFILE_TYPE(7) = 'z',
PROFILE_LOCATION(7) = 0,
PROFILE_ISKIP(7) = 1,
PROFILE_QUANTITY(8) = 'TEMPERATURE',
PROFILE_QUANTITY_INDEX(8) = 0,
PROFILE_TYPE(8) = 'z',
PROFILE_LOCATION(8) = 0,
PROFILE_ISKIP(8) = 1,
PROFILE_QUANTITY(9) = 'POROSITY',
PROFILE_QUANTITY_INDEX(9) = 0,
PROFILE_TYPE(9) = 'z',

PROFILE_LOCATION(9) = 0,
PROFILE_ISKIP(9) = 1,
PROFILE_QUANTITY(10) = 'M/M0',
PROFILE_QUANTITY_INDEX(10) = 0,
PROFILE_TYPE(10) = 'z',
PROFILE_LOCATION(10) = 0,
PROFILE_ISKIP(10) = 1,
PROFILE_QUANTITY(11) = 'YI',
PROFILE_QUANTITY_INDEX(11) = 5,
PROFILE_TYPE(11) = 'z',
PROFILE_LOCATION(11) = 0,
PROFILE_ISKIP(11) = 1,
/

&GPYRO_SPROPS

NSSPEC = 5,
NAME(1) = 'Hetron',
K0Z(1) = 0.23,
NKZ(1) = 0,
R0(1) = 1200,
NR(1) = 0,
C0(1) = 1400,
NC(1) = 0,
EMIS(1) = 0.84,
KAPPA(1) = 1000000,
TMELT(1) = 3000,
DHMELT(1) = 0,
SIGMA2MELT(1) = 0,
GAMMA(1) = 0,
PERMZ(1) = 1D-10,
RS0(1) = 1200,
PORE_DIAMETER(1) = 0.0005,
K0X(1) = 0.2,
NKX(1) = 0,
PERMX(1) = 1D-10,
NAME(2) = 'Hetron_residue',
K0Z(2) = 0.19,
NKZ(2) = 0,
R0(2) = 253,
NR(2) = 0,
C0(2) = 1900,
NC(2) = 0,
EMIS(2) = 0.90,
KAPPA(2) = 1000000,
TMELT(2) = 3000,
DHMELT(2) = 0,

SIGMA2MELT(2) = 0,
GAMMA(2) = 0.00348,
PERMZ(2) = 1D-10,
RS0(2) = 253,
PORE_DIAMETER(2) = 0.0005,
K0X(2) = 0.2,
NKX(2) = 0,
PERMX(2) = 1D-10,
NAME(3) = 'ATH',
K0Z(3) = 1.220,
NKZ(3) = 0,
R0(3) = 2300,
NR(3) = 0,
C0(3) = 1200,
NC(3) = 0,
EMIS(3) = 0.81,
KAPPA(3) = 1000000,
TMELT(3) = 3000,
DHMELT(3) = 0,
SIGMA2MELT(3) = 0,
GAMMA(3) = 0.000,
PERMZ(3) = 1D-10,
RS0(3) = 2300,
PORE_DIAMETER(3) = 0.0005,
K0X(3) = 0.2,
NKX(3) = 0,
PERMX(3) = 1D-10,
NAME(4) = 'ATH_residue',
K0Z(4) = 0.240,
NKZ(4) = 0.0,
R0(4) = 1558,
NR(4) = 0.0,
C0(4) = 1200,
NC(4) = 0.0,
EMIS(4) = 0.89,
KAPPA(4) = 1000000,
TMELT(4) = 3000,
DHMELT(4) = 0,
SIGMA2MELT(4) = 0,
GAMMA(4) = 0.00475,
PERMZ(4) = 1D-10,
RS0(4) = 1558,
PORE_DIAMETER(4) = 0.0005,
K0X(4) = 0.2,
NKX(4) = 0,
PERMX(4) = 1D-10,

NAME(5) = 'glass',
K0Z(5) = 0.18,
NKZ(5) = 0.59,
R0(5) = 2600,
NR(5) = 0.0,
C0(5) = 400,
NC(5) = 0.53,
EMIS(5) = 0.88,
KAPPA(5) = 1D6,
TMELT(5) = 3000,
DHMELT(5) = 0,
SIGMA2MELT(5) = 0,
GAMMA(5) = 0.00769,
PERMZ(5) = 1D-10,
RS0(5) = 2600,
PORE_DIAMETER(5) = 0.0005,
K0X(5) = 0.2,
NKX(5) = 0,
PERMX(5) = 1D-10,
/

&GPYRO_LAYERS

NLAYERS = 1,
X1(1) = -1,
X2(1) = 1,
Z1(1) = 0,
Z2(1) = 0.009,
NZCELLS_PER_LAYER(1) = 381,
NXCELLS_PER_LAYER(1) = 1,
HCRZ(1) = 0,
HCRX(1) = 0,
TINITIAL(1) = 300,
SOLVE_POROSITY_IN_LAYER(1) = .FALSE.,
YI0(1,1) = 0.4,
YI0(1,2) = 0,
YI0(1,3) = 0.1,
YI0(1,4) = 0,
YI0(1,5) = 0.5,
/

&GPYRO_RXNS

NRXNS = 2,
CFROM(1) = 'Hetron',
CTO(1) = 'Hetron_residue',
Z(1) = 5000000000000000,
E(1) = 195,

DHS(1) = 0 ,
DHV(1) = 172000 ,
CHI(1) = 1 ,
ORDER(1) = 1.125 ,
ORDERO2(1) = 0 ,
IKINETICMODEL(1) = 0 ,
IO2TYPE(1) = 0 ,
M(1) = 0 ,
KCAT(1) = 0 ,
ICAT(1) = 0 ,
CFROM(2) = 'ATH' ,
CTO(2) = 'ATH_residue' ,
Z(2) = 250000000000 ,
E(2) = 140.1 ,
DHS(2) = 0 ,
DHV(2) = 1000000 ,
CHI(2) = 1 ,
ORDER(2) = 1.24 ,
ORDERO2(2) = 0 ,
IKINETICMODEL(2) = 0 ,
IO2TYPE(2) = 0 ,
M(2) = 0 ,
KCAT(2) = 0 ,
ICAT(2) = 0 ,
/

&GPYRO_HGRXNS
NHGRXNS = 0,
/

&GPYRO_GPROPS
NGSPEC = 1,
IBG = 1,
IO2 = 2,
CPG = 1000,
NAME(1) = 'pyrolysate' ,
YJ0(1) = 1 ,
M(1) = 44 ,
SIGMA(1) = 5.061 ,
EPSOK(1) = 254 ,
B(1) = 0 ,
TONSET(1) = 653 ,
TSPAN(1) = 50 ,
/

&GPYRO_GYIELDS

```
GYIELDS(1,1) = 1,  
GYIELDS(1,2) = 1,  
/
```

```
&GPYRO_HGYIELDS  
/
```

```
&GPYRO_SEBCPATCH  
NSEBCPATCH = 2,  
T(1) = 0,  
X1(1) = -1,  
X2(1) = 1,  
Z1(1) = 0,  
Z2(1) = 0,  
QE(1) = 50000,  
HC(1) = 10,  
TINF(1) = 300,  
RERADIATION(1) = .TRUE.,  
TFIXED(1) = -1,  
T(2) = 0,  
X1(2) = -1,  
X2(2) = 1,  
Z1(2) = 0.009,  
Z2(2) = 0.009,  
QE(2) = 0,  
HC(2) = 10,  
TINF(2) = 300,  
RERADIATION(2) = .FALSE.,  
TFIXED(2) = -1,  
/
```

```
&GPYRO_GMBCPATCH  
NGMBCPATCH = 0,  
/
```

```
&GPYRO_GSBCPATCH  
NGSBCPATCH = 0,  
/
```

```
&GPYRO_GEBCPATCH  
NGEBCPATCH = 0,  
/
```

```
&GPYRO_QE  
NQE = 1,  
QE(1) = 50000,
```

```
HC0(1) = 10,  
NHC(1) = 0,  
DELTA0(1) = 0.009,  
NCELL(1) = 91,  
L(1) = 0.01,  
NBC(1) = 1,  
TIG(1) = 10000,  
QFL(1) = 0,  
TSTOP(1) = 1600,  
MIG(1) = 3,  
TMPIG(1) = 350,  
ZEROD(1) = .FALSE.,  
BETA(1) = 5,  
YJINF(1,1) = 1,  
/  

```

```
&GA_GENINPUT NGEN = 100,  
NINDIV = 200,  
MAXCOPIES = 4,  
LINUX = .TRUE.,  
SIMULATED_EXPERIMENTAL_DATA = .FALSE.,  
RESTART = .FALSE.,  
FITMIN = 0,  
FITCLIP = 0,  
FITEXPONENT = 2,  
WHOLEGENEFRACTION = 0.3,  
BRUTE_FORCE = .FALSE.,  
KILL_NONCONVERGED_SOLNS = .TRUE.,  
/  
&GA_PHI  
NPHI = 0,  
/  

```

```
&GA_VARS  
NGENE = 0,  
/  

```

[9.11.6. 0.25 mm Coating](#)

```
&GPYRO_GENERAL  
DT0 = 0.1,  
TAMB = 300,  
TREF = 300,  
P0 = 101300,  
GX = 0,  
GZ = 0,  
THERMAL_EQUILIBRIUM = .TRUE.,
```

```
VHLC = 0,  
HCV = 1000000,  
NU_A = 2,  
NU_B = 1,  
NU_C = 0.5,  
NTDMA_ITERATIONS = 1000,  
NSSPECIESITERNS = 1,  
NCONTINUITYITERNS = 1,  
ALPHA = 1,  
TMPTOL = 0.0001,  
HTOL = 0.00000001,  
YITOL = 0.0001,  
PTOL = 0.0001,  
YJTOL = 0.0001,  
HGTOL = 0.1,  
EXPLICIT_T = .FALSE.,  
SOLVE_GAS_YJ = .TRUE.,  
SOLVE_GAS_ENERGY = .FALSE.,  
SOLVE_PRESSURE = .FALSE.,  
SOLVE_POROSITY = .FALSE.,  
PROPERTY_LINTERP = .FALSE.,  
USE_TOFH_NEWTON = .TRUE.,  
SHYI_CORRECTION = .TRUE.,  
NCOEFF_UPDATE_SKIP = 1,  
FDSMODE = .FALSE.,  
CONVENTIONAL_RXN_ORDER = .FALSE.,  
TWOD = .FALSE.,  
USE_BC_PATCHES = .TRUE.,  
NOCONSUMPTION = .FALSE.,  
EPS = 0.0000000001,  
GAS_DIFFUSION = .FALSE.,  
FRONT_GAS_DIFFUSION = .FALSE.,  
BLOWING = .FALSE.,  
MINIMUM_CONDUCTIVITY = 0,  
CONSTANT_DHVOL = .TRUE.,  
FULL_QSG = .FALSE.,  
GASES_PRODUCED_AT_TSOLID = .FALSE.,  
/  
  
&GPYRO_OUTPUT  
CASENAME = '100_133mixedcoat_3mm',  
DUMP_ENERGY_BALANCE = .FALSE.,  
N_POINT_QUANTITIES = 1,  
N_PROFILE_QUANTITIES = 11,  
N_SMOKEVIEW_QUANTITIES = 0,  
DUMP_EVERYTHING = .FALSE.,
```

DTDUMP_GA = 1,
DTDUMP_POINT = 1,
DTDUMP_PROFILE = 1,
DTDUMP_SMOKEVIEW = 1,
TMP_REDUCED_DTDUMP = 5000,
REDUCED_DTDUMP = 0.0001,
DTMIN_KILL = 0.0000001,
POINT_QUANTITY(1) = 'MLR',
POINT_QUANTITY_INDEX(1) = 0,
POINT_Z(1) = 0,
POINT_X(1) = 0,
PROFILE_QUANTITY(1) = 'BULK_DENSITY',
PROFILE_QUANTITY_INDEX(1) = 0,
PROFILE_TYPE(1) = 'z',
PROFILE_LOCATION(1) = 0,
PROFILE_ISKIP(1) = 1,
PROFILE_QUANTITY(2) = 'REACTION_RATE_K',
PROFILE_QUANTITY_INDEX(2) = 1,
PROFILE_TYPE(2) = 'z',
PROFILE_LOCATION(2) = 0,
PROFILE_ISKIP(2) = 1,
PROFILE_QUANTITY(3) = 'REACTION_RATE_K',
PROFILE_QUANTITY_INDEX(3) = 2,
PROFILE_TYPE(3) = 'z',
PROFILE_LOCATION(3) = 0,
PROFILE_ISKIP(3) = 1,
PROFILE_QUANTITY(4) = 'YI',
PROFILE_QUANTITY_INDEX(4) = 1,
PROFILE_TYPE(4) = 'z',
PROFILE_LOCATION(4) = 0,
PROFILE_ISKIP(4) = 1,
PROFILE_QUANTITY(5) = 'YI',
PROFILE_QUANTITY_INDEX(5) = 2,
PROFILE_TYPE(5) = 'z',
PROFILE_LOCATION(5) = 0,
PROFILE_ISKIP(5) = 1,
PROFILE_QUANTITY(6) = 'YI',
PROFILE_QUANTITY_INDEX(6) = 3,
PROFILE_TYPE(6) = 'z',
PROFILE_LOCATION(6) = 0,
PROFILE_ISKIP(6) = 1,
PROFILE_QUANTITY(7) = 'YI',
PROFILE_QUANTITY_INDEX(7) = 4,
PROFILE_TYPE(7) = 'z',
PROFILE_LOCATION(7) = 0,
PROFILE_ISKIP(7) = 1,

PROFILE_QUANTITY(8) = 'TEMPERATURE',
PROFILE_QUANTITY_INDEX(8) = 0,
PROFILE_TYPE(8) = 'z',
PROFILE_LOCATION(8) = 0,
PROFILE_ISKIP(8) = 1,
PROFILE_QUANTITY(9) = 'POROSITY',
PROFILE_QUANTITY_INDEX(9) = 0,
PROFILE_TYPE(9) = 'z',
PROFILE_LOCATION(9) = 0,
PROFILE_ISKIP(9) = 1,
PROFILE_QUANTITY(10) = 'M/M0',
PROFILE_QUANTITY_INDEX(10) = 0,
PROFILE_TYPE(10) = 'z',
PROFILE_LOCATION(10) = 0,
PROFILE_ISKIP(10) = 1,
PROFILE_QUANTITY(11) = 'YI',
PROFILE_QUANTITY_INDEX(11) = 5,
PROFILE_TYPE(11) = 'z',
PROFILE_LOCATION(11) = 0,
PROFILE_ISKIP(11) = 1,
/

&GPYRO_SPROPS

NSSPEC = 5,
NAME(1) = 'Hetron',
K0Z(1) = 0.23,
NKZ(1) = 0,
R0(1) = 1200,
NR(1) = 0,
C0(1) = 1400,
NC(1) = 0,
EMIS(1) = 0.84,
KAPPA(1) = 1000000,
TMELT(1) = 3000,
DHMELT(1) = 0,
SIGMA2MELT(1) = 0,
GAMMA(1) = 0,
PERMZ(1) = 1D-10,
RS0(1) = 1200,
PORE_DIAMETER(1) = 0.0005,
K0X(1) = 0.2,
NKX(1) = 0,
PERMX(1) = 1D-10,
NAME(2) = 'Hetron_residue',
K0Z(2) = 0.19,
NKZ(2) = 0,

R0(2) = 253,
NR(2) = 0,
C0(2) = 1900,
NC(2) = 0,
EMIS(2) = 0.90,
KAPPA(2) = 1000000,
TMELT(2) = 3000,
DHMELT(2) = 0,
SIGMA2MELT(2) = 0,
GAMMA(2) = 0.00348,
PERMZ(2) = 1D-10,
RS0(2) = 253,
PORE_DIAMETER(2) = 0.0005,
K0X(2) = 0.2,
NKX(2) = 0,
PERMX(2) = 1D-10,
NAME(3) = 'ATH',
K0Z(3) = 1.220,
NKZ(3) = 0,
R0(3) = 2300,
NR(3) = 0,
C0(3) = 1200,
NC(3) = 0,
EMIS(3) = 0.81,
KAPPA(3) = 1000000,
TMELT(3) = 3000,
DHMELT(3) = 0,
SIGMA2MELT(3) = 0,
GAMMA(3) = 0.000,
PERMZ(3) = 1D-10,
RS0(3) = 1200,
PORE_DIAMETER(3) = 0.0005,
K0X(3) = 0.2,
NKX(3) = 0,
PERMX(3) = 1D-10,
NAME(4) = 'ATH_residue',
K0Z(4) = 0.240,
NKZ(4) = 0.0,
R0(4) = 1558,
NR(4) = 0.0,
C0(4) = 1200,
NC(4) = 0.0,
EMIS(4) = 0.89,
KAPPA(4) = 1000000,
TMELT(4) = 3000,
DHMELT(4) = 0,

SIGMA2MELT(4) = 0,
GAMMA(4) = 0.00475,
PERMZ(4) = 1D-10,
RS0(4) = 1558,
PORE_DIAMETER(4) = 0.0005,
K0X(4) = 0.2,
NKX(4) = 0,
PERMX(4) = 1D-10,
NAME(5) = 'glass',
K0Z(5) = 0.18,
NKZ(5) = 0.59,
R0(5) = 2600,
NR(5) = 0.0,
C0(5) = 400,
NC(5) = 0.53,
EMIS(5) = 0.88,
KAPPA(5) = 1D6,
TMELT(5) = 3000,
DHMELT(5) = 0,
SIGMA2MELT(5) = 0,
GAMMA(5) = 0.00769,
PERMZ(5) = 1D-10,
RS0(5) = 2600,
PORE_DIAMETER(5) = 0.0005,
K0X(5) = 0.2,
NKX(5) = 0,
PERMX(5) = 1D-10,
/

&GPYRO_LAYERS

NLAYERS = 2,
X1(1) = -1,
X2(1) = 1,
Z1(1) = 0,
Z2(1) = 0.00025,
NZCELLS_PER_LAYER(1) = 381,
NXCELLS_PER_LAYER(1) = 1,
HCRZ(1) = 10000,
HCRX(1) = 0,
TINITIAL(1) = 300,
SOLVE_POROSITY_IN_LAYER(1) = .FALSE.,
YI0(1,1) = 0,
YI0(1,2) = 0,
YI0(1,3) = 0,
YI0(1,4) = 0,
YI0(1,5) = 1,

ICAT(2) = 0 ,
/

&GPYRO_HGRXNS
NHGRXNS = 0,
/

&GPYRO_GPROPS
NGSPEC = 1,
IBG = 1,
IO2 = 2,
CPG = 1000,
NAME(1) = 'pyrolysate' ,
YJ0(1) = 1 ,
M(1) = 44 ,
SIGMA(1) = 5.061 ,
EPSOK(1) = 254 ,
B(1) = 0 ,
TONSET(1) = 653 ,
TSPAN(1) = 50 ,
/

&GPYRO_GYIELDS
GYIELDS(1,1) = 1,
GYIELDS(1,2) = 1,
/

&GPYRO_HGYIELDS
/

&GPYRO_SEBCPATCH
NSEBCPATCH = 2,
T(1) = 0,
X1(1) = -1,
X2(1) = 1,
Z1(1) = 0,
Z2(1) = 0,
QE(1) = 50000,
HC(1) = 10,
TINF(1) = 300,
RERADIATION(1) = .TRUE.,
TFIXED(1) = -1,
T(2) = 0,
X1(2) = -1,
X2(2) = 1,
Z1(2) = 0.00925,

Z2(2) = 0.00925,
QE(2) = 0,
HC(2) = 10,
TINF(2) = 300,
RERADIATION(2) = .FALSE.,
TFIXED(2) = -1,
/

&GPYRO_GMBCPATCH
NGMBCPATCH = 0,
/

&GPYRO_GSBCPATCH
NGSBCPATCH = 0,
/

&GPYRO_GEBCPATCH
NGEBCPATCH = 0,
/

&GPYRO_QE
NQE = 1,
QE(1) = 50000,
HC0(1) = 10,
NHC(1) = 0,
DELTA0(1) = 0.00925,
NCELL(1) = 93,
L(1) = 0.01,
NBC(1) = 1,
TIG(1) = 10000,
QFL(1) = 0,
TSTOP(1) = 1600,
MIG(1) = 3,
TMPIG(1) = 350,
ZEROD(1) = .FALSE.,
BETA(1) = 5,
YJINF(1,1) = 1,
/

&GA_GENINPUT NGEN = 100,
NINDIV = 200,
MAXCOPIES = 4,
LINUX = .TRUE.,
SIMULATED_EXPERIMENTAL_DATA = .FALSE.,
RESTART = .FALSE.,
FITMIN = 0,

```
FITCLIP = 0,  
FITEXPONENT = 2,  
WHOLEGENEFRAC = 0.3,  
BRUTE_FORCE = .FALSE.,  
KILL_NONCONVERGED_SOLNS = .TRUE.,
```

```
/  
&GA_PHI  
NPHI = 0,  
/
```

```
&GA_VARS  
NGENE = 0,  
/
```

[9.11.7. 0.5 mm Coating](#)

```
&GPYRO_GENERAL  
DT0 = 0.1,  
TAMB = 300,  
TREF = 300,  
P0 = 101300,  
GX = 0,  
GZ = 0,  
THERMAL_EQUILIBRIUM = .TRUE.,  
VHLC = 0,  
HCV = 1000000,  
NU_A = 2,  
NU_B = 1,  
NU_C = 0.5,  
NTDMA_ITERATIONS = 1000,  
NSSPECIESITERNS = 1,  
NCONTINUITYITERNS = 1,  
ALPHA = 1,  
TMPTOL = 0.0001,  
HTOL = 0.00000001,  
YITOL = 0.0001,  
PTOL = 0.0001,  
YJTOL = 0.0001,  
HGTOL = 0.1,  
EXPLICIT_T = .FALSE.,  
SOLVE_GAS_YJ = .TRUE.,  
SOLVE_GAS_ENERGY = .FALSE.,  
SOLVE_PRESSURE = .FALSE.,  
SOLVE_POROSITY = .FALSE.,  
PROPERTY_LINTERP = .FALSE.,  
USE_TOFH_NEWTON = .TRUE.,  
SHYI_CORRECTION = .TRUE.,
```

```
NCOEFF_UPDATE_SKIP = 1,  
FDSMODE = .FALSE.,  
CONVENTIONAL_RXN_ORDER = .FALSE.,  
TWOD = .FALSE.,  
USE_BC_PATCHES = .TRUE.,  
NOCONSUMPTION = .FALSE.,  
EPS = 0.0000000001,  
GAS_DIFFUSION = .FALSE.,  
FRONT_GAS_DIFFUSION = .FALSE.,  
BLOWING = .FALSE.,  
MINIMUM_CONDUCTIVITY = 0,  
CONSTANT_DHVOL = .TRUE.,  
FULL_QSG = .FALSE.,  
GASES_PRODUCED_AT_TSOLID = .FALSE.,  
/  

```

```
&GPYRO_OUTPUT  
CASENAME = '100_133mixedcoat_5mm',  
DUMP_ENERGY_BALANCE = .FALSE.,  
N_POINT_QUANTITIES = 1,  
N_PROFILE_QUANTITIES = 11,  
N_SMOKEVIEW_QUANTITIES = 0,  
DUMP_EVERYTHING = .FALSE.,  
DTDUMP_GA = 1,  
DTDUMP_POINT = 1,  
DTDUMP_PROFILE = 1,  
DTDUMP_SMOKEVIEW = 1,  
TMP_REDUCED_DTDUMP = 5000,  
REDUCED_DTDUMP = 0.0001,  
DTMIN_KILL = 0.0000001,  
POINT_QUANTITY(1) = 'MLR',  
POINT_QUANTITY_INDEX(1) = 0,  
POINT_Z(1) = 0,  
POINT_X(1) = 0,  
PROFILE_QUANTITY(1) = 'BULK_DENSITY',  
PROFILE_QUANTITY_INDEX(1) = 0,  
PROFILE_TYPE(1) = 'z',  
PROFILE_LOCATION(1) = 0,  
PROFILE_ISKIP(1) = 1,  
PROFILE_QUANTITY(2) = 'REACTION_RATE_K',  
PROFILE_QUANTITY_INDEX(2) = 1,  
PROFILE_TYPE(2) = 'z',  
PROFILE_LOCATION(2) = 0,  
PROFILE_ISKIP(2) = 1,  
PROFILE_QUANTITY(3) = 'REACTION_RATE_K',  
PROFILE_QUANTITY_INDEX(3) = 2,
```

PROFILE_TYPE(3) = 'z',
PROFILE_LOCATION(3) = 0,
PROFILE_ISKIP(3) = 1,
PROFILE_QUANTITY(4) = 'YI',
PROFILE_QUANTITY_INDEX(4) = 1,
PROFILE_TYPE(4) = 'z',
PROFILE_LOCATION(4) = 0,
PROFILE_ISKIP(4) = 1,
PROFILE_QUANTITY(5) = 'YI',
PROFILE_QUANTITY_INDEX(5) = 2,
PROFILE_TYPE(5) = 'z',
PROFILE_LOCATION(5) = 0,
PROFILE_ISKIP(5) = 1,
PROFILE_QUANTITY(6) = 'YI',
PROFILE_QUANTITY_INDEX(6) = 3,
PROFILE_TYPE(6) = 'z',
PROFILE_LOCATION(6) = 0,
PROFILE_ISKIP(6) = 1,
PROFILE_QUANTITY(7) = 'YI',
PROFILE_QUANTITY_INDEX(7) = 4,
PROFILE_TYPE(7) = 'z',
PROFILE_LOCATION(7) = 0,
PROFILE_ISKIP(7) = 1,
PROFILE_QUANTITY(8) = 'TEMPERATURE',
PROFILE_QUANTITY_INDEX(8) = 0,
PROFILE_TYPE(8) = 'z',
PROFILE_LOCATION(8) = 0,
PROFILE_ISKIP(8) = 1,
PROFILE_QUANTITY(9) = 'POROSITY',
PROFILE_QUANTITY_INDEX(9) = 0,
PROFILE_TYPE(9) = 'z',
PROFILE_LOCATION(9) = 0,
PROFILE_ISKIP(9) = 1,
PROFILE_QUANTITY(10) = 'M/M0',
PROFILE_QUANTITY_INDEX(10) = 0,
PROFILE_TYPE(10) = 'z',
PROFILE_LOCATION(10) = 0,
PROFILE_ISKIP(10) = 1,
PROFILE_QUANTITY(11) = 'YI',
PROFILE_QUANTITY_INDEX(11) = 5,
PROFILE_TYPE(11) = 'z',
PROFILE_LOCATION(11) = 0,
PROFILE_ISKIP(11) = 1,
/

&GPYRO_SPROPS

NSSPEC = 5,
NAME(1) = 'Hetron',
K0Z(1) = 0.23,
NKZ(1) = 0,
R0(1) = 1200,
NR(1) = 0,
C0(1) = 1400,
NC(1) = 0,
EMIS(1) = 0.84,
KAPPA(1) = 1000000,
TMELT(1) = 3000,
DHMELT(1) = 0,
SIGMA2MELT(1) = 0,
GAMMA(1) = 0,
PERMZ(1) = 1D-10,
RS0(1) = 1200,
PORE_DIAMETER(1) = 0.0005,
K0X(1) = 0.2,
NKX(1) = 0,
PERMX(1) = 1D-10,
NAME(2) = 'Hetron_residue',
K0Z(2) = 0.19,
NKZ(2) = 0,
R0(2) = 253,
NR(2) = 0,
C0(2) = 1900,
NC(2) = 0,
EMIS(2) = 0.90,
KAPPA(2) = 1000000,
TMELT(2) = 3000,
DHMELT(2) = 0,
SIGMA2MELT(2) = 0,
GAMMA(2) = 0.00348,
PERMZ(2) = 1D-10,
RS0(2) = 253,
PORE_DIAMETER(2) = 0.0005,
K0X(2) = 0.2,
NKX(2) = 0,
PERMX(2) = 1D-10,
NAME(3) = 'ATH',
K0Z(3) = 1.220,
NKZ(3) = 0,
R0(3) = 2300,
NR(3) = 0,
C0(3) = 1200,
NC(3) = 0,

EMIS(3) = 0.81,
KAPPA(3) = 1000000,
TMELT(3) = 3000,
DHMELT(3) = 0,
SIGMA2MELT(3) = 0,
GAMMA(3) = 0.000,
PERMZ(3) = 1D-10,
RS0(3) = 1200,
PORE_DIAMETER(3) = 0.0005,
K0X(3) = 0.2,
NKX(3) = 0,
PERMX(3) = 1D-10,
NAME(4) = 'ATH_residue',
K0Z(4) = 0.240,
NKZ(4) = 0.0,
R0(4) = 1558,
NR(4) = 0.0,
C0(4) = 1200,
NC(4) = 0.0,
EMIS(4) = 0.89,
KAPPA(4) = 1000000,
TMELT(4) = 3000,
DHMELT(4) = 0,
SIGMA2MELT(4) = 0,
GAMMA(4) = 0.00475,
PERMZ(4) = 1D-10,
RS0(4) = 1558,
PORE_DIAMETER(4) = 0.0005,
K0X(4) = 0.2,
NKX(4) = 0,
PERMX(4) = 1D-10,
NAME(5) = 'glass',
K0Z(5) = 0.18,
NKZ(5) = 0.59,
R0(5) = 2600,
NR(5) = 0.0,
C0(5) = 400,
NC(5) = 0.53,
EMIS(5) = 0.88,
KAPPA(5) = 1D6,
TMELT(5) = 3000,
DHMELT(5) = 0,
SIGMA2MELT(5) = 0,
GAMMA(5) = 0.00769,
PERMZ(5) = 1D-10,
RS0(5) = 2600,

DHS(1) = 0 ,
DHV(1) = 172000 ,
CHI(1) = 1 ,
ORDER(1) = 1.125 ,
ORDERO2(1) = 0 ,
IKINETICMODEL(1) = 0 ,
IO2TYPE(1) = 0 ,
M(1) = 0 ,
KCAT(1) = 0 ,
ICAT(1) = 0 ,
CFROM(2) = 'ATH' ,
CTO(2) = 'ATH_residue' ,
Z(2) = 250000000000 ,
E(2) = 140.1 ,
DHS(2) = 0 ,
DHV(2) = 1000000 ,
CHI(2) = 1 ,
ORDER(2) = 1.24 ,
ORDERO2(2) = 0 ,
IKINETICMODEL(2) = 0 ,
IO2TYPE(2) = 0 ,
M(2) = 0 ,
KCAT(2) = 0 ,
ICAT(2) = 0 ,
/

&GPYRO_HGRXNS
NHGRXNS = 0,
/

&GPYRO_GPROPS
NGSPEC = 1,
IBG = 1,
IO2 = 2,
CPG = 1000,
NAME(1) = 'pyrolysate' ,
YJ0(1) = 1 ,
M(1) = 44 ,
SIGMA(1) = 5.061 ,
EPSOK(1) = 254 ,
B(1) = 0 ,
TONSET(1) = 653 ,
TSPAN(1) = 50 ,
/

&GPYRO_GYIELDS

```
GYIELDS(1,1) = 1,  
GYIELDS(1,2) = 1,  
/
```

```
&GPYRO_HGYIELDS  
/
```

```
&GPYRO_SEBCPATCH  
NSEBCPATCH = 2,  
T(1) = 0,  
X1(1) = -1,  
X2(1) = 1,  
Z1(1) = 0,  
Z2(1) = 0,  
QE(1) = 50000,  
HC(1) = 10,  
TINF(1) = 300,  
RERADIATION(1) = .TRUE.,  
TFIXED(1) = -1,  
T(2) = 0,  
X1(2) = -1,  
X2(2) = 1,  
Z1(2) = 0.0095,  
Z2(2) = 0.0095,  
QE(2) = 0,  
HC(2) = 10,  
TINF(2) = 300,  
RERADIATION(2) = .FALSE.,  
TFIXED(2) = -1,  
/
```

```
&GPYRO_GMBCPATCH  
NGMBCPATCH = 0,  
/
```

```
&GPYRO_GSBCPATCH  
NGSBCPATCH = 0,  
/
```

```
&GPYRO_GEBCPATCH  
NGEBCPATCH = 0,  
/
```

```
&GPYRO_QE  
NQE = 1,  
QE(1) = 50000,
```

```
HC0(1) = 10,  
NHC(1) = 0,  
DELTA0(1) = 0.0095,  
NCELL(1) = 96,  
L(1) = 0.01,  
NBC(1) = 1,  
TIG(1) = 10000,  
QFL(1) = 0,  
TSTOP(1) = 1600,  
MIG(1) = 3,  
TMPIG(1) = 350,  
ZEROD(1) = .FALSE.,  
BETA(1) = 5,  
YJINF(1,1) = 1,  
/  

```

```
&GA_GENINPUT NGEN = 100,  
NINDIV = 200,  
MAXCOPIES = 4,  
LINUX = .TRUE.,  
SIMULATED_EXPERIMENTAL_DATA = .FALSE.,  
RESTART = .FALSE.,  
FITMIN = 0,  
FITCLIP = 0,  
FITEXPONENT = 2,  
WHOLEGENEFRACTION = 0.3,  
BRUTE_FORCE = .FALSE.,  
KILL_NONCONVERGED_SOLNS = .TRUE.,  
/  
&GA_PHI  
NPHI = 0,  
/  

```

```
&GA_VARS  
NGENE = 0,  
/  

```

[9.11.8. 1 mm Coating](#)

```
&GPYRO_GENERAL  
DT0 = 0.1,  
TAMB = 300,  
TREF = 300,  
P0 = 101300,  
GX = 0,  
GZ = 0,  
THERMAL_EQUILIBRIUM = .TRUE.,
```

```
VHLC = 0,  
HCV = 1000000,  
NU_A = 2,  
NU_B = 1,  
NU_C = 0.5,  
NTDMA_ITERATIONS = 1000,  
NSSPECIESITERNS = 1,  
NCONTINUITYITERNS = 1,  
ALPHA = 1,  
TMPTOL = 0.0001,  
HTOL = 0.00000001,  
YITOL = 0.0001,  
PTOL = 0.0001,  
YJTOL = 0.0001,  
HGTOL = 0.1,  
EXPLICIT_T = .FALSE.,  
SOLVE_GAS_YJ = .TRUE.,  
SOLVE_GAS_ENERGY = .FALSE.,  
SOLVE_PRESSURE = .FALSE.,  
SOLVE_POROSITY = .FALSE.,  
PROPERTY_LINTERP = .FALSE.,  
USE_TOFH_NEWTON = .TRUE.,  
SHYI_CORRECTION = .TRUE.,  
NCOEFF_UPDATE_SKIP = 1,  
FDSMODE = .FALSE.,  
CONVENTIONAL_RXN_ORDER = .FALSE.,  
TWOD = .FALSE.,  
USE_BC_PATCHES = .TRUE.,  
NOCONSUMPTION = .FALSE.,  
EPS = 0.0000000001,  
GAS_DIFFUSION = .FALSE.,  
FRONT_GAS_DIFFUSION = .FALSE.,  
BLOWING = .FALSE.,  
MINIMUM_CONDUCTIVITY = 0,  
CONSTANT_DHVOL = .TRUE.,  
FULL_QSG = .FALSE.,  
GASES_PRODUCED_AT_TSOLID = .FALSE.,  
/  
  
&GPYRO_OUTPUT  
CASENAME = '100_133mixedcoat_1mm',  
DUMP_ENERGY_BALANCE = .FALSE.,  
N_POINT_QUANTITIES = 1,  
N_PROFILE_QUANTITIES = 11,  
N_SMOKEVIEW_QUANTITIES = 0,  
DUMP_EVERYTHING = .FALSE.,
```

DTDUMP_GA = 1,
DTDUMP_POINT = 1,
DTDUMP_PROFILE = 1,
DTDUMP_SMOKEVIEW = 1,
TMP_REDUCED_DTDUMP = 5000,
REDUCED_DTDUMP = 0.0001,
DTMIN_KILL = 0.0000001,
POINT_QUANTITY(1) = 'MLR',
POINT_QUANTITY_INDEX(1) = 0,
POINT_Z(1) = 0,
POINT_X(1) = 0,
PROFILE_QUANTITY(1) = 'BULK_DENSITY',
PROFILE_QUANTITY_INDEX(1) = 0,
PROFILE_TYPE(1) = 'z',
PROFILE_LOCATION(1) = 0,
PROFILE_ISKIP(1) = 1,
PROFILE_QUANTITY(2) = 'REACTION_RATE_K',
PROFILE_QUANTITY_INDEX(2) = 1,
PROFILE_TYPE(2) = 'z',
PROFILE_LOCATION(2) = 0,
PROFILE_ISKIP(2) = 1,
PROFILE_QUANTITY(3) = 'REACTION_RATE_K',
PROFILE_QUANTITY_INDEX(3) = 2,
PROFILE_TYPE(3) = 'z',
PROFILE_LOCATION(3) = 0,
PROFILE_ISKIP(3) = 1,
PROFILE_QUANTITY(4) = 'YI',
PROFILE_QUANTITY_INDEX(4) = 1,
PROFILE_TYPE(4) = 'z',
PROFILE_LOCATION(4) = 0,
PROFILE_ISKIP(4) = 1,
PROFILE_QUANTITY(5) = 'YI',
PROFILE_QUANTITY_INDEX(5) = 2,
PROFILE_TYPE(5) = 'z',
PROFILE_LOCATION(5) = 0,
PROFILE_ISKIP(5) = 1,
PROFILE_QUANTITY(6) = 'YI',
PROFILE_QUANTITY_INDEX(6) = 3,
PROFILE_TYPE(6) = 'z',
PROFILE_LOCATION(6) = 0,
PROFILE_ISKIP(6) = 1,
PROFILE_QUANTITY(7) = 'YI',
PROFILE_QUANTITY_INDEX(7) = 4,
PROFILE_TYPE(7) = 'z',
PROFILE_LOCATION(7) = 0,
PROFILE_ISKIP(7) = 1,

PROFILE_QUANTITY(8) = 'TEMPERATURE',
PROFILE_QUANTITY_INDEX(8) = 0,
PROFILE_TYPE(8) = 'z',
PROFILE_LOCATION(8) = 0,
PROFILE_ISKIP(8) = 1,
PROFILE_QUANTITY(9) = 'POROSITY',
PROFILE_QUANTITY_INDEX(9) = 0,
PROFILE_TYPE(9) = 'z',
PROFILE_LOCATION(9) = 0,
PROFILE_ISKIP(9) = 1,
PROFILE_QUANTITY(10) = 'M/M0',
PROFILE_QUANTITY_INDEX(10) = 0,
PROFILE_TYPE(10) = 'z',
PROFILE_LOCATION(10) = 0,
PROFILE_ISKIP(10) = 1,
PROFILE_QUANTITY(11) = 'YI',
PROFILE_QUANTITY_INDEX(11) = 5,
PROFILE_TYPE(11) = 'z',
PROFILE_LOCATION(11) = 0,
PROFILE_ISKIP(11) = 1,
/

&GPYRO_SPROPS

NSSPEC = 5,
NAME(1) = 'Hetron',
K0Z(1) = 0.23,
NKZ(1) = 0,
R0(1) = 1200,
NR(1) = 0,
C0(1) = 1400,
NC(1) = 0,
EMIS(1) = 0.84,
KAPPA(1) = 1000000,
TMELT(1) = 3000,
DHMELT(1) = 0,
SIGMA2MELT(1) = 0,
GAMMA(1) = 0,
PERMZ(1) = 1D-10,
RS0(1) = 1200,
PORE_DIAMETER(1) = 0.0005,
K0X(1) = 0.2,
NKX(1) = 0,
PERMX(1) = 1D-10,
NAME(2) = 'Hetron_residue',
K0Z(2) = 0.19,
NKZ(2) = 0,

R0(2) = 253,
NR(2) = 0,
C0(2) = 1900,
NC(2) = 0,
EMIS(2) = 0.90,
KAPPA(2) = 1000000,
TMELT(2) = 3000,
DHMELT(2) = 0,
SIGMA2MELT(2) = 0,
GAMMA(2) = 0.00348,
PERMZ(2) = 1D-10,
RS0(2) = 253,
PORE_DIAMETER(2) = 0.0005,
K0X(2) = 0.2,
NKX(2) = 0,
PERMX(2) = 1D-10,
NAME(3) = 'ATH',
K0Z(3) = 1.220,
NKZ(3) = 0,
R0(3) = 2300,
NR(3) = 0,
C0(3) = 1200,
NC(3) = 0,
EMIS(3) = 0.81,
KAPPA(3) = 1000000,
TMELT(3) = 3000,
DHMELT(3) = 0,
SIGMA2MELT(3) = 0,
GAMMA(3) = 0.000,
PERMZ(3) = 1D-10,
RS0(3) = 1200,
PORE_DIAMETER(3) = 0.0005,
K0X(3) = 0.2,
NKX(3) = 0,
PERMX(3) = 1D-10,
NAME(4) = 'ATH_residue',
K0Z(4) = 0.240,
NKZ(4) = 0.0,
R0(4) = 1558,
NR(4) = 0.0,
C0(4) = 1200,
NC(4) = 0.0,
EMIS(4) = 0.89,
KAPPA(4) = 1000000,
TMELT(4) = 3000,
DHMELT(4) = 0,

SIGMA2MELT(4) = 0,
GAMMA(4) = 0.00475,
PERMZ(4) = 1D-10,
RS0(4) = 1558,
PORE_DIAMETER(4) = 0.0005,
K0X(4) = 0.2,
NKX(4) = 0,
PERMX(4) = 1D-10,
NAME(5) = 'glass',
K0Z(5) = 0.18,
NKZ(5) = 0.59,
R0(5) = 2600,
NR(5) = 0.0,
C0(5) = 400,
NC(5) = 0.53,
EMIS(5) = 0.88,
KAPPA(5) = 1D6,
TMELT(5) = 3000,
DHMELT(5) = 0,
SIGMA2MELT(5) = 0,
GAMMA(5) = 0.00769,
PERMZ(5) = 1D-10,
RS0(5) = 2600,
PORE_DIAMETER(5) = 0.0005,
K0X(5) = 0.2,
NKX(5) = 0,
PERMX(5) = 1D-10,
/

&GPYRO_LAYERS

NLAYERS = 2,
X1(1) = -1,
X2(1) = 1,
Z1(1) = 0,
Z2(1) = 0.001,
NZCELLS_PER_LAYER(1) = 381,
NXCELLS_PER_LAYER(1) = 1,
HCRZ(1) = 10000,
HCRX(1) = 0,
TINITIAL(1) = 300,
SOLVE_POROSITY_IN_LAYER(1) = .FALSE.,
YI0(1,1) = 0,
YI0(1,2) = 0,
YI0(1,3) = 0,
YI0(1,4) = 0,
YI0(1,5) = 1,

X1(2) = -1,
X2(2) = 1,
Z1(2) = 0.001,
Z2(2) = 0.010,
NZCELLS_PER_LAYER(2) = 381,
NXCELLS_PER_LAYER(2) = 1,
HCRZ(2) = 0,
HCRX(2) = 0,
TINITIAL(2) = 300,
SOLVE_POROSITY_IN_LAYER(2) = .FALSE.,
YI0(2,1) = 0.2145,
YI0(2,2) = 0,
YI0(2,3) = 0.2855,
YI0(2,4) = 0,
YI0(2,5) = 0.5,
/

&GPYRO_RXNS
NRXNS = 2,
CFROM(1) = 'Hetron',
CTO(1) = 'Hetron_residue',
Z(1) = 5000000000000000,
E(1) = 195,
DHS(1) = 0,
DHV(1) = 172000,
CHI(1) = 1,
ORDER(1) = 1.125,
ORDERO2(1) = 0,
IKINETICMODEL(1) = 0,
IO2TYPE(1) = 0,
M(1) = 0,
KCAT(1) = 0,
ICAT(1) = 0,
CFROM(2) = 'ATH',
CTO(2) = 'ATH_residue',
Z(2) = 2500000000000000,
E(2) = 140.1,
DHS(2) = 0,
DHV(2) = 1000000,
CHI(2) = 1,
ORDER(2) = 1.24,
ORDERO2(2) = 0,
IKINETICMODEL(2) = 0,
IO2TYPE(2) = 0,
M(2) = 0,
KCAT(2) = 0,

ICAT(2) = 0 ,
/

&GPYRO_HGRXNS
NHGRXNS = 0,
/

&GPYRO_GPROPS
NGSPEC = 1,
IBG = 1,
IO2 = 2,
CPG = 1000,
NAME(1) = 'pyrolysate' ,
YJ0(1) = 1 ,
M(1) = 44 ,
SIGMA(1) = 5.061 ,
EPSOK(1) = 254 ,
B(1) = 0 ,
TONSET(1) = 653 ,
TSPAN(1) = 50 ,
/

&GPYRO_GYIELDS
GYIELDS(1,1) = 1,
GYIELDS(1,2) = 1,
/

&GPYRO_HGYIELDS
/

&GPYRO_SEBCPATCH
NSEBCPATCH = 2,
T(1) = 0,
X1(1) = -1,
X2(1) = 1,
Z1(1) = 0,
Z2(1) = 0,
QE(1) = 50000,
HC(1) = 10,
TINF(1) = 300,
RERADIATION(1) = .TRUE.,
TFIXED(1) = -1,
T(2) = 0,
X1(2) = -1,
X2(2) = 1,
Z1(2) = 0.01,

Z2(2) = 0.01,
QE(2) = 0,
HC(2) = 10,
TINF(2) = 300,
RERADIATION(2) = .FALSE.,
TFIXED(2) = -1,
/

&GPYRO_GMBCPATCH
NGMBCPATCH = 0,
/

&GPYRO_GSBCPATCH
NGSBCPATCH = 0,
/

&GPYRO_GEBCPATCH
NGEBCPATCH = 0,
/

&GPYRO_QE
NQE = 1,
QE(1) = 50000,
HC0(1) = 10,
NHC(1) = 0,
DELTA0(1) = 0.010,
NCELL(1) = 101,
L(1) = 0.01,
NBC(1) = 1,
TIG(1) = 10000,
QFL(1) = 0,
TSTOP(1) = 1600,
MIG(1) = 3,
TMPIG(1) = 350,
ZEROD(1) = .FALSE.,
BETA(1) = 5,
YJINF(1,1) = 1,
/

&GA_GENINPUT NGEN = 100,
NINDIV = 200,
MAXCOPIES = 4,
LINUX = .TRUE.,
SIMULATED_EXPERIMENTAL_DATA = .FALSE.,
RESTART = .FALSE.,
FITMIN = 0,

```
FITCLIP = 0,  
FITEXPONENT = 2,  
WHOLEGENEFRACTION = 0.3,  
BRUTE_FORCE = .FALSE.,  
KILL_NONCONVERGED_SOLNS = .TRUE.,
```

```
/  
&GA_PHI  
NPHI = 0,  
/
```

```
&GA_VARS  
NGENE = 0,  
/
```

9.11.9. Layered FRP

```
&GPYRO_GENERAL  
DT0 = 0.1,  
TAMB = 300,  
TREF = 300,  
P0 = 101300,  
GX = 0,  
GZ = 0,  
THERMAL_EQUILIBRIUM = .TRUE.,  
VHLC = 0,  
HCV = 1000000,  
NU_A = 2,  
NU_B = 1,  
NU_C = 0.5,  
NTDMA_ITERATIONS = 1000,  
NSSPECIESITERNS = 1,  
NCONTINUITYITERNS = 1,  
ALPHA = 1,  
TMPTOL = 0.0001,  
HTOL = 0.00000001,  
YITOL = 0.0001,  
PTOL = 0.0001,  
YJTOL = 0.0001,  
HGTOL = 0.1,  
EXPLICIT_T = .FALSE.,  
SOLVE_GAS_YJ = .TRUE.,  
SOLVE_GAS_ENERGY = .FALSE.,  
SOLVE_PRESSURE = .FALSE.,  
SOLVE_POROSITY = .FALSE.,  
PROPERTY_LINTERP = .FALSE.,  
USE_TOFH_NEWTON = .TRUE.,  
SHYI_CORRECTION = .TRUE.,
```

```
NCOEFF_UPDATE_SKIP = 1,  
FDSMODE = .FALSE.,  
CONVENTIONAL_RXN_ORDER = .FALSE.,  
TWOD = .FALSE.,  
USE_BC_PATCHES = .TRUE.,  
NOCONSUMPTION = .FALSE.,  
EPS = 0.0000000001,  
GAS_DIFFUSION = .FALSE.,  
FRONT_GAS_DIFFUSION = .FALSE.,  
BLOWING = .FALSE.,  
MINIMUM_CONDUCTIVITY = 0,  
CONSTANT_DHVOL = .TRUE.,  
FULL_QSG = .FALSE.,  
GASES_PRODUCED_AT_TSOLID = .FALSE.,  
/  

```

```
&GPYRO_OUTPUT  
CASENAME = '100_133layeredRerad',  
DUMP_ENERGY_BALANCE = .FALSE.,  
N_POINT_QUANTITIES = 1,  
N_PROFILE_QUANTITIES = 11,  
N_SMOKEVIEW_QUANTITIES = 0,  
DUMP_EVERYTHING = .FALSE.,  
DTDUMP_GA = 1,  
DTDUMP_POINT = 1,  
DTDUMP_PROFILE = 1,  
DTDUMP_SMOKEVIEW = 1,  
TMP_REDUCED_DTDUMP = 5000,  
REDUCED_DTDUMP = 0.0001,  
DTMIN_KILL = 0.0000001,  
POINT_QUANTITY(1) = 'MLR',  
POINT_QUANTITY_INDEX(1) = 0,  
POINT_Z(1) = 0,  
POINT_X(1) = 0,  
PROFILE_QUANTITY(1) = 'BULK_DENSITY',  
PROFILE_QUANTITY_INDEX(1) = 0,  
PROFILE_TYPE(1) = 'z',  
PROFILE_LOCATION(1) = 0,  
PROFILE_ISKIP(1) = 1,  
PROFILE_QUANTITY(2) = 'REACTION_RATE_K',  
PROFILE_QUANTITY_INDEX(2) = 1,  
PROFILE_TYPE(2) = 'z',  
PROFILE_LOCATION(2) = 0,  
PROFILE_ISKIP(2) = 1,  
PROFILE_QUANTITY(3) = 'REACTION_RATE_K',  
PROFILE_QUANTITY_INDEX(3) = 2,
```

PROFILE_TYPE(3) = 'z',
PROFILE_LOCATION(3) = 0,
PROFILE_ISKIP(3) = 1,
PROFILE_QUANTITY(4) = 'YI',
PROFILE_QUANTITY_INDEX(4) = 1,
PROFILE_TYPE(4) = 'z',
PROFILE_LOCATION(4) = 0,
PROFILE_ISKIP(4) = 1,
PROFILE_QUANTITY(5) = 'YI',
PROFILE_QUANTITY_INDEX(5) = 2,
PROFILE_TYPE(5) = 'z',
PROFILE_LOCATION(5) = 0,
PROFILE_ISKIP(5) = 1,
PROFILE_QUANTITY(6) = 'YI',
PROFILE_QUANTITY_INDEX(6) = 3,
PROFILE_TYPE(6) = 'z',
PROFILE_LOCATION(6) = 0,
PROFILE_ISKIP(6) = 1,
PROFILE_QUANTITY(7) = 'YI',
PROFILE_QUANTITY_INDEX(7) = 4,
PROFILE_TYPE(7) = 'z',
PROFILE_LOCATION(7) = 0,
PROFILE_ISKIP(7) = 1,
PROFILE_QUANTITY(8) = 'TEMPERATURE',
PROFILE_QUANTITY_INDEX(8) = 0,
PROFILE_TYPE(8) = 'z',
PROFILE_LOCATION(8) = 0,
PROFILE_ISKIP(8) = 1,
PROFILE_QUANTITY(9) = 'POROSITY',
PROFILE_QUANTITY_INDEX(9) = 0,
PROFILE_TYPE(9) = 'z',
PROFILE_LOCATION(9) = 0,
PROFILE_ISKIP(9) = 1,
PROFILE_QUANTITY(10) = 'M/M0',
PROFILE_QUANTITY_INDEX(10) = 0,
PROFILE_TYPE(10) = 'z',
PROFILE_LOCATION(10) = 0,
PROFILE_ISKIP(10) = 1,
PROFILE_QUANTITY(11) = 'YI',
PROFILE_QUANTITY_INDEX(11) = 5,
PROFILE_TYPE(11) = 'z',
PROFILE_LOCATION(11) = 0,
PROFILE_ISKIP(11) = 1,
/

&GPYRO_SPROPS

NSSPEC = 5,
NAME(1) = 'Hetron',
K0Z(1) = 0.23,
NKZ(1) = 0,
R0(1) = 1200,
NR(1) = 0,
C0(1) = 1400,
NC(1) = 0,
EMIS(1) = 0.84,
KAPPA(1) = 1000000,
TMELT(1) = 3000,
DHMELT(1) = 0,
SIGMA2MELT(1) = 0,
GAMMA(1) = 0,
PERMZ(1) = 1D-10,
RS0(1) = 1200,
PORE_DIAMETER(1) = 0.0005,
K0X(1) = 0.2,
NKX(1) = 0,
PERMX(1) = 1D-10,
NAME(2) = 'Hetron_residue',
K0Z(2) = 0.19,
NKZ(2) = 0,
R0(2) = 253,
NR(2) = 0,
C0(2) = 1900,
NC(2) = 0,
EMIS(2) = 0.90,
KAPPA(2) = 1000000,
TMELT(2) = 3000,
DHMELT(2) = 0,
SIGMA2MELT(2) = 0,
GAMMA(2) = 0.00348,
PERMZ(2) = 1D-10,
RS0(2) = 253,
PORE_DIAMETER(2) = 0.0005,
K0X(2) = 0.2,
NKX(2) = 0,
PERMX(2) = 1D-10,
NAME(3) = 'ATH',
K0Z(3) = 1.220,
NKZ(3) = 0,
R0(3) = 2300,
NR(3) = 0,
C0(3) = 1200,
NC(3) = 0,

EMIS(3) = 0.81,
KAPPA(3) = 1000000,
TMELT(3) = 3000,
DHMELT(3) = 0,
SIGMA2MELT(3) = 0,
GAMMA(3) = 0.000,
PERMZ(3) = 1D-10,
RS0(3) = 2300,
PORE_DIAMETER(3) = 0.0005,
K0X(3) = 0.2,
NKX(3) = 0,
PERMX(3) = 1D-10,
NAME(4) = 'ATH_residue',
K0Z(4) = 0.240,
NKZ(4) = 0.0,
R0(4) = 1558,
NR(4) = 0.0,
C0(4) = 1200,
NC(4) = 0.0,
EMIS(4) = 0.89,
KAPPA(4) = 1000000,
TMELT(4) = 3000,
DHMELT(4) = 0,
SIGMA2MELT(4) = 0,
GAMMA(4) = 0.00475,
PERMZ(4) = 1D-10,
RS0(4) = 1558,
PORE_DIAMETER(4) = 0.0005,
K0X(4) = 0.2,
NKX(4) = 0,
PERMX(4) = 1D-10,
NAME(5) = 'glass',
K0Z(5) = 0.18,
NKZ(5) = 0.59,
R0(5) = 2600,
NR(5) = 0.0,
C0(5) = 400,
NC(5) = 0.53,
EMIS(5) = 0.88,
KAPPA(5) = 1D6,
TMELT(5) = 3000,
DHMELT(5) = 0,
SIGMA2MELT(5) = 0,
GAMMA(5) = 0.00769,
PERMZ(5) = 1D-10,
RS0(5) = 2600,

PORE_DIAMETER(5) = 0.0005,
K0X(5) = 0.2,
NKX(5) = 0,
PERMX(5) = 1D-10,
/

&GPYRO_LAYERS

NLAYERS = 15,
X1(1) = -1,
X2(1) = 1,
Z1(1) = 0,
Z2(1) = 0.000395,
NZCELLS_PER_LAYER(1) = 381,
NXCELLS_PER_LAYER(1) = 1,
HCRZ(1) = 10000,
HCRX(1) = 0,
TINITIAL(1) = 300,
SOLVE_POROSITY_IN_LAYER(1) = .FALSE.,
YI0(1,1) = 0.429,
YI0(1,2) = 0,
YI0(1,3) = 0.571,
YI0(1,4) = 0,
YI0(1,5) = 0,
X1(2) = -1,
X2(2) = 1,
Z1(2) = 0.000395,
Z2(2) = 0.000895,
NZCELLS_PER_LAYER(2) = 381,
NXCELLS_PER_LAYER(2) = 1,
HCRZ(2) = 10000,
HCRX(2) = 0,
TINITIAL(2) = 300,
SOLVE_POROSITY_IN_LAYER(2) = .FALSE.,
YI0(2,1) = 0,
YI0(2,2) = 0,
YI0(2,3) = 0,
YI0(2,4) = 0,
YI0(2,5) = 1,
X1(3) = -1,
X2(3) = 1,
Z1(3) = 0.000895,
Z2(3) = 0.00168,
NZCELLS_PER_LAYER(3) = 381,
NXCELLS_PER_LAYER(3) = 1,
HCRZ(3) = 10000,
HCRX(3) = 0,

TINITIAL(3) = 300,
SOLVE_POROSITY_IN_LAYER(3) = .FALSE.,
YI0(3,1) = 0.429,
YI0(3,2) = 0,
YI0(3,3) = 0.571,
YI0(3,4) = 0,
YI0(3,5) = 0,
X1(4) = -1,
X2(4) = 1,
Z1(4) = 0.00168,
Z2(4) = 0.00218,
NZCELLS_PER_LAYER(4) = 381,
NXCELLS_PER_LAYER(4) = 1,
HCRZ(4) = 10000,
HCRX(4) = 0,
TINITIAL(4) = 300,
SOLVE_POROSITY_IN_LAYER(4) = .FALSE.,
YI0(4,1) = 0,
YI0(4,2) = 0,
YI0(4,3) = 0,
YI0(4,4) = 0,
YI0(4,5) = 1,
X1(5) = -1,
X2(5) = 1,
Z1(5) = 0.00218,
Z2(5) = 0.002965,
NZCELLS_PER_LAYER(5) = 381,
NXCELLS_PER_LAYER(5) = 1,
HCRZ(5) = 10000,
HCRX(5) = 0,
TINITIAL(5) = 300,
SOLVE_POROSITY_IN_LAYER(5) = .FALSE.,
YI0(5,1) = 0.429,
YI0(5,2) = 0,
YI0(5,3) = 0.571,
YI0(5,4) = 0,
YI0(5,5) = 0,
X1(6) = -1,
X2(6) = 1,
Z1(6) = 0.002965,
Z2(6) = 0.003465,
NZCELLS_PER_LAYER(6) = 381,
NXCELLS_PER_LAYER(6) = 1,
HCRZ(6) = 10000,
HCRX(6) = 0,
TINITIAL(6) = 300,

SOLVE_POROSITY_IN_LAYER(6) = .FALSE.,
YI0(6,1) = 0,
YI0(6,2) = 0,
YI0(6,3) = 0,
YI0(6,4) = 0,
YI0(6,5) = 1,
X1(7) = -1,
X2(7) = 1,
Z1(7) = 0.003465,
Z2(7) = 0.00425,
NZCELLS_PER_LAYER(7) = 381,
NXCELLS_PER_LAYER(7) = 1,
HCRZ(7) = 10000,
HCRX(7) = 0,
TINITIAL(7) = 300,
SOLVE_POROSITY_IN_LAYER(7) = .FALSE.,
YI0(7,1) = 0.429,
YI0(7,2) = 0,
YI0(7,3) = 0.571,
YI0(7,4) = 0,
YI0(7,5) = 0,
X1(8) = -1,
X2(8) = 1,
Z1(8) = 0.00425,
Z2(8) = 0.00475,
NZCELLS_PER_LAYER(8) = 381,
NXCELLS_PER_LAYER(8) = 1,
HCRZ(8) = 10000,
HCRX(8) = 0,
TINITIAL(8) = 300,
SOLVE_POROSITY_IN_LAYER(8) = .FALSE.,
YI0(8,1) = 0,
YI0(8,2) = 0,
YI0(8,3) = 0,
YI0(8,4) = 0,
YI0(8,5) = 1,
X1(9) = -1,
X2(9) = 1,
Z1(9) = 0.00475,
Z2(9) = 0.005535,
NZCELLS_PER_LAYER(9) = 381,
NXCELLS_PER_LAYER(9) = 1,
HCRZ(9) = 10000,
HCRX(9) = 0,
TINITIAL(9) = 300,
SOLVE_POROSITY_IN_LAYER(9) = .FALSE.,

YI0(9,1) = 0.429,
YI0(9,2) = 0,
YI0(9,3) = 0.571,
YI0(9,4) = 0,
YI0(9,5) = 0,
X1(10) = -1,
X2(10) = 1,
Z1(10) = 0.005535,
Z2(10) = 0.006035
NZCELLS_PER_LAYER(10) = 381,
NXCELLS_PER_LAYER(10) = 1,
HCRZ(10) = 10000,
HCRX(10) = 0,
TINITIAL(10) = 300,
SOLVE_POROSITY_IN_LAYER(10) = .FALSE.,
YI0(10,1) = 0,
YI0(10,2) = 0,
YI0(10,3) = 0,
YI0(10,4) = 0,
YI0(10,5) = 1,
X1(11) = -1,
X2(11) = 1,
Z1(11) = 0.006035,
Z2(11) = 0.00682,
NZCELLS_PER_LAYER(11) = 381,
NXCELLS_PER_LAYER(11) = 1,
HCRZ(11) = 10000,
HCRX(11) = 0,
TINITIAL(1) = 300,
SOLVE_POROSITY_IN_LAYER(11) = .FALSE.,
YI0(11,1) = 0.429,
YI0(11,2) = 0,
YI0(11,3) = 0.571,
YI0(11,4) = 0,
YI0(11,5) = 0,
X1(12) = -1,
X2(12) = 1,
Z1(12) = 0.00682,
Z2(12) = 0.00732,
NZCELLS_PER_LAYER(12) = 381,
NXCELLS_PER_LAYER(12) = 1,
HCRZ(12) = 10000,
HCRX(12) = 0,
TINITIAL(12) = 300,
SOLVE_POROSITY_IN_LAYER(12) = .FALSE.,
YI0(12,1) = 0,

YI0(12,2) = 0,
YI0(12,3) = 0,
YI0(12,4) = 0,
YI0(12,5) = 1,
X1(13) = -1,
X2(13) = 1,
Z1(13) = 0.00732,
Z2(13) = 0.008105,
NZCELLS_PER_LAYER(13) = 381,
NXCELLS_PER_LAYER(13) = 1,
HCRZ(13) = 10000,
HCRX(13) = 0,
TINITIAL(13) = 300,
SOLVE_POROSITY_IN_LAYER(13) = .FALSE.,
YI0(13,1) = 0.429,
YI0(13,2) = 0,
YI0(13,3) = 0.571,
YI0(13,4) = 0,
YI0(13,5) = 0,
X1(14) = -1,
X2(14) = 1,
Z1(14) = 0.008105,
Z2(14) = 0.008605,
NZCELLS_PER_LAYER(14) = 381,
NXCELLS_PER_LAYER(14) = 1,
HCRZ(14) = 10000,
HCRX(14) = 0,
TINITIAL(14) = 300,
SOLVE_POROSITY_IN_LAYER(14) = .FALSE.,
YI0(14,1) = 0,
YI0(14,2) = 0,
YI0(14,3) = 0,
YI0(14,4) = 0,
YI0(14,5) = 1,
X1(15) = -1,
X2(15) = 1,
Z1(15) = 0.008605,
Z2(15) = 0.009,
NZCELLS_PER_LAYER(15) = 381,
NXCELLS_PER_LAYER(15) = 1,
HCRZ(15) = 0,
HCRX(15) = 0,
TINITIAL(15) = 300,
SOLVE_POROSITY_IN_LAYER(15) = .FALSE.,
YI0(15,1) = 0.429,
YI0(15,2) = 0,

YI0(15,3) = 0.571,
YI0(15,4) = 0,
YI0(15,5) = 0,
/

&GPYRO_RXNS

NRXNS = 2,
CFROM(1) = 'Hetron',
CTO(1) = 'Hetron_residue',
Z(1) = 5000000000000000,
E(1) = 195,
DHS(1) = 0,
DHV(1) = 172000,
CHI(1) = 1,
ORDER(1) = 1.125,
ORDERO2(1) = 0,
IKINETICMODEL(1) = 0,
IO2TYPE(1) = 0,
M(1) = 0,
KCAT(1) = 0,
ICAT(1) = 0,
CFROM(2) = 'ATH',
CTO(2) = 'ATH_residue',
Z(2) = 2500000000000000,
E(2) = 140.1,
DHS(2) = 0,
DHV(2) = 1000000,
CHI(2) = 1,
ORDER(2) = 1.24,
ORDERO2(2) = 0,
IKINETICMODEL(2) = 0,
IO2TYPE(2) = 0,
M(2) = 0,
KCAT(2) = 0,
ICAT(2) = 0,
/

&GPYRO_HGRXNS

NHGRXNS = 0,
/

&GPYRO_GPROPS

NGSPEC = 1,
IBG = 1,
IO2 = 2,
CPG = 1000,

```
NAME(1) = 'pyrolysate' ,  
YJ0(1) = 1 ,  
M(1) = 44 ,  
SIGMA(1) = 5.061 ,  
EPSOK(1) = 254 ,  
B(1) = 0 ,  
TONSET(1) = 653 ,  
TSPAN(1) = 50 ,  
/  

```

```
&GPYRO_GYIELDS  
GYIELDS(1,1) = 1,  
GYIELDS(1,2) = 1,  
/  

```

```
&GPYRO_HGYIELDS  
/  

```

```
&GPYRO_SEBCPATCH  
NSEBCPATCH = 2,  
T(1) = 0,  
X1(1) = -1,  
X2(1) = 1,  
Z1(1) = 0,  
Z2(1) = 0,  
QE(1) = 50000,  
HC(1) = 10,  
TINF(1) = 300,  
RERADIATION(1) = .TRUE.,  
TFIXED(1) = -1,  
T(2) = 0,  
X1(2) = -1,  
X2(2) = 1,  
Z1(2) = 0.009,  
Z2(2) = 0.009,  
QE(2) = 0,  
HC(2) = 10,  
TINF(2) = 300,  
RERADIATION(2) = .FALSE.,  
TFIXED(2) = -1,  
/  

```

```
&GPYRO_GMBCPATCH  
NGMBCPATCH = 0,  
/  

```



```
&GPYRO_GSBPCATCH  
NGSBPCATCH = 0,  
/
```

```
&GPYRO_GEBPCATCH  
NGEBPCATCH = 0,  
/
```

```
&GPYRO_QE  
NQE = 1,  
QE(1) = 50000,  
HCO(1) = 10,  
NHC(1) = 0,  
DELTA0(1) = 0.009,  
NCELL(1) = 91,  
L(1) = 0.01,  
NBC(1) = 1,  
TIG(1) = 10000,  
QFL(1) = 0,  
TSTOP(1) = 1600,  
MIG(1) = 3,  
TMPIG(1) = 350,  
ZEROD(1) = .FALSE.,  
BETA(1) = 5,  
YJINF(1,1) = 1,  
/
```

```
&GA_GENINPUT NGEN = 100,  
NINDIV = 200,  
MAXCOPIES = 4,  
LINUX = .TRUE.,  
SIMULATED_EXPERIMENTAL_DATA = .FALSE.,  
RESTART = .FALSE.,  
FITMIN = 0,  
FITCLIP = 0,  
FITEXPONENT = 2,  
WHOLEGENEFAC = 0.3,  
BRUTE_FORCE = .FALSE.,  
KILL_NONCONVERGED_SOLNS = .TRUE.,  
/  
&GA_PHI  
NPHI = 0,  
/
```

```
&GA_VARS  
NGENE = 0,
```

/